Structure and functional characterization of recombinant chondroitin sulphate AC lyase of family 8 polysaccharide lyase (*Ps*PL8A) from *Pedobacter saltans* for its *in vitro* applications in therapeutics and production of chondroitin oligosaccharide with anti-cancer and prebiotic properties

A Thesis

Submitted in partial fulfillment of the requirements for the Degree of

Doctor of Philosophy

by

Aruna Rani

Under supervision of

Professor Arun Goyal

August 2017

DEPARTMENT OF BIOSCIENCES AND BIOENGINEERING

INDIAN INSTITUTE OF TECHNOLOGY GUWAHATI

GUWAHATI – 781039, ASSAM, INDIA

Structure and functional characterization of recombinant chondroitin sulphate AC lyase of family 8 polysaccharide lyase (*Ps*PL8A) from *Pedobacter saltans* for its *in vitro* applications in therapeutics and production of chondroitin oligosaccharide with anti-cancer and prebiotic properties

PhD Thesis

by

Aruna Rani

August 2017

DEPARTMENT OF BIOSCIENCES AND BIOENGINEERING

INDIAN INSTITUTE OF TECHNOLOGY GUWAHATI

GUWAHATI – 781039, ASSAM, INDIA

INDIAN INSTITUTE OF TECHNOLOGY GUWAHATI

DEPARTMENT OF BIOSCIENCES & BIOENGINEERING

STATEMENT

I do hereby declare that the content embodied in this thesis entitled as "**Structure and functional characterization of recombinant chondroitin sulphate AC lyase of family 8 polysaccharide lyase (*Ps*PL8A) from *Pedobacter saltans* for its *in vitro* applications in therapeutics and production of chondroitin oligosaccharide with anti-cancer and prebiotic properties"** is the result of investigations carried out by me in the Department of Biosciences and Bioengineering, Indian Institute of Technology Guwahati, Guwahati, India under the guidance of Professor Arun Goyal.

In keeping with the general practice of reporting scientific observations, due acknowledgements have been made wherever the work described is based on the findings of other investigators.

August, 2017 Aruna Rani

(11610622)

INDIAN INSTITUTE OF TECHNOLOGY GUWAHATI

DEPARTMENT OF BIOSCIENCES & BIOENGINEERING

CERTIFICATE

It is certified that the work described in this thesis entitled **"Structure and functional characterization of recombinant chondroitin sulphate AC lyase of family 8 polysaccharide lyase (*Ps*PL8A) from *Pedobacter saltans* for its *in vitro* applications in therapeutics and production of chondroitin oligosaccharide with anti-cancer and prebiotic properties"** by **Aruna Rani (Roll No. 11610622)** for the award of degree of Doctor of Philosophy is an authentic record of the results obtained from the research work carried out under my supervision at the Department of Biosciences & Bioengineering, Indian Institute of Technology Guwahati, Guwahati, India and this work has not been submitted elsewhere for a degree.

Dr. Arun Goyal *(MTech, PhD)*
(FAMI, FBRS, FABAP, FNABS, FNAAS, FIFIB)
Professor
(Thesis Supervisor)
Department of Biosciences & Bioengineering
Indian Institute of Technology Guwahati
Guwahati, 781 039, India

ACKNOWLEDGEMENTS

This thesis has been kept on track and been seen through to completion with the support and encouragement of many people including my supervisor, doctoral committee members, my family, my friends and colleagues. I would like to thank all those people who made this thesis possible and an unforgettable experience for me. At the end of my thesis, it is a pleasant task to express my thanks to all those who contributed in many ways and had profound impact in the success of this study deserves special acknowledgment.

Firstly, from the depth of my heart I express my deep sincere gratitude to the Almighty for the Blessings and strength bestowed upon me to complete this work.

At this moment of accomplishment, I am extremely indebted to my thesis supervisor, Professor Arun Goyal, Department of Biosciences and Bioengineering, IIT Guwahati. This work would not have been possible without his guidance, support and encouragement. Under his guidance I successfully overcame many difficulties and learned a lot. I earnestly thank him for inculcating in me scientific temperament and appreciable work ethics which helped me to achieve this goal. I am indebted to him for introducing me into the realm of this interesting work, training me with the techniques, giving me the freedom in designing and conducting the experiments. He has not only guided me in research, also his invaluable suggestion helped me to become a stronger person in life.

I would also like to express my sincere gratitude to all my doctoral committee members Dr. Nitin Chaudhury, Dr. Ajai B. Kunnumakkara, Prof. Tharmalingam Punniyamurthy for their valuable suggestions and constructive criticism during my progress presentations that has led to the successful completion of my thesis.

I am thankful to Department of Biosciences & Bioengineering and Central Instrumentation Facility (CIF), IITG for providing me instruments for my research work.

I would also like to express my sincere gratitude to Prof. M.N. Gupta, Department of Chemistry, IIT Delhi and his PhD student Joyeeta Mukherjee for Circular Dichroism (CD) analysis of my recombinant protein. I sincerely thank Dr. Ashish and his student Ms. Kunzes Dolma from Institute of Microbial Technology Chandigarh for Small Angle X-ray Scattering (SAXS) analysis.

I would also like to thank the present and previous heads of the Department of Biotechnology, IIT Guwahati, Prof. Kannan Pakshirajan, Prof. Venkata. V. Dasu, Prof. Arun Goyal for providing me with the necessary facilities.

I am also thankful to my seniors Dr. Shadab Ahamed, Dr. Rishikesh Shukla, Dr. Shraddha Shukla, Dr. T.J.M. Rao, Dr. Saprativ P. Das, Dr. Deeplina Das, Dr. Arabinda Ghosh, Dr. Damini Kothari, Dr. A.K. Verma, Dr. Soumyadeep Chakraborty for their help and suggestions. I am immensely thankful to my research group members Arun, Rwivoo, Kedar, Vikky, Shweta, Karthika, Sumitha, Abhijeet, Priyanka, Krishan and Subashree.

My greatest appreciation and friendship goes to my closest friends, Dr. Shalini Singh, Keshav, Sambhavi and Vibha who were always a great support in all my struggles and frustrations during my stay in IIT Guwahati. They were always cheering me up and stood by me through the good times and bad times. I am also thankful to Dr. Himangshu Sonowal for his valuable suggestions for cell culture experiments and analysis. I am thankful to my friends Dipti, Ruchi, Ruchira, Archita, Anuma, Haripriya and many more, who made my stay at the campus a memorable one by their company and moral support during the tenure of my PhD.

I wish to acknowledge the support received from other teaching and non-teaching staff of the Department of Biosciences and Bioengineering, IIT Guwahati.

I wish to acknowledge IIT Guwahati, Ministry of Human Resource and Development (MHRD) for providing financial assistance and experimental facilities and also Council of Scientific and Industrial research (CSIR), Govt. of India, New Delhi for providing me fellowship through its sponsored project.

My PhD endeavor would not have been successful without the love, trust, support and blessings of my parents, my brother, sisters and my furry family member lucky. I owe my achievements to my family.

Aruna Rani
August 2017

SYNOPSIS

Introduction

Proteoglycans (PGs) are glycoconjugates consisting of protein and polysaccharide glycosaminoglycans (GAGs). PGs are generally found on the cell surfaces, extracellular matrix (ECM) and in basement membranes of animal tissues (Ly *et at*., 2010; Li *et al*., 2012). PGs are involved in various biological functions including cell migration, proliferation, microbial recognition, adhesion, pathogenesis, cell-matrix interactions, chemokine and cytokine activation etc. (Cattaruzza *et al.,* 2006; Kreuger *et al.,* 2006; Garner *et al.,* 2008; Shaya *et al.,* 2008; Ly *et al.,* 2010). GAGs are highly charged linear chains of polysaccharides. GAGs are the natural heteropolysaccharides that are present in every mammalian tissue (Afratis *et al.,* 2012). GAGs are the side chains of PGs and are involved in various biological activities (Shaya *et al.,* 2008). On the basis of the structural configuration, GAGs have been categorized into 4 major types: hyaluronan, chondroitin/dermatan sulphates (CS/DS), heparan sulphate (HS) and keratan sulphate (Iozzo *et al.,* 1998; Capila *et al.,* 2002; Esko *et al.,* 2002; Linhardt *et al.,* 2004).

Among four Chondroitin sulphate (CS) is belonging to one of four major categories of the GAGs, and is an unbranched polymeric chain of repeating disaccharide unit. The disaccharide unit is consisting of N-acetyl-D- galactosamine (GalNAc) and glucuronic acid (GlcA) linked by [-4)GlcA(β1→3)GalNAc(β1-]$_n$ linkages (Shaya *et al.,* 2008). The main application of CS is in the treatment of osteoarthritis because of its anti-inflammatory action. Other potential applications of CS are its use as antiviral and

anti-infective agent, scaffolds for tissue regeneration and engineering and as biomarkers in cancer detection.

On the basis of substrate specificity, the chondroitin degrading enzymes (chondroitin lyases) are categorized mainly into three types such as chondroitin AC lyase, chondroitin B lyase and chondroitin ABC lyase (Fig. 1.6) (Linhardt *et al.,* 1994; Lunin *et al.,* 2004; Prabhakar *et al.,* 2006; Lemmnitzer *et al.,* 2014). Chondroitin AC lyase degrades both CS-A and CS-C and to a lesser extent hyaluronan (Gu *et al.,* 1995; Linhardt *et al.,* 2006). Chondroitin B lyase specifically degrades only dermatan sulphate as its sole substrate. They are not able to act on CS-A, CS-C and hyaluronan. Chondroitin ABC lyase is a broad specificity enzyme and is able to depolymerize CS-A, CS-C, DS and also hyaluronan to some extent (Shaya *et al.,* 2008).

The family 8 polysaccharide lyase (PL8) currently contain 27 well characterized sequences. The enzyme reported in family 8 have shown activities like chondroitin AC lyase (EC 4.2.2.5), chondroitin ABC lyase (EC 4.2.2.20), hyaluronate lyase (EC 4.2.2.1) and xanthan lyase (EC 4.2.2.12) (http://www.cazy.org/PL8.html). Chondroitin sulphate lyases of families 8 catalyze the cleavage of β-(1,4)-glycosidic bond between hexosamine and uronic acid residue by β-elimination and generate Δ4,5 unsaturated uronate oligosaccharides as the product, which exhibits a maximum absorbance at 232 nm (A_{232}). The main structural fold present in family 8 polysaccharide lyase is $(\alpha/\alpha)_{5,6}$ β toroid domain, which contains five α-helical hairpins and in some proteins a sixth hairpin is assembled from two additional antiparallel helices, one at the N-terminus and the other at the C-terminus of this domain. This domain is followed by a C-terminal antiparallel β-sandwich domain containing four β-sheets (Féthière *et al.,*

1999; Garron *et al.,* 2010). The PL8 family contains lyases that can depolymerize several different types of substrates such as CS-A, CS-B, CS-C, HA and xanthan. All these enzymes, with exception of hyaluronate lyase, contain structural ions, calcium or sodium, coordinated mainly by aspartate side chains. Despite similarities in their structures, none of these metal ion sites are conserved across this enzyme family (Garron *et al.,* 2010). There are nearly 930 bacterial, 2 eukaryotic and 1 archaeal sequences in family 8 polysaccharide lyase (http://www.cazy.org/PL8.html). Among which 27 sequences are characterized and 9 crystal structures have been determined till date (January 2017) (http://www.cazy.org/PL8.html).

The present work entitled as "Structure and functional characterization of recombinant chondroitin sulphate AC lyase of family 8 polysaccharide lyase (*Ps*PL8A) from *Pedobacter saltans* for its *in vitro* applications in therapeutics and production of chondroitin oligosaccharide with anti-tumor and prebiotic property" has been divided into 7 chapters. This study deals with the cloning, expression and purification of a family 8 polysaccharide lyase *Ps*PL8A (Fig. 1) from *Pedobacter saltans* DSM 12154. Biochemical and functional characterization of *Ps*PL8A was extensively carried out to determine its affinity towards different glycosaminoglycan substrate and understand its mode of action. Structural characteristics, substrate binding analysis and mutagenesis of active ste residues of chondroitin AC lyase (*Ps*PL8A) was studied. The anti-proliferative effect of chondroitin AC lyase (*Ps*PL8A) on human melanoma (SK-Mel 28) and fibrosarcoma (HT-1080) cell lines were determined. CS polysaccharide was isolated from chicken keel bone cartilage. The composition, structure, surface, thermal analysis, antioxidant activity and biocompatibility was explored. CS-Keel disaccharide

(CSD) was produced by chondroitin AC lyase (*Ps*PL8A) degradation of isolated CS-Keel polysaccharide and the prebiotic and anticancer potential of CSD was studied extensively for functional food preparation and prevention of gastrointestinal disorders.

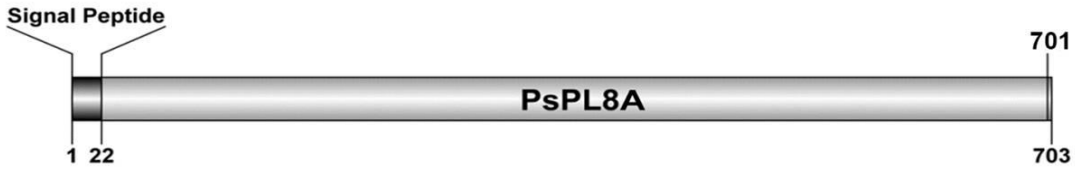

Fig. 1 Molecular architecture of chondroitin AC lyase (*Ps*PL8A) from *Pedobacter saltans* showing boundaries and designation of different domains. It consist a signal peptide of N-terminal 22 amino acids long signal peptide followed by the GAG lyase domain from 23 to 701 amino acids, a 679 amino acid domain.

Chapter 1 is the General Introduction which embodies the brief review of literature dedicated to the importance of different carbohydrates and their structural features. It mainly describes the types of glycosaminoglycans (GAG) present in mammalian body, their classification and application. The chapter also focuses on the polysaccharide lyase enzymes having the capability to degrade these GAG polysaccharides. It illustrates sequence-similarity based classification of chondroitin lyases belonging to different polysaccharide lyase (PL) families. It also describes different PLs categorized in to various 'clans' based on fold of proteins or core structural features. This chapter elaborately reviewed family 8 polysaccharide lyase (PL8). The chapter reviews about the type of structural core architecture seen in chondroitin lyases of family 8 PLs, their enzyme activities, substrate specificity, active site and active site residues. Previously characterized recombinant family 8 chondritin sulphate lyases, such as chondroitin AC lyase, chondroitin ABC lyase and chondroitin B lyase from different bacteria. A brief review on different chondroitin lyases and their mode of

action during enzymatic reaction has been included. A detailed account of applications of chondroitin sulpahte lyases in various therapeutic field has also been provided.

Significance of the work has been elaborated in this chapter. Chondroitin sulphate is a part of connective tissues and involved in major biological processes such as resiliency, structural integrity of cartilage and maintenance of synovial fluid in the bone joints owing to its polyanionic structure (Raynauld *et al.*, 2016). CS also acts as free radical scavenger and decreases DNA fragmentation, protein degradation and cell death rate. CS is commercially available from various sources such as, bovine cartilage, bovine trachea and shark fin. The increasing demand and the high cost of CS has led to the exploitation of shark and bovine which impart a strong impact on the ecological balance. CS is also in high demand for its applications in tissue engineering, pharmaceutical, cosmetic and food industries. All these reasons make it essential for researchers to seek for more different animal sources of CS isolation and its physicochemical characterization. Recruitment of CS lyase to modulate structure and functionality of CS polysaccharides might be effective in this regard. Substrate specificity of the enzyme requires precise understanding to manipulate the targeted polysaccharide. Analytical tools like mass spectrometry, NMR and FTIR can facilitate this pursuit. Novel CS lyases can be identified by screening new microbes from various taxonomic groups. Production of anti-inflammatory and anti-oxidative oligosaccharides might be employed to tackle allergic, auto-immune diseases and cancer. CS lyase-based manipulation of cancer hallmarks, the altered cell surface receptors can be crucial towards cancer mitigation. CS lyase has shown synergistic effect with other therapeutic

agents which requires assessment. Overall, a plethora of approaches can be undertaken to enrich CS lyase research in discovery of their optimal biological efficiency.

The aim of present study was to explore the new recombinant chondroitin AC lyase, *Ps*PL8A from *Pedobactor saltans*. The specific primers will be designed to amplify gene and it will be subsequently cloned into an expression vector followed by expression in *E. coli*. The substrate specificity and various biochemical and functional properties of *Ps*PL8A will be determined. The reaction conditions for enzyme assay, kinetic parameters and mode of catalysis will be investigated. The *in-vitro* therapeutic potential of *Ps*PL8A will be studied on the human melanoma and fibrosarcoma cell lines. The present study will unfold the avenue for the potential application of *Ps*PL8A as antitumor agent. The structural analysis of *Ps*PL8A will involve the homology modelling, docking and circular dichroism study to determine the overall structure feature and key amino acid residues and their role in catalysis of *Ps*PL8A. desired mutants of key residues of *Ps*PL8A and deciphering.

The other part of the investigation involves the isolation, complete physicochemical and structural characterization of a chondroitin sulphate from the poultry waste, chicken keel bone cartilage. The CS-keel will be analyzed for its various physicochemical properties and its antioxidant and emulsifying potentials. The recombinant *Ps*PL8A will be utilized for the production of CS-keel oligosaccharide by degrading CS-keel polysaccharide. The CS-keel disaccharide will be studied for their anticancer potential on human colon cancer cell lines. *In vitro* prebiotic potential of purified CS-keel disaccharide for functional foods will be investigated.

Chapter 2 describes amplification and cloning of the gene encoding family 8 polysaccharide lyase *Ps*PL8A from the genomic DNA of *Pedobacter saltans* DSM 1214 (GenBank accession no. ADY54337.1). The molecular architecture revealed the presence of 22 amino acid signal peptide followed by the catalytic family 8 polysaccharide module (*Ps*PL8A). The ORF encoding *Ps*PL8A was PCR amplified that showed a band of 2037 bp. The PCR amplified gene fragment encoding *Ps*PL8A was cloned into pGEM-T Easy vector for TA cloning and transformed using *E. coli* (XL10 Gold) competent cells. Positive clones were selected by blue-white colony screening, and plasmid DNA was isolated for restriction digestion. *NheI* and *XhoI* digested plasmid DNA gave bands of 3 kb and 2 kb for pGEM-T Easy vector and the insert gene fragment encoding *Ps*PL8A, respectively. The restriction enzyme digested gene fragment encoding *Ps*PL8A was ligated to linearized pET-28a(+) expression vector. The ligated product was transformed using *E. coli* DH5α competent cells. The positive clone containing recombinant plasmid DNA was screened by restriction enzyme digestion using restriction enzymes, *Nhe*I and *Xho*I. The restriction enzyme digested products displayed 5.4 kb and 2 kb bands for pET-28a(+) vector and insert fragment for gene encoding *Ps*PL8A, respectively. The positive clone containing recombinant plasmid DNA was used for transformation of *E. coli* (BL21) competent cells. The recombinant protein *Ps*PL8A was hyper-expressed at 24 ºC after IPTG induction. The purified recombinant *Ps*PL8A protein displayed a band of approximately, 77 kDa on SDS-PAGE. The amount of protein obtained from 100 ml culture of the recombinant *Ps*PL8A protein after Immobilized metal ion affinity chromatography (IMAC) purification was 3.5 mg.

Chapter 3 describes the biochemical and functional characterisation of chondroitin AC lyase (*Ps*PL8A). *Ps*PL8A showed maximum enzyme activity at optimum pH 7.2 and was active within the pH range of 6.8-7.6. The optimal temperature of *Ps*PL8A was 39ºC and it showed ~100% retention of activity within temperature range 30 - 40ºC. Both the enzymes showed high activity towards pectic polysaccharides. *Ps*PL8A showed maximum activity with chondroitin 4-sulphate, C4S (489 U/mg) followed by chondroitin 6-sulphate, C6S (214 U/mg) and hyaluronic acid (43 U/mg). 100 mM Na^{+}, 20 mM Ca^{2+} and 20 mM Co^{2+} ions enhanced the *Ps*PL8A activity by 2 fold implying that these ions might play a role of essential cofactors. A 1.5 fold rise in enzyme activity of *Ps*PL8A was observed with 20 mM Mg^{2+} ion concentration. However, the enzyme activity of *Ps*PL8A was adversely affected at the low concentrations of Zn^{2+}, Al^{3+}, EDTA and SDS. A 5 M Urea and 3 M GuHCl imparts the peak shift hence indicating loss of structural integrity of *Ps*PL8A. The melting study of *Ps*PL8A revealed that it starts unfolding at 45ºC and the protein got completely distorted at 60ºC.

The time dependent TLC analysis of *Ps*PL8A degraded products of C4S revealed initial concomitant endo- and exo-lytic mode and later shifting to exolytic mode of catalysis. *Ps*PL8A released di-, hexa-, octa- and dodeca-saccharide as analyzed by ESI–MS. C4S disaccharide gave peaks at m/z 458 in (ESI–MS) and at m/z 300 in MS/MS modes. ^{1}H- and ^{13}C-NMR analyses confirmed the presence of N-acetylgalactosamine and glucuronic acid in C4S disaccharide. The *Ps*PL8A enzyme and its degradation products unfolds the avenue for its potential applications in spinal cord

nerve injury system and as antitumor, antiangiogenic, anti-metastatic agent and for immune-modulating and anti-inflammatory effects.

Chapter 4 focuses on the structural aspects of *Ps*PL8A. The structure of chondroitin AC lyase (*Ps*PL8A) of family 8 polysaccharide lyase was characterized. Multiple sequence alignment of *Ps*PL8A with previously known chondroitin lyases revealed the conserved and semi-conserved amino acid residues. The 3-Dimensional structure showed a N-terminal $(\alpha/\alpha)_6$ incomplete toroidal fold and a layered β sandwich structure at C-terminal. Ramchandran plot displayed 98.5% residues in the favoured region and 1.2% in the generously allowed region. The secondary structure of *Ps*PL8A prediction by PsiPred and confirmation by CD analysis revealed the presence of 27.31% α helices 22.7% β sheets and rest 49.9% random coils. The protein melting study of *Ps*PL8A showed that the protein completely unfolds at 60ºC. SAXS showed the *Ps*PL8A structure in solution form. Kratky plot gave indication that protein is fully folded in solution. The *ab initio* derived dummy atom model of *Ps*PL8A superposed well with its modeled structure with some α-helices and loop region not superposing with dummy atom model. ITC analysis of Y212F and H203A with C4S polysaccharide, showed moderate quantitative binding by Y212F (Ka = 9.56 ± 3.81×10^5) and no binding with H203A. The roles of catalytic residues Y212 and H203 or R266 as probable general base and general acid, respectively were confirmed by site-directed mutagenesis. The involvement of Y212, H203 and R266 residues in substrate binding was confirmed by ITC and docking analyses. The structural characterization of chondroitin AC lyase (*Ps*PL8A) has enabled in elucidation of the catalytic mechanism. The residues Y212 and H203 or R266 might act as general base and general acid

respectively, during catalysis. N153 and E349 are likely contributing in charge neutralization and stabilizing the enolate anion intermediate during β-elimination. The structural characterization will enable to elucidate the complete mechanism underlying the mode catalysis of chondroitin AC lyase (*Ps*PL8A). However, the future challenge includes to determine the crystal structure of *Ps*PL8A by X-ray crystallography.

Chapter 5 describes the anti-proliferative effect of chondroitin AC lyase (*Ps*PL8A) on human melanoma (SK-Mel 28) and fibrosarcoma (HT-1080) cell lines. The treatment of normal mouse fibroblast L929 cell lines with chondroitin AC lyase (*Ps*PL8A) imparts no cytotoxicity displaying 95-98% cell viability. The human melanoma SK-Mel 28 and fibrosarcoma HT-1080 cell lines treated with chondroitin AC lyase (*Ps*PL8A) showed 58% and 59% inhibition of cell proliferation, respectively after 24h of treatment. Mode of cell death was studied by Annexin-V FITC using flow cytometry and fluorescence microscopy. The chondroitin AC lyase treated SK-Mel 28 and HT-1080 cell lines displayed ~27% and 17% apoptosis, respectively as observed by flow cytometry analysis. The *Ps*PL8A treated SK-Mel 28 and HT-1080 cells showed significantly strong green fluorescence of cell membrane after staining with annexin-V FITC under fluorescence microscopy, displaying the apoptosis. The SK-Mel 28 and HT-1080 treated with chondroitin AC lyase (*Ps*PL8A) and staining with JC-1 dye gave green fluorescence, hence indicating the dissipation of mitochondrial potential. The chondroitin AC lyase inhibiting the melanoma and fibrosarcoma cell proliferation and leading to their apoptotic cell death prospects a potential target for therapeutic approach in cancer treatment.

Chapter 6 describes the isolation of natural chondroitin sulphate from the poultry waste, its structural and thermal characterization, antioxidant and biocompatible properties for potential biomedical application. Chicken keel bone cartilage was explored for cheaper and sustainable source for isolation of chondroitin sulfate (CS) for its future use in tissue engineering and pharmaceutical industry. HPSEC analysis displayed two peaks of 100 kDa for CS-Keel polysaccharide and 1 kDa for protein. DLS analysis of CS-Keel displayed polydispersity. CS-Keel yield was 15% and 53±5% uronic acid content. The quantified percentages of UA-GalNAc4S and UA-GalNAc6S disaccharide in CS-Keel were 58% and 42%, respectively. FT-IR identified CS-Keel to be chondroitin 4-sulphate. ^{1}H-NMR of CS-Keel confirmed the presence of N-acetylgalactosamine and Glucuronic acid. FESEM demonstrated layer structure and AFM displayed the size of CS-Keel fibres. DSC, TGA and DTG studies of CS-Keel showed T_d at 243ºC. The composition, structure, surface and thermal analysis of CS-Keel displayed that it can serve as a strong candidate in tissue scaffolds for biomedical engineering. *In vitro* cell proliferation assay and morphological analysis of mouse fibroblast L929 cell lines confirmed the biocompatibility of CS-Keel. CS-Keel (5 mg/ml) exhibited ~49% antioxidant activity against DPPH and 22% against superoxide radical protecting from oxidative damage. CS-Keel demonstrated better (70.3%) emulsifying activity than commercial sodium alginate (60.2%). Therefore, CS-Keel can be used for functional food applications enriching the nutritional values. CS-Keel also enables future prospects for analysis of its chondroprotective and anti-inflammatory properties for osteoarthritis treatment. Future challenges include its utilization in

nanomedicine to develop an efficient delivery vehicle for therapeutic agents, to further enhance its specificity and finally to have controlled drug release.

Chapter 7 describes about the preparation and purification of Prebiotic chondroitin sulphate disaccharide isolated from chicken keel bone exhibiting anticancer potential against human colon adenocarcinoma HT-29 cells. Chondroitin Sulphate-Keel disaccharide (CSD) was produced by chondroitin AC lyase (*Ps*PL8A) degradation of CS-Keel polysaccharide isolated from chicken keel cartilage. *Ps*PL8A showed specific activity, 340±5 U/mg with CS-Keel polysaccharide. Time dependent TLC analysis showed the presence of higher oligosaccharide till 30 min after which the disaccharide was the major product. CSD was purified by gel filtration using Bio-Gel P2 matrix and the ESI-MS and MS/MS analysis showed peak at 300 m/z, confirming it to be chondroitin 4-sulpahte disaccharide. The structural characterization of CSD by FTIR and NMR showed the presence of N-acetylgalactosamine and glucuronic acid. CSD displayed prebiotic properties by showing 23.7% hydrolysis to gastric juice, comparable to commercial inulin (25.2%) at pH 1.0. CSD showed a positive prebiotic score for *Lactobacillus acidophilus* NRRL B-4495(0.57) and *Bifidobacterium infantis* NRRL B-41661 (0.58). CSD was fermented by probiotic bacteria into Short Chain Fatty Acid (SCFA) products such as acetate, propionate and butyrate. MTT assay and morphological analysis confirmed that CSD (0.5 mg/ml) does not decrease the viability of mouse fibroblast (L929) cell lines and showed anti-proliferative potential against human colon cancer (HT-29) cell lines displaying 80% inhibition. CSD treated HT-29 cells also displayed the nuclear fragmentation on observation by DAPI dye. CSD treated HT-29 cells showed more intense staining of nuclei with DAPI as compared with the

untreated cells because of chromatin condensation. CSD treated HT-29 cells exhibited apoptotic body formation, which confirms apoptosis as major mode of cell death as observed by annexin-V-FITC and PI staining. Colonic microflora has a profound influence on health. CSD having the prebiotic and anticancer properties can be used to manipulate the colonic microflora to improve gut health and can specifically target intestinal bowel disorders, colorectal cancer and maintain the gastrointestinal health. Future challenges includes the study of the prebiotic and anti-colorectal cancer potential of CSD under *in vivo* conditions.

CONTENTS

Chapter 2. Cloning, expression and purification of chondroitin sulphate AC lyase of family 8 polysaccharide lyase (*Ps*PL8A) from *Pedobacter saltans* DSM12145

Chapter 1

General Introduction

1. Introduction

Proteoglycans (PGs) are glycoconjugates consisting of protein and polysaccharide glycosaminoglycans (GAGs). PGs are generally found on the cell surfaces, extracellular matrix (ECM) and in basement membranes of animal tissues (Ly *et at*., 2010; Li *et al*., 2012). PGs are involved in various biological functions including cell migration, proliferation, microbial recognition, adhesion, pathogenesis, cell-matrix interactions, chemokine and cytokine activation etc. (Cattaruzza *et al.,* 2006; Kreuger *et al.*, 2006; Garner *et al.*, 2008; Shaya *et al.*, 2008; Ly *et al.*, 2010). GAGs are highly charged linear chains of polysaccharides. GAGs are the side chains of PGs and are involved in various biological activities (Shaya *et al.*, 2008).

1.1 Glycosaminoglycans

GAGs are the natural heteropolysaccharides that are present in every mammalian tissue (Afratis *et al.*, 2012). GAGs are composed of disaccharide repeats

of two hexose monosaccharide units, D-galactosamine/D-glucosamine and D-glucuronic acid/L-Iduronic acid (Shaya *et al.*, 2008; Igarashi *et al.*, 2013). The two monosaccharide units are connected by β-(1→3)-glycosidic linkage while the two disaccharide units are connected by β-(1→4)-glycosidic linkage and forms an unbranched chain (Linhardt *et al.*, 2006; Igarashi *et al.*, 2013). On the basis of the structural configuration, GAGs have been categorized into 4 major types: hyaluronan, chondroitin/dermatan sulphates (CS/DS), heparan sulphate (HS) and keratan sulphate (Iozzo *et al.*, 1998; Capila *et al.*, 2002; Esko *et al.*, 2002; Linhardt *et al.*, 2004). The 3 important GAGs and the structure of CS are shown in Fig. 1.1.1. The backbone of these GAGs is linear with repetitive units, having variations in (i) sulfation at different carbon positions, (ii) uronate epimerization and (iii) acetylation at the amino group of the galactosamine (Huang *et al.*, 2003; Yamada *et al.*, 2008; Huang *et al.*, 2011).

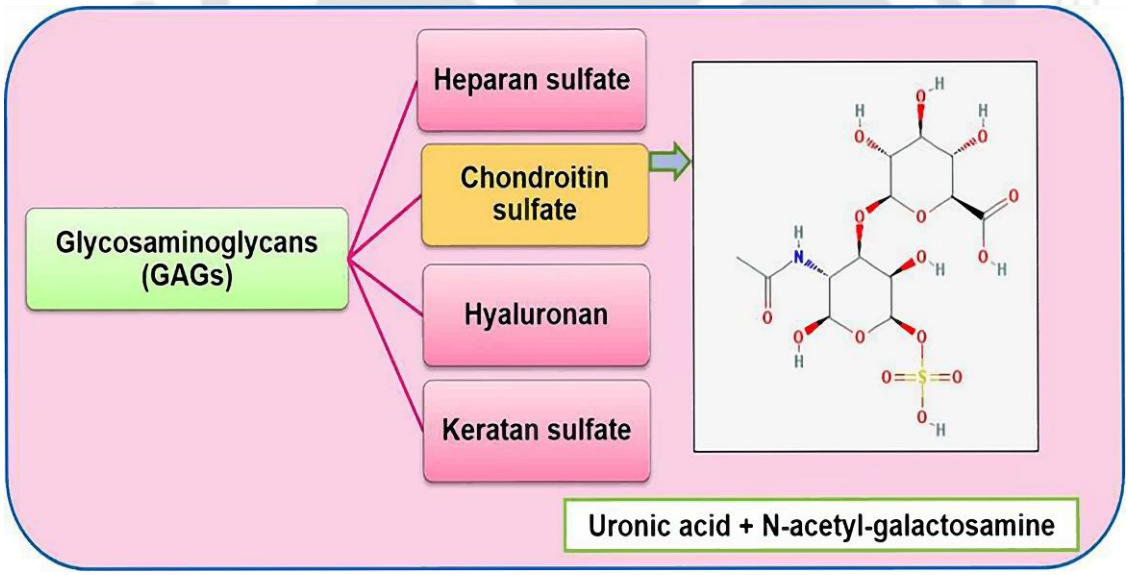

Fig. 1.1.1 Types of GAGs. (The chemical structure of chondroitin sulphate is referred from Pubchem).

Chondroitin sulphate/Dermatan sulphate (CS/DS) are the GAGs made up of alternating units of N-acetyl-D- galactosamine (GalNAc) and glucuronic acid

(GlcA)/Iduronic acid (IdoA) (Shaya *et al.*, 2008). The polysaccharide chain is sulphated at C2 position of uronic acid and/or at C4/C6 position of N-acetyl-D- galactosamine residue (Huang *et al.,* 2003). Though, the GAG subclass HS has been studied extensively for its ubiquitous role in cell signalling and developmental process (Sugahara *et al.*, 2000). In this regard, CS/DS has been only meagerly explored, though CS forms a key component of bone synovial fluid.

Existing studies report that CS/DS interact with various growth factors and adhesion molecules and play crucial role in cell proliferation, differentiation, migration, central nervous system (CNS) development, infection, wound repair and other important physiological events (Esko *et al.,* 2002; Sugahara *et al.,* 2003; Rauch *et al.,* 2006; Uyama *et al.,* 2007). CS/DS chains have been exploited as the cell surface receptors by the malarial parasites and HSV-1 virus which might be of therapeutic significance (Banfield *et al.,* 1995; Mårdberg *et al.,* 2002; Brustoski *et al.,* 2005). The biological functions of GAGs hinge on their architecture, which makes the GAG-degrading enzymes crucial for deciphering their structure and function. The major source of these enzymes are microorganisms, such as *Flavobacterium heparinum* (Pojasek *et al.,* 2001), *Arthrobacter aurescens* (Lunin *et al.,* 2004) and *Bacteroides species* (Hong *et al.,* 2002; Shaya *et al.,* 2008). Chondroitin 4-sulphate (CS-A), chondroitin 6-sulphate (CS-C) and DS are found within the extracellular matrix (ECM) or on cell membranes attached to a variety of proteins, including decorin, biglycan and aggrecan (Kresse *et al.,* 2001; Matuszewski *et al*., 2012). The CS-degrading enzymes, chondroitin lyases (CS lyases) have been classified into family 6, 8 and 23 polysaccharide lyase in the CaZy database (Cantarel *et al*., 2009). The CS degrading enzyme are also known as chondroitinases. CS lyase degrades CS by β-elimination

mechanism and generates an unsaturated hexenuronic acid residue and a new reducing end (Cantarel *et al*., 2009). These enzymes have been cloned, expressed and purified from various bacterial sources such as *Flavobacterium heparinum* (Gu *et al*., 1995; Pojasek *et al.*, 2001), *Bacteroides thetaiotaomicron* (Shaya *et al*., 2008), *Arthrobacter aurescens* (Lunin *et al*., 2004) *Bacteroides stercoris* HJ-15 (Hong *et al.*, 2002), *Serratia marcescens* (Ke *et al.*, 2005) and virus *Autographa californica* nucleopolyhedrovirus (ODV-E66) (Sugiura *et al.*, 2011).

1.2 Chondroitin Sulphate

Among four Chondroitin sulphate (CS) is belonging to one of four major categories of the GAGs, and is an unbranched polymeric chain of repeating disaccharide unit. The disaccharide unit is consisting of N-acetyl-D- galactosamine (GalNAc) and glucuronic acid (GlcA) linked by [-4)GlcA(β1→3)GalNAc(β1-]$_n$ linkages (Shaya *et al.*, 2008). The basic structure of the CS disaccharide unit was first reported in 1913 in which glucuronic acid (GlcA) was identified and within the course of the following 2 years, the structure of the other subunit *N*-acetylgalactosamine (Gal*N*Ac) was also reported (Levene and La Forge, 1914; Kwok *et al.*, 2012). CS is regio-selectivel y O-sulphated at position 4 or 6 of GalNAc which gives rise to two isomers, chondroitin 4-sulphate (CS-A) and chondroitin 6-sulphate (CS-C), respectively (Fig. 1.2.1A & 1.2.1B) (Murata *et al.*, 1985; Habuchi *et al.*, 2000; Jin *et al.*, 2010). Dermatan sulphate or chondroitin sulphate B (CS-B) is composed of repeating units of iduronic acid (IdoA), the epimeric form of glucuronic acid and N-acetyl-D-galactosamine (GalNAc) (Fig. 1.2C) (Halldórsdóttir *et al.*, 2006). The sulfation is present in position 4 or 6 of the GalNAc and position 2 of the IdoA (Halldórsdóttir *et al.*, 2006).

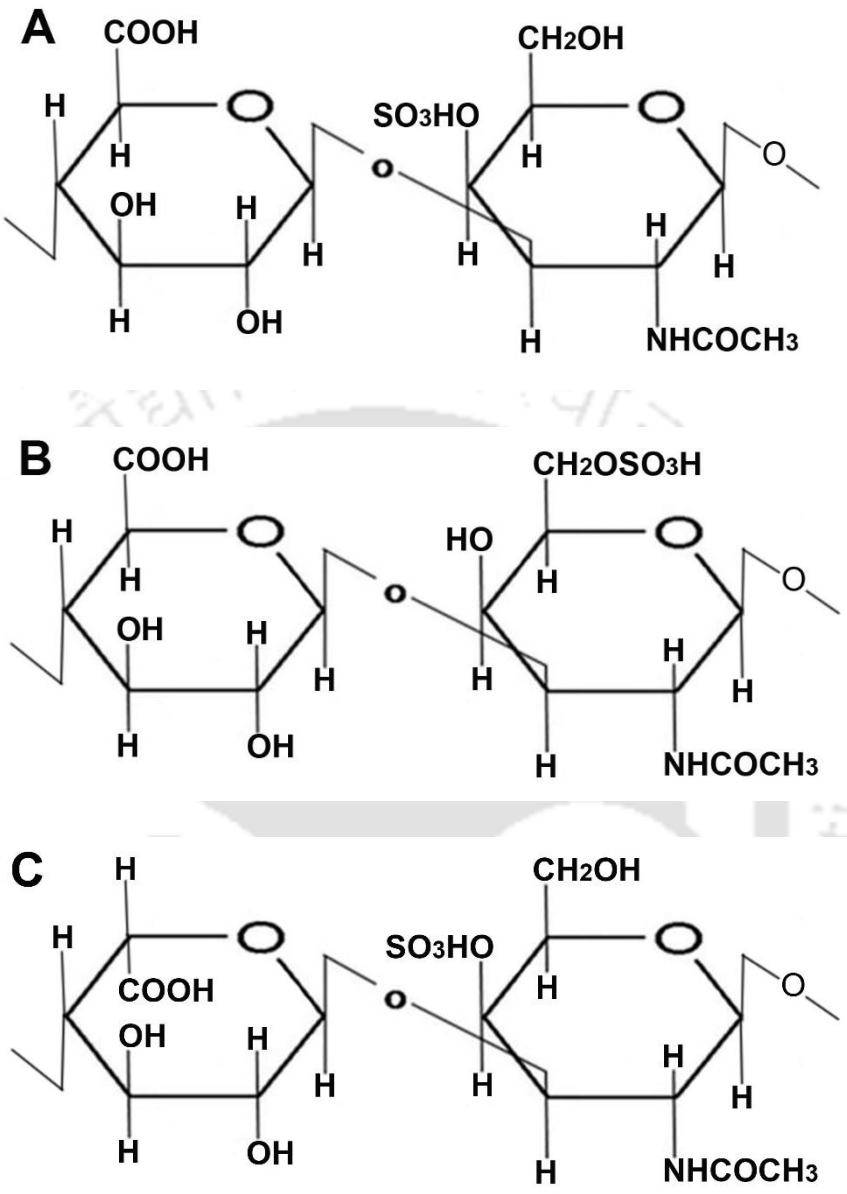

Fig. 1.2.1 (A) Chondroitin 4- sulphate, consist of an alternating copolymer of β-glucuronic acid-(1-3)-N-acetyl-β-galactosamine-4-sulphate, (B) Chondroitin 6-sulphate consist of an alternating copolymer of β-glucuronic acid-(1-3)-N-acetyl-β-galactosamine-6-sulphate and (C) Dermatan sulphate consist of an alternating copolymer of β-iduronic acid-(1-3)-N-acetyl-β-galactosamine-4-sulphate.

1.3 Chondroitin sulphate proteoglycans

CS are generally found as the GAG chains bound to serine residue of the protein core linked through a tetrasaccharide linkage region made up of xylose-galactose-galactose-glucuronic acid and forming a proteoglycan (PG) (Fig. 1.3.1) (Kresse *et al.*, 2001; Silbert *et al.*, 2002). Aggrecan, a major PG of the cartilage mainly consists of CS (Kempson *et al.*, 1980; Linhardt *et al.*, 2006). The presence of negative charge on the CS confers osmotic effect to the cartilage resisting shrinkage (Linhardt *et al.*, 2006; Kwok *et al.*, 2012). CS is responsible for the resiliency and structural integrity of the cartilage tissue. Clinical studies have demonstrated a favorable therapeutic effect of CS in the treatment of Osteoarthritis (Henrotin *et al.*, 2010). Other CS proteoglycans (CSPGs) such as neurocan, versican, brevican and phosphacan have been found as the major components in nervous system (Herndon *et al.*, 1990; Kwok *et al.*, 2012).

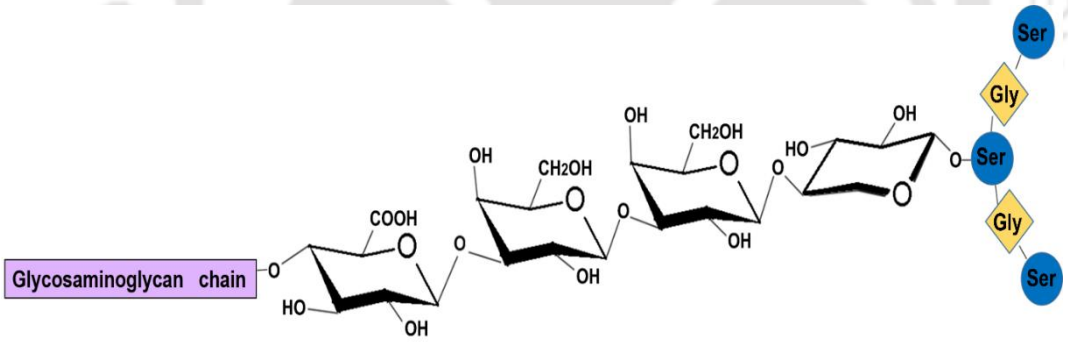

Fig. 1.3.1 Structure of Proteoglycan.

1.3.1 Biosynthesis of chondroitin sulphate proteoglycans

The biosynthesis of CSPGs requires an array of enzymes present in endoplasmic reticulum (ER) and Golgi apparatus. The core protein is assembled in Golgi apparatus whereas the CS chain is synthesized in the ER (Linhardt *et al.*, 2006; (Laremore *et al.*, 2009; Mikami *et al.*, 2013). The tetrasaccahride linker region (Xyl-Gal-Gal-GlcA) starts associating with the protein in the ER (Sugahara *et al.*, 2000; Linhardt *et al.*, 2006;

Mikami *et al.,* 2013). Xyl residue of the tetrasaccharide attaches to the serine residue of the protein with xylosyl transferase in ER. Further, two Gal are added in Golgi body through the action of galactosyltransferase I and galactosyltransferase II, whereas GlcA is added by glucuronyltransferase I, completing the linker (Sugahara *et al.,* 2000; Sugahara *et al.,* 2003; Laremore *et al.,* 2009; Mikami *et al.,* 2013). Subsequent addition of GalNAc and GlcA to the linker region occurs by a multitude of enzymes including GalNAc transferase, GlcA transferases, chondroitin synthases, CS N-acetyl galactosaminyl transferases I and II, CS glucuronyltransferase and chondroitin sulphate polymerizing factor (Kitagawa *et al.,* 2001; Kwok et al., 2012).

1.4 Application of Chondroitin sulphate

The main application of CS is in the treatment of osteoarthritis because of its anti-inflammatory action. Other potential applications of CS are its use as antiviral and anti-infective agent, scaffolds for tissue regeneration and engineering and as biomarkers in cancer detection.

1.4.1 CS in osteoarthritis treatment

CS is a part of connective tissues and involved in major biological processes such as resiliency, structural integrity of cartilage and maintenance of synovial fluid in the bone joints owing to its polyanionic structure (Fig. 1.4.1) (Luo *et al.,* 2002, Henrotin *et al.,* 2010). Low-molecular weight CS are beneficial for treatment and prevention of osteoarthritis because it inhibits cartilage degrading enzymes (Lauder *et al.,* 2009; Schiraldi *et al.,* 2010). CS showed chondroprotective properties as a result of increase in the biosynthesis of connective tissue components such as, collagen, proteoglycan and hyaluronan and hence increase of the viscosity of the synovial fluid at disease sites (Schiraldi *et al.,* 2010). At present in the United States of America several CS

containing products, often combined with glucosamine, are marketed as "dietary supplements" (Schiraldi *et al.*, 2010).

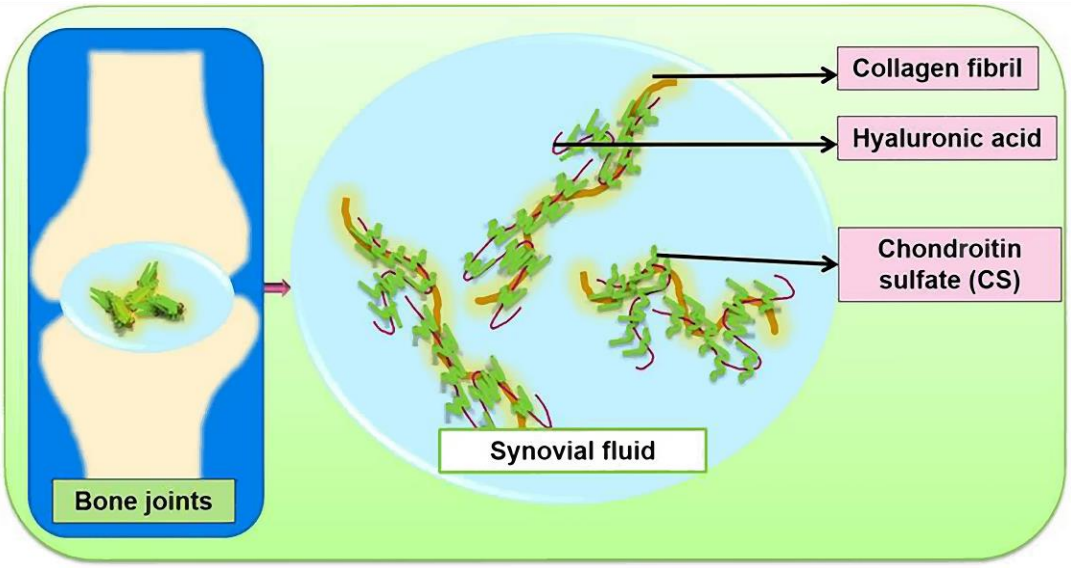

Fig. 1.4.1 Configuration of Chondroitin sulphate along with collagen fibrils and hyalunoric acid in synovial fluid**.**

1.4.2 CS as anti-inflammatory agent

CS supplements have an effect in relieving pain and stiffness caused by arthritis with fewer side effects as compared with conventional drugs. The beneficial effects of CS have been reported for joint pains, stiffness and swelling in osteoarthritis patents (Hochberg *et al.*, 2015; Raynauld *et al.*, 2016). CS binds to (Tumor Necrosis Factor) TNF-α, inhibits its activity and hence reduces inflammation of joints (Tully *et al.*, 2006; Lauder *et al.*, 2009). CS may also influence inflammatory processes by inhibiting the expression of pro-inflammatory molecules such as reducing Interleukin-1β induced Nuclear Factor- KappaB (NF-ĸB) nuclear translocation and TNF- α induced signalling (Lauder *et al.*, 2009).

1.4.3 CS in tissue engineering

CS alone or in combination with hyaluronic acid or chitosan were used to formulate scaffolds that mediate and accelerate the regeneration of damaged tissues, bone repair, cartilage and cutaneous wounds (Bianchera *et al.,* 2014). CS-hydrogels are appealing materials for biomedical application as they enhance wound healing by reepithelialization and neovascularization (Bianchera *et al.,* 2014). A research report describes the application of bi-layer gelatin-chondrointin-6-sulfate-hyaluronic acid (gelatin-C6S-HA) biomatrices in tissue engineered skin substitutes (Wang *et al.,* 2006). The results demonstrated the feasibility of these scaffolds to overcome the shortage of skin autograft by *in vitro* culturing the keratinocytes and dermal fibroblasts (Wang *et al.,* 2006).

1.4.4 Anti-oxidative properties of CS

CS also acts as free radical scavenger and decreases DNA fragmentation, protein degradation and cell death rate (Campo *et al.,* 2006; Henrotin *et al.,* 2010). This antioxidant activity, caused by the chelation of transition metals such as Cu^{2+} and Fe^{2+} is also believed to be partially responsible for the chondroprotective effects of CS (Campo *et al.,* 2006).

1.4.5 CS as biomarker in cancer cell biology and treatment

During recent years, cell biology studies have revealed that the altered structure of glycosaminoglycans in several diseases indicate their importance as biomarkers for disease diagnosis and progression, as well as pharmacological targets (Fig. 1.4.2) (Afratis *et al.,* 2012; Poh *et al.,* 2015). CSPGs are able to regulate key cellular processes, including proliferation, apoptosis, migration, adhesion and invasion. Versican and decorin are the major CSPGs, and are over-expressed in the stroma of a

wide variety of malignant tumors, including osteosarcoma, testicular tumors, breast, pancreatic and colon cancer (Theocharis *et al.*, 2006; Skandalis *et al.*, 2011).

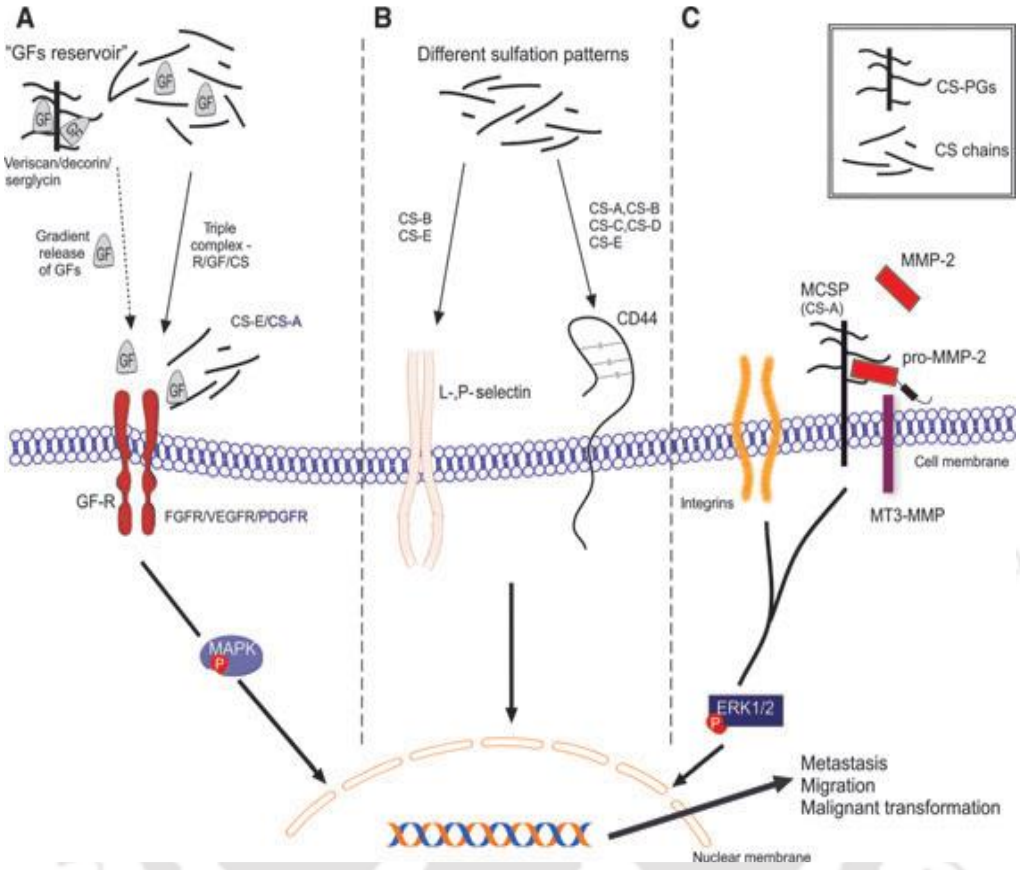

Fig. 1.4.2 CS-mediated signaling pathways and biological actions. The CS chains shown are either components of CSPGs or exogenously added free chains bearing various sulphation patterns. (A) Release of growth factors (GFs) from CS chains or delivery of GFs through CS chains creating a triple complex with receptors of growth factors (GF-R), leading to activation of the mitogen-activated protein kinase (MAPK) pathway and malignant transformation. (B) The importance of the CS sulphation pattern in interactions with cell membrane receptors such as L- and P-selectins and CD44. (C) Specific role of CS-A chains of melanoma chondroitin sulphate proteoglycans (MCSP) in activation of MMP2 through a triple complex with pro-MMP2 and MT3-MMP, promoting metastasis (adapted from Afratis *et al.*, 2012).

16 different CS disaccharides were synthesized and their inhibitory effect on the proliferation of breast cancer cells (MDA-MB-231, MCF-7 and T47D) were studied

(Poh *et al.*, 2015). The role of CS as pharmacological agent may be achieved via direct uptake of CS or as part of drug delivery system targeting cancer. Modified molecules called neoglycans are able to promote apoptosis of multiple myeloma cells (Afratis *et al.*, 2010). These carbodiimide-modified CS chains were demonstrated to reduce or even abolish tumor growth when directly injected in nude mice with breast cancer without causing toxicity (Pumphrey *et al.*, 2002; Afratis *et al.*, 2012). The over-expression of CS in several metastatic tumors enables selective delivery of anti-cancer drugs by polyethylene glycol-coated liposomes (Lee *et al.*, 2002; Afratis *et al.*, 2012).

1.5 Carbohydrate active enzymes

Carbohydrates are dynamic molecules that are constantly synthesized and broken down in animal and plants. There are varieties of enzymes involved in the synthesis as well as breakdown of carbohydrates. Carbohydrate modifying enzymes are divided into four classes: glycoside hydrolases (GHs), glycosyltransferases (GTs), polysaccharide lyases (PLs) and carbohydrate esterases (CEs). The glycosyltransferases (GTs) are mainly involved in the formation of the glycosidic bond or biosynthesis of carbohydrates. The polysaccharide lyases (PLs), carbohydrate esterase (CEs) and glycoside hydrolases (GHs) are concerned with the breakdown of polysaccharides. The carbohydrate-active enzymes are grouped into different families based on amino acid sequence similarity and are listed in the continually updated carbohydrate-active enzyme (CAZy) database (www.cazy.org) (Cantarel *et al*., 2009). The polysaccharide lyases are classified into 24 families and among them, the chondroitin degrading enzymes have been reported in families 6, 8 and 23.

1.5.1 Family 8 polysaccharide lyase

The family 8 polysaccharide lyase (PL8) currently contain 27 well characterized sequences. The enzyme reported in family 8 have shown activities like chondroitin AC lyase (EC 4.2.2.5), chondroitin ABC lyase (EC 4.2.2.20), hyaluronate lyase (EC 4.2.2.1) and xanthan lyase (EC 4.2.2.12) (http://www.cazy.org/PL8.html). Chondroitin sulphate lyases of families 8 catalyze the cleavage of β-(1,4)-glycosidic bond between hexosamine and uronic acid residue by β-elimination and generate Δ4,5 unsaturated uronate oligosaccharides as the product, which exhibits a maximum absorbance at 232 nm (A_{232}). The main structural fold present in family 8 polysaccharide lyase is $(\alpha/\alpha)_{5,6}$ β toroid domain, which contains five α-helical hairpins and in some proteins a sixth hairpin is assembled from two additional antiparallel helices, one at the N-terminus and the other at the C-terminus of this domain. This domain is followed by a C-terminal antiparallel β-sandwich domain containing four β-sheets (Féthière *et al.,* 1999; Garron *et al.,* 2010). The PL8 family contains lyases that can depolymerize several different types of substrates such as CS-A, CS-B, CS-C, HA and xanthan. All these enzymes, with exception of hyaluronate lyase, contain structural ions, calcium or sodium, coordinated mainly by aspartate side chains. Despite similarities in their structures, none of these metal ion sites are conserved across this enzyme family (Garron *et al.,* 2010). There are nearly 930 bacterial, 2 eukaryotic and 1 archaeal sequences in family 8 polysaccharide lyase (http://www.cazy.org/PL8.html). Among which 27 sequences are characterized and 9 crystal structures have been determined till date (January 2017) (http://www.cazy.org/PL8.html).

1.6 Classification of chondroitin degradation enzymes

The enzymes capable of degrading GAGs have been studied in order to understand the structure of GAGs and harness their therapeutic effects by manipulating cell signaling, differentiation, migration and adhesion (Iozzo *et al.*, 1993; Iozzo *et al.*, 1998; Lander *et al.*, 2000; Sugahara *et al.*, 2000; Bao *et al.*, 2004). In many cases, the GAG chains serves as the receptor for various microbes, viruses and pathogens, hence involved in pathogenesis (Rostand *et al.*, 1997; Giroglou *et al.*, 2001; Liu *et al.*, 2002; Yamada *et al.*, 2008). Designing GAG-based therapeutic drugs to tackle the pathogenic and inflammatory diseases requires holistic understanding of the related enzymes (Linhardt *et al.*, 2006).

A number of microorganisms such as *Proteus vulgaris* (Prabhakar *et al.*, 2006), *Arthrobacter aurescens* (Linhardt *et al.*, 1994; Lunin *et al.*, 2004) and *Bacteroides stercoris* HJ-15 (Hong *et al.*, 2002) elaborate and recruit the GAG-degrading enzymes for invading the host tissues to derive the nutrients. The GAG-degrading enzymes include heparinases I, II, III, chondroitin lyases and hyaluronan lyases. Chondroitin layses have been expressed by number of soil and intestinal bacteria (Lunin *et al.*, 2004; Shaya *et al.*, 2008) such as *Arthrobacter aurescens* (Linhardt *et al.*, 1994; Lunin *et al.*, 2004), *Bacteroides thetaiotaomicron* WAL2926 (Shaya *et al.*, 2008) and *Bacteroides stercoris* HJ-15 (Hong *et al.*, 2002).

On the basis of substrate specificity, the chondroitin lyases are categorized mainly into three types such as chondroitin AC lyase, chondroitin B lyase and chondroitin ABC lyase (Fig. 1.6.1) (Linhardt *et al.*, 1994; Lunin *et al.*, 2004; Prabhakar *et al.*, 2006; Lemmnitzer *et al.*, 2014).

1.6.1 Chondroitin AC lyase

Chondroitin AC lyase degrades both CS-A and CS-C and to a lesser extent hyaluronan (Gu *et al.,* 1995; Linhardt *et al.,* 2006). It cannot degrade dermatan sulphate, as it is unable to break the glycosidic bond between hexosamine and iduronic acid residues (Gu *et al.,* 1995; Linhardt *et al.,* 2006). Chondroitin AC lyase has been isolated from bacteria including *Flavobacterium heparinus* (*Pedobacter heparinus*) (Gu *et al.,* 1995; Féthière *et al.,* 1999; Pojasek *et al.,* 2001), *Arthrobacter aurescens* (Lunin *et al.,* 2004; Lemmnitzer *et al.,* 2014), *Bacteroides stercoris* HJ-15 (Hong *et al.,* 2002) and *Serratia marcescens* (Ke *et al.,* 2005). Heparin and dermatan sulphate potentially act as the inhibitors of these enzymes (Pojasek *et al.,* 2001; Rye *et al.,* 2002).

1.6.2 Chondroitin B lyase /Dermatan lyase

Chondroitin B lyase specifically degrades only dermatan sulphate as its sole substrate. They are not able to act on CS-A, CS-C and hyaluronan. The endo acting chondroitin B lyase from *Pedobacter heparinus* has been studied extensively (Huang *et al.,* 1999; Pojasek *et al.,* 2001).

1.6.3 Chondroitin ABC lyase

Chondroitin ABC lyase is a broad specificity enzyme and is able to depolymerize CS-A, CS-C, DS and also hyaluronan to some extent (Shaya *et al.,* 2008). This subgroup of lyases have been identified from *Bacteroides stercoris* HJ-15 (Hong *et al.,* 2002), *Proteus vulgaris* (Jandik *et al.,* 1994; Prabhakar *et al., 2005;* Prabhakar *et al.,* 2009) and *Bacteroides thetaiotaomicron* WAL2926 (Shaya *et al.,* 2008).

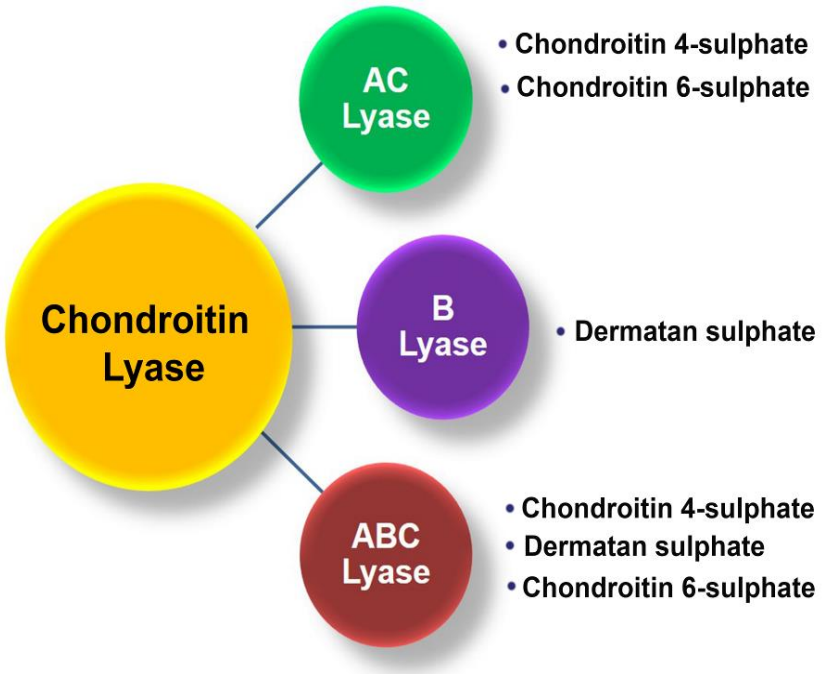

Fig. 1.6.1 Classification of chondroitin lyase enzymes

Recently, a chondroitinase has been reported from occlusion-derived virus envelope protein 66 (ODV-E66) of *Autographa californica* nucleopolyhedrovirus (Sugiura *et al.*, 2011). This chondroitin-degrading enzyme specifically degrades chondroitin, chondroitin 6-sulphate and hyaluronan, but inactive towards chondroitin 4-sulphate, DS and heparin (Sugiura *et al.*, 2011). ODV-E66 chondroitinases has been included as a new member with unique substrate specificity under family 23 in polysaccharide lyases (http://www.cazy.org/PL23.html). This enzyme appears promising in unravelling baculovirus infection mechanisms.

1.7 Structure of chondroitin lyases

1.7.1 Crystal structure of chondroitin AC lyase

Substantial information on structural variations of these enzymes have accumulated over the years. Crystal structure of chondroitin AC lyase from *Flavobacterium heparinum* (FlavoAC) (Féthière *et al.*, 1999) and *Arthrobacter*

aurescens (ArthroAC) (Lunin *et al.*, 2004) have been solved under native as well as substrate complexation states. Site of lysis varies in that FlavoAC is endolytic whereas ArthroAC is exolytic (Jandik *et al.*, 1998). As per the three dimensional structure, FlavoAC consists of two domains, a N-terminal domain of around 300 amino acids arranged as α-helices and the C-terminal domain spanning 370 residues are configured as four antiparallel β-sheets. The N-terminal domain imparts the protein a double layered horseshoe structure $(\alpha/\alpha)_5$ toroidal (doughnut-shaped) topology (Féthière *et al.*, 1999) (Fig.1.7.1A). Site-directed mutagenesis of *F. heparinum* revealed that His225Ala, Tyr234Phe and Arg288Ala render the enzyme inactive (Blain *et al.*, 2002) Crucial catalytic function of residues His225, Tyr234, Arg288, and Glu371came forth. From high resolution electron density maps and subsequent mass spectrometry studies, ArthroAC conformation was found to be an α+β (Lunin *et al.*, 2004). The N-terminal contains 13 α helices, 10 out of which forms an $(\alpha/\alpha)_5$ toroidal topology (Lunin *et al.*, 2004). The C-terminal domain is entirely made up of antiparallel β-strands arranged into four β-sheets (Lunin *et al.*, 2004). Structural comparison of ArthroAC (Exolytic) and FlavoAC (Endolytic) explains the difference in their mode of action. At the N-terminal domain, ArthroAC has insertions of 15 residues (Arg23-Ser38) and 25 residues (Thr343-Gly366) as compared to FlavoAC (Lunin *et al.*, 2004). These two insertions form a loop, preventing the binding of large oligosaccharide to the active site cavity (Lunin *et al.*, 2004).

1.7.2 Crystal structure of chondroitin B lyase

The only chondroitin B lyase reported till date is from *Flavobacterium heparinum* (*Pedobacter heparinus*). The crystal structure of enzyme was determined at 1.7 Å in both native and in complex with dermatan sulphate disaccharide (Huang *et al.*,

1999). The chondroitin B lyase contains a right-handed parallel β-helix fold, as the other members of the polysaccharide lyase family such as pectate lyase (Yoder *et al.,* 1993; Jurnak, *et al.,* 1994; Jenkins *et al.,* 1998). Overall β-helix is an L-shaped structure, made up of three β-sheets. The two sheets are arranged parallel to each other, while third one is perpendicular to the second β-sheet. The β-strands of the adjacent sheets were connected by turns or loop (Fig. 1.7.1B). A positively charged cleft within the fold is involved in binding of the substrate. The two residues Arg318 and Arg364 are responsible for interacting with sulphate group of N-acetylgalactosamine moiety, while Glu333 possibly act as general base (Huang *et al.*, 1999).

In 2004, the crystal structure of chondroitin B lyase from *Flavobacterium heparinum,* complexed with DS and CS oligosaccharide was reported (Michel *et al.*, 2004). Complex of enzyme with DS hexasaccharide revealed the presence of +2 and +1 subsites (Michel *et al.,* 2004). This study also revealed the presence of Ca^{2+} binding site coordinated by conserved acidic residues and by the carboxyl group of the L-iduronic acid at the +1 subsite. Subsequently the kinetics and mutagenesis studies explains the absolute requirement of Ca^{2+} ion for catalysis. The residues Lys250 and Arg271 act as general base and acid, respectively and are involved in the catalysis (Michel *et al.,* 2004).

1.7.3 Crystal structure of Chondroitin ABC lyase

The crystal structure of chondroitin ABC lyase I from *Proteus vulgaris* was determined at 1.9 Å in 2003 (Huang *et al.,* 2003). The enzyme has broad specificity and is endolytic and degrades all three types of substrates *viz.* chondroitin A, chondroitin C and dermatan sulphate (Huang *et al.,* 2003). This 110 kDa protein consists of 3 domains. The N-terminal domain composed of 209 amino acids is the most flexible

domain. This domain is made up of jellyroll fold which consists of a two-layered bent β-sheet sandwich with one short α-helix. It shows the fold similarity with the ligand binding domains especially, carbohydrate binding domains (CBMs) of xylanases, glucanases and lectins (Huang *et al.,* 2003). This structural similarity of N-terminal domain suggests that this domain helps in binding of long glycosaminoglycan chains of substrate (Prabhakar *et al.,* 2006). The central or catalytic domain is the helical domain consisting 15 α-helices. Central domain is formed by 10 α-helices, which is arranged into an incomplete toroid $(\alpha/\alpha)_5$ structure (Fig. 1.7.1C). The structure superimposition and amino acid comparison shows that this domain shares structural similarity with catalytic domains of chondroitin AC lyase from *Flavobacterium heparinum* and hyaluronidases. The C-terminal domain is made up of 404 amino acids constituting four antiparallel β-sheets. This domain is homologous to the non-catalytic C-terminal domain of chondroitin AC lyase of *Flavobacterium heparinum* (FlavoAC) (Huang *et al.,* 2003; Linhardt *et al.,* 2006).

The three domains are arranged in linear fashion. The N- and C-terminal domains are attached to the catalytic domain. The N-terminal domain interacts with the first several α-helices of the toroid, while the C-terminal domain interacts with the tips of few α-helices and intervening loops (Huang *et al*., 2003). Arg500 plays a crtical role in binding the acidic group of glucuronic acid. The chondroitin ABC lyase of *Proteus vulgaris* and chondroitin AC lyase of *Flavobacterium heparinum* share the same catalytic residues, while residues involved in substrate binding sites are not conserved. Arg500 plays important role in charge neutralization of acidic group of uronic acid in either conformation (Glucuronic acid or Iduronic acid), giving this enzyme the ability to catalyze both glucuronic and iduronic acid moieties (Linhardt *et al.,* 2006). Crystal

structure of an another exo acting chondroitin ABC lyase from *Bacteroides thetaiotaomicron* (BactABC) is available (Shaya *et al.*, 2008). In spite of having no sequence similarity, its central domain shows structural similarty to the catalytic domains of chondroitin AC from *Pedobacter heparinus* and *Arthrobacter aurescens* (Lunin *et al.*, 2004), hyaluronate lyase (Li *et al.*, 2000), xanthan lyase (Hashimoto *et al.*, 2003) and alginate lyase (Yoon *et al.*, 1999). The C-terminal is a 420 amino acid long domain, consisting of stack of four antiparallel β-sheets. The residues His454, Tyr461, Arg514 and Glu628 forms a catalytic tetrad. Chondroitin ABC lyase BactABC from *Bacteroides thetaiotaomicron* has single substrate-binding site and two partially overlapping active sites catalyzing the reactions for CS and DS (Shaya *et al.*, 2008). A substrate-induced conformational change brings all catalytically essential residues close to each other (Shaya *et al.*, 2008).

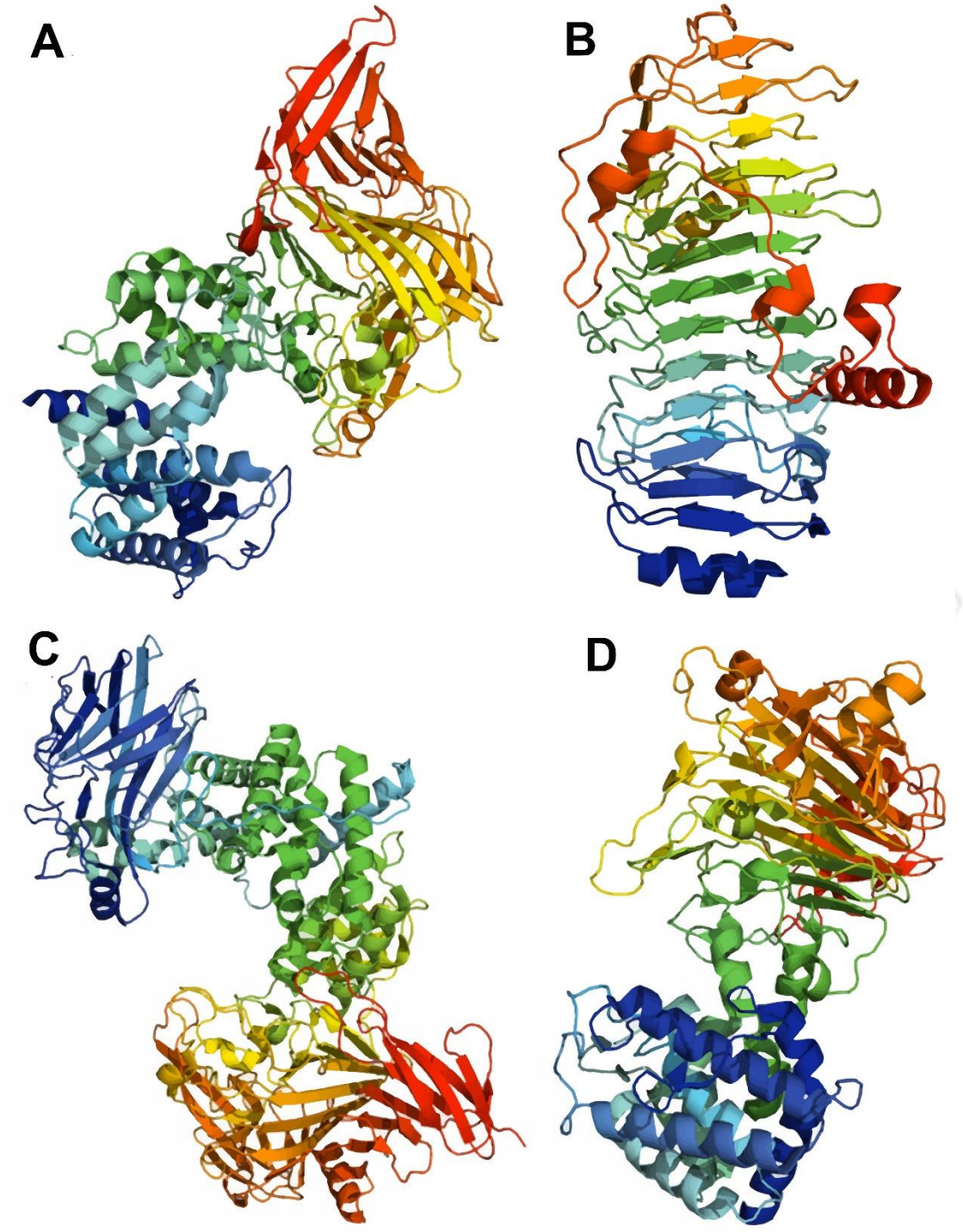

Fig. 1.7.1 Structures of chondroitin lyases (a) Chondroitin AC lyase from *Flavobacterium heparinum* (PDBid_1HM2), (b) Chondroitin B lyase from *Flavobacterium heparinum* (PDBid_1DBG), (c) Chondroitin ABC lyase from *Proteus vulgaris* (PDBid_1HN0), (d) Chondroitin lyase from *Autographa californica nucleopolyhedrovirus* (PDBid_3VSM).

1.7.4 Crystal structure of chondroitin lyase from *Autographa californica nucleopolyhedrovirus*

Chondroitin lyase (ODV-E66) from *Autographa californica nucleopolyhedrovirus* is the first viral chondroitin lyase cloned from baculovirus envelope protein that has a molecular size of 61 kDa. The chondroitin lyase ODV-E66 has low sequence similarity with bacterial chondroitin lyases. The crystal structure of native ODVE66 was determined at 2.0 Å resolution (Kawaguchi *et al.,* 2013) The native ODV-E66 protein is composed of two domains. The N-terminal domain is an α-helix rich domain, it containing 8 α-helices and four short β-strands. This domain is composed of 202 amino acids forming α/α toroid topology. The C-terminal domain is composed of 431 amino acids and is a β strand rich domain. It contains 31 β-strands and 12 short α-helices and forms an anti-parallel β-sandwich structure (Fig. 1.7.1D). The structural features of this enzyme are very similar to chondroitin AC lyase and chondroitin ABC lyase of the family 8 polysaccharide lyase (Kawaguchi *et al.,* 2013). The structure and mutation analysis of enzyme confirmed that the Asn236, His291, Tyr299, Arg345 and Glu395 residues are involved in catalysis. The residues Asn236 and His291 help in neutralizing the negative charge on the carboxyl group of glucuronic acid. The Tyr299 abstracts a proton from C-5 residue of glucuronic acid and act as catalytic base. An unsaturated sugar with a new reducing end is generated by breaking the glycosidic bond with help of residues Arg345, Tyr299, His291 and Glu395 (Kawaguchi *et al.,* 2013).

1.8 Reaction mechanism of Chondroitin sulphate lyase

Glycosaminoglycan degradation can be achieved by two classes of enzymes involving distinct reaction mechanisms. Based on the mechanism of GAG degradation

these enzymes are classified as the hydrolases and lyases (Rye *et al.*, 2002). The GAG hydrolases are present in the eukaryotic system, while the GAG lyases are present in prokaryotes. The hydrolytic breakdown of glycosidic bond, present between the hexosamine and hexuronic acid involves the addition of the water molecule. It involves the breakdown of glycosyl-oxygen bond of the glycosidic linkage. Whereas, the lyases act *via* elimination mechanism resulting in oligosaccharides with unsaturated uronic acid residues at the nonreducing end in which, the oxygen-aglycon bond of the glycosidic linkage is broken (Fig. 1.8.1) (Zechel *et al.*, 2000; Linhardt *et al.*, 2006).

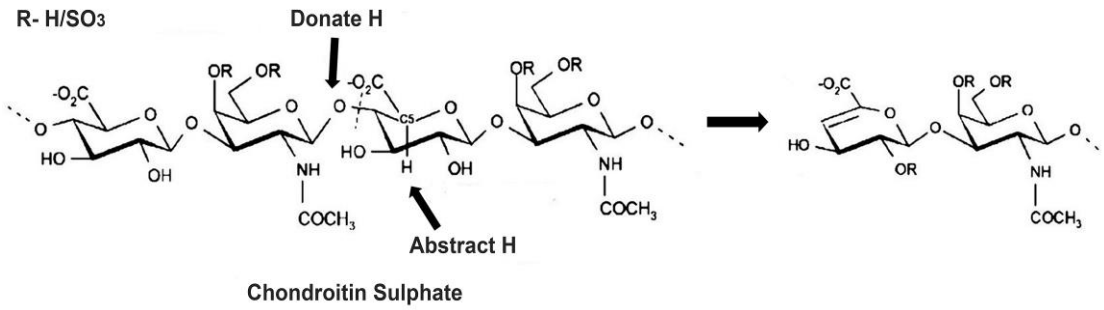

Fig. 1.8.1 β-elimination mechanism for degradation of chondroitin sulphate in prokaryotes. The bond between N-acetylgalactosamine & Glucouronic acid is broken resulting in oligosaccharides with unsaturated uronic acid residues at the nonreducing end (adapted from Shaya *et al.*, 2008).

The elimination mechanism followed by lyases is characterized by the abstraction of the relatively acidic proton at C-5 of the hexuronic acid by a general base. This is further followed by the generation of a C4-C5 double bond at the uronic acid ring present at the nonreducing end (Rye *et al.*, 2002; Linhardt *et al.*, 2006). The catalytic mechanism followed by the lyases was elucidated in detail defining the three basic steps involved in the catalysis *viz.* (1) abstraction of the C-5 proton on the sugar ring of a uronic acid or ester by a basic amino acid side chain, (2) stabilization of the resulting anion by charge delocalization into the C-6 carbonyl group and (3) lytic

cleavage of the β-(1→4)-glycosidic linkage, facilitated by proton donation from a catalytic acid, which finally yield a hexenuronic acid at the newly formed non-reducing chain end (Yip *et al.*, 2004; Yip *et al.*, 2006; Lombard *et al.*, 2010). Depending on the monosaccharide composition of the substrate and its conformation in the lyase active site, the proton removed from C-5 and the departing oxygen on C-4 may lay either syn or anti to each other (Fig. 1.8.2) (Lombard et al., 2010).

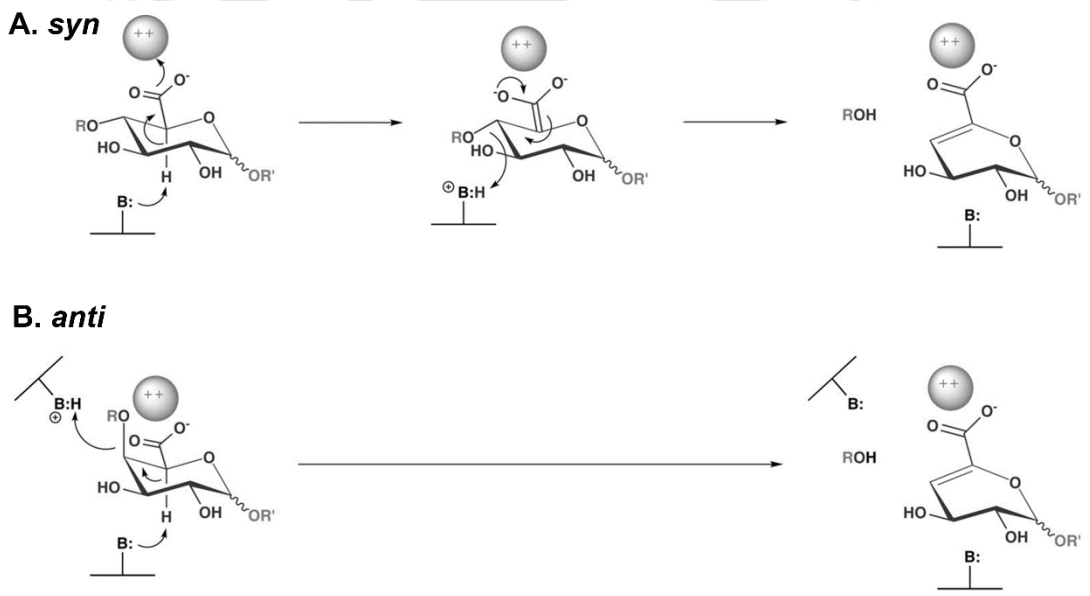

Fig. 1.8.2 (A) syn-β-elimination and (B) anti-β-elimination, as in α-(1,4)-linked polysaccharide lyase. In both, polysaccharides are cleaved to produce an 4,5 unsaturated galacturonate moiety at the newly formed non-reducing end of the chain. As the cleavage is caused in the polysaccharide chain, the C-5 proton adjacent to the carbonyl group is abstracted by a basic amino acid at the catalytic centre (B:). Removal of the glycosidic oxygen is facilitated by proton donation from an acidic amino acid residue (B:H). Syn elimination is commonly found in chondroitin lyase, while anti elimination is observed in pectate lyase or pectin lyase (adapted from Lombard *et al.*, 2010).

Some specific microorganisms express the GAG-degrading lyases and utilize their end products as the source of carbon. Different categories of CS lyases have a distinct substrate specificity for degradation of chondroitin sulphate. The Chondroitn ABC lyase shows wide substrate specificity and degrades the CS/DS containing either glucuronic acid or iduronic acid. The two chondroitin ABC lyases (PvulABCI and PvulABCII) from *Proteus vulgaris* have been studied including the site-directed mutagenesis for identifying the active site residues involved in catalysis (Prabhakar *et al.,* 2006; Prabhakar *et al.,* 2009). The commensal human intestinal bacterium *B. thetaiotaomicron* and *B. stercoris* genome has large number of genes encoding enzymes involved in GAG degradation (Ahn *et al.,* 1998; Kim *et al.,* 2000). The chondroitin ABC lyase from *Bacteroides thetaiotaomicron* WAL2926 possesses the broad specificity with an ability to act on both epimers of uronic acid. The conservative replacement of active site key residue by site-directed mutagenesis revealed the role of His345 as the general base, which initiates the degradation of dermatan sulphate by abstracting the C5 proton. While the residues Tyr461 and His454 act as general base in performing CS degradation. Tyr461 also act as the general acid by protonating the leaving group and leads to the completion of CS/DS degradation (Xu *et al.,* 2003; Shaya *et al.,* 2008). The chondroitin lyase B from *Flavobacterium heparinum* (*Pedobacter heparinus*) specifically degrades only DS by accepting iduronic acid, while chondroitin AC lyase cleaves both CS-A and CS-C and accepts only glucuronic acid (Gu *et al.,* 1995; Pojasek *et al.,* 2001).

1.9 Production, purification and characterization of Chondroitin Sulphate lyases

In order to viably employ these enzymes for therapeutic purposes, their production, purification without denaturation and structural elucidation is paramount. The sections below illuminate on these aspects. A chondroitin sulphate lyase secreting strain, *Arthrobacter aurescens* was isolated and its chondroitin sulphate degradation properties were studied (Hiyama *et al.,* 1975). Later, two chondroitin ABC lyases were isolated and characterized from *Bacteroides thetaiotaomicron* (Linn *et al.,* 1983). On growing *Bacteroides thetaiotaomicron* in medium containing chondroitin sulphate as the sole carbon source, chondroitin lyase activity was detected in crude cell extracts. The two chondroitin lyases with similar molecular weights were found active against chondroitin sulphate A, B and C.

Chondroitin sulphate lyases have been purified by the ammonium sulphate precipitation, ion-exchange chromatography and gel filtration (Gu *et al.,* 1995; Hong *et al.,* 2002; Ke *et al.,* 2005). Two distinct chondroitin ABC lyases obtained from chondroitin sulphate-induced *Proteus vulgaris* NCTC 4636 were fractionated into an endoeliminase capable of depolymerizing chondroitin sulphate producing the end products, the mixture of D-unsaturated tetra- and di-saccharides and an exo-eliminase preferentially acting on chondroitin sulphate tetra- and hexa-saccharides to yield the disaccharides (Hamai *et al.,* 1997). Two novel enzymes, chondroitin ABC and chondroitin AC lyases were purified and characterized from *Bacteroides stercoris* HJ-15, a human intestinal isolate (Hong *et al.,* 2002). Chondroitin ABC lyase expressed as a single subunit of 116 kDa, while chondroitin AC lyase was composed of two identical subunits of 84 kDa. Both chondroitin lyases were potently inhibited by Cu^{2+}, Zn^{2+} and *p*-chloromercuriphenyl sulfonic acid. Chondroitin AC lyase from *Bacteroides stercoris*

HJ-15 showed maximum activity at pH 5.8 and temperature 45ºC (Hong *et al.*, 2002). While the chondroitin ABC lyase showed maximum activity at pH 7.0 and 40ºC. A chondroitinase AC, purified from *Serratia marcescens* showed optimum activity at pH 7.5 and 40ºC and was composed of two identical subunits of 35 kDa (Ke *et al.*, 2005).

The gene encoding chondroitin AC lyase *Flavobacterium heparinum* designated *cslA* was expressed in *E. coli*. The *cslA* sequence revealed an open reading frame of 2,103 bp coding for peptide of 700 amino acid (aa) residues, while mature form consists of 678 aa and a molecular size of 77169 Da. The chondroitin AC lyase from *Flavobacterium heparinum* was cloned and expressed in *E. coli* (Pojasek *et al.*, 2001). The purification of recombinant chondroitin AC lyase was achieved by including an N-terminal 6x histidine tag using IMAC. The end products, the disaccharides of chondroitin 4-sulphate and chondroitin 6-sulphate after exhaustive digestion by chondroitin AC lyase from *Flavobacterium heparinum* were analyzed by strong-anion exchange chromatography (SAX-HPLC) (Pojasek *et al.*, 2001). The chondroitin AC lyase enzyme displayed an optimum pH 8.0 and optimum temperature 35ºC (Pojasek *et al.*, 2001). The recombinant chondroitin ABC lyase from *Bacteroides thetaiotaomicron* WAL2926 was purified by IMAC followed by gel filtration (Shaya *et al.*, 2008).

An endo acting chondroitinase ABCI from *Proteus vulgaris* was cloned and expressed in *E. coli*. The putative catalytic residues His-501, Tyr-508, Arg-560 and Glu-653 were predicted via site-directed mutagenesis (Prabhakar *et al.*, 2005). A chondroitin ABC lyase from *Bacteroides thetaiotaomicron* was characterized and the 3D structure was determined. Its catalysis was stimulated by presence of Ca^{2+} and Mg^{2+} ions, particularly against dermatan sulphate (DS) (Shaya *et al.*, 2008). Degradation of

DS and CS by chondroitin ABC lyase yielded only disaccharide products, pointing to an exolytic mode of action. The enzyme showed maximum activity at pH 7.6 and 37ºC (Shaya *et al.,* 2008). The expression, purification and biochemical characterization of chondroitinase ABC II from *Proteus vulgaris* was carried out (Prabhakar *et al.,* 2009). The site-directed mutagenesis of the four critical residues *viz.* Arg513, His453, Tyr460 and Glu608 to Ala resulted in a completely inactive enzyme (Prabhakar *et al.,* 2009). The *Proteus vulgaris* chondroitinase ABC (a mixture of PvulABCI and PvulABCII) is the only commercially available preparation (Seikagaku, Tokyo, Japan). A novel chondroitin lyase with distinct substrate specificity was cloned from occlusion-derived virus envelope protein 66 (ODV-E66) of *Autographa californica* nucleopolyhedrovirus (Sugiura *et al.,* 2011). The enzyme shows activity over a wide range of pH (4–9) and temperature (30–60°C) and was unaffected by divalent metal ions like Ca^{2+}, Mg^{2+} Mn^{2+} and Co^{2+} and EDTA. The recombinant enzyme shows highest activity with chondroitin followed by chondroitin 6-sulphate and degrade hyaluronan to a minimal extent, but it did not show activity with dermatan sulphate and heparin. This enzyme specifically acts on glucuronate residues present in non-sulphated and chondroitin 6-sulphate structures but not in chondroitin 4-sulphate (Sugiura *et al.,* 2011). Properties of some of the well characterized chondroitin lyases have been listed in Table 1.9.1

Table 1.9.1 Some characterized chondroitin lyases and their sources

Organism	Enzyme	Substrate specifity	Molecular weight (Da)	Mode of action	Reference
Flavobacterium heparinum	Chondroitin AC lyase	C4S, C6S, HA	74,000	Endo	(Gu *et al.*, 1995)
Arthrobacter aurescens	Chondroitin AC lyase	C4S, C6S, HA	79,840	Exo	(Lunin *et al.*, 2004; 51)
Bacteroides stercoris HJ-15	Chondroitinase AC	C4S, C6S, HA	84,000	Endo	(Hong *et al.*, 2002)
Bacteroides stercoris HJ-15	Chondroitin ABC lyase	C4S, C6S, DS	116,000	Exo	(Hong *et al.*, 2002)
Serratia marcescens	Chondroitinase AC	C4S, C6S, HA	35,000	-	(Ke *et al.*, 2005)
Proteus vulgaris	Chondroitinase ABC-II	C4S, C6S, DS	100,000	Exo	(Prabhakar *et al.*, 2009)
Bacteroides thetaiotaomicron WAL2926	Chondroitin sulphate ABC lyase	C4S, C6S, DS	115,200	Exo	(Shaya *et al.*, 2008)
Proteus vulgaris	Chondroitinase ABC-I	C4S, C6S, DS	105.000	Endo	(Prabhakar *et al.*, 2005)
Autographa californica Nucleopolyhedrovirus	Chondroitin lyase	Chondroitin, C6S, HA	74,300	Endo	(Sugiura *et al.*, 2011)

1.10 Established and emerging applications of Chondroitin sulphate lyases

Chondroitin Sulphate lyases are involved in some validated functions such as the inhibition of cell proliferation, differentiation and migration and some possible functions such as antitumor, pathogenic infection control, wound repair and neuro-generation. (Pojasek *et al.*, 2001; Sugahara *et al.*, 2003; Rauch *et al.*, 2006; Uyama *et al.*, 2007). Recruitment of CS lyase for meddling with cancer cell surface receptors can offer exciting therapeutic possibilities. Also, therapeutic oligosaccharides appear to be another crucial implication of the CS lyases. Among the prospective roles, reinnervation is perhaps, the most promising application of this enzyme. The scope and progress on the applications of these lyases have been discussed below.

1.10.1 Chondroitin sulphate oligosaccharide production and their structure determination

The GAGs have complex structures. CS and DS contain linear and highly sulphated polysaccharide chains. The sulphate groups are bound to C-4 or C-6 positions of the disaccharide units of these CS/DS polysaccharides which leads to the structural diversity (Ly *et al.,* 2010; Li *et al.,* 2012). The molecular weights of the CS/DS also vary depending on the number of disaccharide units present in the chain. Because of the structural complexity, it is difficult to characterize the degradation products of these polysaccharides and understand their structure and function relationships as an anti-inflammatory and therapeutic agent (Kimata *et al.,* 1973; Toida *et al.,* 1993; Scott *et al.,* 2001; Lemmnitzer *et al.,* 2014). Chondroitin lyases cleave the β (1→4) linkage, of the CS/DS polysaccharides [-3)GalNAc β(1→4)GlcA/IdoAα(1-] and generate the oligosaccharides (Pojasek *et al.,* 2001; Linhardt *et al.,* 2006; Shaya *et al.,* 2008).

The oligosaccharides generated by enzymatic degradation can be separated by various techniques including Strong anion exchange High performance liquid chromatography (SAX-HPLC) (Linhardt *et al.,* 1994; Yang *et al.,* 2000) and polyacrylamide gel electrophoresis (PAGE) (Linhardt *et al.,* 1991; Linhardt *et al.,* 1994), Gel permeation chromatography (GPC) (Yang *et al.,* 2000; Lemmnitzer *et al.,* 2014) and capillary electrophoresis (CE) (Al-Hakim *et al.,* 1991; Pervin *et al.,* 1993; Pervin *et al.,* 1994). The structure analysis of the oligosaccharides involves the exhaustive depolymerization of the substrates by the enzymes. Controlled degradation of substrate can also be carried out in order to attain maximum number of oligosaccharides. The separation of the oligosaccharide mixture can be achieved by gel permeation chromatography (Yang *et al.,* 2000; Lemmnitzer *et al.,* 2014). The purified

oligosaccharide was analyzed by PAGE analysis and further purified by SAX-HPLC (Linhardt *et al.,* 2006; Mourier et al., 2015). ESI-MS, MALDI-MS and MALDI-TOF methods can be used to determine the molecular weight (Linhardt *et al.,* 2006; Nimptsch *et al.,* 2009; Schiller *et al.,* 2010; Fenn *et al.,* 2011; Lemmnitzer *et al.,* 2014). The refined chemical structure of the oligosaccharides can be further resolved by mass and 1D/2D nuclear magnetic resonance (NMR) spectroscopy (Linhardt *et al.,* 1991; Yang et al., 2000; Schiller *et al.,* 2010; Lemmnitzer *et al.,* 2014).

1.10.2 CS oligosaccharides with anti-inflammatory properties

As mentioned before, PGs are complex biomolecules with role in myriad biological process. CS lyases are capable of modulating their structure and ultimately the function, by selectively degrading their CS chains (Linhardt *et al.,* 2006; Ly *et al.,* 2010; Li *et al.,* 2012) CS lyase degradation products vary in size, such as disaccharide, tetrasaccharide and hexasaccharide. These oligosaccharides have been found to exhibit toll-like receptor TLR9-mediated anti-inflammation responses (Jin *et al.,* 2010). The TLR9 receptor coordinates innate immune system, being expressed on both phagocytes (macrophages, dendritic cells) and lymphocytes (B cells) (Visintin, *et al.,* 2001; Wagner *et al.,* 2002; Verstak *et al.,* 2007; Jin *et al.,* 2010; Fenn *et al.,* 2011). Interlukien-6 (IL-6) is known to be a multifunctional cytokine that regulates the immune response and inflammation (Hirano *et al.,* 1998; Ly *et al.,* 2002; Kumagai *et al.,* 2008). TLR 9 induces IL-6 secretion in the macrophage cells, as demonstrated *in vitro* through macrophage-like J774.1 cells (Jin *et al.,* 2010). The induction of IL-6 was dramatically suppressed by the disaccharide derived from CS-A, while the CS-A polysaccharide had no effect on IL-6 secretion (Ly *et al.,* 2002; Jin *et al.,* 2010). The CS-A derived disaccharide restrains IL-6 secretion at both transcription and translation levels in

macrophage-like J774.1 cells (Jin *et al.,* 2010). Such studies unfold the future avenues for the CS lyases application in production of oligosaccharides with anti-inflammatory properties.

1.10.3 Antitumor activity of chondroitin lyases

PGs are involved in cellular communication and cancer biology Linhardt *et al.,* 1994; Iozzo *et al.,* 2011). Metastasis of tumors occur by rapid and dynamic regulation of cancer cell surface adhesion factors, and angiogenesis (formation of new blood vessels) (Eisenmann *et al.,* 1999; Denholm *et al.,* 2001; Ishihara *et al.,* 2002; Iozzo *et al.,* 2011). Metastasis of tumors involves a complex sequence of events, called as the "metastatic cascade" (Sneath *et al.,* 1998; Denholm *et al.,* 2001). Chondroitin sulphate chains as a part of PGs have important role in the process of tumor growth and metastasis (Fig. 1.9) (Iida *et al.,* 1996; Sneath *et al.,* 1998; Eisenmann *et al.,* 1999; Denholm *et al.,* 2001; Yamada *et al.,* 2008). Much of the research has focused on understanding the role for cell surface PGs in modulating the adhesion as well as the motility of malignant melanoma cells (Iida *et al.,* 1994; Iida *et al.,* 1996; Eisenmann *et al.,* 1999; Iozzo *et al.,* 2011). Melanoma cells express CS proteoglycan 4 (CSPG4). CSPG4 is the transmembrane protein which traverses cell membrane and modulates integrin function and enhances growth factor receptor-regulated pathways including extracellular signal-regulated protein kinases (ERK) 1,2 (Price *et al.,* 2011).

Chondroitinase AC from *Flavobacterium heparinum*, removes and degrades GAGs from PGs and thereby modulating the interactions involved in tumor cell invasion and proliferation. Chondroitin lyases has been reported to possess the antitumor potential (Denholm *et al.,* 2001). Chondroitinase AC inhibited melanoma invasion and proliferation as well as endothelial proliferation and angiogenesis

(Denholm *et al.,* 2001). Apoptosis of melanoma and endothelial cells, as measured by the caspase-3 activity, was also increased by chondroitinase AC, but not by chondroitinase B. The latter also inhibited endothelial and melanoma proliferation and invasion, but to a lesser extent than chondroitinase AC (Denholm *et al.,* 2001).

Oncolytic viruses are genetically engineered viruses that kill cancer cells and remain harmless to the normal tissue. After being injected into a tumor, they infect cancer cells and multiply inside them, when a cancer cell is killed they move on to spread and infect other cancer cells. This strategy has been facilitated by chondroitinase ABC I (Dmitrieva *et al.,* 2011; Kim *et al.,* 2014). Chondroitinase ABC (Chase-ABC) is a bacterial enzyme that can remove a major glioma ECM component, CS GAGs from PGs without any deleterious effects *in vivo*. This enzymatic treatment is capable of promoting the spread of the viruses, increasing the efficacy of the viral treatment and antitumor efficacy (Dmitrieva *et al.,* 2011; Kim *et al.,* 2014).

1.10.4 Neuronal Regeneration

Appreciation of CS lyase for neural therapy is rather a nascent field. Extracellular matrix (ECM) of nervous system is replete with CS/DS, which occur in variable saccharide and sulfation site. These modifications directly influence the neural wiring and dictating anomalies (Flangea *et al.,* 2006). CS lyase might be employed to modulate their distribution in the ECM. Loss of neural functions has devastating consequences which can be deteriorated by CS/DS, produced in high amount of scarred neurons (Sharma *et al.,* 2012). CSPG prevent the repair of spinal cord following damage by hindering axonal regeneration from astrocytes (Massey *et al.,* 2008; Kuffler *et al.,* 2009; Bartus *et al.,* 2014). Removal of the CSPGs inhibitors from dorsal root ganglia has been observed to resume synaptic links (Kuffler *et al.,* 2009). Administration of chondroitin

ABC lyases to distal graft in spinal cord injury rat models augmented axonal regeneration (Tom et al., 2009). An engineered CS lyase ABC administered to rat model with neural impairment *via* lentiviral vector modulated the CSPG and repaired the nerves. The mechanism was found to be phenotypic changes of phagocytic cells like macrophages. CS lyase ABC gene therapy can ameliorate neural injuries improved by axonal repair and better sensorimotor function (Bartus *et al.,* 2014).

Another rat study revealed that CS lyase ABC is capable of degrading the pooled CSPGs post neural injury due to hypertension stroke. The depletion CSPGs due to the lyase activity was accompanied with elevated level of growth-associated protein-43 (GAP-43) and synaptophysin (SYN). This finding confirmed the neural revitalizing property of CS lyases (Chen *et al.,* 2014). Rejuvenation of the scarred nerves *via* remodelling of ECM, by augmenting GAP-43 and myelin basic protein (MBP), while suppressing glial fibrillary acidic protein (GFAP) level was corroborated by rat studies (Zang *et al.,* 2012). Schwann cells engineered to secrete neurotrophin and CS lyase ABC was demonstrated to promote axon growth and synaptic plasticity. The neurotrophic evidence was evaluated through higher axons and myelin sheath on them (Kanno *et al.,* 2014). Further, supporting the beneficial role of CS lyases on nervous system, from rat study it was demonstrated that the axonal sprouting post lesion is not random but in sync with normal neural circuitry, hence dismiss any malfunction risks like seizures (Harris *et al.,* 2015). In another striking study, CS lyase ABC treatment of rats was shown to modulate immune response by inducing M2 macrophage polarization (Didangelos *et al.,* 2014). As a response to the enzyme activity, anti-inflammatory cytokine IL-10 level improved while proinflammatory cytokine IL-12B level dwindled (Didangelos *et al.,* 2014).

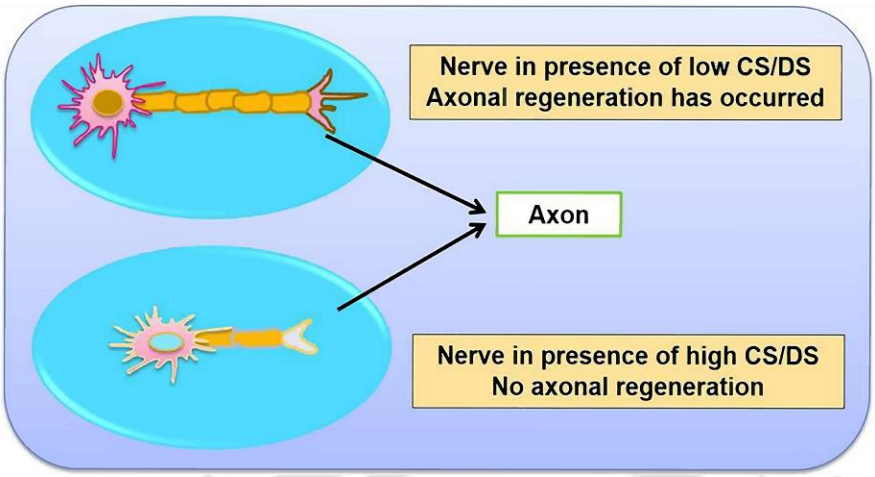

Fig. 1.10.1 Neural regeneration blocking effect of Chondroitin/Dermatan sulphate**.**

Apart from neuroprotective role, the CS lyase enzyme-based studies are providing crucial insights on neural architecture and behaviour with aging. A mass spectrometry study showed that digestion of mice brain DS/CS with CS lyase B and AC I liberates variable oligosaccharides for mice of different age group (Robu *et al.*, 2015). The rodents with older brain had DS with higher sulfation degree whereas those with younger brain had more nonsulphated CS (Zhao *et al.*, 2013; Robu *et al.*, 2015). Such interesting findings might encourage similar studies on human subjects. The delineated findings are only few of the possible neurotrophic roles of CS lyase, which ought to be pursued further. Fig. 1.10.1 illustrates the effect of CS/DS on neuronal regeneration. Among all applications, reinnervation seems most exciting, as neural regeneration was assumed impossible until recent past. The neurotrophic role of CS lyase is a reassuring domain, which must be investigated further.

1.11 The microorganism

Pedoabcter saltans belongs to family *Sphingobacteriaceae*. The genus name is derived from the Latinized Greek word 'pedon' meaning 'the ground, earth' and the word 'bacter' meaning 'rod', yielding '*Pedobacter*', the 'rod from soil' (Styen *et al.*, 1998). The species epithet is derived from the Latin word 'saltare' meaning 'to dance', yielding 'saltans', referring to the gliding motility of the strain (Styen *et al.*, 1998). *P. saltans* was isolated from soil in Iceland. The temperature range for growth of *P. saltans* is normally between 5°C and 30°C (Styen *et al.*, 1998) The cells of *P. saltans* are short rods (0.5 x 0.7-1.0 µm) with rounded or slightly tapering ends (Fig. 1.11.1). *P. saltans* is aerobic, gram-negative and non-spore-forming (Styen *et al.*, 1998; Liolios *et al.*, 2011). *Pedobacter saltans* is a heparinolytic bacterium and has been identified with features like degradation of chondroitin sulphate and heparin (Liolios *et al.*, 2011). Thus cloning and biochemical characterization of polysaccharide lyase family 8 from *Pedobacter saltans* in *E.coli* as a host may find a new area of research, its scale up and overproduction may accomplish the therapeutic need of chondroitin and hepain degrading enzymes.

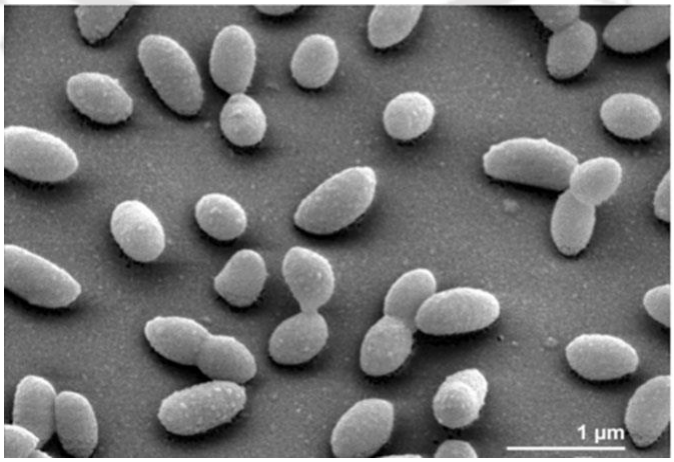

Fig. 1.11.1 Scanning electron microscope (SEM) image of *Pedobacter saltans* (adapted from Liolios *et al.*, 2011).

1.12 Significance and specific objectives of the present study

CS is a part of connective tissues and involved in major biological processes such as resiliency, structural integrity of cartilage and maintenance of synovial fluid in the bone joints owing to its polyanionic structure (Raynauld *et al.,* 2016). CS also acts as free radical scavenger and decreases DNA fragmentation, protein degradation and cell death rate. CS is commercially available from various sources such as, bovine cartilage, bovine trachea and shark fin. The increasing demand and the high cost of CS has led to the exploitation of shark and bovine which impart a strong impact on the ecological balance. CS is also in high demand for its applications in tissue engineering, pharmaceutical, cosmetic and food industries. All these reasons make it essential for researchers to seek for more different animal sources of CS isolation and its physicochemical characterization. Recruitment of CS lyase to modulate structure and functionality of CS polysaccharides might be effective in this regard. Substrate specificity of the enzyme requires precise understanding to manipulate the targeted polysaccharide. Analytical tools like mass spectrometry, NMR and FTIR can facilitate this pursuit. Novel CS lyases can be identified by screening new microbes from various taxonomic groups. Production of anti-inflammatory and anti-oxidative oligosaccharides might be employed to tackle allergic, auto-immune diseases and cancer. CS lyase-based manipulation of cancer hallmarks, the altered cell surface receptors can be crucial towards cancer mitigation. CS lyase has shown synergistic effect with other therapeutic agents which requires assessment. Overall, a plethora of approaches can be undertaken to enrich CS lyase research in discovery of their optimal biological efficiency.

The aim of present study was to explore the new recombinant chondroitin AC lyase, *Ps*PL8A from *Pedobactor saltans*. The specific primers will be designed to amplify gene and it will be subsequently cloned into an expression vector followed by expression in *E. coli*. The substrate specificity and various biochemical and functional properties of *Ps*PL8A will be determined. The reaction conditions for enzyme assay, kinetic parameters and mode of catalysis will be investigated. The *in-vitro* therapeutic potential of *Ps*PL8A will be studied on the human melanoma and fibrosarcoma cell lines. The present study will unfold the avenue for the potential application of *Ps*PL8A as antitumor agent. The structural analysis of *Ps*PL8A will involve the homology modeling, docking, circular dichroism, SAXS and site-directed mutagenesis analyses to determine the overall structure, key amino acid residues and their role in catalysis.

The other part of the investigation involves the isolation, complete physicochemical and structural characterization of a chondroitin sulphate from the poultry waste, chicken keel bone cartilage. The CS-keel will be analyzed for its various physicochemical properties and its antioxidant and emulsifying potentials. The recombinant *Ps*PL8A will be utilized for the production of CS-keel oligosaccharide by degrading CS-keel polysaccharide. The CS-keel disaccharide will be studied for their anticancer potential on human colon cancer cell lines. *In vitro* prebiotic potential of purified CS-keel disaccharide for functional foods will be investigated.

1.12.1 Specific objectives of the present study

1. Cloning, expression and purification of family 8 polysaccharide lyase (*Ps*PL8A) from *Pedobacter saltans.*
2. Biochemical and functional characterization of chondroitin sulphate AC lyase (*Ps*PL8A) from *Pedobacter saltans* DSM 12145
3. Insights into the structural characteristics and substrate binding analysis of chondroitin AC lyase (*Ps*PL8A) from *Pedobacter saltans.*
4. Antitumor effect of chondroitin AC lyase (*Ps*PL8A) from *Pedobacter saltans* on melanoma and fibrosarcoma cell lines by *in vitro* analysis.
5. Physicochemical, antioxidant and biocompatible properties of chondroitin sulphate isolated from chicken keel bone for potential biomedical applications.
6. Prebiotic chondroitin sulphate disaccharide isolated from chicken keel bone exhibiting anticancer potential against human colon adenocarcinoma HT-29 cells

1.13 References

Afratis, N., Gialeli, C., Nikitovic, D., Tsegenidis, T., Karousou, E., Theocharis, A.D., Pavão, M.S., Tzanakakis, G.N. and Karamanos, N.K. (2012). Glycosaminoglycans: key players in cancer cell biology and treatment. *FEBS Journal*, *279*(7), 1177-1197.

Ahn, M.Y., Shin, K.H., Kim, D.H., Jung, E.A., Toida, T., Linhardt, R.J. and Kim, Y.S. (1998). Characterization of a Bacteroides species from human intestine that degrades glycosaminoglycans. *Canadian Journal of Microbiology*, *44*(5), 423-429.

Al-Hakim, A., Linhardt, R.J. (1991). Capillary electrophoresis for the analysis of chondroitin sulfate-and dermatan sulfate-derived disaccharides. *Analytical Biochemistry*, *195*(1), 68-73.

Banfield, B.W., Leduc, Y., Esford, L., Visalli, R.J., Brandt, C.R. and Tufaro, F. (1995). Evidence for an interaction of herpes simplex virus with chondroitin sulfate proteoglycans during infection. *Virology*, *208*(2), 531-539.

Bao, X., Nishimura, S., Mikami, T., Yamada, S., Itoh, N. and Sugahara, K. (2004). Chondroitin sulfate/dermatan sulfate hybrid chains from embryonic pig brain, which contain a higher proportion of L-iduronic acid than those from adult pig brain, exhibit neuritogenic and growth factor binding activities. *Journal of Biological Chemistry*, *279*(11), 9765-9776.

Bartus, K., James, N.D., Didangelos, A., Bosch, K.D., Verhaagen, J., Yáñez-Muñoz, R.J., Rogers, J.H., Schneider, B.L., Muir, E.M. and Bradbury, E.J. (2014). Large-scale chondroitin sulfate proteoglycan digestion with chondroitinase gene therapy

leads to reduced pathology and modulates macrophage phenotype following spinal cord contusion injury. *Journal of Neuroscience, 34*(14), 4822-4836.

Bianchera, A., Salomi, E., Pezzanera, M., Ruwet, E., Bettini, R. and Elviri, L. (2014) Chitosan hydrogels for chondroitin sulphate controlled release: An analytical characterization. *Journal of Analytical Methods in Chemistry* http://dx.doi.org/10.1155/2014/808703, Article ID 808703.

Blain, F., Tkalec, A.L., Shao, Z., Poulin, C., Pedneault, M., Gu, K., Eggimann, B., Zimmermann, J. and Su, H. (2002). Expression system for high levels of GAG lyase gene expression and study of the hepA upstream region in *Flavobacterium heparinum*. *Journal of Bacteriology*, *184*(12), 3242-3252.

Brustoski, K., Kramer, M., Möller, U., Kremsner, P.G. and Luty, A.J. (2005). Neonatal and maternal immunological responses to conserved epitopes within the DBL-γ3 chondroitin sulfate A-binding domain of *Plasmodium falciparum* erythrocyte membrane protein 1. *Infection and Immunity*, *73*(12), 7988-7995.

Campo, G.M., Avenoso, A., Campo, S., Ferlazzo, A.M. and Calatroni, A. (2006) Chondroitin sulphate: antioxidant properties and beneficial effects. *Mini Reviews in Medicinal Chemistry*, *6*(12), 1311-1320.

Cantarel, B.L., Coutinho, P.M., Rancurel, C., Bernard, T., Lombard, V. and Henrissat, B. (2009). The Carbohydrate-Active EnZymes database (CAZy): an expert resource for glycogenomics. *Nucleic Acids Research*, *37*(suppl 1), D233-D238.

Capila, I. and Linhardt, R.J. (2002). Heparin–protein interactions. *Angewandte Chemie International Edition*, *41*(3), 390-412.

Cattaruzza, S. and Perris, R. (2006). Approaching the proteoglycome: molecular interactions of proteoglycans and their functional output. *Macromolecular Bioscience*, *6*(8), 667-680.

Chen, X.R., Liao, S.J., Ye, L.X., Gong, Q., Ding, Q., Zeng, J.S. and Yu, J. (2014). Neuroprotective effect of chondroitinase ABC on primary and secondary brain injury after stroke in hypertensive rats. *Brain Research, 1543*, 324-333.

Denholm, E.M., Lin, Y.Q. and Silver, P.J. (2001). Anti-tumor activities of chondroitinase AC and chondroitinase B: inhibition of angiogenesis, proliferation and invasion. *European Journal of Pharmacology*, *416*(3), 213-221.

Didangelos, A., Iberl, M., Vinsland, E., Bartus, K. and Bradbury, E.J. (2014). Regulation of IL-10 by chondroitinase ABC promotes a distinct immune response following spinal cord injury. *Journal of Neuroscience*, *34*(49), 16424-16432.

Dmitrieva, N., Yu, L., Viapiano, M., Cripe, T.P., Chiocca, E.A., Glorioso, J.C. and Kaur, B. (2011). Chondroitinase ABC I–mediated enhancement of oncolytic virus spread and antitumor efficacy. *Clinical Cancer Research, 17*(6), 1362-1372.

Eisenmann, K.M., McCarthy, J.B., Simpson, M.A., Keely, P.J., Guan, J.L., Tachibana, K., Lim, L., Manser, E., Furcht, L.T. and Iida, J. (1999). Melanoma chondroitin sulphate proteoglycan regulates cell spreading through Cdc42, Ack-1 and p130cas. *Nature Cell Biology*, *1*(8), 507-513.

Esko, J.D. and Selleck, S.B. (2002). Order Out of Chaos: Assembly of ligand binding sites in heparan sulfate 1. *Annual Review of Biochemistry*, *71*(1), 435-471.

Fenn, L.S. and McLean, J.A. (2011). Structural resolution of carbohydrate positional and structural isomers based on gas-phase ion mobility-mass spectrometry. *Physical Chemistry Chemical Physics*, *13*(6), 2196-2205.

Féthière, J., Eggimann, B. and Cygler, M. (1999). Crystal structure of chondroitin AC lyase, a representative of a family of glycosaminoglycan degrading enzymes. *Journal of Molecular Biology*, *288*(4), 635-647.

Flangea, C., Schiopu, C., Sisu, E., Serb, A., Przybylski, M., Seidler, D.G. and Zamfir, A.D. (2009). Determination of sulfation pattern in brain glycosaminoglycans by chip-based electrospray ionization ion trap mass spectrometry. *Analytical and Bioanalytical Chemistry*, *395*(8), 2489.

Garner, O.B., Yamaguchi, Y., Esko, J.D. and Videm, V. (2008). Small changes in lymphocyte development and activation in mice through tissue-specific alteration of heparan sulphate. *Immunology*, *125*(3), 420-429.

Garron, M.L. and Cygler, M. (2010). Structural and mechanistic classification of uronic acid-containing polysaccharide lyases. *Glycobiology*, *20*(12), 1547-1573.

Giroglou, T., Florin, L., Schäfer, F., Streeck, R.E. and Sapp, M. (2001). Human papillomavirus infection requires cell surface heparan sulfate. *Journal of Virology*, *75*(3), 1565-1570.

Gu, K., Linhardt, R.J., Laliberte, M. and Zimmermann, J. (1995). Purification, characterization and specificity of chondroitin lyases and glycuronidase from *Flavobacterium heparinum*. *Biochemical Journal*, *312*(2), 569-577.

Habuchi, O. (2000). Diversity and functions of glycosaminoglycan sulfotransferases. *Biochimica et Biophysica Acta (BBA)-General Subjects*, *1474*(2), 115-127.

Halldórsdóttir, A.M., Zhang, L. and Tollefsen, D.M. (2006). N-Acetylgalactosamine 4, 6-O-sulfate residues mediate binding and activation of heparin cofactor II by porcine mucosal dermatan sulfate. *Glycobiology*, *16*(8), 693-701.

Hamai, A., Hashimoto, N., Mochizuki, H., Kato, F., Makiguchi, Y., Horie, K. and Suzuki, S. (1997). Two distinct chondroitin sulfate ABC lyases an endoeliminase yielding tetrasaccharides and an exoeliminase preferentially acting on oligosaccharides. *Journal of Biological Chemistry*, *272*(14), 9123-9130.

Harris, N.G., Nogueira, M.S., Verley, D.R. and Sutton, R.L. (2013). Chondroitinase enhances cortical map plasticity and increases functionally active sprouting axons after brain injury. *Journal of Neurotrauma*, *30*(14), 1257-1269.

Hashimoto, W., Nankai, H., Mikami, B. and Murata, K. (2003). Crystal structure of Bacillus sp. GL1 xanthan lyase, which acts on the side chains of xanthan. *Journal of Biological Chemistry*, *278*(9), 7663-7673.

Henrotin, Y., Mathy, M., Sanchez, C. and Lambert, C (2010). Chondroitin sulfate in the treatment of osteoarthritis: from in vitro studies to clinical recommendations. *Therapeutic Advances in Musculoskeletal Disease*, *2*(6), 335-348.

Herndon, M.E. and Lander, A.D. (1990). A diverse set of developmentally regulated proteoglycans is expressed in the rat central nervous system. *Neuron*, *4*(6), 949-961.

Hirano, T. (1998). Interleukin 6 and its receptor: ten years later. *International Reviews of Immunology*, *16*(3-4), 249-284.

Hiyama, K., and Okada, S. (1975). Amino acid composition and physicochemical characterization of chondroitinase from *Arthrobacter aurescens*. *Biochemical Journal*, *78*(6), 1183.

Hochberg, M.C., Martel-Pelletier, J., Monfort, J., Möller, I., Castillo, J.R., Arden, N., Berenbaum, F., Blanco, F.J., Conaghan, P.G., Doménech, G. and Henrotin, Y. (2015). Combined chondroitin sulfate and glucosamine for painful knee osteoarthritis: a multicentre, randomised, double-blind, non-inferiority trial versus celecoxib. *Annals of the Rheumatic Diseases*, annrheumdis, 1-8.

Hong, S.W., Kim, B.T., Shin, H.Y., Kim, W.S., Lee, K.S., Kim, Y.S. and Kim, D.H. (2002). Purification and characterization of novel chondroitin ABC and AC lyases from *Bacteroides stercoris* HJ-15, a human intestinal anaerobic bacterium. *European Journal of Biochemistry*, *269*(12), 2934-2940.

Huang, R., Pomin, V.H. and Sharp, J.S. (2011). LC-MSn analysis of isomeric chondroitin sulfate oligosaccharides using a chemical derivatization strategy. *Journal of the American Society for Mass Spectrometry*, *22*(9), 1577-1587.

Huang, W., Lunin, V., Li, Y., Suzuki, S., Sugiura, N., Miyazono, H. and Cygler, M. (2003). Crystal structure of *Proteus vulgaris* chondroitin sulfate ABC lyase I at 1.9 Å resolution. *Journal of Molecular Biology*, *328*(3), 623-634.

Huang, W., Matte, A., Li, Y., Kim, Y.S., Linhardt, R.J., Su, H. and Cygler, M. (1999). Crystal structure of chondroitinase B from *Flavobacterium heparinum* and its complex with a disaccharide product at 1.7 A resolution. *Journal of Molecular Biology*, *294*(5),1257–1269.

Igarashi, N., Takeguchi, A., Sakai, S., Akiyama, H., Higashi, K. and Toida, T. (2013). Effect of molecular sizes of chondroitin sulfate on interaction with L-

selectin. *International Journal of Carbohydrate Chemistry, 2013*. dx.doi.org/10.1155/2013/856142, Article ID 856142.

Iida, J., Meijne, A.M., Knutson, J.R., Furcht, L.T. and McCarthy, J.B. (1996). Cell surface chondroitin sulfate proteoglycans in tumor cell adhesion, motility and invasion. In *Seminars in Cancer Biology, 7*(3), 155-162. Academic Press.

Iida, J., Milius, R.P., Oegema, T.R., Furcht, L.T. and McCarthy, J. B. (1994). Role of cell surface proteoglycans in tumor cell recognition of fibronectin. *Trends in Glycoscience and Glycotechnology*, *6***,** 1-16.

Iozzo, R. V. (1998). Matrix proteoglycans: from molecular design to cellular function. *Annual Review of Biochemistry*, *67*(1), 609-652.

Iozzo, R.V. and Cohen, I. (1993). Altered proteoglycan gene expression and the tumor stroma. *Experientia*, *49*(5), 447-455.

Iozzo, R.V. and Sanderson, R.D. (2011)**.** Proteoglycans in cancer biology, tumour microenvironment and angiogenesis. *Journal of Cellular and Molecular Medicine, 15*(5), 1013-1031.

Ishihara, K. and Hirano, T. (2002). IL-6 in autoimmune disease and chronic inflammatory proliferative disease. *Cytokine & Growth Factor Reviews*, *13*(4), 357-368.

Jandik, K.A., Gu, K. and Linhardt, R.J. (1994). Action pattern of polysaccharide lyases on glycosaminoglycans. *Glycobiology*, *4*(3), 289-296.

Jenkins, J. Mayans, O. and Pickersgill, R. (1998). Structure and evolution of parallel β-helix proteins. *Journal of Structural Biology*, *122*(1), 236-246.

Jin, M., Iwamoto, T., Yamada, K., Satsu, H., Totsuka, M. and Shimizu, M. (2010). Disaccharide derived from chondroitin sulfate A suppressed CpG-induced IL-6 secretion in macrophage-like J774. 1 cells. *Cytokine*, *51*(1), 53-59.

Jurnak, F., Yoder, M.D., Pickergill, R. and Jenkins, J. (1994). Parallel β-domains: A new fold in protein structures. *Current Opinion in Structural Biology*, *4*(6), 802-806.

Kanno, H., Pressman, Y., Moody, A., Berg, R., Muir, E.M., Rogers, J.H., Ozawa, H., Itoi, E., Pearse, D.D. and Bunge, M.B. (2014). Combination of engineered Schwann cell grafts to secrete neurotrophin and chondroitinase promotes axonal regeneration and locomotion after spinal cord injury. *Journal of Neuroscience*, *34*(5), 1838-1855.

Kawaguchi, Y., Sugiura, N., Kimata, K., Kimura, M. and Kakuta, Y. (2013). The crystal structure of novel chondroitin lyase ODV-E66, a baculovirus envelope protein. *FEBS Letters*, *587*(24), 3943-3948.

Ke, T., Zhangfu, L., Qing, G., Yong, T., Hong, J., Hongyan, R., Kun, L. and Shigui, L. (2005). Isolation of *Serratia marcescens* as a chondroitinase-producing bacterium and purification of a novel chondroitinase AC. *Biotechnology Letters*, *27*(7), 489-493

Kempson, G. E. (1980). The mechanical properties of articular cartilage. *The Joints and Synovial Fluid*, *2*, 177-238.

Kim, B.T., Kim, W.S., Kim, Y.S., Linhardt, R.J. and Kim, D. H. (2000). Purification and characterization of a novel heparinase from *Bacteroides stercoris* HJ-15. *Journal of Biochemistry*, *128*(2), 323-328.

Kim, Y., Lee, H.G., Dmitrieva, N., Kim, J., Kaur, B. and Friedman, A. (2014). Choindroitinase ABC I-mediated enhancement of oncolytic virus spread and antitumor efficacy: a mathematical model, *Plos One*, e102499.

Kimata, K., Okayama, M., Oohira, A. and Suzuki, S. (1973) Cyto-differentiation and proteoglycan biosynthesis. *Molecular and Cellular Biochemistry*, *1*(2), 211-228.

Kitagawa, H., Uyama, T. and Sugahara, K. (2001). Molecular cloning and expression of a human chondroitin synthase. *Journal of Biological Chemistry*, *276*(42), 38721-38726.

Kresse, H. and Schönherr, E. (2001). Proteoglycans of the extracellular matrix and growth control. *Journal of Cellular Physiology*, *189*(3), 266-274.

Kreuger, J., Spillmann, D., Li, J.P. and Lindahl, U. (2006). Interactions between heparan sulfate and proteins: the concept of specificity. *The Journal of Cell Biology*, *174*(3), 323-327.

Kuffler, D.P., Sosa, I.J. and Reyes, O. (2009). Schwann cell chondroitin sulfate proteoglycan inhibits dorsal root ganglion neuron neurite outgrowth and substrate specificity via a soma and not a growth cone mechanism. *Journal of Neuroscience Research*, *87*(13), 2863-2871.

Kumagai, Y., Takeuchi, O. and Akira, S. (2008). TLR9 as a key receptor for the recognition of DNA. *Advanced Drug Delivery Reviews*, *60*(7), 795-804.

Kwok, J.C.F., Warren, P. and Fawcett, J.W. (2012). Chondroitin sulfate: a key molecule in the brain matrix. *The International Journal of Biochemistry & Cell Biology*, *44*(4), 582-586.

Lander, A.D. and Selleck, S.B. (2000). The Elusive Functions of Proteoglycans In Vivo Veritas. *The Journal of Cell Biology*, *148*(2), 227-232.

Laremore, T.N., Zhang, F., Dordick, J.S., Liu, J. and Linhardt, R.J. (2009). Recent progress and applications in glycosaminoglycan and heparin research. *Current Opinion in Chemical Biology*, *13*(5), 633-640.

Lauder, R.M. (2009). Chondroitin sulphate: a complex molecule with potential impacts on a wide range of biological systems. *Complementary Therapies in Medicine*, *17*(1), 56-62.

Lee, C.M., Tanaka, T., Murai, T., Kondo, M., Kimura, J., Su, W., Kitagawa, T., Ito, T., Matsuda, H. and Miyasaka, M. (2002). Novel chondroitin sulfate-binding cationic liposomes loaded with cisplatin efficiently suppress the local growth and liver metastasis of tumor cells *in vivo*. *Cancer Research*, 62(15), 4282-4288.

Lemmnitzer, K., Schiller, J., Becher, J., Möller, S. and Schnabelrauch, M. (2014). Improvement of the digestibility of sulfated hyaluronans by bovine testicular hyaluronidase: A UV spectroscopic and Mass spectrometric study. *BioMed Research International*, doi.org/10.1155/2014/986594, Article ID 986594.

Levene, P. A., and La Forge, F. B. (1914). On chondroitin sulphuric acid. *Studies from the Rockefeller Institute for Medical Research*, *19*, 233.

Li, L., Ly, M. and Linhardt, R.J. (2012). Proteoglycan sequence. *Molecular BioSystems*, *8*(6), 1613-1625

Li, S., Kelly, S.J., Lamani, E., Ferraroni, M. and Jedrzejas, M.J. (2000). Structural basis of hyaluronan degradation by *Streptococcus pneumoniae* hyaluronate lyase. *The EMBO Journal*, *19*(6), 1228-1240.

Linhardt, R. J. (1994). Analysis of glycosaminoglycans with polysaccharide lyases. In: Varki, A., editor. Current Protocols in Molecular Biology, Analysis of Glycoconjugates. Wiley Interscience; Boston, Vol. 2. pp. 17.13.17-17.13.32.

Linhardt, R.J. and Toida, T. (2004). Role of glycosaminoglycans in cellular communication. *Accounts of Chemical Research*, *37*(7), 431-438.

Linhardt, R.J., Al-Hakim, A., Liu, J., Hoppensteadt, D., Mascelanni, P. and Fareed, J. (1991). Structural features of dermatan sulfates and their relationship to anticoagulant and antithrombotic activities. *Biochemical Pharmacology*, *42*(8), 1609-1619.

Linhardt, R.J., Avci, F.Y., Toida, T., Kim, Y.S. and Cygler, M. (2006). CS lyases: structure, activity, and applications in analysis and the treatment of diseases. *Advances in Pharmacology*, *53*, 187-215.

Linn, S., Chan, T., Lipeski, L. and Salyers, A.A. (1983). Isolation and characterization of two chondroitin lyases from *Bacteroides thetaiotaomicron*. *Journal of Bacteriology*, *156*(2), 859-866.

Liolios, K., Sikorski, J., Lu, M., Nolan, M., Lapidus, A., Lucas, S. and Kyrpides, N. C. (2011) Complete genome sequence of the gliding, heparinolytic *Pedobacter saltans* type strain (113T). *Standards in Genomic Science, 5*. 30-40.

Liu, J. and Thorp, S.C. (2002). Cell surface heparan sulfate and its roles in assisting viral infections. *Medicinal Research Reviews*, *22*(1), 1-25.

Lombard, V., Bernard, T., Rancurel, C., Brumer, H., Coutinho, P. and Henrissat, B. (2010). A hierarchical classification of polysaccharide lyases for glycogenomics. *Biochemical Journal*, *432*, 437-444.

Lunin, V.V., Li, Y., Linhardt, R.J., Miyazono, H., Kyogashima, M., Kaneko, T., Bell, A.W. and Cygler, M. (2004). High-resolution crystal structure of *Arthrobacter aurescens* chondroitin AC lyase: an enzyme–substrate complex defines the catalytic mechanism. *Journal of Molecular Biology*, *337*(2), 367-386.

Luo, X.M., Fosmire, G.J. and Leach, R.M. (2002) Chicken keel cartilage as a source of chondroitin sulfate. *Poultry Science*, *81*(7), 1086-1089.

Ly, M., Laremore, T.N. and Linhardt, R.J. (2010). Proteoglycomics: recent progress and future challenges. *Omics: A Journal of Integrative Biology*, *14*(4), 389-399.

Mårdberg, K., Trybala, E., Tufaro, F. and Bergström, T. (2002). Herpes simplex virus type 1 glycoprotein C is necessary for efficient infection of chondroitin sulfate-expressing gro2C cells. *Journal of General Virology*, *83*(2), 291-300.

Massey, J.M., Amps, J., Viapiano, M.S., Matthews, R.T., Wagoner, M.R., Whitaker, C.M. and Onifer, S.M. (2008). Increased chondroitin sulfate proteoglycan expression in denervated brainstem targets following spinal cord injury creates a barrier to axonal regeneration overcome by chondroitinase ABC and neurotrophin-3. *Experimental Neurology*, *209*(2), 426-45.

Matuszewski, P.E., Chen, Y.L., Szczesny, S.E., Lake, S.P., Elliott, D.M., Soslowsky, L.J. and Dodge, G.R. (2012). Regional variation in human supraspinatus tendon proteoglycans: decorin, biglycan, and aggrecan. *Connective Tissue Research*, *53*(5),343-348.

Michel, G., Pojasek, K., Li, Y., Sulea, T., Linhardt, R.J., Raman, R., Prabhakar, V., Sasisekharan, R. and Cygler, M. (2004). The structure of chondroitin B lyase complexed with glycosaminoglycan oligosaccharides unravels a calcium-dependent catalytic machinery. *Journal of Biological Chemistry*, *279*(31), 32882-32896.

Mikami, T. and Kitagawa, H. (2013). Biosynthesis and function of chondroitin sulfate. *Biochimica et Biophysica Acta (BBA)-General Subjects*, *1830*(10), 4719-4733.

Mourier, P., Anger, P., Martinez, C., Herman, F. and Viskov, C. (2015). Quantitative compositional analysis of heparin using exhaustive heparinase digestion and strong anion exchange chromatography. *Analytical Chemistry Research*, *3*, 46-53.

Murata, K. and Yokoyama, Y. (1985). Enzymatic analysis with chondrosulfatases of constituent disaccharides of sulfated chondroitin sulfate and dermatan sulfate isomers by high-performance liquid chromatography. *Analytical Biochemistry*, *149*(1), 261-268.

Nimptsch, A., Schibur, S., Schnabelrauch, M., Fuchs, B., Huster, D. and Schiller, J. (2009). Characterization of the quantitative relationship between signal-to-noise (S/N) ratio and sample amount on-target by MALDI-TOF MS: determination of chondroitin sulfate subsequent to enzymatic digestion. *Analytica Chimica Acta Journal*, *635*(2), 175-182.

Pervin, A., Alhakim, A. and Linhardt, R.J. (1994). Separation of glycosaminoglycan-derived oligosaccharides by capillary electrophoresis using reverse polarity. *Analytical Biochemistry*, *221*(1), 182-188.

Pervin, A., Gu, K. and Linhardt, R.J. (1993). Capillary electrophoresis to measure sulfoesterase activity on chondroitin sulfate and heparin derived disaccharides. *Applied and Theoretical Electrophoresis*, *3*(6), 297-297.

Poh, Z. W., Gan, C. H., Lee, E. J., Guo, S., Yip, G. W. and Lam, Y. (2015). Divergent synthesis of chondroitin sulfate disaccharides and identification of sulfate motifs that inhibit triple negative breast cancer. *Scientific Reports*, *5*.

Pojasek, K., Shriver, Z., Kiley, P., Venkataraman, G. and Sasisekharan, R. (2001). Recombinant expression, purification, and kinetic characterization of

chondroitinase AC and chondroitinase B from *Flavobacterium heparinum*. *Biochemical and Biophysical Research Communications*, *286*(2), 343-351.

Prabhakar, V., Capila, I., Raman, R., Srinivasan, A., Bosques, C.J., Pojasek, K. and Sasisekharan, R. (2006). The catalytic machinery of chondroitinase ABC I utilizes a calcium coordination strategy to optimally process dermatan sulfate. *Biochemistry*, *45*(37), 11130-11139.

Prabhakar, V., Capila, I., Soundararajan, V., Raman, R. and Sasisekharan, R. (2009). Recombinant expression, purification, and biochemical characterization of chondroitinase ABC II from *Proteus vulgaris*. *Journal of Biological Chemistry*, *284*(2), 974-982.

Prabhakar, V., Raman, R., Capila, I., Bosques, C.X., Pojasek, K. and Sasisekharan, R. (2005). Biochemical characterization of the chondroitinase ABC I active site. *Biochemical Journal*, *390*, 395-405.

Price, M.A., Colvin Wanshura, L.E., Yang, J., Carlson, J., Xiang, B., Li, G., Ferrone, S., Dudek, A.Z., Turley, E.A. and McCarthy, J.B. (2011). CSPG4, a potential therapeutic target, facilitates malignant progression of melanoma. *Pigment Cell & Melanoma Research*, *24*(6),1148-1157.

Pumphrey, C. Y., Theus, A. M., Li, S., Parrish, R. S., & Sanderson, R. D. (2002). Neoglycans, Carbodiimide-modified Glycosaminoglycans. *Cancer Research*, *62*(13), 3722-3728.

Rauch, U. and Kappler, J. (2006). Chondroitin/dermatan sulfates in the central nervous system: their structures and functions in health and disease. *Advances in Pharmacology*, *53*, 337-356.

Raynauld, J.P., Pelletier, J.P., Abram, F., Delorme, P. and Martel-Pelletier, J. (2016). Long-term effects of glucosamine/chondroitin sulfate on the progression of structural changes in knee osteoarthritis: 6-year follow-up data from the osteoarthritis initiative. *Arthritis Care & Research*, *68*(10), 1560-1566.

Robu, A.C. Popescu, L. Munteanu, C.V. Seidler, D.G. and Zamfir, A.D. (2015). Orbitrap mass spectrometry characterization of hybrid chondroitin/dermatan sulfate hexa-saccharide domains expressed in brain. *Analytical Biochemistry*, *485*, 122-131.

Ronca, F., Palmieri, L., Panicucci, P., and Ronca, G. (1998). Anti-inflammatory activity of chondroitin sulfate. *Osteoarthritis and Cartilage*, *6*, 14-21.

Rostand, K.S. and Esko, J.D. (1997). Microbial adherence to and invasion through proteoglycans. *Infection and Immunity*, *65*(1), 1.

Rye, C.S. and Withers, S.G. (2002). Elucidation of the Mechanism of Polysaccharide Cleavage by Chondroitin AC Lyase from *Flavobacterium heparinum*. *Journal of the American Chemical Society*, *124*(33), 9756-9767.

Schiller, J., Becher, J., Möller, S., Nimptsch, K., Riemer, T. and Schnabelrauch, M. (2010). Synthesis and characterization of chemically modified hyaluronan and chondroitin sulfate. *Mini-Reviews in Organic Chemistry*, *7*(4), 290-299.

Schiraldi, C., Cimini, D., and De Rosa, M. (2010). Production of chondroitin sulfate and chondroitin. *Applied microbiology and biotechnology*, *87*(4), 1209-1220.

Scott, J.E. (2001). Structure and function in extracellular matrices depend on interactions between anionic glycosaminoglycans. *Pathologie Biologie*, *49*(4), 284-289.

Sharma, K., Selzer, M.E. and Li, S. (2012). Scar-mediated inhibition and CSPG receptors in the CNS. *Experimental Neurology*, *237*(2), 370-378.

Shaya, D., Hahn, B.S., Bjerkan, T.M., Kim, W.S., Park, N.Y., Sim, J.S., Kim, Y.S. and Cygler, M. (2008). Composite active site of chondroitin lyase ABC accepting both epimers of uronic acid. *Glycobiology*, *18*(3), 270-277.

Shaya. D., Hahn, B.S., Park, N.Y., Sim, J.S., Kim, Y.S. and Cygler, M. (2008). Characterization of chondroitin sulfate lyase ABC from *Bacteroides thetaiotaomicron* WAL2926. *Biochemistry, 47*, 6650-6661.

Silbert, J.E. and Sugumaran, G. (2002). Biosynthesis of chondroitin/dermatan sulfate. *International Union of Biochemistry and Molecular Biology Life*, *54*(4), 177-186.

Skandalis, S.S., Labropoulou, V.T., Ravazoula, P., Likaki-Karatza, E., Dobra, K., Kalofonos, H.P., Karamanos, N.K and Theocharis, A.D (2011). Versican but not decorin accumulation is related to malignancy in mammographically detected high density and malignant-appearing microcalcifications in non-palpable breast carcinomas. *BMC Cancer*, *11*, 314.

Sneath, R.J. and Mangham, D.C. (1998). The normal structure and function of CD44 and its role in neoplasia. *Molecular Pathology, 51*(4), 191.

Steyn, P. L., Segers, P., Vancanneyt, M., Sandra, P., Kersters, K. and Joubert, J. J. (1998) Classification of heparinolytic bacteria into a new genus, *Pedobacter*, comprising four species: *Pedobacter heparinus* comb. nov. *Pedobacter piscium* comb. nov., *Pedobacter africanus* sp. nov. and *Pedobacter saltans* sp. nov. Proposal of the family Sphingobacteriaceae fam. nov. *International Journal of Systematic and Evolutionary Bacteriology*, *48*, 165-177.

Sugahara, K. and Kitagawa, H. (2000). Recent advances in the study of the biosynthesis and functions of sulfated glycosaminoglycans. *Current Opinion in Structural Biology*, *10*(5), 518-527.

Sugahara, K., Mikami, T., Uyama, T., Mizuguchi, S., Nomura, K. and Kitagawa, H. (2003). Recent advances in the structural biology of chondroitin sulfate and dermatan sulfate. *Current Opinion in Structural Biology*, *13*(5), 612-620.

Sugiura, N., Setoyama, Y., Chiba, M., Kimata, K. and Watanabe, H. (2011). Baculovirus envelope protein ODV-E66 is a novel chondroitinase with distinct substrate specificity. *Journal of Biological Chemistry*, *286*(33), 29026-29034.

Theocharis, A.D., Tsolakis, I., Tzanakakis, G.N. and Karamanos, N.K. (2006). Chondroitin sulfate as a key molecule in the development of atherosclerosis and cancer progression. *Advances in Pharmacology*, *53*, 281-295.

Toida, T., Toyoda, H. and Imanari, T. (1993). High-resolution proton nuclear magnetic resonance studies on chondroitin sulfates. *Analytical Sciences*, *9*(1), 53-58.

Tom, V. J., Sandrow-Feinberg, H.R., Miller, K., Santi. L., Connors, T., Lemay, M.A. and Houlé, J.D. (2009). Combining peripheral nerve grafts and chondroitinase promotes functional axonal regeneration in the chronically injured spinal cord. *The Journal of Neuroscience*, *29*(47), 14881-14890.

Tully, S.E., Rawat, M. and Hsieh-Wilson, L.C. (2006). Discovery of a TNF-α antagonist using chondroitin sulfate microarrays. *Journal of the American Chemical Society*, *128*(24), 7740-7741.

Uyama, T., Kitagawa, H. and Sugahara, K. (2007). In *Comprehensive Glycoscience*, Kamerling J.P. Ed.: Elsevier: Amsterdam, vol. *3*, pp, 79-104.

Verstak, B., Hertzog, P. and Mansell, A. (2007). Toll-like receptor signalling and the clinical benefits that lie within. *Inflammation Research*, *56*(1), 1-10.

Visintin, A., Mazzoni, A., Spitzer, J.H., Wyllie, D.H., Dower, S.K. and Segal, D.M. (2001). Regulation of Toll-like receptors in human monocytes and dendritic cells. *The Journal of Immunology*, *166*(1), 249-255.

Wagner, H. (2002). Interactions between bacterial CpG-DNA and TLR9 bridge innate and adaptive immunity. *Current Opinion in Microbiology*, *5*(1), 62-69.

Wang, T.W., Sun, J.S., Wu, H.C., Tsuang, Y.H., Wang, W.H. and Lin, F.H. (2006). The effect of gelatin–chondroitin sulfate–hyaluronic acid skin substitute on wound healing in SCID mice. *Biomaterials*, *27*(33), 5689-5697

Xu, J., Bjursell, M.K., Himrod, J., Deng, S., Carmichael, L.K., Chiang, H.C. and Gordon, J.I. (2003). A genomic view of the human-*Bacteroides thetaiotaomicron* symbiosis. *Science*, *299*(5615), 2074-2076.

Yamada, S. and Sugahara, K. (2008). Potential therapeutic application of chondroitin sulfate/dermatan sulfate. *Current Drug Discovery Technologies*, *5*, 289-301.

Yang, H.O., Gunay, N.S., Toida, T., Kuberan, B., Yu, G., Kim, Y.S. and Linhardt, R.J. (2000). Preparation and structural determination of dermatan sulfate-derived oligosaccharides. *Glycobiology*,*10*(10):1033-1040.

Yip, V.L. and Withers, S.G. (2006). Breakdown of oligosaccharides by the process of elimination. *Current Opinion in Chemical Biology*, *10*(2), 147-155.

Yip, V.L., Varrot, A., Davies, G.J., Rajan, S.S., Yang, X., Thompson, J. and Withers, S.G. (2004). An unusual mechanism of glycoside hydrolysis involving redox and elimination steps by a family 4 β-glycosidase from *Thermotoga maritima*. *Journal of the American Chemical Society*, *126*(27), 8354-8355.

Yoder, M.D., Lietzke, S.E. and Jurnak, F. (1993). Unusual structural features in the parallel β-helix in pectate lyases. *Structure*, *1*(4), 241-251.

Yoon, H.J., Mikami, B., Hashimoto, W. and Murata, K. (1999). Crystal structure of alginate lyase A1-III from *Sphingomonas* species A1 at 1.78 Å resolution. *Journal of Molecular Biology*, *290*(2), 505-514.

Zechel, D.L. and Withers, S.G. (2000). Glycosidase mechanisms: anatomy of a finely tuned catalyst. *Accounts of Chemical Research*, *33*(1), 11-18.

Zhang, T., Shen, Y., Lu, L., Fan, Z. and Huo, W. (2013). Effect of chondroitinase ABC on axonal myelination and glial scar after spinal cord injury in rats. *Chinese Journal of Reparative and Reconstructive Surgery*, *27*(2), 145-150.

Zhao, R.R. and Fawcett, J. W. (2013). Combination treatment with chondroitinase ABC in spinal cord injury-breaking the barrier. *Neuroscience Bulletin*, *29*(4), 477-483.

Chapter 2

Cloning, expression and purification of chondroitin sulphate AC lyase of family 8 polysaccharide lyase (*Ps*PL8A) from *Pedobacter saltans* DSM12145

2.1 Introduction

Proteoglycans are the major constituent of extracellular matrix in animals (Yamada *et al*., 2008). These proteoglycans are made up of protein core and the Glycosaminoglycan (GAG) chains. GAG are highly charged linear heteropolysaccharide chains composed of an alternating repeating disaccharide units of two six membered sugar rings, a hexosamine (D-glucosamine, GlcNAc, or D-galactosamine, GalNAc) linked to a uronic acid (D-glucuronic acid, GlcA, or L-iduronic acid, IdoA) (Shaya *et al.,* 2008). These monosaccharide units can either be sulphated or non-sulphated. The molecular weight and sulphation of these chains depends upon its location and the type of tissue (Bulow and Hobert 2006; Ernst *et al*., 1995; Afratis *et al.,* 2012). GAGs are classified into four main categories, heparin/heparan sulphate, keratan sulphate, hyaluronic acid, chondroitin sulphate (CS) or dermatan sulphate (DS). GAG with an exception of hyaluronic acid are attached

through a serine residue to the protein core and forms proteoglycan. Chondroitin sulphate is composed of Glucuronic acid (GlcA) attached to N-acetylgalactosamine (GalNAc) through a β-(1→3) linkage and these disaccharide units are connected *via* β-(1→4) glycosidic linkage forming a polysaccharide chain (Galtrey *et al.*, 2007). CS can be regioselectively sulphated at 4-O or 6-O positions of N-acetylgalactosamine and hence classified as chondroitin 4-sulphate (C4S) or chondroitin 6-sulphate (C6S), respectively (Habuchi *et al.*, 2000). CS chains play important roles in various biological functions such as cell adhesion, proliferation, differentiation, signalling, inflammation, organ morphogenesis, inflammation and infection by interacting with cytokines and myriad growth factors (Iozzo *et al.*, 1998; Denholm *et al.*, 2001).

Polysaccharide lyases (EC 4.2.2.-) are group of enzymes belonging to carbohydrate active enzymes and have been classified into 23 families (March 2016), on the basis of sequence similarity according to the CAZy database (Cantarel *et al.*, 1999). These 23 PL families contain nearly 1884 species of bacteria, 130 species of archaea, and 65 species of eukaryotes (www.cazy.org). Chondroitin lyase has been reported from families 6, 8 and 23 that degrades chondroitin sulphate *via* β elimination mechanism and generating Δ4,5 unsaturated products.

Microorganisms are the major sources of CS degrading enzymes, particularly soil bacteria which may depend upon connective tissues of animal carcasses as a nutrient source (Sutherland 1995). Chondroitin lyases have been previously reported from *Bacteroides thetaiotaomicron* (Shaya *et al.*, 2008), *Pedobacter heparinus* (previously known as *Flavobacterium heparinum*) (Fethiere *et al.*, 1999; Pojasek *et al.*, 2001), *Arthrobacter aurescens* (Lunin *et al.*, 2004) and *Bacteroides stercoris* HJ-15

(Shim *et al.*, 2008). In recent times chondroitin lyases have emerged as major therapeutic agents in clinical field (Denholm *et al.*, 2001; Didangelos *et al.*, 2014).

The gene sequence with locus name, Pedsa_3808 (http://www.cazy.org/PL8_bacteria.html) having GenBank accession no. ADY54337.1 belonging to family 8 polysaccharide lyase (PL8) from *Pedobacter saltans* DSM 12145 was identified. The putative chondroitin AC lyase (*Ps*PL8A) was cloned and expressed in *E. coli*. The sequence of gene and protein was retrieved from CAZy database. The molecular architecture of *Ps*PL8A from *Pedobacter saltans* shows a signal peptide of N-terminal 22 amino acids long signal peptide followed by the GAG lyase domain from 23 to 701 amino acids, a 679 amino acid domain (Fig. 2.1.1). The recombinant *Ps*PL8A protein containing the N-terminal His6-tags was purified by immobilized metal ion affinity chromatography (IMAC). The expression and purification of the recombinant *Ps*PL8A protein was analysed by SDS-PAGE and its further biochemical, functional and structural characterization was carried out.

Fig. 2.1.1 Molecular architecture of *Ps*PL8A showing boundaries and designation of different domains.

2.2 Materials and Methods

2.2.1 Chemicals, reagents and kits

The oligonucleotide primers for PCR amplification of *Ps*PL8A was procured from Eurofins, India. BIOTAQ DNA polymerase was supplied by Bioline, UK. The dNTPs and $MgCl_2$ were obtained from Sigma Aldrich, USA. PCR tubes (0.2 ml) were from Axygen, Germany. pGEM-T Easy vector system for TA cloning was purchased from Promega, USA. Restriction enzymes *Nhe*I, and *Xho*I were purchased from Promega, USA. The expression vector pET-28a(+), were purchased from Novagen, Germany. T_4 DNA ligase, 10x ligase buffer were purchased from Promega, USA. RNase solution (20 mg/ml), glacial acetic acid (99.9 % pure), Trizma base (Tris free base), ethidium bromide, Bradford reagent, nuclease free water (pH 8.0) and components of polyacrylamide gel electrophoresis were obtained from Sigma Aldrich, USA. The GenElute plasmid miniprep isolation kit and GenElute gel-extraction kit was from Sigma Aldrich, USA. The DNA was run on agarose gel prepared using Agrose, with low EEO from Sigma Aldrich, USA. DNA marker Hyperladder I was purchased from Bioline, UK. Page Ruler protein marker was procured from Fermentas, Germany. Disodium ethylenediamine tetra acetate salt (EDTA), glucose, sodium hydroxide, sodium dodecyl sulphates (SDS), LB medium and SOC medium components were supplied by Himedia Pvt. Ltd, India. The antibiotics, ampicillin and kanamycin were procured from Sigma Aldrich, USA. SDS-PAGE was performed using Mini-PROTEAN Tetra Cell purchased from Bio-Rad Laboratories (India) Private Limited. The protein staining dye Coomassie Brilliant Blue R250 was procured from Himedia and methanol from Merck, India. The genomic DNA of *Pedobacter saltans* DSM12145

was purchased from Leibniz Institute DSMZ - German Collection of Microorganisms and Cell Cultures.

2.2.2 Microorganisms

Escherichia coli DH5α and XL-10 Gold cells used for transformation and amplification of recombinant plasmid were procured from Novagen (Germany). *E. coli* BL-21 (DE3) cells for expression of recombinant proteins were obtained from Novagen (Germany).

2.2.3 PCR amplification of gene encoding *Ps*PL8A

The ORF encoding *Ps*PL8A with GenBank accession no. ADY54337.1 was amplified from genomic DNA of *Pedobacter saltans* using two oligonucleotide primers containing *NheI* and *XhoI* restriction sites. The sequence details of primers are mentioned in Table 2.2.1. Amplification of gene (2037 bp) encoding a 679 amino acid domain (*Ps*PL8A) was carried out following the schematic representation in Fig. 2.2.1. The components of 50 µl PCR reaction mixture and the conditions of PCR cycles for amplification are given in Tables 2.2.2 and 2.2.3, respectively. PCR amplification was performed using a thermal cycler (TAKARA Bio, Japan). The amplified PCR product was run on 0.8% (w/v) agarose gel in presence of DNA marker (Hyperladder I) as mentioned in Section 2.2.5.

Fig. 2.2.1 Schematic representation of PCR amplification of a 2037 bp gene encoding *Ps*PL8A from *Pedobacter saltans*.

Table 2.2.1 Oligonucleotide primers used for cloning *Ps*PL8A from *Pedobacter saltans.* The nucleotides shown in bold are the restriction enzyme sites.

Primer name	Primer sequence
*Ps*PL8A-F	5'CGC**GCTAGC**CAAAAGCAGACATTTGAACTG-3'
*Ps*PL8A-R	5'-GCGC**CTCGAG**TTAAACTTTTTCTGATTTGGT-3'

Table 2.2.2 PCR reaction setup for amplification of gene encoding *Ps*PL8A.

PCR components	Volume (µl)	Final concentration
10x reaction buffer	5.0	1x
$MgCl_2$ (50 mM)	2.5	2.5mM
dNTP mix (100 mM)	1.0	2 mM
Forward primer (15 µM)	1.5	0.45 µM
Reverse primer (15 µM)	1.5	0.45 µM
Sigma water, pH 8.0	36.5	--
Genomic DNA (2.22 ng/µl)	1.0	0.044 ng
Taq DNA polymerase (2.5 U/µl)	1.0	0.025U/ µl
Total	50.0	--

Table 2.2.3 Conditions for PCR thermal cycles for amplification of gene encoding *Ps*PL8A.

Steps		Time (min)
I. Denaturation at 94°C		4
II. 30 cycles of	i) Denaturation at 94°C	0.5
	ii) Annealing at 55°C	1.5
	iii) Extension at 72°C	2
III. Final extension at 72°C		10

2.2.4 Agarose gel electrophoresis of PCR amplified gene encoding *Ps*PL8A

The PCR amplified gene encoding *Ps*PL8A was run on 0.8% agarose gel prepared in 1x TAE buffer. A stock solution of TAE buffer was prepared according to Sambrook and Russell (2001) keeping the concentrations of components to 10x (400 mM Tris-acetate, 10 mM EDTA pH 8.0). The gel was prepared by dissolving agarose (400 mg for 0.8% gel) in 50 ml of 1x TAE buffer by heating in a microwave oven to

get a clear solution. Then 5.0 µl of ethidium bromide (5.0 mg/ml) was added when the solution temperature was around 50°C. The solution was mixed well and poured on the casting apparatus, combs were placed and the gel was allowed to solidify. For separating of PCR amplicon, 1x TAE (Tris-acetate-EDTA) buffer was used for preparing of agarose gel and also as an electrophoresis running buffer (Sambrook and Russel, 2001). The DNA sample and DNA loading dye were mixed in 4:1 ratio and the gel run at 60 Volt for 70% migration of the leading dye. The bands were then visualized under UV illumination in a gel documentation system (BioRad XR Gel documentation system).

2.2.4.1 DNA loading dye

The DNA or sample loading dye was prepared by mixing the components mentioned below in Table 2.2.4. A 5x stock solution of DNA loading dye was prepared and mixed with 4 volumes of DNA to make it to 1x before loading on to agarose gel. The final pH of the DNA loading dye adjusted to pH 8.0.

Table 2.2.4 Composition of 5x DNA loading dye.

Components	Final concentration (5x)
Tris-HCl	50 mM
Glycerol	25% (w/v)
EDTA	5.0 mM
Bromophenol blue	0.2% (w/v)
Xylene cyanol	0.2% (w/v)

2.2.5 Extraction of DNA from agarose gel

The PCR amplified DNA was purified from agarose gel using a kit (GenElute Gel Extraction Kit, Sigma Aldrich, USA), following the protocol provided by the

manufacturer as discussed in Section 2.2.5.1. The extracted DNA was eluted in 40 µl elution buffer supplied with the kit.

2.2.5.1 DNA gel extraction protocol

1. 1.5 ml sterile, empty microcentrifuge tubes were weighed and weight noted.
2. The PCR DNA was excised from gel using sharp sterile scalpel and transferred to an empty preweighed micro-centrifuge tubes. The tube was weighed again and the weight of excised gel was determined by subtracting the empty tube weight.
3. Now, 3 volumes of Gel solubilization solution was added to every 1 volume of gel (100 mg ~ 100 µl).
4. The microcentrifuge tube containing excised gel was incubated at 50°C for 10 min (or until the gel slice dissolved completely) indicated by the yellow colour of the solution.
5. 1 gel volume of isopropanol was added to this solution for PCR amplicons to get higher yield of DNA fragments <500 bp and >4 kb.
6. GenElute binding column G was placed in 2 ml collection tube provided with the kit. 500 µl of column preparation solution were added to each column membrane and centrifuged at 16,000*g* for 1 min. The flow through was discarded before the next step.
7. The solution containing PCR-amplified product (>700 µl) was added to DNA binding column and centrifuged at 16,000*g* for 1 min at room temperature discarding the flow through. If the volume was more than 700 µl, the remaining solution was centrifuged similarly and again the flow through was discarded.

8. 700 µl of Wash solution was added to each DNA bound spin column and the mixture centrifuged at 16,000*g* for 1 min at room temperature, discarding the flow through. The column was given an additional spin of 1 min at 16,000*g* to completely remove the residual ethanol.
9. Now the column containing bound DNA was placed in a fresh 1.5 ml sterile microcentrifuge tube. 30 µl of DNAse free water (Sigma-Aldrich, USA) or elution buffer (10 mM Tris-Cl, pH 8.5) was added at the centre of the column. The column was incubated for 2 min at room temperature and centrifuged at 16,000*g* for 1 min. For efficient recovery of DNA, the elution solution was preheated to 65°C prior to adding it to the membrane. Eluting at 65°C improves DNA recoveries by 2 to 3-fold.
10. The PCR-amplicon was eluted from GenElute spin columns and collected in 1.5 ml sterile microcentrifuge tube. The eluted PCR-amplified DNA was stored at -20°C for further use.

2.2.6 Preparation of Luria-Bertani (LB) medium

The most commonly used LB medium for growing *E. coli* cells was prepared by dissolving the ingredients (Table 2.2.5) in 800 ml of deionized water. The pH was adjusted to 7.2 and final volume was made up to 1 litre. 100 ml of LB medium was transferred to 250 ml conical flask and autoclaved at 121°C at 15 psi for 20 min. The filter sterilized antibiotics (ampicillin or kanamycin) were added in laminar air flow or near the flame to the autoclaved and cooled LB medium prior to inoculation.

Table 2.2.5 Composition of Luria-Bertani medium (Sambrook *et al*., 1989).

Components	Final concentration (%, w/v)
Tryptone	1.0
Yeast extract powder	0.5
Sodium chloride	1.0

2.2.6.1 Preparation of LB-agar medium

LB agar medium was prepared by adding 2% (w/v) Agar type I in LB liquid medium. The medium was autoclaved as described in Section 2.2.6 cooled to around 50-55°C and appropriate amount of antibiotic was added under laminar air flow. 20-25 ml of LB agar medium supplemented with antibiotic was poured in sterile petri plates and allowed to solidify for 15- 20 min.

2.2.7 Preparation of SOC medium

The SOC (super optimal medium with catabolic repression) was prepared using ingredients detailed in Table 2.2.6. It is a modified SOB medium with added glucose (Hanahan, 1983; Deutscher, 2008; Park *et al.*, 2012). Bactotryptone, yeast extract powder and NaCl were autoclaved separately. 1 M stock solutions of KCl, $MgCl_2$, $MgSO_4$ and glucose were filter-sterilized and required quantities added to above solution in the laminar hood to finally make SOC medium.

Table 2.2.6 Composition of SOC medium (Sambrook *et al*., 1989).

Components	Final concentration
Bactotryptone	2.0 (%, w/v)
Yeast extract powder	0.5 (%, w/v)
NaCl	10 mM
KCl	2.5 mM
$MgCl_2$	10 mM
$MgSO_4$	10 mM
Glucose	20 mM

2.2.8 Preparation of *E. coli* (XL10 Gold) and DH5α competent cells

Day 1

1. 50 µl of culture of *E. coli* (DH5α) or XL10 Gold cells from glycerol stocks were inoculated into 5.0 ml LB medium (Sambrook *et al*., 1989) contained, in test tube and grown overnight at 37ºC and 180 rpm.
2. 0.1 M $CaCl_2$ solution was filter-sterilized by passing through 0.22 µm filter in laminar air flow and kept in refrigerator.

Day 2

3. 1.0 ml overnight grown culture from day 1 was inoculated into 100 ml LB medium and incubated at 37ºC with 180 rpm till cell OD at 550 nm reached 0.4-0.6.
4. Micro-centrifuge tubes, 50 ml centrifuge tubes (round bottom) and micro tips were autoclaved and prechilled by keeping on ice bath placed in a laminar air flow.
5. 40 ml culture was transferred aseptically to round bottom centrifuge tubes.
6. The tubes were centrifuged at 4ºC with 4000g for 10 min.
7. The step was repeated to centrifuge the entire 100 ml culture.
8. The cell pellet was resuspended in 3-4 ml sterilized, ice-chilled 0.1 M $CaCl_2$ solution followed by making up the final volume to 20 ml. The cell suspension in centrifuge tubes was kept on ice for 10 min.
9. The tubes were centrifuged again at 4000g at 4ºC for 10 min.
10. The supernatant was carefully removed and the cell pellet was resuspended in 3.0 ml of sterilized ice chilled 0.1 M $CaCl_2$ solution.

11. 200 µl of competent cells were aliquoted into each 1.5 ml microcentrifuge tube containing 10 (%, v/v) glycerol (final concentration) and kept at -80ºC for further use.

12. The transformation efficiency was calculated using the following formula,

$$\text{Transformation efficiency} = \frac{\text{No. of colonies on LB plate}}{\text{Amount of insert (µg)}} = \text{cfu/µg}$$

2.2.9 Cloning of PCR amplified gene encoding *Ps*PL8A into pGEM-T Easy vector

PCR amplified gene encoding *Ps*PL8A was subjected to TA cloning after gel extraction. The description of pGEM-T Easy vector construct from Promega, USA is given in section 2.2.9.1. Ligation reaction was setup following the protocol mentioned in section 2.2.9.2.

2.2.9.1 Description of pGEM-T Easy vector

The pGEM-T Easy Vector Systems (Fig. 2.2.2) are convenient for the cloning of PCR products. The vectors are prepared upon linearization of pGEM-5Zf(+) vector (GenBank accession no. X65308) with EcoR V, and adding a 3´- terminal thymidine to both the ends. These single 3´-T overhangs at the insertion site greatly improve the efficiency of ligation of a PCR product into the plasmids by preventing recircularization of the vector and providing a compatible overhang for PCR products generated by certain thermostable polymerases. These polymerases often add a single deoxyadenosine, in a template-independent fashion, to the 3´-ends of the amplified fragments. The high copy number pGEM-T Easy vectors contain T7 and SP6 RNA polymerase promoters flanking a multiple cloning region within the alpha-peptide coding region of the enzyme beta-galactosidase. Hence, successful insertion of the PCR DNA encoding *Ps*PL8A will interrupt the coding sequence of β-galactosidase and the

recombinant clones can be identified by colour screening on indicator plates. Clones containing PCR products produce white colonies, whereas blue colonies usually do not contain any clone. Rarely the blue colonies may contain positive clone, which happens when the PCR fragments are cloned in-frame with the lacZ gene.

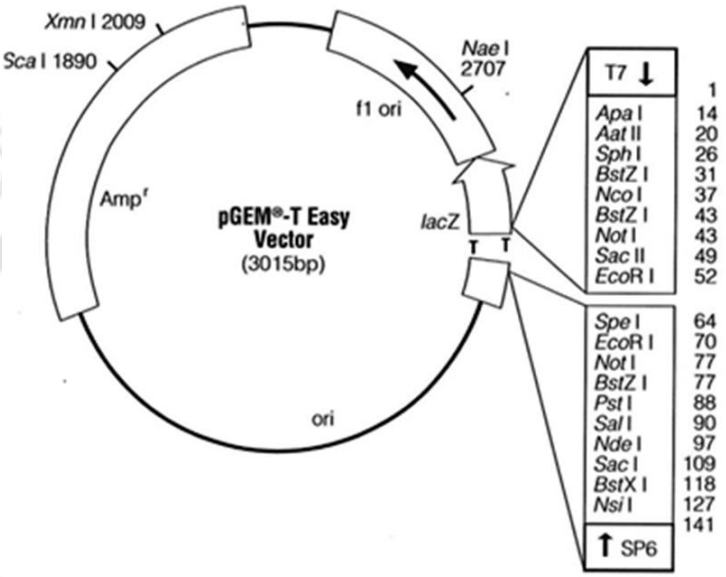

Fig. 2.2.2 pGEM-T Easy vector map and sequence reference points.

2.2.9.2 Ligation of PCR amplified gene encoding *Ps*PL8A into pGEM-T Easy vector

The gel extracted PCR DNA encoding *Ps*PL8A was ligated to pGEM-T Easy vector following the components of ligation reaction as mentioned in Table 2.2.7. The ligation reaction was setup in 0.5 ml microcentrifuge tube and incubated at 16°C overnight to get maximum number of transformants. The reaction was setup at an insert: vector molar ratio of 3:1, where the amount of insert required in a reaction is calculated using the following formula (Engler *et al*., 1982),

$$\frac{\text{amount of vector(ng)} \times \text{size of insert(kb)}}{\text{size of vector (kb)}} \times \text{insert :vector molar ratio} = \text{amount of insert (ng)}$$

$$\frac{25\ (\text{ng}) \times 2.037(\text{kb})}{3.015\ (\text{kb})} \times \frac{3}{1} = 50.67\ \text{ng}$$

Table 2.2.7 Components for ligation reaction setup for TA cloning of PCR amplicon.

Reaction components	
2x Rapid Ligation Buffer	5.0 µl
pGEM®-T Easy Vector (50 ng)	0.5 µl (25 ng)
PCR product encoding *Ps*PL8A	2.5 µl (~51 ng)
T4 DNA Ligase (3 units/µl)	1.0 µl
Nuclease-free water	1.0 µl
Total	10.0 µl

2.2.9.3 Transformation of ligated product after TA cloning

The *E. coli* DH5α competent cells were transformed with pGEM-T Easy cloned plasmid DNA containing gene encoding *Ps*PL8A. Preparation of XL-10 Gold *E. coli* competent cell preparation has described in Section 2.2.8. The step-wise transformation protocol is described below:

1. The microcentrifuge tube containing XL-10 Gold competent cell (200 µl) was taken out from -80°C and kept on ice for 5 min, followed by addition of 10 µl of ligation mixture (the mixture was given a very short spin prior to use).
2. The tube was gently tapped 4-5 times and kept on ice for 30 min.
3. The cells were given a heat shock at 42°C for 40s.
4. The cells were immediately transferred to ice for 2-3 min.
5. 800 µl of super optimal medium with catabolite repression (SOC) (Hanahan, 1983; Sambrook *et al*., 1989; shown in Section 2.2.7) was added to the transformed cells (previously incubated at 37°C).
6. The transformed cells were incubated at 37°C in a shaking incubator at 220 rpm for 1h.
7. The cells were harvested by centrifugation at 2000*g* at 25°C for 5 min.

8. 800 µl supernatant was discarded and the cell pellet resuspended in remaining 200 µl supernatant.
9. The 200 µl cells were spread plated on LB agar plates as described in Section 2.2.6.1 supplemented with antibiotics ampicillin, IPTG (Isopropyl β-D-1-thiogalactopyranoside) and X-Gal (5-bromo-4-chloro-3-indolyl-β-D-galactoside) at a final concentration of 100 µg/ml, 0.5 mM and 80 µg/ml, respectively.
10. The LB agar plates were incubated overnight at 37°C.

2.2.9.4 Screening of positive TA clones of *Ps*PL8A

Positive TA clones of *Ps*PL8A were identified by the process of blue white screening. Overnight grown plates were observed for blue white colonies. White colonies containing the positive clones were picked up in a laminar air flow and grown in 5 ml LB medium supplemented with ampicillin (100 µg/ml) and incubated at 37ºC, 180 rpm for overnight. The positive TA clones produce white colonies are unable to produce β-galactosidase because of the interrupted *lacZ* gene induced by the presence of the insert DNA. In absence of β-galactosidase the cells cannot degrade X-Gal and produce blue colour colonies.

2.2.9.5 Isolation of plasmid DNA from positive colonies by Non-ionic detergent (NID) method

The plasmid DNA was isolated from grown *E. coli* (XL10 Gold) cells which were picked from the LB plates after transformation of the ligated TA cloned product of gene encoding *Ps*PL8A. NID method as described below was employed for isolation of plasmid (Lezin *et al.*, 2011). The composition of NID buffers is given in Table 2.2.8.

1. 5 ml of grown cultures (XL10 Gold) were centrifuged at 7000*g* for 1 min.
2. After drawing 150 µl extraction buffer into a pipette tip, the pellet was loosened off the tube wall with the tip without releasing the buffer. Then the extraction buffer was added and the cell pellet resuspended.
3. The bacterial suspension was incubated at 65°C for 5 min.
4. Suspension was centrifuged at 13000*g* for 10 min or until a tight cell pellet was formed. The pellet was removed with a toothpick.
5. 100 µl isopropanol was added, followed by mixing and centrifugation of the solution at 7000*g* for 10 min at 25ºC.
6. DNA usually forms film-like precipitates that adhere well to tube walls and are invisible in isopropanol solutions. After discarding the supernatant, the DNA was centrifuged after adding 70% ethanol. Ethanol was removed, and the DNA pellet was dissolved in 20-50 µl TE buffer.

Table 2.2.8 Composition of NID extraction buffer for plasmid isolation.

Components	**Final Concentration**
Tris-HCl, pH 8.0	50 mM
Sucrose	5% (w/v)
EDTA	50 mM
NH_4Cl	75 mM
TritonX-100	0.5% (v/v)
Lysozyme	100 µg/ml
RNaseA	25 µg/ml
$CaCl_2$	50 mM

A 100x enzyme stock containing 10 mg/ml lysozyme and 2.5 mg/ml of RNaseA prepared in 50% glycerol and 50 mM Tris-HCl pH 8 was stored at −20°C and used repeatedly.

2.2.9.6 Screening of recombinant plasmid DNA for identification of positive TA clones by restriction digestion analysis

15 µl of recombinant plasmid DNA from of TA clone of *Ps*PL8A isolated by NID method as described in Section 2.2.9.5, was taken in a fresh sterile microcentrifuge tube for restriction enzyme digestion analysis. The recombinant plasmid DNA was digested with restriction enzymes, *Nhe*I and *Xho*I, to check for positive clones. A 30 µl reaction mixture was set up as mentioned in Table 2.2.9. The reaction mixture was incubated in a water bath at 37ºC for 2h. The digested product was run on 0.8% agarose gel as described in Section 2.2.4. The digested pGEM-T Easy vector and the insert DNA encoding *Ps*PL8A were visualized by placing the gel under UV transilluminator. The digested gene fragment encoding *Ps*PL8A of 2 kb expected size was confirmed as a positive TA clone. Glycerol stocks of *E. coli* (XL 10 Gold) cells containing the positive TA clone containing *Ps*PL8A was prepared in glycerol (~22.5 % v/v) and stored at -80°C.

Table 2.2.9 Restriction enzyme digestion set up of recombinant plasmid DNA.

Digestion set up	**1x (µl)**
10x buffer	3.0
DNAse free water	10.0
Recombinant plasmid DNA (approx. 60 ng)	15.0
*Nhe*I (10 U/µl)	1.0
*Xho*I (10 U/µl)	1.0
Total	30.0

2.2.10 Cloning of restriction digestion product of *Ps*PL8A to pET-28a(+) expression vector

The pET-28a(+) vector is commonly used for cloning and expression of recombinant proteins in *E. coli*. It is a modified form of pBR322 vector with a strong expressing T7 promotor system originally developed by Studier and colleagues (Studier and Moffatt, 1986; Studier *et al.,* 1990). It is possible to control expression levels in pET vectors by simply by manipulating the concentration of inducer. The desired genes to be cloned in pET vectors are under the influence of bacteriophage T7 transcription and the expression is induced by T7 RNA polymerase in the host cell. An additional advantage with pET system is, its ability to maintain target genes transcriptionally silent in the uninduced state. The His_6-Tag is useful and easy to purify recombinant protein in a single step by making use of affinity chromatography. The pET-28a(+) vector is incorporated with an N-terminal His_6-Tag/thrombin/T7-Tag configuration in addition to an optional C-terminal His_6-Tag sequence (Fig. 2.2.3). The thrombin tag can be used to remove the His_6-Tag, during structural and western blotting detection of the recombinant protein. The location of His-Tag, T7 coding sequence, T7 terminator, kanamycin coding region and f1 origin are depicted in the Fig. 2.2.3.

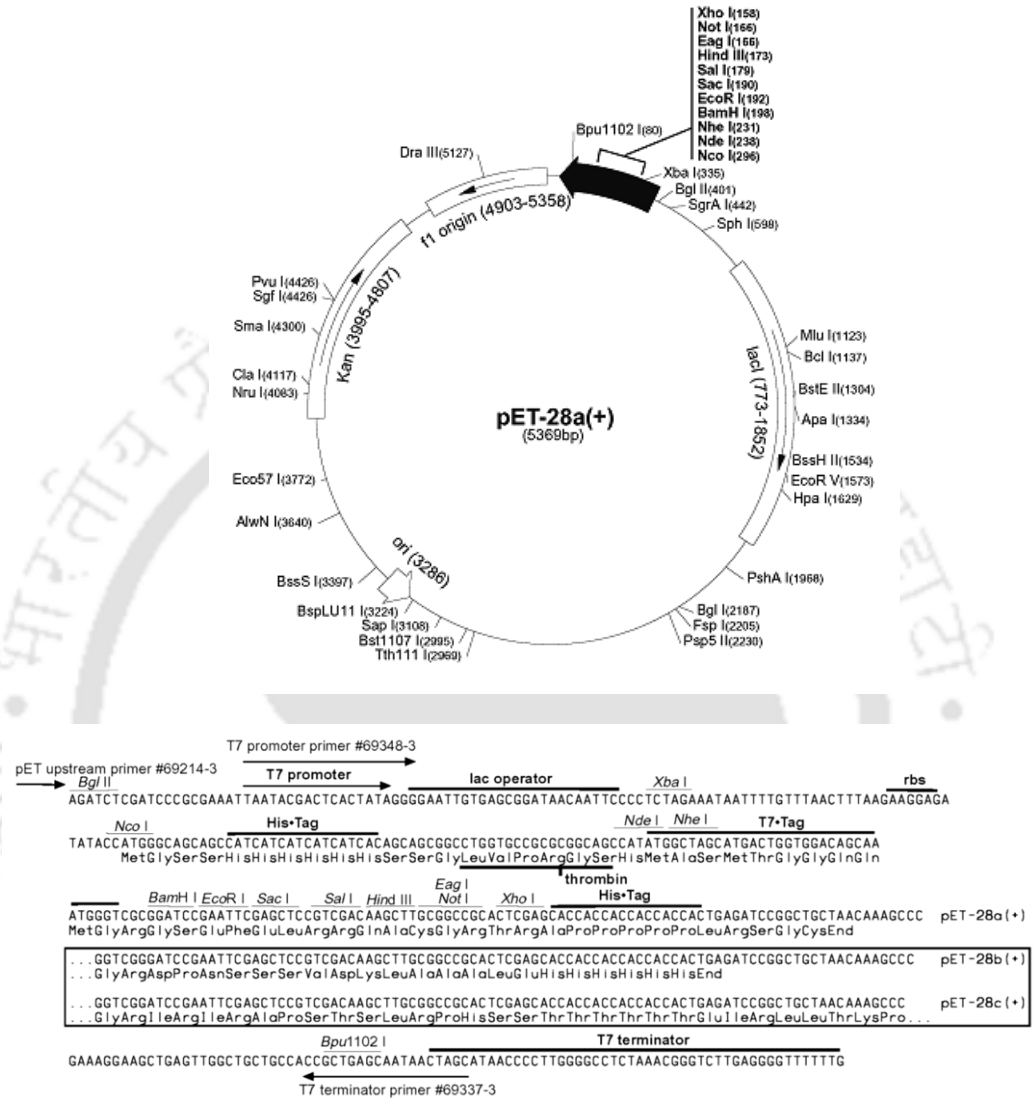

Fig. 2.2.3 Restriction map of the pET-28a(+) expression vector showing multiple cloning site (158-203 bp), restriction enzyme sites, N-terminal His_6-Tag coding sequence (270-287 bp), C-terminal His_6-Tag coding sequence (140-157 bp), T7 promoter (370-386), T7 terminator (26-72 bp), pBR322 origin (3286 bp), kanamycin marker (3995-4807 bp) and a f1 origin (4903-5358). *Nhe*I cuts at 231 and *Xho*I at 158 (Novagen, Germany).

The pET-28a(+) vector was digested with *Nhe*I and *Xho*I restriction enzymes to prepare for cloning of PCR amplified DNA fragment and extracted from subcloning to pGEM-T Easy vector encoding of *Ps*PL8A. A stock solution (100 ng/µl) of pET 28a(+) was prepared from the supplied stock of 10 µg using DNase free water (pH 8.0). The

restriction enzyme digestion of pET-28a(+) vector was carried out as described earlier (Table 2.2.9). The digestion mixture was incubated in a water bath at 37°C for 2h. The *Nhe*I-*Xho*I digested pET-28a(+) vector was purified from agarose gel as described in Section 2.2.5.

2.2.10.1 Ligation of gene encoding *Ps*PL8A insert to pET-28a(+) expression vector

The *Nhe*I-*Xho*I digested fragment of gene encoding *Ps*PL8A from TA clone in Section 2.2.9.6 was cloned into pET-28a(+) vector, which was also digested with same restriction enzymes as described in Section 2.2.10. The ligation reaction was setup using the reaction components mentioned in Table 2.2.10 and incubated at 16°C overnight to get maximum number of transformants. The reaction was setup at an insert: vector molar ratio of 3:1, where the amount of insert is calculated as mentioned below.

$$\frac{50\ (\text{ng}) \times 2.037\ (\text{kb})}{5.369\ (\text{kb})} \times \frac{3}{1} = 57\ \text{ng}$$

Table 2.2.10 Components for ligation reaction setup for gene insert encoding *Ps*PL8A from TA clone to pET-28a(+) expression vector.

Reaction components	**(µl)**
10x Rapid Ligation Buffer	2.0
pET-28a(+) Vector (100 ng)	0.5 (50 ng)
TA clone digested product	2.0 (57 ng)
T4 DNA Ligase (3 units/µl)	1.0
Nuclease-free water	4.5
Total	10.0 µl

2.2.10.2 Transformation of ligated product of gene encoding *Ps*PL8A into pET 28a(+) using *E. coli* DH5α cells

The *E. coli* DH5α competent cells were transformed with construct of pET-28a(+) vector ligated to gene encoding *Ps*PL8A. Transformation protocol was followed as mentioned in Section 2.2.9.3. The transformed DH5α cells were plated on LB plates supplemented with kanamycin (50 µg/ml) and incubated overnight at 37°C.

2.2.10.3 Isolation of plasmid DNA from pET-28a(+) ligation products containing colonies by miniprep kit

Overnight incubated LB kanamycin plates were observed for colonies of DH5α cell. Colonies preferably from the centre of the plate were randomly picked under a laminar air flow and grown overnight in 5 ml LB medium supplemented with kanamycin (50 µg/ml). The plasmid DNA from the 10 ml culture was isolated by GenElute plasmid miniprep Kit (Sigma-Aldrich, USA) following the protocol mentioned below in Section 2.2.10.3.1.

2.2.10.3.1 Plasmid isolation protocol by miniprep kit

1. 9 ml from each of the grown culture was taken and transferred to 2.0 ml microcentrifuge tube aseptically.
2. The cells were then centrifuged at 14,000*g* for 1 min and the process was repeated 5 times with another 2 ml of grown culture.
3. The resulting cell pellet was resuspended in 200 µl resuspension solution and vortexed. RNase in final concentration of 20 µg/ml was added to the re-suspension solution prior to use.
4. 200 µl of lysis solution was added to the tube and the tube was inverted gently 5-6 times to ensure mixing and allowed to stand for 2-5 min.

5. 350 µl of neutralization solution was added to the mixture and the tube was inverted again for 4–6 times to mix properly.
6. The mixture was centrifuged at 16,000g for 10 min.
7. The DNA binding columns were prepared or activated by adding 500 µl of column preparation solution to binding column and centrifuging at 14,000*g* for 1 min. The flow through accumulated in collection tube was discarded.
8. The clear lysate was then transferred to activated DNA binding column, centrifuged at 14,000*g* for 1 min and the flow through in the collection tube was discarded again.
9. The plasmid DNA bound to column was washed with 700 µl wash solution and spun at 14,000*g* for 1 min. The flow through was discarded and the column was given another 1 min spin at 14,000g for removing the wash solution completely.
10. The DNA binding column was transferred to a fresh sterile microcentrifuge tube and 25 µl of TE buffer solution or DNAse free water was added at the centre of binding column. The microcentrifuge tube was allowed to stand for 10 min at room temperature and then plasmid DNA was eluted by centrifugation at 14,000*g* for 1 min. The plasmid DNA then got collected in the sterile microcentrifuge tube.
11. The eluted plasmid DNA in sterile microcentrifuge tube was stored at -20°C.

2.2.10.4 Screening of recombinant plasmid DNA for positive pET-28a(+) clones by restriction digestion

15 µl of recombinant plasmid DNA from pET-28a(+) clones containing gene encoding *Ps*PL8A that was isolated in the last step, was taken in a fresh sterile microcentrifuge tube for restriction enzyme digestion analysis. The recombinant plasmid DNA was digested with restriction enzymes, *Nhe*I and *Xho*I, to check for positive clones. A 30 µl reaction mixture set up as mentioned in the Table 2.2.9. The digestion reaction protocols and identification of digested products were done following the methods mentioned in Section 2.2.9.6. The positive clone was confirmed by gene sequencing using T7 universal primers (Forward primer: TAATACGACTCACTATAGGG and Reverse primer: GCTAGTTATTGCTCAGCGG from SciGenom Labs Pvt. Ltd, India.

2.2.11 Preparation of competent *E. coli* BL-21 cells

The competent *E. coli* BL-21 (DE3) cells were prepared by calcium chloride method following the protocol as discussed in Section 2.2.8. Finally, 10% (v/v) glycerol (final concentration) was added to competent cells and 200 µl aliquots were made in sterile microcentrifuge tubes and stored at -80°C for further use.

2.2.12 Transformation of recombinant plasmids containing gene encoding *Ps*PL8A using *E. coli* (BL21) cells for expression

10 µl of the recombinant plasmid of positive pET-28a(+) clones containing gene insert encoding *Ps*PL8A isolated in Section 2.2.10.3 was used for transformation of 200 µl *E. coli* (BL-21) cells for hyper-expression of *Ps*PL8A following the transformation protocol described in Section 2.2.9.3. The transformed *E. coli* (BL-21) cells were plated on LB agar plates supplemented with kanamycin (50 µg/ml) and grown overnight at 37°C.

2.2.13 Hyper-expression of recombinant *Ps*PL8A

The overnight grown LB kanamycin plate was observed for *E. coli* BL-21 cell colonies. The colonies from centre of the plate were randomly picked under a laminar air flow and grown in two tubes containing 5 ml LB medium supplemented with kanamycin (50 µg/ml) by incubating the tubes at 37°C and 180 rpm. The cells were grown till mid-exponential phase or the cell OD reached $A_{550} \approx 0.6$. 1 ml of this culture, containing uninduced cells was used for sample preparation for SDS-PAGE analysis and stored for glycerol stock prepration. The remaining 4 ml culture in two tubes were then induced with 1 mM IPTG for hyper-expression of recombinant proteins and further incubated for 24h at 24ºC and 8h at 37ºC, 180 rpm. Expression of recombinant proteins in each colony was analysed after running the uninduced and induced cultures separately on SDS-PAGE (Section 2.2.14). Comparing their expression level, the colonies containing each recombinant plasmid were selected for glycerol stock preparation and stored at -80°C for further use.

2.2.14 Sodium dodecyl sulphate-Polyacrylamide gel electrophoresis (SDS-PAGE) analysis of recombinant proteins

The recombinant protein *Ps*PL8A was analysed on SDS-PAGE gel on the basis of its molecular size. PAGE was used to separate components of a protein mixture based on their size (Laemmli, 1970; Sambrook *et al*., 1989). Analysis of expression and purification of *Ps*PL8A was done using 10% SDS-PAGE. The SDS-PAGE gel was prepared by using the ingredients mentioned in Tables 2.2.11 and 2.2.12.

Table 2.2.11 Composition of SDS-PAGE components for preparation of resolving gel.

Components	**Resolving gel (10%) volume (ml)**
Acrylamide solution (30%, w/v)	3.3
Deionized water	1.4
SDS (10%, w/v)	1.0
Glycerol (50%, v/v)	1.0
1.5 M Tris-HCl (pH 8.8)	3.3
Ammonium persulphate (APS) (10%, w/v)	0.1
TEMED	0.01

Table 2.2.12 Composition of SDS-PAGE components for preparation of stacking gel.

Components	**Stacking gel (4%) volume (ml)**
*Acrylamide solution (30%, w/v)	0.7
Deionized water	2.8
SDS (10%, w/v)	0.5
0.5 M Tris-HCl (pH 6.8)	1.0
Ammonium persulphate APS (10%, w/v)	0.05
†TEMED	0.005

*Acrylamide solution composed of 29.2% of Acrylamide and 0.8% N,N'-Methylene Bis acrylamide.

†TEMED: Tetramethylethylenediamine

SDS-PAGE was run in 1x Tris-Glycine (pH 8.3) running buffer at constant current 30 mA for Miniprotean system (BioRad). The expressed and purified protein sample was viewed after staining the gel with staining solution. Staining solution was prepared by dissolving Coomassie Brilliant Blue (CBB) R-250 dye (0.25% w/v) in 50 ml deionized water, 40 ml methanol and 10 ml glacial acetic acid. The gel was destained by immersing it in destaining solution containing 50 ml deionized water, 40 ml

methanol and 10 ml glacial acetic acid with gentle rocking and periodic change of destaining solution, until the protein bands were clearly visible.

2.2.15 Purification of recombinant *Ps*PL8A protein

The *E. coli* BL-21(DE3) cells harbouring recombinant plasmids were grown in 100 ml LB medium supplemented with kanamycin (50 µg/ml) in 250 ml flask. The recombinant protein containing a His_6-tag at the N-terminal was purified by a single step purification method based on immobilized metal-ion affinity chromatography (IMAC) as described in Section 2.2.15.1. The purification of recombinant protein was carried out using 1.0 ml sepharose column (GE Healthcare, HiTrap chelating HP). The composition of binding as well as elution buffers used for affinity column purification is mentioned in Table 2.2.13.

Table 2.2.13 Composition of buffers required for purification of recombinant protein by IMAC.

Buffers	Composition
Equilibration buffer	50 mM Tris-HCl, pH 7.2
	300 mM NaCl, 60 mM Imidazole
Elution buffer	50 mM Tris-HCl, pH 7.2
	300 mM NaCl, 500 mM Imidazole
Cleaning buffer	50 mM Tris-HCl, pH 8.0
	500 mM NaCl, 50 mM EDTA

2.2.15.1 Purification protocol for recombinant *Ps*PL8A protein by IMAC

1. The bacterial cells (100 ml culture) were harvested by centrifugation at 8,000*g* and at 4°C. The cell pellet was re-suspended in 5 ml of 50 mM Tris-HCl buffer, pH 7.2 containing 1 mM phenylmethanesulfonyl fluoride (PMSF).

2. The cells were sonicated (Sonics, vibra cells) by keeping on ice for 30 min with 10 s ON and 15 s OFF pulse at 33% amplitude and centrifuged at 12,000*g* at 4ºC for 45 min to get the crude cell free extract.
3. The cell free extract was passed through a 0.22 µm filter membrane before loading into 1 ml HiTrap chelating column.
4. The column was pre-washed with 5 volumes of filtered and degassed water using peristaltic pump.
5. Column was charged using 2.0 ml of 0.1 M $NiSO_4$ solution and the unbound nickel was washed away by running 5 volumes of water.
6. Then the column was equilibrated by running 5 volumes of equilibration buffer (Table 2.2.13) using the peristaltic pump at 1 ml/min flow rate.
7. The filtered cell free extract containing recombinant protein was loaded on to the column at a flow rate of 0.5 ml/min.
8. The column was then washed with 50-60 column volumes of equilibration buffer to remove the unbound proteins.
9. The retained protein of interest was then eluted by using elution buffer under a gradient of 0-500 mM imidazole concentration and 1 ml fractions were collected.
10. The column was cleaned by using the cleaning buffer as mentioned in Table 2.2.13, and then washed with 5 volumes of water and incubated in 1N NaOH at 4°C for 2h.
11. The column was then washed with 50 volumes of water to remove NaOH, and finally stored in 20% (v/v) ethanol at 4°C.

The purified recombinant *Ps*PL8A protein was dialyzed against 50 mM Tris-HCl buffer, pH 7.2 containing 150 mM NaCl. The purity and molecular mass of recombinant proteins was verified by SDS-PAGE as described in Section 2.2.14.

2.2.16 Protein concentration determination of purified *Ps*PL8A protein

The concentration of purified *Ps*PL8A protein was determined by taking its absorbance at 280 nm A_{280} using the formula mentioned below (Layne, 1957; Stoscheck, 1990). The measurement of A_{280} was taken after appropriate dilution of the protein sample, on spectrophotometer (Cary 100, Varian) having a path length of 1 cm. The molar extinction co-efficient of 140150 $M^{-1}cm^{-1}$ for *Ps*PL8A protein was used to calculate its concentration.

$$\text{Concentration of protein (mg/ml)} = \frac{A_{280} \times Mw\ (Da) \times D.F}{\varepsilon \times 1\ cm}$$

Where,

A_{280} = Absorbance at 280 nm
Mw = Molecular weight of protein in Daltons
D.F =Dilution factor
ε = Molar Extinction coefficient
Path length = 1 cm

2.3 Results and Discussion

2.3.1 PCR amplification of gene encoding family 8 polysaccharide lyase *Ps*PL8A

The DNA sequence of 2037 base pairs, encoding *Ps*PL8A with putative chondroitin AC lyase activity was amplified by PCR. The analysis of deduced amino acid sequence of the protein gave an insight about the existence of N-terminal signal sequence with a cleavage site predicted between Ala22 and Gln23 suggesting the extracellular nature of *Ps*PL8A. *Ps*PL8A was amplified from genomic DNA of *Pedobacter saltans* DSM 12145 strain using the conditions as mentioned in Section 2.2.3 and detected on 0.8% agarose gel and shown below (Fig. 2.3.1). The PCR product was purified from gel using gel extraction kit as mentioned in Section 2.2.5 and stored at -20°C for subsequent TA cloning.

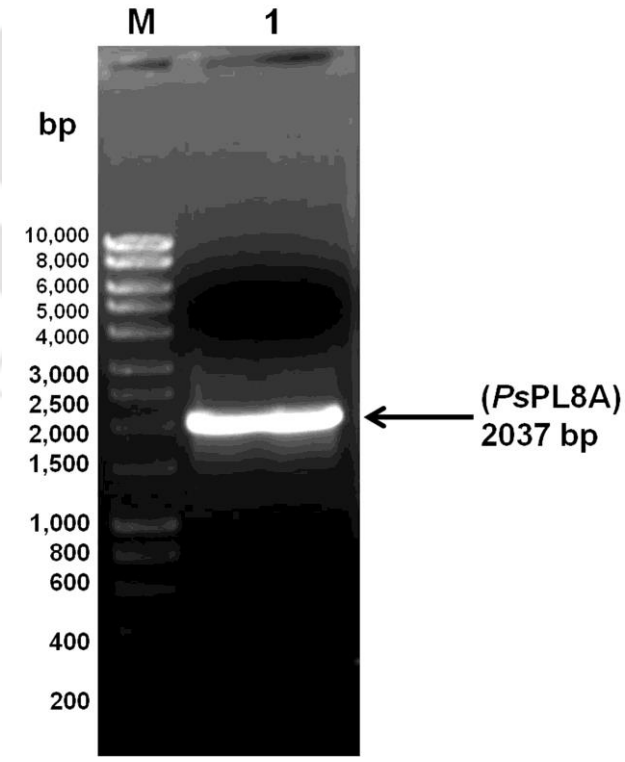

Fig. 2.3.1 Agarose gel (0.8% w/v) showing PCR amplification of gene encoding *Ps*PL8A (lane 1), of size 2037 bp, Where M is marker lane (200 bp-10 kb) Hyperladder I (Bioline).

2.3.2 Cloning of gene encoding *Ps*PL8A to pGEM-T Easy vector

The PCR amplified product of gene encoding *Ps*PL8A with 3'-A overhangs was ligated to pGEM-T Easy vector following the method described in Section 2.2.9.2. In TA cloning Taq DNA polymerase adds 3'-A overhang to the end of PCR product due to its terminal transferase activity. This makes it possible to clone the PCR product directly into a linearized cloning pGEM-T Easy vector with 3'-T overhangs. The ligated product was transformed using *E. coli* (XL 10 Gold) competent cells and positive clones were selected by blue-white colony selection as described in Section 2.2.9.3. The colonies carrying the recombinant plasmids were white, whereas colonies devoid were blue. The transformation efficiency of *E. coli* XL-10 Gold cells was calculated as $2x10^6$ CFU/µg.

2.3.2.1 Isolation of plasmid DNA harbouring the gene encoding *Ps*PL8A

Plasmid DNA from positive colonies after TA cloning was successfully isolated by NID method as mentioned in Section 2.2.9.5. The isolated plasmid was visualized on an agarose gel. Positive clone was confirmed after restriction digestion of this isolated plasmid DNA.

2.3.2.2 Restriction digestion of isolated plasmid DNA for confirmation of TA clone

The isolated TA cloned plasmid DNA was digested with *Nhe*I and *Xho*I restriction enzymes to confirm and prepare the insert DNA of *Ps*PL8A for further cloning into pET-28a(+) expression vector. The plasmid DNA after restriction digestion was run on 0.8% agarose gel. After *NheI* and *XhoI* digestion, pGEM-T Easy vector was visualized on agarose gel at around 3 kb while digested fragment of *Ps*PL8A of around 2 kb (Fig. 2.3.2). The digested fragment of DNA encoding *Ps*PL8A was gel

eluted and prepared for cloning into pET-28a(+) vector. The expression vector pET-28a (+) was also linearized after restriction digestion by *Nhe*I and *Xho*I, and used for ligation with the insert.

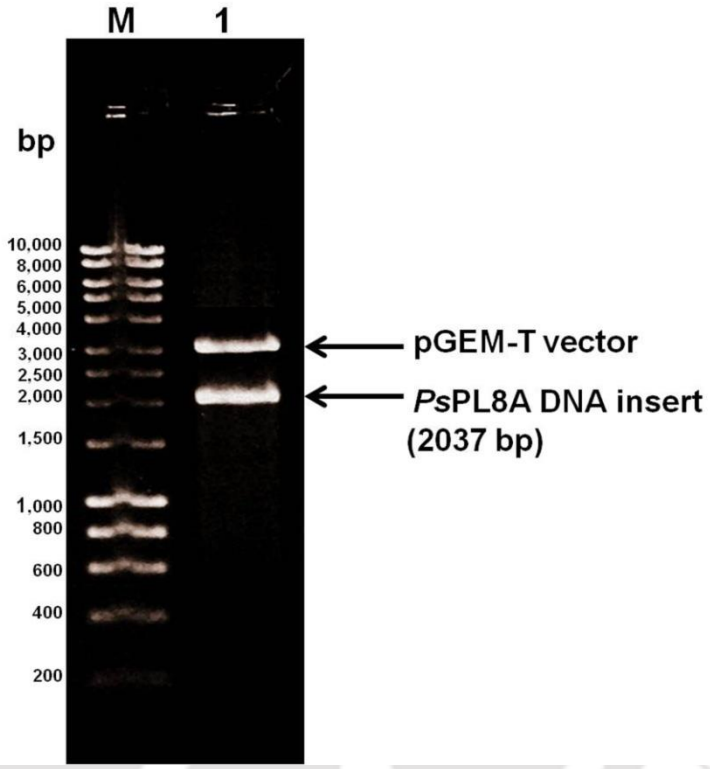

Fig. 2.3.2 Agarose gel (0.8%) showing *Nhe*I-*Xho*I digested TA clone plasmid DNA. Lane 1: Gene encoding *Ps*PL8A insert fragment of 2 kb and pGEM-T Easy vector of 3 kb, Where M is marker lane (200 bp-10 kb) Hyperladder I (Bioline).

2.3.3 Cloning of gene encoding *Ps*PL8A into pET-28a(+) vector

The restriction enzyme digested fragment of gene encoding *Ps*PL8A was ligated to the linearized fragment of pET-28a(+) vector following the protocol mentioned in Section 2.2.10.1. The ligated product was used for transformation of *E. coli* DH5α competent cells and grown overnight on kanamycin supplemented LB agar plates incubated at 37°C. The transformation efficiency of *E. coli* DH5α competent cells was 1.2×10^6 CFU/µg.

2.3.3.1 Isolation of recombinant plasmid DNA harbouring the gene encoding *Ps*PL8A

Plasmid DNA from grown colonies after cloning into pET-28a(+) was isolated using Plasmid miniprep kit following the protocol mentioned in Section 2.2.10.3.1. The isolated plasmid was visualized on 0.8% agarose gel. Positive clones were confirmed after restriction digestion of this isolated plasmid DNA.

2.3.3.2 Restriction digestion of isolated plasmid DNA for confirmation of positive clone

The isolated plasmid DNA was digested with *Nhe*I and *Xho*I restriction enzymes for confirming the positive clones. The plasmid DNA after restriction digestion was run on 0.8% agarose gel. *NheI* and *XhoI* digested fragment of gene encoding *Ps*PL8A and pET-28a(+) vector were visualized on agarose gel at around 2 kb and 5.4 kb, respectively (Fig 2.3.3). The positive clone was confirmed by gene sequencing from SciGenom Labs Pvt. Ltd, India (Fig. 2.3.4). The chromatograms generated after forward and reverse sequencing reactions are given in Fig 2.3.5.

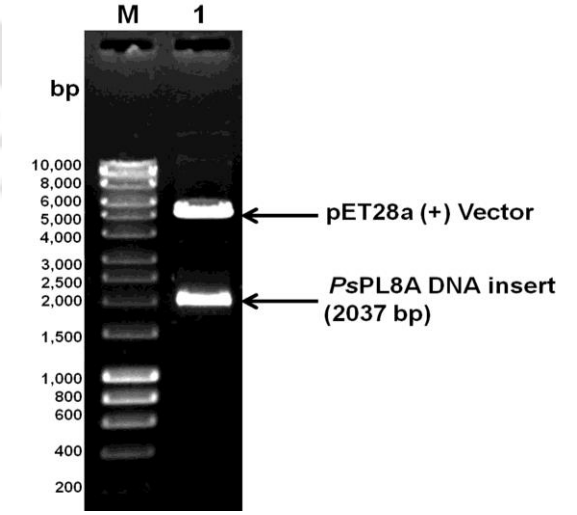

Fig. 2.3.3 Agarose gel (0.8%) showing *Nhe*I-*Xho*I digested pET-28a(+) cloned plasmid DNA. Lane 1: Gene encoding *Ps*PL8A insert fragment of 2 kb and pET-28a(+) vector of 5.4 kb, Where M is marker lane (200 bp-10 kb) Hyperladder I (Bioline).

5´-CAAAAGCAGACATTTGAACTGATTATGGGGCGCGTAGCCGAAGATAATGCGGTTACTA
AACCCAAACAGGTAGATGCTGCGGCAATTAAATTATTTGATAAGTGGCAGGAAGATGGCA
GTTGGTCTGATATCAATTACAAAGCTATAGATATTACCAAATGGCAACCGTCTACGCATTT
AGACAGATTAAGAACTATTGTTAATGCTTATACGGATAAAGATGGTAGCTTTTACGGTAA
CCCGCAGATATTTAATAAAATACAAAATGCTTTGGCGTTTTGGTACGATCAGGATCCTAAA
AGTGACAACTGGTGGCATAACGAGATAGATGTTCCGCAAAAACTGGGCGAACTATTAATT
TCTTTAAGGTACGGAAGTCAGAAACTATCAAAAGAATTAGAAGCCAATTTAATAGAGCGC
ATGAAGCGTGGCGTTGCCGAGAAAAAAACCGGAGCCAACAAAACGGATATTGCTTTACAT
TATTTCTATAGAGCTTTACTTACCCAGGATAAAGCTTTATTGAAACTGGCAGTAGACCAGC
TTTTAGAACCGGTTGCGCTGGTAGACGGGGCAGAGGGTTTGCAATATGATTACTCTTATAT
GCAACACGGGCCACAGCTATACATCTCTGGTTACGGAGCGGTTTATCTGACAGGTATTGTA
AAAATAGGGAAGTACGTAGCGAATACACCTTATGCCATGTCTAAAGAGCAAGTCGCTTTA
TTCTCTAAATTCTATAGAGACGTGTATTTGAAGACTTTTAGGTCAAAATATATCGATTTTA
ACGTAGAGGGAAGAGGGATTAGCAGGAAAGACATTTTAAAGAAAACTTCAGAAAAATAC
CGAATCAATAATGCTAAACTAATTGATCCTAAAAATGCAGACGATTGGGAAAATAACCGT
TTGAGGGTAGACAGCGCAGAGGCACCAAGTTTTAAAGTAACTCCTTACCACCAGCATTTC
TGGAAAGCGGATTATACATTGCATATTCGTCCGAATTATTCTTTCAACGTTAGAATTGCCA
GTAACAGAACCAATAGAAGCGAATCTGGTAATAAGGAAAATTTGTATGGTCGTTACCTTT
CTGATGGGGCTACAAACATACAGGTTAATGGACCAGAATATTTTAATATTATGCCTATCTG
GGAATGGGATAAAATTCCGGGAACGACCAGCGTAGATAATAAAGAAGATTTATTGTTAGA
TAAGTTTTGGGGGCATTTAGGAGATAATGCATTTGCCGGAGGGGTGTCAGACCAGGTTTA
TGGTGCGACAGCTTATCAGTTGGATTATGACAATGTATTGGCTAAAAAAGCGTGGTTCTTC
TTTGATGATGAGATTGTTTGCTTAGGTGCAGATATCCATTCTAAAGACGAAAGAAATGTGA
CTACTACGCTTAACCAGACCTGGTTAAACGGAAAAGTGTCATCTTCTGTAGCTGATATTAA
AACGGAAAGTCCAGAGCAAATGAATATTGCAGCAAATGGATGGTTGTTCCATAACGGAGT
AGCTTATGTATTCCCTAAGCCAAGCCAGGTTAATGTTAGCACAGCGACGCAAACGGGTTC
CTGGTACAAGATTAATAATTCGTTTGGTAAAGCAGAAGTTTCCGGCTCGGTATTTAAAGCA
TGGATAGACCATGGTAAACAACCCGAAGGTGCAGATTATGCTTATATCGTACTGCCGGGA
TTAAAAGACGCAGCTGCTTTAAAGAAATACAATTCGCCTATAGAAATTGTTAGAAACGAT
AAAGATGTACAGGCAGTTTTCCATAAGAAACTGAATTTGACACAAGTGGTATTCTATACA
GCAGGTACAGCTACAGTAAGTGGTTTAGAAATTACGGTAGACAAGCCATCGGTATTGATG
GTGAAATCTCTAAAAGGAGCCGAAAAAGAAGTTCTGGTAGCAGATCCTTTGCAAAAAGAA
ACAGCATTAAAAGTAAGTCTTAAAAATGCCAAAAATGGTGTTCAAAAAGATTTGTCAATT
ACTTTACCGACTGGGCCATATAAAGGTTCTACCAAATCAGAAAAAGTT-**3´**

Fig. 2.3.4 Nucleotide sequence of *Ps*PL8A gene (2037bp) from *Pedobacter saltans.*

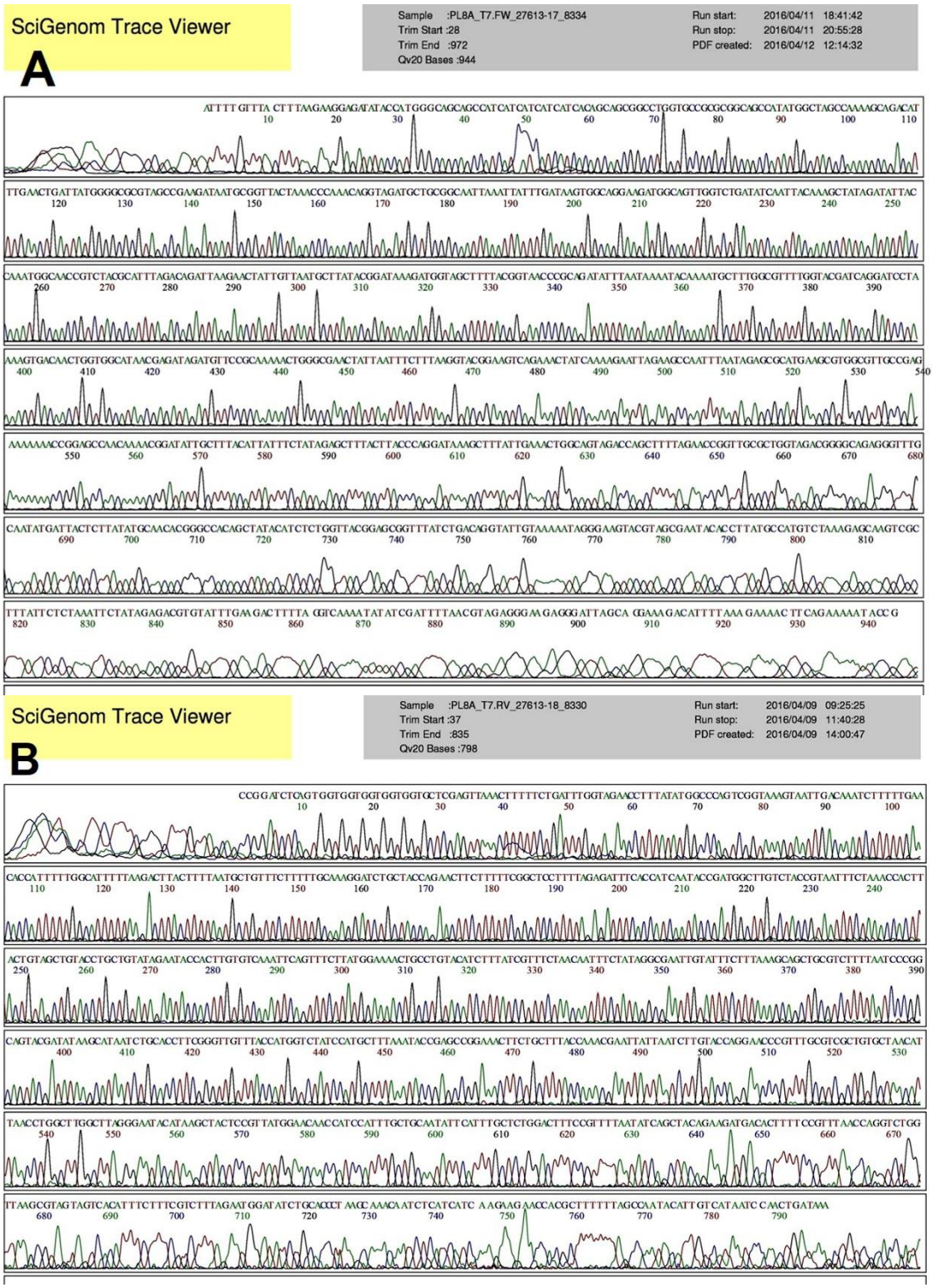

Fig. 2.3.5 Sequencing chromatogram of *Ps*PL8A gene sequence from *Pedobacter saltans* (A) PCR amplification using Forward T7 primer and (B) Reverse T7 primer.

2.3.4 Hyper-expression and purification of recombinant *Ps*PL8A protein

The *E. coli* (BL-21) competent cells were transformed with recombinant plasmid DNA containing pET-28a(+) and the gene encoding *Ps*PL8A. The transformation efficiency of *E. coli* BL-21 (DE3) cells was 1.8 x 10^6 CFU/µg. The colonies were picked randomly and grown in 5 ml LB medium supplemented with kanamycin (50 µg/ml) as described in Section 2.2.13. The cells were induced for hyperexpression of protein at mid exponential stage as described in Section 2.2.13. Hyper-expression of protein was analyzed on SDS-PAGE by loading uninduced as well as the induced cells of recombinant protein on adjacent wells, as depicted in Fig. 2.3.6

The hyper-expressed recombinant *Ps*PL8A protein was purified by immobilized metal ion affinity chromatography as described in Section 2.2.15 and then dialyzed for removal of imidazole and salt. Fig. 2.3.7 shows SDS-PAGE (10.5%) analysis of expression and purification of *Ps*PL8A. The purified *Ps*PL8A (Fig. 2.9, lane 6) showed a band of molecular size of approximately, 77 kDa. The theoretical molecular mass calculated from *Ps*PL8A sequence included the N-terminal amino acids with the His6 tag (MGSSHHHHHHSSGLVPRGSHMAS) was 77.2 kDa. The molecular size of the *Ps*PL8A obtained from SDS-PAGE was in agreement with the theoretically expected value. The recombinant *Ps*PL8A expressed as a soluble protein as most of the protein could be seen in cell free extract and almost none with the cell debris pellet.

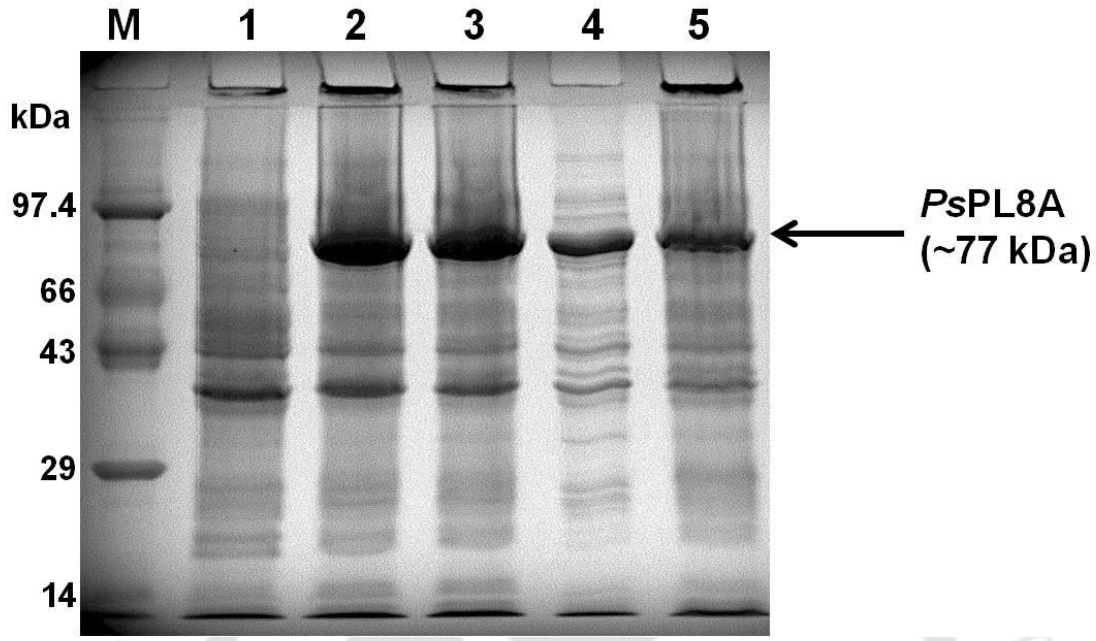

Fig. 2.3.6 SDS-PAGE (10.5%) gel showing expression of recombinant *Ps*PL8A in *E. coli* BL-21 cells, Lane M: Protein marker (Genei), Lane 1: Uninduced cells, Lane 2-3: Induced cells at 24ºC and Lane 4-5: Induced cells at 37ºC.

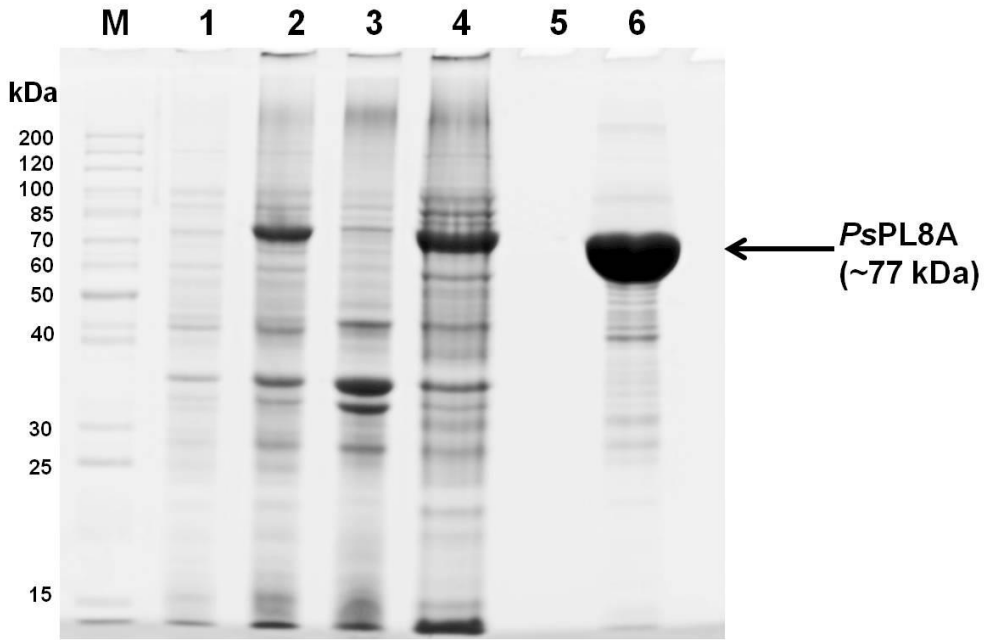

Fig. 2.3.7 SDS-PAGE (10.5%) gel showing expression and purification of recombinant *Ps*PL8A in *E. coli* BL-21 cells, Lane M: Page Ruler marker (Fermentas), Lane 1: Uninduced cells, Lane 2: Induced cells, Lane 3: Cell pellet (cell debris after sonication), Lane 4: Cell free extract, Lane 5: Last column wash, Lane 6: Purified dialyzed *Ps*PL8A (77 kDa approx.).

2.3.5 Protein estimation of expressed and purified recombinant *Ps*PL8A protein

The amount of purified recombinant *Ps*PL8A protein obtained from 100 ml of LB grown grown cultures was calculated using the formula mentioned in Section 2.2.16 and is listed in Table 2.3.1. The concentration of recombinant *Ps*PL8A protein purified after HiTrap column and after dialysis was 1.75±0.18 mg/ml (Table 2.3.1). The total volume of recombinant *Ps*PL8A enzyme after dialysis was 2 ml.

Table 2.3.1 Purified recombinant *Ps*PL8A protein obtained from 100 ml LB culture.

Recombinant protein	Protein concentration (mg/ml)	Volume of purified protein after dialysis (ml)	Total amount of purified protein (mg)
*Ps*PL8A	1.75±0.18	2.0	3.5±0.18

2.4 Conclusions

The gene encoding the family 8 polysaccharide lyase (*Ps*PL8A) was cloned from the genomic DNA of *Pedobacter saltans* DSM 12145 (GenBank accession no. ADY54337.1). The molecular architecture revealed the presence of 22 amino acid signal peptide followed by the catalytic family 8 polysaccharide module (*Ps*PL8A). The ORF encoding *Ps*PL8A was PCR amplified that showed a band of 2037 bp. The PCR amplified gene fragment encoding *Ps*PL8A was cloned into pGEM-T Easy vector for TA cloning and transformed using *E. coli* (XL10 Gold) competent cells. Positive clones were selected by blue-white colony screening, and plasmid DNA was isolated for restriction digestion. *NheI* and *XhoI* digested plasmid DNA gave bands of 3 kb and 2 kb for pGEM-T Easy vector and the insert gene fragment encoding *Ps*PL8A, respectively. The restriction enzyme digested gene fragment encoding *Ps*PL8A was ligated to linearized pET-28a(+) expression vector. The ligated product was transformed using *E. coli* DH5α competent cells. The positive clone containing recombinant plasmid DNA was screened by restriction enzyme digestion using restriction enzymes, *Nhe*I and *Xho*I. The restriction enzyme digested products displayed 5.4 kb and 2 kb bands for pET-28a(+) vector and insert fragment for gene encoding *Ps*PL8A, respectively. The positive clone containing recombinant plasmid DNA was used for transformation of *E. coli* (BL21) competent cells. The recombinant protein *Ps*PL8A was hyper-expressed at 24ºC after IPTG induction. The purified recombinant *Ps*PL8A protein displayed a band of approximately, 77 kDa on SDS-PAGE. The amount of protein obtained from 100 ml culture of the recombinant *Ps*PL8A protein after Immobilized metal ion affinity chromatography (IMAC) purification was 3.5 mg.

2.5 References

Afratis, N., Gialeli, C., Nikitovic, D., Tsegenidis, T., Karousou, E., Theocharis, A.D. and Karamanos, N. K. (2012) Glycosaminoglycans: key players in cancer cell biology and treatment. *FEBS Journal*, *279*(7), 1177-1197.

Bulow, H.E. and Hobert, O. (2006) The molecular diversity of glycosaminoglycans shapes animal development. *Annual Review of Cell and Developmental Biology*, *22*, 375-407.

Cantarel, B.L., Coutinho, P.M., Rancurel, C., Bernard, T., Lombard, V. and Henrissat, B. (1999) The Carbohydrate-Active EnZymes database (CAZy): an expert resource for Glycogenomics. *Nucleic Acids Research, 37,* D 233-238.

Denholm, E.M., Lin, Y.Q. and Silver, P.J. (2001) Anti-tumor activities of chondroitinase AC and chondroitinase B: Inhibition of angiogenesis, proliferation and invasion. European *Journal of Pharmacology*, *416*(3), 213-221.

Deutscher, J. (2008) The mechanisms of carbon catabolite repression in bacteria. *Current Opinion in Microbiology*, *11*(2), 87-93.

Didangelos, A., Iberl, M., Vinsland, E., Bartus, K. and Bradbury, E.J. (2014) Regulation of IL-10 by chondroitinase ABC promotes a distinct immune response following spinal cord injury. *The Journal of Neuroscience*, *34*(49), 16424-16432.

Engler, M.J. and Richardson, D.C. (1982) DNA ligases. In P.D. Boyer (ed.), *The Enzymes*. Academic Press, San Diego. *15*, 3-30.

Ernst, S., Langer, R., Cooney, C.L. and Sasisekharan, R. (1995) Enzymatic degradation of glycosaminoglycans. *Critical Reviews in Biochemistry and Molecular Biology*, *30*(5), 387-444.

Fethiere, J., Eggimann, B. and Cygler, M. (1999) Crystal structure of chondroitin AC lyase, a representative of a family of glycosaminoglycan degrading enzymes. *Journal of Molecular Biology, 288*(4), 635-647.

Galtrey, C.M. and Fawcett, J.W. (2007) The role of chondroitin sulfate proteoglycans in regeneration and plasticity in the central nervous system. *Brain Research Reviews, 54*(1), 1-18.

Habuchi, O. (2000) Diversity and functions of glycosaminoglycan sulfotransferases. *Biochimica et Biophysica Acta (BBA)-General Subjects, 1474*(2), 115-127.

Hanahan, D. (1983) Studies on transformation of *Escherichia coli* with plasmids. *Journal of Molecular Biology, 166*(4), 557-580.

Iozzo, R.V. (1998) Matrix proteoglycans: from molecular design to cellular function. *Annual Review of Biochemistry, 67*, 609-652.

Laemmli, U.K., 1970. Cleavage of structural proteins during the assembly of the head of bacteriophage T4. *Nature, 227*(5259), 680-5.

Layne, E. (1957) Spectrophotometric and Turbidimetric Methods for Measuring Proteins. *Methods in Enzymology, 3*, 447-455.

Lezin, G., Kosaka, Y., Yost, H.J., Kuehn, M.R. and Brunelli, L. (2011) A one-step miniprep for the isolation of plasmid DNA and lambda phage particles. *PLoS One, 6*(8) e23457.

Lunin, V.V., Li, Y., Linhardt, R. J., Miyazono, H., Kyogashima, M., Kaneko, T., Bell, A.W. and Cygler, M. (2004) High resolution crystal structure of *Arthrobacter aurescens* chondroitin AC lyase: enzyme-substrate complex defines the catalytic mechanism. *Journal of Molecular Biology, 337*(2), 367-386.

Park, J.M., Vinuselvi, P. and Lee, S.K. (2012) The mechanism of sugar-mediated catabolite repression of the propionate catabolic genes in *Escherichia coli*. *Gene*, *504*(1), 116-121.

Pojasek, K., Shriver, Z., Kiley, P., Venkataraman, G. and Sasisekharan, R. (2001) Recombinant expression, purification, and kinetic characterization of chondroitinase AC and chondroitinase B from *Flavobacterium heparinum*. *Biochemical and Biophysical Research Communications*, *286*(2), 343-351.

Sambrook, J., Fritsch, E.F. and Maniatis, T. (1989) In (2nd ed.) Molecular Cloning: A Laboratory Manual, Vol. 1. *Plainview, Cold Spring Harbor Laboratory Press, Woodbury, New York.*

Sambrook, J. and Russel, D.W. (2001) In (3rd ed.) Molecular Cloning: A Laboratory Manual, Vol. 1. *Cold Spring Harbor Laboratory Press, Woodbury, New York.*

Shaya, D., Hahn, B.S., Park, N.Y., Sim, J.S., Kim, Y.S. and Cygler, M. (2008) Characterization of chondroitin sulfate lyase ABC from *Bacteroides thetaiotaomicron* WAL2926. *Biochemistry, 47*(25), 6650-6661.

Shim, K.W. and Kim, D.H. (2008) Cloning and expression of chondroitinase AC from *Bacteroides stercoris* HJ-15. *Protein Expression and Purification*, *58*(2), 222-228.

Stoscheck, C.M. (1990) Quantitation of Protein. *Methods in Enzymology, 182*, 50-69.

Studier, F.W. and Moffatt, B.A. (1986) Use of bacteriophage T7 RNA polymerase to direct selective high-level expression of cloned genes. *Journal of Molecular Biology, 189*(1), 113-130.

Studier, F.W., Rosenberg, A.H., Dunn, J.J. and Dubendorff, J.W. (1990) Use of T7 RNA polymerase to direct expression of cloned genes. *Methods Enzymology, 185*, 60-89.

Sutherland, I.W. (1995) Polysaccharide lyases. *FEMS Microbiology Reviews,16*(4), 323-347.

Yamada, S. and Sugahara, K. (2008) Potential therapeutic application of chondroitin sulfate/dermatan sulphate. *Current Drug Discovery Technologies*, *5*(4), 289-30.

Chapter 3

Biochemical and functional characterization of chondroitin sulphate AC lyase (*Ps*PL8A) from *Pedobacter saltans* DSM 12145

3.1 Introduction

Proteoglycans (PGs) are glycoconjugates consisting of protein and polysaccharide glycosaminoglycans (GAGs). PGs are generally found on the cell surfaces, extracellular matrix (ECM) and in basement membranes of animal tissues (Ly *et al*., 2010; Li *et al*., 2012). Glycosaminoglycans (GAGs) such as chondroitin sulfate (CS) are the chief natural polysaccharides which reside in biological tissues mainly in extracellular matrix (Shaya *et al.*, 2008). These CS along with adhesion molecules and growth factors are involved in central nervous system (CNS) development, cell adhesion, proliferation, differentiation, signalling, inflammation and pathogenesis (Iozzo *et al*., 1998; Denholm *et al.*, 2001; Cattaruzza *et al*., 2006; Ly *et al*., 2010). Chondroitin sulfate/Dermatan sulphate (CS/DS) are the GAGs made up of alternating units of N-acetyl-D-galactosamine (GalNAc) and glucuronic acid (GlcA)/Iduronic acid (IdoA) (Shaya *et al.*, 2008). The polysaccharide chain is sulfated at C2 position of

uronic acid and/or at C4/C6 position of N-acetyl-D-galactosamine residue (Huang *et al.,* 2003). The biological functions of GAGs hinge on their architecture, which makes the GAG-degrading enzymes crucial for deciphering their structure and function. The major source of these enzymes are microorganisms, such as *Arthrobacter aurescens* (Lunin *et al*., 2004), *Bacteroides species* (Shaya *et al*., 2008; Hong *et al*., 2002), *Pedobacter heparinus* (previously known as *Flavobacterium heparinum*) (Pojasek *et al*., 2001) and virus *Autographa californica* nucleopolyhedrovirus ODV-E66 (Sugiura *et al*., 2011). *Pedobacter saltans* is gram negative, soil isolate and strictly aerobic bacterium. It was reported to possess chondroitin sulphate degradation and heparinolytic activity (Steyn *et al*., 1998; Liolios *et al*., 2011).

The enzymatic degradation of GAGs involves mainly two classes of enzymes, hydrolases and lyases. The hydrolase enzymes are present in the eukaryotic sources, it act on the hexosamine-hexuronic acid bond *via* hydrolytic mechanism by the addition of a water molecule. The hydrolase enzymes produce the saturated disaccharide products (Lunin *et al.,* 2004). The GAG lyases from prokaryotic origin depolymerize GAGs *via* a β elimination mechanism and cleave the oxygen–aglycone linkage through proton abstraction from C5 carbon of uronic acid, producing an unsaturated disaccharide product with a double bond between C4 and C5 at uronic acid ring The Δ4,5 unsaturated oligosaccharide shows maximum absorption at 232 nm (A_{232}) (Pojasek *et al*., 2001; Hong *et al.*, 2002; Lunin *et al.,* 2004).

Biochemical and functional characterization of *Ps*PL8A is essential to understand the mechanism of catalysis and to determine their substrate specificity. In the present study *Ps*PL8A, a chondroitin AC lyase enzyme was biochemically and functionally characterized. The enzyme activity of *Ps*PL8A against various

glycosaminoglycans polysaccharides were determined. The parameters for *Ps*PL8A enzyme activity such as optimum temperature, optimum pH, thermal stability, pH stability and kinetic parameters were determined. Effects of various metal ions on the activity of *Ps*PL8A was also studied. TLC, ESI-MS and NMR analysis were performed to elucidate the mode of catalysis of *Ps*PL8A.

3.2 Materials and Methods

3.2.1 Substrates and reagents

Chondroitin 6-sulphate disaccharide (Δdi-6S) sodium salt (Dextra Laboratories Ltd., UK), Chondroitin 6-sulphate (C6S) sodium salt from shark cartilage, Chondroitin 4-sulphate sodium salt (C4S) from bovine trachea, Chondroitin sulphate B sodium salt (Dermatan sulphate) from porcine intestinal mucosa, Hyaluronic acid sodium salt from *Streptococcus equi*, Heparin sodium salt**,** Chondroitin 4-sulphate disaccharide (Δdi-4S) sodium salt, N-Acetyl-D-galactosamine, Trizma (Tris base), glycine, sodium hydroxide, Disodium 2-[2-carboxylatomethyl-(carboxymethyl)-amino]-ethyl-(carboxymethyl)-amino] acetate (disodium EDTA) were procured from Sigma-Aldrich Pvt. Ltd., USA. Diphenylamine and salts of metal ions *viz.* Ca^{2+}, Mg^{2+}, Ni^{2+}, Zn^{2+}, Mn^{2+}, Cu^{2+}, Co^{2+}, Al^{3+} and Li^{+} were procured from Himedia Laboratories Pvt. Ltd., India. N-Butanol, ethanol, acetic acid, sulphuric acid, aniline, H_3PO_4 and ethyl acetate were purchased from Merck Limited, India. Readymade silica coated aluminium TLC plates obtained from Merck, Germany.

3.2.2 Enzyme activity assay

The enzyme assay of *Ps*PL8A was carried out by incubating 0.1 µg of enzyme in 1 ml reaction mixture containing 1 mg/ml of C4S substrate. The enzyme reaction was performed under optimum reaction conditions of 50 mM Tris-HCl buffer, pH 7.2 at 39°C for 5 min. The unsaturated oligosaccharide product formation was monitored by an increase in the absorbance at 232 nm (A_{232}) as a function of time on a UV-Visible spectrophotometer (Varian, Cary 100). The absorbance observed was converted to units using molar absorption coefficient (3800 M^{-1} cm^{-1}) for Δ4,5 unsaturated double bond formed in the reaction. One unit of enzyme activity was defined as amount of enzyme

that liberates 1 µmol of unsaturated oligosaccharides product per min as calculated using a molar absorption coefficient of 3800 M^{-1} cm^{-1} (Pojasek *et al.,* 2001).

3.2.2.1 Calculation of enzyme activity

The activity of the enzyme was expressed as U/ml and the specific activity as U/mg of protein. 1 Unit of enzyme was defined as the amount of enzyme that forms 1 µmol of unsaturated oligosaccharides product per min. The enzyme activity of *Ps*PL8A was calculated as described below,

$$\text{Enzyme activity (U/ml)} = \frac{\Delta A_{232} \times 1000}{\varepsilon \times t \times v}$$

Where,

ΔA_{232} = Absorbance of unsaturated CS oligosaccharides
ε = Molar extinction of unsaturated CS oligosaccharides at A_{232}, 3800 $M^{-1}cm^{-1}$
t = Time of reaction in min
v = Volume of enzyme used in reaction in ml

$$\text{Specific activity (U/mg)} = \frac{\text{Enzyme activity (U/ml)}}{\text{Concentration of protein used in reaction (mg/ml)}}$$

3.2.3 Substrate specificity of *Ps*PL8A

Recombinant *Ps*PL8A was assayed against several polysaccharides, to determine its substrate specificity. According to several reports of family 8 polysaccharide lyase, it has been found that these enzymes could have putative activity against glycosaminoglycans. Hence the major substrates were Chondroitin 4-sulphate sodium salt from bovine trachea, chondroitin sulphate B sodium salt (dermatan sulphate) from porcine intestinal mucosa, hyaluronic acid sodium salt from *Streptococcus equi,* heparin sodium salt and chondroitin 6-sulphate sodium salt from shark cartilage. The enzyme activity of *Ps*PL8A was determined by incubating 1 mg/ml of substrate at optimum conditions of temperature and pH. The increase in A_{232} was

measured from time zero as a function of time on a UV-Visible spectrophotometer (Varian, Cary 100). The enzyme activity and specific activity were calculated by using the formula mentioned in Section 3.2.2.1.

3.2.4 Determination of optimum temperature of *Ps*PL8A

The optimum temperature of *Ps*PL8A was determined by incubating the 0.1 µg of enzyme in 1 ml reaction mixture containing 1 mg/ml chondroitin 4-sulphate in 50 mM Tris-HCl buffer, pH 7.2 in the temperature range 20ºC - 60ºC for 5 min. Specific activity at different temperatures was determined from amount of unsaturated chondroitin oligosaccharide produced at A_{232} nm as mentioned earlier in Section 3.2.2.1.

3.2.5 Determination of optimum pH of *Ps*PL8A

The optimum pH of *Ps*PL8A was determined by performing enzyme assays at optimum temperature (39ºC). Two buffer systems 50 mM sodium phosphate for pH 6-8 and 50 mM Tris-HCl for pH 7-9 were used to determine the optimum pH of *Ps*PL8A. The optimum pH of *Ps*PL8A was determined by incubating the 0.1 µg of enzyme in 1 ml reaction mixture containing 1 mg/ml of chondroitin 4-sulphate incubated at 39°C for 5 min under pH range of pH 6-9. The absorbance was measured at A_{232} nm to calculate the specific activity as mentioned earlier in Section 3.2.2.1.

3.2.6 Determination of temperature stability of *Ps*PL8A

The thermal stability of enzyme was studied by incubating 100 µl enzyme (10 µg/ml) in 50 mM Tris-HCl buffer, pH 7.2 (optimized pH) for 30 min at different temperatures varying from 20ºC to 50ºC. After incubation 10 µl of enzyme was assayed in a 1 ml reaction mixture containing 1 mg/ml of C4S in 50 mM Tris-HCl buffer, pH 7.2 for the residual activity at optimum temperature 39ºC for 5 min. The specific activity for *Ps*PL8A enzyme was calculated as mentioned earlier in Section 3.2.2.1.

3.2.7 Determination of pH stability of *Ps*PL8A

The pH stability analysis of *Ps*PL8A was carried out by incubating the 100 µl enzyme (10 µg/ml) in 50 mM buffer (sodium phosphate, pH 6-8 or Tris-HCl, pH 7-9). The enzyme was incubated for 30 min at 25ºC. The residual activity of the incubated was calculate by assaying 10 µl of *Ps*PL8A enzyme in a 1ml reaction mixture containing 1 mg/ml C4S dissolved in 50 mM Tris-HCl buffer, pH 7.2 at optimum temperature of 39ºC for 5 min. The specific activity for *Ps*PL8A enzyme was calculated as mentioned earlier in Section 3.2.2.1.

3.2.8 Determination of kinetic parameters of *Ps*PL8A

The kinetic parameters of *Ps*PL8A were determined under optimized condition of pH and temperature. The concentration of substrate chondroitin 4-sulphate was varied in a range of 0.1- 3.0 mg/ml. A 0.1 µg of *Ps*PL8A enzyme was assayed in 1 ml reaction mixture containing 50 mM Tris-HCl buffer, pH 7.2 and varying concentration of C4S (0.1-3.0 mg/ml). The reaction was done at optimum temperature, 39ºC for 5 min and the unsaturated product formed was monitored spectophotometrically at A_{232} nm. The specific activity was calculated as mentioned earlier in Section 3.2.2. The kinetic parameters, K_m, V_{max}, k_{cat} and k_{cat}/K_m, of *Ps*PL8A were calculated by obtaining initial reaction rate as a function of substrate concentration. k_{cat} and K_m were determined using the Michaelis-Menten plot and Lineweaver-Burk plot.

3.2.9 Effect of metal ions on activity of *Ps*PL8A

The activity of *Ps*PL8A was studied in the presence of varying concentrations of different metal ions mixed with 1.0 mg/ml of chondroitin 4-sulphate in 1 ml reaction mixture. A control without metal ions was also run in parallel. The reaction was carried out in 50 mM Tris-HCl, buffer pH 7.2 and at a temperature of 39°C. The assay was

carried out by monitoring unsaturated product formation by an increase in A_{232} as a function of time as mentioned earlier in Section 3.2.2.1. The effects of metals ion on the activity of *Ps*PL8A was studied using varying concentration of corresponding salts of metal ions *viz.* NaCl (10-500 mM), KCl (10-400 mM), $CaCl_2$ (5-100 mM), $MgCl_2$ (5-80 mM), $CoCl_2$ (5-200 mM), $CuCl_2$ (0.01-0.5 mM), FeCl2 (0.01-1 mM), $ZnSO_4$ (0.1–1.0 mM), $NiSO_4$ (0.05–1 mM), $AlCl_3$ (1–10 mM), EDTA (1-10 mM) and SDS (0.1-2 mM).

3.2.10 Structural stability of *Ps*PL8A in presence of chaotropic agents

The structural stability of *Ps*PL8A was monitored in presence of chaotropic agents like guanidine hydrochloride (GuHCl) or urea, under an isothermal condition by fluorescence studies. 1 ml reaction was setup using 20 µg of *Ps*PL8A in 50 mM Tris-HCl buffer, pH 7.2 with varying concentrations of GuHCl (0 - 7 M) or urea (0 - 5 M). The above solutions were incubated at room temperature for 3h. The fluorescence spectrum of *Ps*PL8A at each concentration of GuHCl or Urea was recorded on spectrofluorometer (Fluoromax 4, Jobin). The tryptophan residues of the samples were excited at a wavelength of 295 nm and the emission spectrum was recorded in the wavelength range, 310-400 nm. The loss in structural integrity of *Ps*PL8A was monitored by the shifting of the emission spectrum peak to a higher wavelength. A control sample (buffer and chaotropic agent) without *Ps*PL8A was used for each concentration of the chaotropic agent.

3.2.11 Thin layer chromatography analysis of degraded products of C4S by *Ps*PL8A

The mode of action of *Ps*PL8A on its substrate C4S was determined by analysing its degraded products released at different time intervals by thin layer chromatography (TLC). Separate reactions were set up in which *Ps*PL8A was incubated in a 1 ml reaction mixture containing, 1.0 mg/ml C4S in 50 mM Tris-HCl buffer, pH 7.2 and incubated at 39°C. Different reactions were set up for each time interval (0 min, 1 min, 2 min, 5 min, 10 min, 15 min, 20 min, 25 min, 30 min, 35 min, 45 min, 1 h, 2 h, 4 h, 8 h, 12 h, 16 h and 24 h). After completion of the time interval the degraded products were separated by precipitating the undigested polysaccharides and protein by adding equal volume of absolute ethanol and by centrifuging at 13,000*g* for 10 min. The supernatant containing enzyme degraded products were collected in separate micro- centrifuge tubes and concentrated from 1 ml to 100 µl by heating at 60°C. A 0.5 µl of concentrated products were applied as a spot on TLC plate (Merck, Germany) and run under a solution containing 1-butanol, water and acetic acid in the ratio 5:3:2 (v/v) (Lojkwoska *et al.,* 1995). The TLC plates were stained by diphenylamine: aniline: phosphoric acid reagent (1 ml of 37.5% HCL, 2 ml aniline, 10 ml of 85% H_3PO_4, 100 ml of ethyl acetate and 2 g of diphenylamine) and visualized after incubating at 80°C for 30 min (Zhang *et al.,* 2009). Standard oligosaccahrides like D-glucuronic acid, N-acetyl galactosamine, ΔC6S disaccharide and ΔC4S disaccharide were used to analyze the degradation product formed from different substrates upon enzymatic treatment.

3.2.12 ESI-Mass Spectrometric analysis of *Ps*PL8A degraded product of C4S

The reaction of *Ps*PL8A was carried out in a 1 ml reaction mixture containing, 1.0 mg/ml C4S in 50 mM Tris-HCl buffer, pH 7.2 and incubated at 39°C for 2 min, 30

min, 1 h, 2 h and 24 h. The 1 ml reaction mixture was treated with equal volume of ethanol and centrifuged at 13,000*g* for 10 min to precipitate and separate the polysaccharide and protein. After centrifugation the supernatant was collected and concentrated to 100 µl in hot air oven at 60°C. The samples containing the oligosaccharides were diluted in 1:1 (v/v) ratio by methanol and 20 µl was used for analysis. The samples after 2 min, 30 min, 1 h, 2 h and 24 h reaction with *Ps*PL8A were then analyzed by Electron Spray Ionization (ESI) mass spectrometer (Waters, Q-TOF Premier) in MS mode without any purification. The reaction product of 24 h was analysed by both MS and tandem MS (MS/MS) mode. ESI-MS and tandem MS analyses were carried out in negative ion mode, where the parameters for ESI-MS analysis were; capillary voltage 3 eV, collision energy 5 eV, ionization energy 1 eV, desolvation temperature 250°C and the source temperature of 80°C. The tandem MS analysis was carried out by nanospray ionization using the voltage 3 eV, collision energy 20 eV and collision-induced dissociation was performed on ion of interest using the argon gas.

3.2.13 ^{1}H- and ^{13}C- NMR spectroscopic analysis of *Ps*PL8A degraded C4S disaccharide

The final degraded disaccharide product of C4S by enzyme *Ps*PL8A after reaction completion at 24 h was analysed by ^{1}H- and ^{13}C- Nuclear magnetic resonance (NMR) spectroscopy. The enzyme reaction was carried out in 1 ml reaction mixture containing 1.0 mg/ml of C4S in 50 mM Tris-HCl buffer, pH 7.2 and 0.5 µg of *Ps*PL8A enzyme and incubated at 39°C for 24 h. The undigested polysaccharide and protein were precipitated by adding equal volume of absolute ethanol with gentle mixing and subsequently centrifuged at 13,000 g for 10 min. After centrifugation the supernatant

was collected and lyophilized. The sample was dissolved in D_2O (99.96%) (Merck Germany) at concentrations of 5 mg/ml (for ^{1}H-NMR) and 20-30 mg/ml (for ^{13}C-NMR). The ^{1}H- and ^{13}C- NMR spectra were acquired at 25ºC at 600 MHz NMR spectrometer (Bruker, Avance III HD, MA, USA) fitted with a 5-mm probe and equipped with topspin software package from Bruker for analysis.

3.3 Results and Discussion

3.3.1 Substrate specificity of *Ps*PL8A

The enzyme activity of *Ps*PL8A was determined under the optimized conditions as described in Section 3.2.2.1. The activity of *Ps*PL8A with various glycosaminoglycan (GAG) substrates is reported in Table 3.3.1. *Ps*PL8A is a characteristic chondroitin AC lyase and preferentially cleaves chondroitin 4-sulphate and chondroitin 6-sulphate, though it also acts against hyaluronic acid. *Ps*PL8A was predominantly active towards chondroitin sulphate substrates. It displayed highest activity towards C4S (489.0±11 U/mg) followed by C6S (214.0±2.0 U/mg) and hyaluronic acid (43.2±1.2 U/mg), but did not show any activity with dermatan sulphate and heparin. Chondroitin AC lyase reported earlier from *Flavobacterium heparinum*, showed activity towards C4S and C6S (Pojasek *et al*., 2001). Chondroitin AC lyase reported from *Bacteroides stercoris* HJ-15 displayed higher activity with C4S followed by hyaluronic acid and C6S (Hong *et al*., 2002; Shim *et al*., 2008). Another report on chondroitin lyase from Baculovirus envelope protein ODV-E66 does not degrade C4S, whereas it degrades most efficiently, the chondroitin without sulphation followed by C6S and hyaluronic acid to lesser extent (Sugiura et al., 2011). Chondroitin AC lyase from *Serratia marcescens* GT596 showed enzyme activity with chondroitin 4-sulphate notably lower activity than with chondroitin 6-sulphate (Ke *et al*., 2005). The spectrophotometric assay method used to evaluate the activity of *Ps*PL8A provides evidence that *Ps*PL8A enzyme belongs to polysaccharide lyase 8 family. The β-elimination reaction mechanism followed by *Ps*PL8A was confirmed spectrophotometrically by measuring the Δ4,5 unsaturated oligosaccharides by the increase in absorbance at 232 nm (A_{232}).

Table 3.3.1 Substrate specificity of *Ps*PL8A against various glycosaminoglycan substrates.

Substrate (1 mg/ml)	Specific Activity (U/mg)
Chondroitin 4-sulphate	489.0±11
Chondroitin 6-sulphate	214.0±2.0
Hyaluronic acid	43.2±1.2
Dermatan sulphate	NA
Heparin	NA

NA- No Activity

The reaction was carried out under optimised conditions of 50 mM Tris-HCl buffer, pH 7.2 at 39ºC as described in the "Material and Methods" section 3.2.2.1.
The assays were performed in triplicates.

3.3.2 Optimum temperature for activity of *Ps*PL8A

The optimum temperature for the activity of chondroitin AC lyase *Ps*PL8A was determined after performing assay with C4S under varying temperatures 20ºC - 60ºC. *Ps*PL8A displayed an optimum temperature of 39°C and retained ~90% of activity within the temperature range 35-40°C (Fig 3.3.1). Chondroitin AC lyase from *Flavobacterium heparinum* (Pojasek *et al*., 2001) and *Bacteroides stercoris* HJ-15 (Hong *et al*., 2002) displayed optimum temperatures 35ºC and 45ºC, respectively. The optimum temperature of chondroitin AC lyase from *Serratia marcescens* was 40ºC (Ke *et al*., 2005). Chondroitin lyase from Baculovirus envelope protein ODV-E66 showed an optimum temperature of 37ºC (Sugiura *et al*., 2011). *Ps*PL8A displayed an optimum temperature of 39ºC which is in the range of human physiological conditions. Therefore, *Ps*PL8A can serve as a potential candidate for therapeutic applications such as neuronal reinnervation and antitumor agent.

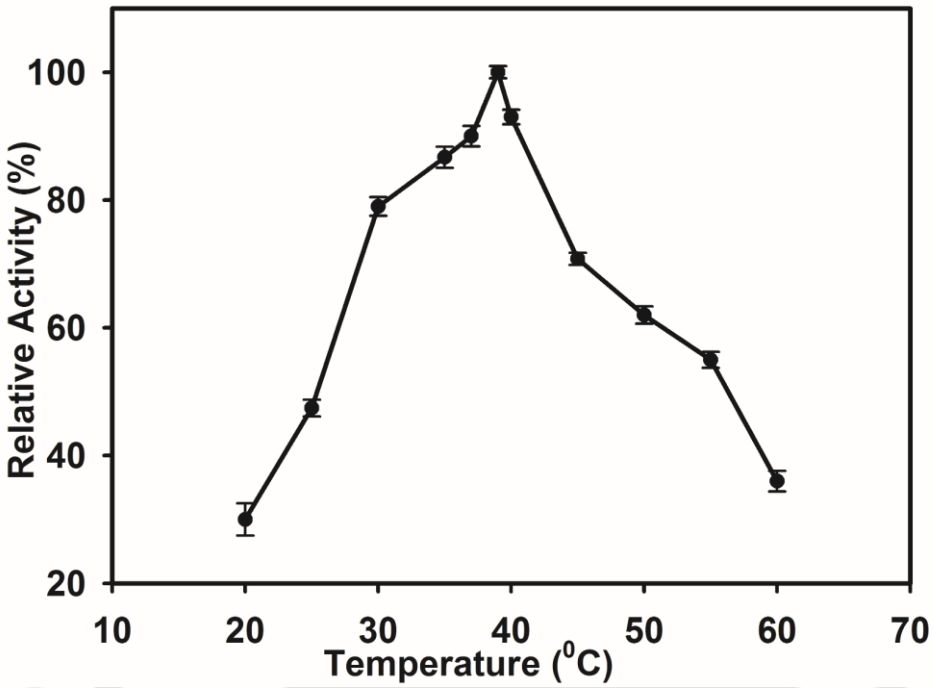

Fig. 3.3.1 Optimum temperature for activity of *Ps*PL8A.

3.3.3 Optimum pH for activity of *Ps*PL8A

The effect of pH on the activity of the recombinant *Ps*PL8A was determined using C4S as substrate. The result showed the *Ps*PL8A enzyme was active under human physiological pH conditions (pH 7.2). *Ps*PL8A displayed optimum pH of 7.2 and retained 90% activity within the pH range 6.9 -7.6 (Fig. 3.3.2). Chondroitin AC lyase from *Flavobacterium heparinum* (Pojasek *et al.*, 2001) and *Bacteroides stercoris* HJ-15 (Hong *et al.*, 2002) displayed optimum pH of 8.0 and 5.8, respectively. The optimum pH of chondroitin AC lyase from *Serratia marcescens* was 7.5 (Ke *et al.*, 2005). Chondroitin lyase from Baculovirus envelope protein ODV-E66 showed an optimum pH of 7 (Sugiura *et al.*, 2011).

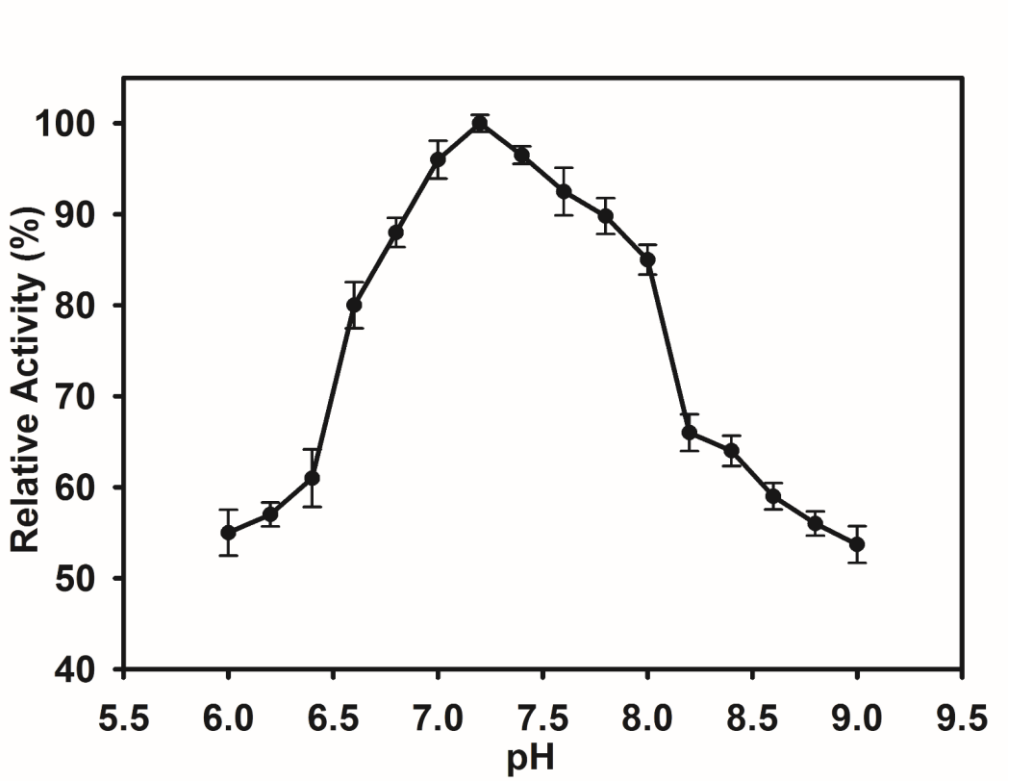

Fig. 3.3.2 Optimum of pH for the activity of *Ps*PL8A.

3.3.4 Thermal stability of *Ps*PL8A

The thermal stability of *Ps*PL8A displayed ~100% retention of activity within temperature range 30-40°C after 30 min incubation (Fig 3.3.3). However, at higher temperature, 50°C there was a sharp decrease in the residual activity suggesting significant decrease in the enzyme stability (Fig. 3.3.3). The most accepted explanation loss of enzyme activity at high temperature is the opening or uncoiling of the protein architecture, which results in decreased stability and consequently lowering the activity (Branden *et al*., 1991; Creighton., 1992). The opening of protein tertiary structure changes the conformation of protein architecture that directly affects the velocity of enzyme catalyzed reaction.

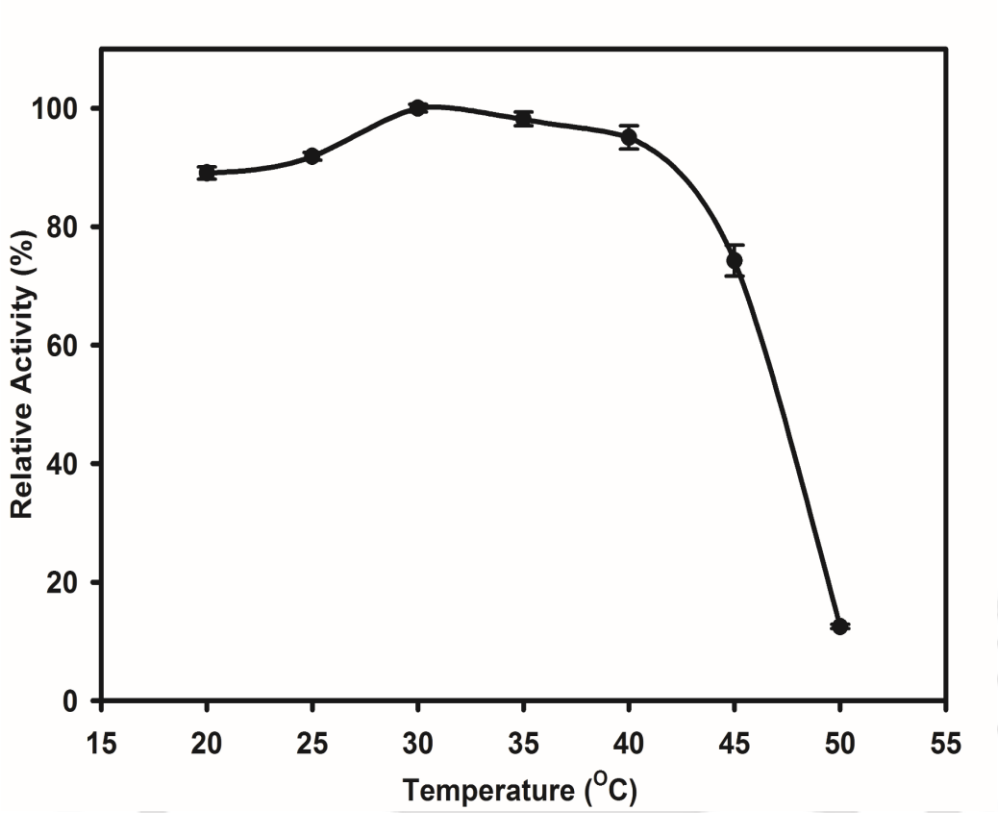

Fig 3.3.3 Thermal stability for the activity of *Ps*PL8A.

3.3.5 pH stability of *Ps*PL8A

The pH stability profile displayed retaining of approximately, ~90% of enzyme activity for 30 min in the pH range 6.8-7.6 and most stable at pH 7.2 (Fig 3.3.4). The pH stability of an enzyme depends on two factors, i) type of enzyme and direct involvement of ionic groups in the catalytic mechanism and ii) participation of charged groups in the stabilization of the protein structure (Branden *et al*., 1991). Enzyme catalysis occurs by interaction of ionic groups from amino acid side chains at the active centre of the enzyme. These ionic groups get protonated during catalysis to carry out a successful reaction. As the pH deviates from the optimum pH value the protonation state of ionic groups involved may alter and hinders proper catalysis of the substrate, thus resulting in a lower activity.

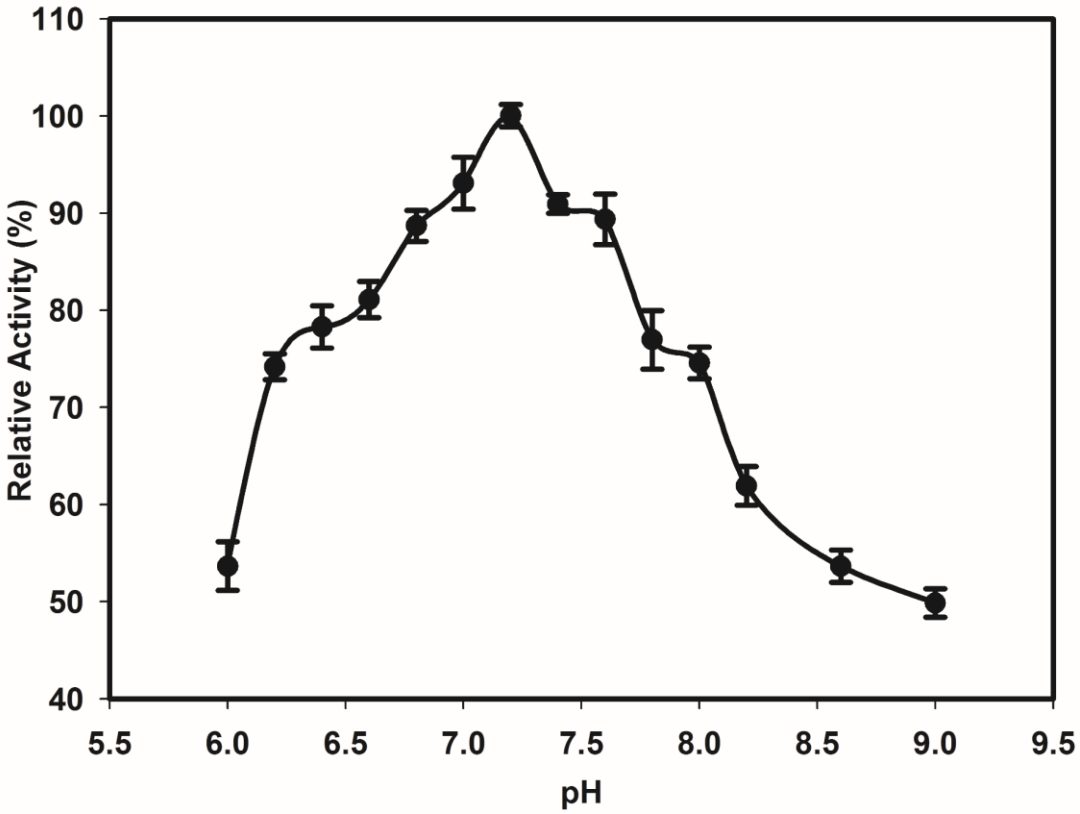

Fig. 3.3.4 pH stability of *Ps*PL8A.

3.3.6 Kinetic parameters of *Ps*PL8A

Kinetic parameters of *Ps*PL8A were determined against C4S and are presented in Table 3.3.2. The data revealed that *Ps*PL8A displayed K_m and V_{max} values of 1.1± 0.01 mg/ml and 526±28 U mg^{-1}, respectively using C4S. It gave the turnover number (k_{cat}) of 679.6 s^{-1} and (k_{cat}/K_m) as 617.8 s^{-1} mg^{-1} ml using C4S as substrate.

Table 3.3.2 Kinetic parameters of *Ps*PL8A with Chondroitin 4-sulphate (C4S). One unit of enzyme was defined as the amount of enzyme that forms 1 µmol of unsaturated oligosaccharides product per min.

Enzyme	Substrate	k_{cat} (S^{-1})	K_m (mg/ml)	k_{cat}/K_m (s^{-1} mg^{-1} ml)
***Ps*PL8A**	**C4S**	679.6	1.1± 0.01	617.8

All experiments were performed in triplicate following the method mentioned in Section 3.2.7.

3.3.7 Effect of metal ions on the activity of *Ps*PL8A

The performance of *Ps*PL8A under the influence of various monovalent and divalent metal ions as well as detergent, using C4S as substrate was investigated and the results are shown in Table 3.3.3. The activity of *Ps*PL8A with no additive was taken as 100%. The presence of 100 mM Na^+ (Fig. 3.3.5A) or 20 mM Ca^{2+} (Fig 3.3.5C) or 20 mM Co^{2+} (Fig. 3.3.5 E) ions concentration enhanced the activity of *Ps*PL8A by ~2 fold. A 100 mM concentration of K^+ ion enhanced the enzyme activity of *Ps*PL8A by 1.9 fold (Fig. 3.3.5.B). A 20 mM Mg^{2+} ion concentration caused ~1.4 fold rise *Ps*PL8A activity (Fig. 3.3.5D). The enzyme activity of *Ps*PL8A was reduced to 15.5% by 1 mM Zn^{2+} ions (Fig. 3.3.5.F). 1 mM Fe^{2+} ion concentration reduced the enzyme activity of *Ps*PL8A by 1.2%. The enzyme activity of *Ps*PL8A was reduced to 2.2% by 0.1 mM Cu^{2+} ion concentration and reduced to 5.4% by 10 mM concentration of Al^{3+} ions (Fig. 3.3.5G). The enzyme activity of *Ps*PL8A was adversely affected at the low concentrations of Zn^{2+}, Al^{3+}, EDTA (Fig. 3.3.5H) and SDS (Fig. 3.3.5I), while enzyme activity of *Ps*PL8A was completely inhibited at very low concentrations of Fe^{2+} or Cu^{2+} ions. The results of metal ion study gave a lucid idea that Ca^{2+} or Co^{2+} ions might be required by *Ps*PL8A as cofactors for increasing its the activity. It was earlier reported that chondroitin lyase from Baculovirus envelope protein ODV-E66 remains unaffected by the addition of divalent metal ions (Sugiura *et al*., 2011). Chondroitin AC lyase from *Bacteroides stercoris* HJ-15 displayed only a 5% and 2% increase in the activity by 1 mM Ca^{2+} or Mg^{2+} ion concentrations, respectively (Hong *et al*., 2002). The enzyme activity of chondroitin AC lyase from marine *Arthrobacter sp*. MAT3885 remains unaffected by addition of metal ions such as Na^+, K^+, Mg^{2+}, Ca^{2+}, Fe^{2+}, Co^{2+}, Cu^{2+} and Ni^{2+}, while the addition of Mn^{2+} increased the activity by only 20% (Kale *et al*., 2015).

The HA/CS-degrading activity of HCLase from marine bacterium was significantly inhibited by 5 mM concentration of divalent metal salts $CaCl_2$, $MgCl_2$, $MnCl_2$ and $CoCl_2$ suggesting that the activity is independent of divalent metal ions (Han *et al*., 2014). The present study of metal ions with *Ps*PL8A indicated that the divalent Ca^{2+} or Co^{2+} ion(s) might be present at the catalytic site and involved in catalysis enhancing the enzyme activity of *Ps*PL8A.

Table 3.3.3 Effect of metal ions on the activity of *Ps*PL8A**.**

Metal ion/ Reagent	**Concentration (mM)**	**Relative activity (%)**
Control	--	100
Na^+	100	209
K^+	100	185
Ca^{2+}	20	190
Co^{2+}	20	185
Mg^{2+}	20	136
Zn^{2+}	1.0	15.2
Fe^{2+}	1.0	1.2
Cu^{2+}	0.1	2.2
Al^{3+}	10.0	5.4
SDS	1.0	1.1
EDTA	10.0	1.4

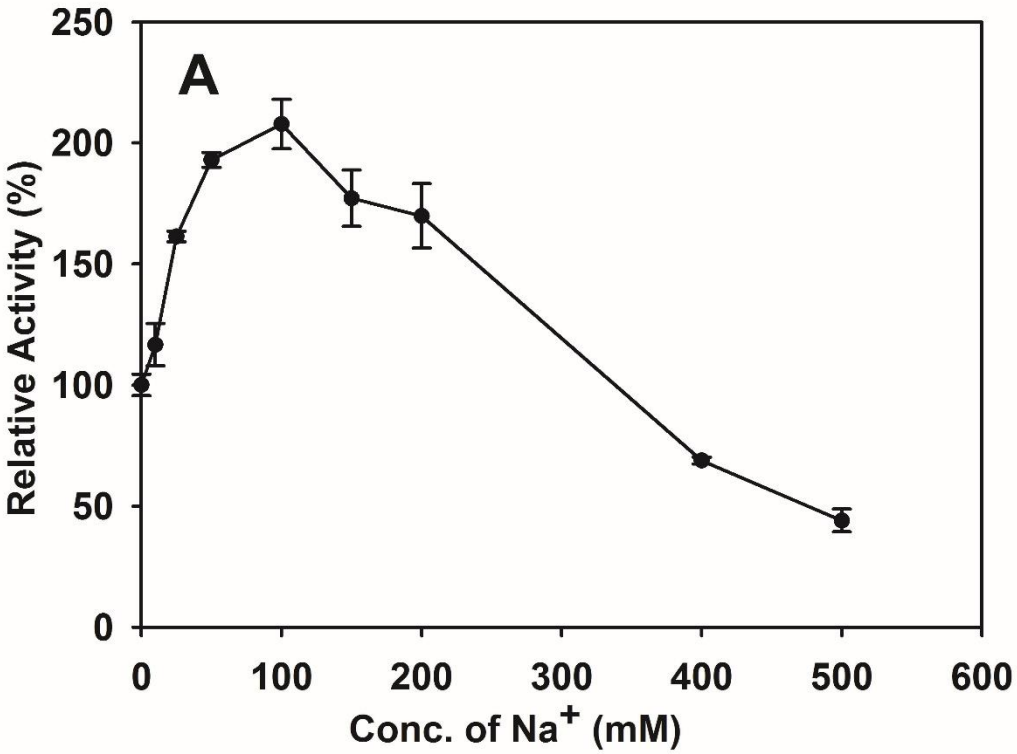

Fig. 3.3.5A Effect of Na^+ ion on enzyme activity of *Ps*PL8A.

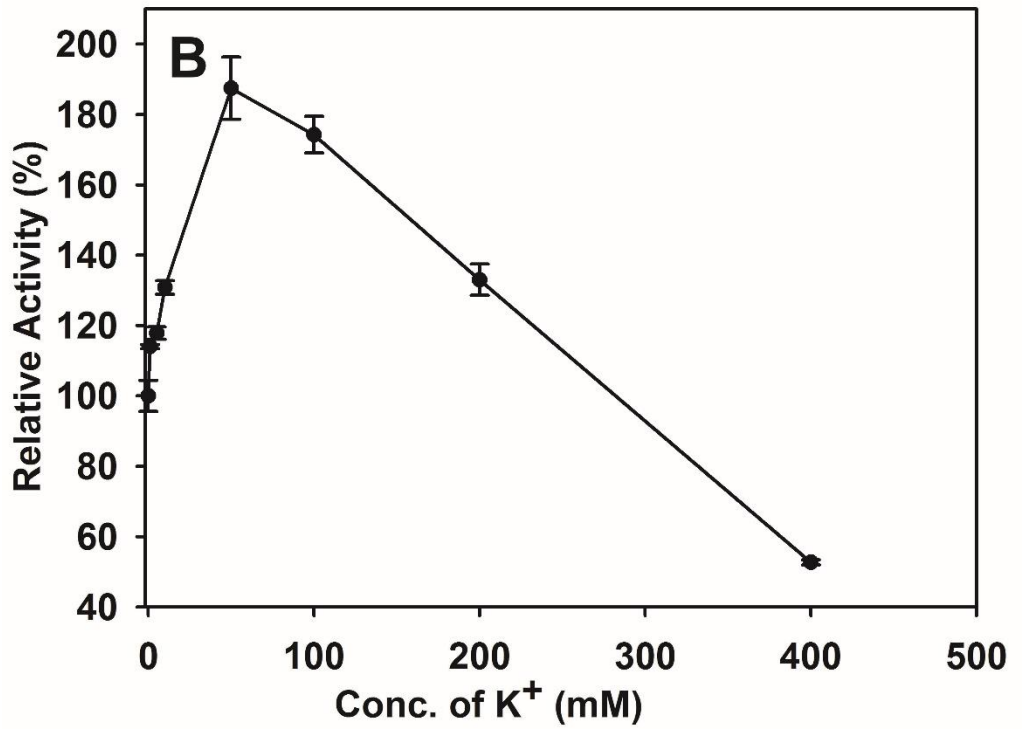

Fig. 3.3.5B Effect of K^+ ion on enzyme activity of *Ps*PL8A.

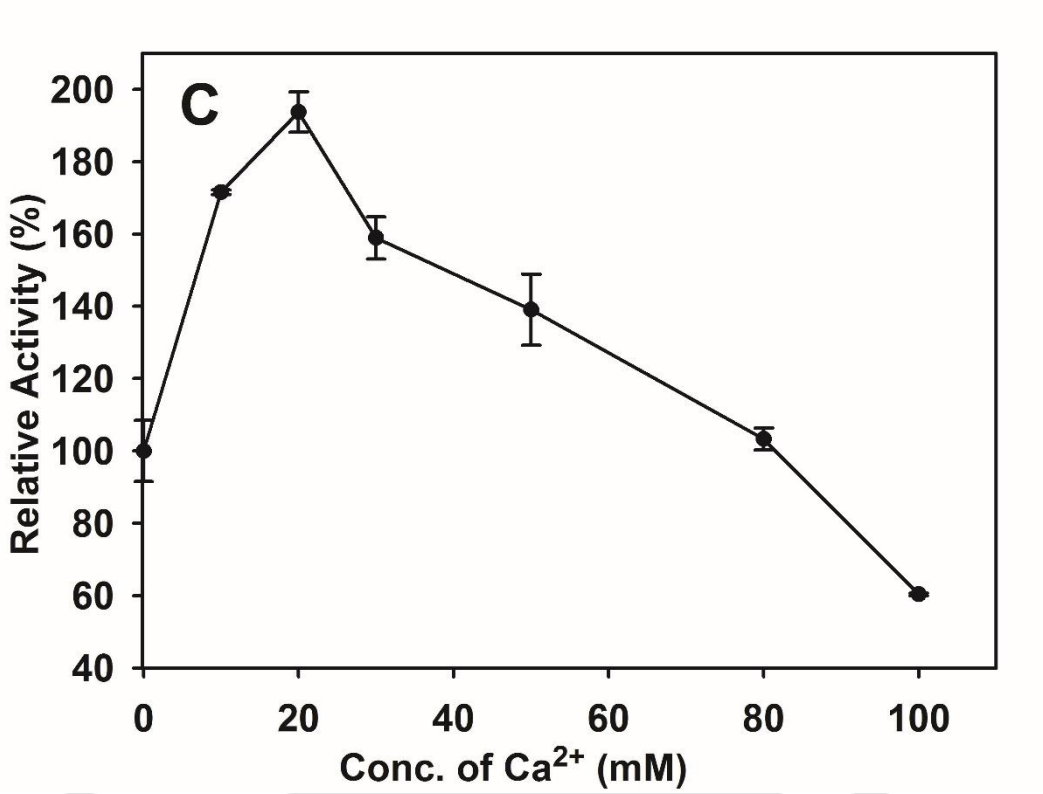

Fig. 3.3.5C Effect of Ca^{2+} ion on enzyme activity of *Ps*PL8A.

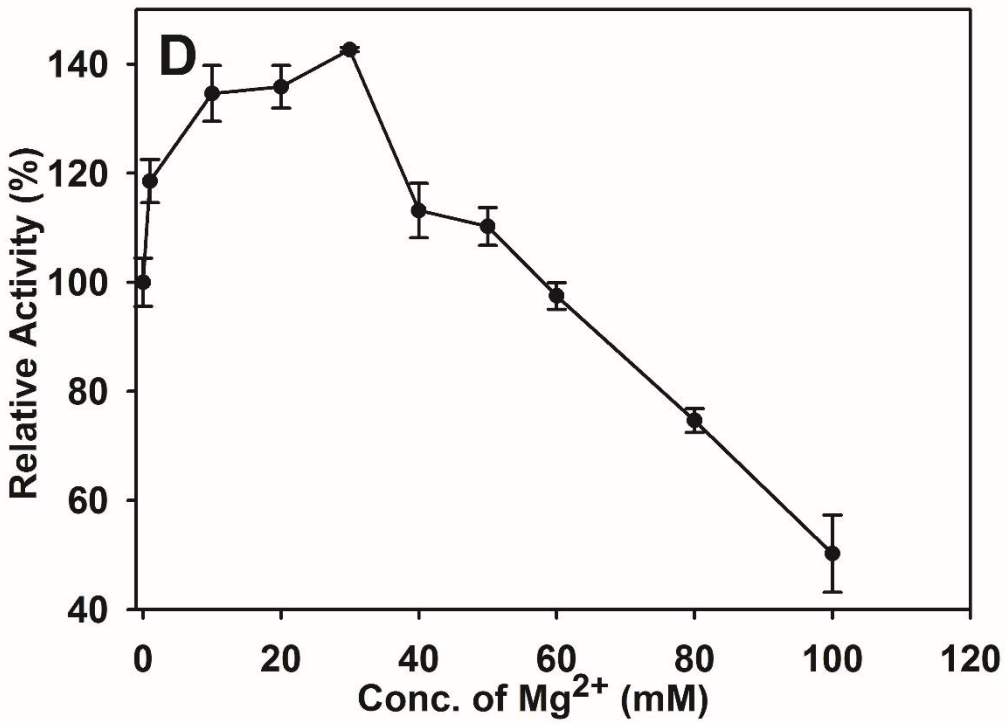

Fig. 3.3.5D Effect of Mg^{2+} ion on enzyme activity of *Ps*PL8A.

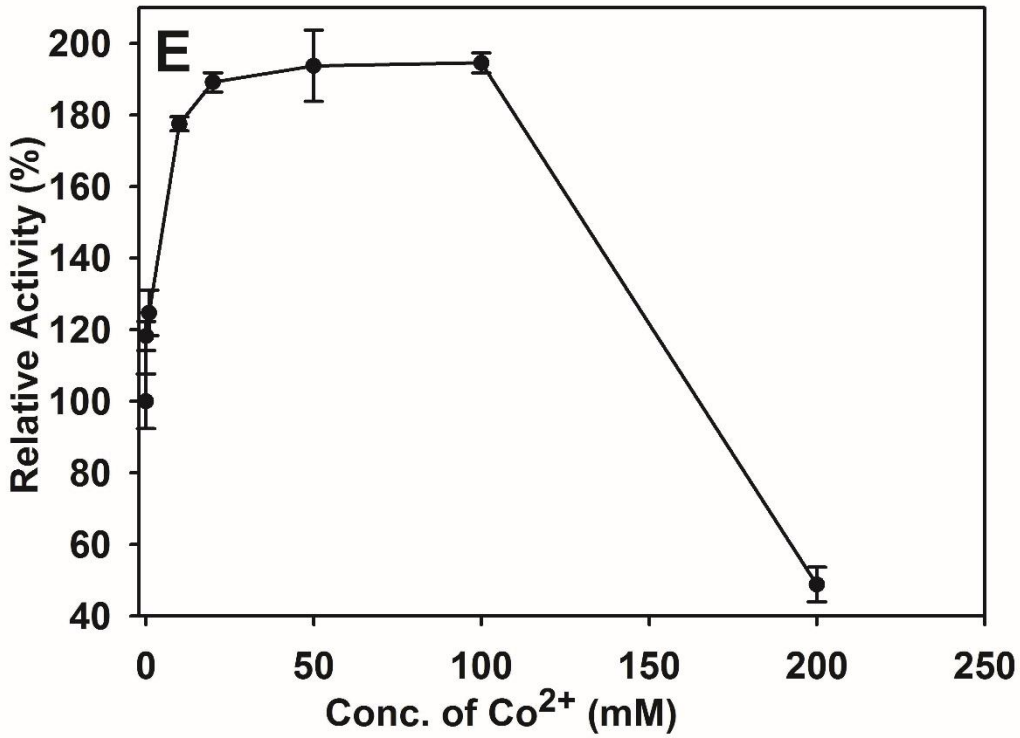

Fig. 3.3.5E Effect of Co^{2+} ion on enzyme activity of *Ps*PL8A**.**

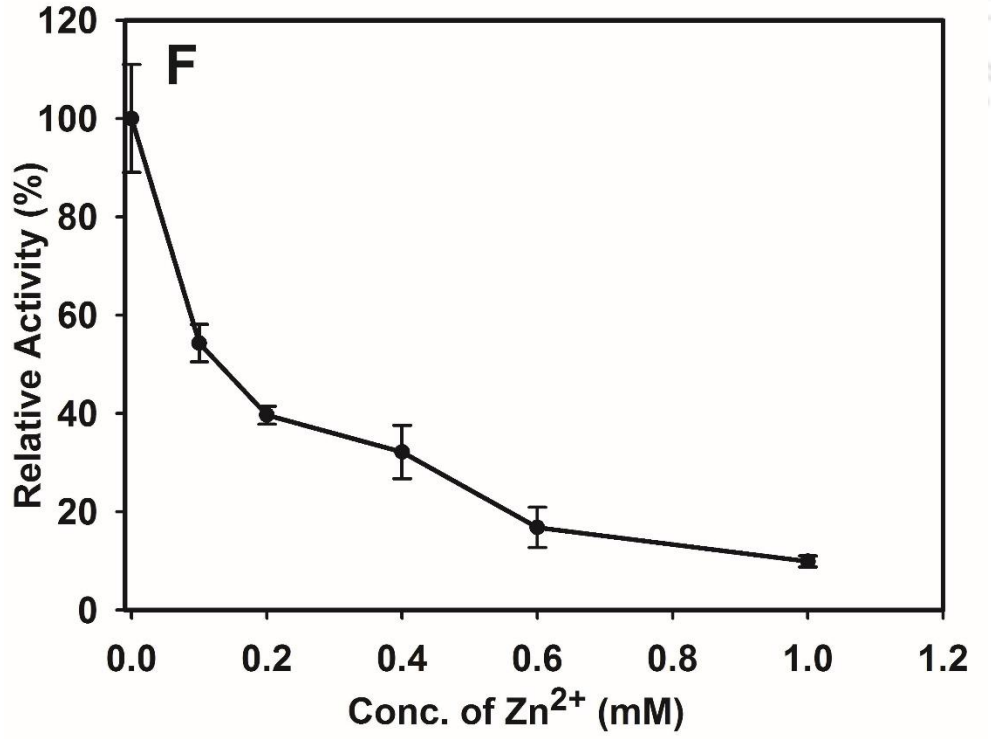

Fig. 3.3.5F Effect of Zn^{2+} ion on enzyme activity of *Ps*PL8A.

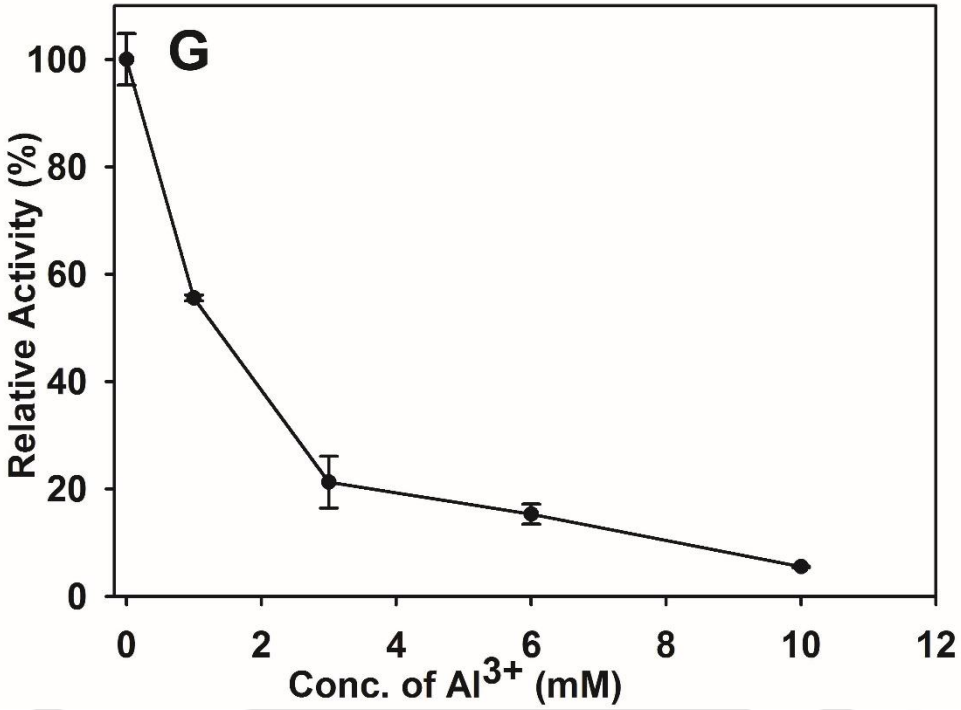

Fig. 3.3.5G Effect of Al^{3+} on enzyme activity of *Ps*PL8A.

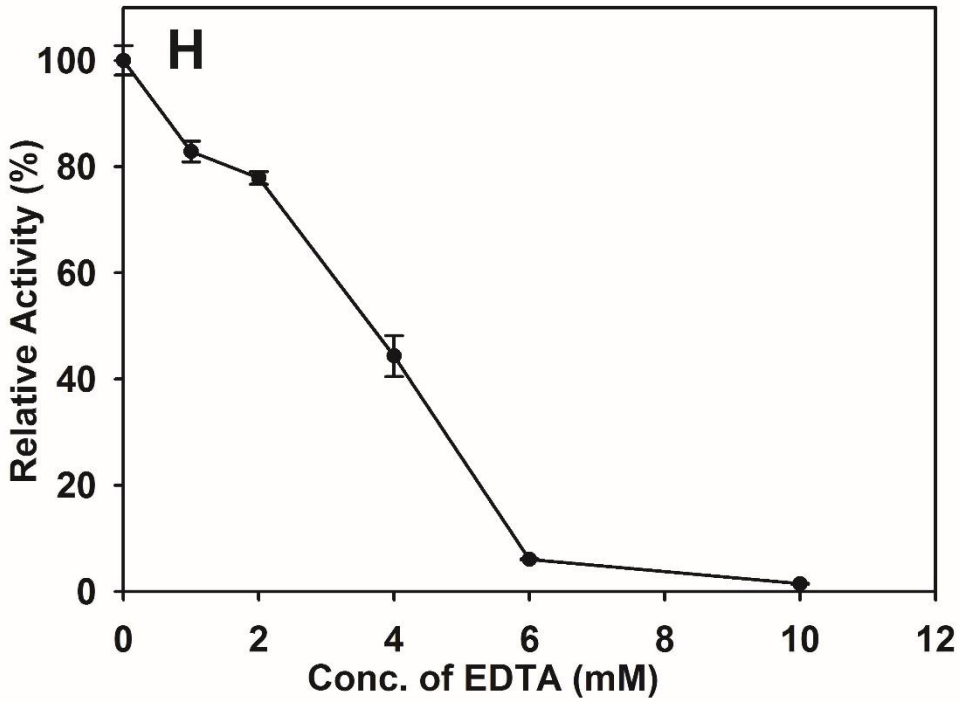

Fig. 3.3.5H Effect of EDTA on enzyme activity of *Ps*PL8A.

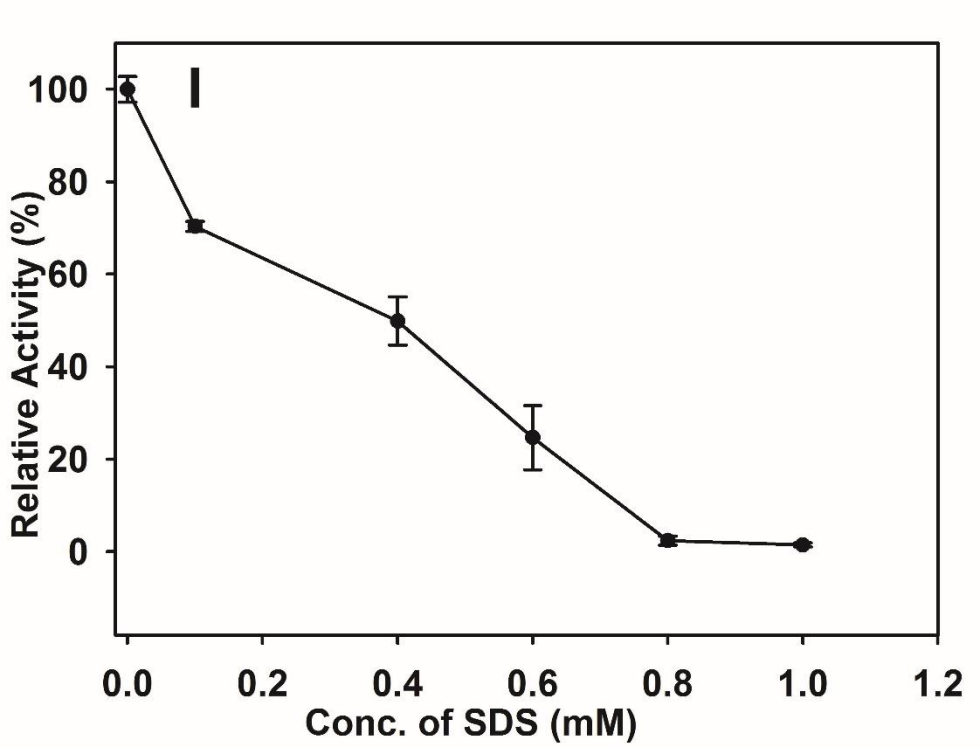

Fig. 3.3.5I Effect of SDS on enzyme activity of *Ps*PL8A.

3.3.8 Structural stability of *Ps*PL8A in presence of chaotropic agents

The effect of chaotropic agents *viz.* Urea and Guanidine hydrochloride (GuHCl) on structural integrity of *Ps*PL8A was studied. The chaotropic agents at different concentrations were incubated with *Ps*PL8A and changes were monitored by fluorescence spectroscopy. Excitation wavelength was kept at 295 nm, whereas, the fluorescence emission was recorded from 310-400 nm for each sample. A peak at 330 nm was observed for *Ps*PL8A protein. The peak of *Ps*PL8A shifted to higher wavelength (from 330 nm to 340 nm) at 5 M Urea concentration (Fig. 3.3.6A), while in presence of 3 M GuHCl the peak corresponding to *Ps*PL8A shifted from 330 nm to 341 nm (Fig. 3.3.6B) indicating the loss of structural integrity of *Ps*PL8A protein.

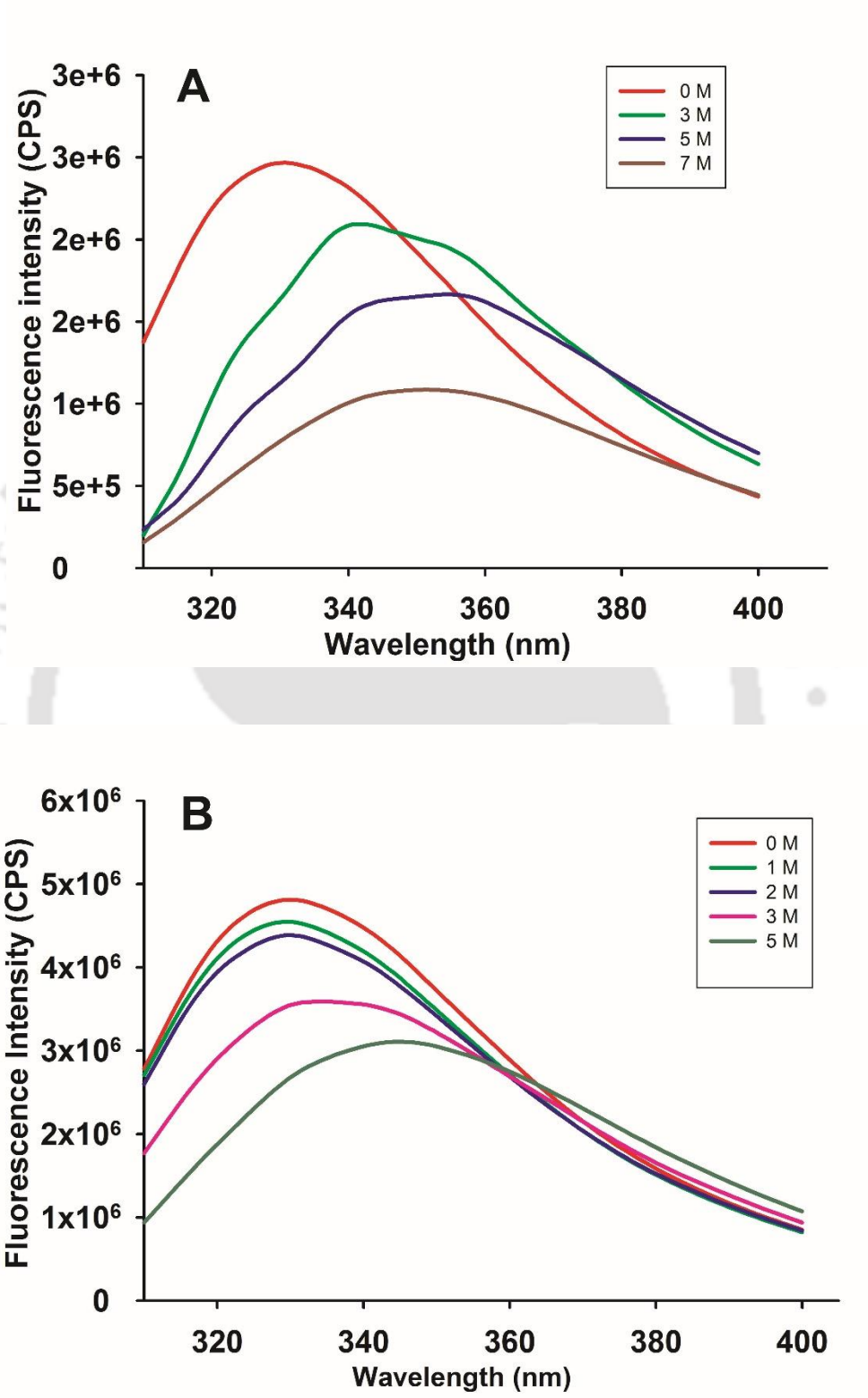

Fig. 3.3.6 Tryptophan emission spectra of *Ps*PL8A in presence of different concentration of chaotropic agents (A) Guanidine hydrochloride (GuHCl) and (B) Urea.

3.3.9 Thin layer chromatography analysis of degraded products of C4S by *Ps*PL8A

The products released by the enzymatic degradation of *Ps*PL8A with C4S were determined by TLC (Fig. 3.3.7). The salient feature of *Ps*PL8A catalysis involved only the β-(1→4)-bond cleavage by β elimination mechanism. The time dependent C4S degradation by *Ps*PL8A in TLC analysis showed simultaneous endo- and exo-lytic cleavage pattern for first hour producing a series of higher oligosaccharides along with the ΔC4S disaccharide (Fig. 3.3.7). After 1 h of the reaction *Ps*PL8A started utilizing the higher oligosaccharides, chopping off them, producing only the ΔC4S disaccharide as the sole product that continued till 24 h. This result displayed the initial concomitant endo- and exo-lytic cleaving property of *Ps*PL8A and finally shifting to only exo-lytic mode. The previous reports suggest that chondroitin AC lyase from *Flavobacterium heparinum* cleaves endolytically the substrates (Hiyama et al., 1976; Jandik et al., 1995; Pojasek et al., 2001) whereas for chondroitin AC lyases from *Arthrobacter auresus* the exolytic action was reported (Hiyama et al., 1976; Jandik et al., 1995; Linhardt et al., 200; Lunin et al., 2004).

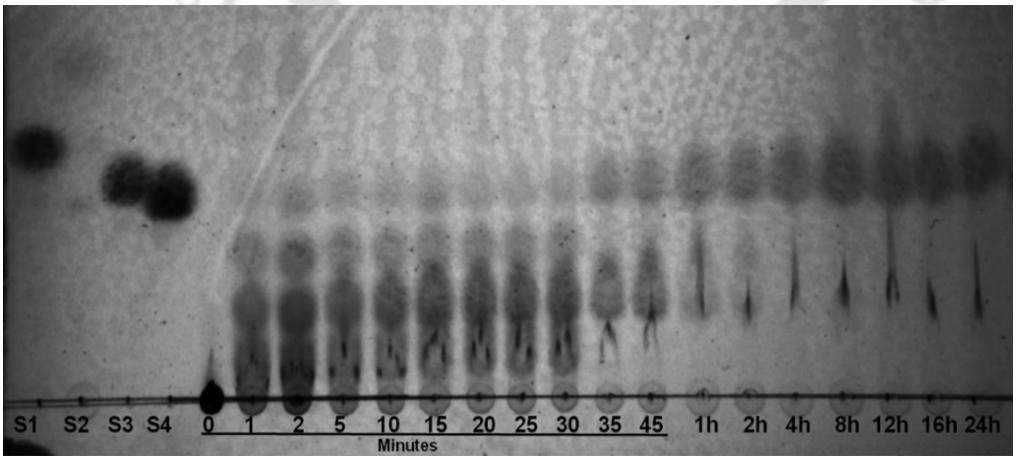

Fig. 3.3.7 Time dependant TLC analysis of *Ps*PL8A degraded products of C4S using the standards *viz.* S1: D-glucuronic acid, S2: N-acetyl galactosamine, S3: ΔC6S disaccharide and S4: ΔC4S disaccharide.

3.3.10 ESI-MS and MS/MS analysis of *Ps*PL8A degraded product of C4S

The supernatant containing degraded products of C4S after *Ps*PL8A treatment for 2 min, 30 min, 1 h, 2h and 24h were subjected to ESI-MS and MS/MS analyses. The ESI-MS analysis of 2 min sample showed the presence of mono sulphated unsaturated disaccharide UA-GalNAc4S with m/z 458, triply charged penta-sulphated unsaturated hexa-saccharide UA-GalNAc-$[GlcA\text{-}GalNAc]_3(4S)_5$ with m/z 508.14, triply charged tetra-sulphated unsaturated octa-saccharide UA-GalNAc-$[GlcA\text{-}GalNAc]_4(4S)_4$ as a sodium adduct with m/z 616.11 and triply charged unsaturated hexa-sulphated dodeca-saccharide UA-GalNAc-$[GlcA\text{-}GalNAc]_6(4S)_6$ as a tri sodium adduct with m/z 939.07 (Fig. 3.3.8A). The m/z values assigned to the degraded products corroborated well with CS oligosaccharides reported earlier by Zaia *et al*., 2001 and Zamfir *et al*., 2003. The ESI-MS analysis further supported the contention elucidated from the TLC data of concomitant occurrence of endo- and exo-lytic mode of *Ps*PL8A catalysis. In 30 min sample, the percent intensities of the hexa-saccharide and octa-saccharide peaks were lower as compared with that of 2 min sample, inferring the degradation of the same with time (Fig. 3.3.8B). The 1 h, 2 h and 24 h samples displayed the peak of only mono-sulphated unsaturated disaccharide with m/z 458, suggesting the complete degradation of the higher oligosaccharides by *Ps*PL8A (Fig. 3.3.8C, D & E).

Tandem MS mode can be used to differentiate the isomeric species. In order to determine the type of sulphated unsaturated disaccharide MS/MS was performed on the mono-sulphated unsaturated disaccharide with m/z 458. MS/MS of mono-sulphated unsaturated disaccharide (m/z 458) in 24 h sample showed a distinct peaks of m/z 300 which uniquely identify the ΔC4S disaccharide (ΔUA-GalNAc4S) (Fig. 3.3.8F). The results of *Ps*PL8A degraded products from C4S was in accordance with the results

reported earlier, where a detail ESI-MS analysis and MS/MS analysis of chondroitin disaccharides have been performed (Desaire *et al*., 2000; Flangea *et al*., 2009).

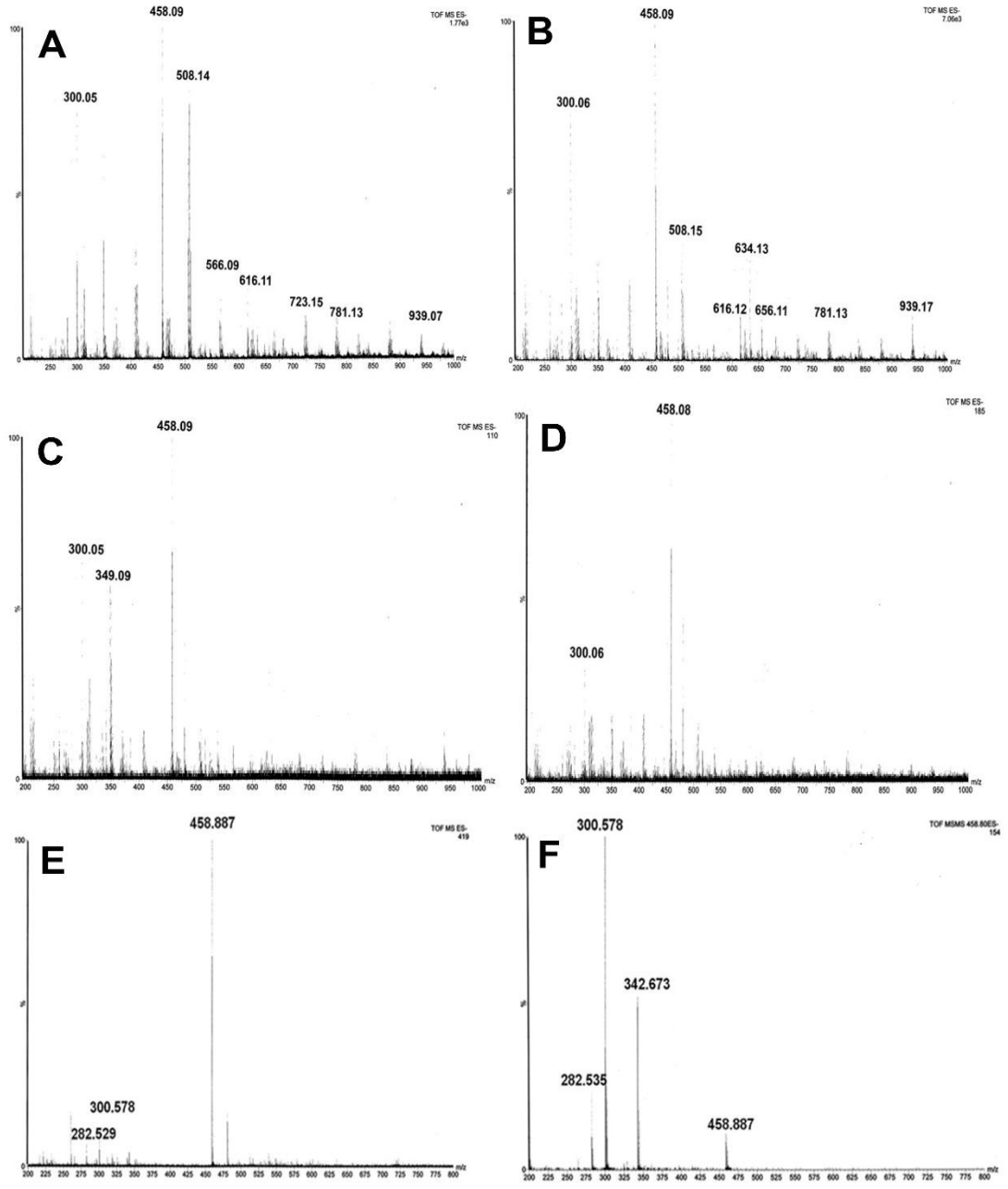

Fig. 3.3.8 ESI-Mass spectrometric analysis of *Ps*PL8A degraded product of C4S. (A) MS analysis of 2 min sample (B) MS analysis of 30 min sample (C) MS analysis of 1 h sample, (D) MS analysis of 2 h sample, (E) MS analysis of 24 h sample showing ΔC4S disaccharide (ΔUA-GalNAc4S) having single peak at *m/z* 458, (F) MS/MS analysis of ΔC4S disaccharide (ΔUA-GalNAc4S) showing a peak at *m/z* 300.

3.3.11 ^{1}H- and ^{13}C- NMR spectroscopic analysis of disaccharide from *Ps*PL8A degraded C4S

The ^{1}H-NMR and ^{13}C- spectra of chondroitin 4-sulphate disaccharide product (Fig. 3.3.9A) released after 24 h of C4S degradation by *Ps*PL8A is shown in Fig. 3.3.9B & C, respectively. The characteristic signals of the protons and ^{13}C- chemical shifts were assigned according to the previous studies done by Yamada *et al*, 1992; Huckerby *et al.*, 2001 and Lauder *et al.*, 2011. The ^{1}H-NMR spectra for ΔC4S disaccharide was recorded at 25ºC, which showed the prominent signal at 5.94 ppm for anomeric proton resonance of H-4* for GlcA ring (Fig. 3.3.9B). In the GlcA ring, the H-1* proton shows response at 5.24 ppm, while the H-2* and H-3* gave the proton responses at 3.83 ppm and 3.98 ppm, respectively. Similarly, for the GalNAc ring in the ΔC4S disaccharide the ^{1}H-NMR chemical shift of H-4, indicates the sulphation with a resonance at 4.65 ppm. The GalNAc ring has the acetylation -NAc(CH_3) which shows proton resonance at 2.08 ppm, this value corroborates well with the previous reports (Yamada *et al.*, 1992; Huckerby *et al.*, 2001; Lauder *et al.*, 2011). The correlation for rest of the protons of GalNAc ring were also made, the H-1, H-2, H-3, H-5, H-6a and H-6b show the proton resonances at 4.77 ppm, 4.14 ppm, 4.17 ppm, 4.28, 3.77 ppm and 3.70 ppm, respectively, which also showed similarity with previous reports (Yamada *et al.*, 1992; Huckerby *et al.*, 2001; Lauder *et al.*, 2011). The bulk of proton resonance of ΔC4S disaccharide lies in the range of 3.7-4.8 ppm (Fig. 3.3.9B). The results for the ^{1}H- NMR chemical shifts of ΔC4S disaccharide (ΔGlcA-GalNAc4S**)** are summarised in Table 3.3.3. The 1-D 600 MHz ^{13}C spectrum was acquired for ΔC4S disaccharide and the peaks were assigned for carbon atoms (Fig. 3.3.9C). The chemical shifts of C-1*, C-2*, C-3*, C-4*, C-5* and C-6* carbon atoms of GlcA residue were detected at 106.6 ppm,

70.32 ppm, 68.47 ppm, 106.8 ppm, 145.4 ppm and 169.15 ppm, respectively. The chemical shift of another residue GalNAc of ΔC4S disaccharide was also assigned. The acetyl (-$COCH_3$) group present in GalNAc gave the chemical shift at 22.19 ppm, while the sulphation present at C-4 gave the shift at 77.2 ppm. The chemical shift for C-1, C-2, C-3, C-5 and C-6 for GalNAc were 99.91 ppm, 58.55 ppm, 76.15 ppm, 75.67 ppm and 64.4 ppm, respectively. The carbonyl (-C=O) group present in GalNAc gave the shift at 174.69 ppm (Fig. 3.3.9C). The chemical shifts assigned to both the residues GlcA and GalNAc of ΔC4S disaccharide were in agreement with the previous reports (Yamada *et al*, 1992; Huckerby *et al*, 2001; Lauder *et al*, 2011). ^{13}C- NMR chemical shifts of ΔC4S disaccharide (ΔGlcA-GalNAc4S) are summarised in Table 3.3.4.

Table 3.3.4 ^{1}H- NMR and ^{13}C- NMR chemical shifts of ΔGlcA-GalNAc4S**.**

Residue	**Proton**	**^{1}H Chemical Shift (ppm)**	**Carbon**	**^{13}C Chemical Shift (ppm)**
GlcA	H-1*	5.24	C-1*	106.6
	H-2*	3.83	C-2*	70.32
	H-3*	3.98	C-3*	68.47
	H-4*	5.94	C-4*	106.8
			C-5*	145.4
			C-6*	169.15
GalNAc	H-1	4.77	C-1	99.91
	H-2	4.14	C-2	58.55
	H-3	4.17	C-3	76.15
	H-4	4.65	C-4	77.20
	H-5	4.28	C-5	75.67
	H-6a	3.77	C-6	64.4
	H-6b	3.70	(-$NAcCH_3$)	22.19
	(CH_3)	2.08	C=O	174.69

** mark signifies the proton and carbon atom belonging to GlcA residue*

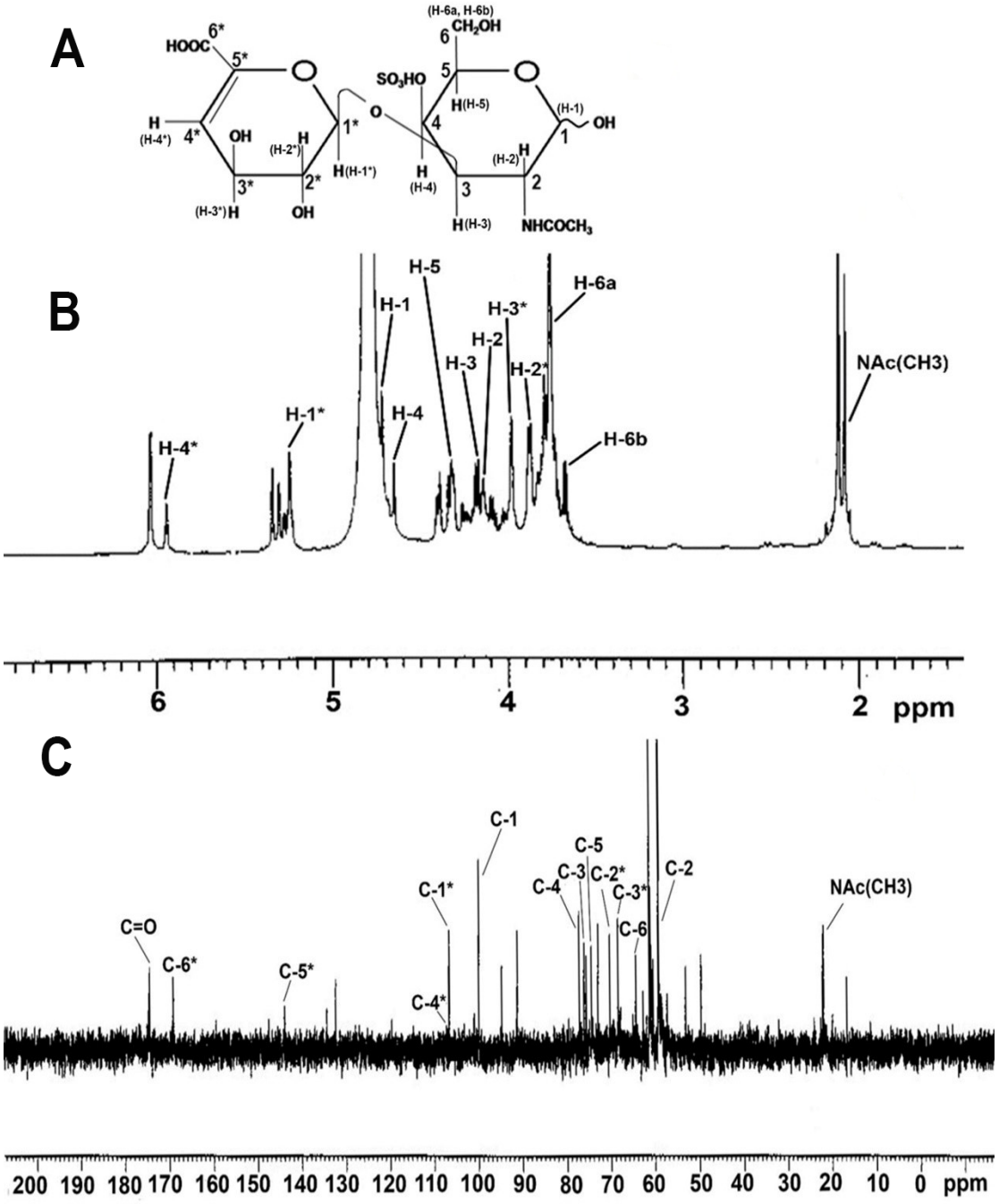

Fig. 3.3.9 (A) The chemical structure of ΔC4S (ΔUA-GalNAc4S) disaccharide (B) 1D ^{1}H-NMR spectrum (600 MHz) and (C) ^{13}C-NMR spectrum of degraded product ΔC4S (ΔUA-GalNAc4S) disaccharide obtained after 24 h reaction of 1 mg/ml C4S with *Ps*PL8A (as described in Materials and Methods).

The TLC and ESI-MS and MS/MS results conclusively demonstrated that *Ps*PL8A initially degrades the C4S substrate by a concomitant endo- and exo-lytic mode and produces higher oligosaccharides such as hexasaccharide, octasaccharide and dodecasacchride along with ΔC4S disaccharide. After ~1h of reaction the enzyme starts utilizing the higher oligosaccharides and further fragmenting them into the lowest possible oligosaccharide i.e. ΔC4S disaccharide displaying its prominent exolytic mode of catalysis in the later stage as depicted in Fig. 3.3.10.

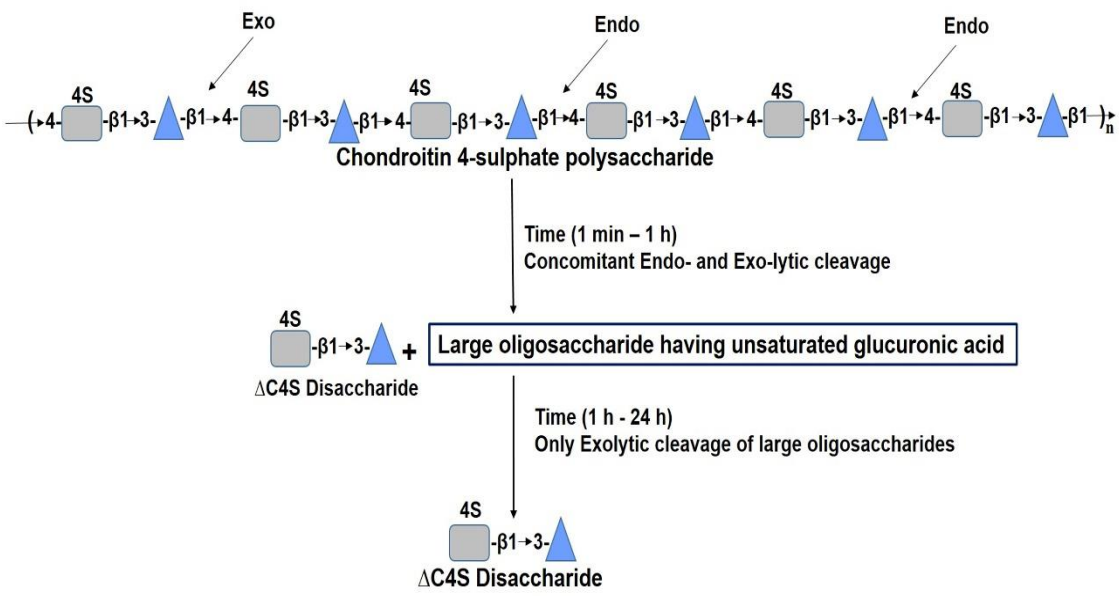

Fig. 3.3.10 Endo- and exo-lytic cleavage pattern of chondroitin 4-sulphate degradation by *Ps*PL8A. ▲ Represents the glucuronic acid residue (GlcA) and ▢ represents GalNAc residue having sulphation at 4C- position.

3.4 Conclusions

Chondroitin AC lyase (*Ps*PL8A) from *Pedobactor saltans* showed maximum enzyme activity at optimum pH 7.2 and was active within the pH range of 6.8-7.6. The optimal temperature of *Ps*PL8A was 39ºC and it showed ~100% retention of activity within the temperature range, 30 - 40ºC. *Ps*PL8A showed maximum activity with chondroitin 4-sulphate, C4S (489 U/mg) followed by chondroitin 6-sulphate, C6S (214 U/mg) and hyaluronic acid (43 U/mg). 100 mM Na^{+}, 20 mM Ca^{2+} and 20 mM Co^{2+} ions enhanced the *Ps*PL8A activity by 2 fold implying that these ions might play a role of essential cofactors. A 1.5 fold rise in enzyme activity of *Ps*PL8A was observed with 20 mM Mg^{2+} ion concentration. However, the enzyme activity of *Ps*PL8A was adversely affected at the low concentrations of Zn^{2+}, Al^{3+}, EDTA and SDS. At 5 M Urea concentration the peak of *Ps*PL8A shifted from 330 nm to 340 nm, while in presence of 3 M GuHCl the peak corresponding to *Ps*PL8A shifted from 330 nm to 341 nm indicating the loss of structural integrity of *Ps*PL8A protein. The time dependent TLC analysis of *Ps*PL8A degraded products of C4S revealed initial concomitant endo- and exo-lytic mode and later shifting to exolytic mode of catalysis. *Ps*PL8A released di-, hexa-, octa- and dodeca-saccharide as analyzed by ESI–MS and MS/MS analyses. ^{1}H- and ^{13}C-NMR analyses of C4S disaccharide confirmed the presence of N-acetylgalactosamine and glucuronic acid. The *Ps*PL8A enzyme and its degradation products unfolds the avenue for its potential applications in spinal cord nerve injury system and as antitumor, antiangiogenic, anti-metastatic agent and for immune-modulating and anti-inflammatory effects.

3.5 References

Branden, C. and Tooze, J. (1991) In Introduction to Protein Structure, (2nd ed.), Garland publishing, Taylor and Francis Group, Ney York, NY.

Cattaruzza, S. and Perris, R**.** (2006) Approaching the proteoglycome: molecular interactions of proteoglycans and their functional output. *Macromolecular Bioscience*, *6*(8), 667-680.

Creighton, T. E. (1992) In Proteins: Structures and Molecular Properties, (2nd ed.), Freeman, W. H. & Company, Macmillan Higher Education, Ney York, NY.

Denholm, E. M., Lin, Y. Q. and Silver, P. J. (2001) Anti-tumor activities of chondroitinase AC and chondroitinase B: Inhibition of angiogenesis, proliferation and invasion. European *Journal of Pharmacology*, *416*(3), 213-221.

Desaire, H. and Leary, J. A. (2000) Detection and quantification of the sulphated disaccharides in chondroitin sulfate by electrospray tandem masss pectrometry. *Journal of The American Society for Mass Spectrometery*, *11*(10), 916–920.

Flangea, C., Serb, A. F., Schiopu, C., Tudor, S., Sisu, E., Seidler, D. G. and Zamfir, A. D. (2009) Discrimination of GalNAc (4S/6S) sulfation sites in chondroitin sulfate disaccharides by chip-based nanoelectrospray multistage mass spectrometry. *Central European Journal of Chemistry*, *7*(4), 752–759.

Han, W., Wang, W., Zhao, M., Sugahara, K. and Li, F. (2014) A novel eliminase from a marine bacterium that degrades hyaluronan and chondroitin sulfate. *The Journal of Biological Chemistry*, *289*(40), 27886-27898.

Hiyama, K. and Okada, S. (1976) The mode of action of two chondroitinase-AC preparations of different origin. *Journal of Biochemistry*, *80*(6), 1201–1207.

Hong, S. W., Kim, B. T., Shin, H. Y., Kim, W. S., Lee, K. S., Kim, Y. S. and Kim, D. H. (2002) Purification and characterization of novel chondroitin ABC and AC lyases from *Bacteroides stercoris* HJ-15, a human intestinal anaerobic bacterium. *European Journal of Biological Chemistry*, *269*(12), 2934-2940.

Huang, W., Lunin, V., Li, Y., Suzuki, S., Sugiura, N., Miyazono, H. and Cygler, M. (2003) Crystal structure of *Proteus vulgaris* chondroitin sulfate ABC lyase I at 1.9 Å resolution. *Journal of Molecular Biology*, *328*(3), 623-634.

Huckerby, T. N., Lauder, R. M., Brown, G. M., Nieduszynski, I. A., Anderson, K., Boocock, J., Sandall, P. L. and Weeks, S. D. (2001) Characterization of oligosaccharides fromthe chondroitin sulfates, *European Journal of Biochemistry, 268*(5), 1181–1189.

Iozzo, R.V. (1998) Matrix proteoglycans: from molecular design to cellular function. *Annual Review of Biochemistry*, 67, 609-652.

Jandik, K. A., Gu, K. and Linhardt, R. J. (1994) Action pattern of polysaccharide lyases on glycosaminoglycan. *Glycobiology, 4*(3), 289–296.

Kale, V., Friðjónsson, Ó., Jónsson, J. Ó., Kristinsson, H. G., Ómarsdóttir, S. and Hreggviðsson, G. Ó. (2015) Chondroitin lyase from a marine Arthrobacter sp. mat3885 for the production of chondroitin sulfate disaccharides. *Marine Biotechnology, 17*(4), 479-492.

Ke, T., Zhangfu, L., Qing, G., Yong, T., Hong, J., Hongyan, R. and Shigui, L. (2005) Isolation of *Serratia marcescens* as a chondroitinase-producing bacterium and purification of a novel chondroitinase AC. *Biotechnology Letters, 27*(7), 489-493.

Lauder, R. M., Huckerby, T. N., Nieduszynski, I. A. and Sadler, I. H. (2011) Characterisation ofoligosaccharides from the chondroitin/dermatan sulphates:

^{1}H and ^{13}C NMR studies of oligosaccharides generated by nitrous acid depolymerisation. *Carbohydrate Research*, *346*(14), 2222–2227.

Li, L., Ly, M. and Linhardt, R. J. (2012) Proteoglycan sequence. *Molecular BioSystems*, *8*(6), 1613-1625.

Linhardt, R. J. (2001) Analysis of glycosaminoglycans with polysaccharide lyases. *Current Protocols in Molecular Biology*, 48, III:17.13B:17.13B. 1–17.13B.16.

Liolios, K., Sikorski, J., Lu, M., Nolan, M., Lapidus, A., Lucas, S. and Kyrpides, N. C. (2011) Complete genome sequence of the gliding, heparinolytic *Pedobacter saltans* type strain (113T). *Standards in Genomic Science*, *5*(1), 30-40.

Lojkwoska, E., Masclaux, C., Boccara, M., Robert-Baudouy, J. and Hugouvieux-Cotte-Pattat, N. (1995) Characterization of pelL gene encoding a novel pectate lyase of *Erwinia chrysanthemi* 3937. *Molecular Microbiology*, *16*(6), 1183–1195.

Lunin, V.V., Li, Y., Linhardt, R. J., Miyazono, H., Kyogashima, M., Kaneko, T., Bell, A.W. and Cygler, M. (2004) High resolution crystal structure of *Arthrobacter aurescens* chondroitin AC lyase: enzyme-substrate complex defines the catalytic mechanism. *Journal of Molecular Biology*, *337*(2), 367-386.

Ly, M., Laremore, T. N. and Linhardt, R. J. (2010) Proteoglycomics: recent progress and future challenges. *Omics: A Journal of Integrative Biology*, *14*(4), 389-399.

Pojasek, K., Shriver, Z., Kiley, P., Venkataraman, G. and Sasisekharan, R. (2001) Recombinant expression, purification, and kinetic characterization of chondroitinase AC and chondroitinase B from *Flavobacterium heparinum*. *Biochemical and Biophysical Research Communications*, *286*(2), 343-351.

Shaya, D., Hahn, B. S., Park, N. Y., Sim, J. S., Kim, Y. S. and Cygler, M. (2008) Characterization of chondroitin sulfate lyase ABC from *Bacteroides thetaiotaomicron* WAL2926. *Biochemistry, 47*(25), 6650-6661.

Shim, K. W. and Kim, D. H. (2008) Cloning and expression of chondroitinase AC from *Bacteroides stercoris* HJ-15. *Protein Expression and Purification, 58*(2), 222-228.

Steyn, P. L., Segers, P., Vancanneyt, M., Sandra, P., Kersters, K. and Joubert, J. J. (1998) Classification of heparinolytic bacteria into a new genus, *Pedobacter*, comprising four species: *Pedobacter heparinus* comb. nov. *Pedobacter piscium* comb. nov., *Pedobacter africanus* sp. nov. and *Pedobacter saltans* sp. nov. Proposal of the family Sphingobacteriaceae fam. nov. *International Journal of Systematic and Evolutionary Bacteriology*, *48*(1), 165-177.

Sugiura, N., Setoyama, Y., Chiba, M., Kimata, K. and Watanabe, H. (2011) Baculovirus envelope protein ODV-E66 is a novel chondroitinase with distinct substrate specificity. *Journal of Biological Chemistry, 286*(33), 29026-29034.

Yamada, S., Yoshida, K., Sugiura, M. and Sugahara, K. (1992) One-and two-dimensional ^{1}H-NMR characterization of two series of sulfated disaccharides prepared from chondroitin sulfate and heparan sulfate/heparin by bacterial eliminase digestion. *Journal of Biochemistry, 112*(4), 440–447.

Zaia, J. and Costello, C. E. (2001) Compositional analysis of glycosaminoglycans by electrospray mass spectrometry. *Analytical Chemistry*, *73*(2), 233–239.

Zamfir, A., Seidler, D. G., Kresse, H. and Peter-Katalini´c, J. (2003) Structural investigation of chondroitin/dermatan sulfate oligosaccharides from human skin fibroblast decorin. *Glycobiology*, *13*(11), 733–742.

Zhang, Z., Xiao, Z. and Linhardt, R. J. (2009) Thin layer chromatography for the separation and analysis of acidic carbohydrates. *Journal of Liquid Chromatography and Related Technologies*, *32*(11-12), 1711-1732.

Chapter 4

Insights into the structural characteristics and substrate binding analysis of chondroitin AC lyase (*Ps*PL8A) from *Pedobacter saltans*

4.1 Introduction

Carbohydrates are dynamic molecules that are constantly synthesized and broken down in animal and plants. There are varieties of enzymes involved in the synthesis as well as breakdown of carbohydrates. The carbohydrate-active enzymes are grouped into different families based on amino acid sequence similarity and are listed in the continually updated carbohydrate-active enzyme (CAZy) database (www.cazy.org) (Cantarel *et al.*, 2009). The carbohydrate active enzymes belonging to the polysaccharide lyase (PL) class are relatively less explored enzymes. The PL family enzymes degrade the acidic polysaccharide such as pectin, glycosaminoglycans (GAG) and alginate. GAG are highly sulphated linear and anionic polysaccharide made up of repeating disaccharide units of hexosamine and uronic acid residues (Rye *et al.*, 2002). These GAG chains are linked through glycosidic linkage to serine residue of core

protein and hence form proteoglycans (PG) (Féthière *et al.,* 1999). GAG are classified into four major classes: Chondroitin Sulphate (CS)/Dermatan Sulphate (DS), Heparin/Heparan Sulphate, Hyaluronic acid (HA) and Keratan sulphate (KS). CS consisted of N-acetyl-galactosamine (sulphated at C4/C6) linked via β-(1→3) linkage to D-glucuronic acid and the two disaccharide are linked by β-(1→4) glycosidic bond (Prabhakar *et al.,* 2005; Rani *et al.,* 2017). CS lyase catalyze the cleavage of β-(1→4) glycosidic bond between hexosamine and uronic acid residue of CS by β-elimination and generate Δ4,5 unsaturated uronate oligosaccharides that exhibits absorbance maxima at 232 nm (A_{232}) (Gacesa 1987; Rye *et al.,* 2006). The plausible mechanism proposed by Gacesa et al in 1987 includes three steps: i) negative charge present on the carboxylate anion of glucuronic acid can be neutralized by positive charge amino acid/divalent metal ion, ii) Abstraction of C-5 proton by general base and iii) β-elimination of 4-O glycosidic bond.

The crystal structures of chondroitin AC lyase (Féthière *et al.,* 1999; Lunin *et al.,* 2004), Hyaluronate lyase (Li *et al.,* 2000), chondroitin ABC lyase (Huang *et al.,* 2003) have been reported. The structural fold present in family 8 polysaccharide lyase is $(\alpha/\alpha)_{5,6}$ β toroid domain, that contains five α-helical hairpins and in some proteins a sixth hairpin is assembled from two additional antiparallel helices, one at the N-terminus and the other at the C-terminus of this domain. This domain is followed by a C-terminal antiparallel β-sandwich domain containing four β-sheets (Féthière *et al.,* 1999; Garron *et al.,* 2010). Chondroitin AC lyase from *Flavobacterium heparinum* consists of two domains, a N-terminal domain of around 300 amino acids arranged as α-helices and the C-terminal domain spanning 370 residues are configured as four antiparallel β-sheets. The N-terminal domain imparts the protein a double layered

horseshoe structure $(\alpha/\alpha)_5$ toroidal (doughnut-shaped) topology (Féthière *et al.*, 1999). The putative catalytic residues His, Tyr, Arg, Glu and Cys have been previously proposed which act as general base by abstracting C-5 proton of uronic acid and the residues acting as general acid initially neutralizes the negative charge on the carboxylate ion (Rye *et al.*, 2002). The complete mechanism of the catalysis by chondroitin lyases is still not known.

Small-angle scattering (SAS) of X-rays (SAXS) is an established powerful method for the analysis of biological macromolecules in solution. SAXS provides low-resolution, three-dimensional structures, using *ab initio* and rigid body modeling (Mertens *et al.*, 2010). It allows one to assess the oligomeric state of proteins. SAXS is a powerful tool for structure validation and is highly complementary to X-ray crystallography and NMR techniques (Mertens *et al.*, 2010). In the present study the 3-dimensional structure of *Ps*PL8A from *Pedobacter saltans* was developed by homology modeling. The structure of *Ps*PL8A in solution state was determined by SAXS. Secondary structure elements were evaluated by CD and Psipred analyses. The docking study of *Ps*PL8A with various CS ligands and site directed mutagenesis was performed to ascertain the catalytic centre and residues involved in *Ps*PL8A catalysis.

4. 2 Material and methods

4.2.1 Materials

Chondroitin 4 sulphate, Trizma base, Sodium chloride, Calcium chloride, EDTA, phenyl methane sulfonyl fluoride (PMSF), Isopropyl-1-thio-β-D-galactopyranoside (IPTG), Kanamycin and Imidazole were procured from Sigma-Aldrich USA. Genomic DNA of *Pedobacter saltans* DSM12145 was purchased from Leibniz Institute DSMZ - German Collection of Microorganisms and Cell Cultures. *Escherichia coli* DH5α cells used for transformation of recombinant plasmid and *E. coli* BL-21 (DE3) cells for expression of recombinant proteins were purchased from Novagen (Germany).

4.2.2 Sequence retrieval and alignment of *Ps*PL8A

The protein sequence of *Ps*PL8A belonging to family 8 polysaccharide lyase (PL8) from *Pedobacter saltans* DSM 12145 was retrieved from the CAZy Database (http://www.cazy.org/PL8_bacteria.html). The sequence has a GenBank accession no. ADY54337.1. BLAST analysis of the query sequence was performed with known PDB structures from X-ray or NMR data (Altschul *et al.*, 1990). The N-terminal signal peptide sequence was identified by using signalIP. *Ps*PL8A sequence was aligned with the previously reported sequence of chondroitin AC lyase sequences from *Pedobacter heparinus* (previously known as *Flavobacterium heparinum*) and *Arthrobacter aurescens*. Multiple Sequence alignment (MSA) was done by using Clustal omega (http://www.ebi.ac.uk/Tools/msa/clustalo/) available at EMBL-EBI page. The MSA sequence file was viewed under ESPript 3.0 to analyse the conserved and semi-conserved residues present in the sequence of *Ps*PL8A.

4.2.3 Homology modeling of *Ps*PL8A

The 3-Dimensional structure of *Ps*PL8A was modelled by using Modeller 9v12 (http://salilab.org/modeller/). MODELLER is used for homology or comparative modeling of protein three-dimensional structures (Webb and Sali., 2014). The comparative protein structure modeling was done based on related known templates satisfying the spatial restraints (Sali and Blundell., 1993). The query sequence *Ps*PL8A was align with the best matched template of known protein sequence, PDB id: 1CB8_A from *Pedobacter heparinus*. After the optimization of molecular probability density by modeller, 15 independent models were generated. Further refining of structure was achieved by the loop optimization method in modeller. Discrete optimized protein score (DOPE) was generated for each model after loop refinement until a negative DOPE score was attained. The modeled structure with the least DOPE score was selected as best model for further studies.

4.2.4 Structure refinement and quality assessment of modelled *Ps*PL8A

The modelled structure with least DOPE value was refined and energy minimized by using 3Drefine: Protein structure refinement server (http://sysbio.rnet.missouri.edu/3Drefine/). The spatial structure of protein is critical for predicting the biological function on basis of its structure and docking studies (Mendez *et al.,* 2005; Bhattacharya *et al.,* 2016). The 3Drefine server utilizes iterative optimization of hydrogen bonding network along with atomic-level energy minimization on the optimized model for the refinement of modeled protein structure (Bhattacharya *et al.,* 2016). The structure generated after energy minimization was validated by using structure analysis and verification server (SAVES) at NIH–MBI laboratory page (http://nihserver.mbi.ucla.edu/SAVES/). The overall compatibility of

3D model generated with its own amino acid sequence was analysed by using Verify3D. ERRAT plot was generated which determines the overall quality of modeled structure. Ramachandran plot was generated using PROCHECK, where the possible and permitted torsional angles, backbone phi (ϕ) and psi (ϕ) dihedral angles were defined. Protein Structure Analysis (ProSA) web Server (https://prosa.services.came.sbg.ac.at/prosa.php) was used to analyse steriochemical quality of modelled structure. Active site involves key amino acid residues which participate in the reaction mechanism. Generally, these residues are conserved within the family. Therefore, to identify the active site residues, we performed structure alignment of *Ps*PL8A with template protein (1CB8_A) of family PL8 using PyMOL(http://www.PyMOL.org).

4.2.5 Secondary structure of *Ps*PL8A

4.2.5.1 Secondary structure prediction tools

The secondary structure of *Ps*PL8A was predicted by using the secondary structure prediction tool PsiPred (http://bioinf.cs.ucl.ac.uk/psipred/). PsiPred software gave the percentage of the secondary structure elements, *viz*, α helices, β strands and random coils present in the structure. The topology diagram of modelled structure was generated by using PDBSum (http://www.ebi.ac.uk/thornton-srv/databases/pdbsum/Generate.html).

4.2.5.2 Circular Dichroism (CD) analysis of *Ps*PL8A

*Ps*PL8A was cloned, expressed, purified and biochemically characterized in our earlier report (Rani and Goyal., 2016). The secondary structure of *Ps*PL8A was analysed using 0.332 µM of *Ps*PL8A in 50 mM Tris-HCl, pH 7.2. CD spectrum of *Ps*PL8A was recorded in the Far UV range (190-250 nm) on a spectropolarimeter (J-

815, Jasco Corporation, Tokyo) at 25°C using a sample cell with path length of 0.1 cm. The CD spectrum was collected at a scanning rate of 50 nm/min and 1 nm bandwidth with an average of six scans. The CD spectra was corrected for buffer contributions and the percentage of different secondary structures present in *Ps*PL8A were determined by using K2D3 server (http:// k2d3.ogic.ca/). The molar residual ellipticity (mre) was calculated from the ellipticity (θ) values at each wavelength (Kelly *et al.,* 2005). The mre values were analysed from 190 to 240 nm by K2D3 server. The data of secondary structure of *Ps*PL8A observed by CD analysis were compared with that obtained from PsiPred prediction.

4.2.6 Molecular docking studies of *Ps*PL8A

Molecular docking analysis of *Ps*PL8A was performed using Autodock 4.2.1. along with the viewer MGLTools1.5.6 (http://mgltools.scripps.edu/). Autodock uses novel and robust docking method by implementing new scoring function that estimates the free energy change during ligand binding (Goodsell *et al.,* 1990). Chondroitin 4-sulphate disaccharide, chondroitin 4-sulphate tetrasaccharide and chondroitin 6-sulphate disaccharide were used as docking ligand. Ligand PDBs were obtained from pubchem (http://pubchem.ncbi.nlm.nih.gov) or from ligand were drawn in chemsketch and converted into PDB files by OpenBabel 2.3.2a software. At first, the PDB files of protein and ligand were converted to PDBQT files by assigning gasteiger charges. Thereafter, non-polar hydrogens were merged and their charges were assigned to carbon atoms. Grid box having dimension of 52, 92, 84 (*x*, *y*, *z* coordinates) with 0.375 Å grid point spacing was assigned around active site. Lamarckian Genetic Algorithm (LGA) was implemented for docking simulation and conformational search (Morris *et al.*, 1998). Number of GA runs was set to 100. All other parameters were set to default

and the different conformations were generated. The best conformation was selected after evaluating the lowest binding energy of each conformation. The docked conformation and interaction energies were saved and analyzed for protein-ligand complex with a minimum lowest free energy of binding (Δ G). The generated protein-ligand complexes were viewed in SPDB viewer (Guex and Peitsch., 1997) and PyMOL (http://www.PyMOL.org) to detect the hydrophobic interactions and polar contacts.

4.2.7 Protein melting studies of *Ps*PL8A

The protein melting curve of *Ps*PL8A was generated by subjecting the recombinant protein to varying temperatures and thereafter measuring the change in the absorbance at 280 nm (A_{280}) by a UV-Visible spectrophotometer (Varian, Carry 100-Bio) following the method described previously (Dvortsov *et al.*, 2009). 30 µg of purified *Ps*PL8A in 1 ml 50 mM Tris-HCl, buffer, pH 7.2 was used. The absorbance at 280 nm (A_{280}) was measured by increasing the temperature at 5°C per min from 25°C to 100°C using a peltier temperature controller. The protein solution was kept at a particular temperature for 3 min to attain the equilibrium and the melting curve of *Ps*PL8A was acquired. The melting curve of *Ps*PL8A was also studied in presence of 20 mM Ca^{2+} ion or 5 mM EDTA. A curve of absorbance at 280 nm versus temperature was plotted to generate the melting profile of *Ps*PL8A.

4.2.8 Structure analysis of *Ps*PL8A in solution by Small Angle X-ray Scattering (SAXS)

4.2.8.1 SAXS data acquisition

The SAXS data for the *Ps*PL8A were collected using a one-dimensional CMOS Mythen detector (Dectris, Baden, Switzerland) on the SAXSpace instrument (Anton Paar GmbH, Graz, Austria). The radiation wavelength and the ratio of the sample to-

detector distance were set to 1.5418 Å and 317 mm, respectively. For SAXS measurement, *Ps*PL8A (12 mg/ml) was used and passed through 0.22 µm filter (Millipore, USA). The sample was centrifuged at 24,000***g*** for 15 min at 4 °C prior to acquiring the scattering data. Two frames of 30 min at 10°C were collected using 60 µl of *Ps*PL8A was used in a thermostated quartz capillary having 1 mm diameter. The images recorded on the CMOS Mythen detector were reduced in SAXStreat software to calibrate the position of the primary beam. SAXSquant software was used to subtract buffer contribution to obtain the scattering intensity I, as a function of momentum-transfer vector s ($s= 4\sin\theta/\lambda$ where λ and θ represent the wavelength of the X-rays and the scattering angle, respectively.

4.2.8.2 SAXS data processing

Initial data processing was done using PRIMUS software. The radius of gyration, Rg was computed from Guinier equation (Guinier *et al.,* 1995) and by indirect Fourier transform method using Gnom package (Semenyuk *et al.,* 1991). The distance distribution function p(r) also was calculated using Gnom, and the maximum diameter, D_{max} was obtained. The *ab initio* method was used to determine the low resolution shapes of the *Ps*PL8A from the scattering curve by Dammif (Franke and Svergun 2009). The reconstructions of *Ps*PL8A were performed using 20 independent runs of Dammif. These solutions were subsequently checked by Damaver to create the final *ab initio* shape (Volkov *et al.,* 2003). The modeled structures of the *Ps*PL8A were positioned in the envelopes using PyMOL.

4.2.9 Site directed mutagenesis of *Ps*PL8A by Megaprimer PCR method

4.2.9.1 Cloning of *Ps*PL8A mutants

Five mutants *viz*. N153A, H203A, Y212F, R266A and E349A were generated on the basis of the identified residues involved in active site of *Ps*PL8A. The site-directed mutagenesis was performed by megaprimer PCR approach (Ke *et al.*, 1997). Primers designed to introduce single amino acid mutation were prefabricated with *NheI* and *XhoI* restriction enzyme sites. The details of primers used for mutants are listed in Table 4.2.1. The PCR was carried out in two steps to introduce the single point mutations and 2037 bp amplicon was amplified for each mutant. The PCR amplification condition and reaction set up are given in Table 4.2.2 and Table 4.2.3, respectively. The PCR products and vector pET28a(+) were digested with *NheI* and *XhoI* enzymes and were ligated in 3:1 ratio of vector: insert. The ligation mix was incubated overnight at 16ºC. 5 µl of ligated product was transformed using 200 µl of *E. coli* DH5α competent cells prepared earlier. Cells were plated on LB agar plate containing kanamycin (50 µg/ml) and incubated at 37ºC overnight under static condition. The colonies were picked and grown on 5 ml LB broth containing Kanamycin at 37ºC 180 rpm for 12h. The grown culture was centrifuged at 8000g at 4°C for 10 min and the recombinant plasmid was isolated by Non-ionic detergent (NID) method (Lezin *et al.*, 2011). The clone for the mutants *viz.* N153A, Y212F, H203A, R266A and E349A were screened by restriction digestion of respective plasmids.

Table. 4.2.1 Details of Primers used for site-directed mutagenesis.

Primer	Primer sequence
FPL8A	CGCGCTAGCCAAAAGCAGACATTTGAACTGATTATGGGGCG CGTAGCC
RN153A	GTAAAGCAATATCCGTTTTGGCGGCTCCGGTTTTTTTCTCGG
RH203A	TATAGCTGTGGCCCGGCTTGCATATAAGAGTAATCATATTGC AAAC
RY212F	TAAACCGCTCCGAAACCAGAGATGTATAGCTGTGGC
RR266A	TTTCCTGCTAATCCCTGCTCCCTCTACGTTAAAATCGATATAT TTTGAC
FE349A	CAGTAACAGAACCAATAGAAGCGCATCTGGTAATAAGGAAA ATTTGT
RPL8A	GCGCCTCGAGTTAAACTTTTTCTGATTTGGTAGAACCTTTAT ATGGCCCAGTCGG

Table. 4.2.2 PCR amplification conditions for site directed mutagenesis.

Mutant	1st PCR (T_m in °C)	1st PCR amplicon (bp)	2nd PCR (T_m in °C)	2nd PCR amplicon (bp)
N153A	57	459	63	2037
H203A	59	609	63	2037
Y212F	61	636	63	2037
R266A	59	798	63	2037
E349A	61	1047	63	2037

Table. 4.2.3 PCR reaction setup

Reaction Component	Final Concentration	Volume Used (µl)
10X Reaction Buffer	1x	1.0
10mM dNTPs	1 mM	0.8
Template (genomic DNA, 2.2ng/ µl)	pg/µl	1.0
Forward Primer	0.5 µM	0.5
Reverse Primer	0.5 µM	0.5
Taq DNA Polymerase (NEB)	0.025 U/ µl	0.5
Nuclease Free Water	-	5.7
Total Reaction Volume		10 µl

4.2.9.2 Expression and purification of *Ps*PL8A mutants

E. coli BL21 (DE3) cells were used as host for expression of the mutants *viz.* N153A, Y212F, H203, E349A and R266A. The expression of R266A was not found in *E.coli* BL-21 cells, so its expression was further studied in *E.coli* BL-21 pLysS cells. The cells were grown in 100 ml LB medium supplemented with kanamycin (50 µg/ml) incubated at 37ºC with shaking at 180 rpm to mid exponential phase till the absorbance at 550 nm (A_{550}) reached 0.6. At this point isopropyl-1-thio-β-D-galactopyranoside (IPTG) was added to a final concentration of 1.0 mM and culture was incubated at 24°C with shaking at 180 rpm. The cells were harvested by centrifugation at 8,000 g and 4°C for 10 min. The cell pellet was resuspended in 5 ml of 50 mM Tris-HCl buffer, pH 7.2 containing 1 mM phenyl methane sulfonyl fluoride (PMSF). The cells were sonicated (Sonics, vibra cells) by keeping on ice for 30 min with 10 s on and 15 s off pulse at 33% amplitude. The sonicated cells were centrifuged at 18,000***g*** and 4ºC for 45 min. The cell free supernatant was subjected to immobilized metal ion affinity chromatography (IMAC) for purification. The cell free extract was filtered through a 0.45 mm membrane and loaded on to a 1 ml HiTrap chelating column (GE Healthcare) equilibrated with 50 mM Tris-HCl buffer, pH 7.2 containing 300 mM NaCl and 60 mM imidazole. After extensively washing the column with 50 ml of same buffer the bound protein was eluted with 50 mM Tris-HCl buffer, pH 7.2 containing 300 mM NaCl and 350 mM Imidazole. SDS polyacrylamide gel electrophoresis (10.5% w/v) was used to assess the molecular weight and purity of recombinant *Ps*PL8A mutant proteins.

4.2.9.3 Activity assay of *Ps*PL8A mutants with chondroitin 4-sulphate substrate

The enzyme assay of wild type *Ps*PL8A and mutants were performed by incubating 0.15 µg of enzyme in 1 ml reaction mixture by containing 1 mg/ml of C4S substrate at optimum reaction conditions in 50 mM Tris-HCl buffer, pH 7.2 at 39°C for 5 min (Rani and Goyal. 2016). The unsaturated oligosaccharide product formation was monitored by an increase in the absorbance at 232 nm (A_{232}) as a function of time on a UV-Visible spectrophotometer (Varian, Cary 100). The absorbance observed was converted to units using molar absorption coefficient (3800 M^{-1} cm^{-1}) for Δ4,5 unsaturated double bond formed in the reaction. One unit of enzyme activity was defined as amount of enzyme that liberates 1 µmol of unsaturated oligosaccharides product per min as calculated using a molar absorption coefficient of 3800 M^{-1} cm^{-1} (Pojasek *et al.*, 2001).

4.2.9.4 Ligand binding studies of mutants by Isothermal Titration Calorimetry (ITC)

The binding of *Ps*PL8A mutants, Y212F and H203A with C4S polysaccharide was quantified by ITC (MICROCAL iTC 200, Malvern UK) using protocol described by Bolam *et al.*, 2004. Titration of mutant proteins and C4S polysaccharide was carried out using 50 mM Tris-HCl buffer, pH 7.2 at 25°C. the reaction cell was filled by protein (Y212F or H203A) at a concentration of 80 µM, while the syringe was filled with 20 mg/ml (0.2%, w/v) of C4S polysaccharide.

4.3 Results and discussion

4.3.1 Sequence analysis of *Ps*PL8A

The BLAST analysis of PsPL8A sequence having GenBank accession no. ADY54337.1 from *Pedobacter saltans* displayed the sequence similarity with previously characterized chondroitin AC lyase. *Ps*PL8A showed 55% sequence identity and 95% query coverage with chondroitinase AC from *Flavobacterium heparinum* (1CB8_A). *Ps*PL8A further showed 26% and 25% sequence identity with chondroitin AC lyase belonging to *Streptomyces coelicolor* A3 (2WDA_A) and *Arthrobacter aurescens* (1RW9_A), respectively. Multiple sequence alignment of *Ps*PL8A with the above mentioned chondroitin AC lyase sequences gave critical information about the conserved and semi conserved amino acid residue regions (Fig. 4.3.1). The SignalP 3.0 server deduced a N-terminal signal peptide sequence with a cleavage site between Ala22 and Gln23. The signal peptide consisted of 22 amino acids from N-terminal and consisted of a 679 amino acid *Ps*PL8A domain.

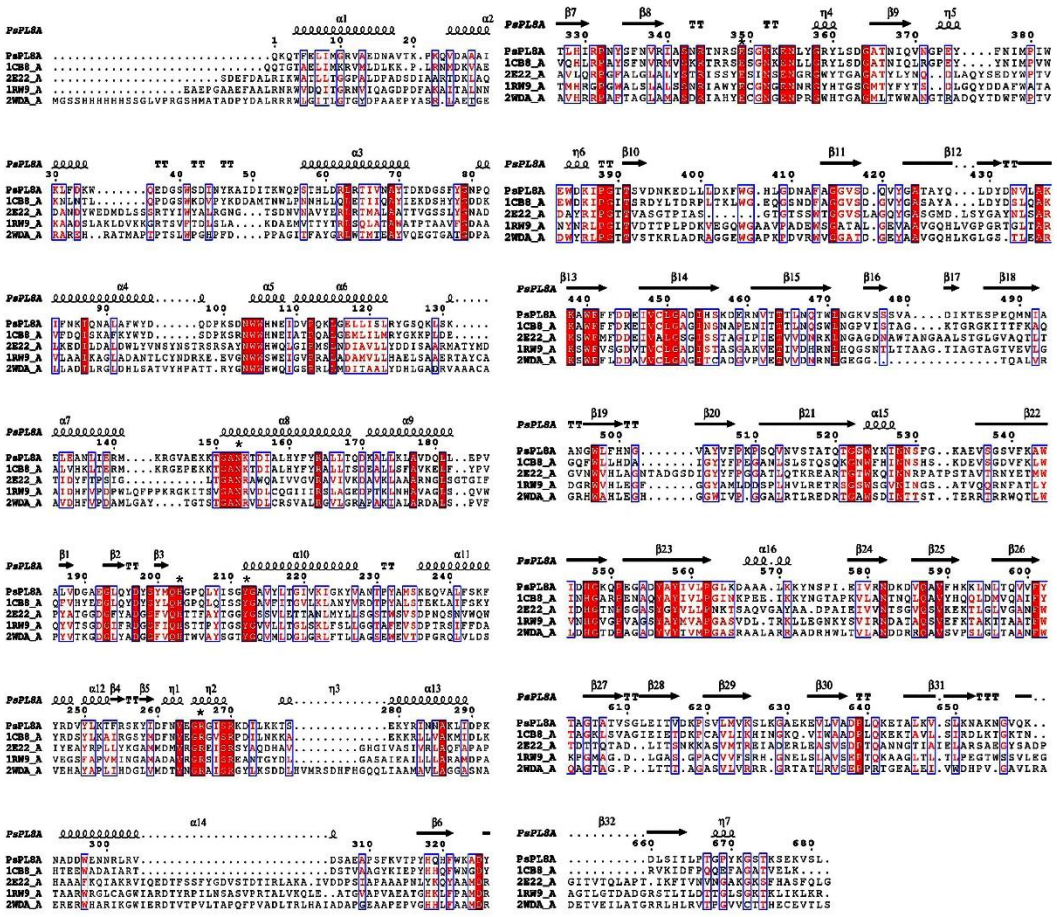

Fig. 4.3.1 Multiple sequence alignment of *Ps*PL8A from *Pedobacter saltans* with chondroitin AC lyases from *Flavobacterium heparinum* (1CB8_A), *Arthrobacter aurescens* (1RW9_A), *Streptomyces coelicolor* A3 (2WDA_A) and xanthan lyase from *Bacillus Sp* (2E22_A). The conserved residues are shown in red background and semi conserved residues are shown in box. Conserved catalytic residues are marked as asterisks. The figure was developed by EsPript3.0 (http://espript.ibcp.fr/).

4.3.2 Homology modeling and structure validation of *Ps*PL8A

Modeled structure of *Ps*PL8A showed that it consists of two domains, a N-terminal domain having $(\alpha/\alpha)_6$ toroidal topology and C-terminal made up of antiparallel β-sheet folding structure (Fig. 4.3.2A). This $(\alpha/\alpha)_6$ toroidal fold and antiparallel β-sandwich structure are the conventional fold being assigned to the PL8 family (Féthière *et al.*, 1999; Lunin *et al.*, 2004; Garron and Cygler., 2012). The N-terminal of *Ps*PL8A

is made up of nearly 330 amino acids forming a doubly layered horseshoe shaped or open toroid structure. The rest of 350 amino acids fold in a four layered β sandwich structure forming a C-terminal of *Ps*PL8A. The twelve alpha helices (α1-α12) in N-terminal are arranged in $(\alpha/\alpha)_6$ incomplete toroidal fold and these helices are linked with each other by the random coils. C-terminal is made up of β sheets with an exception of small α helix present between the β sheet S3 and S4. The chondroitin AC lyase from *Flavobacterium heparinum* also revealed the presence of small α helix in its C-terminal domain (Féthière *et al.*, 1999). The N-terminal and C-terminal domain of *Ps*PL8A are linked by helix α12 and β sheet (S1) through the random coils. The quality of modeled structure after energy minimization was assessed on the tools available at SAVES server. Ramachandran plot developed by PROCHECK displayed that 98.5% residues were in the favoured region, 1.2% in the generously allowed region while only 0.5% of the residues were in the disallowed region (Fig. 4.3.2B). This implied that dihedral angles, phi (ϕ) and psi (ψ) of the modeled *Ps*PL8A structure have occupied favourable positions. The ERRAT plot also confirmed that modeled structure of *Ps*PL8A to be of satisfactory quality, with a quality factor of 90.89% (Fig. 4.3.2C). ProSA results indicate that the modelled protein is error free and reside in the x-ray zone with a score of -9.45 (Fig. 4.3.2D). The active site residues of *Ps*PL8A involved in catalysis were obtained by superposing the modeled *Ps*PL8A with the available structure of chondroitin AC lyase from *Flavobacterium heparinum* 1CB8_A. The superposition showed that the critical active site residues were conserved and aligned spatially. Asp153, His203, Tyr212, Arg266 and Glu349 were the active site residues of *Ps*PL8A (Fig. 4.3.3).

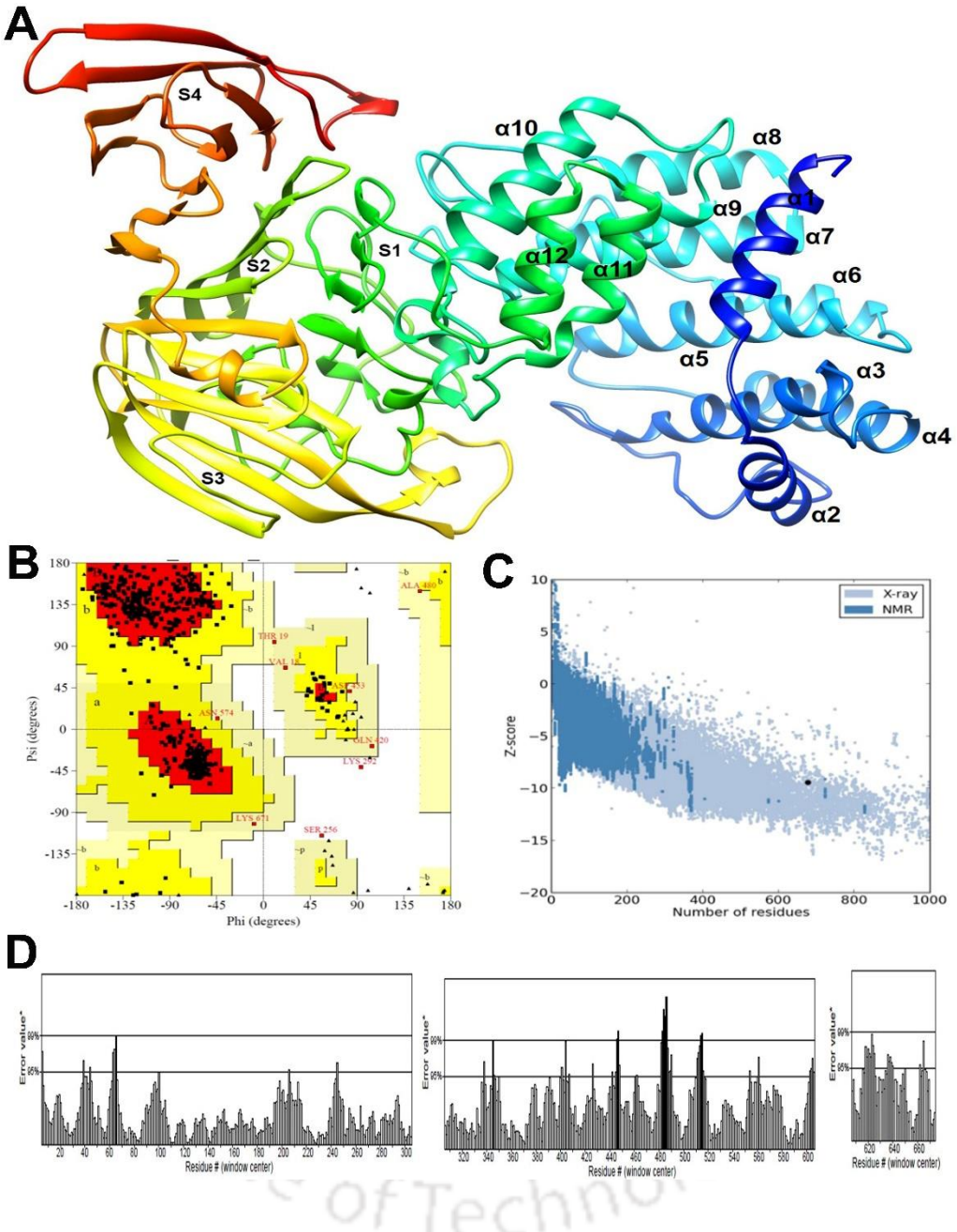

Fig. 4.3.2 Three dimensional predicted structure of *Ps*PL8A. (A) Cartoon representation of the modelled *Ps*PL8A structure, displaying two domains, a N-terminal domain having $(\alpha/\alpha)_6$ toroidal topology and C-terminal made up of antiparallel β-sheet folding structure. Quality assessment of modeled *Ps*PL8A structure by (B) Ramachandran plot. (C) ERRAT plot. (D) Z-score plot by ProSA-web server.

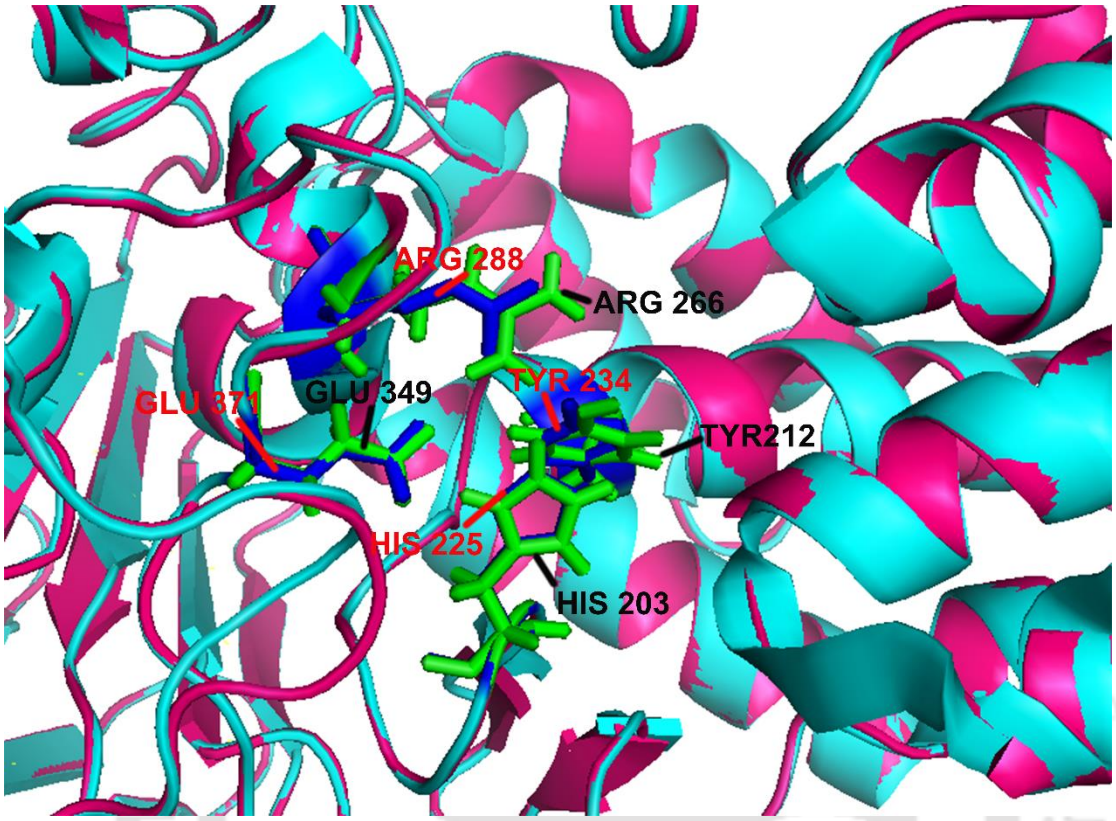

Fig. 4.3.3 Superposition of modeled structure of *Ps*PL8A (shown in magenta) with chondroitin AC lyase (1CB8_A) (shown in light-blue) from *Flavobacterium heparinum* showing the binding cleft. The residues from the binding cleft of *Ps*PL8A are marked in green and those from chondroitin AC lyase (1CB8_A) are marked in dark blue. The figure was generated using the PyMol program (http://www.pymol.org).

4.3.3 Secondary structure analysis of *Ps*PL8A by Psipred and CD

The secondary structure prediction analysis of *Ps*PL8A was done by using the Psipred software. The predicted secondary structure of *Ps*PL8A showed it contains 24.92% α helices, 21.68% β sheets and 53.4% random coils (Fig. 4.3.4) (Table. 4.3.1). Circular dichroism (CD) analysis was performed using K2D3 server and the CD spectrum of *Ps*PL8A was compared with the secondary structure of previously available proteins (Jeune *et al.,* 2012). The CD spectrum of *Ps*PL8A revealed that it contains 27.31% α helices, 22.7% β sheets and rest 49.9% random coils (Fig. 4.3.5). (Table. 4.3.1). The results of Psipred for secondary structural element of *Ps*PL8A well

corroborated with those of CD analysis. The results from the homology modeling of *Ps*PL8A also showed the presence of the α helices rich N-terminal domain and C-terminal consisting predominantly of β sheets. The overall structure of *Ps*PL8A matches well with previously solved crystal structure of chondroitin AC lyase form *Flavobacterium heparinum* and *Arthrobacter aurescens* (Féthière *et al.*, 1999; Lunin *et al.*, 2004). The results of Psipred and CD analyses further consolidate the authenticity of modeled *Ps*PL8A structure.

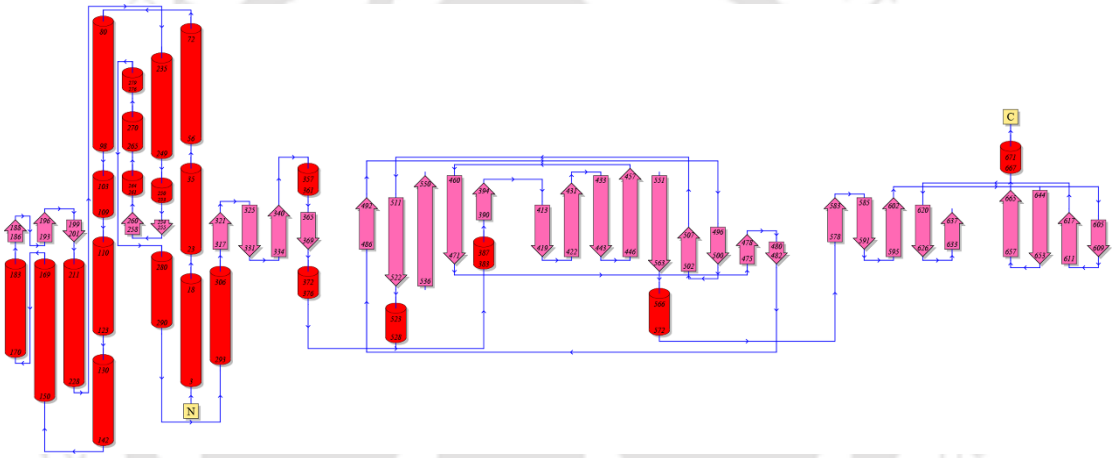

Fig. 4.3.4 Topology diagram of modelled *Ps*PL8A displaying the orientation of the secondary structures (thick arrows represent the β-strand and cylinders represent α-helix).

Table 4.3.1 Secondary structure elements of *Ps*PL8A.

Secondary structure element	Percentage predicted by PSIPRED	Percentage analysis by CD spectrum
α helix	24.92	27.31
β strand	21.68	22.70
random coils	53.40	49.99

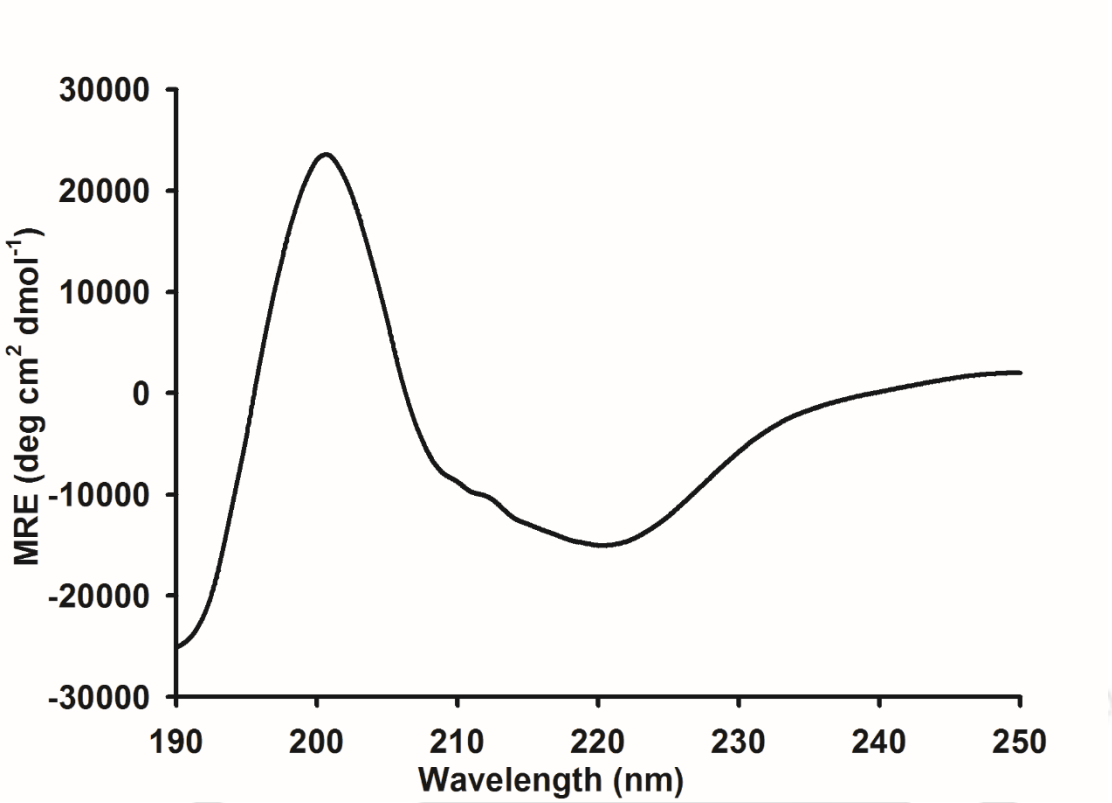

Fig. 4.3.5 Far UV CD spectrum of *Ps*PL8A.

4.3.4 Protein melting study of *Ps*PL8A

The melting curve of *Ps*PL8A displayed a single peak at 60°C. The protein starts unfolding at 45ºC and as the temperature increases it completely melts at 60ºC (Fig. 4.3.6). In our previous biochemical characterization study of *Ps*PL8A (Rani and Goyal., 2016), it was observed that the enzyme activity get enhanced by 2 fold in presence of 20 mM Ca^{2+} ions. Therefore, melting study of *Ps*PL8A was also studied in presence of 20 Mm Ca^{2+} ion, but there was no change in the melting temperature. This indicated that Ca^{2+} ion enhances only the enzyme activity of *Ps*PL8A but does not impart any structural stability to it. Melting study of *Ps*PL8A with 5 mM EDTA showed that it starts unfolding at 42ºC and gets completely melts at 52 ºC. This 8ºC decrease in

melting temperature of *Ps*PL8A in presence of EDTA might be due to chelation of the inherent divalent metal ion present in the protein structure.

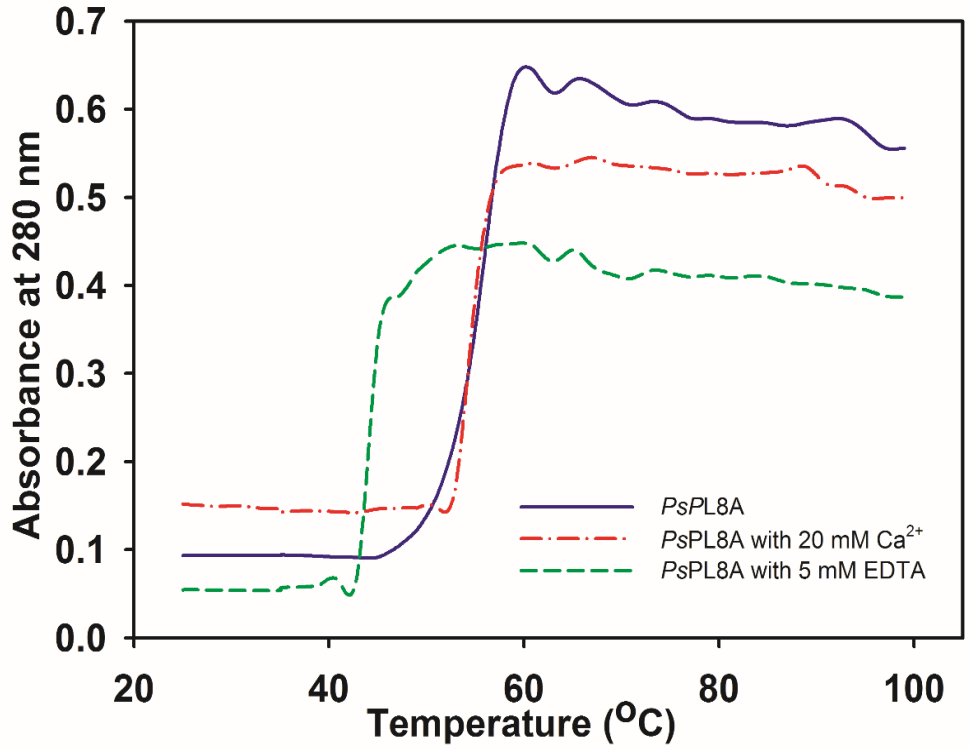

Fig. 4.3.6 Protein-melting analysis displaying melting curve of *Ps*PL8A (——), in presence of 20 mM Ca^{2+} ions (-·-·-) and of 5 mM EDTA (---).

4.3.5 Docking analysis and ligand binding interaction of *Ps*PL8A

The previously reported cocrystal structure of chondroitin AC lyase from *Flavobacterium heparinum* with CS/DS oligosaccharide (Huang *et al.*, 2001; Lunin *et al.*, 2004) and *Arthrobacter aurescens* (Féthière *et al.*, 1999) guided the location of catalytic core and conserved active site residues of *Ps*PL8A. The docking of *Ps*PL8A with C4S disaccharide (Fig. 4.3.7A), C6S disaccharide (Fig. 4.3.8A) and C4S tetrasaccharide (Fig. 4.3.9A) was performed to obtain best fit conformation of the ligands. The result of docking studies is summarized in Table 4.3.2. The docking analysis of *Ps*PL8A showed best binding affinity with C6S disaccharide with binding

energy of -8.00 kcal/mol followed by C4S disaccharide (-7.40 kcal/mol) and C4S tetrasaccharide (-7.20 kcal/mol). The ligand binding study of *Ps*PL8A with C4S disaccharide revealed that substrate binding cavity is formed by α10, α11, α12 helices of N-terminal $(\alpha/\alpha)_6$ incomplete toroid domain and is enclosed by the loop region from the C-terminal (Fig. 4.3.7B & C). The catalytic core is majorly formed by the N-terminal α-helical domain and is broad enough to hold the CS polysaccharide chain. The presence of basic amino acids such as His203, Arg 266, Arg 270, Lys 271 and Lys 276 residues in the catalytic cavity might create the positive charge and hence contribute to the binding of acidic CS polysaccharide. The presence of basic residues (His225, Arg288, Arg292, Lys298 and Lys 299) was also observed in the catalytic core of chondroitin AC lyase from *Flavobacterium heparinum* (Féthière *et al.*, 1999). His203 and R266 residues of *Ps*PL8A lies in the stretch of well conserved residues and corresponds to the His225 and R288 of chondroitin AC lyase from *Flavobacterium heparinum* (Féthière *et al.*, 1999). The aromatic residues such as Trp105, Tyr208 and Tyr 212 might help in the accommodation of the sugar ring of the CS substrate. The docking analysis of *Ps*PL8A was also studied with C6S disaccharide (Fig. 4.3.8B & C) and C4S tetrasaccharide (Fig. 4.3.9B & C). This docking study showed that polar interactions taking place between active site amino acid residues and the ligand molecule (Table. 4.3.2). The docking result inferred that Asn153, His203, Tyr212, Arg266, Glu349 are the key catalytic residues of *Ps*PL8A. A similar catalytic tetrad including His225, Tyr234, Arg288 and Glu371 were reported in the chondroitin AC lyase from *Flavobacterium heparinum.* In addition to these critical active site residues, there are several other residues in *Ps*PL8A, such as Trp105, Tyr 208, Gly211, Val215

and Arg270 that are proximal to the CS substrate and hence could play a key role in positioning the substrate for enzyme action.

Table. 4.3.2 Amino acid residues of *Ps*PL8A showing polar interaction and residues within 4Å of distance around the ligand at docking site.

Ligand	Binding Energy (kcal/mol)	Polar Interactions	Residues within 4Å
C6S disaccharide	-8.0	His 203, Gly211,Val 215, Arg266, Gly267, Arg270, Asn352, Trp 405	Asn 103, Trp105, Asn 153, Tyr 208, Tyr212, Gly265
C4S disaccharide	-7.4	Asn103, Asn153, Tyr212, Arg266, Arg270, Asn 352,	Trp 105, Val215, Lys271, Ile 273, Trp 405, Phe531
C4S tetrasaccharide	-7.2	Gly211, Ala214, Glu264, Gly267, Arg270, Lys275	Ile 51, Asn 103, Trp 105, His106, Tyr212, Val215, Arg266, Asn 352

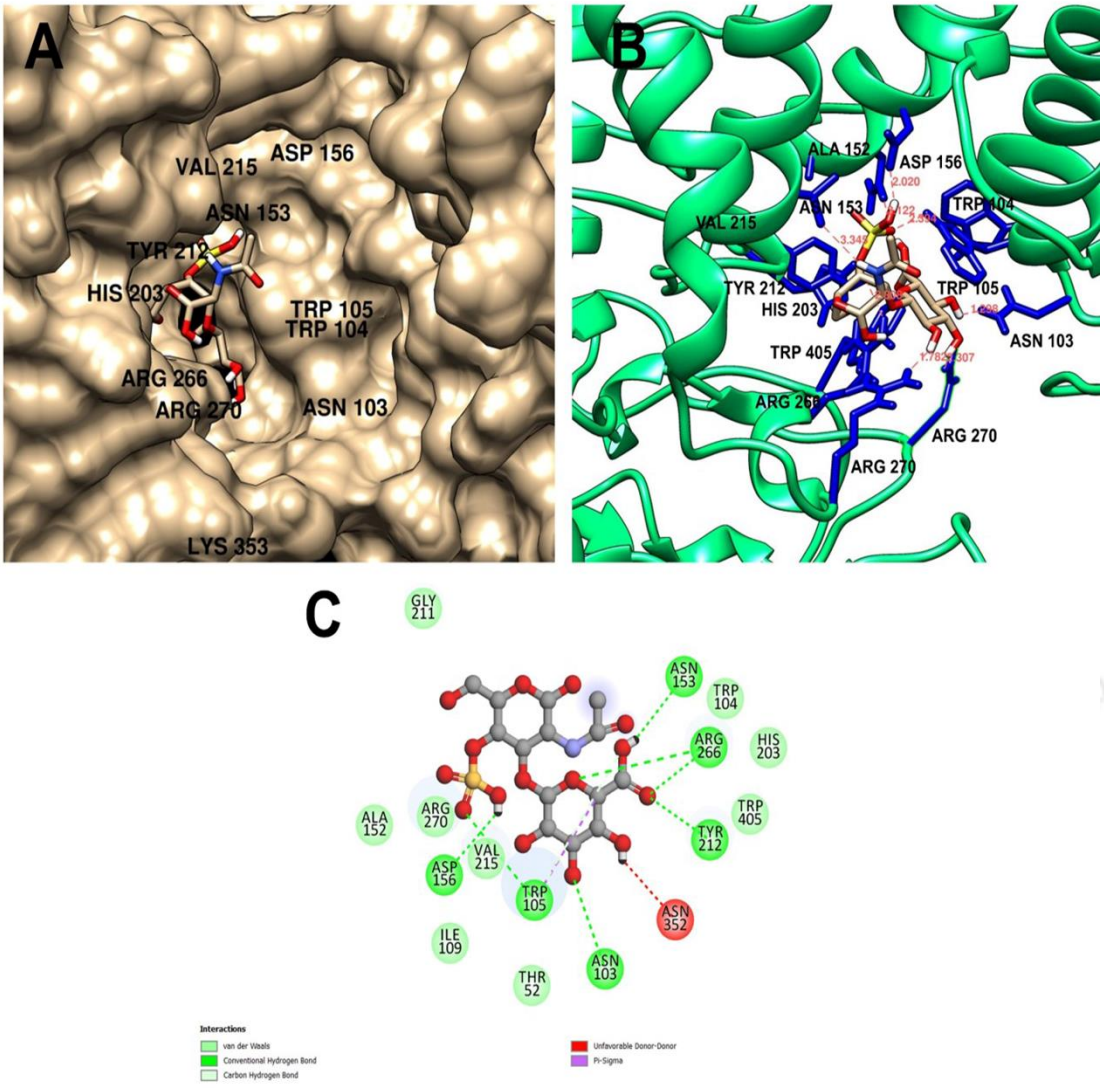

Fig. 4.3.7 (A) Surface view of the active site cleft of *Ps*PL8A showing the binding with ligand C4S disaccharide (B) C4S disaccharide interacting with the active site amino acid residues of *Ps*PL8A. (- - -) represents the hydrogen bond and the residues labelled are within 4Å radius forming hydrophobic interaction with the ligand, (C) 2D LigPlot of C4S disaccharide interacting with the active site amino acid residues of *Ps*PL8Agenerated in Discovery studio visualizer-Accelrys.

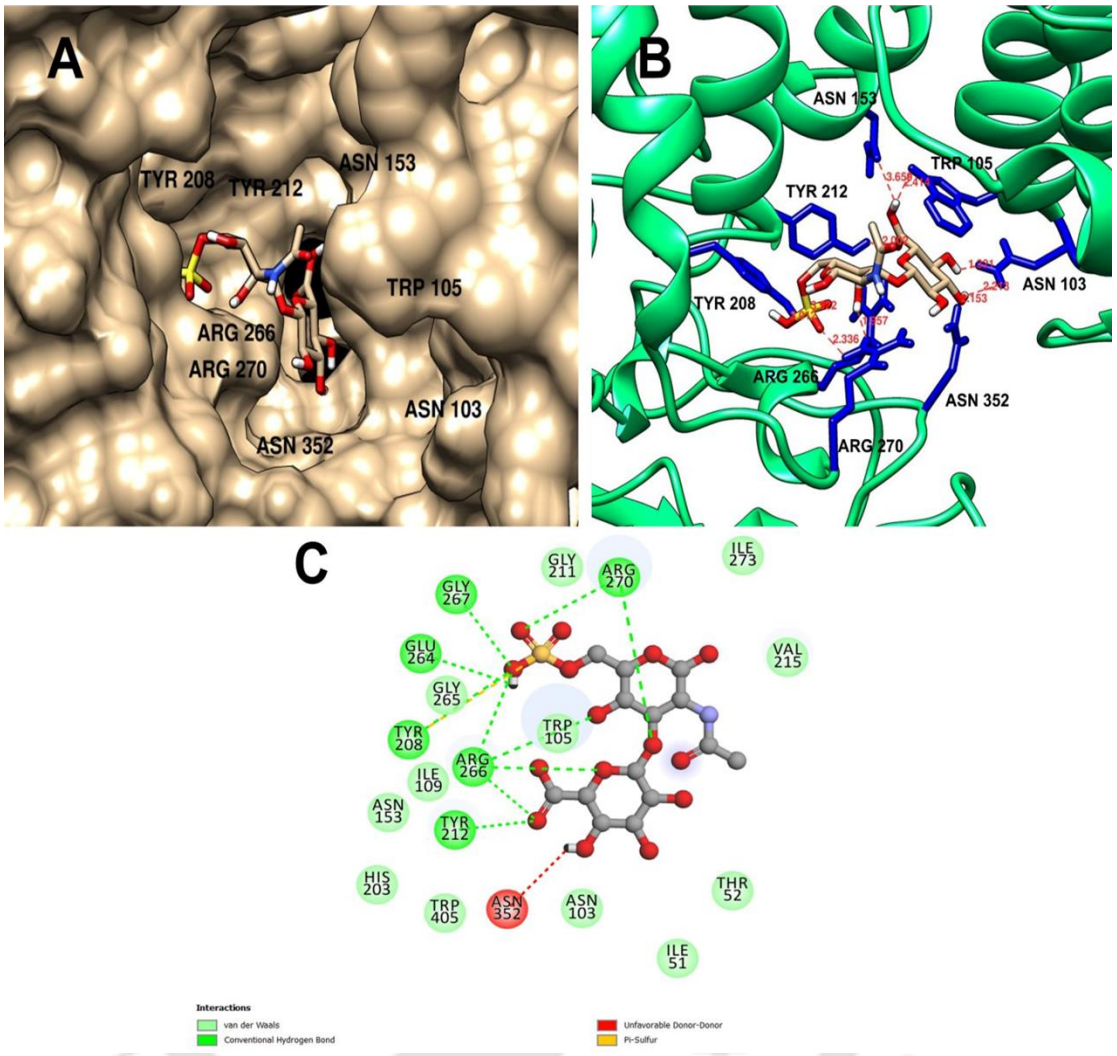

Fig. 4.3.8 (A) Surface view of the active site cleft of *Ps*PL8A displaying the binding with ligand C6S disaccharide (B) C6S disaccharide interacting with the active side amino acid residues of *Ps*PL8A. (- - -) represents the hydrogen bond and the residues labeled are within 4Å radius forming hydrophobic interaction with the ligand, (C) 2D LigPlot of C6S disaccharide interacting with the active site amino acid residues of *Ps*PL8A generated in Discovery studio visualizer-Accelrys.

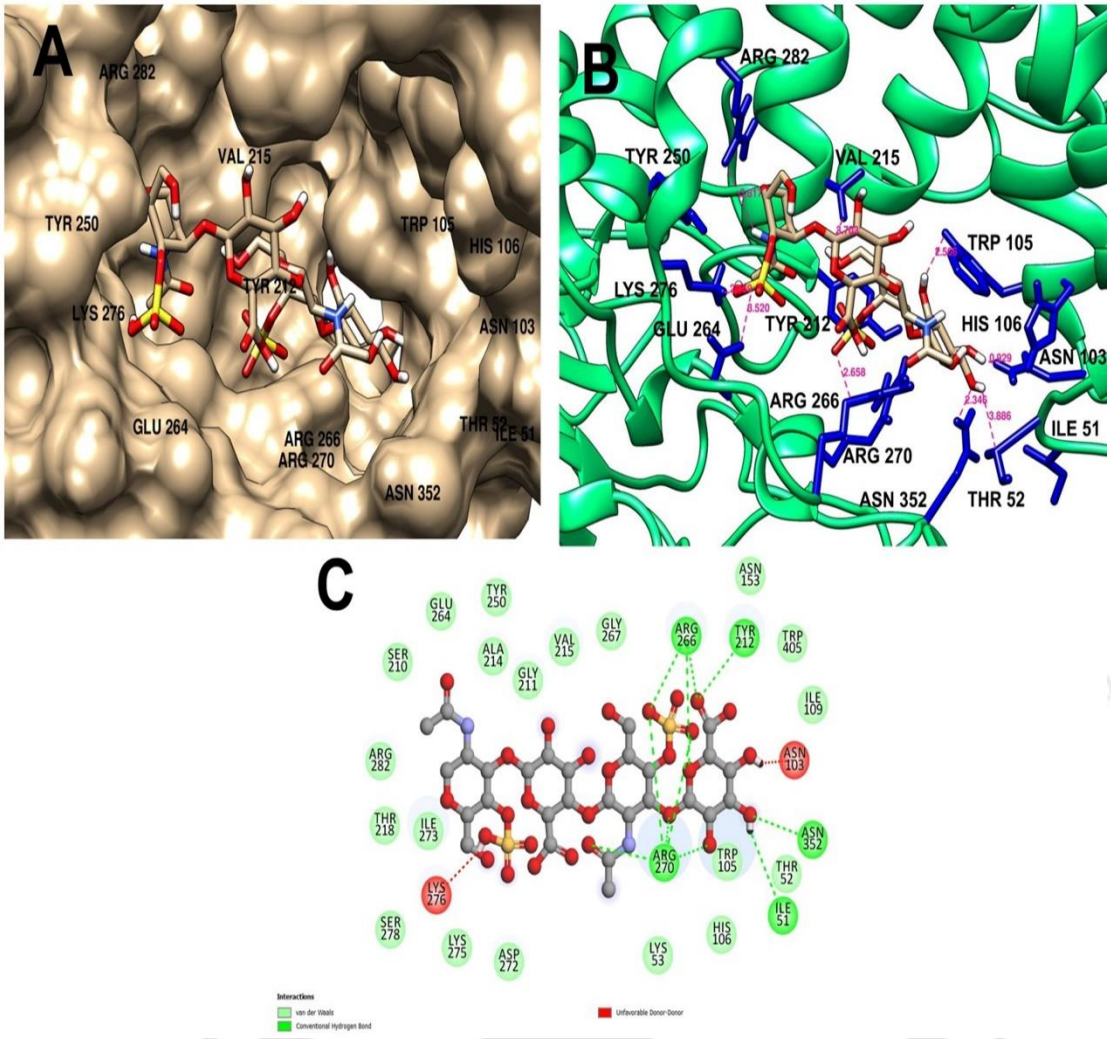

Fig. 4.3.9 (A) Surface view of the active site cleft of *Ps*PL8A showing the binding with ligand C4S tetrasaccharide (B) C4S tetrasaccharide interacting with the active site amino acid residues of *Ps*PL8A. (- - -) represents the hydrogen bond and the residues labeled are within 4Å radius forming hydrophobic interaction with the ligand, (C) 2D LigPlot of C4S tetrasaccharide interacting with the active site amino acid residues of *Ps*PL8A generated in Discovery studio visualizer-Accelrys.

4.3.6 Structure analysis of *Ps*PL8A by Small Angle X-ray Scattering (SAXS)

SAXS analysis of *Ps*PL8A was performed using scattering data collected at 12 mg/ml concentration (Fig. 4.3.10A). Guinier analysis for *Ps*PL8A indicate that the predominant shape by a radius of gyration (Rg) 3.19± 0.09 nm. Alternatively, Guinier approximation of a rod shape *Ps*PL8A implied an RC value of ~1.57 nm (Fig. 4.3.10B). The linearity of the Guinier plot in the low q-region shows that the scattered intensities follow the Guinier law and suggesting the length of *Ps*PL8A about 10 nm. The Kratky plot analysis of the *Ps*PL8A indicated that it is fully folded state in solution (Fig. 4.3.10C). The distribution profile of interatomic vectors [P(r)] evaluated by the indirect Fourier transform over a range of 0.01-0.3 concluded that the predominant solution shape of *Ps*PL8A are similar (modeled structure and ab initio generated model) and characterized by a D_{max} and Rg value of 12 nm and 3.3 nm, respectively (Fig. 4.3.10D). Experimentally obtained parameters matched with the modeled *Ps*PL8A structure parameters, which supported that the solution shape of *Ps*PL8A is in good correlation with modeled structure and its homologous crystal structures. Multiple independent cycles of *ab initio* modelling by DAMMIF were computed without symmetry restrictions and were averaged by DAMAVER to produce a low-resolution *ab initio* shape for *Ps*PL8A (Fig. 4.3.10E). The Dummy Atom Molecule of the *Ps*PL8A is elongated, and clearly reveals a single domain. The *ab initio* derived dummy atom model superpose well with the modeled *Ps*PL8A while, few α-helices and loop region protruding the dummy atom model of *Ps*PL8A derived from the SAXS Data. These regions outside the envelop may be due to the flexibility of the loops (Fig. 4.3.10F).

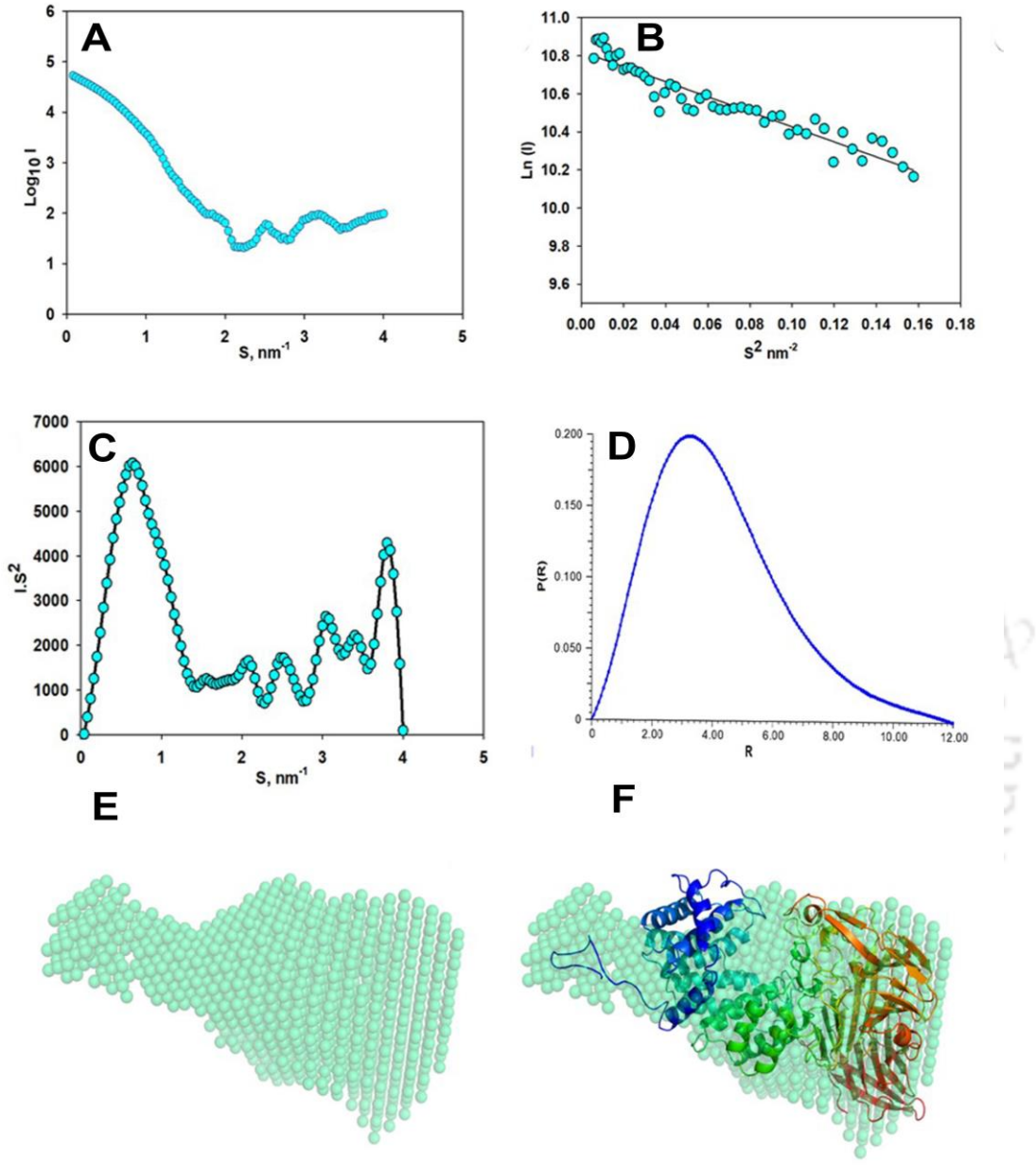

Fig. 4.3.10 Small Angle X-ray Scattering analysis of *Ps*PL8A (A) SAXS intensity profiles from samples of *Ps*PL8A, (B) Guinier plot of the SAXS intensities, *Ps*PL8A. The straight line was obtained by least-squares fitting in the region, (C) Kratky plots of the SAXS datasets confirmed the globular nature of the scattering *Ps*PL8A, (D) P(r) curves of the predominant scattering dataset of *Ps*PL8A plotted as a function of r, (E) *Ab initio* model of *Ps*PL8A generated by constructing independent dummy atom residue models using DAMMIF and averaging with DAMAVER. (F) Superposition of *ab initio* and modeled *Ps*PL8A. Images were generated using PyMol ver. 1.3 Schrödinger, LLC.

4.3.7 Construction of *Ps*PL8A mutants by Site-directed mutagenesis

Based on the structural model of *Ps*PL8A and molecular docking studies with C4S disaccharide/tetrasaccharide, the putative catalytic residues N153, H203, Y212, R266 and E349 were selected for site-directed mutagenesis. The DNA sequence of 2037 base pairs encoding mutants N153A, H203A, Y212F, R266A and E349A was amplified by a two-step PCR megaprimer approach (Fig. 4.3.11). A single point mutation was introduced in each mutant. The *Ps*PL8A mutants were cloned in pET28a(+) expression vector and the positive clones were screened by restriction digestion (Fig. 4.3.11).

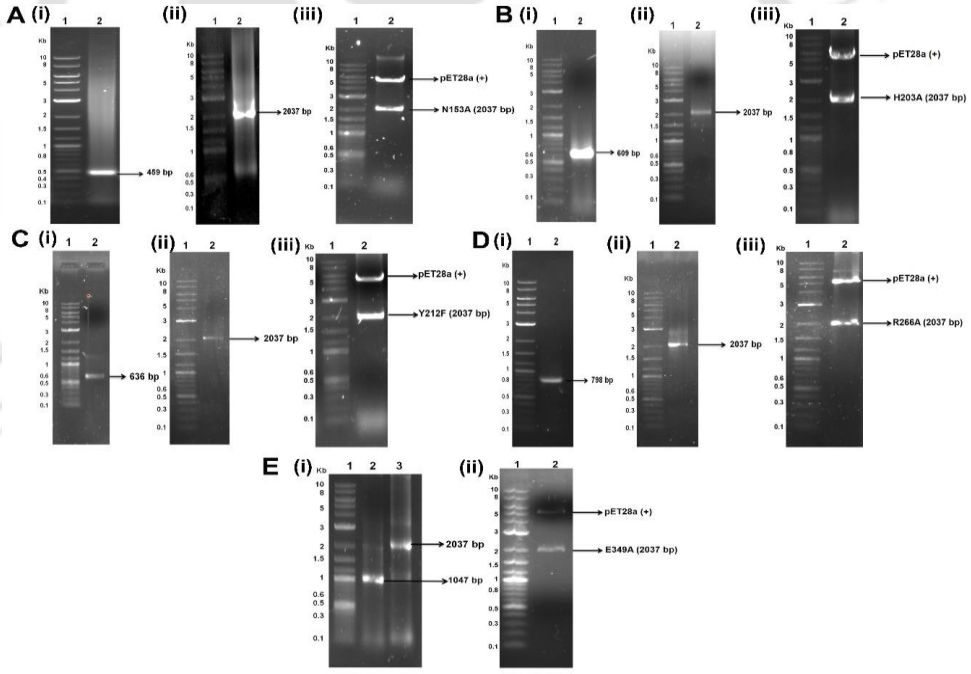

Fig. 4.3.11 Site-directed mutagenesis of *Ps*PL8A by Megaprimer approach (A) N153A, (B) H203A, (C) Y212F, (D) R266A (i) 1st round PCR in lane 2, (ii) 2nd round PCR amplification of 2037 bp in lane 2, (iii) clone confirmation by restriction digestion showing band of pET28a(+) at 5.34 bp and mutant at 2037 bp (Lane 2), where Lane 1 is marker (NEB log2 DNA ladder) and (E) E349A mutant (i) 1st round PCR in lane 2, 2nd round PCR in lane 3 and (ii) clone confirmation by restriction digestion.

The recombinant proteins were purified to apparent homogeneity level by immobilised metal ion chromatography (IMAC). The expression and purification of the five recombinant *Ps*PL8A mutants was analysed by SDS-PAGE (10.5%, w/v) gel and all showed a molecular size of approximately, 77 kDa (4.3.12).

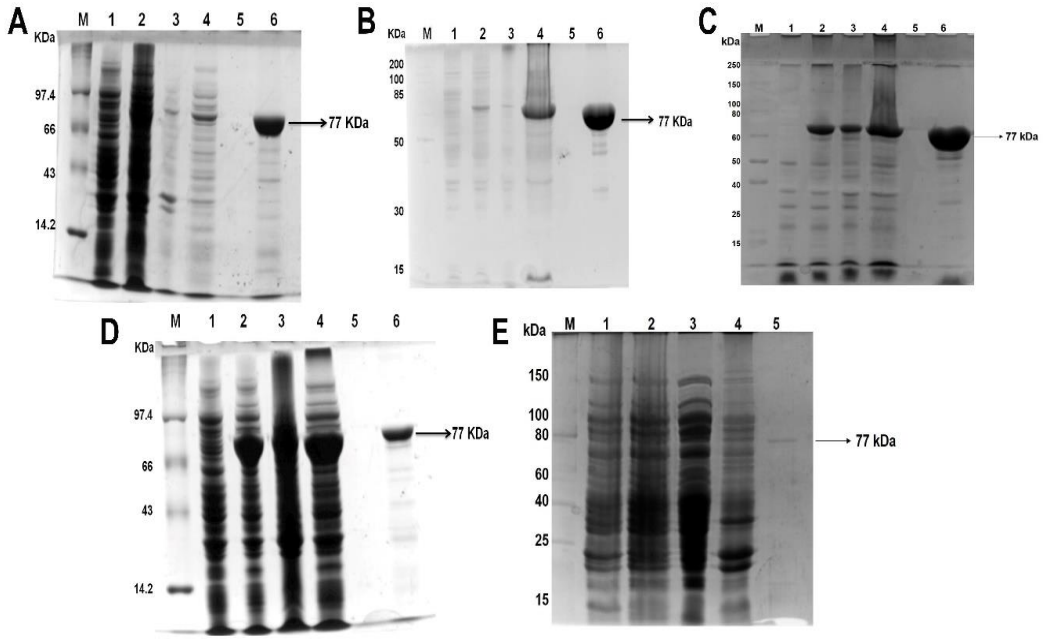

Fig. 4.3.12 SDS-PAGE (10.5%, w/v) gel showing over-expression and purification of *Ps*PL8A mutants using *E. coli* BL21 (DE3) cells; (A) N153A, (B) H203A, (C) Y212F, (D) E349A, Lane 1: Uninduced BL21 (DE3) cells, Lane 2: Induced BL21 (DE3) cells, Lane 3: Cell pellet after sonication, Lane 4: Cell free extract, Lane 5: Last wash from the column and Lane 6: Purified recombinant *Ps*PL8A mutant enzyme: Lane M: Protein marker (Genei and fermentas), (E) Over-expression and purification of R266A in *E. coli* BL-21 pLysS cells, Lane 1: Uninduced BL21 (DE3) cells, Lane 2: Induced BL21 (DE3) cells, Lane 3: Cell pellet after sonication, Lane 4: Cell free extract, Lane 5: Purified recombinant R266A mutant enzyme.

4.3.8 Binding and activity analysis of mutants and catalytic mechanism of *Ps*PL8A

The mutants N153A, H203A, Y212F, R266A and E349A were developed as mentioned in section 3.7, in order to probe the role of these residues in catalysis. The specific activity of all mutants was determined and compared with the wild-type

*Ps*PL8A (Table 4.3.3). The results showed that the mutants N153A, H203A, Y212F, R266A and E349A gave 0.66%, 0.13%, 3.8%, 0.38% and 0.80% relative activity against C4S substrate taking the wild-type *Ps*PL8A activity as 100%. All the mutants showed no activity against C6S substrate when assayed under the same conditions. The complete loss in activity of the mutant proteins showed that these residues are critical and catalytic residues of *Ps*PL8A.

Table 4.3.3. Enzyme activity of *Ps*PL8A mutants.

Enzyme	**Relative Activity (%)**	
	Chondroitin4-Sulphate	**Chondroitin 6-Sulphate**
*Ps*PL8A (wild type)	100	100
N153A	0.66	ND
H203A	0.13	ND
Y212F	3.80	ND
R266A	0.38	ND
E349A	0.80	ND

ND: Not detected

*Ps*PL8A showed an initial random endolytic mode generating higher C4S oligosaccharide up to dodeca-saccharide along with C4S disaccharide, while disaccharide was the major product observed after 1 h of catalysis as previously reported (Rani and Goyal., 2016). One of the plausible explanation for this mode of catalysis could be, since the catalytic cleft is formed by N-terminal and two-three loop region from C-terminal, the catalytic core of *Ps*PL8A is not rigid and the loops might be flexible enough for periodically opening and allowing the entry of CS chain inside to the catalytic groove. Such catalytic core was also reported for chondroitin AC lyase from *Flavobacterium heparinum* (Hung *et al.,* 2001). Initially as the substrate enters

the catalytic core, *Ps*PL8A enzyme starts acting randomly and generates the higher oligosaccharide as well as the disaccharide, while with time it degrades all higher oligosaccharide to final disaccharide product, suggesting its more affinity towards disaccharide. The docking study with C4S disaccharide and tetra saccharide revealed that it has higher binding affinity with C4S disaccharide (-5.14 kcal) as compared with tetrasaccharide (-4.1kcal). The tunnel like catalytic core of cellobiohydrolase also showed the evidence of local conformational changes upon binding of the polysaccharide (Varrot *et al.,* 1999; Zou *et al.,* 1999). The crystal structure of endolytic chondroitin AC lyase from *Flavobacterium heparinum* showed the catalytic tunnel which is not rigid and having flexible loops (Huang *et al.,* 2001) while, the catalytic core of exolytic *Arthrobacter aurescens* (Lunin *et al.,* 2004) was covered by the two loops, restricting the movement of only two to three sugar residues.

In β-elimination a general base is required to abstract the proton from C-5 of the uronic acid, generating an enolate anion intermediate, followed by proton donation by a general acid or water molecule and concomitant release of the leaving group (Gacesa *et al.,* 1987). Three probable theories for catalytic mechanism of chondroitin AC lyase from *Flavobacterium heparinum* have been proposed (Huang *et al.,* 2001) *viz.* i) His acting as general base while Tyr as general acid, ii) Tyr acting as both general acid and base iii) Tyr acting as general base and Arg as general acid. In other study it was suggested that Tyr242 acts as a general base in chondroitin AC lyase enzyme from *Flavobacterium heparinum* (Rye *et al.,* 2006). The structure comparison, mutagenesis and binding results of *Ps*PL8A indicated the roles of Y212 and H203 or R266 as probable general base and general acid, respectively. The residues N153 and E349 of

*Ps*PL8A, are likely contributing to the charge neutralization and stabilization of the enolate anion intermediate during β-elimination.

4.3.9 Ligand binding studies of Y212F and H203A by Isothermal Titration Calorimetry (ITC)

The binding of mutants Y212F and H203A with C4S polysaccharide by ITC analysis showed that H203A has no binding with C4S polysaccharide (Fig. 4.3.13), implicating that mutation of His203 residue with alanine leads to the loss of activity as well as the ligand binding affinity. However, Y212F showed weak binding against C4S polysaccharide (Fig. 4.3.14) as it also retained ~4% relative activity (Table 4.3.3). This revealed that Y212 residue is involved in the catalysis and substrate binding. Similarly, the crystal structure analysis of Y242F mutant of chondroitin AC lyase from *Flavobacterium heparinum* complex with CS-tetrasaccharide showed binding at the same position of catalytic site as that of the wild-type enzyme, suggesting the involvement of Tyr242 in catalysis and substrate binding (Huang *et al.*, 2001).

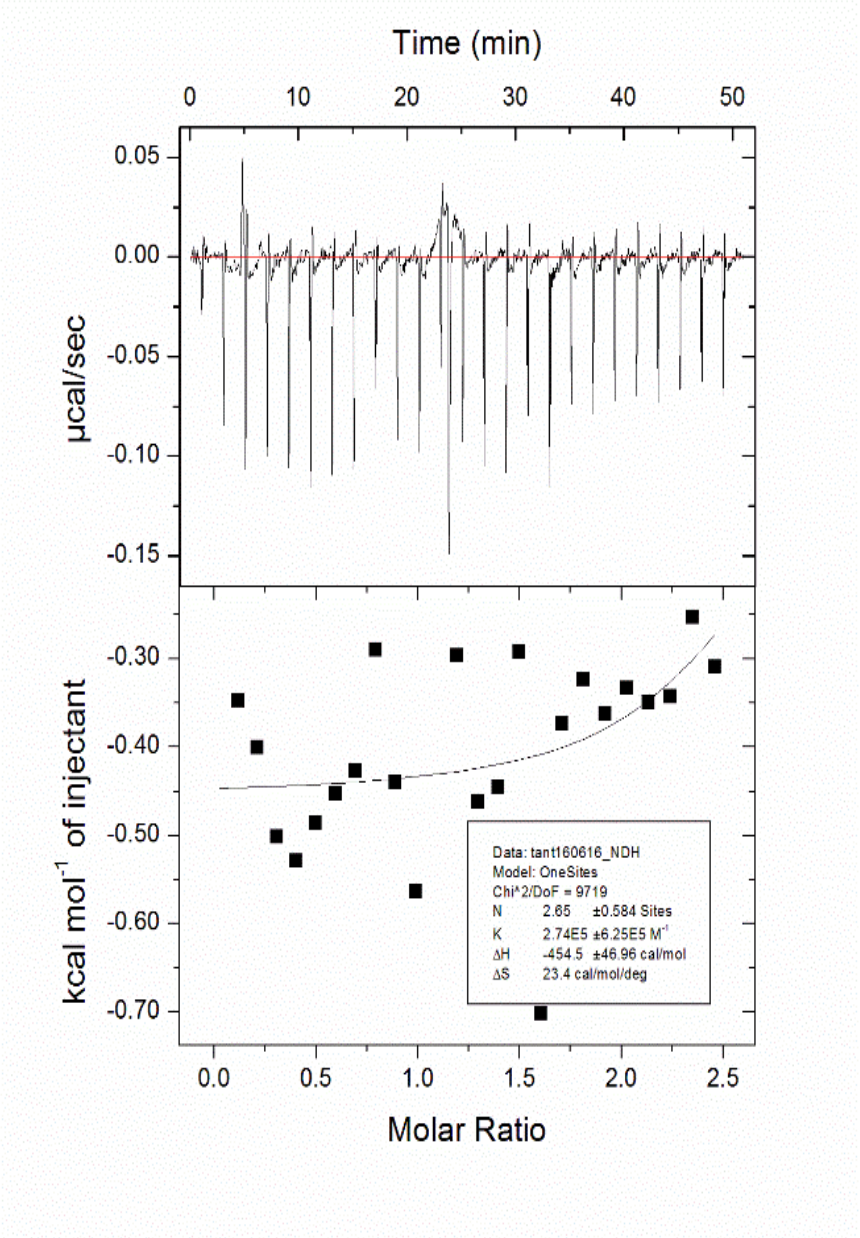

Fig. 4.3.13 Representative ITC data of *Ps*PL8A mutant, H203A with C4S polysaccharide. The ligand C4S polysaccharide (20 mg/ml) in syringe was titrated with 80 µM of protein in the cell. The top half of each panel shows the raw ITC heat while the bottom half represents the integrated peak areas fitted to a single-site binding model with MicroCal Origin Ver. 8.0 ITC was carried out using 50 mM Tris-HCl buffer, pH 7.2.

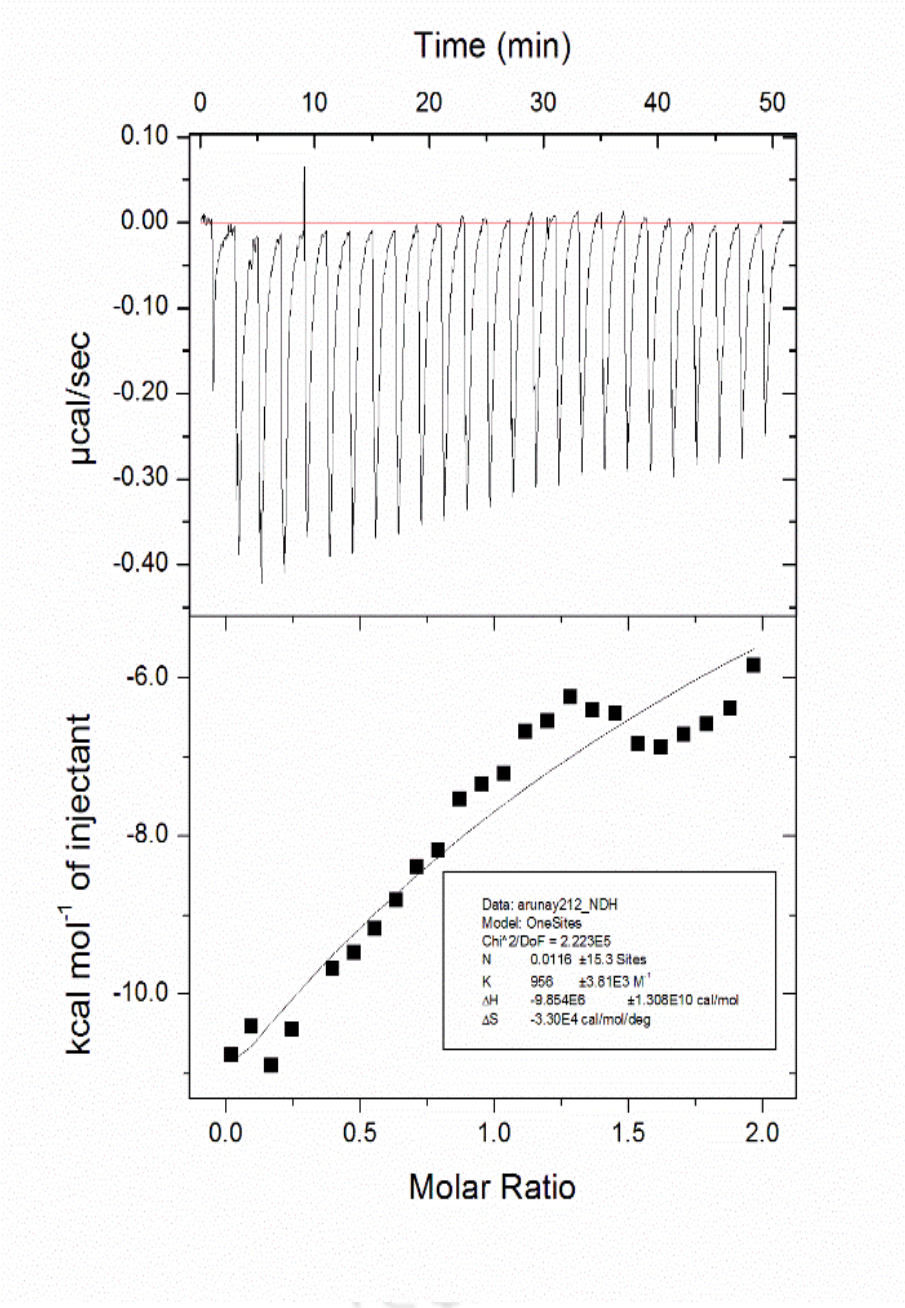

Fig. 4.3.14 Representative ITC data of *Ps*PL8A mutant, Y212F with C4S polysaccharide The ligand C4S polysaccharide (20 mg/ml) in syringe was titrated with 80 µM of protein in the cell. The top half of each panel shows the raw ITC heat while the bottom half represents the integrated peak areas fitted to a single-site binding model with MicroCal Origin Ver. 8.0. ITC was carried out using 50 mM Tris-HCl buffer, pH 7.2.

4.4 Conclusions

The structure of chondroitin AC lyase (*Ps*PL8A) of family 8 polysaccharide lyase was characterized. Multiple sequence alignment of *Ps*PL8A with previously known chondroitin lyases revealed the conserved and semi-conserved amino acid residues. The 3-Dimensional structure showed a N-terminal $(\alpha/\alpha)_6$ incomplete toroidal fold and a layered β sandwich structure at C-terminal. Ramchandran plot displayed 98.5% residues in the favoured region and 1.2% in the generously allowed region. The secondary structure of *Ps*PL8A prediction by PsiPred and confirmation by CD analysis revealed the presence of 27.31% α helices 22.7% β sheets and rest 49.9% random coils. The protein melting study of *Ps*PL8A showed that the protein completely unfolds at 60ºC. SAXS showed the *Ps*PL8A structure in solution form. Kratky plot gave indication that protein is fully folded in solution. The *ab initio* derived dummy atom model of *Ps*PL8A superposed well with its modeled structure with some α-helices and loop region not superposing with dummy atom model. ITC analysis of Y212F and H203A with C4S polysaccharide, showed moderate quantitative binding by Y212F (Ka = 9.56 ± 3.81×10^5) and no binding with H203A. The roles of catalytic residues Y212 and H203 or R266 as probable general base and general acid, respectively were confirmed by site-directed mutagenesis. The involvement of Y212 and H203 residues in substrate binding was confirmed by ITC and docking analyses. The structural characterization of chondroitin AC lyase (*Ps*PL8A) has enabled in elucidation of the catalytic mechanism. The residues Y212 and H203 or R266 might act as general base and general acid respectively, during catalysis. N153 and E349 are likely contributing in charge neutralization and stabilizing the enolate anion intermediate during β-elimination. The structural characterization will enable to

elucidate the complete mechanism underlying the mode catalysis of chondroitin AC lyase (*Ps*PL8A). However, the future challenge includes to determine the crystal structure of *Ps*PL8A by X-ray crystallography.

4.5 References

Altschul, S. F., Gish, W., Miller, W., Myers, E. W., and Lipman, D. J. (1990). Basic local alignment search tool. *Journal of Molecular Biology*, *215*(3), 403-410.

Bhattacharya, D., Nowotny, J., Cao, R., and Cheng, J. (2016). 3Drefine: an interactive web server for efficient protein structure refinement. *Nucleic Acids Research*, gkw336.

Bolam, D. N., Xie, H., Pell, G., Hogg, D., Galbraith, G., Henrissat, B., and Gilbert, H. J. (2004). X4 modules represent a new family of carbohydrate-binding modules that display novel properties. *Journal of Biological Chemistry*, *279*(22), 22953-22963.

Cantarel, B.L., Coutinho, P.M., Rancurel, C., Bernard, T., Lombard, V. and Henrissat, B. (2009). The Carbohydrate-Active EnZymes database (CAZy): an expert resource for glycogenomics. *Nucleic Acids Research*, *37*(suppl 1), D233-D238.

Dvortsov, I. A., Lunina, N. A., Chekanovskaya, L. A., Schwarz, W. H., Zverlov, V. V., and Velikodvorskaya, G. A. (2009). Carbohydrate-binding properties of a separately folding protein module from β-1, 3-glucanase Lic16A of *Clostridium thermocellum*. *Microbiology*, *155*(7), 2442-2449.

Féthière, J., Eggimann, B., and Cygler, M. (1999). Crystal structure of chondroitin AC lyase, a representative of a family of glycosaminoglycan degrading enzymes. *Journal of Molecular Biology*, *288*(4), 635-647.

Franke, D., and Svergun, D. I. (2009). DAMMIF, a program for rapid ab-initio shape determination in small-angle scattering. *Journal of Applied Crystallography*, *42*(2), 342-346.

Gacesa, P. (1987). Alginate-modifying enzymes: a proposed unified mechanism of action for the lyases and epimerases. *FEBS Letters*, *212*(2), 199-202.

Garron, M. L., and Cygler, M. (2010). Structural and mechanistic classification of uronic acid-containing polysaccharide lyases. *Glycobiology*, *20*(12), 1547-1573.

Goodsell, D. S., and Olson, A. J. (1990). Automated docking of substrates to proteins by simulated annealing. *Proteins: Structure, Function and Bioinformatics*, *8*(3), 195-202.

Guex, N., and Peitsch, M. C. (1997). SWISS-MODEL and the Swiss-Pdb Viewer: an environment for comparative protein modeling. *Electrophoresis*, *18*(15), 2714-2723.

Guiner, A., Fournet, G., and Walker, C. B. (1955). Small angle scattering of X-rays. *J. Wiley & Sons, New York*.

Huang, W., Boju, L., Tkalec, L., Su, H., Yang, H. O., Gunay, N. S., Linhardt, R.J., Kim, Y.S., Matte, A. and Cygler, M. (2001). Active site of chondroitin ac lyase revealed by the structure of enzyme- oligosaccharide complexes and mutagenesis. *Biochemistry*, *40*(8), 2359-2372.

Huang, W., Lunin, V., Li, Y., Suzuki, S., Sugiura, N., Miyazono, H., and Cygler, M. (2003). Crystal structure of *Proteus vulgaris* chondroitin sulfate ABC lyase I at 1.9 Å resolution. *Journal of Molecular Biology*, *328*(3), 623-634.

Ke, S. H., and Madison, E. L. (1997). Rapid and efficient site-directed mutagenesis by single-tube 'megaprimer'PCR method. *Nucleic Acids Research*, *25*(16), 3371-3372.

Kelly, S. M., Jess, T. J., and Price, N. C. (2005). How to study proteins by circular dichroism. *Biochimica et Biophysica Acta (BBA)-Proteins and Proteomics*, *1751*(2), 119-139.

Lezin, G., Kosaka, Y., Yost, H. J., Kuehn, M. R., and Brunelli, L. (2011). A one-step miniprep for the isolation of plasmid DNA and lambda phage particles. *PloS One*, *6*(8), e23457.

Li, S., Kelly, S. J., Lamani, E., Ferraroni, M., and Jedrzejas, M. J. (2000). Structural basis of hyaluronan degradation by *Streptococcus pneumoniae* hyaluronate lyase. *The EMBO Journal*, *19*(6), 1228-1240.

Louis-Jeune, C., Andrade-Navarro, M. A., and Perez-Iratxeta, C. (2012). Prediction of protein secondary structure from circular dichroism using theoretically derived spectra. *Proteins: Structure, Function, and Bioinformatics*, *80*(2), 374-381.

Lunin, V. V., Li, Y., Linhardt, R. J., Miyazono, H., Kyogashima, M., Kaneko, T., Bell, A.W and Cygler, M. (2004). High-resolution crystal structure of *Arthrobacter aurescens* chondroitin AC lyase: an enzyme–substrate complex defines the catalytic mechanism. *Journal of Molecular Biology*, *337*(2), 367-386.

Méndez, R., Leplae, R., Lensink, M. F., and Wodak, S. J. (2005). Assessment of CAPRI predictions in rounds 3–5 shows progress in docking procedures. *Proteins: Structure, Function, and Bioinformatics*, *60*(2), 150-169.

Mertens, H. D., and Svergun, D. I. (2010). Structural characterization of proteins and complexes using small-angle X-ray solution scattering. *Journal of Structural Biology*, *172*(1), 128-141.

Morris, G. M., Goodsell, D. S., Halliday, R. S., Huey, R., Hart, W. E., Belew, R. K., and Olson, A. J. (1998). Automated docking using a Lamarckian genetic

algorithm and an empirical binding free energy function. *Journal of Computational Chemistry*, *19*(14), 1639-1662

Pojasek, K., Shriver, Z., Kiley, P., Venkataraman, G., and Sasisekharan, R. (2001). Recombinant expression, purification, and kinetic characterization of chondroitinase AC and chondroitinase B from *Flavobacterium heparinum*. *Biochemical and Biophysical Research Communications*, *286*(2), 343-351.

Prabhakar, V., Raman, R., Capila, I., Bosques, C. J., Pojasek, K., and Sasisekharan, R. (2005). Biochemical characterization of the chondroitinase ABC I active site. *Biochemical Journal*, *390*(2), 395-405.

Rani, A., and Goyal, A. (2016). A new member of family 8 polysaccharide lyase chondroitin AC lyase (*Ps*PL8A) from *Pedobacter saltans* displays endo-and exo-lytic catalysis. *Journal of Molecular Catalysis B: Enzymatic*, *134*, 215-224.

Rani, A., Patel, S., and Goyal, A. (2017). Chondroitin sulfate (CS) lyases: Structure, function and application in therapeutics. *Current protein & peptide science*, DOI: 10.2174/1389203718666170102112805.

Rye, C. S., and Withers, S. G. (2002). Elucidation of the Mechanism of Polysaccharide Cleavage by Chondroitin AC Lyase from *Flavobacterium heparinum*. *Journal of the American Chemical Society*, *124*(33), 9756-9767.

Rye, C. S., Matte, A., Cygler, M., and Withers, S. G. (2006). An atypical approach identifies TYR234 as the key base catalyst in chondroitin AC lyase. *ChemBioChem*, *7*(4), 631-637.

Šali, A., and Blundell, T. L. (1993). Comparative protein modelling by satisfaction of spatial restraints. *Journal of Molecular Biology*, *234*(3), 779-815.

Semenyuk, A. V., and Svergun, D. I. (1991). GNOM–a program package for small-angle scattering data processing. *Journal of Applied Crystallography*, *24*(5), 537-540.

Volkov, V. V., and Svergun, D. I. (2003). Uniqueness of *ab initio* shape determination in small-angle scattering. *Journal of Applied Crystallography*, *36*(3), 860-864.

Webb, B., and Sali, A. (2014). Protein structure modeling with modeller. *Protein Structure Prediction*, 1-15.

Zou, J. Y., Kleywegt, G. J., Ståhlberg, J., Driguez, H., Nerinckx, W., Claeyssens, M., Koivula, A., Teeri, T.T. and Jones, T. A. (1999). Crystallographic evidence for substrate ring distortion and protein conformational changes during catalysis in cellobiohydrolase Ce16A from *Trichoderma reesei*. *Structure*, *7*(9), 1035-1045.

Chapter 5

Antitumor effect of chondroitin AC lyase (*Ps*PL8A) from *Pedobacter saltans* on melanoma and fibrosarcoma cell lines by *in vitro* analysis

5.1 Introduction

Glycosaminoglycans (GAGs) are the natural heteropolysaccharides that are present in every mammalian tissue (Afratis *et al.,* 2012). GAGs are composed of disaccharide repeats of two hexose monosaccharide units, D-galactosamine/D-glucosamine and D-glucuronic acid/L-Iduronic acid (Igarashi *et al.,* 2013). Proteoglycans (PGs) are glycoconjugates consisting of protein and polysaccharide glycosaminoglycans (GAGs). PGs are generally found on the cell surfaces, extracellular matrix (ECM) and in basement membranes of animal tissues (Li *et al*., 2012). Chondroitin sulphate (CS) are the GAG chains that bound to serine residue of the protein core linked through a tetrasaccharide linkage region consisting of xylose-galactose-galactose-glucuronic acid and forming a proteoglycan (PG) (Kresse *et al.,* 2001). CS is involved in various biological functions including cell migration,

proliferation, microbial recognition, adhesion, pathogenesis, cell-matrix interactions, chemokine and cytokine activation etc. (Cattaruzza *et al.*, 2006; Garner *et al.*, 2008). GAGs are highly charged linear chains of polysaccharides. In the recent years, cell biology studies have revealed that the altered structure of glycosaminoglycans in several diseases indicate their importance as biomarkers for disease diagnosis and progression, as well as pharmacological targets (Afratis *et al.*, 2012; Poh *et al.*, 2015). CSPGs are able to regulate key cellular processes, including proliferation, apoptosis, migration, adhesion and invasion. Versican and decorin are the major CSPGs and are over-expressed in the stroma of a wide variety of malignant tumors, including osteosarcoma, testicular tumors, breast, pancreatic and colon cancer (Theocharis *et al.*, 2006; Skandalis *et al.*, 2011).

The enzymes capable of degrading GAGs have been studied in order to understand the structure of GAGs and harness their therapeutic effects by manipulating cell signaling, differentiation, migration and adhesion (Sugahara *et al.*, 2003; Bao *et al.*, 2004). Designing GAG-based therapeutic drugs to tackle the pathogenic and inflammatory diseases requires complete understanding of GAG degrading enzymes (Linhardt *et al.*, 2006). Chondroitin sulphate lyases have been reported to exhibit the functions such as the inhibition of cell proliferation, differentiation and migration and some possible functions such as antitumor, pathogenic infection control, wound repair and neuro-generation. (Sugahara *et al.*, 2003; Rauch *et al.*, 2006; Uyama *et al.*, 2007). PGs are involved in cellular communication and cancer biology (Iozzo *et al.*, 2011). Metastasis of tumors involves a complex sequence of events, called as the “metastatic cascade” (Sneath *et al.*, 1998; Denholm *et al.*, 2001). Chondroitin sulphate chains as a part of PGs have important role in the process of tumor growth and metastasis (Iida *et*

al., 1996; Sneath *et al.,* 1998; Eisenmann *et al.,* 1999; Denholm *et al.,* 2001; Yamada *et al.,* 2008). Chondroitin lyases has been reported to possess the antitumor potential (Denholm *et al.,* 2001). Chondroitin AC lyase from *Flavobacterium heparinum* inhibited melanoma (SK-Mel2) invasion and proliferation as well as endothelial proliferation and angiogenesis (Denholm *et al.,* 2001). Recruitment of CS lyase for meddling with cancer cell surface receptors can offer exciting therapeutic possibilities. These observations have prompted the researchers to explore the possible role of chondroitin sulphate lyases in understanding the cancer biology. Chondroitin AC lyase (*Ps*PL8A) degrades the CS chains and hence can be potentially utilized to treat and control the progression of melanoma and fibrosarcoma. In the present chapter the effect of chondroitin AC lyase (*Ps*PL8A) on mouse fibroblast (L929), melanoma (SK-Mel-28) and fibrosarcoma (HT-1080) cell lines was explored. The mode of cell death and changes in mitochondrial membrane potential was studied after treatment of these cancer cells with chondroitin AC lyase (*Ps*PL8A).

5.2 Materials and Methods

5.2.1 Chemicals and reagents

Dulbecco's Modified Eagle Medium (DMEM) low glucose medium, minimum essential medium (MEM), 1-diphenyl-2-picrylhydrazyl (DPPH), MTT [3-(4,5-dimethylthiazol-2-yl)-2,5-diphenyltetrazolium bromide and Mitochondria Staining Kit were procured from Sigma-Aldrich, USA. Fetal bovine serum (FBS), 50 µg/ml streptomycin and 50 IU/ml penicillin were purchased from Gibco, USA. Phosphate buffer saline (PBS), DAPI dye (4´,6-diaminidino-2-phenylindole) and Trypsin-EDTA solution were purchased from Hi-Media Pvt. Ltd., India. FITC (Fluorescein isothiocyanate)-Annexin V and Propidium iodide (PI) cell apoptosis kit were purchased from Invitrogen, Ltd. UK.

5.2.2 Expression and purification of chondroitin AC lyase (*Ps*PL8A)

The gene encoding *Ps*PL8A cloned in pET28a(+) and expressed in *E. coli* BL21 (DE3) cells as described earlier (Rani and Goyal., 2016) was used in the present study. The chondroitin AC lyase (*Ps*PL8A) was purified by immobilized metal ion affinity chromatography and dialysed in Tris-HCl buffer, pH 7.2. The purity of protein, whether it is free from other host cell proteins was checked on SDS-PAGE using a 10.5% (w/v) gel as described in section 2.2.14 of chapter 2. Chondroitin AC lyase (*Ps*PL8A) was filtered through a 0.22 µm filter (Millipore, USA) prior to use in all experiments.

5.2.3 Mammalian cell culture and maintenance of cell lines

The mouse fibroblast cell line (L929), Human melanoma (SK-Mel28) and Fibrosarcoma HT-1080 were procured from National Centre for Cell Science (NCCS), Pune, India. All cell lines were cultured in DMEM low glucose medium supplemented with 10% (v/v) heat-inactivated fetal bovine serum (FBS) (Gibco, USA), 50 µg/ml

streptomycin and 50 IU/ml penicillin (Gibco, USA) incubated at 37ºC under 5% CO_2. The cells were grown in T-25 and T-75 flasks at 37ºC under 5% CO_2 in a regulated CO_2 incubator. After the cells reached confluent stage, they were washed several times with 1XPBS (pH 7.4) and harvested with 0.25% (v/v) trypsin-EDTA solution for further experiments. All the three cell lines were stored at -80ºC in freezing medium (Invitrogen, USA) for long term storage.

5.2.4 Sub-culturing of cells

The media was removed carefully and discarded from the culture flask of L929, SK-Mel28 and HT-1080. The cells were then washed with 1xPBS (pH 7.4) gently by adding it to the side of the flask opposite the attached cell layer to avoid disturbing the cell layer. The PBS was discarded and the cells were treated with 1x Trypsin EDTA solution for 2-3 min at 37°C and observed under microscope (Nikon, TS2R, Japan) at 40x magnification for detachment. After ≥ 90% of the cells have detached, 2 ml of complete medium was added to the detached cells and centrifuged at 200*g* at 4ºC for 10 min. The supernatant was discarded and the cells were re-suspended in 1 ml of complete medium. A split ratio of 1:10 (1 ml of above cell suspension in 9 ml complete medium) was used for sub-culturing cells.

5.2.5 *In vitro* cell proliferation assay of L929, SK-Mel28 and HT-1080 cells with *Ps*PL8A

The effect of chondroitin AC lyase (*Ps*PL8A) enzyme on L929, SK-Mel28 and HT-1080 cells viability was analysed by MTT [3-(4,5-dimethylthiazol-2-yl)-2,5-diphenyltetrazolium bromide] assay (Mosmann, 1983). The cells were seeded at a density of $2x10^4$ cells/well in 96 well plates which were incubated at 37ºC under 5% CO_2 for overnight for cell adherence. After the incubation, the medium was completely

removed and the L929, SK-Mel 28 and HT-1080 cells were gently washed with 1x phosphate buffer saline (PBS) (pH 7.4). After the PBS wash the cells were exposed to different concentrations varying between (0.0013 µM -1.3 µM) of the *Ps*PL8A enzyme dissolved in serum-free DMEM medium (incomplete). The incomplete DMEM medium without *Ps*PL8A enzyme was used as a negative control. The plates were incubated at 37ºC in 5% CO_2 for 12h and 24h. MTT assay was carried out after 12h and 24h by removing the medium and washing the wells with 200 µl of 1x phosphate buffer saline (PBS) pH 7.4. A 100 µl of MTT (0.5 mg/ml) was added to each well and plate was incubated at 37ºC in 5% CO_2 for 4h. After the incubation, MTT was removed from the wells and the formazan formed was dissolved by adding 100 µl of dimethyl sulfoxide. The absorbance at 570 nm (A_{570}) was monitored by a 96-well microplate reader (Tecan, Infinite 200 Pro, Switzerland). The cell viability (%) was calculated according to Meerloo *et al.,* (2011).

$$\text{Viability (\%)} = (N_t/N_c) \text{ X } 100$$

Where, N_t is the absorbance of treated cells and N_c is the absorbance of untreated cells.

5.2.6 Mode of cell death by Annexin-FITC assay by microscopy

The mode of cell death of SK-Mel 28 and HT-1080 cells after *Ps*PL8A enzyme treatment was analysed by staining the cells with annexin-V-FITC and PI staining kit from Invitrogen, Ltd. UK. The cells were seeded at the density of $2x10^6$ cells in a 24 well cell culture plate. After overnight incubation, the cells were treated with *Ps*PL8A enzyme at a concentration of 1.3 µM dissolved in incomplete DMEM medium, and incubated at 37ºC in 5% CO_2 incubator for 24h. The cells in only incomplete DMEM medium were used as control. After treatment, the cells were washed with cold 1x PBS

solution and incubated with 1x annexin-binding buffer, pH 7.4. The cells were treated with PI (100 µg/ml) and annexin-V-FITC dye at the concentration as mentioned by manufacturer (Invitrogen, Ltd. UK) for 15 min at 25°C and kept in dark. The stain was removed and 400 µl of 1x annexin-binding buffer was added and cells were observed under fluorescence microscope (Nikon, TS2R, Japan) with UV excitation/emission at 494/518 nm and 535/617 nm for annexin V-FITC and PI, respectively. The cells showing green fluorescence were considered as apoptotic and red cells were dead or necrotic.

5.2.7 Apoptosis analysis of SK-Mel 28 and HT-1080 cell lines by Flow cytometry

Analysis of apoptotic/necrotic features by flow cytometry was performed using an annexin V-fluorescein isothiocyanate (FITC) apoptosis kit from Invitrogen, Ltd., UK. The untreated SK-Mel 28 and HT-1080 cells at a cell density of 2×10^6 cells/ml were used. and staining with annexin V-FITC and propidium iodide (PI) was performed according to the instructions given by the manufacturer as mentioned in section 5.2.5. Similarly, *Ps*PL8A enzyme (1.3 µM) treated SK-Mel 28 and HT-1080 cells at a cell density of 2×10^6 cells/ml, were analyzed for apoptosis/necrosis by flow cytometery. The fluorescence of the stained cells was detected with a flow cytometer (BD FACSCalibur, BD bioscience, USA), and the results were analyzed using Flow Jo software.

5.2.8 Mitochondrial cell potential analysis of SK-Mel 28 and HT-1080 cells

The dissipation of the mitochondrial electrochemical potential gradient (Dy) is known as an early event in apoptosis. Any event leading to the changes in mitochondrial inner membrane can be detected by using a cationic dye JC-1 (5,5',6,6'-tetrachloro-1,1',3,3'-tetraethylbenzimidazolocarbocyanineiodide). Mitochondrial cell potential

analysis was carried out by using mitochondrial electrochemical gradient kit from Sigma Aldrich, USA. The JC-1 Staining solution was prepared as per manufacturer instruction by mixing 25 µl of the 200X JC-1 Stock solution in 4 ml of ultrapure water in an appropriate tube**.** The solution was mixed by inversion or brief vortex of the tube. The tube was incubated for 2 minutes at 25°C to ensure that the JC-1 is completely dissolved. 1 ml of the JC-1 staining buffer 5X was added to the tube and mixed by inversion. The working solution of JC-1 dye was prepared by adding equal volume of complete DMEM medium to the previously prepared staining solution of JC-1 dye. The adherent SK-Mel 28 and HT-1080 cells were stained by the working solution of JC-1 dye. The growth medium was aspirated from the flask and the cells were overlaid with the 400 µl working solution of JC-1 dye. The cells were incubated for 20 minutes at 37°C in a humidified atmosphere containing 5% CO_2. The staining solution was aspirated and the cells were washed three times with ice cold 1X JC-1 buffer and then twice by DMEM complete medium. The cells were overlayed with the growth medium and were observed under fluorescence microscope (Nikon, TS2R, Japan). Both the untreated and *Ps*PL8A treated SK-Mel 28 and HT-1080 cells were observed under fluorescence microscope (Nikon, TS2R, Japan) under 20X magnification. The cells treated with 0.1 µM valinomycin were used as positive control

5.2.9 Statistical analysis

All experiments were performed in triplicates (n= 3). The results were presented as mean of three determinations ± SD (standard deviation).

5.3 Result and Discussion

5.3.1 *In vitro* cell proliferation assay of L929, SK-Mel28 and HT-1080 cells treated with *Ps*PL8A

The effect of *Ps*PL8A in the concentration range, 0.0013 µM -1.3 µM was studied on mouse fibroblast L929 cells, human melanoma SK-Mel 28 and fibrosarcoma (HT-1080) cells. The L929 cells treated with *Ps*PL8A showed no significant change in the proliferation of the cells displaying 95-98% cell viability (Fig. 5.3.1). Chondroitin AC lyase (*Ps*PL8A) imparts no cytotoxicity to the mouse fibroblast cells with increase in time as well as concentration. The proliferation of human melanoma (SK-Mel 28) and fibrosarcoma (HT-1080) cell lines were studied after treatment with *Ps*PL8A (0.0013 µM-1.3 µM). An overall 58% and 59% inhibition of SK-Mel 28 (Fig. 5.3.2A) and HT-1080 (Fig. 5.3.3A) cells proliferation, respectively was observed with 1.3 µM of *Ps*PL8A after 24h of incubation. The IC_{50} value for SK-Mel 28 cell lines at 12h and 24h were 0.68 µM and 0.54 µM, respectively (Fig. 5.3.2B). While, for HT-1080 the IC_{50} value at 12h and 24h were 0.15 µM and 0.11 µM, respectively (Fig. 5.3.3B). The IC_{50} value was calculated using GraphPad Prism software. Chondroitin AC lyase and chondroitin B lyase inhibited the proliferation of SK-Mel 2 human melanoma cells (Denholm *et al.,* 2001). Chondroitin AC lyase from *Flavobacterium heparinum* inhibited melanoma invasion and proliferation as well as endothelial proliferation and angiogenesis (Denholm *et al.,* 2001). Melanoma cells express CS proteoglycan 4 (CSPG4). CSPG4 is the transmembrane protein which traverses cell membrane and modulates integrin function and enhances growth factor receptor-regulated pathways including extracellular signal-regulated protein kinases (ERK) 1,2 (Price *et al.,* 2011).

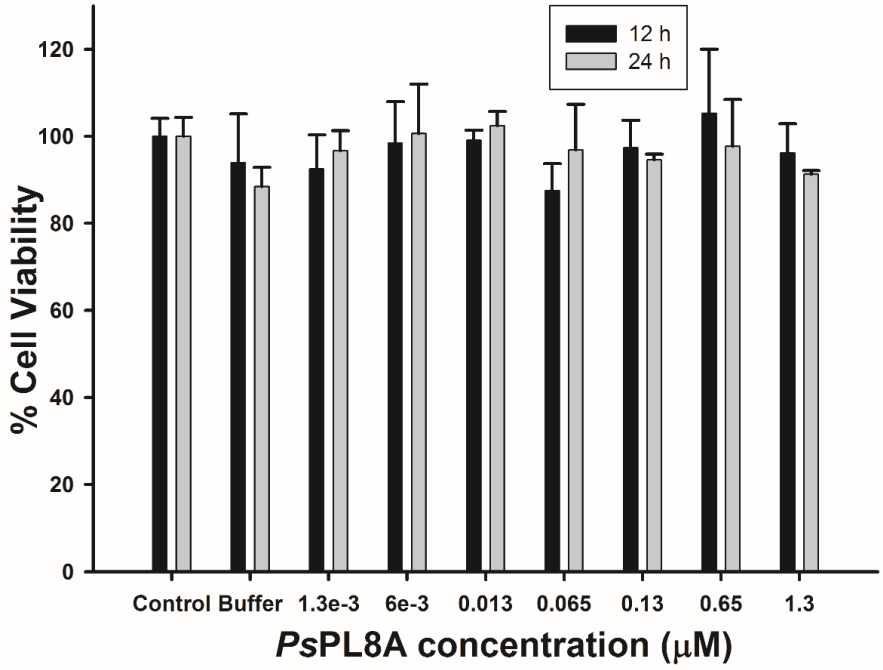

Fig. 5.3.1 *In vitro* cell proliferation assay (MTT) showing percent cell viability of mouse fibroblast L929 cells treated with varying concentration (0.0013-1.3 µM) of *Ps*PL8A.

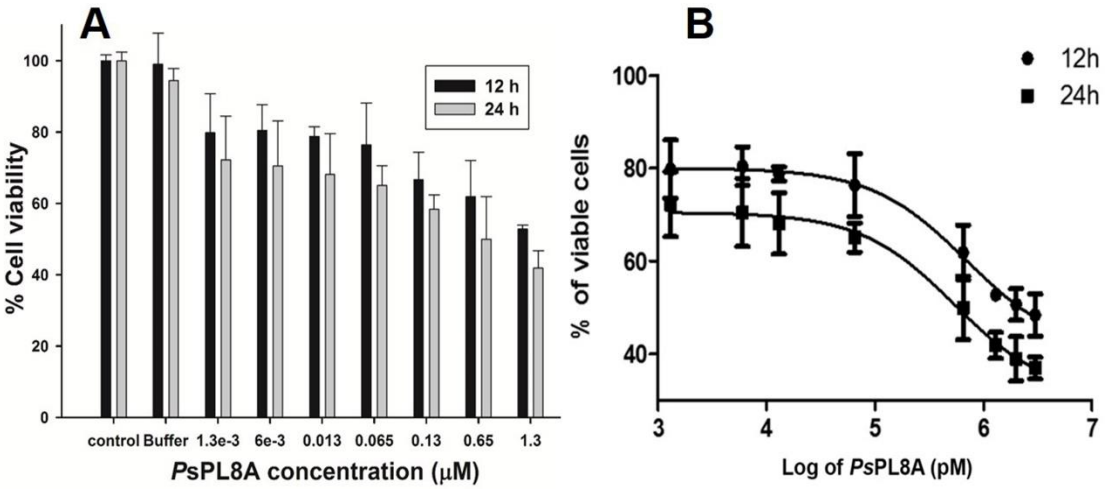

Fig. 5.3.2 (A) *In vitro* cell proliferation assay (MTT) showing percent cell viability of Human melanoma SK-Mel 28 cells treated with varying concentration (0.0013-1.3 µM) of *Ps*PL8A (B) IC_{50} curve for SK-Mel 28.

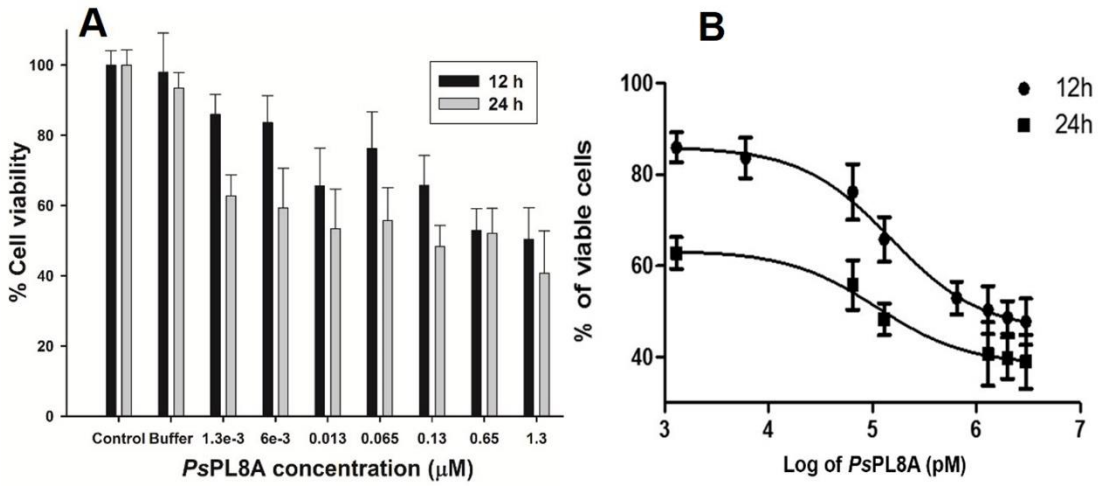

Fig. 5.3.3 (A) *In vitro* cell proliferation assay (MTT) showing percent cell viability of Human fibrosarcoma HT-1080 cells treated with varying concentration (0.0013-1.3 µM) of *Ps*PL8A (B) IC_{50} curve for HT-1080.

5.3.2 Apoptosis analysis of SK-Mel 28 and HT-1080 cell lines by Fluorescence microscopy

Apoptosis is the mode of cell death that is distinguished from necrosis by characteristics morphological and biochemical changes. These changes include compaction and fragmentation of the nuclear chromatin, shrinkage of the cytoplasm and loss of membrane asymmetry. A plasma protein phosphatidylserine gets translocated from the inner to outer side during apoptosis. The annexien-V FITC dye binds the phosphatidylserine, exposed from the membrane and hence stains the apoptotic cells, while PI stains the dead or necrotic cells. The apoptotic/necrotic mode of cell death was analysed by staining the untreated and *Ps*PL8A treated SK-Mel 28 and HT-1080 cells with annexin V-FITC and PI. The untreated SK-Mel 28 (Fig. 5.3.4 A & B) and HT-1080 (Fig. 5.3.5 A & B) cells showed no or faint green fluorescence after staining, demonstrating the viability of cells. The *Ps*PL8A (1.3 µM) treated SK-Mel 28 (Fig. 5.3.4 C & D) and HT-1080 (Fig. 5.3.5 C & D) cells showed significantly

strong green fluorescence of cell membrane with annexin-V FITC displaying membrane blebbing. The annexin-V FITC binds strongly in the *Ps*PL8A treated cells due to the loss of integrity of cellular membrane confirming the presence of apoptotic bodies after the *Ps*PL8A treatment. The dead cells showed both the membrane staining by annexin-V as well as nuclear staining by propidium iodide.

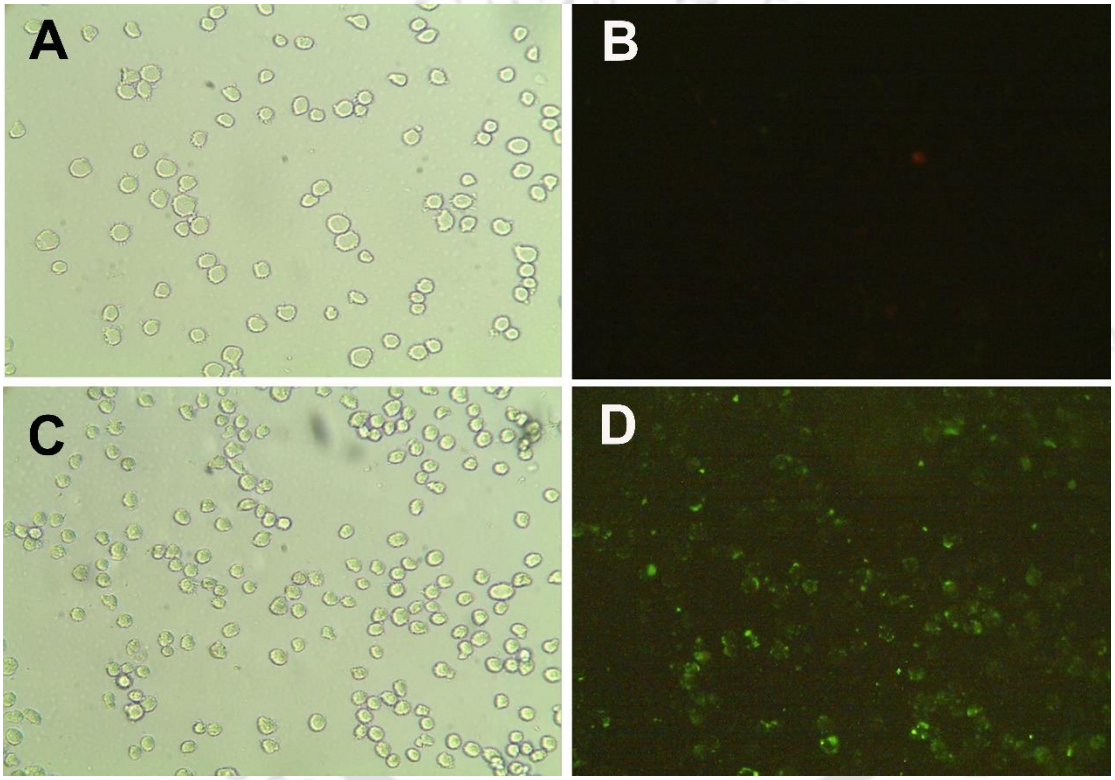

Fig. 5.3.4 Apoptosis analysis of SK Mel-28 cells by fluorescence under 20X magnification, untreated SK-Mel 28 cells under (A) Phase contrast microscope (B) fluorescence microscope. Treated SK-Mel 28 *Ps*PL8A enzyme (1.3 µM) cells under (C) Phase contrast microscope (D) fluorescence microscope.

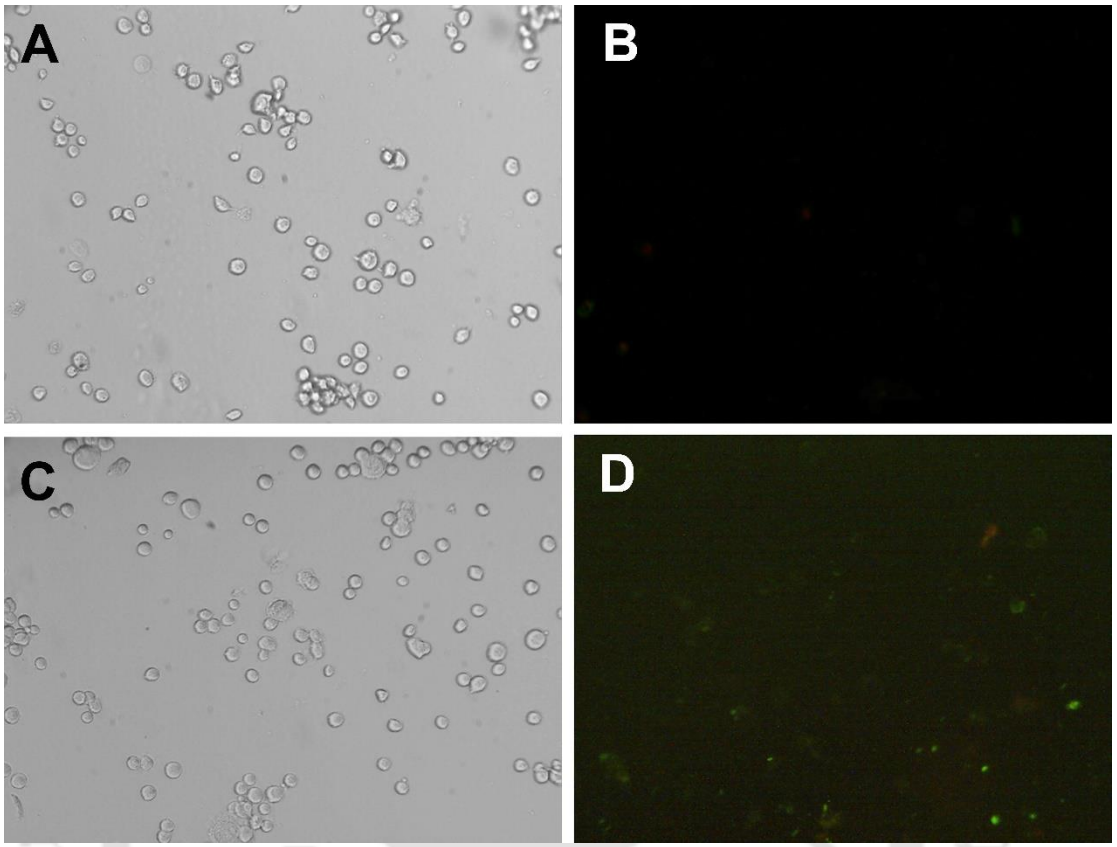

Fig. 5.3.5 Apoptosis analysis of SK Mel-28 cells by fluorescence under 20X magnification, untreated SK-Mel 28 cells under (A) Phase contrast microscope (B) fluorescence microscope. Treated SK-Mel 28 *Ps*PL8A enzyme (1.3 µM) cells under (C) Phase contrast microscope (D) fluorescence microscope.

5.3.3 Mode of cell death analysis by flow cytometry

The mode of cell death after *Ps*PL8A (1.3 µM) treatment was also studied by flow cytometric analysis of SK-Mel 28 and HT-1080 cells after staining with annexin V-FITC and propidium iodide. The untreated (negative control) SK-Mel 28 (Fig. 5.3.6A) and HT-1080 cells (Fig. 5.3.7A) did not show staining with either annexin V-FITC or propidium iodide and hence the cell population was present in the lower left quadrant. SK-Mel 28 (Fig. 5.3.6B) and HT-080 (Fig. 5.3.7B) treated with *Ps*PL8A (1.3 µM) for 24 h showed both annexin V-FITC and propidium iodide binding, indicating

apoptosis-like cell death. The flow cytometry analysis showed that *Ps*PL8A treated SK-Mel 28 and HT-1080 cell lines results ~27% and 17% apoptosis, respectively. The results of annexin-V FITC and PI staining by both microscopic analysis and flow cytometry suggested that *Ps*PL8A treatment induce the cell death in human melanoma and fibrosarcoma cells by apoptosis. Apoptosis of melanoma (SK-Mel 2) cells by chondroitin AC lyase from *Flavobacterium heparinum* was also reported in a previous study (Denholm *et al.*, 2000).

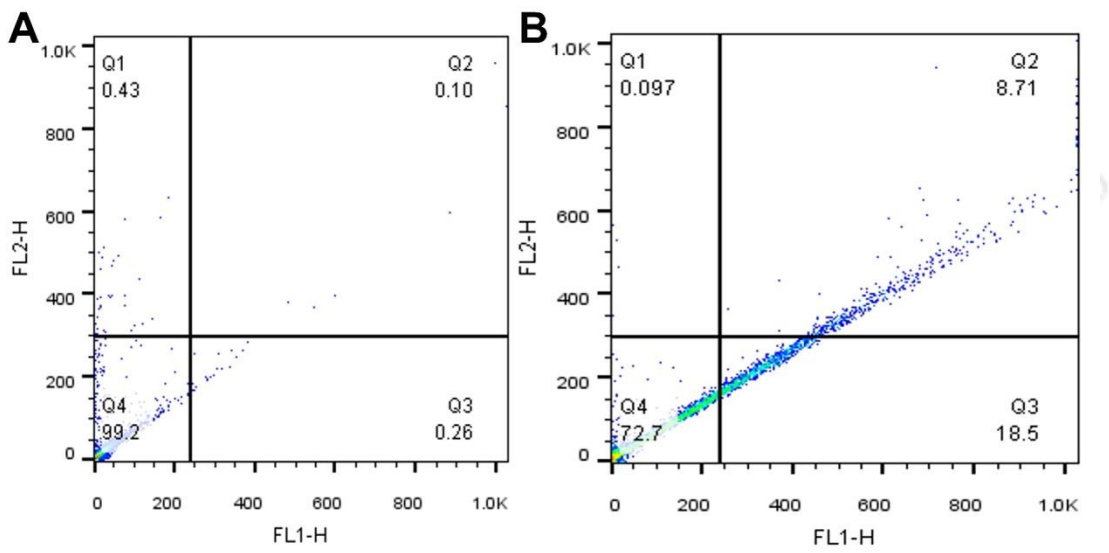

Fig. 5.3.6 Apoptosis analysis of SK Mel-28 cells by flow cytometry (A) untreated SK-Mel 28 cells and (B) *Ps*PL8A enzyme (1.3 µM) treated SK-Mel 28 cells.

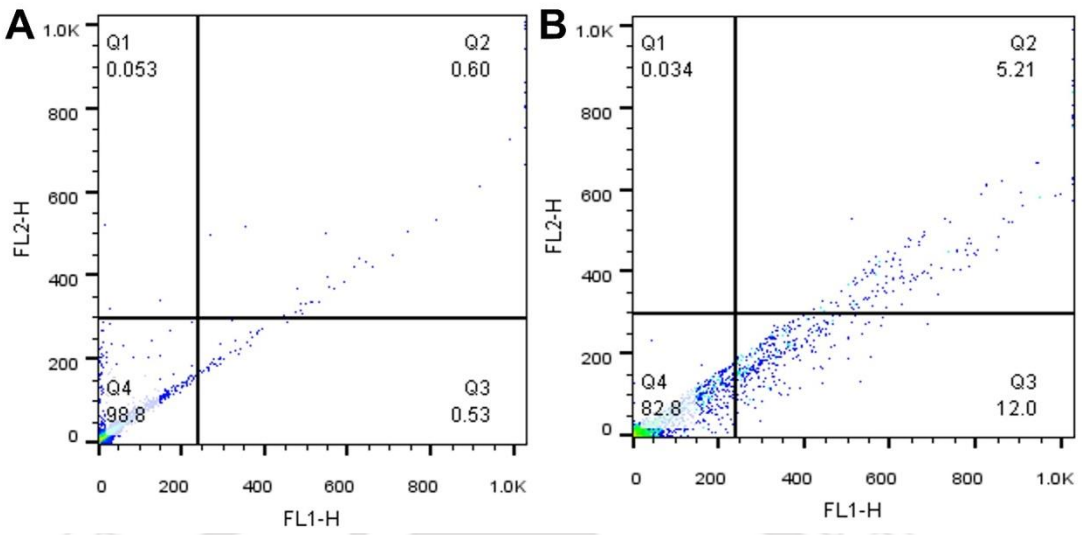

Fig. 5.3.7 Apoptosis analysis of HT-1080 cells by flow cytometry (A) untreated cells and (B) *Ps*PL8A enzyme (1.3 µM) treated cells.

5.3.4 Mitochondrial cell potential analysis of SK-Mel 28 and HT-1080 cells with *Ps*PL8A

Fluorescent probes for monitoring mitochondrial membrane potential ($\Delta\psi_m$) are frequently used for assessing mitochondrial function (Perry *et al*., 2011). The $\Delta\psi_m$ is a key indicator of cell health or injury. In normal cells, due to the electrochemical potential gradient, the dye concentrates in the mitochondrial matrix, where it forms red fluorescent aggregates (J-aggregates) (Cossarizza *et al*., 1993). The dissipation of mitochondrial potential is one of the early event in apoptosis of cells. Any event that dissipates the mitochondrial membrane potential prevents the accumulation of the JC-1 dye in the mitochondria and thus, the dye is dispersed throughout the entire cell leading to a shift from red (J-aggregates) to green fluorescence (JC-1 monomers) (Cossarizza *et al*., 1993). The JC-1 accumulates within mitochondria in inverse proportion to $\Delta\psi_m$ according to the Nernst equation. More polarized mitochondria (i.e., hyperpolarized, where the interior is more negative) will accumulate more cationic dye,

and depolarized mitochondria (interior is less negative) accumulate less dye. The effect of *Ps*PL8A treatment on SK-Mel 28 and HT-1080 was studied using JC-1 dye. The untreated SK-Mel 28 (Fig. 5.3.8 A & B) and HT-1080 (Fig. 5.3.9 A & B) were used as negative controls which gave red fluorescence with JC-1 dye. This indicated the maintenance of mitochondrial potential gradient among normal cells. The SK-Mel 28 (Fig. 5.3.8 C & D) and HT-1080 (Fig. 5.3.9 C & D) upon treatment with *Ps*PL8A (1.3 µM) for 24 h, the JC-1 dye gave green fluorescence due to dissipation of mitochondrial potential. The positive control of SK-Mel 28 and HT-1080 cells treated with valinomycin was kept, which is dissipates the mitochondrial electrochemical potential by permeabilizing the mitochondrial membrane for K^+ ions. The SK-Mel 28 (Fig. 5.3.8 E & F) and HT-1080 cells (Fig. 5.3.9 E & F) treated with 0.1 µM of valinomycin showed green fluorescence due to dissipation of mitochondrial potential. The results JC-1 dye staining suggested that *Ps*PL8A treatment dissipates the mitochondrial potential gradient of in human melanoma and fibrosarcoma cells. This disruption of mitochondrial potential of human melanoma and fibrosarcoma cells by *Ps*PL8A treatment signifies the early event leading to cell death by apoptosis. The data of mitochondrial cell potential further contended the data of Annexin-V FITC results for apoptosis mode of cell death.

Glycosaminoglycans can regulate the cell activation by triggering various signal transduction pathways. The chondroitin sulphate affects the cell proliferation of melanoma predominantly by their relative abundance and their interaction with the various cell receptors (Denholm *et al.,* 2000; Price *et al.,* 2011). Previous studies suggest that various CSPG regulate basic fibroblast growth factor, hepatocyte growth factor and interferon- γ with their respective receptors (Lyon *et al.,* 1998; Hurt-Camejo

et al., 1999; Denholm *et al.*, 2001). Cluster of differentiation 44 (CD44) and chondroitin sulfate proteoglycan 4 (CSPG4) are the two cell surface antigens having associated chondroitin sulphate proteoglycans that are involved in tumor growth and invasion of melanoma. (Price *et al.*, 2011) CSPG4 proteoglycan was identified as a highly immunogenic tumor antigen on the surface of melanoma cells and is associated with melanoma tumor formation (Price *et al.*, 2011). CSPG4 is highly expressed in majority of human melanoma cells and was deciphered to be involved in its progression (Campoli *et al.*, 2010; Price *et al.*, 2011). CSPG4 is also associated with the progression of other cancers including oligodendrocytomas, gliomas, triple-negative breast carcinomas and squamous cell carcinoma (Price *et al.*, 2011). Removing cellular and extracellular chondroitin sulfate can also reduce the cell activation through signalling pathways, which occurs during adhesion (Denholm *et al.*, 2001). These observations have prompted the researchers to explore the possible role of chondroitin sulphate lyases in understanding the cancer biology. Chondroitin AC lyase (*Ps*PL8A) degrades the CS chains and hence can be potentially utilized to treat and control the progression of melanoma and fibrosarcoma.

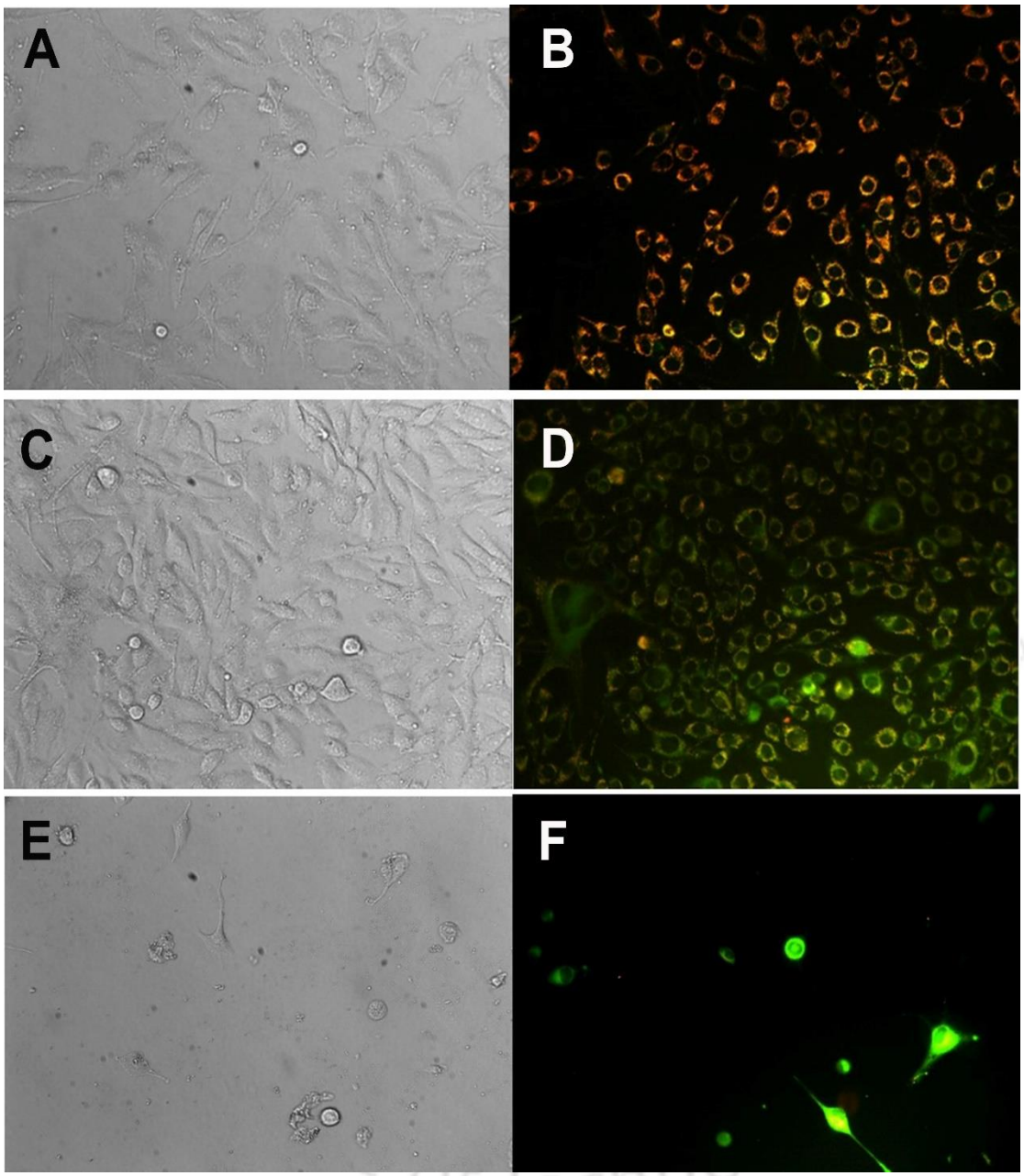

Fig. 5.3.8 Mitochondrial cell potential analysis of untreated SK-Mel 28 cells (A) Phase contrast microscope (B) fluorescence microscope. Cells treated with 1.3 µM *Ps*PL8A enzyme under (C) Phase contrast microscope (D) fluorescence microscope. Positive control of SK-Mel 28 cells treated with 0.1 µM Valinomycin under (E) Phase contrast microscope (F) under fluorescence microscope.

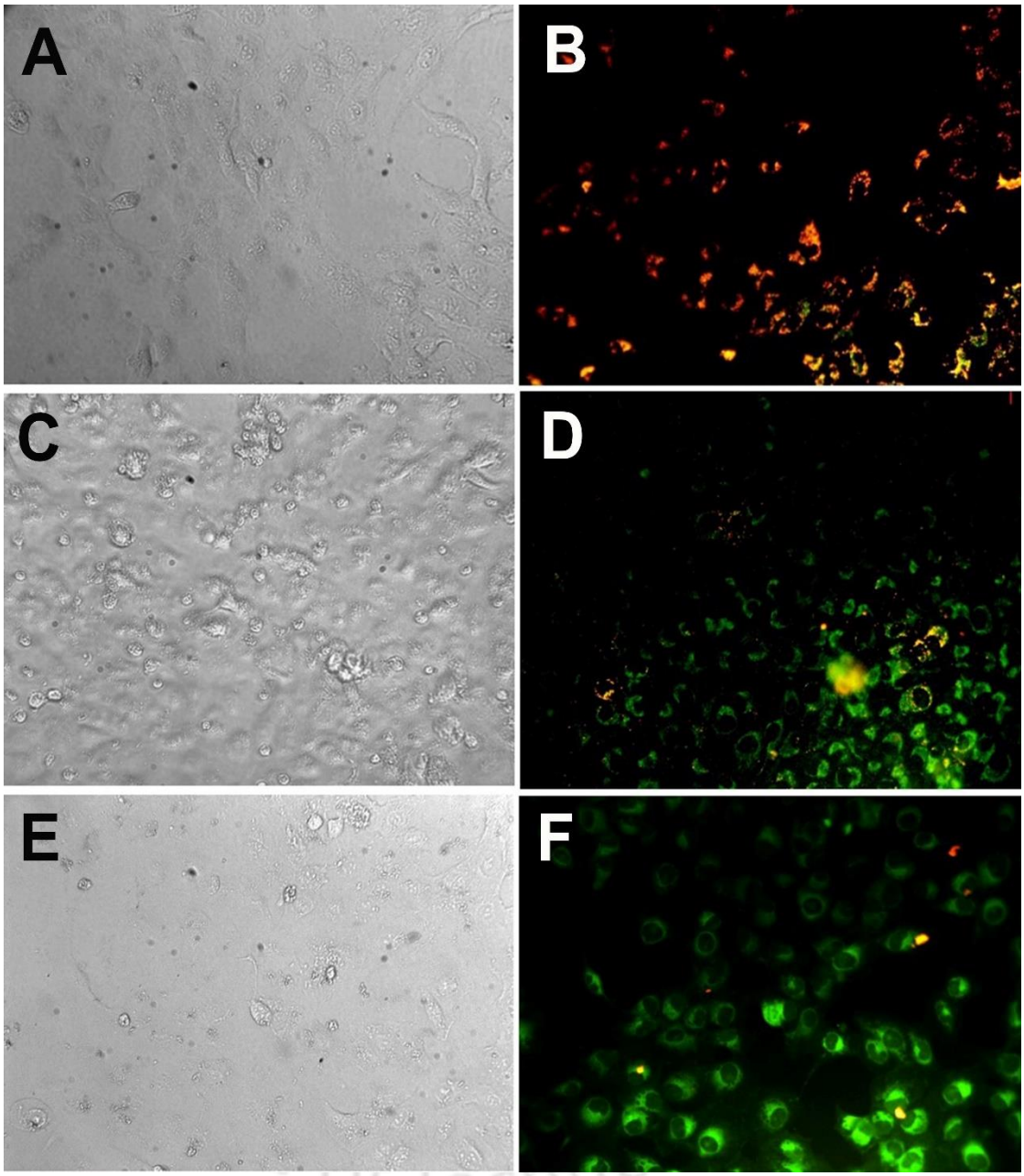

Fig. 5.3.9 Mitochondrial cell potential analysis of untreated HT-1080 cells (A) Phase contrast microscope (B) fluorescence microscope. Cells treated with 1.3 µM *Ps*PL8A enzyme under (C) Phase contrast microscope (D) fluorescence microscope. Positive control of HT-1080 cells treated with 0.1 µM Valinomycin under (E) Phase contrast microscope (F) under fluorescence microscope.

5.4 Conclusions

The anti-proliferative effect of chondroitin AC lyase (*Ps*PL8A) on human melanoma (SK-Mel 28) and fibrosarcoma (HT-1080) cell lines were determined in the present study. The treatment of mouse fibroblast L929 cell lines with chondroitin AC lyase (*Ps*PL8A) imparts no cytotoxicity displaying 95-98% cell viability. The human melanoma SK-Mel 28 and fibrosarcoma HT-1080 cell lines treated with chondroitin AC lyase (*Ps*PL8A) showed 58% and 59% inhibition of cell proliferation, respectively after 24h of treatment. Mode of cell death was studied by Annexin-V FITC using flow cytometry and fluorescence microscopy. The chondroitin AC lyase treated SK-Mel 28 and HT-1080 cell lines displayed ~27% and 17% apoptosis, respectively as observed by flow cytometry analysis. The *Ps*PL8A treated SK-Mel 28 and HT-1080 cells showed significantly strong green fluorescence of cell membrane after staining with annexin-V FITC under fluorescence microscopy, displaying the apoptosis. The SK-Mel 28 and HT-1080 treated with chondroitin AC lyase (*Ps*PL8A) and staining with JC-1 dye gave green fluorescence, hence indicating the dissipation of mitochondrial potential. The chondroitin AC lyase inhibiting the melanoma and fibrosarcoma cell proliferation and leading to their apoptotic cell death prospects a potential target for therapeutic approach in cancer treatment.

5.5 References

Afratis, N., Gialeli, C., Nikitovic, D., Tsegenidis, T., Karousou, E., Theocharis, A.D., Pavão, M.S., Tzanakakis, G.N. and Karamanos, N.K. (2012). Glycosaminoglycans: key players in cancer cell biology and treatment. *FEBS Journal*, *279*(7), 1177-1197.

Bao, X., Nishimura, S., Mikami, T., Yamada, S., Itoh, N. and Sugahara, K. (2004). Chondroitin sulfate/dermatan sulfate hybrid chains from embryonic pig brain, which contain a higher proportion of L-iduronic acid than those from adult pig brain, exhibit neuritogenic and growth factor binding activities. *Journal of Biological Chemistry*, *279*(11), 9765-9776.

Campoli, M., Ferrone, S., and Wang, X. (2010). Functional and clinical relevance of chondroitin sulfate proteoglycan 4. *Advances in Cancer Research*, *109*, 74.

Cattaruzza, S. and Perris, R. (2006). Approaching the proteoglycome: molecular interactions of proteoglycans and their functional output. *Macromolecular Bioscience*, *6*(8), 667-680.

Cossarizza, A., Ceccarelli, D., and Masini, A. (1996). Functional heterogeneity of an isolated mitochondrial population revealed by cytofluorometric analysis at the single organelle level. *Experimental Cell Research*, *222*(1), 84-94.

Denholm, E.M., Lin, Y.Q. and Silver, P.J. (2001). Anti-tumor activities of chondroitinase AC and chondroitinase B: inhibition of angiogenesis, proliferation and invasion. *European Journal of Pharmacology*, *416*(3), 213-221.

Eisenmann, K.M., McCarthy, J.B., Simpson, M.A., Keely, P.J., Guan, J.L., Tachibana, K., Lim, L., Manser, E., Furcht, L.T. and Iida, J. (1999). Melanoma chondroitin

sulphate proteoglycan regulates cell spreading through Cdc42, Ack-1 and p130cas. *Nature Cell Biology*, *1*(8), 507-513.

Garner, O.B., Yamaguchi, Y., Esko, J.D. and Videm, V. (2008). Small changes in lymphocyte development and activation in mice through tissue-specific alteration of heparan sulphate. *Immunology*, *125*(3), 420-429.

Hurt-Camejo, E., Rosengren, B., Sartipy, P., Elfsberg, K., Camejo, G., and Svensson, L. (1999). CD44, a cell surface chondroitin sulfate proteoglycan, mediates binding of interferon-γ and some of its biological effects on human vascular smooth muscle cells. *Journal of Biological Chemistry*, *274*(27), 18957-18964.

Igarashi, N., Takeguchi, A., Sakai, S., Akiyama, H., Higashi, K. and Toida, T. (2013). Effect of molecular sizes of chondroitin sulfate on interaction with L-selectin. *International Journal of Carbohydrate Chemistry*, dx.doi.org/10.1155/2013/856142.

Iida, J., Meijne, A.M., Knutson, J.R., Furcht, L.T. and McCarthy, J.B. (1996). Cell surface chondroitin sulfate proteoglycans in tumor cell adhesion, motility and invasion. In *Seminars in Cancer Biology*, *7*(3), 155-162. Academic Press.

Iozzo, R.V. and Sanderson, R.D. (2011). Proteoglycans in cancer biology, tumour microenvironment and angiogenesis. *Journal of Cellular and Molecular Medicine*, *15*(5), 1013-1031.

Kresse, H. and Schönherr, E. (2001). Proteoglycans of the extracellular matrix and growth control. *Journal of Cellular Physiology*, *189*(3), 266-274.

Li, L., Ly, M. and Linhardt, R.J. (2012). Proteoglycan sequence. *Molecular BioSystems*, *8*(6), 1613-1625.

Linhardt, R.J., Avci, F.Y., Toida, T., Kim, Y.S. and Cygler, M. (2006). CS lyases: structure, activity, and applications in analysis and the treatment of diseases. *Advances in Pharmacology*, *53*, 187-215.

Lyon, M., Deakin, J. A., Rahmoune, H., Fernig, D. G., Nakamura, T., and Gallagher, J. T. (1998). Hepatocyte growth factor/scatter factor binds with high affinity to dermatan sulfate. *Journal of Biological Chemistry*, *273*(1), 271-278.

Mosmann, T. (1983) Rapid colorimetric assay for cellular growth and survival: application to proliferation and cytotoxicity assays. *Journal of Immunological Methods*, *65*(1-2), 55-63.

Perry, S. W., Norman, J. P., Barbieri, J., Brown, E. B., and Gelbard, H. A. (2011). Mitochondrial membrane potential probes and the proton gradient: a practical usage guide. *Biotechniques*, *50*(2), 98.

Poh, Z. W., Gan, C. H., Lee, E. J., Guo, S., Yip, G. W. and Lam, Y. (2015). Divergent synthesis of chondroitin sulfate disaccharides and identification of sulfate motifs that inhibit triple negative breast cancer. *Scientific Reports*, *5*.

Price, M.A., Colvin Wanshura, L.E., Yang, J., Carlson, J., Xiang, B., Li, G., Ferrone, S., Dudek, A.Z., Turley, E.A. and McCarthy, J.B. (2011). CSPG4, a potential therapeutic target, facilitates malignant progression of melanoma. *Pigment Cell & Melanoma Research*, *24*(6),1148-1157.

Rani, A., and Goyal, A. (2016). A new member of family 8 polysaccharide lyase chondroitin AC lyase (*Ps*PL8A) from *Pedobacter saltans* displays endo-and exo-lytic catalysis. *Journal of Molecular Catalysis B: Enzymatic*, *134*, 215-224.

Rauch, U. and Kappler, J. (2006). Chondroitin/dermatan sulfates in the central nervous system: their structures and functions in health and disease. *Advances in Pharmacology, 53*, 337-356.

Skandalis, S.S., Labropoulou, V.T., Ravazoula, P., Likaki-Karatza, E., Dobra, K., Kalofonos, H.P., Karamanos, N.K and Theocharis, A.D. (2011) Versican but not decorin accumulation is related to malignancy in mammographically detected high density and malignant-appearing microcalcifications in non-palpable breast carcinomas. *BMC Cancer 11*, 314.

Sneath, R.J. and Mangham, D.C. (1998). The normal structure and function of CD44 and its role in neoplasia. *Molecular Pathology, 51*(4), 191.

Sugahara, K., Mikami, T., Uyama, T., Mizuguchi, S., Nomura, K. and Kitagawa, H. (2003). Recent advances in the structural biology of chondroitin sulfate and dermatan sulfate. *Current Opinion in Structural Biology*, *13*(5), 612-620.

Theocharis, A.D., Tsolakis, I., Tzanakakis, G.N. and Karamanos, N.K. (2006). Chondroitin sulfate as a key molecule in the development of atherosclerosis and cancer progression. *Advances in Pharmacology, 53*, 281-295.

Uyama, T., Kitagawa, H. and Sugahara, K. (2007). In *Comprehensive Glycoscience*, Kamerling J.P. Ed.: Elsevier: Amsterdam, vol. *3*, pp, 79-104.

Van Meerloo, J., Kaspers, G.J. and Cloos, J. (2011) Cell sensitivity assays: the MTT assay. *Cancer Cell Culture: Methods and Protocols*, 237-245.

Yamada, S. and Sugahara, K. (2008). Potential therapeutic application of chondroitin sulfate/dermatan sulfate. *Current Drug Discovery Technologies*, *5*(4), 289-301.

Chapter 6

Physicochemical, antioxidant and biocompatible properties of chondroitin sulphate isolated from chicken keel bone for potential biomedical applications

6.1 Introduction

The waste by products from slaughter house and poultry industries can serve as the major sources of cartilage. Cartilage mainly constitutes glycosaminoglycans (GAGs) and collagens (Garnjanagoonchorn *et al.*, 2007; Vázquez *et al.*, 2013). GAGs are heteropolysacchrides made up of disaccharide repeats of D-galactosamine/D-glucosamine and D-glucuronic acid/L-Iduronic acid. GAGs are abundant in the cartilages (Iozzo *et al.*, 1998). The cartilage matrix is composed of fine mesh of collagen embedded with hyaluronic acid (HA), chondroitin sulphate (CS), various glycoproteins and proteoglycans (PGs). CS is composed of N-acetyl galactosamine (GalNAc) and glucuronic acid (GlcA), linked by β-(1→3)-glycosidic bond, while the two disaccharides are linked by β-(1→4) linkage. CS has been classified as chondroitin 4-sulfate (CS-A), chondroitin 6-sulfate (CS-C) and dermatan sulfate (DS/CS-B) with

sulfation at C4 and C6 positions of GalNAc residue, respectively and C4 of GalNAc/C2 of GlcA for DS (Schiller *et al.,* 2012).

CS is a part of connective tissues and involved in major biological processes such as resiliency, structural integrity of cartilage and maintenance of synovial fluid in the bone joints owing to its polyanionic structure (Luo *et al.,* 2002, Henrotin *et al.,* 2010). Low molecular weight CS is used as oral nutraceutical supplement for joint disorder treatment (Hochberg *et al.,* 2008; Henrotin *et al.,* 2012; Raynauld *et al.,* 2016). The beneficial effects of CS have been reported for joint pains, stiffness and swelling in osteoarthritis patents (Hochberg *et al.,* 2015; Raynauld *et al.,* 2016). CS alone or in combination with HA or chitosan were used to formulate scaffolds that mediate and accelerate the regeneration of damaged tissues, bone repair, cartilage and cutaneous wounds (Bianchera *et al.,* 2014). CS-hydrogels are appealing materials for biomedical application as they enhance wound healing by reepithelialization and neovascularization (Bianchera *et al.,* 2014). CS also acts as free radical scavenger and decreases DNA fragmentation, protein degradation and cell death rate (Campo *et al.,* 2006; Henrotin *et al.,* 2010). The partially purified CS was also used as food preservative and emulsifying agent (Hamano *et al.,* 1989; Vázquez *et al.,* 2013).

CS is commercially available from various sources such as, bovine cartilage, bovine trachea and shark fin. The increasing demand and the high cost of CS has led to the exploitation of shark and bovine which impart a strong impact on the ecological balance (Field *et al.,* 2010; Vázquez *et al.,* 2013). CS has been isolated from other sources *viz.* ray fish and crocodile cartilages (Garnjanagoonchorn *et al.,* 2007), broiler chicken carcasses (Nakano *et al.,* 2012; Srichamroen *et al.,* 2013), duck trachea (Vittayanont *et al.,* 2014), chicken keel cartilage (Luo *et al.,* 2002; Khan *et al.,* 2013),

Bony fishes (Maccari *et al.*, 2015) and sea cucumber (Zou *et al.*, 2016). Production of bioengineered chondroitin using a non-pathogenic *E. coli* strain by metabolic engineering approach has been reported (He *et al.*, 2015). However, the bioengineering approach has the disadvantages of relatively high cost and the lack of commercializable sulfation method for CS production. All these reasons make it essential for researchers to seek for more different animal sources of CS isolation. CS is also in high demand for its applications in tissue engineering, pharmaceutical, cosmetic and food industries. This makes it essential to rigorously characterize the physicochemical, biocompatible and antioxidant properties of CS. Most of the reports however, have focused on isolation and partial characterization of CS. This is the first study on the isolation, complete physicochemical and structural characterization of a CS from chicken keel bone cartilage that displayed biocompatible, antioxidant and emulsifying potentials. These preliminary results will facilitate further exploration of CS-Keel for emulsifying and antioxidant activities under *in vivo* studies.

6.2 Materials and Methods

6.2.1 Substrates and reagents

Keel bone cartilage of chicken was collected from the waste of a local slaughter house, Guwahati, Assam, India. Papain from *Carica papaya*, Carbazole reagent and Phosphate buffer saline (PBS) were purchased from Himedia Pvt. Ltd., India. Chondroitin 4-sulphate sodium salt (C4S) from bovine trachea, Chondroitin 6-sulfate sodium salt (C6S), D-Glucuronic acid (GlcA), Potassium bromide (KBr), 1-diphenyl-2-picrylhydrazyl (DPPH), MTT [3-(4,5-dimethylthiazol-2-yl)-2,5-diphenyltetrazolium bromide, Chondroitin 4-sulphate disaccharide (UA-GalNAc4S) and UA2S-GalNAc were purchased from Sigma-Aldrich, USA. Chondroitin 6-sulphate disaccharide (UA-GalNAc6S) was purchased from Dextra Laboratories Ltd., U.K. Trizma (Tris base), disodium EDTA, Sodium acetate, Cysteine-HCl, Sodium hydroxide, Sodium borohydride, $NaNO_3$, Ascorbic acid, n-Hexadecane, Dulbecco's Modified Eagle Medium (DMEM) low glucose medium were procured from Sigma-Aldrich, USA. D_2O (99.96%) and ethanol were purchased from Merck, Germany. Fetal bovine serum (FBS), 50 µg/ml streptomycin and 50 IU/ml penicillin were purchased from Gibco.

6.2.2 Isolation of CS from the Keel bone cartilage

CS was isolated from keel cartilage using the method of Lauder et al., 2000. One hundred gram of cartilage was diced and boiled for 15 min to remove the meat and connective tissues. The remaining cartilage was washed with Milli-Q water and wet weight was taken. This was digested with papain (1U/100 mg tissue) in 100 ml of 0.1 M sodium acetate buffer, pH 6.8 containing 2.4 mM EDTA and 10 mM cysteine HCl and incubated at 65°C for 24h. GAG containing CS was precipitated from soluble fraction by adding 4 volumes of ethanol and the solution was cooled to 4°C and allowed

to stand overnight. It was centrifuged at 13,000***g*** and 4°C for 30 min and the pellet was resuspended in minimum volume of 50 mM sodium acetate buffer (pH 6.8). The CS-Keel was precipitated by dropwise addition of 2 volumes of ethanol with constant stirring at 25°C. The solution was cooled to 4°C and allowed to stand overnight for recovery of CS-rich precipitate which was resuspended in 5 ml of 50 mM sodium acetate buffer (pH 6.8) and dialyzed overnight against distilled water. The dialysed CS was lyophilized. The residual amino acids were removed by treating 18 g of lyophilized CS-Keel resuspended in 5 ml Milli-Q water with 0.05 M NaOH and 1M sodium borohydride at 45ºC for 12h. CS-Keel was precipitated by neutralizing with 5 ml**,** 1 M sodium acetate. The CS-Keel precipitate was resuspended and dialysed against Milli-Q water to remove the excess salts and finally lyophilized for further use.

6.2.3 Determination of molecular weight of CS-Keel by HPSEC and particle size by DLS

The molecular mass of CS-keel (1 mg/ml) was determined using high performance size exclusion chromatography (HPSEC) system consisting of Phenomenex Polysep-GFC-P6000 column connected with a guard column Phenomenex Polysep-GFC-P and Prominence, UFLC (Shimadzu, Japan) equipped with RI detector. 10 µl samples each of CS-Keel, standards and reference (1 mg/ml) were loaded and eluted using 0.1M $NaNO_3$ with a flow rate of 0.5 ml/min. C4S and C6S (Sigma Aldrich, USA.) each at 1 mg/ml were used as reference. The standard dextran T20, T40, T70, T100, T200 and T500 (1 mg/ml) were used as standards to calculate the molecular weight of CS-Keel. The particle size of CS-keel (1 mg/ml in 0.1M $NaNO_3$) was determined by Dynamic Light Scattering (DLS) (Zetasizer nano, Malvern, UK).

6.2.4 Composition analysis of CS-Keel

The CS-Keel polysaccharide was purified by HPSEC. A stock solution (10 mg/ml) of isolated crude CS-Keel was prepared. 50 µl of CS-keel solution was applied to Phenomenex Polysep-GFC-P6000 column connected with a guard column Phenomenex Polysep-GFC-P and Prominence, UFLC (Shimadzu, Japan) equipped with RI and UV detector. The UV detector was set at 280 nm to identify the peak specifically for the protein. The peak corresponding to CS-Keel (100 kDa) was eluted and collected. This process was repeated 10 times for collection of enough CS keel for Carbazole assay. The eluted purified CS-Keel fractions were mixed and lyophilised. The protein content of the purified and lyophilised CS-Keel was estimated by method of Lowry *et al.,* 1951 using bovine serum albumin (BSA) as standard in the concentration range, 25-500 µg/ml. The carbazole assay is used for quantification of uronic acid present in GAG and is based on the quantitative concentration-dependent colour reaction between carbazole and the uronic acid. The uronic acid content of purified lyophilised CS-Keel was estimated by carbazole method (Frazier *et al.*, 2008). C4S and GlcA were used as standards at a concentration range, 4 - 40 µg/ml

6.2.5 Quantification of CS disaccharides in CS-Keel by enzymatic digestion

The enzymatic depolymerisation of CS-Keel was achieved by using chondroitin AC lyase (*Ps*PL8A) from *Pedobacter saltans* (Rani and Goyal., 2016). The digestion of CS-Keel with 5 µg/ml of *Ps*PL8A was carried out in a 1 ml reaction mixture containing, 5.0 mg/ml CS-Keel in 50 mM Tris-HCl buffer, pH 7.2 and incubating the reaction at 39°C for 24 h (Rani and Goyal., 2016). 1 ml reaction mixture was then treated with 1 ml absolute ethanol and centrifuged at 13000g at 25ºC for 10 min to precipitate the undigested CS-Keel (Rani and Goyal 2016). The glucuronic acid content

in the un-digested and the digested sample in the supernatant was quantified by carbazole assay (Frazier *et al.,* 2008). The sample was analysed by Electron Spray Ionization (ESI) mass spectrometer (Waters, Q-TOF Premier) in both MS and tandem MS (MS/MS) mode. ESI-MS and tandem MS analyses were carried out in negative ion mode, where the parameters for ESI-MS analysis were; capillary voltage 3 eV, collision energy 5 eV, ionization energy 1 eV, desolvation temperature 250°C and the source temperature of 80°C. The tandem MS analysis was carried out by nanospray ionization using the voltage 3 eV, collision energy 20 eV and collision-induced dissociation was performed on ion of interest using the argon gas. The detection and quantification of disaccharide composition was analysed by electronspray tandem mass spectrometery (Desaire *et al.,* 2000a). The relative abundance of product ions for pure isomeric standards (UA-GalNAc4S and UA-GalNAc6S) were used in a binary system. The disaccharide composition of digested CS-Keel was quantified based on the MS/MS spectra of all standards (Desaire *et al.,* 2000a).

6.2.6 Fourier transform infrared (FT-IR) spectroscopic analysis of CS-Keel

FT-IR spectroscopy was used for determining the functional groups present in CS-Keel. CS-Keel was pressed into KBr pellet (sample: KBr, 1:100) using 15 Ton Hydraulic Press. FTIR spectrophotometer (Perkin Elmer, Spectrum Two, USA) was used to obtain the spectrum in 4000-500 cm^{-1} region in the transmission mode with 32 scans per min. The spectral resolution was 4 cm^{-1}.

6.2.7 ^{1}H-NMR spectroscopic analysis of CS-Keel

CS-Keel (5 mg/ml) was dissolved in D_2O (99.96%) (Merck, Germany) and ^{1}H-NMR spectrum was acquired at 25ºC using 600 MHz NMR spectrometer (Bruker,

Avance III-HD, USA) fitted with a 5-mm probe and equipped with topspin software (Bruker) for analysis.

6.2.8 Scanning electron microscopy (SEM) analysis of CS-Keel bone

5 mg of CS-Keel was fixed on the SEM stubs using double sided carbon tape, then coated with ~10 nm thick layer of gold. The samples were observed in a scanning electron microscope (Zeiss, Sigma, Germany) at an accelerating voltage of 2.5 kV at 500x and 1000x magnifications.

6.2.9 Atomic Force Microscopic (AFM) analysis of CS-Keel

A stock solution of CS-Keel (5 mg/ml) was prepared in Milli-Q water. The solution was diluted to make final concentrations of 0.01, 0.05 and 1.0 mg/ml. 10 µl of each diluted CS-Keel solution was dropped on the surface of mica sample carrier and allowed to dry at 25°C and analysed using semi-contact imaging mode. AFM analysis was performed using atomic force microscope (Agilent 5500, USA). The data obtained were processed using WSxM 5.0 Develop 7.0 software (Horcas *et al.*, 2007).

6.2.10 Thermogravimetric Analysis (TGA) and Derivative Thermogravimetric Analysis (DTG) of CS-Keel

The TGA and DTG of CS-Keel was carried out using thermal analyser (Hitachi STA7200, Japan) operating at atmospheric pressure under nitrogen gas flow rate of 100 ml/min. The CS-Keel (6.5 mg) was placed in a Al_2O_3 crucible and heated at a linear heating rate of 10ºC min^{-1} over a temperature range, 30ºC-600ºC and the corresponding weight loss was determined.

6.2.11 Differential scanning calorimeter (DSC) analysis of CS-Keel

The DSC analysis of CS-Keel was carried out using thermal analyser (STA 449-F3, Germany) operating at atmospheric pressure under argon gas at a flow rate of 100

ml/min. The CS-Keel (3 mg) was placed in an Al_2O_3 crucible and heated at a linear heating rate of 10ºC min^{-1} over a temperature range, 25ºC-800ºC and enthalpy changes were determined.

6.2.12 *In vitro* cell proliferation assay of CS- Keel

The mouse fibroblast cell line (L929) was procured from National Centre for Cell Science, Pune, India. The L929 cells were cultured in Dulbecco's Modified Eagle Medium (DMEM) low glucose medium supplemented with 10% (v/v) heat-inactivated fetal bovine serum (FBS) (Gibco), 50 µg/ml streptomycin and 50 IU/ml penicillin (Gibco) incubated at 37ºC under 5% CO_2. The effect of CS-Keel on L929 cells viability was analysed by MTT [3-(4,5-dimethylthiazol-2-yl)-2,5-diphenyltetrazolium bromide] assay (Mosmann, 1983). The cells were seeded at a density of $2x10^4$ cells/well in a 96 well plate and incubated at 37ºC in 5% CO_2 for 16h for cell adherence. After incubation, the medium was completely removed and the cells were exposed to different concentrations (0.5 mg/ml to 5 mg/ml) of CS-Keel dissolved in serum-free DMEM medium (incomplete). The incomplete DMEM medium without CS-Keel was used as negative control. The plate was incubated at 37ºC in 5% CO_2 for 12h and 24h. MTT assay was done after 12h and 24h by removing the medium and washing the wells with 200 µl of 1x phosphate buffer saline (PBS). 100 µl of MTT (0.5 mg/ml) was added to each well and plate was incubated at 37ºC in 5%CO_2 for 4h. After the incubation, MTT was removed from the wells and the formazan formed was dissolved by adding 100 µl of dimethyl sulfoxide. The absorbance at 570 nm was monitored by a 96-well microplate reader (Tecan, Infinite 200 Pro, Switzerland). The cell viability (%) was calculated according to Meerloo et al., 2011.

6.2.13 Microscopic analysis of CS-Keel treated L929 cells

The surface morphology of L929 cells was observed after treating with CS-Keel for 24h. The L929 cells were maintained and seeded as described in the section 2.10. The cells were treated with 5 mg/ml of CS-Keel dissolved in incomplete DMEM medium. The cells in only incomplete DMEM medium were used as control. After 24h of treatment, the cells were observed under microscope (Nikon, TS100F, Japan) and photomicrographs were taken and processed using imaging software (Nikon NIS-Element).

6.2.14 DPPH radical scavenging activity of CS-Keel

1-diphenyl-2-picrylhydrazyl (DPPH) scavenging activity was measured by the method of Lee et al., 2010. 100 µl of 0.5 mM DPPH in ethanol was mixed with 100 µl of different concentrations (0.25 mg/ml-5 mg/ml) of CS-Keel dissolved in 50 mM Tris-HCl buffer (pH 7.2). The reaction mixture was incubated in dark at 37°C for 30 min and 50 mM Tris-HCl was used as blank. The absorbance at 517 nm was measured using a microplate reader (Tecan, Infinite 200 Pro, Switzerland). The DPPH scavenging activity was calculated according to Lee *et al.*, 2010.

6.2.15 Assay of inhibition of ascorbate autoxidation

The ascorbate inhibition assay was performed according to method of Lin et al., 1999. 0.01 ml of varying concentrations (0.5 mg/ml-5 mg/ml) of CS-Keel was added to 0.98 ml of 0.2 mM sodium phosphate buffer, pH 7.0 and 0.01 ml of 5 mM ascorbic acid solution (Sigma Aldrich, USA). A blank was set up in parallel to the reaction with distilled water in place of CS-Keel. The 1 ml reaction mixture was transferred to the UV cuvette and incubated at 37ºC and the absorbance at 265 nm was observed as a function of time for 10 min on a UV-Visible spectrophotometer (Varian, Cary 100).

The percentage inhibition of ascorbate autoxidation was calculated as mentioned by Lin *et al.,* 1999.

6.2.16 Emulsifying properties of CS-Keel

The emulsifying property of CS-Keel was analyzed by method described by Bramhachari *et al.,* 2007. 0.5 mg of CS-Keel was dissolved in 0.5 ml of Milli-Q water by heating at 100ºC. The 1x PBS, pH 7.4 was used to make up the reaction volume to 2 ml. 0.5 ml of n-Hexadecane was added to 2 ml reaction for emulsion formation and mixed by vigorous vortexing for 2 min. The absorbance at 0 min (A_0) was measured at 540 nm immediately after mixing the content. The reaction sample was incubated at 25ºC and decrease in absorbance (A_t) was recorded at 30 and 60 min. The negative control consisted of 2 ml of 1x PBS and 0.5 ml n-hexadecane without CS keel, while the commercial guar gum was used as positive control. The emulsifying activity was calculated according to Bramhachari *et al.,* 2007.

6.2.17 Statistical analysis

All experiments were performed in triplicates (n = 3). The results were presented as means of three determinations ± SD (standard deviation).

6.3 Results and Discussion

6.3.1 Extraction and molecular weight determination of CS-Keel

The chondroitin sulphate (CS) was isolated from the poultry waste of keel bone cartilage and 15% (g/g of cartilage) yield was achieved after lyophilisation (Fig.6.3.1A). The molecular mass of references chondroitin 4-sulphate and chondroitin 6-sulphate were 70 kDa (Fig 6.3.1B) and 110 kDa, (Fig 6.3.1C) respectively as determined by HPSEC. The molecular weight of CS-Keel was 100 kDa (Fig. 6.3.1D). Another peak of 1 kDa appeared which might be due to the presence of small peptides or stretches of amino acids along with CS-Keel. The protein contamination varies significantly depending on the source of cartilage. Two contaminating proteins, 77.8 kDa and 50.5 kDa were found in extracted GAG from chicken keel bone, which reduced the overall yield of CS content (Khan *et al.*, 2013). The DLS analysis of CS-Keel solution revealed polydispersity (Fig. 6.3.1E). The CS-Keel sample contained two peaks with hydrodynamic diameter of 255 nm and 44 nm which might be possibly corresponding to 100 kDa for CS-Keel polysaccharide and 1 kDa for peptide peaks. The CS polysaccharide was reported to be polydispersed as well as large differences were also observed the average molecular weights of preparations from different sources (Hjertquist and Wasteson., 1971).

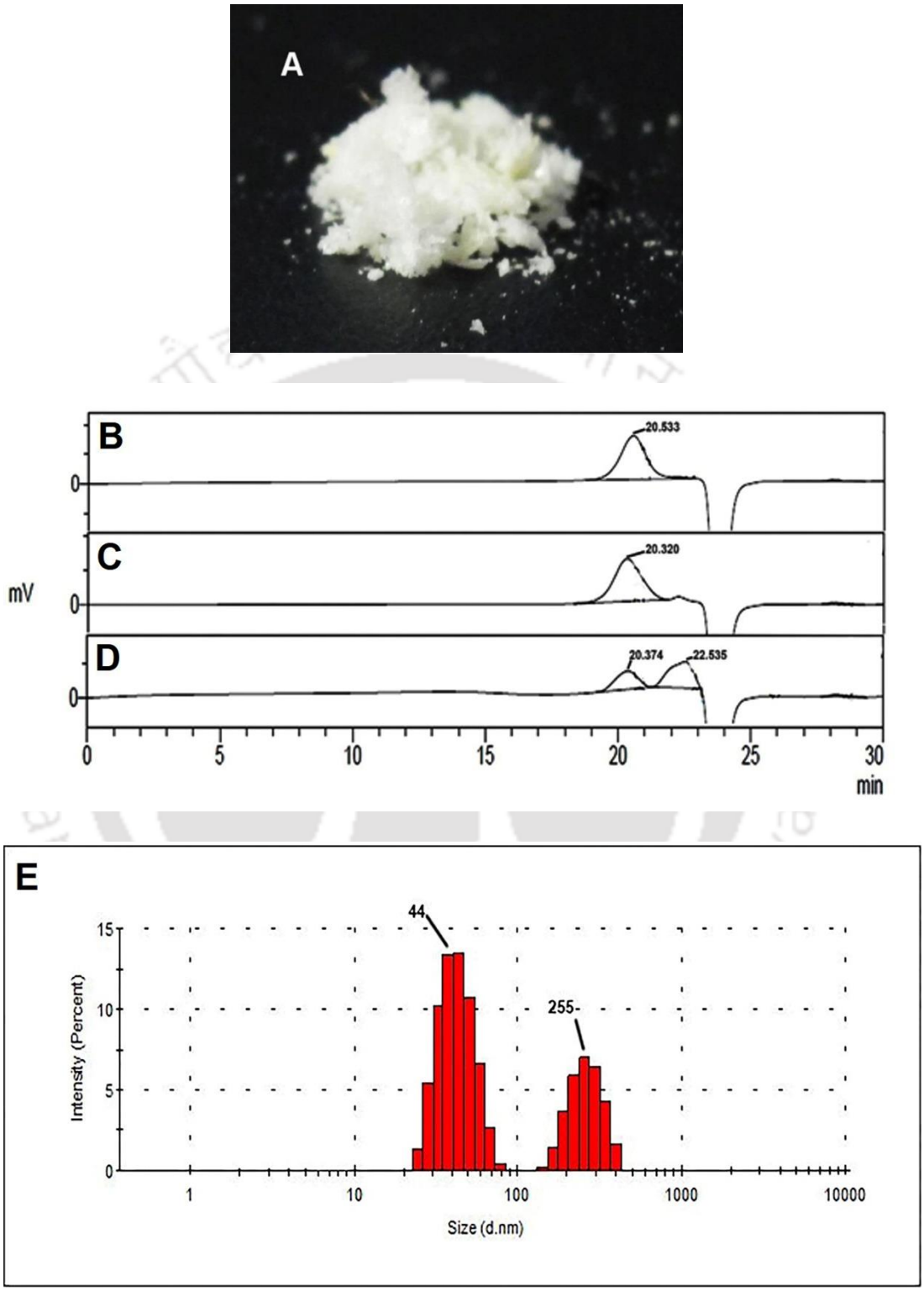

Fig. 6.3.1 (A) Digital image of isolated lyophillized CS-Keel polysaccharide. HPSEC chromatogram of (B) C4S from Sigma (C) C6S from Sigma (D) Isolated CS-Keel and (E) DLS analysis of CS-Keel in the range of 0-10000 d.nm (hydrodynamic radius).

6.3.2 Compositional analysis of HPSEC purified CS-Keel

The uronic acid content of HPSEC purified CS-Keel as assayed by Carbazole method was 53±5% (g/g of purified CS-Keel). The protein content analysis of purified CS-Keel showed that there was no trace of protein.

6.3.3 Quantification of CS disaccharides in CS-Keel by enzymatic digestion

Mass spectrometry (MS) is being used as a powerful tool for structural analysis of isolated polysaccharides (Desaire *et al.*, 2000b). MS provides advantage in terms of accurate analysis and low sample consumption as compared to HPAEC and HPLC-UV detection (Desaire *et al.*, 2000b). CS-Keel was digested with chondroitin AC lyase (*Ps*PL8A) and its disaccharide composition was quantified by MS and MS/MS analysis. The MS analysis of three standard disaccharides UA-GalNAc4S (Fig. 6.3.2A), UA-GalNAc6S (Fig. 6.3.2C) and UA2S-GalNAc gave a major ion peak at m/z 458. The peak at m/z 458 was selected for MS/MS analysis for the three disaccharide standards. After MS/MS the UA-GalNAc4S (Fig. 6.3.2B), UA-GalNAc6S (Fig. 6.3.2D) and UA2S-GalNAc (data not shown) standards gave major peak at m/z 300, m/z 282 and m/z 237 respectively. The MS analysis of digested CS-Keel sample gave major ion peak at m/z 458 (Fig. 6.3.2E). The MS/MS analysis of CE-Keel sample gave two peaks, one major peak at m/z 300 and other at m/z 282, which signifies the presence of UA-GalNAc4S, UA-GalNAc6S disaccharides in the sample (Fig. 6.3.2F). The absence of any peak at m/z 237 rules out the presence of UA2S-GalNAc in the CS-Keel sample.

The quantification of disaccharides in CS-Keel was done by using protocol described by Desaire *et al.*, 2000a. The contribution of ions with m/z 282 and m/z 300 (as percentage of total ion current) were determined for the two standard disaccharide

UA-GalNAc4S, UA-GalNAc6S from their MS/MS chromatograms. The binary equations were derived using these values

$$3.3 \times A + 55.5 \times B = C_{282} \quad (1)$$

$$73.5 \times A + 5.14 \times B = C_{300} \quad (2)$$

Where, A and B are the apparent percentages of UA-GalNAc4S, UA-GalNAc6S disaccharide in CS-Keel sample, and C_{282} and C_{300} are the percentage contribution of two diagnostic ions in the sample. The value of A and B were calculated by inserting the values of C_{282} and C_{300} in the sample. A normalization factor was used as reported earlier (Desaire *et al.*, 2000a) as many factors including the differences in the respective ionization efficiencies of the isomers might influence the peak intensities in the sample. The normalization factor for m/z 300 was 0.677, while for m/z 282 was 1.8 (Table 6.3.1). After normalizing, the observed values for A and B were then converted to the actual relative molar percentages of UA-GalNAc4S and UA-GalNAc6S disaccharide in CS-Keel sample by dividing each normalized value by the sum of the two normalized values (Desaire *et al.*, 2000a). The quantified percentages of UA-GalNAc4S and UA-GalNAc6S disaccharide in CS-Keel sample were 58% and 42%, respectively (Table 6.3.1).

Table. 6.3.1 Quantification of UA-GalNac4S and UA-GalNAc6S in CS-Keel by MS/MS.

Contributions of diagnostic ions	A and B	Normalization factor (Norm 1)	Ratios (A or B x Norm 1)	Calculated % of Disaccharides
m/z 300 = 48.20	A = 64.33	0.677	43.55	58 % (UA-GalNAc4S)
m/z 282 = 11.90	B = 17.78	1.80	32.00	42 % (UA-GalNAc6S)

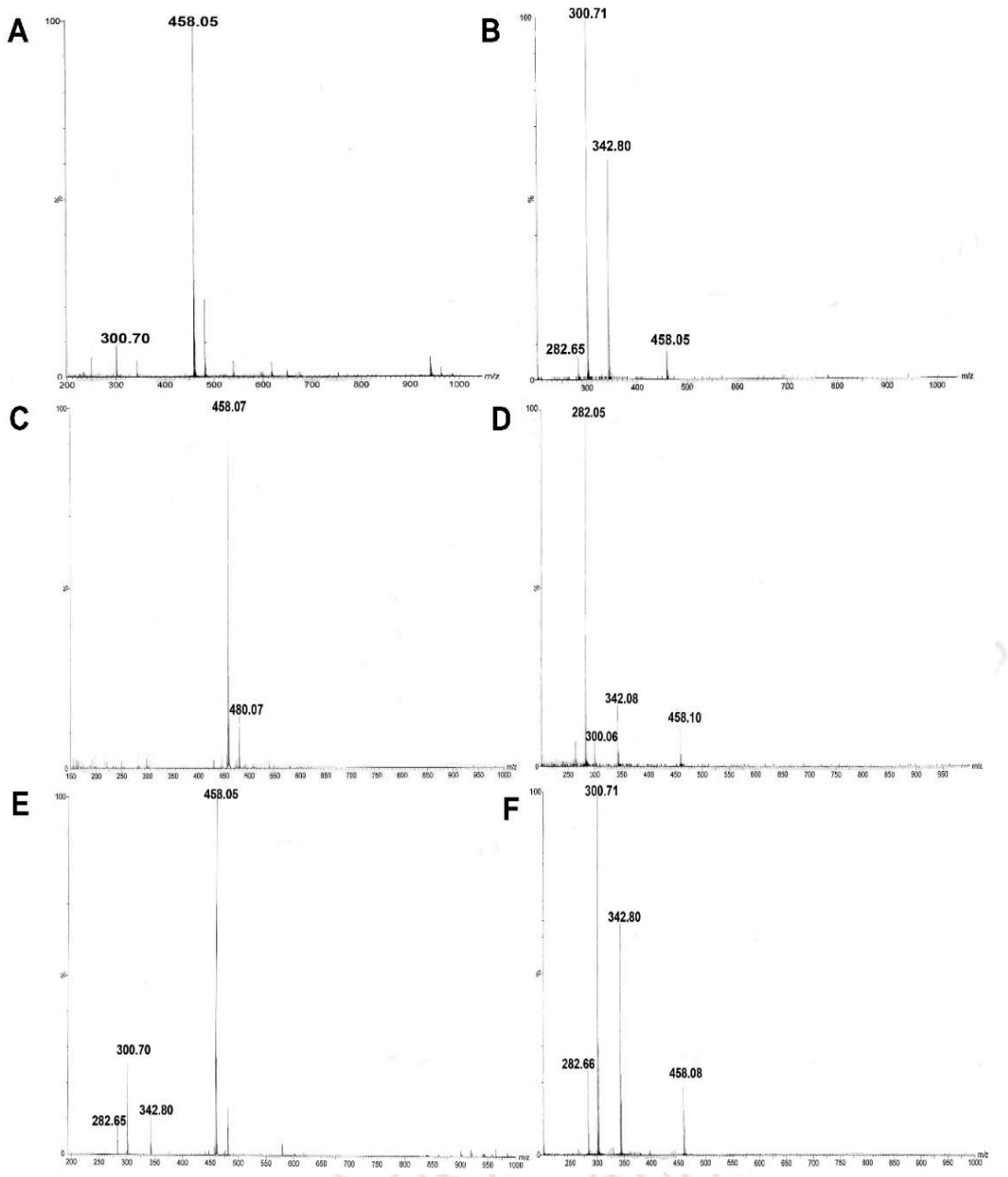

Fig. 6.3.2 ESI-Mass spectrometric analysis of (A) MS analysis of standard UA-GalNAc4S, (B) MS/MS analysis of standard UA-GalNAc4S, (C) MS analysis of standard UA-GalNAc6S, (D) MS/MS analysis of standard UA-GalNAc6S, (E) MS analysis of enzymatic digested sample of CS-Keel and (F) MS/MS analysis of enzymatic digested sample of CS-Keel.

6.3.4 Identification of type of chondroitin sulphate in CS-Keel by FT-IR

The FT-IR spectrum of commercial C4S and C6S showed the corresponding peaks of sulphation at 856.9 cm^{-1} and 826.1 cm^{-1}, respectively (Fig. 6.3.3A & B). The isolated CS-Keel spectrum displayed a distinct peak of sulphate group at 856.9 cm^{-1} indicating the polysaccharide being C4S (Fig. 6.3.3C). The peaks assigned for sulphation in present study corroborated with the previous findings by Garnjanagoonchorn *et al.,* 2007 and Wang *et al.,* 2009. The peaks for various other functional groups were analysed. The peak at 1411.2 cm^{-1} represented the coupling of C-O stretching vibration, OH variable angle vibration and existence of free COO^- groups. While the peaks at 1257.9 cm^{-1} and 1057.4 cm^{-1} signify S=O and -C-O-S stretching vibrations, respectively, as also reported earlier by Khan *et al.,* 2013. The presence of the amide group in the CS-Keel was depicted by the peak at 1664 cm^{-1} as shown earlier by Wang *et al.,* 2003.

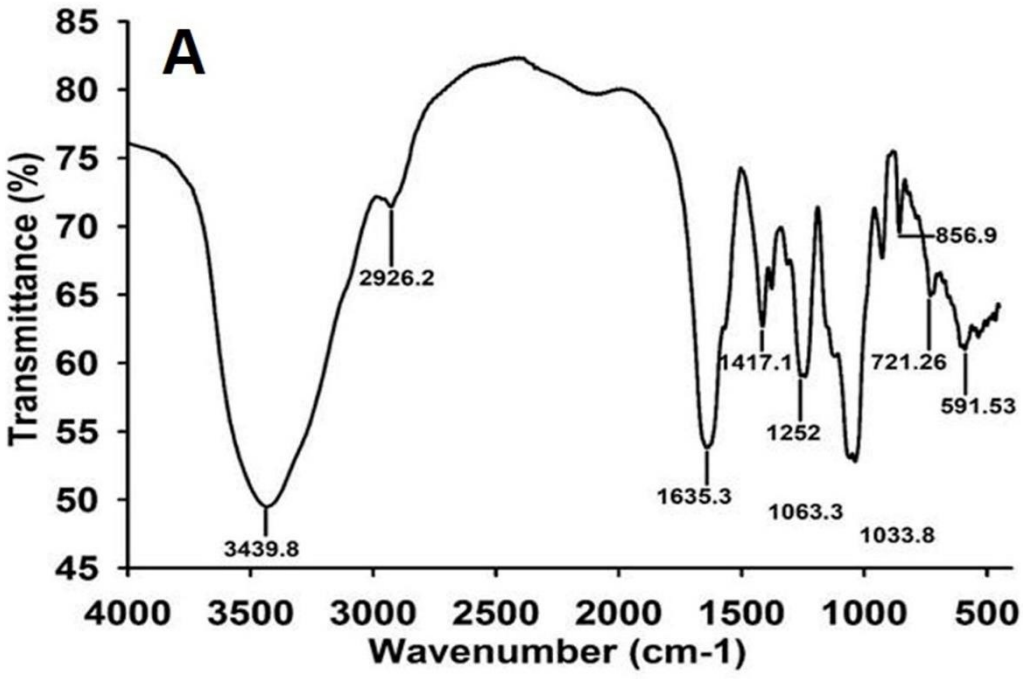

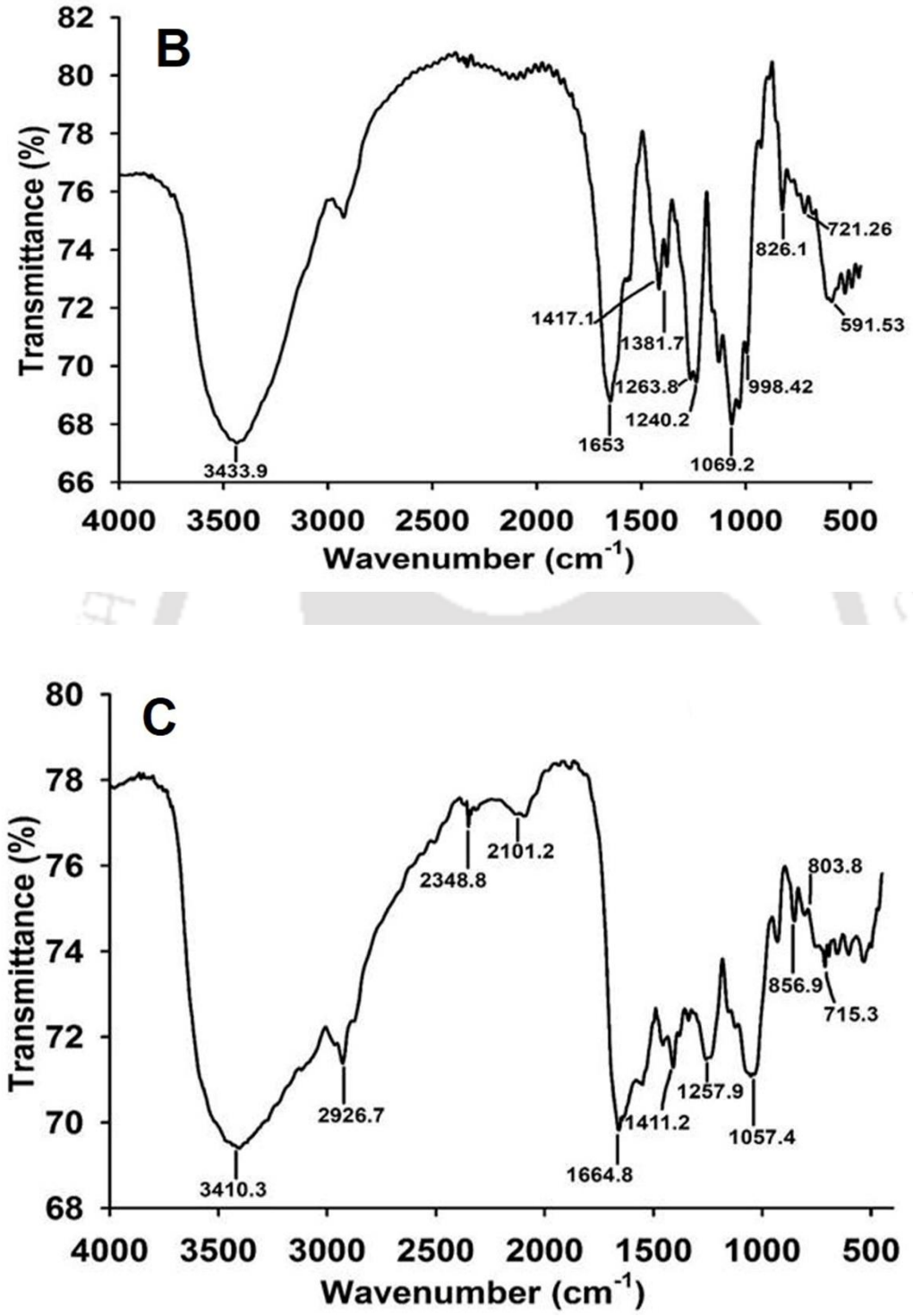

Fig. 6.3.3 FT-IR spectra of (A) standard chondroitin 4-suphate (B) standard chondroitin 6-sulphate (C) chondroitin sulphate isolated from chicken keel bone cartilage (CS-Keel).

6.3.5 ^{1}H-NMR analysis of CS-Keel

The ^{1}H-NMR spectrum of CS-Keel was obtained at 600 MHz (Fig. 6.3.4). The characteristic signals of protons were assigned using previously reported chondroitin sulphate from porcine trachea, bovine trachea and shark cartilage (Mucci *et al.,* 2000) and from *Scyliorhinus canicula* (Gargiulo *et al.*, 2009). The presence of broad range (3.4 to 4.6 ppm) of proton NMR spectrum confirms the polysaccharide nature of CS-Keel (Table 6.3.2). CS-Keel showed prominent signals of GlcA for H-1* and H-2* protons at 4.51 ppm and 3.41 ppm, respectively. The protons, H-3*, H-4* and H-5* of GlcA showed the resonances at 3.63 ppm, 3.71 ppm and 3.84 ppm, respectively. The protons of the GlcA ring resonate in the range, 3.4 -4.5 ppm, which is similar as previously reported (Mucci *et al.,* 2000). Proton resonance at 2.08 ppm proves the existence of methyl group of N-acetylgalactosamine residue as also reported earlier by Gargiulo *et al.,* 2009. The proton resonances of GalNAc residues, appeared in the regions, 3.6-3.8 ppm and 4.0-4.7 ppm. H-5 and H-6 protons of GalNAc showed the signals at 3.62 ppm and 3.87 ppm, respectively and the rest of the protons in the 4.0-4.7 ppm region (Fig. 6.3.4). H-1, H-2, H-3 and H-4 protons of GalNAc gave resonances at 4.61 ppm, 4.07 ppm, 4.03 and 4.72 ppm as also reported earlier by Mucci *et al.,* 2000.

Table 6.3.2 ^{1}H- NMR (600MHz) chemical shift of CS isolated from keel bone cartilage**.**

Residue	Proton	^{1}H Chemical Shift (ppm)
GlcA	H-1*	4.51
	H-2*	3.41
	H-3*	3.63
	H-4*	3.71
	H-5*	3.84
	H-6*	-
GalNAc	H-1	4.61
	H-2	4.07
	H-3	4.03
	H-4	4.72
	H-5	3.87
	H-6	3.62
	NAc(CH_3)	2.08

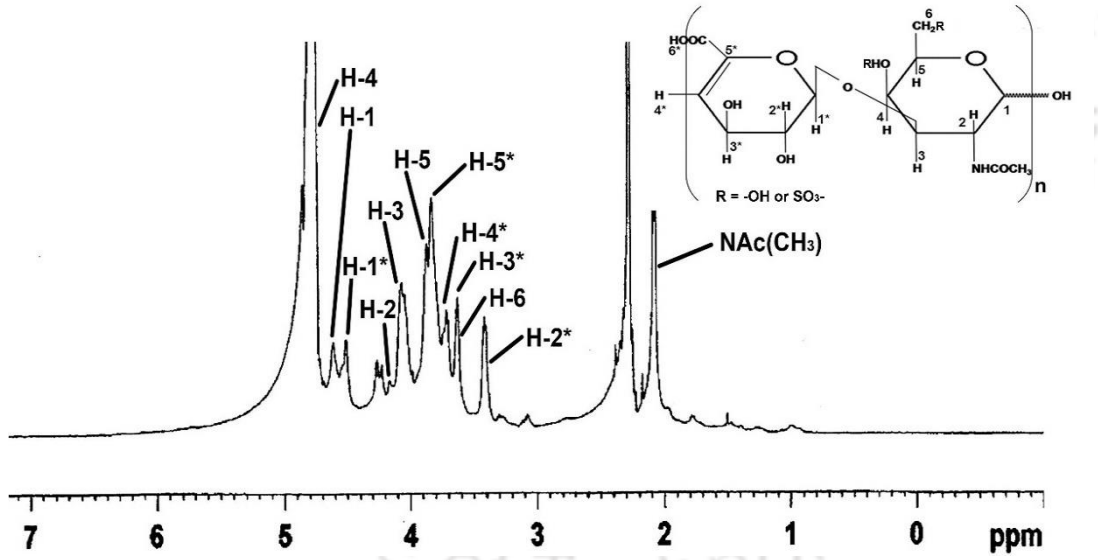

Fig. 6.3.4 ^{1}H-NMR (600 MHz) of CS-Keel polysaccharide.

6.3.6 Surface analysis of CS-Keel by FESEM

Scanning electron microscopy was used for high resolution surface imaging of CS-Keel. The surface morphology of CS-Keel showed rough surface with several layers stacked upon each other (Fig. 6.3.5A). In the previous study of fucosylated chondroitin sulfate from sea cucumber *Acaudina molpadioidea* and *Holothuria nobilis*

also showed the rough surface with several particles stacked together (Zou *et al.*, 2016). The layer structure of CS-Keel also showed the presence of depressions on the surface at regular intervals (Fig. 6.3.5B).

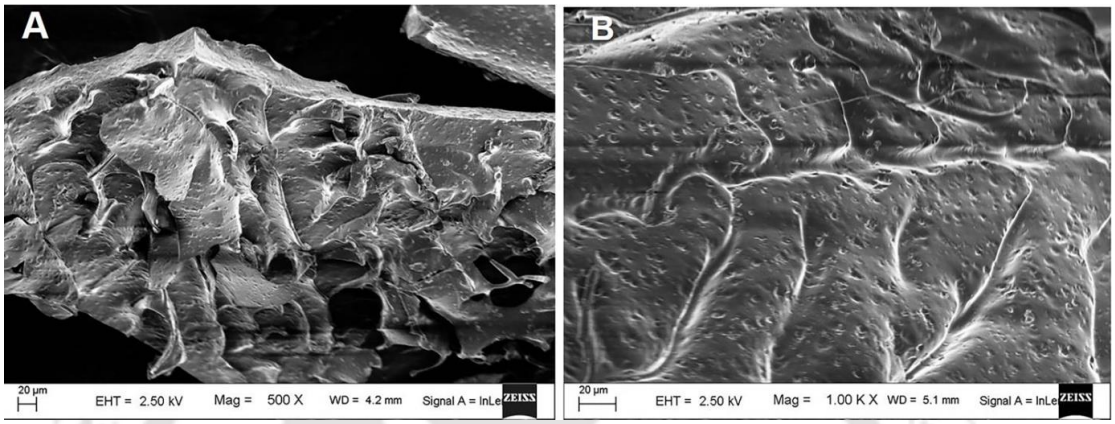

Fig. 6.3.5 FESEM images of CS-Keel at magnifications (A) 500x and (B) 1000x.

6.3.7 Surface analysis of CS-Keel by AFM

AFM is a powerful tool that enables the surface morphology of hydrated and soft samples (Jacoboni *et al.*, 1999). The AFM analysis of CS-Keel bone revealed fibrous structures of irregular shapes arranged randomly throughout the surface (Fig. 6.3.6A & B). The fibrous structures were approximately, 20 nm in height and 300 nm in diameter with variable lengths (Fig. 6.3.6C & D). The distribution of fibrous structure present could be correlated with the concentration of CS-Keel as with the increase in its concentration, the fibrous structure increased and was maximum at 1 mg/ml. Polysaccharides generally form chains of width 0.1 nm to 1 nm (Zou *et al.*, 2016). The large variation in width of the structure could be attributed to the presence of associated core proteins, which form aggregates with CS-Keel polysaccharide chain. The presence of associated proteins was also observed in the HPSEC analysis of CS-Keel as mentioned earlier.

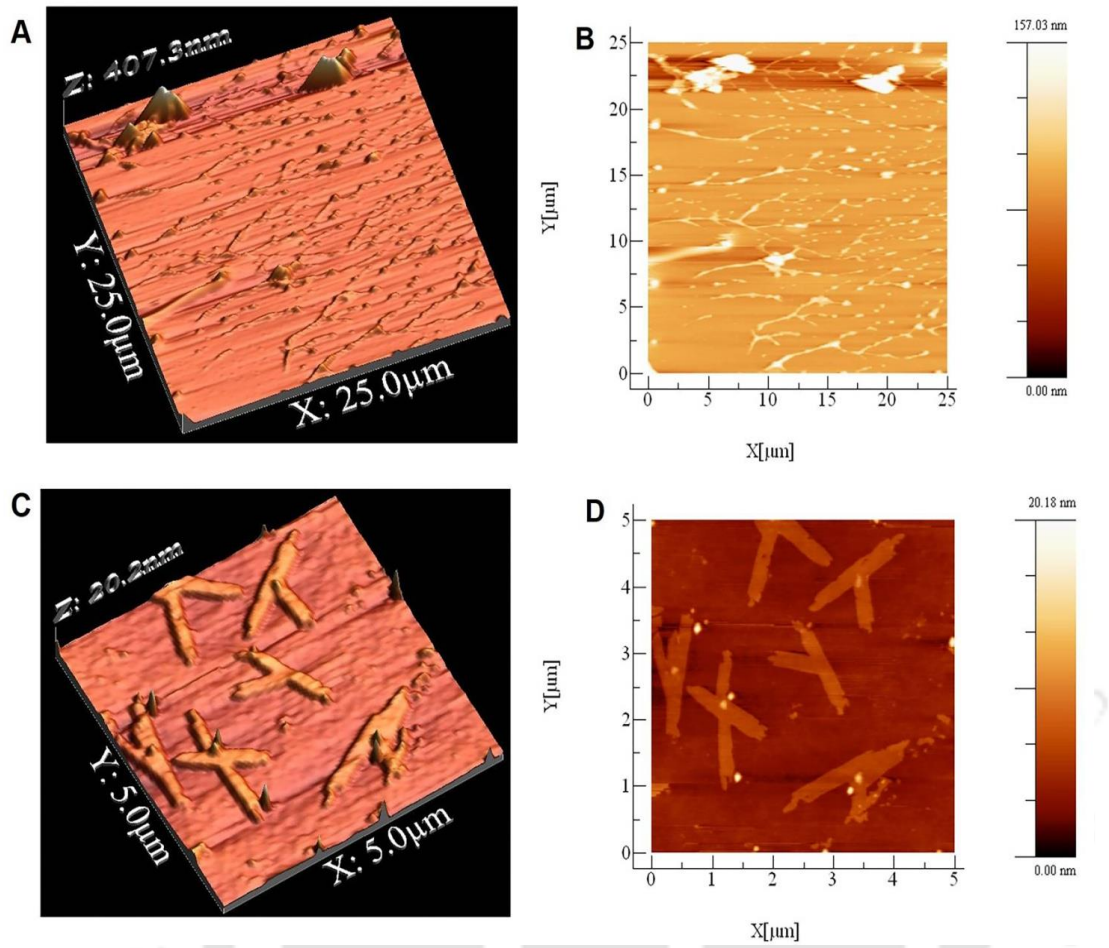

Fig 6.3.6 AFM images of CS-Keel (A) semi-contact mode 3D surface image at 25x25 µm, (B) 2D surface image at 25x25 µm, (C) Magnified 3D surface image at 5x5 µm, showing fibrous structure of CS-Keel and (D) 2D representation of CS-Keel at 5x5 µm.

6.3.8 Thermal properties of CS-Keel by DSC, TGA and DTG analysis

The thermal properties of CS-Keel polysaccharide were studied by TGA, DTG and DSC. The DSC analysis showed, the thermal property of CS-Keel resembles with the behaviour of polysaccharides. The thermal scan of CS-Keel suggested the presence of an endothermic peak at 270.4ºC, which is due to bound water molecule in the CS-Keel polymer chain (Fig. 6.3.7A). The exothermic peak at 451.5ºC is due to the irreversible process of polysaccharide degradation (Fig. 6.3.7A). These properties of

CS-Keel might be due to intermolecular or intramolecular hydrogen bonding and cross linking capacity (Moreno *et al.,* 2008).

TGA of CS-Keel depicted the weight loss of polysaccharide with increase in temperature. The weight loss of CS-Keel was observed in three stages. Initial 15.0% weight loss of CS-Keel occurred between 35ºC to 100ºC. The initial weight loss of polysaccharide CS-Keel was associated with the loss of water and also suggested presence of high content of carboxyl groups which were bound to water molecules as also reported earlier (Wang *et al.,* 2015). A sudden decrease of 43% weight of CS-Keel was observed with in the temperature range, 220ºC-400ºC. The weight loss of CS-Keel gradually decreased further and finally reached 28% at 600ºC (Fig. 6.3.7B). The Derivative thermogravimetric (DTG) curves showed two peaks, at 243ºC and 320ºC. Out of these two, the first sharp peak at 243ºC corresponded to the thermal degradation temperature (T_d) of CS-Keel polysaccharide while the second peak at 320ºC might be due to the presence of protein (Fig. 6.3.7B). The thermal degradation of commercial chondroitin sulphate A isolated from bovine trachea occurred at T_d, 227ºC (Wang *et al.,* 2000). The relatively higher degradation temperature makes CS-Keel a suitable material for tissue scaffolds and joint replacement therapies.

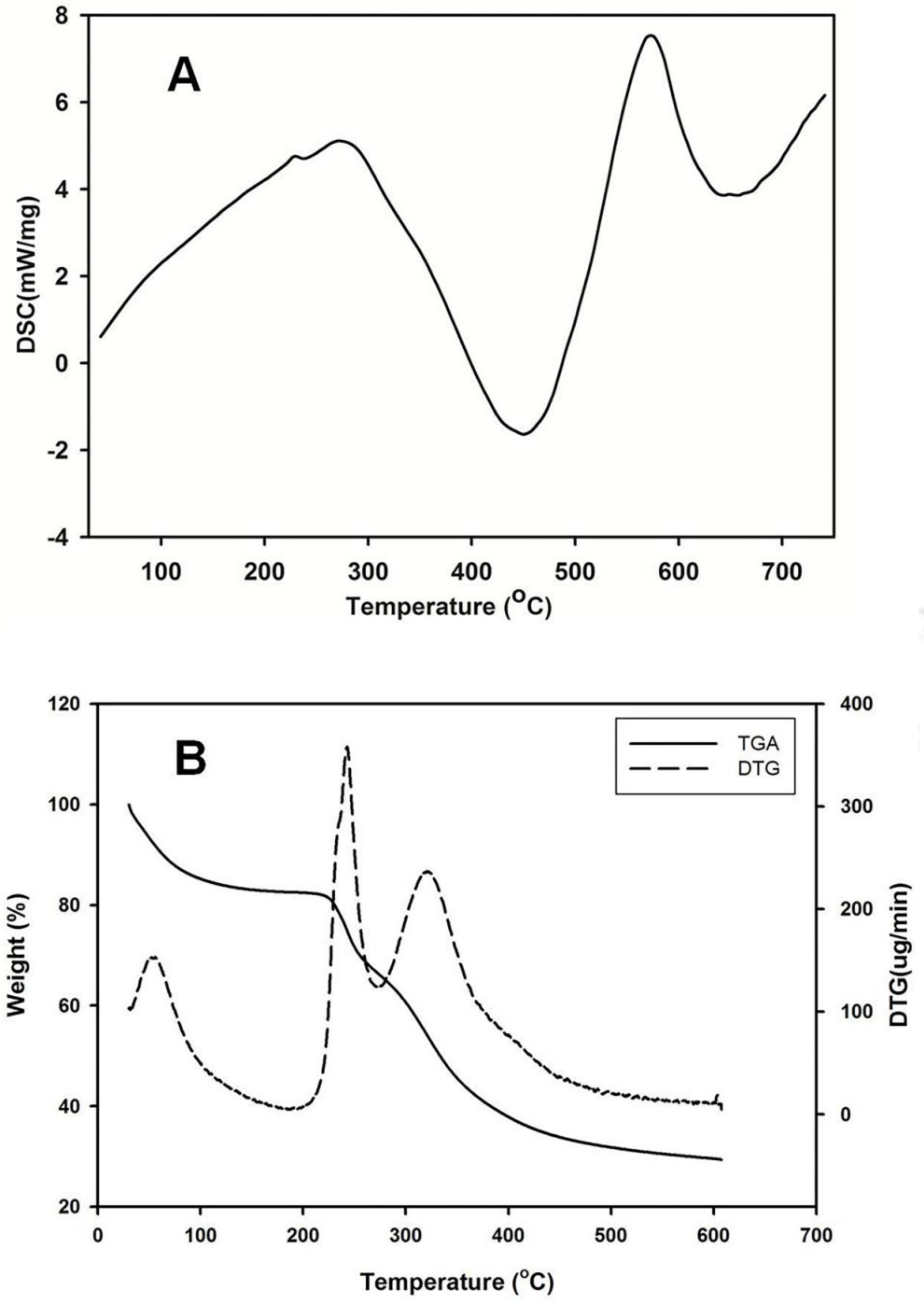

Fig 6.3.7 Thermal property of CS-Keel polysaccharide (A) Differential scanning calorimetery (DSC), (B) Thermogravimetric analysis (TGA) showing thermal stability up to 220ºC and Derivative Thermogravimetric Analysis **(**DTG) showing degradation temperature (T_d) of 243ºC.

6.3.9 *In vitro* cell proliferation assay of CS-Keel polysaccharide

The *in vitro* cell proliferation assay of CS-Keel polysaccharide was determined using MTT. This is widely used method for estimation of cell viability, cytotoxicity and cell proliferation (Mosmann 1983). MTT is a yellow colour compound which on reduction by mitochondrial succinate dehydrogenase in the metabolically active cells yields a purple colour formazan (Meerloo *et al.,* 2011). The mouse fibroblast L929 cells were treated with varying concentrations (0.5 mg/ml to 5 mg/ml) of CS-Keel for 12h and 24h. The CS-Keel was dissolved in serum free DMEM low glucose (incomplete) medium as the presence of serum in complete medium leads to the cell growth and interferes with the cell viability assessment (Barnes and Sato 1980; Meerloo *et al.,* 2011). It was observed that CS-Keel imparts no cytotoxicity on L929 cells with the time as well with increase of its concentration (Fig. 6.3.8). The cell proliferation assay revealed that the viability of CS-Keel treated L929 cells was 98% which was almost similar to the untreated cells at 5 mg/ml after 24h. Hence the results concluded the biocompatible nature of CS-Keel polysaccharide which makes it a prospective candidate for making tissue scaffolds in tissue engineering and as drug delivery agent for controlled release of drugs.

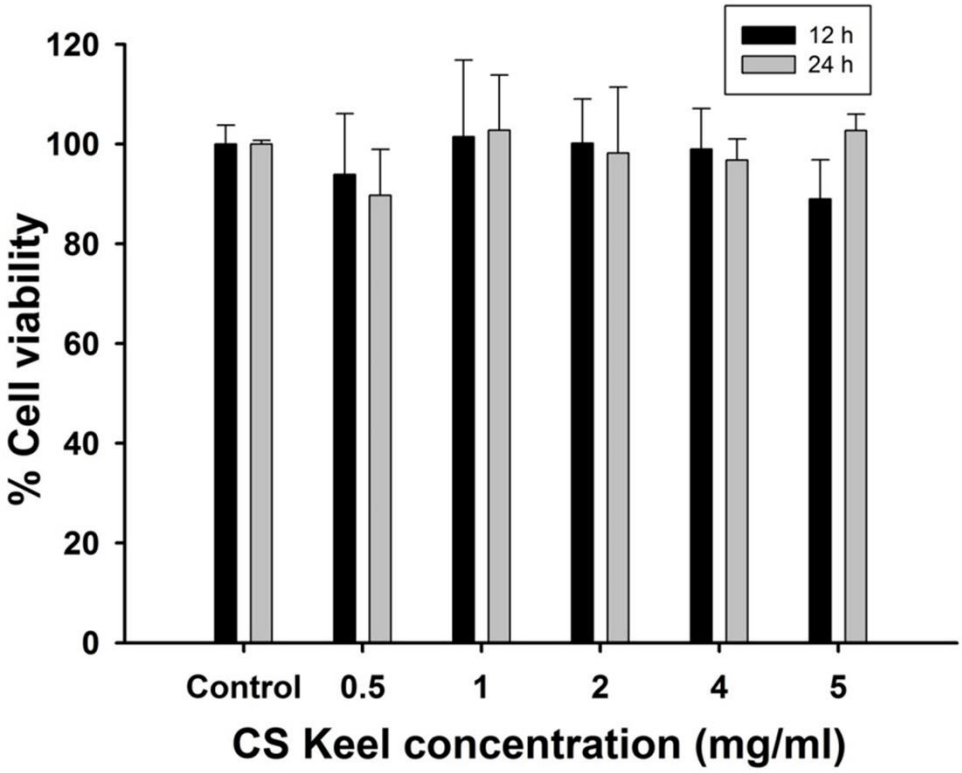

Fig 6.3.8 The *in vitro* cell proliferation assay (MTT) showing percent cell viability of L929 cells treated with varying concentration (0.5 mg/ml -5 mg/ml) of CS Keel.

6.3.10 Microscopic observation of CS-Keel treated L929 cells

The L929 cells under the normal condition exhibit spindle shape when adhered to the surface of culture plate (Theerakittayakorn and Bunprasert., 2011). The microscopic analysis of untreated and CS-Keel treated L929 cells was carried out to study the morphological changes. The bright field microscopic analysis of L929 cells revealed that there was no detectable change in morphology of cells. Both, the untreated (Fig. 6.3.9A & B) and CS-Keel treated cells (Fig. 6.3.9C & D) exhibited the same spindle shape morphology. The surface morphology study analysis further supported the contention elucidated from the MTT assay that CS-Keel polysaccharide is biocompatible.

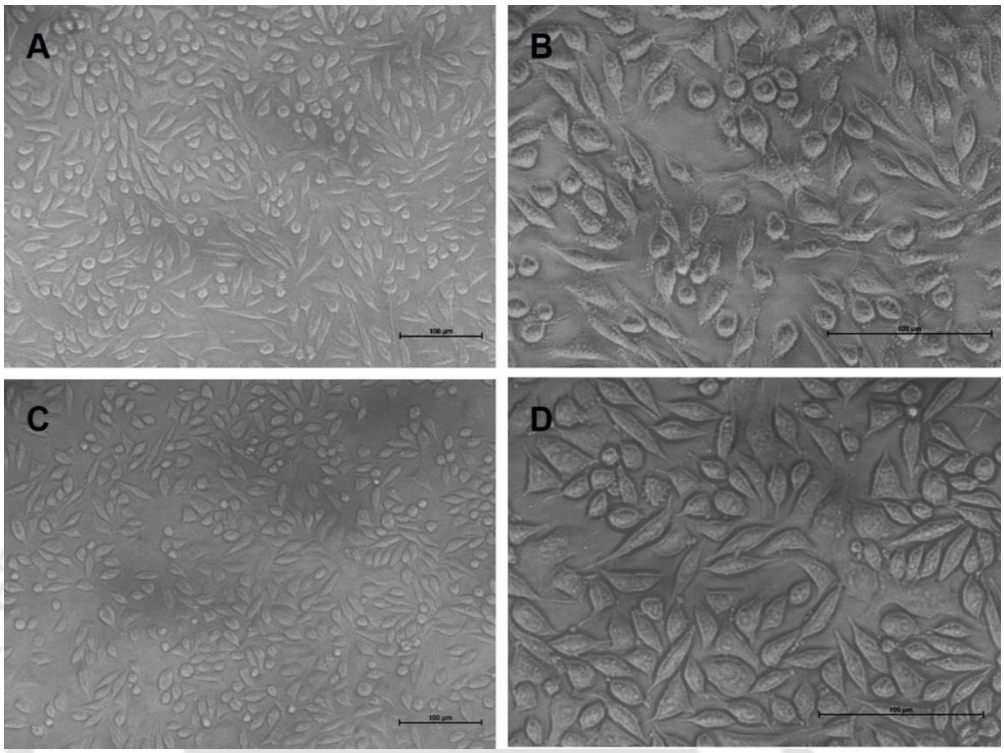

Fig. 6.3.9 Light microscopic images of Untreated L929 cells under (A) 20x (B) 40x magnification and CS-Keel (5 mg/ml) treated cells for 24h under (C) 20x and (D) 40x magnification.

6.3.11 Antioxidant properties of CS-Keel

Antioxidant properties of CS-Keel were assessed by DPPH and inhibition of ascorbate autooxidation method. The DPPH is a free-radical compound, which is widely used to assess the antioxidant nature of compounds. DPPH free radical scavenging activities of the antioxidant compounds is based on their hydrogen donating nature. It receives an electron or hydrogen radical (H•) from antioxidant and become stable in its reduced form. Therefore, the antioxidant activity of a compound can be expressed as its ability in scavenging the DPPH• free radical. The DPPH scavenging activity of CS-Keel in the concentration range of 0.5 mg/ml to 5 mg/ml varied from 8% to 49% (Fig. 6.3.10A). In a previous study, the DPPH radical scavenging activity of

antler CS, bovine cartilage CS and shark cartilage CS at a concentration of 5 mg/ml were measured as 51 ± 1.1%, 8 ± 0.1%, and 5 ± 0.1%, respectively (Kim *et al.*, 2014).

The inhibition of ascorbate autoxidation is the method to assess the superoxide radical suppression generated by oxidation of ascorbate. CS-Keel showed inhibition of ascorbate autoxidation in the range, from 5.0 ± 0.8% to 22 ± 1.6% at concentrations from 0.5 mg/ml to 5 mg/ml (Fig. 6.3.10B). CS-Keel can protect the oxidative damage caused by harmful superoxide radical. The results suggested that CS-Keel possesses strong antioxidant activity preventing the oxidative damage caused by the reactive oxygen species and hence can be used as potential antioxidant agent in pharmaceuticals.

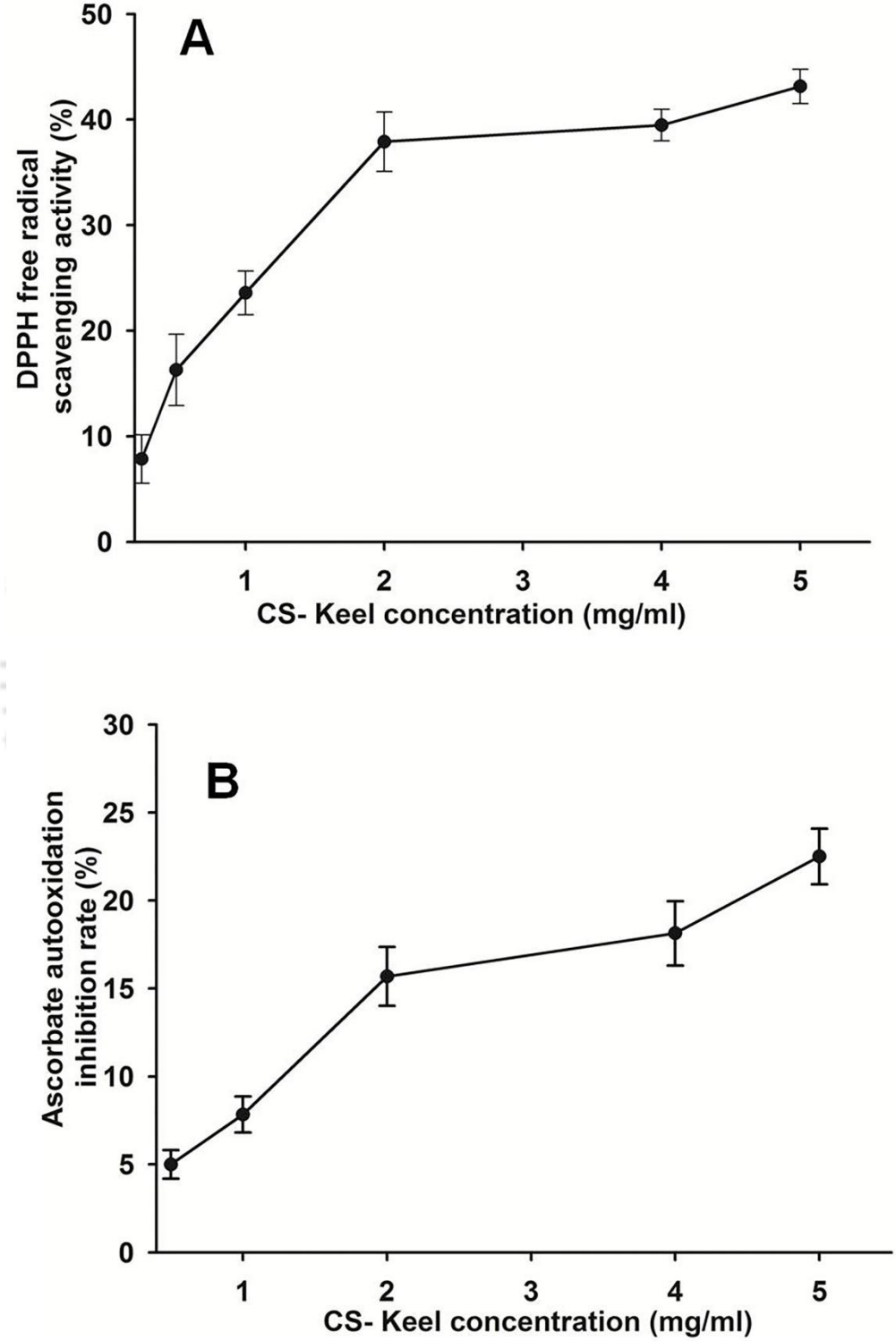

Fig. 6.3.10 *In vitro* antioxidant activity of CS-Keel polysaccharide showing (A) DPPH radicals scavenging activity and (B) Inhibition of ascorbate autooxidation.

6.3.12 Emulsification capacity of CS-Keel

The emulsifying property CS-Keel was determined by its capability of stabilizing the emulsion of hydrocarbon in water. The emulsifying activity of CS-Keel was measured at two different time intervals of 30 min and 60 min against n-hexadecane. CS-Keel stabilized the emulsion of hydrocarbon and retained 72% and 70% of the emulsifying activity at 30 min and 60 min, respectively. The emulsifying activity of the two commercial emulsifiers, guar gum and sodium alginate were also calculated. Guar gum retained 81% and 74% of emulsifying activity after 30 and 60 min, respectively. While emulsifying activity of sodium alginate was 69% and 41% after 30 and 60 min, respectively (Table. 6.3.3). CS-Keel exhibited comparable emulsifying activity than commercial emulsifier guar gum, while better than sodium alginate. Previously the emulsifying capability of commercial CS-A was studied as protein-polysaccharide complex involving lysozyme and CS-A (Kato *et al.*, 1989). The overall finding of the present study suggested that CS-Keel can serve as a potential emulsifier in the food industry.

Table.6.3.3 Emulsifying activity (%) of CS-Keel

Polysaccharide	Emulsifying activity (%) at t=30 min	Emulsifying activity (%) at t=60 min
CS-Keel	72.04	70.3
Guar Gum	81	74
Sodium Alginate	69	41

6.4 Conclusions

Chicken keel bone cartilage was explored for cheaper and sustainable source for isolation of chondroitin sulfate (CS) for its future use in tissue engineering and pharmaceutical industry. HPSEC analysis displayed two peaks of 100 kDa for CS-Keel polysaccharide and 1 kDa for protein. DLS analysis of CS-Keel displayed polydispersity. CS-Keel yield was 15% and 53±5% uronic acid content. The quantified percentages of UA-GalNAc4S and UA-GalNAc6S disaccharide in CS-Keel were 58% and 42%, respectively. FT-IR identified CS-Keel to be chondroitin 4-sulphate. ^{1}H-NMR of CS-Keel confirmed the presence of N-acetylgalactosamine and Glucuronic acid. FESEM demonstrated layer structure and AFM displayed the size of CS-Keel fibres. DSC, TGA and DTG studies of CS-Keel showed T_d at 243ºC. The composition, structure, surface and thermal analysis of CS-Keel displayed that it can serve as a strong candidate in tissue scaffolds for biomedical engineering. *In vitro* cell proliferation assay and morphological analysis of mouse fibroblast L929 cell lines confirmed the biocompatibility of CS-Keel. CS-Keel (5 mg/ml) exhibited ~49% antioxidant activity against DPPH and 22% against superoxide radical protecting from oxidative damage. CS-Keel demonstrated better (70.3%) emulsifying activity than commercial sodium alginate (60.2%). Therefore, CS-Keel can be used for functional food applications enriching the nutritional values. CS-Keel also enables future prospects for analysis of its chondroprotective and anti-inflammatory properties for osteoarthritis treatment. Future challenges include its utilization in nanomedicine to develop an efficient delivery vehicle for therapeutic agents, to further enhance its specificity and finally to have controlled drug release.

6.5 References

Barnes, D. and Sato, G. (1980) Methods for growth of cultured cells in serum-free medium. *Analytical Biochemistry*, *102*(2), 255-270.

Bianchera, A., Salomi, E., Pezzanera, M., Ruwet, E., Bettini, R. and Elviri, L. (2014) Chitosan hydrogels for chondroitin sulphate controlled release: An analytical characterization. *Journal of Analytical Methods in Chemistry*, *2014*. http://dx.doi.org/10.1155/2014/808703, Article ID 808703.

Bramhachari, P.V., Kishor, P.K., Ramadevi, R., Kumar, R., Rao, B.R. and Dubey, S.K. (2007) Isolation and characterization of mucous exopolysaccharide (EPS) produced by *Vibrio furnissii* strain VB0S3. *Journal of Microbiology and Biotechnology*, *17*(1), 44.

Campo, G.M., Avenoso, A., Campo, S., Ferlazzo, A.M. and Calatroni, A. (2006) Chondroitin sulphate: antioxidant properties and beneficial effects. *Mini Reviews in Medicinal Chemistry*, *6*(12), 1311-1320.

Cesaretti, M., Luppi, E., Maccari, F. and Volpi, N. (2003). A 96-well assay for uronic acid carbazole reaction. *Carbohydrate Polymers*, *54*(1), 59-61.

Desaire, H. and Leary, J.A. (2000a) Detection and quantification of the sulfated disaccharides in chondroitin sulfate by electrospray tandem mass spectrometry. *Journal of the American Society for Mass Spectrometry*,*11*(10), 916-920.

Desaire, H. and Leary, J. A. (2000b) Utilization of MS 3 spectra for the multicomponent quantification of diastereomeric N-acetylhexosamines. *Journal of the American Society for Mass Spectrometry*, *11*(12), 1086-1094.

Field, I.C., Meekan, M.G., Buckworth, R.C. and Bradshaw, C.J. (2009) Susceptibility of sharks, rays and chimaeras to global extinction. *Advances in Marine Biology*, *56*, 275-363.

Frazier, S.B., Roodhouse, K.A., Hourcade, D.E. and Zhang, L. (2008) The quantification of glycosaminoglycans: a comparison of HPLC, carbazole, and alcian blue methods. *Open Glycoscience*, *1*, 31- 39.

Gargiulo, V., Lanzetta, R., Parrilli, M. and De Castro, C. (2009) Structural analysis of chondroitin sulfate from *Scyliorhinus canicula*: A useful source of this polysaccharide. *Glycobiology*, *19*(12), 1485-1491.

Garnjanagoonchorn, W., Wongekalak, L. and Engkagul, A. (2007) Determination of chondroitin sulfate from different sources of cartilage. *Chemical Engineering and Processing: Process Intensification*, *46*(5), 465-471.

Hamano, T., Mitsuhashi, Y., Acki, N., Yamamoto, S., Tsuji, S., Ito, Y. and Oji, Y. (1989) High-performance liquid chromatographic assay of chondroitin sulphate in food products. *Analyst*, *114*(8), 891-893.

He, W., Fu, L., Li, G., Jones, J.A., Linhardt, R.J. and Koffas, M. (2015) Production of chondroitin in metabolically engineered *E. coli*. *Metabolic Engineering*, *27*, 92-100.

Henrotin, Y., Mathy, M., Sanchez, C. and Lambert, C. (2010) Chondroitin sulfate in the treatment of osteoarthritis: from in vitro studies to clinical recommendations. *Therapeutic Advances in Musculoskeletal Disease*, *2*(6), 335-348.

Hjertquist, D.S.O. and Wasteson, Å. (1972) The molecular weight of chondroitin sulphate from human articular cartilage. *Calcified Tissue Research*, *10*(1), 31-37.

Hochberg, M.C., Martel-Pelletier, J., Monfort, J., Möller, I., Castillo, J.R., Arden, N., Berenbaum, F., Blanco, F. J., Conaghan, P.G., Doménech, G. and Henrotin, Y. (2015) Combined chondroitin sulfate and glucosamine for painful knee osteoarthritis: a multicentre, randomised, double-blind, non-inferiority trial versus celecoxib. *Annals of the Rheumatic Diseases*, annrheumdis-2014.

Horcas, I., Fernández, R., Gomez-Rodriguez, J.M., Colchero, J., Gómez-Herrero, J.W. S.X.M. and Baro, A.M. (2007) WSXM: a software for scanning probe microscopy and a tool for nanotechnology. *Review of Scientific Instruments*, *78*(1), 013705.

Iozzo, R.V. (1998) Matrix proteoglycans: from molecular design to cellular function. *Annual Review of Biochemistry*, *67*(1), 609-652.

Jacoboni, I., Valdre, U., Mori, G., Quaglino, D. and Pasquali-Ronchetti, I. (1999) Hyaluronic acid by atomic force microscopy. *Journal of Structural Biology*, *126*(1), 52-58.

Kato, A., Sato, T. and Kobayashi, K. (1989) Emulsifying properties of protein–polysaccharide complexes and hybrids. *Agricultural and Biological Chemistry*, *53*(8), 2147-2152.

Khan, H.M., Ashraf, M., Hashmi, A.S., Ahmad, M.U.D. and Anjum, A.A. (2013) Extraction and biochemical characterization of sulphated glycosaminoglycans from chicken keel cartilage. *Pakistan Veterinary Journal*, *33*, 471-475.

Kim, C.T., Gujral, N., Ganguly, A., Suh, J.W. and Sunwoo, H.H. (2014) Chondroitin sulphate extracted from antler cartilage using high hydrostatic pressure and enzymatic hydrolysis. *Biotechnology Reports*, *4*, 14-20.

Lauder, R.M., Huckerby, T.N. and Nieduszynski, I.A. (2000) A fingerprinting method for chondroitin/dermatan sulfate and hyaluronan oligosaccharides. *Glycobiology, 10*(4), 393-401.

Lee, B.J., Kim, J.S., Kang, Y.M., Lim, J.H., Kim, Y.M., Lee, M.S., Jeong, M.H., Ahn, C.B. and Je, J.Y. (2010) Antioxidant activity and γ-aminobutyric acid (GABA) content in sea tangle fermented by *Lactobacillus* brevis BJ20 isolated from traditional fermented foods. *Food Chemistry*, *122*(1), 271-276.

Lowry, O.H., Rosebrough, N.J., Farr, A.L. and Randall, R.J. (1951) Protein measurement with the Folin phenol reagent. *The Journal of Biological Chemistry, 193*(1), 265–275.

Luo, X.M., Fosmire, G.J. and Leach, R.M. (2002) Chicken keel cartilage as a source of chondroitin sulfate. *Poultry Science*, *81*(7), 1086-1089.

Maccari, F., Galeotti, F. and Volpi, N. (2015) Isolation and structural characterization of chondroitin sulfate from bony fishes. *Carbohydrate Polymers*, *129*, 143-147.

Moreno, J.S., Panero, S., Artico, M. and Filippini, P. (2008) Synthesis and characterization of new electroactive polypyrrole-chondroitin sulphate A substrate. *Bioelectrochemistry*, *72*(1), 3-9.

Mosmann, T. (1983) Rapid colorimetric assay for cellular growth and survival: application to proliferation and cytotoxicity assays. *Journal of Immunological Methods*, *65*(1-2), 55-63.

Mucci, A., Schenetti, L. and Volpi, N. (2000) 1-H and 13-C nuclear magnetic resonance identification and characterization of components of chondroitin sulfates of various origin. *Carbohydrate Polymers*, *41*(1), 37-45.

Nakano, T., Pietrasik, Z., Ozimek, L. and Betti, M. (2012) Extraction, isolation and analysis of chondroitin sulfate from broiler chicken biomass. *Process Biochemistry*, *47*(12), 1909-1918.

Rani, A., and Goyal, A. (2016) A new member of family 8 polysaccharide lyase chondroitin AC lyase (*Ps*PL8A) from *Pedobacter saltans* displays endo- and exo-lytic catalysis Journal of Molecular Catalysis B: Enzymatic, *134*, 215-224.

Raynauld, J.P., Pelletier, J.P., Abram, F., Delorme, P. and Martel-Pelletier, J. (2016) Long-term effects of glucosamine/chondroitin sulfate on the progression of structural changes in knee osteoarthritis: 6-year follow-up data from the osteoarthritis initiative. *Arthritis Care & Research*, *68*(10), 1560-1566.

Schiller, J. and Huster, D. (2012) New methods to study the composition and structure of the extracellular matrix in natural and bioengineered tissues. *Biomatter*, *2*(3), 115-131.

Srichamroen, A., Nakano, T., Pietrasik, Z., Ozimek, L. and Betti, M. (2013) Chondroitin sulfate extraction from broiler chicken cartilage by tissue autolysis. *LWT-Food Science and Technology*, *50*(2), 607-612.

Theerakittayakorn, K. and Bunprasert, T. (2011) Differentiation capacity of mouse L929 fibroblastic cell line compared with human dermal fibroblast. *World Academy of Science, Engineering and Technology, International Journal of Medical, Health, Biomedical, Bioengineering and Pharmaceutical Engineering*, *5*(2), 51-54.

Van Meerloo, J., Kaspers, G.J. and Cloos, J. (2011) Cell sensitivity assays: the MTT assay. *Cancer Cell Culture: Methods and Protocols*, 237-245.

Vázquez, J.A., Rodríguez-Amado, I., Montemayor, M.I., Fraguas, J., González, M.D.P. and Murado, M.A. (2013) Chondroitin sulfate, hyaluronic acid and chitin/chitosan production using marine waste sources: Characteristics, applications and eco-friendly processes: A review. *Marine Drugs*, *11*(3), 747-774.

Vittayanont, M. and Jaroenviriyapap, T. (2013) Production of crude chondroitin sulfate from duck trachea. *International Food Research Journal*, *21*(2), 791-797.

Wang, L.F., Shen, S.S. and Lu, S.C. (2003) Synthesis and characterization of chondroitin sulfate–methacrylate hydrogels. *Carbohydrate Polymers*, *52*(4), 389-396.

Wang, P. and Tang, J. (2009) Solvent-free mechanochemical extraction of chondroitin sulfate from shark cartilage. *Chemical Engineering and Processing: Process Intensification*, *48*(6), 1187-1191.

Zou, S., Pan, R., Dong, X., He, M. and Wang, C. (2016) Physicochemical properties and antioxidant activities of two fucosylated chondroitin sulfate from sea cucumber *Acaudina molpadioidea* and *Holothuria nobilis*. *Process Biochemistry*, *51*(5), 650-658.

Chapter 7

Prebiotic chondroitin sulphate disaccharide isolated from chicken keel bone exhibiting anticancer potential against human colon adenocarcinoma HT-29 cells

7.1 Introduction

The connective tissues in mammalians contain extracellular matrix which includes collagens, proteoglycans (PGs), glycosaminoglycans (GAGs) and glycoproteins (Wang et al., 2017). GAGs are anionic, highly sulphated and complex natural heteropolysaccharides (Afratis *et al.*, 2012; Krichen *et al.*, 2017). The major categories of GAGs are Chondroitin sulphate (CS), Dermatan sulphate (DS), Heparin/Heparan sulphate (HS), Keratan sulphate (KS) and Hyaluronic acid (HA) (Nakano *et al.*, 2010). CS consists of N-acetylgalactosamine and glucuronic acid disaccharide repeat which are linked by β-(1→4) glycosidic linkage. CS possesses pharmacological properties *viz.* antioxidant, neuroprotective, antitumor, anti-proliferative, anti-inflammatory, anti-viral and anti-adhesive (Damonte *et al.*, 2004;

Egea *et al.,* 2010; Krichen *et al.,* 2017). These properties of CS are because of specific structural features, especially sulphation and molecular size (Mulloy, 2005).

Despite the beneficial properties of CS, its application in food industries pharmaceuticals and therapeutics has raised concerns due to its poor absorption by intestine after oral administration (1-13% bioavailability) (Baici *et al.*, 1992; Shang *et al.,* 2016; Wang *et al.,* 2017). Therefore, reduction in the molecular weight of the CS polysaccharide by enzymatic hydrolysis may enhance its intestinal absorption (Qian *et al.,* 2013; Xiao *et al.*, 2014; Wang *et al.,* 2017). Prebiotics are the non-digestible food ingredients that are resistant to digestion in the upper gastrointestinal tract and beneficially affect the host by selectively stimulating the growth of beneficial bacteria in the colon, and thus improves host health (Bruno-Barcena *et al.,* 2015). The gut bacteria help in digestion of carbohydrates and lead to the production of short chain fatty acid (SCFA) such as acetic, butyric and propionic acid (Mussatto *et al.,* 2007). These prebiotics also help in curing colon cancer by decreasing the fecal concentration of secondary bile acids, fecal pH, and nitroreductase (Bruno-Barcena *et al.,* 2015). Presently, three commercially available dietary ingredients: galacto-oligosaccharides (GOS), lactulose, and fructo-oligosaccharides (FOS) are being used as food additives in Japan and Europe (Bruno-Barcena *et al.,* 2015). There are no intestinal, pancreatic or brush border enzymes present in human body which can digest the CS (Shang *et al.,* 2016). Hence, CS oligosaccharide/disaccharide could be interesting source to be used as dietary ingredients in food and pharmaceutical industries.

CS interact with growth factors, chemokines, cytokines and their cell surface receptors and thus are involved in various cellular processes such as cell adhesion, proliferation, differentiation, migration and apoptosis (Qiu *et al.,* 2017). Metastasis is

an important characteristic of malignancy. CS has been studied in controlling cell proliferation (Desai *et al.,* 2000; Krichen *et al.,* 2017). Gastric cancer is the second leading cause of death worldwide in which uncontrolled cell growth occurs (Ferlay *et al.,* 2010; Kapoor *et al.,* 2017). Drugs used in chemotherapy imparts toxicity to the surrounding healthy tissues. This leads to the search of natural food and food ingredients which can act as anticancer agents. In previous study, pectic oligosaccharide from tomato have shown inhibition of human gastric carcinoma (AGS) (Kapoor *et al.,* 2017). Chondroitin sulphate disaccharides were chemically synthesised and their inhibitory effects were studied against triple negative breast cancer cells MDA-MB-231 (Poh *et al.,* 2015). However, the chemical synthesis of CS disaccharide has disadvantage of high production cost and therefore it lacks the commercial availability. Marine sulphated GAGs polysaccharide from algae showed antiproliferative activity against HL-60 cancer cell line (Queiroz *et al.,* 2006). However, the poor absorption of the polysaccharide in the intestine is the major drawback. These reasons were the prime, which make the researchers to search for the alternative oligosaccharides for the overall human colon health. In the present study CS-Keel disaccharide (CSD) was produced from CS-Keel polysaccharide by chondroitin AC lyase (*Ps*PL8A) enzymatic digestion, purified and structurally characterized. The prebiotic potential of CS-Keel disaccharide was explored by studying its effect on the growth of probiotic bacteria, gastric juice and SCFA production. The effect of CS-Keel disaccharide was also studied on viability of the human colon adenocarcinoma (HT-29) cell lines. To best of our knowledge, this is the first study reporting the prebiotic activity and colon cancer inhibition properties of CS-Keel disaccharide.

7.2 Materials and Methods

7.2.1 Chemicals and reagents

Chondroitin 4-sulphate disaccharide (UA-GalNAc4S), D-Glucuronic acid (GlcA), N-acetyl-galactosamine, MTT [3-(4,5-dimethylthiazol-2-yl)-2,5-diphenyltetrazolium bromide, Dulbecco's Modified Eagle Medium (DMEM) low glucose medium, Roswell Park Memorial Institute (RPMI 1640) medium were purchased from Sigma-Aldrich, USA. Bio-Gel P-2 (fine mesh) was purchased from Bio-Rad Laboratories, Inc., USA Chondroitin 6-sulphate disaccharide (UA-GalNAc6S) sodium salt (Dextra Laboratories Ltd, U.K). Phosphate buffer saline, DAPI dye (4',6-diaminidino-2-phenylindole) and Trypsin-EDTA solution were purchased from Hi-Media Pvt. Ltd., India. Fetal bovine serum, penicillin-streptomycin antibiotic solution, FITC (Fluorescein isothiocyanate)-Annexin V and Propidium iodide (PI) cell apoptosis kit were purchased from Invitrogen, Ltd. UK.

7.2.2 Isolation of chondroitin sulphate polysaccharide

The chondroitin sulphate polysaccharide (CS-Keel) isolated from chicken keel bone cartilage as reported in our previous chapter 6 (Rani *et al.*, 2017) was used as the polysaccharide material in the present study.

7.2.3 Activity of chondroitin AC lyase (*Ps*PL8A) against CS-Keel polysaccharide

The activity of chondroitin AC lyase (*Ps*PL8A) from *Pedobacter saltans* was analyzed by incubating 0.1 µg of enzyme in 1 ml reaction mixture containing 1 mg/ml of CS-Keel as substrate. The enzyme reaction was carried out under optimum reaction conditions of 50 mM Tris-HCl buffer, pH 7.2 at 39°C for 5 min as reported (Rani and Goyal., 2016). The unsaturated oligosaccharide product formation was monitored by the increase in absorbance at 232 nm (A_{232}) as a function of time on a UV-Visible

spectrophotometer (Varian, Cary 100). One unit of enzyme activity was defined as amount of enzyme that liberates 1 µmole of unsaturated oligosaccharides product per min as calculated using a molar absorption coefficient of 3800 M^{-1} cm^{-1} (Pojasek *et al.*, 2001).

7.2.4 Thin layer chromatography analysis of CS-Keel degradation product

CS-Keel was enzymatically degraded with chondroitin AC lyase, *Ps*PL8A from *Pedobacter saltans* (Rani and Goyal., 2016). CS-Keel (1 mg/ml) was digested with 10 µl of 1 mg/ml stock of *Ps*PL8A in 50 mM Tris-HCl buffer pH 7.2 and was incubated at 39°C. Separate reactions were set up for each time interval *viz.* 0 min, 5 min, 10 min, 15 min, 30 min, 1 h, 2 h, 4 h, 8 h, 12 h and 24 h. After completion of the time interval, 1 ml of absolute ethanol was added to reaction mixture (1 ml) and centrifuged at 13000g at 25°C for 10 min to precipitate and remove the undigested CS-keel. Supernatant was collected in separate 2 ml eppendorf tube and was concentrated to 100 µl by heating at 60°C. 1 µl samples of different time period was applied to TLC plate (Merck, Germany) and run under solvent system containing 1-butanol, water and acetic acid in the ratio 5:3:2 (v/v) (Lojkwoska et al., 1995). The TLC plate was stained and visualized as described previously (Rani and Goyal., 2016).

7.2.5 Purification of CS-Keel disaccharide by size exclusion chromatography

The enzymatic depolymerisation of CS-Keel at 50 mg/ml with 10 µg of *Ps*PL8A enzyme in 1 ml reaction volume was carried out under optimised conditions (50 mM Tris-HCl buffer pH 7.2 at 39°C) for 24 h. A total 20 reactions were set up with 50 mg/ml CS-Keel, to increase the overall yield of oligosaccharide. The reaction was terminated by adding equal volume of ethanol as mentioned in section 2.4 of material and method section. The 20 ml of reaction supernatant was concentrated to a final

volume of 2 ml by evaporation at 60°C in an oven. The supernatant containing 24 h reaction product was purified by size exclusion chromatography (SEC) using XK16/70 column (GE Healthcare) packed with Bio-Gel P-2 (fine mesh) connected to FPLC-AKTA purifier (GE Healthcare). The enzymatic degraded product solution (2 ml) was filtered through 0.22 µm membrane filters (Pall Corporation, USA) and injected into the column through a 2 ml injection loop. The elution was carried out using Milli Q water at a constant flow rate of 0.2 ml/min and fractions of 1 ml were collected. The purified unsaturated CS-Keel oligosaccharide from the column was detected by UV detector at A_{232}. The purified CS-Keel oligosaccharide was freeze dried and stored at -20°C for further use.

7.2.6 Analysis of purified CS-Keel disaccharide (CSD) by TLC, ESI-MS and MS/MS

The purified CSD fractions obtained after SEC (Biogel P2) purification were analyzed by TLC. The fractions obtained under maxima of different fractions in the chromatogram were run on TLC plate (as mentioned in Section 2.4) to identify the purified oligosaccharides. The purified 24 h reaction product fractions were pooled and analysed by Electron Spray Ionization (ESI) mass spectrometer (Waters, Q-TOF Premier) in both MS and tandem MS (MS/MS) mode. ESI-MS and tandem MS analyses were carried out in negative ion mode. The ESI-MS analysis was carried out under following conditions; capillary voltage 3 eV, collision energy 5 eV, ionization energy 1 eV, desolvation temperature 250°C and the source temperature of 80°C. The tandem MS analysis was carried out by nanospray ionization using the voltage 3 eV, collision energy 20 eV and collision-induced dissociation was performed on ion of interest using the argon gas.

7.2.7 Analysis of purified CS-Keel disaccahride by FT-IR

CS-Keel disaccharide was analysed by FT-IR spectroscopy for the presence of various functional groups. CSD was pressed into KBr pellet (sample: KBr, 1:100) using 15 Ton Hydraulic Press. the spectrum in 4000-500 cm^{-1} region in the transmission mode with 32 scans per min was obtained using FTIR spectrophotometer (Perkin Elmer, Spectrum Two, USA). The spectral resolution was 4 cm^{-1}.

7.2.8 ^{1}H and ^{13}C NMR spectroscopic analysis of CS-Keel disaccharide

The purified CSD was dissolved in D_2O (99.96%) (Merck Germany) at 5 mg/ml (for ^{1}H NMR) and 15-20 mg/ml (for ^{13}C NMR) concentrations and filtered using 0.45 µm membrane. The ^{1}H-NMR and ^{13}C NMR spectra were acquired at 25ºC using 600 MHz NMR spectrometer (Bruker, Avance III-HD, USA) fitted with a 5-mm probe and equipped with topspin software (Bruker) for analysis.

7.2.9 Hydrolysis of CS-Keel disaccharide by artificial gastric juice

CS-Keel disaccharide was studied for its hydrolysis in the presence of artificial gastric juice by the method adapted from (Korakli *et al.,* 2002). The artificial gastric juice was composed of 1000 U/ml of pepsin in 1x Phosphate Buffer Saline (PBS) (Al-sheraji et al., 2012). The pH of artificial gastric juice was adjusted to 1, 2, 3 and 4 by 4 N HCl. CS-Keel disaccharide (0.5%, w/v) was dissolved in 20ml of artificial gastric juice of each pH and incubated at 37°C for 5 h. At intervals of 0, 0.5, 1, 2, 3, 4 and 5 h, an aliquot of 500 µl from the reaction mixture was withdrawn. The samples collected were quantified using HPLC system, connected with Phenomenex Rezex ROA-Organic Acid column (Phenomenex, CA, USA) using RI and UV detectors set at 232 nm. The eluent used was 5 mM H_2SO_4 with a flow rate of 0.5 ml/min. C4S disaccharide (Sigma-Aldrich, USA) from 0.05-0.5% (w/v) was used as a standard. The percent hydrolysis of

the sample was estimated by the CS-Keel disaccharide content before and after the reaction using the equation as follows;

$$Hydrolysis\ (\%) = \frac{Initial\ oligosaccharide\ content - Final\ oligosaccharide\ content}{Initial\ oligosaccharide\ content} \times 100$$

7.2.10 Effect of CS-Keel disaccharide on the growth of probiotic bacteria

CS-Keel disaccharide and inulin (standard prebiotic) were studied as carbon source on the growth of probiotic bacteria (*Lactobacillus acidophilus* NRRL B-4495 and *Bifidobacterium infantis* NRRL B-41661) along with non-probiotic enteric bacteria (*E. coli* DH5α and *Enterococcus aerogenes* MTCC7016). MRS medium (pH 6.4) devoid of any carbon source but supplemented with 0.5 mg/ml cysteine (Hongpattarakere et al., 2012) was used to analyze the growth profiles of probiotic bacteria. The probiotic bacterial cultures (~10^6 CFU/ml) were transferred to 5 ml MRS medium containing 1% (w/v) of glucose, or standard prebiotic inulin and 0.5% (w/v) CS-Keel disaccharide and incubated under anaerobic conditions at 37°C for 24 h. TGY medium (pH 7.0) containing tryptone (5 g/l), glucose (1 g/l), yeast extract (5 g/l) and di-potassium hydrogen phosphate K_2HPO_4 (1 g/l) was to evaluate the growth of enteric bacteria. The enteric mixture of non-probiotic *E. coli* DH5α and *E. aerogenes* MTCC 7016 was transferred to 5 ml of TGY medium supplemented with 1% (w/v) of glucose or standard prebiotic inulin or 0.5 % (w/v) CS-Keel disaccharide was incubated under anaerobic conditions at 37°C for 24 h. The microbial growth of probiotic bacteria and enteric bacteria was enumerated after for 12h and 24h by plate count method and expressed as CFU/ml by growing on MRS agar and TGY agar plate, respectively, at 37°C.

The prebiotic activity of CS-Keel disaccharide and inulin was estimated by the method of Huebner *et al.*, 2007.

$$\text{Prebiotic activity score} = \left\{\frac{(\text{Probiotic log CFU } ml^{-1} \text{ on prebiotic at 24h}) - (\text{Probiotic log CFU } ml^{-1} \text{ on prebiotic at 0h})}{(\text{Probiotic log CFU } ml^{-1} \text{ on glucose at 24h}) - (\text{Probiotic log CFU } ml^{-1} \text{ on glucose at 0h})}\right\} - \left\{\frac{(\text{Enteric log CFU } ml^{-1} \text{ on prebiotic at 24h}) - (\text{Enteric log CFU } ml^{-1} \text{ on prebiotic at 0h})}{(\text{Enteric log CFU } ml^{-1} \text{on glucose at 24h}) - (\text{Enteric log CFU } ml^{-1} \text{on glucose at 0h})}\right\}$$

7.2.11 Estimation of short chain fatty acid produce by probiotic bacteria

The short chain fatty acid (SCFA) content produced by probiotic bacteria (*L. acidophilus* NRRL B-4495 and *B. infantis* NRRL B-41661) were analyzed by using the cell free supernatant of probiotic bacteria broth grown in modified MRS media containing either glucose, CS-Keel disaccharide or inulin as mentioned in the previous section. The cell free supernatant was filtered using 0.2 µm membrane and quantified using HPLC system equipped with Phenomenex Rezex ROA-Organic Acid column (Phenomenex, CA, US) and RI detector. The eluent used was 5 mM H_2SO_4 at a flow rate of 0.5 ml/min. Acetic acid, propionic acid and butyric acid (Hi-media Pvt. ltd, India) at 1, 5, 10, 15, 20 mg/ml concentration were used as standards.

7.2.12 Cell culture

7.2.12.1 Maintenance of L929 and HT-29 cell lines

The mouse fibroblast cell line (L929) and human colon cancer cell line (HT-29) were procured from National Centre for Cell Science (NCCS), Pune, India. L929 cells were cultured in DMEM low glucose medium supplemented with 10% (v/v) heat-inactivated fetal bovine serum (FBS) (Gibco, U.S.A), 50 µg/ml streptomycin and 50 IU/ml penicillin (Gibco, U.S.A) incubated at 37ºC under 5% CO_2. HT-29 cells were culture in RPMI medium with 10% FBS and 50 µg/ml streptomycin and 50 IU/ml penicillin (Gibco, U.S.A) incubated at 37ºC under 5% CO_2. The cells were grown in T-

25 flasks at 37ºC under 5% CO_2 in a regulated CO_2 incubator. After cells reached the confluent stage, they were washed several times with 1XPBS (pH 7.4) and harvested with 0.25% trypsin-EDTA solution for further experiments.

7.2.12.2 *In vitro* cell proliferation assay of CS- Keel disaccharide using L929 and HT29 cell lines

. The effect of CS-Keel disaccharide on L929 and HT-29 cells, viability was analysed by MTT [3-(4,5-dimethylthiazol-2-yl)-2,5-diphenyltetrazolium bromide] assay (Mosmann, 1983). The cells were seeded at a density of $2X10^4$ cells/well in two 96 well plates which were incubated at 37ºC under 5% CO_2 for overnight for cell adherence. After incubation, the medium was completely removed and the cells were exposed to different concentrations (0.01 mg/ml to 2 mg/ml) of CS-Keel disaccharide dissolved in serum-free DMEM medium (incomplete) and serum-free RPMI medium, respectively, for L929 and HT-29 cell lines. The incomplete DMEM and RPMI medium without CS-Keel disaccharide were used as negative control for L929 and HT-29 cell lines, respectively. The plates were incubated at 37ºC in 5% CO_2 for 24h and 48h. MTT assay was done after 24h and 48h by removing the medium and washing the wells with 200 µl of 1X phosphate buffer saline (PBS). 100 µl of MTT (0.5 mg/ml) was added to each well and plate was incubated at 37ºC in 5%CO_2 for 4h. After the incubation, MTT was removed from the wells and the formazan formed was dissolved by adding 100 µl of dimethyl sulfoxide. The absorbance at 570 nm was monitored by a 96-well microplate reader (Tecan, Infinite 200 Pro, Switzerland). The cell viability (%) was calculated according to Meerloo *et al.*, (2011).

$$\text{Viability (\%)} = (N_t/N_c) \text{ X } 100$$

Where, N_t is the absorbance of treated cells and N_c is the absorbance of untreated cells.

7.2.12.3 Microscopic analysis of CS-Keel disaccharide treated L929 and HT-29 cells

The mouse fibroblast L929 and human colon cancer cell line (HT-29) cells were maintained and seeded as described in the section 7.2.12.1. The cells were seeded at the density of $2x10^5$ cells in a 24 well cell culture plate. The L929 and human colon cancer cell line (HT-29) were treated with CSD at a concentration of 0.5 mg/ml dissolved in incomplete DMEM and RPMI medium, respectively for 48h. The cells in only incomplete DMEM and RPMI medium were used as control for L929 and HT-29 cells, respectively. The change in morphology of untreated and CSD treated L929 and HT-29 cells were observed after treating with CSD. After 48h of treatment, the cells were observed under microscope (Nikon, TS100F, Japan) and photomicrographs were taken and processed using imaging software (Nikon NIS-Element).

7.2.12.4 Nuclei staining of CS-Keel disaccharide treated HT-29 cells by DAPI

The effect of CSD treatment on the nuclei of HT-29 cells was studied by staining with DAPI dye. The cells were seeded at the density of $2x10^5$ cells in a 24 well cell culture plate. The cells were incubated at 37ºC in 5% CO_2 for overnight for cell adherence. The cells were treated with CSD at a concentration of 0.5 mg/ml dissolved in incomplete RPMI medium, and incubated for 48 h at 37ºC in 5% CO_2 incubator. The cells in only incomplete RPMI medium were used as control. After 48h, the medium was removed and the cells were washed with 1x PBS solution. The DAPI dye stains the cells properly and efficiently when they are under fixed condition. So, the cells were fixed by using 4% paraformaldehyde solution. 500 µl of 4% paraformaldehyde solution was added to each well for 10 min for fixing the cells. After that, the paraformaldehyde solution was removed and cells were washed three-four times with 1x PBS solution.

The cells were treated with DAPI dye solution at a concentration of 350 nM for 10-15 min at 37°C in dark. The stain was removed and the cells were washed several times with 1x PBS solution and was observed under fluorescence microscope (Nikon, TS2R, Japan) with ultraviolet (UV) excitation/emission at 358/461 nm. Cells with nuclei containing condensed chromatin or cells with fragmented nuclei were scored as apoptotic.

7.2.12.5 Mode of cell death analysis of CS-Keel disaccharide treated HT-29 cells

The mode of cell death of CSD treated HT-29 cells was analysed by staining the cells with annexin-V-FITC and PI staining kit from Invitrogen, Ltd UK. The cells were seeded at the density of $2x10^5$ cells in a 24 well cell culture plate. After overnight incubation, the cells were treated with CSD at a concentration of 0.5 mg/ml dissolved in incomplete RPMI medium, and incubated at 37ºC in 5% CO_2 incubator for 48h. The cells in only incomplete RPMI medium were used as control. After treatment, the cells were washed with cold 1x PBS solution and incubated with 1x annexin-binding buffer, pH 7.4. The cells were treated with PI (100 µg/ml) and annexin-V-FITC dye at the concentration as mentioned by manufacturer (Invitrogen, Ltd. UK) for 15 min at room temperature and kept in dark. The stain was removed and 400 µl of 1x annexin-binding buffer was added and cells were observed under fluorescence microscope (Nikon, TS2R, Japan) with UV excitation/emission at 494/518 nm and 535/617 nm for annexin V-FITC and PI, respectively. The cells showing green fluorescence were considered as apoptotic and red cells were dead or necrotic.

7.2.13 Statistical analysis

All experiments were performed in triplicates (n = 3). The results were presented as means of three determinations ± SD (standard deviation).

7.3 Results and Discussion

7.3.1 Enzyme activity of *Ps*PL8A with CS-Keel polysaccharide and TLC analysis

Chondroitin AC lyase **(***Ps*PL8A) showed a specific activity of 340±5.2 (U/mg) with isolated CS-Keel polysaccharide, confirming its chondroitin sulphate nature. The product released by the enzymatic degradation of CS-Keel polysaccharide by *Ps*PL8A was analysed by TLC (Figure. 7.3.1A). The time dependent TLC analysis showed the presence of higher oligosaccharides as well as the disaccharide during initial 30 min of the reaction. However, disaccharide remains the major product of the reaction till 24h. The migration of disaccharide produced after degradation of CS-Keel polysaccharide coincided with that of standard unsaturated chondroitin 4-sulphate (C4S) disaccharide. This confirmed that the CS-Keel polysaccharide contains sulphation at carbon-4 and hence is of predominantly chondroitin 4 sulphate nature.

7.3.2 Purification of CS-Keel Disaccharide

The CS-Keel disaccharide formed after 24h by enzymatic degradation were purified by size exclusion chromatography by using Bio-Gel P2 matrix. The purified CS-Keel disaccharide were detected at A_{232} and collected as 1 ml fractions. A purification chromatogram was developed for CSD, which showed the presence of one major peak at 60 ml, while two small peak at 40 ml and 97 ml were also observed (Fig. 7.3.1B) and analysed by TLC and ESI-MS. Similarly, dermatan oligosaccharide and hyaluronan oligosaccharide were purified by size exclusion chromatography by using Bio-Gel P2 and Bio-Gel P10 column, respectively (Yang *et al.,* 2000; Wang *et al.,* 2016).

7.3.3 TLC and ESI-MS analysis of purified CSD

The purified CS-Keel oligosaccharide samples were analysed by TLC. The fractions at 40 ml, 60 ml, 66 ml and 97 ml were run on TLC. The fractions at 60 ml and 66 ml, which constituted the major peaks were identified as the unsaturated CS-Keel disaccharide. The peak at 40 ml corresponds to left-over un-degraded CS-Keel polysaccharide. While the peak at 97 ml displayed absence of any product and hence may be due to some artefacts observed in purification chromatogram. The purified unsaturated CS-Keel disaccharide was analysed by ESI-MS which showed the presence of a single peak with m/z 458 [Figure. 7.3.1C(i)]. During ESI-MS/MS analysis of unsaturated CS-Keel disaccharide the peak at m/z 458 was further ionized and a peak at m/z 300 was observed which uniquely identifies the presence of CS-Keel disaccharide [Figure. 7.3.1C(ii)]. The result of CS-Keel disaccharide was in accordance with the results reported earlier, where, ESI-MS and MS/MS results of chondroitin disaccharide showed peaks at m/z 458 and m/z 300, respectively (Desaire *et al.*, 2000; Flengea *et al.*, 2009).

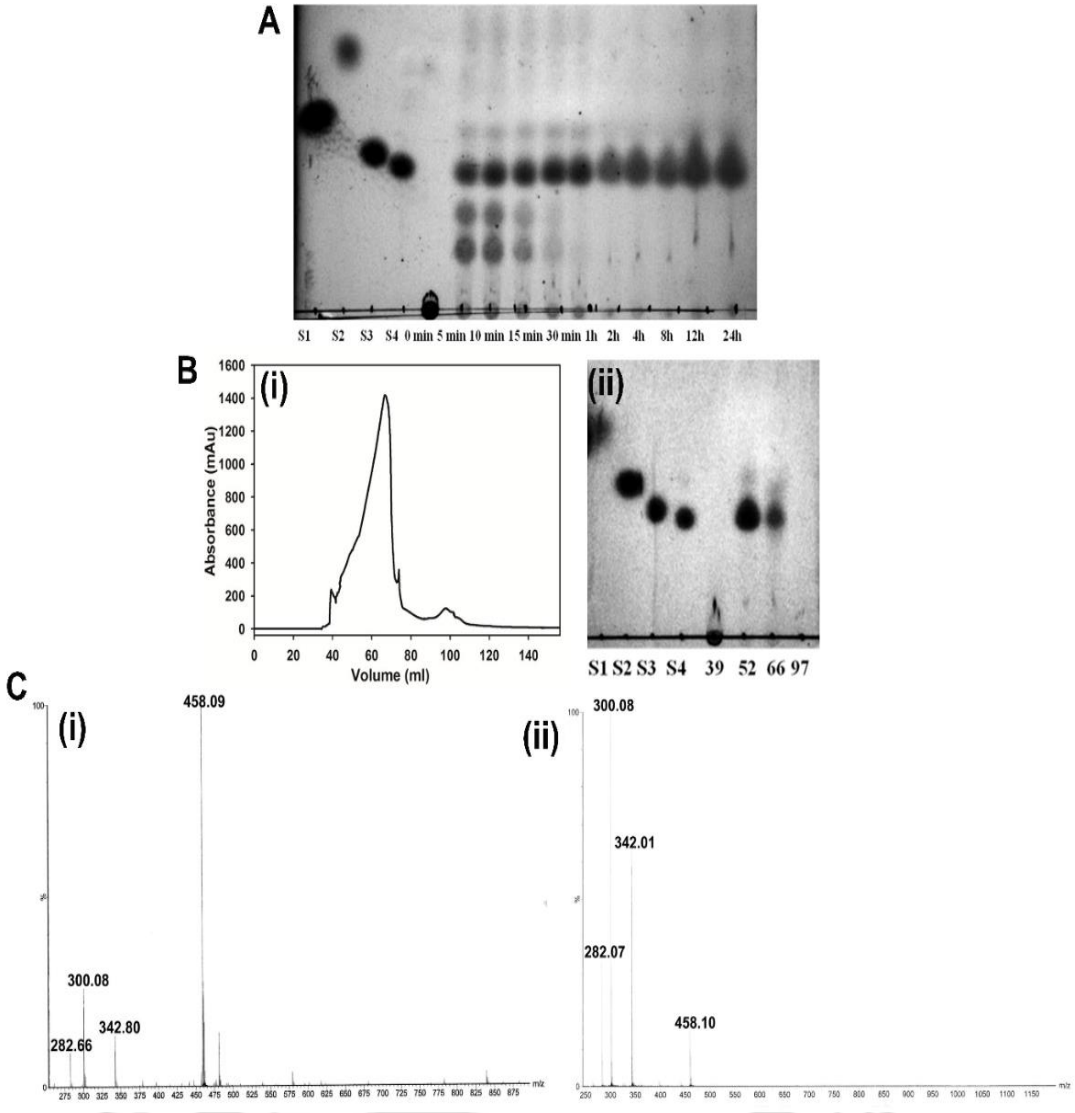

Fig. 7.3.1 (A) Time dependant TLC analysis of degraded products of CS-Keel polysaccharide using *Ps*PL8A and the standards *viz.* S1: D-glucuronic acid, S2: N-acetyl galactosamine, S3: ΔC6S disaccharide and S4: ΔC4S disaccharide, (B) Purification of CS-Keel oligosaccharide, (i) Elution profile by size exclusion chromatography using BioGel P2 matrix, (ii) TLC analyses, (C) ESI-Mass spectrometric analysis of CS-Keel disaccharide (CSD) (i) ESI-MS showing unsaturated CS-Keel disaccharide having single peak at *m/z* 458, (ii) MS/MS analysis of unsaturated CS-Keel disaccharide showing a peak at *m/z* 300.

7.3.4 FT-IR spectroscopic analysis of purified CS-Keel disaccharide

The FT-IR spectrum of CS-Keel disaccharide showed presence of peak at 860 cm^{-1}, which confirms the presence of sulphate group at carbon-4 of N-acetylgalactosamine. The peak for sulphation matches well with the previous report on chondroitin sulphate isolated from shark cartilage (Wang *et al.*, 2009). The presence of peak in the frequency range, 1248-1126 cm^{-1} indicated the presence of 1→4 glycosidic linkage in the disaccharide (Figure. 7.3.2). The spectral range, 1175-1140 cm^{-1} is characteristic of di- and poly-saccharides having 1→4 glycosidic linkage as reported earlier (Nikonenko et al., 2000). The peaks at 1248.6 cm^{-1} and 1056.2 cm^{-1} signify the presence of, S=O and -C-O-S stretching vibrations, respectively, as also reported previously by Khan *et al.*, 2013. A peak at 1645 cm^{-1}in the spectra depicted the amide group, as also shown earlier by Wang *et al.*, (2003).

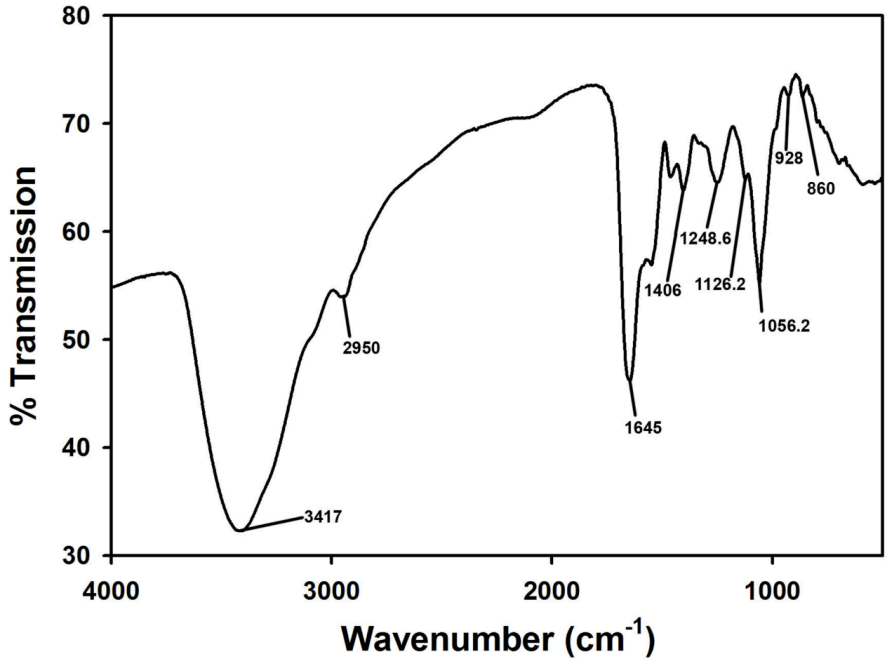

Fig. 7.3.2 FT-IR spectroscopic analysis of purified CS-Keel disaccharide.

7.3.5 ^{1}H NMR and ^{13}C NMR of CS-Keel disaccharide

The ^{1}H and ^{13}C NMR analyses of purified CS-Keel disaccharide were performed which showed the presence of N-acetyl galactosamine (GalNAc) and glucuronic acid (GlcA) in the structure of CSD (Fig. 7.3.3A and 7.3.3B). The characteristic proton signals for GlcA residue showed the resonance of H-1', H-2' and H-3' at 5.25 ppm, 3.833 ppm, 3.978 ppm, respectively. The resonance of H-4' anomeric proton in GlcA residue was observed at 5.94 ppm in the NMR spectrum. In GalNAc residue of CS-Keel disaccharide the proton resonance of H-4 at 4.657 ppm indicated the presence of sulphation in purified CSD. The rest of protons of GalNAc residues H-1, H-2, H-3, H-5, H-6a, H-6b showed resonance at 4.771 ppm, 4.144 ppm, 4.165 ppm, 4.260 ppm, 3.767 ppm and 3.677 ppm, respectively. The presence of acetylation in the GalNAc residue was indicated by the resonance observed at 2.075 ppm (Fig. 7.3.3A). The values for proton resonance of GlcA and GalNAc residues in CSD corroborates well with the previous reports (Yamada *et al*, 1992; Huckerby *et al*, 2001 and Lauder *et al*, 2011). The chemical shift for C-1, C-2, C-3, C-5 and C-6 for GalNAc were observed at 99.89 ppm, 59.26 ppm, 76.10 ppm, 74.43 ppm and 64.39 ppm, respectively in ^{13}C NMR of purified CS-Keel disaccharide (Fig. 7.3.3B). The shift at 22.10 ppm showed the presence of acetylation in GalNAc residue, while carbonyl (-C=O) group was identified by chemical shift at 174.38 ppm. The chemical shift at 77.17 ppm indicated the sulphation at carbon-4 in the GalNAc residue of CS-Keel disaccharide (Fig. 7.3.3B). The chemical shifts assigned to GlcA and GalNAc residues of purified CS-Keel disaccharide were in agreement of previous reports (Yamada *et al*, 1992; Huckerby *et al*, 2001 and Lauder *et al*, 2011). The results for ^{1}H and ^{13}C NMR have been summarized in Table 7.3.1.

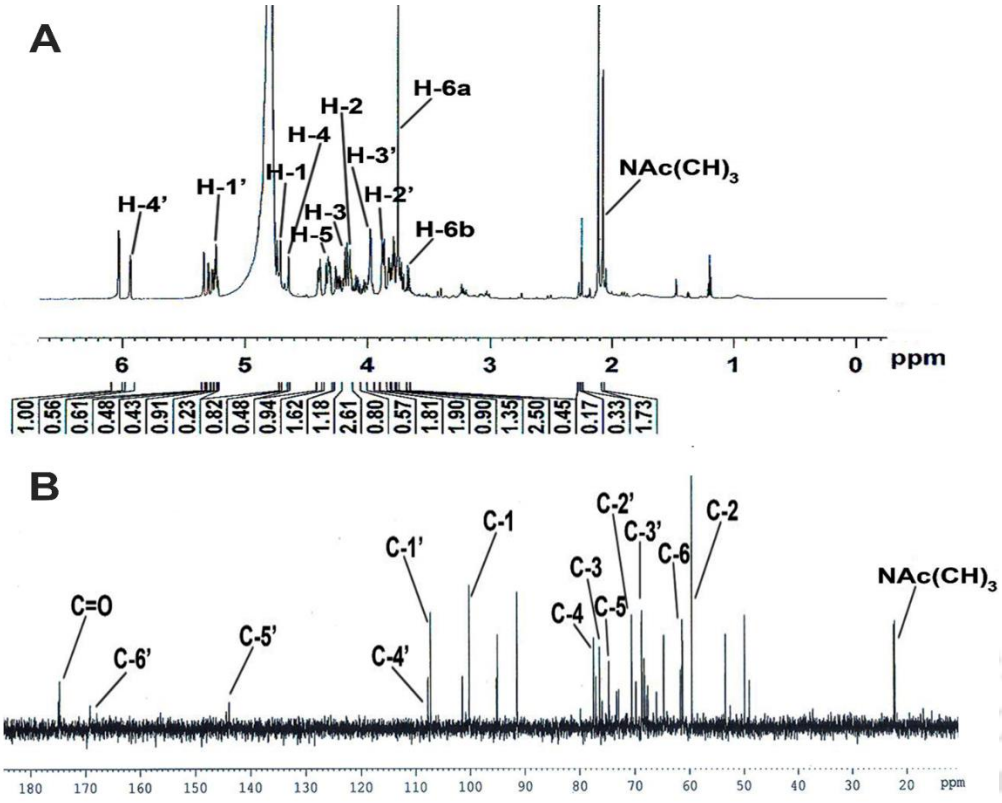

Fig. 7.3.3 NMR (600 MHz) analyses of CS-Keel disaccharide (A) ^{1}H NMR, (B) ^{13}C NMR.

Table 7.3.1 ^{1}H and ^{13}C NMR of purified CS-Keel disaccharide

Residue	Proton	^{1}H Chemical Shift (ppm)	Carbon	^{13}C Chemical Shift (ppm)
GlcA	H-1'	5.250	C-1'	106.97
	H-2'	3.833	C-2'	70.27
	H-3'	3.978	C-3'	68.45
	H-4'	5.940	C-4'	106.97
			C-5'	145.4
			C-6'	169.15
GalNAc	H-1	4.771	C-1	99.89
	H-2	4.144	C-2	59.26
	H-3	4.165	C-3	76.10
	H-4	4.657	C-4	77.17
	H-5	4.260	C-5	74.43
	H-6a	3.767	C-6	64.39
	H-6b	3.677	(-$NAcCH_3$)	22.10
	(CH_3)	2.075	C=O	174.38

H' and C' represents the proton and carbon belonging to GlcA residue in the table.

7.3.6 Effect of artificial gastric juice on CS-Keel disaccharide

The percentage of hydrolysis of CS-Keel disaccharide in the presence of artificial gastric juice was studied at different intervals of time from 1h to 5 h at 37°C. CSD displayed high resistance against artificial gastric juice at different pH from 1.0 to 4.0 (Fig. 7.3.4A). The percent hydrolysis of CSD had uniformly decreased with the increase in the pH, suggesting the higher degradation at higher acidity. CS-Keel disaccharide, after 1h of incubation at 37°C displayed 7.2%, 6.3%, 5.7% and 4.8% hydrolysis at pH 1, 2, 3 and 4, respectively (Fig. 7.3.4A). After 5h incubation at 37°C, CSD displayed 23.7%, 20.6%, 18.3% and 16.2% hydrolysis at pH 1, 2, 3 and 4, respectively (Fig. 7.3.4A). The hydrolysis of CSD (23.7%) is comparatively less with that of commercial prebiotic inulin which was previously reported to show a 25.23% hydrolysis at pH 1 after 5h of incubation (Baruah *et al.*, 2017).

7.3.7 Effect of CS-Keel disaccharide on the growth of probiotic bacteria

The growth of probiotic bacteria namely *L. acidophilus* NRRL B-4495 and *B. infantis* NRRL B-41661 was studied in the presence of CS-Keel disaccharide, inulin and glucose (Table 7.3.2). CSD effected the growth of *L. acidophilus* NRRL B-4495 and *B. infantis* NRRL B-41661 from 6.2 and 6.0 to 9.0 and 9.1 $\log_{10}$ CFU/ml, respectively after 24h. The standard prebiotic inulin stimulated the growth of *L. acidophilus* NRRL B-4495 and *B. infantis* NRRL B-41661 from 6.5 and 6.6 to 9.7 and 9.8 $\log_{10}$ CFU/ml, respectively after 24h (Table 7.3.2). The efficiency of CSD was evaluated using probiotic score which signifies the efficiency of a substrate to effect the growth of probiotic strains than that of non-probiotic strains using a non-prebiotic substrate glucose as a control. CS-Keel disaccharide displayed a positive prebiotic score for both probiotic bacteria *L. acidophilus* NRRL B-4495 and *B. infantis* NRRL B-41661

(Fig 7.3.4B). The prebiotic score of CS-Keel disaccharide for *L. acidophilus* NRRL B-4495 was 0.57 and that of *B. infantis* NRRL B-41661 was 0.58. The prebiotic score for standard prebiotic inulin for *L. acidophilus* NRRL B-4495 was 0.78 and that of *B. infantis* NRRL B-41661 was 0.73. A positive prebiotic activity score is only exhibited by carbohydrates that are metabolized by only probiotic bacteria but not by any other enteric bacteria (Huebner *et al.,* 2007). In a previous study the degradation profile of commercial CS-A polysaccharide by human gut microbiota was studied and a new CS degrading bacterium *Clostridium hathewayi* R4 was isolated from human feces (Shang *et al.,* 2016). The fucosylated-N- acetyl glucosamine disaccharide showed the prebiotic effects under *in vitro* using strains from the *Lactobacillus casei/paracasei/rhamnosus* group and from *Bifidobacterium species* (Becerra *et al.,* 2015). The prebiotics reduced the activity of microbial enzymes involved in the production of toxins and carcinogens as well as reducing the concentration of these metabolites in faeces (Burns *et al.,* 2000; Tuohy *et al.,* 2003). The positive prebiotic score of CS-Keel disaccharide shows that it can serve as prospective prebiotic ingredient for preparation of functional foods.

Table 7.3.2. Growth profile of probiotic and non-probiotic bacteria*

Bacteria	**Glucose**			**Inulin**			**CS-Keel disaccharide**		
	0h	12h	24h	0h	12h	24h	0h	12h	24h
L. acidophilus	7.2 ± 0.07	9.7 ± 0.16	10.2 ± 0.15	6.4± 0.1	9.5 ± 0.11	9.5 ± 0.1	7.3 ± 0.1	9.8 ± 0.1	10.6 ± 0.1
B. infantis	7.1 ± 0.04	10.3 ± 0.2	10.3 ± 0.27	6.6 ± 0.09	9.8 ± 0.73	9.8 ± 0.12	7.1 ± 0.17	9.3 ± 0.17	10.2 ± 0.17
Enteric Mixture	6.6 ± 0.04	9.9 ± 0.17	10.5 ± 0.22	6.7 ± 0.04	7.5 ± 0.12	7.7 ± 0.02	7.7 ± 0.06	8.4 ± 0.12	8.4 ± 0.15

**expressed as log10 CFU/ml*

7.3.8 Estimation of short chain fatty acid produced by probiotic bacteria

The short chain fatty acid namely acetic acid, propionic acid and butyric acid produced from the fermentation of prebiotic substrate was studied using modified MRS media containing either glucose, CS-Keel disaccharide or inulin. In the presence of CSD *L. acidophilus* NRRL B-4495 produced 3.8 mg/ml of acetic acid, 0.75 mg/ml of propionic acid and 0.98 mg/ml of butyric acid (Fig. 7.3.4C). Similarly, *B. infantis* NRRL B-41661 in the presence of CSD produced 3.2 mg/ml of acetic acid, 0.73 mg/ml of propionic acid and 0.96 mg/ml of butyric acid (Fig. 7.3.4C). In the presence of standard prebiotic inulin *L. acidophilus* NRRL B-4495 produced 4.2 mg/ml of acetic acid, 0.88 mg/ml of propionic acid and 0.94 mg/ml of butyric acid. Similarly, *B. infantis* NRRL B-41661 in the presence of standard prebiotic inulin produced 4.7 mg/ml of acetic acid, 0.88 mg/ml of propionic acid and 1 mg/ml of butyric acid (Fig. 7.3.4C). The SCFA produced by the fermentation of CSD was comparable to that of standard prebiotic inulin, proving its potential as a prebiotic substrate. A similar trend in the SCFA production in the presence of inulin and its various substituted forms (acetylated, propionylated, and butyrylated) was seen after 24 h of fermentation by microbiota from batch human fecal fermentation reactions. Gut microbiota utilize the prebiotic as source of carbon, providing up to 50% of the daily energy requirements of colonocytes by fermentation of carbohydrates to organic acids, mainly butyrate (Tuohy *et al.*, 2003). Butyrate promote mucosal cell proliferation, accelerate the healing process and hence provide remission to intestinal bowel disorder patient (Tuohy *et al.*, 2003). These CS-Keel disaccharide gets fermented finally by the gut microbiota to the SCFA including acetate, butyrate and propionate and hence present a suitable functional food ingredient.

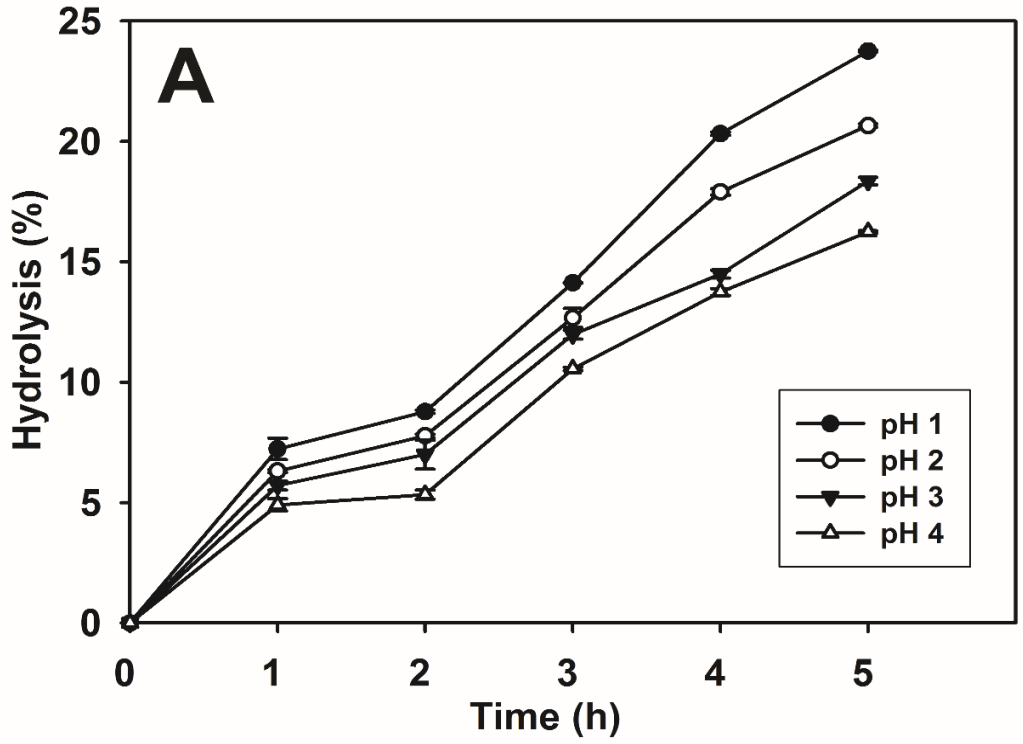

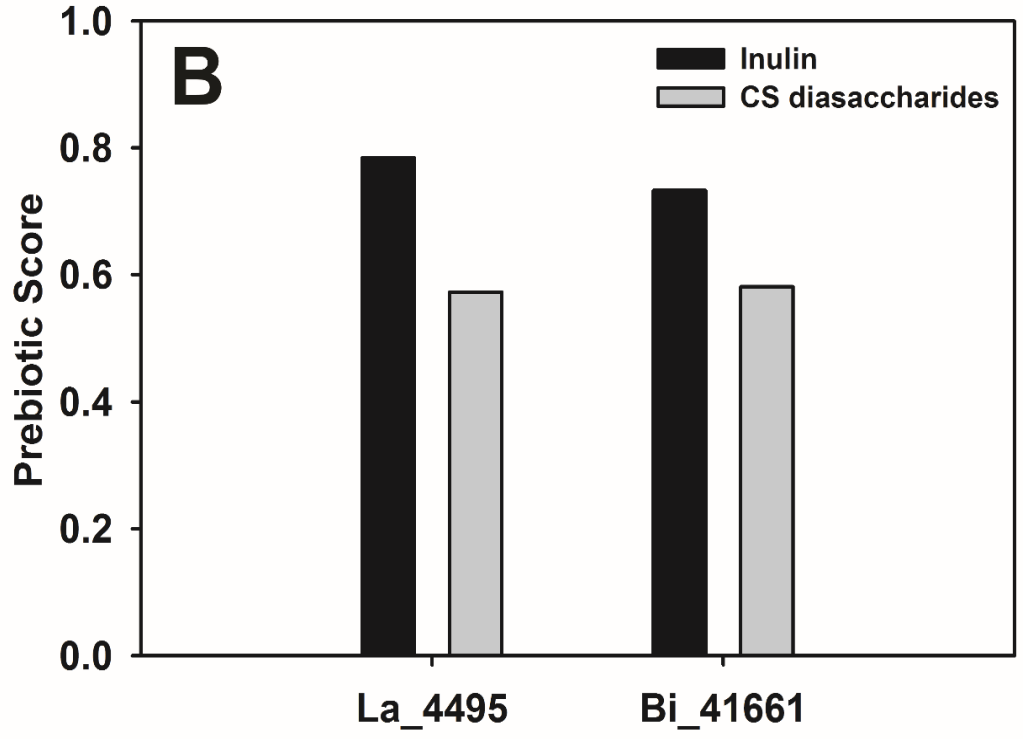

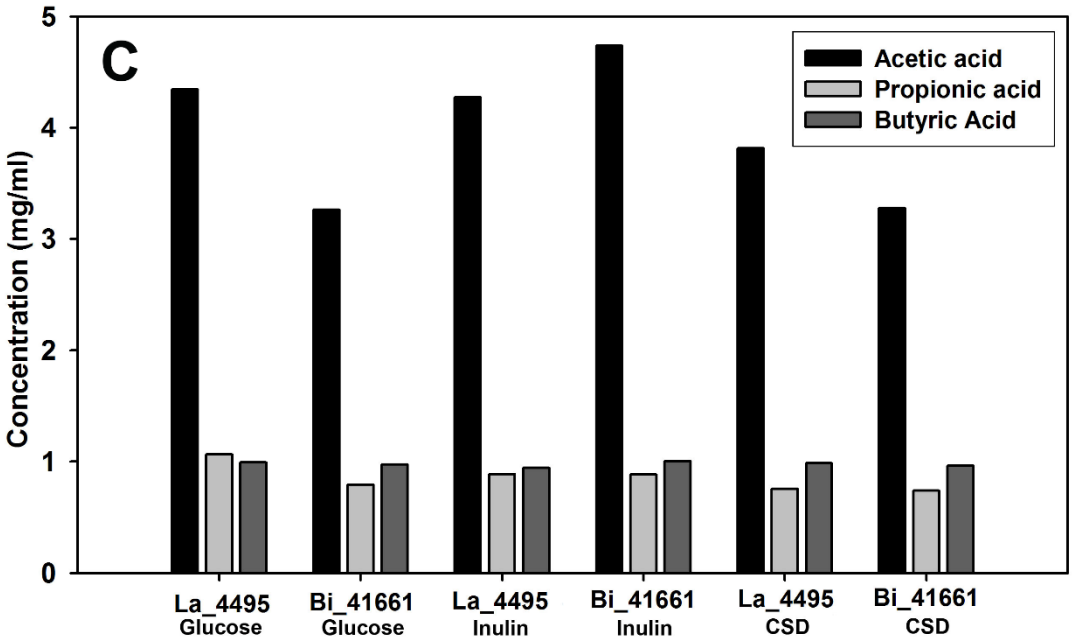

Fig. 7.3.4 (A) Hydrolysis of CS-Keel disaccharide by artificial gastric juice (B) Effect of CS-Keel disaccharide on growth of probiotic bacteria (*L. acidophilus* NRRL B-4495 and *B. infantis* NRRL B-41661) and (C) Short chain fatty acid (SCFA) production by probiotic bacteria in presence of CS-Keel disaccharide, standards glucose and inulin.

7.3.9 *In vitro* cell proliferation assay of CSD effect on L929 and HT29 cell lines

The *in vitro* cell proliferation assay of CS-Keel disaccharide was performed using MTT (Mosmann. 1983). This assay is based on the reduction of MTT into purple coloured formazan compound by metabolically active cells (Meerloo *et al.*, 2011). The effect of CSD in the concentration range, 0.010 mg/ml to 2 mg/ml was studied on normal mouse fibroblast L929 cells and Human colon cancer HT-29 cells. Treatment of L929 cells with CSD showed no alteration in the proliferation of the cells with nearly 93-98% cell viability (Fig. 7.3.5A). Effect of CSD was observed till 48h and it was found that it imparts no cytotoxicity on normal fibroblast cells with increase in time as well as concentration and hence safe for human consumption. The proliferation of Human colon cancer HT-29 cell line was studied after treatment with (0.010 mg/ml-2

mg/ml) of CSD. An overall 80% inhibition of HT-29 cell proliferation was observed with 0.5 mg/ml of CSD after 48h of incubation (Fig. 7.3.5B). Chondroitin sulphate are among the GAG polysaccharide which has been explored for its therapeutic potential. The role of CS as pharmacological agent may be achieved by direct uptake or as part of drug delivery system targeting cancer (Afratis *et al.*, 2010). In a previous study, CS disaccharide of 16 different possible theoretical sulphation were synthesised and the sulphation motifs that inhibit triple negative breast cancer were identified. The highest inhibitory effect was observed for the most aggressive, triple negative breast cancer cell line MDA-MB-23, while no effect was observed with MCF-7, T47D and normal breast cells (MCF-12A) (Poh *et al.*, 2015). Chondroitin sulphate/dermatan sulphate polysaccharide extracted from the skins of grey triggerfish showed inhibition of HCT116 cell lines (Krichen *et al.*, 2017). Antiproliferative activity of many other sulfated polysaccharides such as ulvans inhibiting (CACO-2) cell line (Kunou *et al.*, 1995) and fucans against human leukemia cell line (U-937) (Duarte *et al.*, 2000) has been reported. Such antiproliferative activities has not been studied extensively with disaccharide and oligosaccharides. The CS-Keel disaccharide reported in present study with 80-85% of HT-29 cell inhibition projects a prospective anticancer agent.

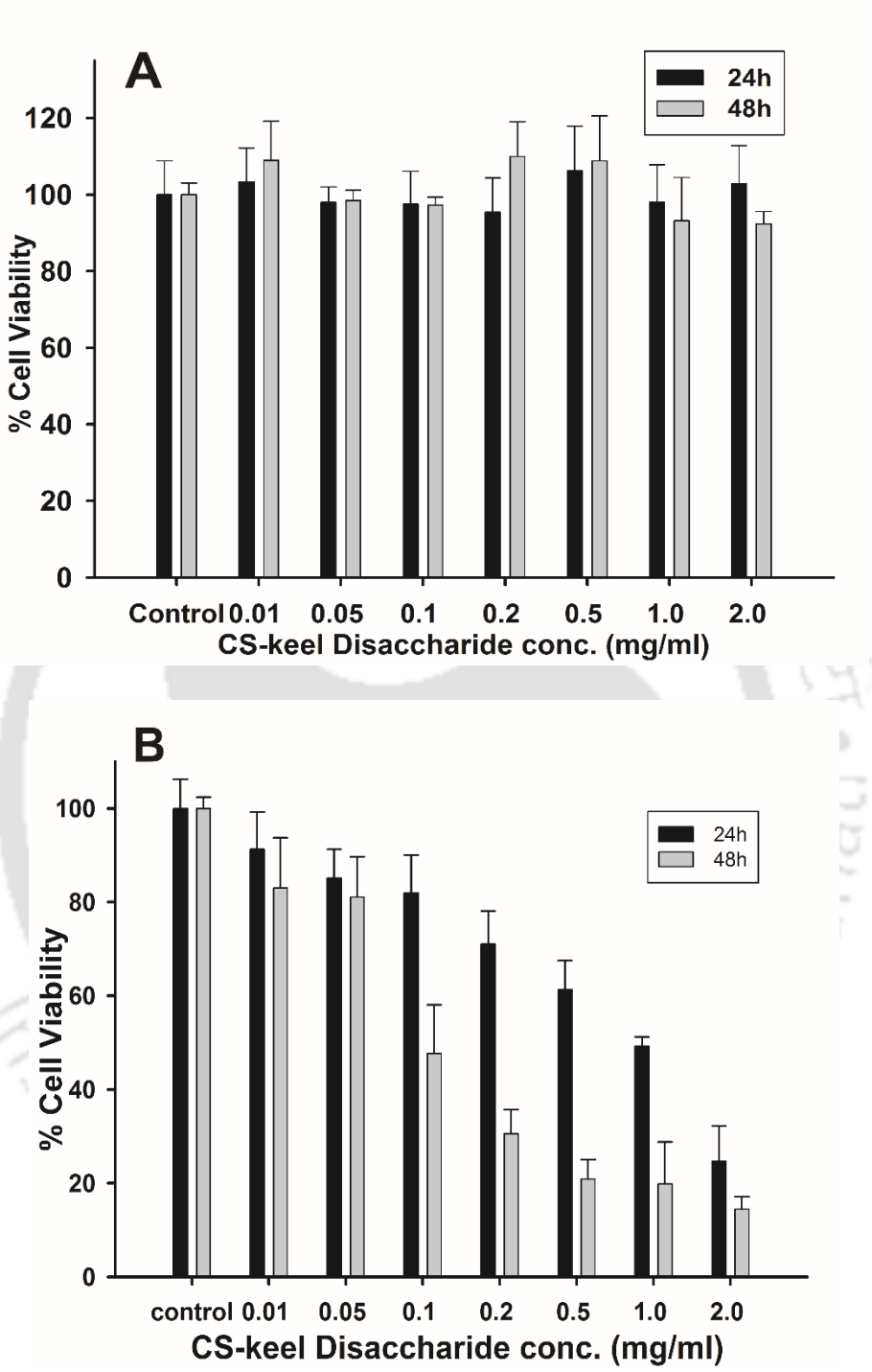

Fig. 7.3.5 The *in vitro* cell proliferation assay (MTT) showing percent cell viability of cells treated with varying concentration (0.01 mg/ml -2 mg/ml) of CS-Keel oligosaccharide (A) Mouse fibroblast L929 cells, (B) Human colon adenocarcinoma HT-29 cells.

7.3.10 Morphological analysis of L929 and HT-29 cell treated with CSD by microscopy

The microscopic analysis of L929 cells was done with and without treatment of CS-Keel disaccharide. The L929 cells exhibit a spindle shape under the normal conditions (Theerakittayakorn and Bunprasert, 2011). The bright field microscopic analysis of untreated cell showed a normal spindle shaped L929 cells (Fig. 7.3.6A & B). The cells after treatment with 2 mg/ml of CSD showed no visible alteration in morphological aspects of L929 cells (Fig. 7.3.6C & D). This revealed that the CSD is non-toxic and showed no antiproliferative activity against normal fibroblast cell lines. The human colorectal adenocarcinoma cells (HT-29) normally exhibit epithelial morphology and forms a monolayer with a typical apical brush border in RPMI medium (Hekmati *et al.*, 1990; Martinez-Maqueda *et al.*, 2015). The untreated HT-29 cells with only incomplete RPMI medium showed a regular monolayer and epithelial shaped cells (Fig. 7.3.7A & B). A 0.5 mg/ml of CS-Keel disaccharide was used for treating the HT-29 cells for 48h. The cells after treatment showed irregular shapes with disrupted cell membrane, also the cells start losing adhesion and getting dislodged from the surface of 24 well plate (Fig. 7.3.7C & D). The microscopic analysis of L929 and HT29 cell lines further strengthened the MTT assay data. The change in morphology and result of MTT assay with 80% inhibition of colon cancer (HT-29) cells growth clearly showed the inhibitory effect of CSD on the proliferation and adhesion of cells.

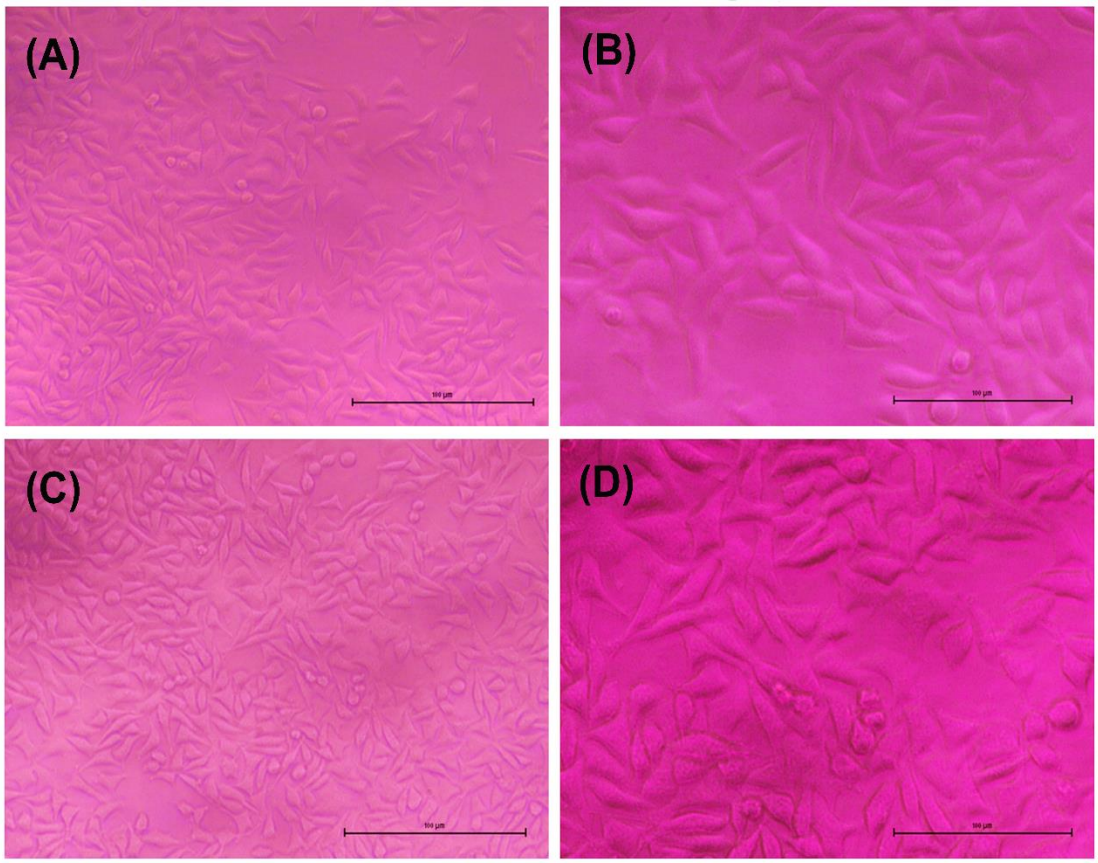

Fig. 7.3.6 Bright field microscopic images of Untreated mouse fibroblast L929 cells under (A) 20x (B) 40x magnification and CS-Keel disaccharide (0.5 mg/ml) treated cells for 48h under (C) 20x and (D) 40x magnification.

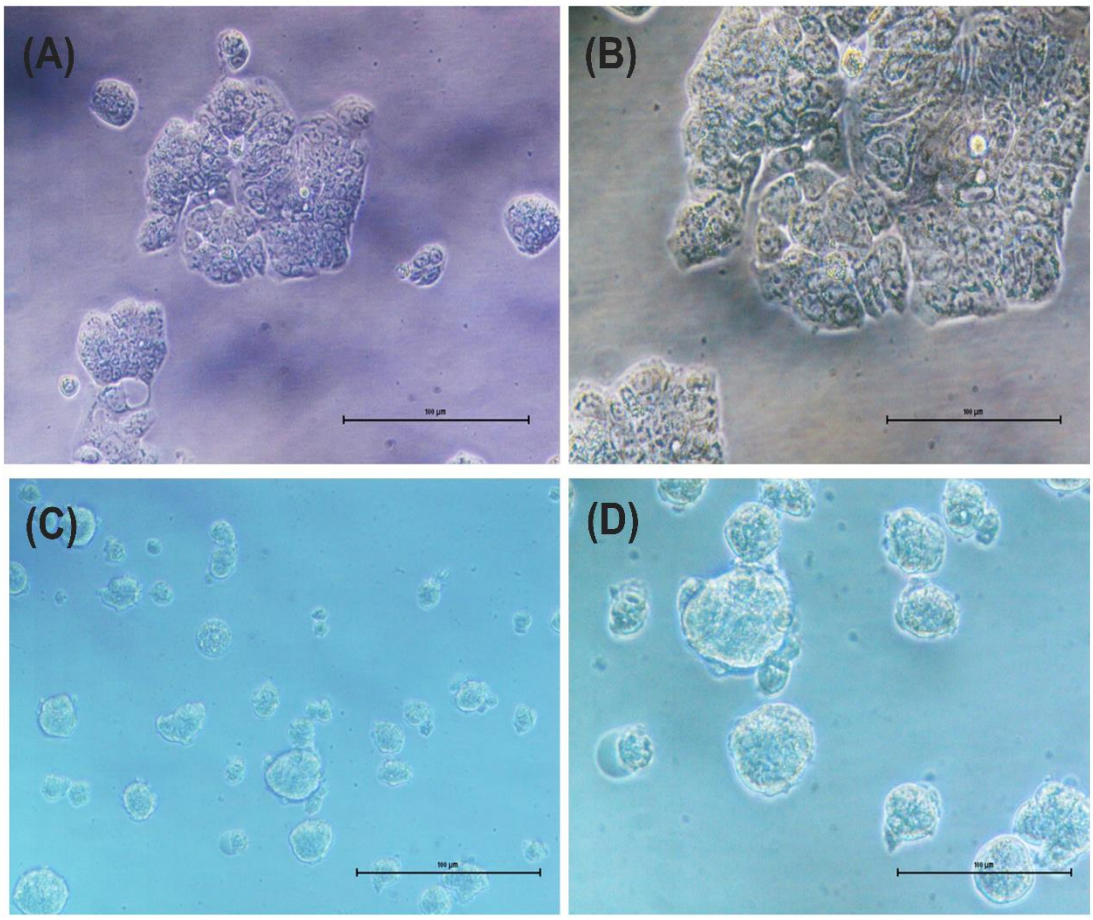

Fig. 7.3.7 Bright field microscopic images of Untreated human colon adenocarcinoma HT-29 cells under (A) 20x (B) 40x magnification and CS-Keel disaccharide (0.5 mg/ml) treated cells for 48h under (C) 20x and (D) 40x magnification.

7.3.11 Nuclear analysis of HT-29 cells by DAPI staining

The HT-29 cells were treated with 0.5 mg/ml of CS-Keel disaccharide for 48 h and the cells were stained with nuclear staining DAPI dye to observe the morphological changes in the nucleus of treated and untreated cells. The cells were observed under fluorescence microscope. DAPI is the fluorogenic dye that binds to the AT-rich region of the DNA and hence can be used for visualizing the nuclear DNA (Tarnowski *et al.*, 1991). Fig. 7.3.8A shows the bright field image of untreated HT-29 cells, in which cells are present in their intact morphology. Untreated cells show intact and round typical nuclei, as observed after DAPI staining (Fig. 7.3.8B). The HT-29 cells treated with CSD

displayed a distorted cell morphology as observed under bright field image (Fig. 7.3.8C). The treated cells showed the morphological changes such as the reduction in cellular volume, shrinkage of cytoplasm, chromatin condensation, bleb formation around nucleus and nuclear fragmentation when observed with DAPI dye (Fig. 7.3.8D). The treated cells showed more intense and bright staining of nuclei with DAPI as compared with the untreated cells, which was due to formation of apoptotic bodies (Fig. 7.3.8D). This is the first study in the effect of CS-Keel disaccharide on the human colon cancer cell lines has been shown. Pectic oligosaccharide isolated from tomato showed the anticancer potential against AGS cell line and hence apoptotic body formation as observed by DAPI and TUNNEL assays (Kapoor *et al.,* 2017).

7.3.12 Mode of cell death analysis by Annexin V-FITC staining

Apoptosis is a regulated process of cell death that is distinguished from necrosis by characteristics morphological and biochemical changes such as compaction and fragmentation of the nuclear chromatin, shrinkage of the cytoplasm and loss of membrane asymmetry. During early stages of apoptosis, the alteration in plasma membrane occurs and phosphatidylserine gets translocated from inner to outer side of the membrane. The annexin-V FITC dye binds the phosphatidylserine, exposed from the membrane and hence stains the apoptotic cells, while PI stains the dead or necrotic cells. The apoptotic/necrotic mode of cell death was analysed by staining the untreated and CSD treated HT-29 cells with annexin V-FITC and PI. HT-29 cells treated with 0.5 mg/ml CSD (Fig. 7.3.8E) showed significantly higher staining and strong green fluorescence of cell membrane with annexin-V FITC. The entry of annexin-V FITC appears to be due to disturbance in the loss of integrity of cellular membrane that confirmed the presence of apoptotic bodies after the CSD treatment (Fig. 7.3.8F). The

dead cells showed membrane staining by both annexin V and nuclear staining by propidium iodide (Fig. 7.3.8G-H). The untreated HT-29 cells showed no or faint green fluorescence after staining, demonstrating the viability of cells (Fig. 7.3.8I & J). The results of DAPI, annexin-V FITC and PI staining suggested that the CS-Keel disaccharide induce the cell death in human colon adenocarcinoma cells by apoptosis. This also demonstrated the promising antiproliferative potential of CSD where by it may be used as an effective agent in treating gastric cancer.

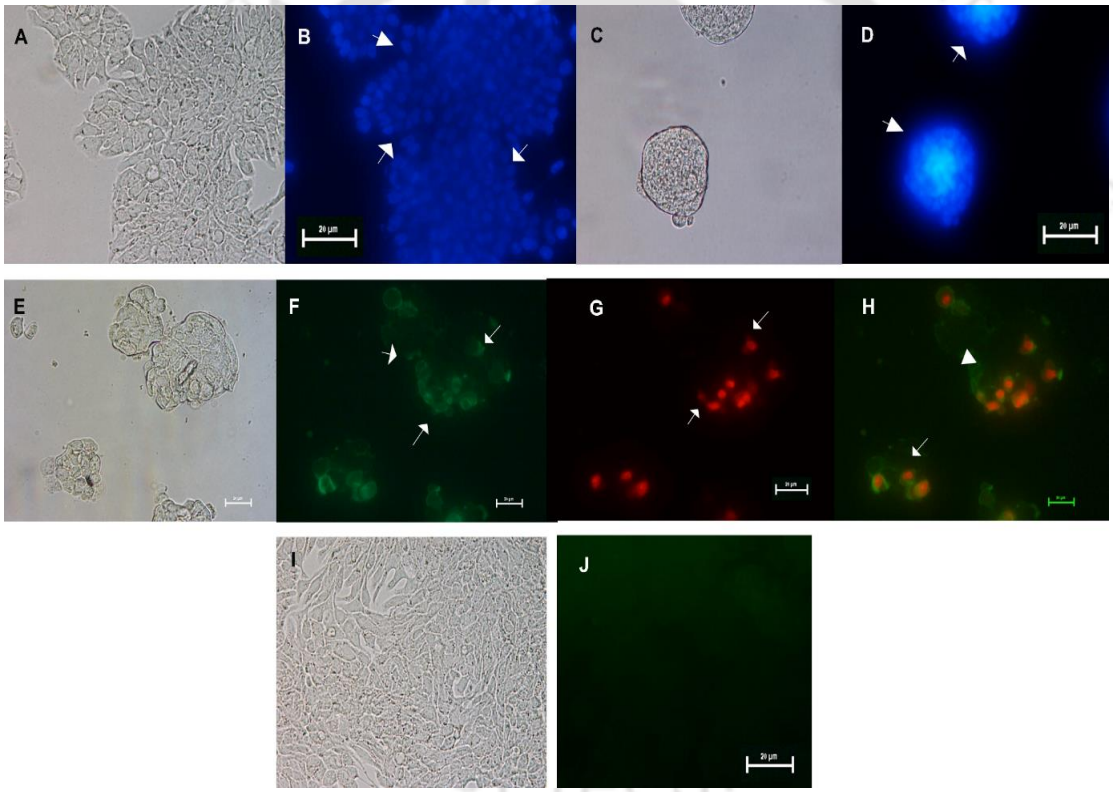

Fig. 7.3.8 Nuclear analysis of HT-29 cells, stained with DAPI under 40X resolution (A) Control untreated cells under bright field microscope, (B) Control untreated cells showing faint fluorescence and less permeability with DAPI, (C) CSD treated cells (0.5 mg/ml) under bright field microscope showing disrupted membrane (D) Treated cells showing high permeability with DAPI and nuclear condensation. Apoptosis/Necrotic analysis of HT-29 cells by Annexin-V-FITC and PI staining under 40X resolution (E)-(H) treated HT-29 cells with 0.5 mg/ml of CSD, (I)-(J) untreated HT-29 cell lines.

7.4 Conclusions

Chondroitin Sulphate-Keel disaccharide (CSD) was produced by chondroitin AC lyase (*Ps*PL8A) degradation of CS-Keel polysaccharide isolated from chicken keel cartilage. *Ps*PL8A showed specific activity, 340±5 U/mg with CS-Keel polysaccharide. Time dependent TLC analysis showed the presence of higher oligosaccharide till 30 min after which the disaccharide was the major product. CSD was purified by gel filtration using Bio-Gel P2 matrix and the ESI-MS and MS/MS analysis showed peak at 300 m/z, confirming it to be chondroitin 4-sulpahte disaccharide. The structural characterization of CSD by FTIR and NMR showed the presence of N-acetylgalactosamine and glucuronic acid. CSD displayed prebiotic properties by showing 23.7% hydrolysis to gastric juice, comparable to commercial inulin (25.2%) at pH 1.0. CSD showed a positive prebiotic score for *Lactobacillus acidophilus* NRRL B-4495(0.57) and *Bifidobacterium infantis* NRRL B-41661 (0.58). CSD was fermented by probiotic bacteria into Short Chain Fatty Acid (SCFA) products such as acetate, propionate and butyrate. MTT assay and morphological analysis confirmed that CSD (0.5 mg/ml) does not decrease the viability of mouse fibroblast (L929) cell lines and showed anti-proliferative potential against human colon cancer (HT-29) cell lines displaying 80% inhibition. CSD treated HT-29 cells also displayed the nuclear fragmentation on observation by DAPI dye. CSD treated HT-29 cells showed more intense staining of nuclei with DAPI as compared with the untreated cells because of chromatin condensation. CSD treated HT-29 cells exhibited apoptotic body formation, which confirms apoptosis as major mode of cell death as observed by annexin-V-FITC and PI staining. Colonic microflora has a profound influence on health. CSD having the prebiotic and anticancer properties can be used to manipulate the colonic microflora

to improve gut health and can specifically target intestinal bowel disorders, colorectal cancer and maintain the gastrointestinal health. Future challenges includes the study of the prebiotic and anti-colorectal cancer potential of CSD under *in vivo* conditions.

7.5 References

Afratis, N., Gialeli, C., Nikitovic, D., Tsegenidis, T., Karousou, E., Theocharis, A. D., Pavão, M. S., Tzanakakis, G. N. and Karamanos, N. K. (2012) Glycosaminoglycans: key players in cancer cell biology and treatment. *FEBS Journal*, *279* (7), 1177-1197.

Al-Sheraji, S. H., Ismail, A., Manap, M. Y., Mustafa, S., Yusof, R. M., and Hassan, F. A. (2012). Fermentation and non-digestibility of Mangifera pajang fibrous pulp and its polysaccharides. *Journal of Functional Foods*, *4*(4), 933-940.

Baici, A., Hörler, D., Moser, B., Hofer, H. O., Fehr, K. and Wagenhäuser, F. J. (1992) Analysis of glycosaminoglycans in human serum after oral administration of chondroitin sulfate. *Rheumatology International*, *12* (3), 81-88.

Baruah, R., Maina, N. H., Katina, K., Juvonen, R., and Goyal, A. (2017). Functional food applications of dextran from Weissella cibaria RBA12 from pummelo (Citrus maxima). *International Journal of Food Microbiology*, *242*, 124-131.

Becerra, J. E., Coll-Marqués, J. M., Rodríguez-Díaz, J., Monedero, V. and Yebra, M. J. (2015) Preparative scale purification of fucosyl-N-acetylglucosamine disaccharides and their evaluation as potential prebiotics and antiadhesins. *Applied Microbiology and Biotechnology*, *99* (1), 7165-7176.

Bruno-Barcena, J. M. and Azcarate-Peril, M. A. (2015) Galacto-oligosaccharides and colorectal cancer: feeding our intestinal probiome. *Journal of Functional Foods*, *12*, 92-108.

Burns, A. J. and Rowland, I. R. (2000) Anti-carcinogenicity of probiotics and prebiotics. *Current Issues in Intestinal Microbiology*, *1*(1), 13-24.

Damonte, E. B., Matulewicz, M. C., and Cerezo, A. S. (2004). Sulfated seaweed polysaccharides as antiviral agents. *Current Medicinal Chemistry*, *11*(18), 2399-2419.

Desai, U., Swanson, R., Bock, S. C., Björk, I. and Olson, S. T. (2000) Role of arginine 129 in heparin binding and activation of antithrombin. *Journal of Biological Chemistry*, *275*(25), 18976-18984.

Desaire, H., and Leary, J. A. (2000). Detection and quantification of the sulfated disaccharides in chondroitin sulfate by electrospray tandem mass spectrometry. *Journal of the American Society for Mass Spectrometry*, *11*(10), 916-920.

Duarte, M. E. R., Noseda, D. G., Noseda, M. D., Tulio, S., Pujol, C. A. and Damonte, E. B. (2001) Inhibitory effect of sulfated galactans from the marine alga *Bostrychia montagnei* on herpes simplex virus replication *in vitro*. *Phytomedicine*, *8* (1), 53-58.

Egea, J., García, A. G., Verges, J., Montell, E., and López, M. G. (2010). Antioxidant, antiinflammatory and neuroprotective actions of chondroitin sulfate and proteoglycans. *Osteoarthritis and Cartilage*, *18*, S24-S27.

Ferlay, J., Shin, H. R., Bray, F., Forman, D., Mathers, C., and Parkin, D. M. (2010). Estimates of worldwide burden of cancer in 2008: GLOBOCAN 2008. *International Journal of Cancer*, *127*(12), 2893-2917.

Flangea, C., Serb, A. F., Schiopu, C., Tudor, S., Sisu, E., Seidler, D. G., and Zamfir, A. D. (2009). Discrimination of GalNAc (4S/6S) sulfation sites in chondroitin sulfate disaccharides by chip-based nanoelectrospray multistage mass spectrometry. *Central European Journal of Chemistry*, *7*(4), 752.

Hekmati, M., Ben-Shaul, Y., and Polak-Charcon, S. (1990). A morphological study of a human adenocarcinoma cell line (HT29) differentiating in culture. Similarities to intestinal embryonic development. *Cell Differentiation and Development*, *31*(3), 207-218.

Hongpattarakere, T., Cherntong, N., Wichienchot, S., Kolida, S., and Rastall, R. A. (2012). In vitro prebiotic evaluation of exopolysaccharides produced by marine isolated lactic acid bacteria. *Carbohydrate Polymers*, *87*(1), 846-852.

Huckerby, T. N., Lauder, R. M., Brown, G. M., Nieduszynski, I. A., Anderson, K., Boocock, J., Sandall, P.L. and Weeks, S. D. (2001). Characterization of oligosaccharides from the chondroitin sulfates. *The FEBS Journal*, *268*(5), 1181-1189.

Huebner, J., Wehling, R. L., and Hutkins, R. W. (2007). Functional activity of commercial prebiotics. *International Dairy Journal*, *17*(7), 770-775.

Kapoor, S. and Dharmesh, S. M. (2017) Pectic Oligosaccharide from tomato exhibiting anticancer potential on a gastric cancer cell line: Structure-function relationship. *Carbohydrate Polymers*, *160*, 52-61.

Korakli, M., Gänzle, M. G., and Vogel, R. F. (2002). Metabolism by bifidobacteria and lactic acid bacteria of polysaccharides from wheat and rye, and exopolysaccharides produced by *Lactobacillus sanfranciscensis*. *Journal of Applied Microbiology*, *92*(5), 958-965.

Krichen, F., Volpi, N., Sila, A., Maccari, F., Mantovani, V., Galeotti, F., Ellouz-Chaabouni, S. and Bougatef, A. (2017) Purification, structural characterization and antiproliferative properties of chondroitin sulfate/dermatan sulfate from

tunisian fish skins. *International Journal of Biological Macromolecules*, *95*, 32-39.

Kunou, M., and Hatanaka, K. (1995). Effects of heparin, dextran sulfate, and synthetic (1→ 6)-α-d-mannopyranan sulfate and acidic fibroblast growth factor on 3T3-L1 fibroblasts. *Carbohydrate Polymers*, *28*(2), 107-112.

Lauder, R. M., Huckerby, T. N., Nieduszynski, I. A., and Sadler, I. H. (2011). Characterisation of oligosaccharides from the chondroitin/dermatan sulphates: ^{1}H and ^{13}C NMR studies of oligosaccharides generated by nitrous acid depolymerisation. *Carbohydrate Research*, *346*(14), 2222-2227.

Lojkowska, E., Masclaux, C., Boccara, M., Robert-Baudouy, J., and Hugouvieux-Cotte-Pattat, N. (1995). Characterization of the pelL gene encoding a novel pectate lyase of Erwinia chrysanthemi 3937. *Molecular Microbiology*, *16*(6), 1183-1195.

Martínez-Maqueda, D., Miralles, B., and Recio, I. (2015). HT29 cell line. In *The Impact of Food Bioactives on Health* (pp. 113-124). Springer International Publishing.

Mosmann, T. (1983). Rapid colorimetric assay for cellular growth and survival: application to proliferation and cytotoxicity assays. *Journal of Immunological Methods*, *65*(1-2), 55-63.

Mulloy, B. (2005). The specificity of interactions between proteins and sulfated polysaccharides. *Anais da Academia Brasileira de Ciencias*, *77*(4), 651-664.

Mussatto, S. I. and Mancilha, I. M. (2007) Non-digestible oligosaccharides: a review. *Carbohydrate Polymers*, *68*, 587-597.

Nakano, T., Betti, M. and Pietrasik, Z. (2010) Extraction, isolation and analysis of chondroitin sulfate glycosaminoglycans. *Recent Patents on Food, Nutrition & Agriculture*, *2*(1), 61-74.

Nikonenko, N. A., Buslov, D. K., Sushko, N. I. and Zhbankov, R. G. (2000) Investigation of stretching vibrations of glycosidic linkages in disaccharides and polysaccarides with use of IR spectra deconvolution. *Biopolymers*, *57*(4), 257-262.

Poh, Z. W., Gan, C. H., Lee, E. J., Guo, S., Yip, G. W. and Lam, Y. (2015) Divergent synthesis of chondroitin sulfate disaccharides and identification of sulfate motifs that inhibit triple negative breast cancer. *Scientific Reports*, *5*, DOI: 10.1038/srep14355.

Pojasek, K., Shriver, Z., Kiley, P., Venkataraman, G., and Sasisekharan, R. (2001). Recombinant expression, purification, and kinetic characterization of chondroitinase AC and chondroitinase B from Flavobacterium heparinum. *Biochemical and Biophysical Research Communications*, *286*(2), 343-351.

Qian, S., Zhang, Q., Wang, Y., Lee, B., Betageri, G. V., Chow, M. S., Huang, M. and Zuo, Z. (2013). Bioavailability enhancement of glucosamine hydrochloride by chitosan. *International Journal of Pharmaceutics*, *455*(1), 365-373.

Qiu, P., Cui, Y., Xiao, H., Han, Z., Ma, H., Tang, Y., Xu, H. and Zhang, L. (2017) 5-Hydroxy polymethoxyflavones inhibit glycosaminoglycan biosynthesis in lung and colon cancer cells. *Journal of Functional Foods*, *30*, 39-47.

Queiroz, K. C., Assis, C. F., Medeiros, V. P., Rocha, H. A., Aoyama, H., Ferreira, C.V. and Leite, E. L. (2006) Cytotoxicity effect of algal polysaccharides on HL60 cells. *Biochemisrty (Moscow), 71*(12), 1312–1315.

Rani, A., Baruah, R. and Goyal, A. (2017) Physicochemical, antioxidant and biocompatible properties of chondroitin sulphate isolated from chicken keel bone for potential biomedical applications. *Carbohydrate Polymers, 159*, 11-19.

Rani, A. and Goyal, A. (2016) A new member of family 8 polysaccharide lyase chondroitin AC lyase (*Ps*PL8A) from *Pedobacter saltans* displays endo- and exo-lytic catalysis. *Journal of Molecular Catalysis B: Enzymatic, 134*, 215-224.

Russell, W. C., Newman, C. and Williamson, D. H. A (1975) simple cytochemical technique for demonstration of DNA in cells infected with mycoplasmas and viruses. *Nature*, *253*(5491), 461-462.

Shang, Q., Yin, Y., Zhu, L., Li, G., Yu, G. and Wang, X. (2016) Degradation of chondroitin sulfate by the gut microbiota of Chinese individuals. *International Journal of Biological Macromolecules, 86*, 112-118.

Tarnowski, B. I., Spinale, F. G. and Nicholson, J.H. (1991) DAPI as a useful stain for nuclear quantitation. *Biotechnic & Histochemistry*, *66*(6), 296-302.

Theerakittayakorn, K., and Bunprasert, T. (2011). Differentiation capacity of mouse L929 fibroblastic cell line compare with human dermal fibroblast. *World Academy of Science, Engineering and Technology, International Journal of Medical, Health, Biomedical, Bioengineering and Pharmaceutical Engineering*, *5*(2), 51-54.

Tuohy, K. M., Probert, H. M., Smejkal, C. W. and Gibson, G. R. (2003) Using probiotics and prebiotics to improve gut health. *Drug Discovery Today*, *8*(15), 692-700.

Van Meerloo, J., Kaspers, G.J. and Cloos, J. (2011) Cell sensitivity assays: the MTT assay. *Cancer Cell Culture: Methods and Protocols*, 237-245.

Wang, H. and Betti, M. (2017) Sulfated glycosaminoglycan-derived oligosaccharides produced from chicken connective tissue promote iron uptake in a human intestinal Caco-2 cell line. *Food Chemistry*, *220*, 460-469.

Wang, L. F., Shen, S. S. and Lu, S. C. (2003) Synthesis and characterization of chondroitin sulfate–methacrylate hydrogels. *Carbohydrate Polymers*, *52*(4), 389-396.

Wang, P. and Tang, J. (2009) Solvent-free mechanochemical extraction of chondroitin sulfate from shark cartilage. *Chemical Engineering and Processing: Process Intensification*, *48*(6), 1187-1191.

Wang, Y., Han, G., Guo, B. and Huang, J. (2016) Hyaluronan oligosaccharides promote diabetic wound healing by increasing angiogenesis. *Pharmacological Reports*, *68*(6), 1126-1132.

Xiao, Y., Li, P., Cheng, Y., Zhang, X., Sheng, J., Wang, D., Li, J., Zhang, Q., Zhong, C., Cao, R. and Wang, F. (2014). Enhancing the intestinal absorption of low molecular weight chondroitin sulfate by conjugation with α-linolenic acid and the transport mechanism of the conjugates. *International Journal of Pharmaceutics*, *465*(1), 143-158.

Yamada, S., Yoshida, K., Sugiura, M., and Sugahara, K. (1992). One-and two-dimensional ^{1}H-NMR characterization of two series of sulfated disaccharides

prepared from chondroitin sulfate and heparan sulfate/heparin by bacterial eliminase digestion. *The Journal of Biochemistry*, *112*(4), 440-447.

Yang, H. O., Gunay, N. S., Toida, T., Kuberan, B., Yu, G., Kim, Y. S. and Linhardt, R. J. (2000) Preparation and structural determination of dermatan sulfate–derived oligosaccharides. *Glycobiology*, *10*(10), 1033-1039.

Journal Publications

Published/accepted

From Thesis:

1. **Aruna Rani,** Arun Dhillon, Kedar Sharma and Arun Goyal **(2017**) Insights into the structural characteristics and substrate binding analysis of chondroitin AC lyase (*Ps*PL8A) from *Pedobacter saltans*. *International Journal of Biological Macromolecule*s. https://doi.org/10.1016/j.ijbiomac.2017.11.087. (JIF 3.67)
2. **Aruna Rani**, Rwivoo Baruah and Arun Goyal **(2017)** Physicochemical, antioxidant and biocompatible properties of chondroitin sulphate isolated from chicken keel bone for potential biomedical applications. *Carbohydrate Polymers*, 159, 11-19. (JIF 4.8)
3. **Aruna Rani**, Seema Patel and Arun Goyal **(2017)** Chondroitin sulphate lyases: structure, function and application in therapeutics. *Current Protein and Peptide Science*. DOI: 10.2174/1389203718666170102112805. (JIF 2.5)
4. **Aruna Rani** and Arun Goyal **(2016)** A new member of family 8 polysaccharide lyase Chondroitin AC lyase (*Ps*PL8A) from *Pedobacter saltans* displays endo- and exo-lytic catalysis. *Journal of Molecular Catalysis B: Enzymatic*, 134, 215-234. (JIF 2.2)

Submitted/to be submitted

5. **Aruna Rani**, Rwivoo Baruah and Arun Goyal **(2017)** Prebiotic chondroitin sulphate disaccharide isolated from chicken keel bone exhibiting anticancer potential against human colon cancer cells. *Nutrition and Cancer* (submitted).
6. **Aruna Rani** and Arun Goyal **(2017)** Antitumor effect of chondroitin AC lyase (*Ps*PL8A) from *Pedobacter saltans* on melanoma and fibrosarcoma cell lines by *in vitro* analysis. *Pharmacological Reports* (Under review).

Other Publications:

1. Jagan Mohan Rao Tingirikari, **Aruna Rani** and Arun Goyal (2017) Synthesis of superparamagnetic nanoparticles and coating with dextran produced by dextransucrase of *Weissella cibaria* JAG8. *Journal of Polymer and the Environment*. 25(3), 569-577. (JIF 2.0)
2. Seema Patel, **Aruna Rani** and Arun Goyal (2017) Insights into the allergenic mechanisms of pollen allergens by protein domain profiling. *Computational Biotechnology and Chemistry*, *70*, 31-39. (JIF 1.0)
3. Soumyadeep Chakraborty, **Aruna Rani** and Arun Goyal (**2017**) From waste to health care product: Colon cancer cells inhibited by pectic oligosaccharide produced from citrus peels by recombinant endo-pectate lyase (PL1B). *Food and Bioproducts processing*. (Under review)
4. Sumitha Banu Jamaldheen, Kedar Sharma, **Aruna Rani**, Vijay S. Moholkar and *Arun Goyal (2017) Comparative study of pretreatment methods on agrowaste Sorghum bicolor towards increasing holocellulose content for biofuel production. *Environmental Progress and Sustainable Energy*. (Submitted)

5. Karthika B., **Aruna Rani**, Kedar Sharma and Arun Goyal (2017) Deciphering the mode of action, structural and biochemical analysis of recombinant heparinase II/III (*Ps*PL12a) a new member of family 12 polysaccharide lyase from *Pedobacter saltans.* Journal of Biotechnology (Submitted).

Book Chapters

1. ***Aruna Rani**, *Damini Kothari and Arun Goyal (2015) Chapter 19, Keratinase in "Current Developments in Biotechnology & Bioengineering", Volume 7: Production, Isolation and Purification of Industrial Products, Eds. Ashok Pandey, Sangeeta Negi, Poonam Nigam, Carlos Ricardo Soccol. http://dx.doi.org/10.1016/B978-0-444-63662-1.00019-1 *Equal contribution.
2. ***Aruna Rani**, *Arun Dhillon, *Soumyadeep Chakraborty and Arun Goyal (2015) Chapter 23, Polysaccharides lysases in "Current Developments in Biotechnology & Bioengineering", Volume VB: Production, Isolation and Purification of Industrial Products, Eds. Ashok Pandey, Sangeeta Negi, Poonam Nigam, Carlos Ricardo Soccol. http://dx.doi.org/10.1016/B978-0-444-63662-1.00023-3 *Equal contribution

Conferences/Symposia/Meetings

International

1. **Aruna Rani**, Rwivoo Baruah and Arun Goyal **(2017)** Recombinant chondroitin AC lyase (*Ps*PL8A) from *Pedobacter saltans* and its applications in therapeutics and functional foods. 7th International Forum on Industrial Bioprocessing (IFIBiop 2017), May 21-24, Wuxi, China.
2. Karthika B., **Aruna Rani**, Kedar Sharma and Arun Goyal **(2017)** Structural and biochemical characterization of recombinant Heparinase II/III of family 12 polysaccharide lyase (PL12) from *Pedobacter saltans*. 7th International Forum on Industrial Bioprocessing (IFIBiop 2017), May 21-24, Wuxi, China.
3. **Aruna Rani**, Kedar Sharma and Arun Goyal **(2017)** Insights into the structural characteristics of chondroitin AC lyase *Ps*PL8A from *Pedobacter saltans*. 12th Carbohydrate Bioengineering Meeting, April 23-26, 2017, Vienna, Austria.
4. **Aruna Rani**, Rwivoo Baruah and Arun Goyal **(2016)** Biocompatible and antioxidant properties of chondroitin sulphate isolated from chicken keel bone for potential biomedical applications. 57th International Annual Conference of the Association of Microbiologists of India (AMI-2016), Nov 24-27, 2016, Gauhati University and IASST, Guwahati, Assam India.
5. Karthika B., Kedar Sharma, **Aruna Rani** and Arun Goyal **(2016)** Cloning, expression, purification and biochemical characterization of Heparinase II/III of family 12 polysaccharide lyase (PL12) from *Pedobacter saltans*. 57th International Annual Conference of the Association of Microbiologists of India (AMI-2016), Nov 24-27, 2016, Gauhati University and IASST, Guwahati, Assam India.
6. **Aruna Rani**, Rwivoo Baruah and Arun Goyal **(2015)** Structural determination of chondroitin oligosaccharide isolated from Keel bone cartilage by recombinant chondroitin AC lyase from *Pedobactor saltans* and its prebiotic potential. 56th

International Annual Conference of Association of Microbiologists of India (AMI), December 7-10, 2015, Jawaher Lal Nehru University, New Delhi.

7. **Aruna Rani** and Arun Goyal **(2015)** Structural and biochemical characterization of endo-acting chondroitin AC lyase a family 8 polysacharide lyase (*Ps*PL8A) from *Pedobacter saltans* DSM 12145, Carbohydrate bioengineering meeting (CBM11), May 2015, Aalto University, Espoo, Finland.
8. **Aruna Rani** and Arun Goyal **(2014)** Effect of metal ions on activity of recombinant Chondroitin lyase (*Ps*PL8A) from *Pedobacter saltans* DSM 12145, 10th European Symposium on Biochemical Engineering Sciences. Lille, France September 7-10, 2014.
9. **Aruna Rani** and Arun Goyal **(2014)** Deciphering the mode of action and kinetic parameters of chondroitin lyase of family 8 polysaccharide lyase (*Ps*PL8A) from *Pedobacter saltans* DSM 12145, International conference on emerging trends in Biotechnology. Jawaharlal Nehru University, New Delhi, November 6-9, 2014.
10. **Aruna Rani** and Arun Goyal **(2014)** Cloning, expression and characterization of family 8 polysaccharide lyase (*Ps*PL8A) from *Pedobacter saltans* (DSM 12145) displaying specificity towards chondroitin sulphate, 27th International carbohydrate symposium (ICS 27), Indian Institute of Science, Bangalore, January 2014.
11. **Aruna Rani** and Arun Goyal **(2013)** Molecular cloning, expression and biochemical characterization of family 8 polysaccharide lyase (*Ps*PL8) enzyme from *Pedobacter saltans* (DSM 12145), 10th Carbohydrate Bioengineering Meeting (CBM10), Prague, Czech Republic, April 2013.

National

1. **Aruna Rani** and Arun Goyal **(2014)** Role of Glycosaminoglycan in cancer biology, National conference on recent advances in cancer biology and therapeutics. Indian Institute of Technology Guwahati, Guwahati, Assam, December 5, 2014.

Workshops attended

1. Participated in Workshop on Flow Cytometry Data Analysis Organized by Department of Biotechnology, IIT Guwahati, 23rd to 24th January 2015.
2. Participated in Technical Writing during Reflux 2.0- Annual Chemical Engineering Symposium, Department of Chemical Engineering, Indian Institute of Technology Guwahati, Assam, held on 9th March, 2014.

VITAE

The author was born on August 18, 1988 in the city of Ghaziabad, (Uttar Pradesh). She passed the Secondary Examination conducted by Central Board of Secondary Education (10th Class), New Delhi in 2003 and Higher Secondary Examination conducted by Central Board of Secondary Education (12th Class), in 2005. She completed B.Tech. (Biotechnology) from University school of biotechnology (USBT), Guru Gobind Singh Indraprastha University, New Delhi in July, 2011. She qualified Graduate Aptitude Test in Engineering (GATE) – 2010 and 2011 in Biotechnology (BT), conducted by Ministry of Human Resource and Development, Govt. of India. She also qualified CSIR- (NET)-JRF-(December, 2010) with All India Rank 341 conducted by Human Resource and Development (HRDG), Council of Scientific and Industrial Research (CSIR), Govt. of India.

Ms. Aruna Rani joined the Ph.D. program in July, 2011 at Department of Biosciences and Bioengineering, Indian Institute of Technology Guwahati, Guwahati 781 039, Assam, India. She successfully completed the course work with 8.67/10 CPI. She received Institute Fellowship (IIT Guwahati) from Aug 2011 to Jul 2016, under the scheme run by the Ministry of Human Resource and Development (MHRD), New Delhi. From September 2016 to May 2017 she received fellowship from a CSIR sponsored project in Department of Biosciences & Bioengineering under Prof. Arun Goyal. She delivered the open (PhD Synopsis) Seminar on 31st July, 2017 and presented her thesis work before the Doctoral Committee and her performance was satisfactory. She submitted the PhD thesis in August 2017.

Journal of Molecular Catalysis B: Enzymatic 134 (2016) 215–224

Contents lists available at ScienceDirect

Journal of Molecular Catalysis B: Enzymatic

journal homepage: www.elsevier.com/locate/molcatb

A new member of family 8 polysaccharide lyase chondroitin AC lyase (*Ps*PL8A) from *Pedobacter saltans* displays endo- and exo-lytic catalysis

Aruna Rani, Arun Goyal*

Department of Biosciences and Bioengineering, Indian Institute of Technology Guwahati, Guwahati 781039, Assam, India

ARTICLE INFO

Article history:
Received 13 June 2016
Received in revised form 1 November 2016
Accepted 2 November 2016
Available online 4 November 2016

Keywords:
Chondroitin AC lyase
Chondroitin 4-sulphate
Chondroitin 6-sulphate
Pedobacter saltans
β-elimination mechanism

ABSTRACT

Chondroitin lyases are therapeutically important enzymes. The functional aspects of a chondroitin AC lyase (*Ps*PL8A) from *Pedobacter saltans* DSM12145 were investigated. *Ps*PL8A was cloned in to pET28a(+) vector, expressed in *E. coli* BL-21(DE3) cells exhibited a molecular size of approximately, 77 kDa. *Ps*PL8A displayed maximum activity with chondroitin 4-sulphate, C4S (489 U mg^{-1}) followed by chondroitin 6-sulphate, C6S (214 U mg^{-1}) and hyaluronic acid (43.2 U mg^{-1}). *Ps*PL8A was maximally active at 39 °C and pH 7.2. 100 mM Na^+ and 20 mM Ca^{2+} ions enhanced the activity of *Ps*PL8A by 2-fold. The time dependent TLC analysis of *Ps*PL8A degraded products of C4S revealed the presence of higher degree of polymerization (DP) chondroitin sulphate (CS) oligosaccharides at initial stage, but after 1 h, only ΔC4S disaccharide was produced as the major product. This result displayed that *Ps*PL8A follows initially a concomitant endo- and exo-lytic mode which finally shifted to exolytic mode of catalysis. The oligosaccharides released were identified as di-, hexa-, octa- and dodeca-saccharide by ESI–MS analysis. The ΔC4S disaccharide showed a peak at *m*/*z* 458 (ESI–MS) while in MS/MS mode it gave the peak at *m*/*z* 300. ESI–MS/MS, ^{1}H- and ^{13}C-NMR analyses confirmed the structure of ΔC4S disaccharide product obtained after 24 h reaction of C4S with *Ps*PL8A. The enzyme reported in present study can be used for cancer mitigation, spinal cord injury treatment and CS oligosaccharides production which act as anti-inflammatory agents. This is the first study reporting the cloning and expression of chondroitin AC lyase from *Pedobacter saltans* DSM 12145.

1. Introduction

Proteoglycans are the major constituent of extracellular matrix (ECM) in animals [1]. These proteoglycans are made up of protein core and the Glycosaminoglycan (GAG) chains. GAGs are highly charged linear heteropolysaccharide chains composed of an alternating repeating disaccharide units of two six membered sugar rings, a hexosamine (N-acetyl glucosamine, GlcNAc, or N-acetyl galactosamine, GalNAc) linked to a uronic acid (D-glucuronic acid, GlcA, or L-iduronic acid, IdoA) [2]. These monosaccharide units can either be sulphated or non-sulphated. The molecular weight and sulphation of these chains depends upon its location and the type of tissue [3–5]. GAGs are classified into four main categories, heparan sulphate, keratan sulphate, hyaluronic acid, chondroitin sulphate (CS) or dermatan sulphate (DS). GAGs with an exception of hyaluronic acid are attached through a serine residue to the protein core and form proteoglycans. Chondroitin sulphate is composed of Glucuronic acid (GlcA) attached through a β-(1 → 3) linkage to N-acetylgalactosamine (GalNAc) and these disaccharides repeat units are connected *via* β-(1 → 4) glycosidic linkage forming a polysaccharide chain [6]. CS can be regioselectively sulphated at 4-O or 6-O positions of N-acetylgalactosamine and hence classified as chondroitin 4-sulphate (C4S) or chondroitin 6-sulphate (C6S), respectively [7]. CS chains play important roles in various biological functions such as cell adhesion, proliferation, differentiation, signalling, inflammation, organ morphogenesis, inflammation, infection and pathogenesis by interacting with cytokines and myriad of growth factors [8–10]. CS also maintains the resiliency and structural integrity of cartilage tissue [11,12].

The enzymatic degradation of GAGs involves mainly two classes of enzymes, hydrolases and lyases. The hydrolase enzymes from eukaryotic sources act *via* hydrolytic mechanism and they degrade the GAGs by cleaving the glycosyl-oxygen bond by the addition of a water molecule and produce saturated disaccharide products. The GAG lyases from prokaryotic origin depolymerize GAGs *via* a β

Abbreviatons: ECM, extracellular matrix; GAG, glycosaminoglycan; GlcNAc, N-acetyl glucosamine; GalNAc, N-acetyl galactosamine; GlcA, D-glucuronic acid; IdoA, L-iduronic acid; CS, chondroitin sulphate; DS, dermatan sulphate; C4S, chondroitin 4-sulphate; C6S, chondroitin 6-sulphate; TLC, thin layer chromatography; IMAC, immobilized metal-ion affinity chromatography; NMR, nuclear magnetic resonance; ESI–MS, Electron Spray Ionization-Mass Spectrometry.

* Corresponding author.
E-mail address: arungoyl@iitg.ernet.in (A. Goyal).

http://dx.doi.org/10.1016/j.molcatb.2016.11.001
1381-1177/

elimination mechanism and cleave the oxygen–aglycone linkage through proton abstraction from C5 carbon of uronic acid, producing an unsaturated disaccharide product with a double bond between C4 and C5 at uronic acid ring [13,14]. Polysaccharide lyases (EC 4.2.2.-) are large group of enzymes belonging to carbohydrate active enzymes and have been classified into 23 families, on the basis of sequence similarity according to the CAZy database [15]. Chondroitin lyase has been reported from family 6, 8 and 23 degrading chondroitin sulphate *via* β elimination mechanism and generating Δ4,5 unsaturated products that shows maximum absorption at 232 nm (A_{232}).

Microorganisms are the major sources of CS degrading enzymes, particularly soil bacteria which may depend upon connective tissues of animal carcasses as a nutrient source [16,17]. Chondroitin lyases have been previously reported from *Bacteroides thetaiotaomicron,* [2] *Pedobacater heparinus,* (previously known as *Flavobacterium heparinum*) [17,18] *Arthrobacter aurescens,* [14] *Bacteroides stercoris* HJ-15 [19]. In recent times chondroitin lyases have emerged as major therapeutic agents in clinical field. Chondroitin lyases have been reported to have antitumor activity, inhibit angiogenesis, neovascularization, proliferation and metastasis in human melanoma (SK-MEL 2) cells [9,20,21]. Chondroitin lyase mediated degradation of upregulated chondroitin sulphate proteoglycans after central nervous system/spinal cord injuries augments the axonal regeneration and improves nerve plasticity [22–26]. CS lyases also impart neuroprotective role by enhancing the anti-inflammatory cytokine IL-10 level, as revealed by a mouse model study [26].

Pedobacter saltans is gram negative, soil isolate and strictly aerobic bacterium. It was reported to possess chondroitin sulphate degradation and heparinolytic activity [27,28]. In the present study chondroitin AC lyase, *Ps*PL8A from *Pedobacter saltans* DSM 12145 was cloned, expressed and biochemically and functionally characterized. To our knowledge *Ps*PL8A is a new member of the family 8 polysaccharide lyase and is the first report on chondroitin AC lyase from *Pedobacter saltans* DSM 12145.

2. Materials and methods

2.1. Bacterial strains and vectors

The genomic DNA of *P. saltans* DSM 12145 was purchased from DSMZ (*Leibniz Institute DSMZ-German Collection of Microorganisms and Cell Cultures*, Germany), *Escherichia coli* DH5α and XL-10 Gold cells Novagen (Madison, WI) were used for transformation and amplification of recombinant plasmid. The *E. coli* BL21 (DE3) cells Novagen (Madison, WI), were used as host cells for expression of recombinant protein. The vectors pET-28a (+) Novagen (Madison, WI) and pGEM-T Easy vector (Promega) were used for cloning and expression, respectively.

2.2. The substrates

Chondroitin 6-sulphate disaccharide (Δdi-6S) sodium salt (Dextra Laboratories Ltd, U.K), Chondroitin 6 – sulphate (C6S) sodium salt from shark cartilage, Chondroitin 4-sulphate sodium salt (C4S) from bovine trachea, Chondroitin sulphate B sodium salt (Dermatan sulphate) from porcine intestinal mucosa, Hyaluronic acid sodium salt from *Streptococcus equi,* Heparin sodium salt, Chondroitin 4-sulphate disaccharide (Δdi-4S) sodium salt, N-Acetyl-D-galactosamine were purchased from Sigma-Aldrich Chemical Company, USA.

2.3. Sequence analysis of Ps*PL8A*

The gene sequence with locus name, Pedsa_3808 (http://www.cazy.org/PL8_bacteria.html) having GenBank accession no. ADY54337.1 belonging to family 8 polysaccharide lyase (PL8) from *Pedobacter saltans* DSM 12145 was identified. BLAST analysis of Pedsa_3808 was performed using protein data bank (pdb) to identify the chondroitin lyase coding region. Conserved Domains Database was referred to for determining the expanse of domains. The subcellular localisation of protein was predicted using PSORT server (http://psort.hgc.jp/form.html). The expected molecular mass of the protein and various physical and chemical parameters including theoretical pI, amino acid composition, atomic composition, extinction coefficient was calculated using ProtParam server of the Swiss Institute of Bioinformatics (http://web.expasy.org/protparam/).

2.4. Amplification of gene encoding Ps*PL8A and cloning*

The ORF encoding *Ps*PL8A was amplified from genomic DNA of *Pedobacter saltans* using two oligonucleotide primers containing *NheI* and *XhoI* restriction sites. The sequence of oligonucleotide primers used for amplification were, forward primer 5′-CGCGCTAGCCAAAAGCAGACATTTGAACTG-3′ and reverse primer 5′-GCGCCTCGAGTTAAACTTTTTCTGATTTGGT-3′. A 50 μl of reaction was set up for PCR containing Mg^{2+} ions (2.5 mM), dNTPs mix (0.2 mM), primers (1.5 μM each), 1.0 μl of Taq DNA polymerase (1 Unit/μl) and 1 μl of 2.22 ng/μl genomic DNA of *P. saltans*. The PCR conditions for amplification of *Ps*PL8A were, initial denaturation 94 °C for 4 min followed by 30 cycles of denaturation at 94 °C for 30 s, annealing temperature at 55 °C for 1 min 30 s, extension at 72 °C for 2 min and final extension at 72 °C for 10 min on thermal cycler (TAKARA Bio, Japan). The amplified PCR product was run on 0.8% agarose gel and purified by GenElute kit (Sigma Chemical Company, USA). The amplified PCR product was ligated to pGEM-T_{Easy} vector containing ampicillin as a resistant marker in a ratio of 3:1 for TA cloning and the ligation mix was incubated overnight at 16 °C. The ligated product was transformed using 200 μl of *E. coli* XL10 GOLD competent cells. After the transformation the cells were spread on LB agar plate containing ampicillin (100 μg/ml), IPTG (100 mM) and X-gal (50 μg/ml) and incubated at 37 °C for overnight. The white colonies were picked on the basis of blue-white colony selection. The positive clones were confirmed by restriction digestion analysis of the recombinant plasmids. The gene was excised from pGEM-T_{Easy} vector using *NheI* and *XhoI* restriction enzymes (Promega, USA) and was cloned into pET28a(+) vector digested with the same set of restriction enzymes. The *E. coli* DH5α cells were used for transformation of above recombinant plasmid. The cells were spread on LB agar plate containing kanamycin (50 μg/ml) and incubated at 37 °C for overnight. The positive clones were screened by restriction digestion analysis of the isolated recombinant plasmid from *E. coli* DH5α cells.

2.5. Expression and purification of Ps*PL8A*

E. coli BL21 (DE3) cells were used as host for expression of *Ps*PL8A. The cells were grown in 100 ml LB medium supplemented with kanamycin (50 μg/ml) incubated at 37 °C with shaking at 180 rpm to mid exponential phase till the absorbance at 550 nm (A_{550}) reached 0.6. At this point isopropyl-1-thio-β-D-galactopyranoside (IPTG) was added to a final concentration of 1.0 mM and culture was incubated at 24 °C with shaking at 180 rpm. The cells were harvested by centrifugation at 8,000*g* and 4 °C for 10 min. The cell pellet was resuspended in 5 ml of 50 mM Tris-HCl buffer pH 7.2 containing 1 mM phenylmethanesulfonyl fluoride (PMSF). The cells were sonicated (Sonics, vibra cells) by keeping

on ice for 30 min with 10 s on and 15 s off pulse at 33% amplitude. The sonicated cells were centrifuged at 16,000 rpm and 4 °C for 45 min. The cell free supernatant was subjected to immobilized metal ion affinity chromatography (IMAC) as the recombinant protein *Ps*PL8A contains N-terminal His_6 tag. The cell free extract was filtered through a 0.45 mm membrane and loaded on to a 1 ml HiTrap chelating column (GE Healthcare) equilibrated with 50 mM Tris-HCl buffer, pH 7.2 containing 300 mM NaCl and 60 mM imidazole. After extensively washing the column with 50 ml same buffer the bound protein was eluted by FPLC (Akta purifier) using a linear gradient of imidazole (0–500 mM) dissolved in 50 mM Tris-HCl buffer, pH 7.2 containing 300 mM NaCl. SDS polyacrylamide gel electrophoresis was used to assess the molecular mass and the purity of recombinant *Ps*PL8A. The enzyme concentration was measured by using molar extinction coefficient (ε) of 140150 M^{-1} cm^{-1} (calculated from sequence at ExPASy server http://web.expasy.org/protparam/) on a NanoDrop spectrophotometer (Thermo, 2000c).

2.6. Activity assay of Ps*PL8A*

The enzyme assay of *Ps*PL8A was carried out by incubating 0.1 μg of enzyme in 1 ml reaction mixture containing 1 mg/ml of C4S substrate. The enzyme reaction was performed under optimum reaction conditions of 50 mM Tris-HCl buffer, pH 7.2 at 39 °C for 5 min. The unsaturated oligosaccharide product formation was monitored by an increase in the absorbance at 232 nm (A_{232}) as a function of time on a UV–vis spectrophotometer (Varian, Cary 100). The absorbance observed was converted to units using molar absorption coefficient (3800 M^{-1} cm^{-1}) for Δ4,5 unsaturated double bond formed in the reaction. One unit of enzyme activity was defined as amount of enzyme that liberates 1 μmol of unsaturated oligosaccharides product per min as calculated using a molar absorption coefficient of 3800 M^{-1} cm^{-1} [18].

2.7. Substrate specificity of Ps*PL8A*

The substrate specificity of *Ps*PL8A was studied against different glycosaminoglycan (GAG) substrates (1 mg/ml) *viz.* Chondroitin 4-sulphate sodium salt from bovine trachea, Chondroitin sulphate B sodium salt (dermatan sulphate) from porcine intestinal mucosa, Hyaluronic acid sodium salt from *Streptococcus equi,* Heparin sodium salt and Chondroitin 6-sulphate sodium salt from shark cartilage. *Ps*PL8A was incubated with 1 mg/ml of substrate in 50 mM Tris-HCl buffer, pH 7.2 in 1 ml reaction mixture at 39 °C for 5 min. The increase in A_{232} was measured from time zero as a function of time on a UV–vis spectrophotometer (Varian, Cary 100).

2.8. Biochemical characterization of Ps*PL8A*

The optimum temperature of *Ps*PL8A was determined by incubating the 0.1 μg of enzyme in 1 ml reaction mixture containing 1 mg/ml chondroitin 4-sulphate in 50 mM Tris-HCl buffer, pH 7.2 in the temperature range 20 °C – 60 °C for 5 min. The thermal stability of enzyme was studied by incubating 100 μl enzyme (10 μg/ml) in 50 mM Tris-HCl buffer (pH 7.2) for 30 min at different temperatures varying from 20 °C to 50 °C. After incubation 10 μl of enzyme was assayed in a 1 ml reaction mixture containing 1 mg/ml of C4S for the residual activity at optimum temperature 39 °C for 5 min. The optimum pH of *Ps*PL8A was determined by incubating the 0.1 μg of enzyme in 1 ml reaction mixture containing 1 mg/ml of chondroitin 4-sulphate incubated at 39 °C for 5 min under pH range of pH 6–9. Two buffer systems 50 mM sodium phosphate for pH 6–8 and 50 mM Tris-HCl for pH 7–9 were used. The activity was measured by monitoring the unsaturated product formation by an increase in A_{232} as a function of time. The pH stability analysis of *Ps*PL8A was carried out by incubating the 100 μl enzyme (10 μg/ml) in 50 mM buffer (sodium phosphate, pH 6–8 or Tris-HCl, pH 7–9) for 30 min at 25 °C. After the incubation 10 μl of enzyme was assayed for the residual activity at optimum temperature of 39 °C for 5 min.

2.9. Kinetic parameters analysis for Ps*PL8A (kcat and km/kcat)*

The kinetic parameters, K_m, V_{max}, k_{cat} and k_{cat}/K_m, of *Ps*PL8A were calculated by obtaining initial reaction rate as a function of substrate concentration. The concentration of substrate chondroitin 4-sulphate was varied in a range of 0.1–3.0 mg/ml and the activity of *Ps*PL8A was assayed under the optimized conditions of temperature, 39 °C and pH 7.2.

2.10. Effect of metal ions on the activity of Ps*PL8A*

The activity of *Ps*PL8A was studied in the presence of varying concentrations of different metal ions mixed with 1.0 mg/ml of chondroitin 4-sulphate in 1 ml reaction mixture. A control without metal ions was also run in parallel. The reaction was carried out in 50 mM Tris-HCl, buffer pH 7.2 and at a temperature of 39 °C. The assay was carried out by monitoring unsaturated product formation by an increase in A_{232} as a function of time as mentioned earlier.

2.11. Thin layer chromatography analysis of degraded products of C4S

The mode of action of *Ps*PL8A on its substrate C4S was determined by analysing its degraded products released at different time intervals by thin layer chromatography (TLC). Separate reactions were set up in which *Ps*PL8A was incubated in a 1 ml reaction mixture containing, 1.0 mg/ml C4S in 50 mM Tris-HCl buffer, pH 7.2 and incubated at 39 °C. Different reactions were set up for each time interval (0 min, 1 min, 2 min, 5 min, 10 min, 15 min, 20 min, 25 min, 30 min, 35 min, 45 min, 1 h, 2 h, 4 h, 8 h, 12 h, 16 h and 24 h). After completion of the time interval the degraded products were separated by precipitating the undigested polysaccharides and protein by adding equal volume of absolute ethanol and by centrifuging at 13,000 *g* for 10 min. The supernatant containing enzyme degraded products were collected in separate micro- centrifuge tubes and concentrated from 1 ml to 100 μl by heating at 60 °C. A 0.5 μl of concentrated products were applied as a spot on TLC plate (Merck, Germany) and run under a solution containing 1-butanol, water and acetic acid in the ratio 5:3:2 (v/v) [29]. The TLC plates were stained by diphenylamine: aniline: phosphoric acid reagent (1 ml of 37.5% HCL, 2 ml aniline, 10 ml of 85% H_3PO_4, 100 ml of ethyl acetate and 2 g of diphenylamine) and visualized after incubating at 80 °C for 30 min [30].

2.12. ESI-Mass spectrometric analysis of Ps*PL8A degraded product of C4S*

The reaction of *Ps*PL8A was carried out in a 1 ml reaction mixture containing, 1.0 mg/ml C4S in 50 mM Tris-HCl buffer, pH 7.2 and incubated at 39 °C for 2 min, 30 min, 1 h, 2 h and 24 h. The 1 ml reaction mixture was treated with equal volume of ethanol and centrifuged at 13,000*g* for 10 min to precipitate and separate the polysaccharide and protein. After centrifugation the supernatant was collected and concentrated to 100 μl in hot air oven at 60 °C. The samples containing the oligosaccharides were diluted in 1:1 (v/v) ratio by methanol and 20 μl was used for analysis. The samples after 2 min, 30 min, 1 h, 2 h and 24 h reaction with *Ps*PL8A were then analyzed by Electron Spray Ionization (ESI) mass spectrometer (Waters, Q-TOF Premier) in MS mode without any purification. The reaction product of 24 h was analysed by both MS and tandem MS (MS/MS) mode. ESI–MS and tandem MS analyses were

carried out in negative ion mode, where the parameters for ESI–MS analysis were; capillary voltage 3 eV, collision energy 5 eV, ionization energy 1 eV, desolvation temperature 250 °C and the source temperature of 80 °C. The tandem MS analysis was carried out by nanospray ionization using the voltage 3 eV, collision energy 20 eV and collision-induced dissociation was performed on ion of interest using the argon gas.

2.13. ^{1}H- and ^{13}C- NMR spectroscopic analysis of Ps*PL8A* degraded disaccharide from C4S

The final degraded disaccharide product of C4S by enzyme *Ps*PL8A after reaction completion at 24 h was analysed by ^{1}H- and ^{13}C- Nuclear magnetic resonance (NMR) spectroscopy. The enzyme reaction was carried out in 1 ml reaction mixture containing 1.0 mg/ml of C4S in 50 mM Tris-HCl buffer, pH 7.2 and 0.5 μg of *Ps*PL8A enzyme and incubated at 39 °C for 24 h. The undigested polysaccharide and protein were precipitated by adding equal volume of absolute ethanol with gentle mixing and subsequently centrifuged at 13,000*g* for 10 min. After centrifugation the supernatant was collected and lyophilized. The sample was dissolved in D_2O (99.96%) (Merck Germany) at concentrations of 5 mg/ml (for ^{1}H NMR) and 20–30 mg/ml (for ^{13}C NMR). The ^{1}H- and ^{13}C-NMR spectra were acquired at 25 °C at 600 MHz NMR spectrometer (Bruker, Avance III HD, MA, USA) fitted with a 5-mm probe and equipped with topspin software package from Bruker for analysis.

3. Results and discussion

3.1. Sequence analysis of Ps*PL8A from* Pedobacter saltans *DSM 12145*

The amino acid sequence of *Ps*PL8A with locus name Pedsa_3808 and GenBank accession no. ADY54337.1 was accessed from CAZy database (http://www.cazy.org/). BLAST analysis of Pedsa_3808 sequence revealed the presence of putative GAG lyase domain belonging to GAG lyase superfamily. The analysis of deduced amino acid sequence of the protein gave an insight about the existence of N-terminal signal sequence with a cleavage site predicted between Ala22 and Gln23 by SignalP 3.0 server (http://www.cbs.dtu.dk/services/SignalP-236 3.0/). The expanse of signal peptide is of 22 amino acids from N-terminal and *Ps*PL8A spans at C-terminal from 23 to 701 amino acids, a 679 amino acid domain (Fig. 1a). It exhibited sequence similarity with chondroitin AC lyase from *Flavobacterium heparinum* (55% identity, PDB id 1HM2_A) and *Arthrobacter aurescens* (25% identity, PDB id 1RW9_A). The subcellular localization score as predicted by PSORT server indicated that the protein encoded by sequence Pedsa_3808 is of extracellular nature.

3.2. Cloning, expression and purification of recombinant Ps*PL8A*

The DNA sequence of 2037 base pairs, encoding *Ps*PL8A was amplified by PCR and ligated to pGEM-T Easy vector for TA cloning. The gene was excised by using *NheI* and *XhoI* restriction enzymes from cloned pGEM-T Easy vector and was ligated to pET28a(+) expression vector as described in methods section. The recombinant protein containing the N-terminal His6-tags was purified by immobilized metal ion affinity chomatography. The expression and purification of the recombinant *Ps*PL8A analysed by SDS-PAGE (10.5%, w/v) gel showed molecular size of approximately, 77 kDa (Fig. 1b). The theoretical molecular mass calculated from *Ps*PL8A sequence included the N-terminal amino acids with the His6 tag (MGSSHHHHHHSSGLVPRGSHMAS) was 77.2 kDa. The molecular size of the *Ps*PL8A obtained from SDS-PAGE was in agreement with the theoretically expected value. The recombinant *Ps*PL8A expressed as a soluble protein. The concentration of purified protein was found to be 3.5 mg/ml from 100 ml culture.

3.3. Substrate specificity of Ps*PL8A*

The β-elimination reaction mechanism followed by *Ps*PL8A was confirmed spectrophotometrically by measuring the Δ4,5 unsaturated oligosaccharides by the increase in absorbance at 232 nm (A_{232}). *Ps*PL8A is a characteristic chondroitin AC lyase and preferentially cleaves chondroitin, though it also acts against hyaluronic acid. *Ps*PL8A was predominantly active towards chondroitin sulphate substrates. It displayed highest activity towards C4S (489.0 ± 11 U/mg) followed by C6S (214.0 ± 2.0 U/mg) and hyaluronic acid (43.2 ± 1.2 U/mg), but did not show any activity with dermatan sulphate and heparin. Chondroitin AC lyase reported earlier from *Flavobacterium heparinum*, showed activity towards C4S and C6S [18]. Chondroitin AC lyase reported from *Bacteroides stercoris* HJ-15 displayed higher activity with C4S followed by hyaluronic acid and C6S [13,19]. Another report on chondroitin lyase from Baculovirus envelope protein ODV-E66 does not degrade C4S, whereas it degrades most efficiently, the chondroitin without sulphation followed by C6S and hyaluronic acid to lesser extent [31]. Chondroitin AC lyase from *Serratia marcescens* GT596 showed enzyme activity with chondroitin 4-sulphate notably lower activity than with chondroitin 6-sulphate [32].

3.4. Biochemical properties of Ps*PL8A*

The effect of the temperature and pH on the activity of the recombinant *Ps*PL8A was determined using C4S as a substrate. *Ps*PL8A displayed an optimum temperature of 39 °C (Fig. 2a) and retained ~90% of activity within the temperature range 35–40 °C. The thermal stability of *Ps*PL8A displayed ~100% retention of activity within temperature range 30–40 °C after 30 min incubation (Fig. 2b). The temperature above 40 °C may be causing the conformational changes leading to loss of enzyme activity. *Ps*PL8A displayed optimum pH of 7.2 and retained 90% activity within the pH range 6.9–7.6 (Fig. 2c). The pH stability profile displayed retaining of approximately, ~90% of enzyme activity for 30 min in the pH range 6.8–7.6 (Fig. 2d).

The chondroitin lyase has the most promising potential in cancer alleviation and spinal cord injuries treatment [9,20–26]. Chondroitin AC lyase from *Flavobacterium heparinum* [18] and *Bacteroides stercoris* HJ-15 [13] displayed optimum pH of 8.0 and 5.8, respectively and the optimum temperatures 35 °C and 45 °C, respectively. However, *Ps*PL8A displayed optimum pH of 7.2 and optimum temperature in the range 35–40 °C, which are human physiological conditions. Therefore, *Ps*PL8A can also serve as a potential candidate for therapeutic applications such as neuronal reinnervation and antitumor agent.

The kinetic parameters of *Ps*PL8A were determined against C4S. *Ps*PL8A displayed K_m and V_{max} values of 1.1 ± 0.01 mg/ml and 526 ± 28 U mg^{-1}, respectively using C4S. It gave the turnover number (k_{cat}) of 679.6 s^{-1} and (k_{cat}/K_m) as 617.8 s^{-1} mg^{-1} ml using C4S as substrate.

3.5. Effect of metal ions on the activity of Ps*PL8A*

The performance of *Ps*PL8A under the influence of various monovalent and divalent salts as well as detergent, using C4S as substrate was investigated and the results are shown in Table 1. The activity of *Ps*PL8A with no additive was taken as 100%. The presence of 100 mM Na^{+} or 20 mM Ca^{2+} or 20 mM Co^{2+} ions concentration enhanced the activity of *Ps*PL8A by ~2 fold. The enzyme activity of *Ps*PL8A was adversely affected at the low concentrations of Zn^{2+}, Al^{3+}, EDTA and SDS, while enzyme activity of *Ps*PL8A was

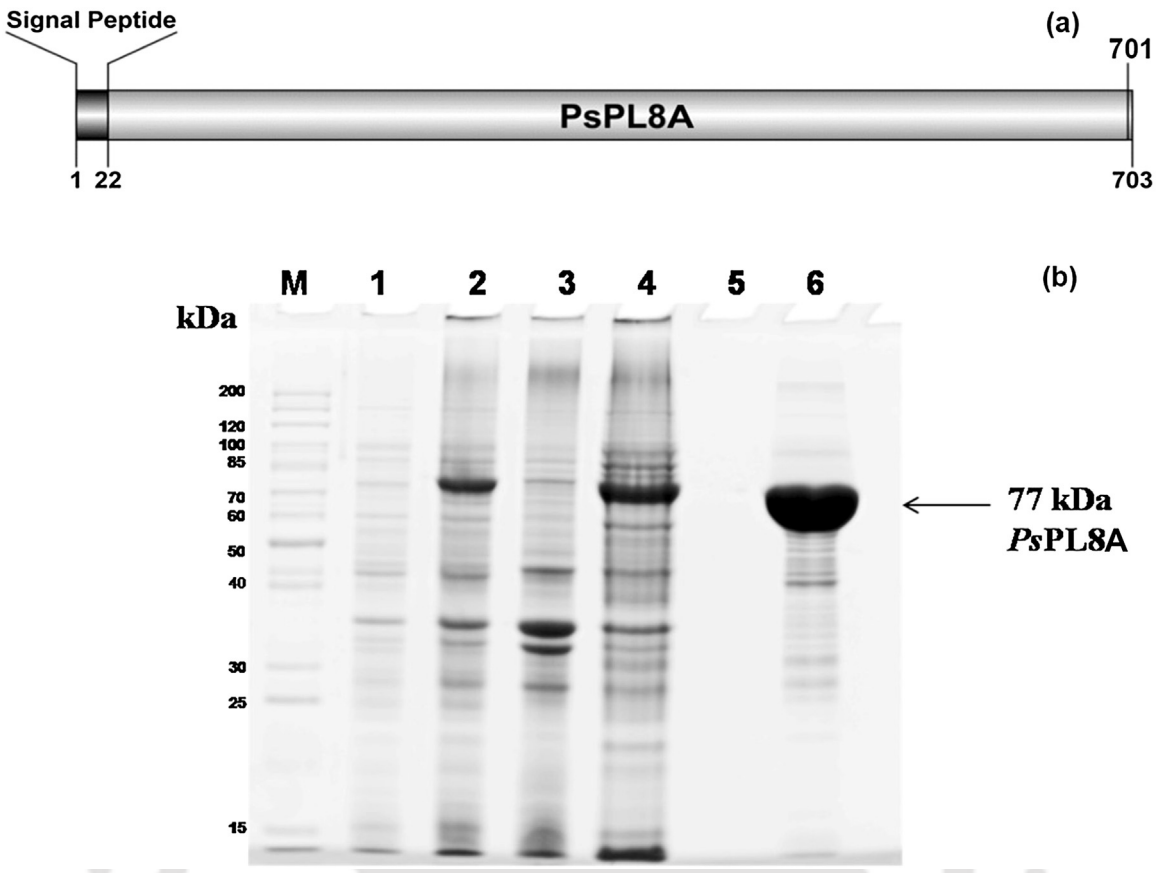

Fig. 1. (a) Molecular architecture of *Ps*PL8A showing an N-terminal signal peptide followed by the catalytic domain (b) SDS-PAGE (10.5%, w/v) gel showing over-expression and purification of *Ps*PL8A using *E. coli* BL21 (DE3) cells; Lane M: Fermentas high range protein molecular mass marker, Lane 1: Uninduced BL21 (DE3) cells, Lane 2: Induced BL21 (DE3) cells, Lane 3: Cell pellet after sonication, Lane 4: Cell free extract, Lane 5: Last wash from the column and Lane 6: Purified recombinant *Ps*PL8A enzyme.

completely inhibited at very low concentrations of Fe^{2+} or Cu^{2+} ions. The results of metal ion study gave a lucid idea that Ca^{2+} or Co^{2+} ions might be required by *Ps*PL8A as cofactors for increasing its the activity. It was earlier reported that chondroitin lyase from Baculovirus envelope protein ODV-E66 remains unaffected by the addition of divalent metal ions [31]. Chondroitin AC lyase from *Bacteroides stercoris* HJ-15 displayed only a 5% and 2% increase in the activity by 1 mM Ca^{2+} or Mg^{2+} ion concentrations, respectively [13]. The enzyme activity of chondroitin AC lyase from marine *Arthrobacter sp*. MAT3885 remains unaffected by addition of metal ions such as Na^{+}, K^{+}, Mg^{2+}, Ca^{2+}, Fe^{2+}, Co^{2+}, Cu^{2+} and Ni^{2+}, while the addition of Mn^{2+} increased the activity by only 20% [33]. The HA/CS-degrading activity of HCLase from marine bacterium was significantly inhibited by 5 mM concentration of divalent metal salts $CaCl_2$, $MgCl_2$, $MnCl_2$ and $CoCl_2$ suggesting that the activity is independent of divalent metal ions [34]. The present metal ions study with *Ps*PL8A indicated that the divalent Ca^{2+} or Co^{2+} ion(s) might be present at the catalytic site and involved in catalysis enhancing enzyme activity of *Ps*PL8A. The modelled structure of *Ps*PL8A was analysed by 3D ligand site server using a structural library of homologous structures with bound ligands to predict the metal binding site. The results revealed the presence of Ca^{2+} ion at the binding site of *Ps*PL8A (Data not shown). This further supports the role of Ca^{2+} or Co^{2+} ion(s) in the catalysis by *Ps*PL8A.

Table 1
Effects of metals ions on *Ps*PL8A activity with chondroitin 4-sulphate as substrate.

Metal ion/Reagent	Concentration (mM)	Relative activity (%)
Control	–	100
Na^{+}	100	209
K^{+}	100	185
Ca^{2+}	20	190
Mg^{2+}	20	136
Co^{2+}	20	185
Zn^{2+}	1.0	15.2
Fe^{2+}	1.0	1.2
Cu^{2+}	0.1	2.2
Al^{3+}	10.0	5.4
SDS	1.0	1.1
EDTA	10.0	1.4

3.6. TLC analysis of enzymatic degradation products of C4S

The products released by the enzymatic degradation of *Ps*PL8A with C4S were determined by TLC (Fig. 3). The salient feature of *Ps*PL8A catalysis involved only the β-(1 → 4)-bond cleavage by β elimination mechanism. The time dependent C4S degradation by *Ps*PL8A in TLC analysis showed simultaneous endo- and exo-lytic cleavage pattern for first hour producing a series of higher oligosaccharides along with the ΔC4S disaccharide (Fig. 3). After 1 h of the reaction *Ps*PL8A started utilizing the higher oligosaccharides, chopping off them, producing only the ΔC4S disaccharide as the sole product that continued till 24 h. This result displayed the initial concomitant endo- and exo-lytic cleaving property of *Ps*PL8A and finally shifting to only exo-lytic mode. The previous reports suggest that chondroitin AC lyase from *Flavobacterium heparinum* cleaves endolytically the substrates [18,35,37], whereas for chondroitin AC lyases from *Arthrobacter auresus* the exolytic action was reported [14,35–37].

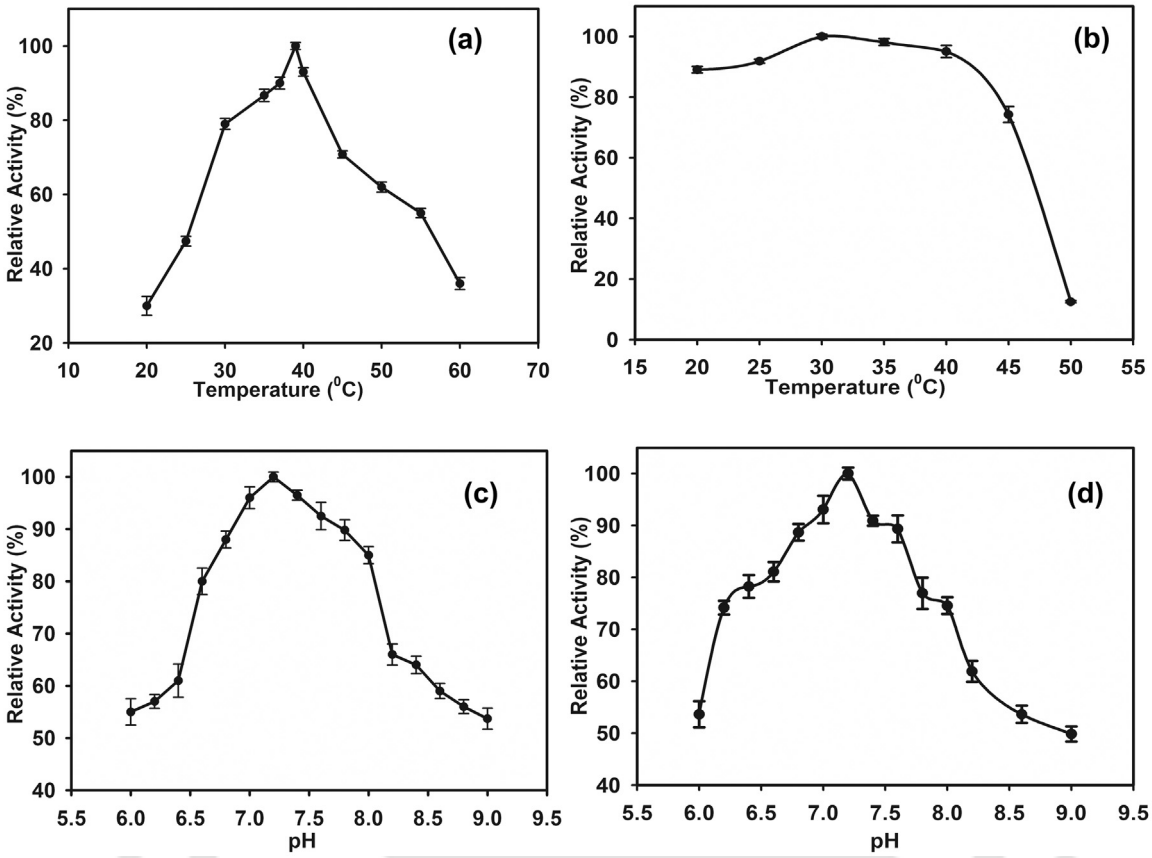

Fig. 2. (a) Effect of temperature on *Ps*PL8A activity with C4S in buffer 50 mM Tris-HCl pH 7.2 (b) Thermal stability of *Ps*PL8A using 50 mM Tris-HCl buffer, pH 7.2, with 30 min incubation of enzyme at 20–50 °C followed by assay 10 μl of enzyme in 1 ml reaction mixture containing 1 mg/ml of C4S for the residual activity at optimum temperature 39 °C for 5 min, (c) Effect of pH on *Ps*PL8A activity. The enzyme was incubated in 50 mM buffer (Sodium phosphate pH 6–8 or Tris-HCl, pH 7–9) and activity was measured at 39 °C for 5 min (d) pH stability of *Ps*PL8A. The enzyme in 50 mM buffer (Sodium phosphate pH 6–8 or Tris-HCl, pH 7–9) was incubated at 25 °C for 30 min followed by activity measurement at 39 °C for 5 min.

3.7. *ESI–MS and MS/MS analysis of* Ps*PL8A degraded product of C4S*

The supernatant containing degraded products of C4S after *Ps*PL8A treatment for 2 min, 30 min, 1 h, 2 h and 24 h were subjected to ESI–MS and MS/MS analyses. The ESI–MS analysis of 2 min sample showed the presence of mono sulphated unsaturated disaccharide UA-GalNAc4S with *m*/*z* 458, triply charged penta-sulphated unsaturated hexa-saccharide UA-GalNAc-[GlcA-GalNAc]$_3$(4S)$_5$ with *m*/*z* 508.14, triply charged tetra-sulphated unsaturated octa-saccharide UA-GalNAc-[GlcA-GalNAc]$_4$(4S)$_4$ as a sodium adduct with *m*/*z* 616.11 and triply charged unsaturated hexa-sulphated dodeca-saccharide UA-GalNAc-[GlcA-GalNAc]$_6$(4S)$_6$ as a tri sodium adduct with *m*/*z* 939.07 (Fig. 4a). The *m*/*z* values assigned to the degraded products corroborated well with CS oligosaccharides reported earlier by Zaia et al., 2001 [38] and Zamfir et al., 2003 [39].

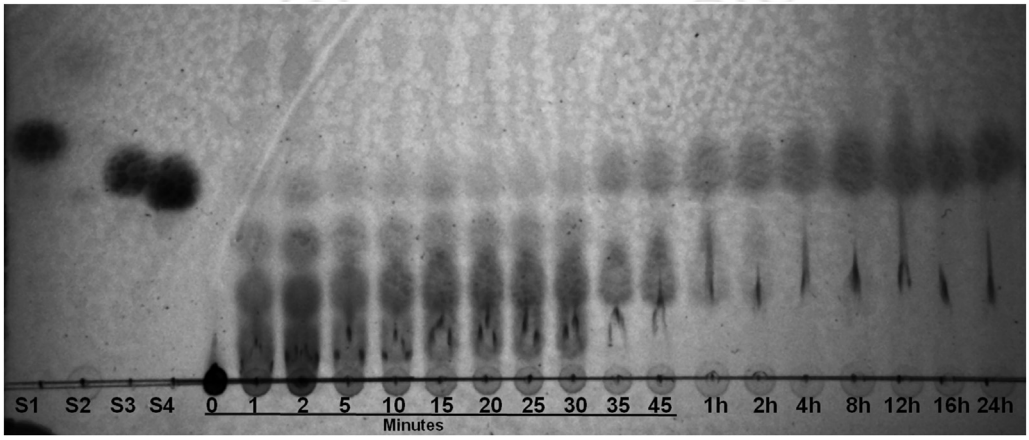

Fig. 3. Time dependant TLC analysis of *Ps*PL8A degraded products of C4S using the standards *viz.* S1: D-glucuronic acid, S2: N-acetyl galactosamine, S3: ΔC6S disaccharide and S4: ΔC4S disaccharide.

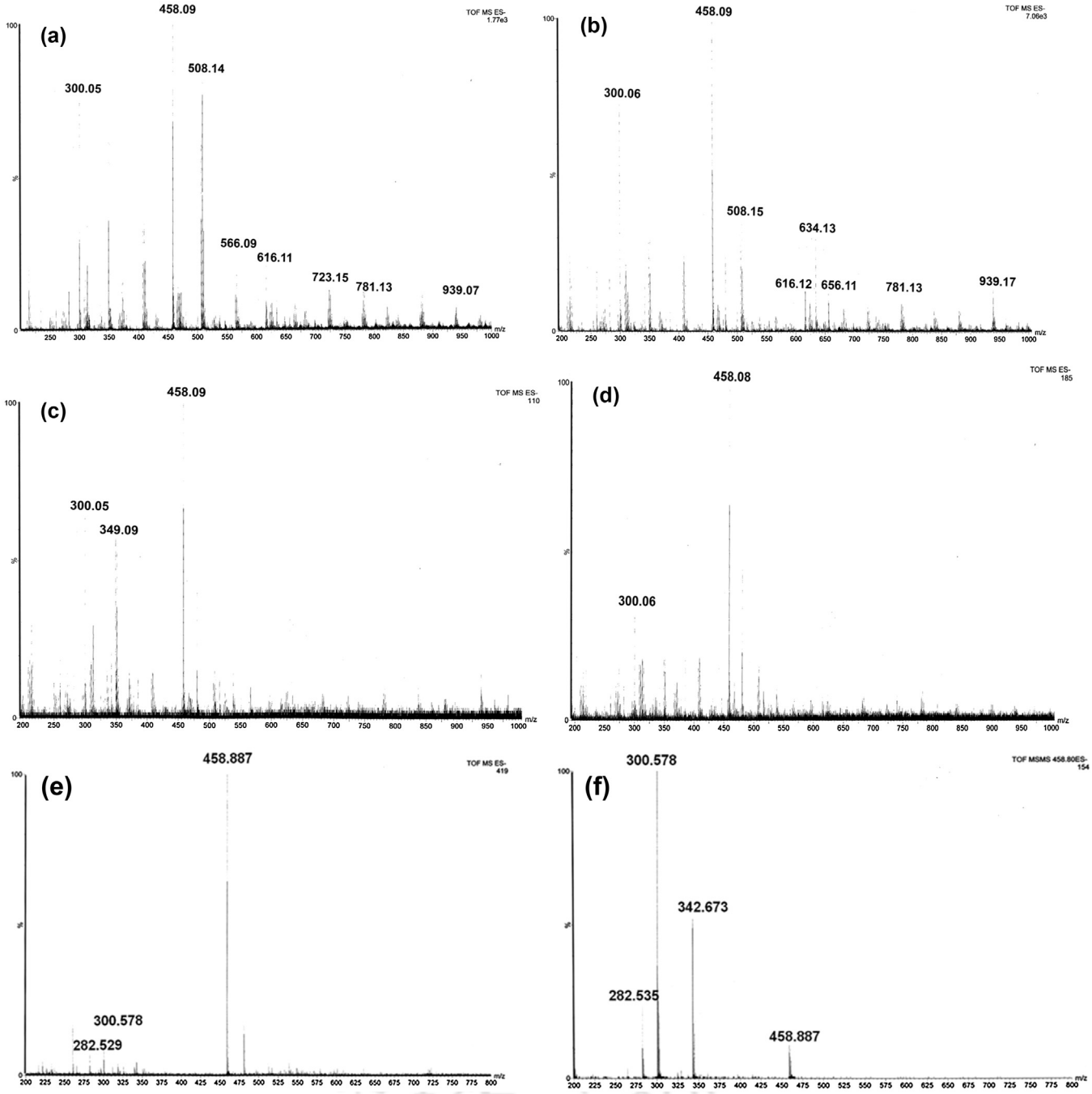

Fig. 4. ESI-Mass spectrometric analysis of *Ps*PL8A degraded product of C4S. (a) MS analysis of 2 min sample (b) MS analysis of 30 min sample (c) MS analysis of 1 h sample, (d) MS analysis of 2 h sample, (e) MS analysis of 24 h sample showing ΔC4S disaccharide (ΔUA-GalNAc4S) having single peak at *m*/*z* 458, (f) MS/MS analysis of ΔC4S disaccharide (ΔUA-GalNAc4S) showing a peak at *m*/*z* 300.

The ESI–MS analysis further supported the contention elucidated from the TLC data of concomitant occurrence of endo- and exo-lytic mode of *Ps*PL8A catalysis. In 30 min sample, the percent intensities of the hexa-saccharide and octa-saccharide peaks were lower as compared with that of 2 min sample, inferring the degradation of the same with time (Fig. 4b). The 1 h, 2 h and 24 h samples displayed the peak of only mono-sulphated unsaturated disaccharide with *m*/*z* 458, suggesting the complete degradation of the higher oligosaccharides by *Ps*PL8A (Fig. 4c–e).

Tandem MS mode can be used to differentiate the isomeric species. In order to determine the type of sulphated unsaturated disaccharide MS/MS was performed on the mono-sulphated unsaturated disaccharide with *m*/*z* 458. MS/MS of mono-sulphated unsaturated disaccharide (*m*/*z* 458) in 24 h sample showed a distinct peaks of *m*/*z* 300 which uniquely identify the ΔC4S disaccharide (ΔUA-GalNAc4S) (Fig. 4f). The results of *Ps*PL8A degraded products from C4S was in accordance with the results reported earlier, where a detail ESI–MS analysis and MS/MS analysis of chondroitin disaccharides have been performed [40,41].

3.8. ^{1}H- and ^{13}C- NMR spectroscopic analysis of disaccharide from Ps*PL8A degraded C4S*

The ^{1}H NMR and ^{13}C- spectra of chondroitin 4-sulphate disaccharide product (Fig. 5a) released after 24 h of C4S degradation by *Ps*PL8A is shown in Fig. 5b & c, respectively. The

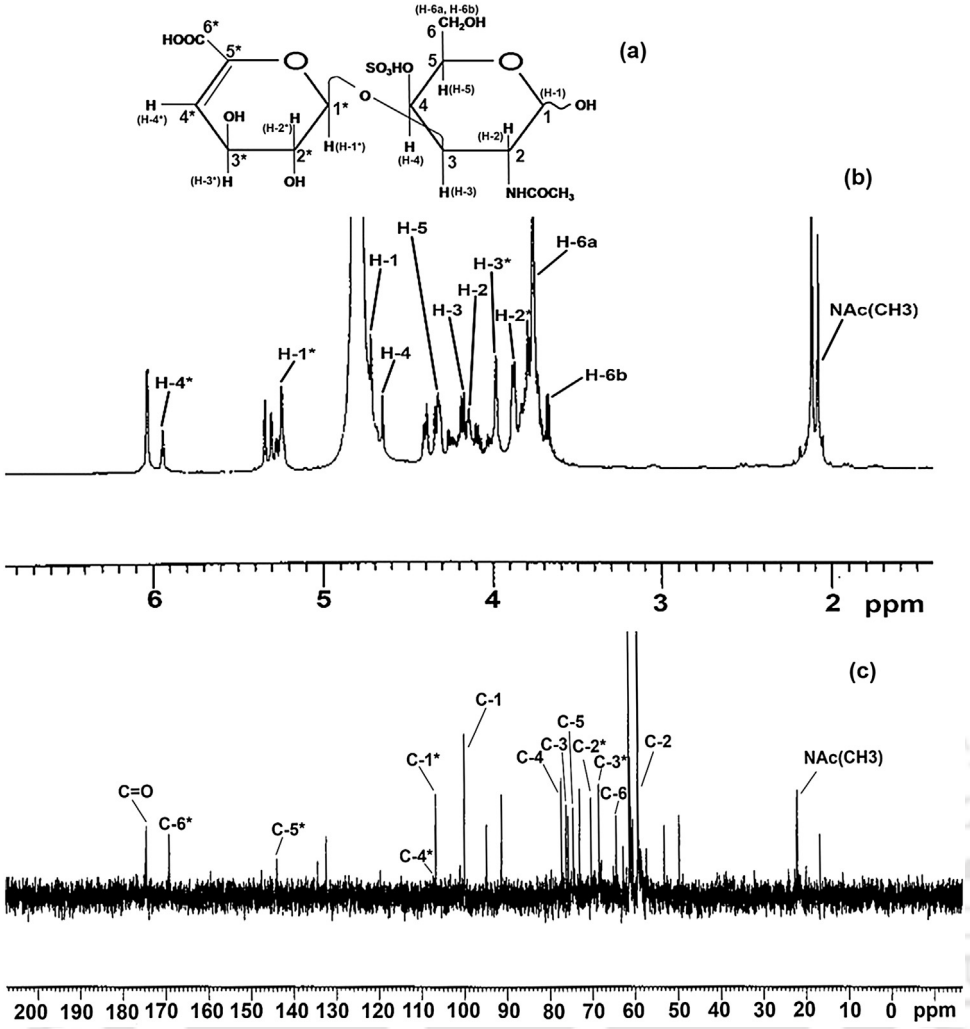

Fig. 5. (a) The chemical structure of ΔC4S (ΔUA-GalNAc4S) disaccharide (b) 1D ^{1}H NMR spectrum (600 MHz) (c) and ^{13}C NMR spectrum of degraded product ΔC4S (ΔUA-GalNAc4S) disaccharide obtained after 24 h reaction of 1 mg/ml C4S with *Ps*PL8A (as described in Methods).

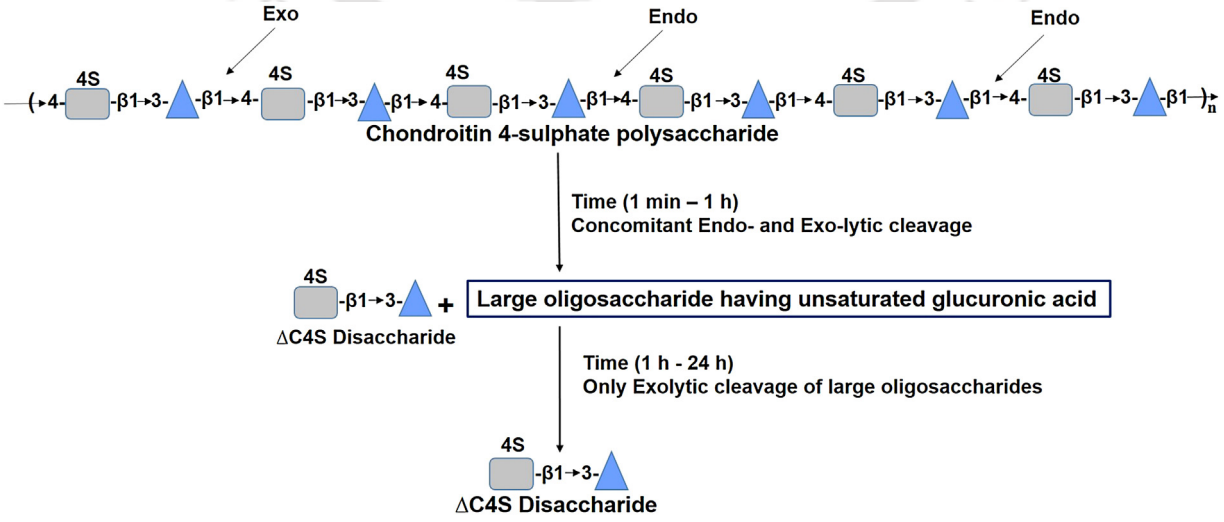

Fig. 6. Endo- and exo-lytic cleavage pattern of chondroitin 4-sulphate degradation by *Ps*PL8A. ▲ represents the glucuronic acid residue (GlcA) and ▭ represents GalNAc residue having sulphation at 4C- position.

Table 2
^{1}H— NMR and ^{13}C— NMR chemical shifts of ΔGlcA-GalNAc4S.

Residue	Proton	^{1}H Chemical Shift (ppm)	Carbon	^{13}C Chemical Shift (ppm)
GlcA	H-1*	5.24	C-1*	106.6
	H-2*	3.83	C-2*	70.32
	H-3*	3.98	C-3*	68.47
	H-4*	5.94	C-4*	106.8
			C-5*	145.4
			C-6*	169.15
GalNAc	H-1	4.77	C-1	99.91
	H-2	4.14	C-2	58.55
	H-3	4.17	C-3	76.15
	H-4	4.65	C-4	77.20
	H-5	4.28	C-5	75.67
	H-6a	3.77	C-6	64.4
	H-6b	3.70	(-NAcCH_3)	22.19
	(CH_3)	2.08	C=O	174.69

"*" mark signifies the proton and carbon atoms belonging to the GlcA residue.

characteristic signals of the protons and ^{13}**C-** chemical shifts were assigned according to the previous studies done by Yamada et al., 1992; Huckerby et al., 2001 and Lauder et al., 2011 [42–44]. The ^{1}H NMR spectra for ΔC4S disaccharide was recorded at 25 °C, which showed the prominent signal at 5.94 ppm for anomeric proton resonance of H-4* for GlcA ring (Fig. 6b). In the GlcA ring, the H-1* proton shows response at 5.24 ppm, while the H-2* and H-3* gave the proton responses at 3.83 ppm and 3.98 ppm, respectively. Similarly, for the GalNAc ring in the ΔC4S disaccharide (Fig. 5a) the ^{1}H NMR chemical shift of H-4, indicates the sulphation with a resonance at 4.65 ppm. The GalNAc ring has the acetylation –NAc(CH_3) which shows proton resonance at 2.08 ppm, this value corroborates well with the previous reports [42–44]. The correlation for rest of the protons of GalNAc ring were also made, the H-1, H-2, H-3, H-5, H-6a and H-6b show the proton resonances at 4.77 ppm, 4.14 ppm, 4.17 ppm, 4.28, 3.77 ppm and 3.70 ppm, respectively, which also showed similarity with previous reports [42–44]. The bulk of proton resonance of ΔC4S disaccharide lies in the range of 3.7–4.8 ppm (Fig. 5b). The results for the ^{1}H- NMR chemical shifts of ΔC4S disaccharide (ΔGlcA-GalNAc4S) are summarised in Table 2. The 1D 600 MHz ^{13}C spectrum was acquired for ΔC4S disaccharide and the peaks were assigned for carbon atoms (Fig. 5c). The chemical shifts of C-1*, C-2*, C-3*, C-4*, C-5* and C-6* carbon atoms of GlcA residue were detected at 106.6 ppm, 70.32 ppm, 68.47 ppm, 106.8 ppm, 145.4 ppm and 169.15 ppm, respectively. The chemical shift of another residue GalNAc of ΔC4S disaccharide was also assigned. The acetyl (-$COCH_3$) group present in GalNAc gave the chemical shift at 22.19 ppm, while the sulphation present at C-4 gave the shift at 77.2 ppm. The chemical shift for C-1, C-2, C-3, C-5 and C-6 for GalNAc were 99.91 ppm, 58.55 ppm, 76.15 ppm, 75.67 ppm and 64.4 ppm, respectively. The carbonyl (—C=O) group present in GalNAc gave the shift at 174.69 ppm (Fig. 5c). The chemical shifts assigned to both the residues GlcA and GalNAc of ΔC4S disaccharide were in agreement with the previous reports [42–44]. ^{13}C- NMR chemical shifts of ΔC4S disaccharide (ΔGlcA-GalNAc4S) are summarised in Table 2.

The TLC and ESI–MS and MS/MS results conclusively demonstrated that *Ps*PL8A initially degrades the C4S substrate by a concomitant endo- and exo-lytic mode and produces higher oligosaccharides such as hexasaccharide, octasaccharide and dodecasacchride along with ΔC4S disaccharide. After ~1 h of reaction the enzyme starts utilizing the higher oligosaccharides and further fragmenting them into the lowest possible oligosaccharide i.e. ΔC4S disaccharide displaying its prominent exolytic mode of catalysis in the later stage as depicted in Fig. 6. The molecular mass and the structure of ΔC4S disaccharide was confirmed by ESI–MS/MS and NMR spectroscopic analysis, respectively. These unsaturated chondroitin sulphate oligosaccharides have promising role as anti-inflammatory agent in therapeutic and clinical fields, however the functions of oligosaccharide in relation to their structures have not yet been fully known [45–47]. The effects of C4S and C6S oligosaccharides and disaccharides on toll-like receptor (TLR) – mediated secretion of interleukin (IL)-6 were compared using macrophage-like cell line J774.1 [46]. Suppression of IL-6 secretion was stronger by smaller sized C4S than that by C4S polysaccharide, particularly C4S disaccharide were effective suppressing agents against TLR-mediated inflammation of macrophages. These immune-modulating effects of C4S disaccharides are helpful in understanding their anti-inflammatory responses. These observations have prompted the researchers to explore the effects of C4S disaccharides and oligosaccharides for the treatment of atherosclerosis, osteoarthritis and degenerative diseases of the central nervous system [48]. Chondroitin AC lyase (*Ps*PL8A) chiefly produced chondroitin disaccharides as the degraded products which can be applied for treatment of allergic reactions and autoimmune diseases.

4. Conclusion

The new recombinant chondroitin AC lyase, *Ps*PL8A from *Pedobactor saltans* being relatively more stable at physiological temperature and pH, than those earlier reported and possessing multi-substrate specificity makes it a promising candidate for therapeutic applications. *Ps*PL8A resulted in formation of chondroitin 4-sulphate disaccharide after completion of the reaction with C4S. The TLC, ESI–MS, tandem MS confirmed the simultaneous exo- and endo-lytic mode of catalysis of *Ps*PL8A. ESI–MS, MS/MS and NMR spectroscopy helps in the structural elucidation of chondroitin 4-sulphate disaccharide. *Ps*PL8A can be used for production of chondroitin oligosaccharide. *Ps*PL8A can also be further used for structure determination of complex GAG polysaccharides. The *Ps*PL8A enzyme and its degradation products in the present study unfolds the avenue for its potential applications in spinal cord nerve injury system and as antitumor, antiangiogenic, anti-metastatic agent and for immune-modulating and anti-inflammatory effects.

Conflict of interest

The authors declare no conflict of interest.

Acknowledgements

The research work was supported by Council of Scientific and Industrial Research (CSIR) project no. 37(1672)/16/EMR-II to AG.

Fellowship provided by Ministry of Human Resource Development, Govt. of India to AR is gratefully acknowledged. The authors thank Central Instrumentation Facility, IIT Guwahati for providing facility for ESI–MS and NMR Spectroscopic analysis.

References

[1] S. Yamada, K. Sugahara, Potential therapeutic application of chondroitin sulfate/dermatan sulphate, Curr. Drug. Discovery Technol. 5 (2008) 289–301.
[2] D. Shaya, B.S. Hahn, N.Y. Park, J.S. Sim, Y.S. Kim, M. Cygler, Characterization of chondroitin sulfate lyase ABC from *Bacteroides thetaiotaomicron* WAL2926, Biochemistry 47 (2008) 6650–6661.
[3] S. Ernst, R. Langer, C.L. Cooney, R. Sasisekharan, Enzymatic degradation of glycosaminoglycans, Crit. Rev. Biochem. Mol. Biol. 30 (1995) 387–444.
[4] H.E. Bulow, O. Hobert, The molecular diversity of glycosaminoglycans shapes animal development, Annu. Rev. Cell Dev. Biol. 22 (2006) 375–407.
[5] N. Afratis, C. Gialeli, D. Nikitovic, T. Tsegenidis, E. Karousou, A.D. Theocharis, N.K. Karamanos, Glycosaminoglycans: key players in cancer cell biology and treatment, FEBS J. 279 (2012) 1177–1197.
[6] C.M. Galtrey, J.W. Fawcett, The role of chondroitin sulfate proteoglycans in regeneration and plasticity in the central nervous system, Brain Res. Rev. 54 (2007) 1–18.
[7] O. Habuchi, Diversity and functions of glycosaminoglycan sulfotransferases, Biochim. Biophys. Acta 1474 (2000) 115–127.
[8] R.V. Iozzo, Matrix proteoglycans: from molecular design to cellular function, Annu. Rev. Biochem. 67 (1998) 609–652.
[9] E.M. Denholm, Y.Q. Lin, P.J. Silver, Anti-tumor activities of chondroitinase AC and chondroitinase B: inhibition of angiogenesis, proliferation and invasion, Eur. J. Pharmacol. 416 (2001) 213–221.
[10] R.V. Iozzo, L. Schaefer, Proteoglycans in health and disease: novel regulatory signaling mechanisms evoked by the small leucine-rich proteoglycans, FEBS J. 277 (2010) 3864–3875.
[11] R.J. Linhardt, F.Y. Avci, T. Toida, Y.S. Kim, M. Cygler, CS lyases: structure, activity, and applications in analysis and the treatment of diseases, Adv. Pharmacol. 53 (2006) 187–215.
[12] J.C.F. Kwok, P. Warren, J.W. Fawcett, Chondroitin sulfate: a key molecule in the brain matrix, Int. J. Biochem. Cell Biol. 44 (2012) 582–586.
[13] S.W. Hong, B.T. Kim, H.Y. Shin, W.S. Kim, K.S. Lee, Y.S. Kim, D.H. Kim, Purification and characterization of novel chondroitin ABC and AC lyases from Bacteroides stercoris HJ-15 a human intestinal anaerobic bacterium, Eur J. Biol. Chem. 269 (2002) 2934–2940.
[14] V.V. Lunin, Y. Li, R.J. Linhardt, H. Miyazono, M. Kyogashima, T. Kaneko, A.W. Bell, M. Cygler, High resolution crystal structure of *Arthrobacter aurescens* chondroitin AC lyase: enzyme-substrate complex defines the catalytic mechanism, J. Mol. Biol. 337 (2004) 367–386.
[15] B.L. Cantarel, P.M. Coutinho, C. Rancurel, T. Bernard, V. Lombard, The carbohydrate-active EnZymes database (CAZy): an expert resource for glycogenomics, Nucleic Acids Res. 37 (1999) D233–238.
[16] I.W. Sutherland, Polysaccharide lyases, FEMS Microbiol. Rev. 16 (1995) 323–347.
[17] J. Fethiere, B. Eggimann, M. Cygler, Crystal structure of chondroitin AC lyase, a representative of a family of glycosaminoglycan degrading enzymes, J. Mol. Biol. 288 (1999) 635–647.
[18] K. Pojasek, Z. Shriver, P. Kiley, G. Venkataraman, R. Sasisekharan, Recombinant expression purification, and kinetic characterization of chondroitinase AC and chondroitinase B from *Flavobacterium heparinum*, Biochem. Biophys. Res. Commun. 286 (2001) 343–351.
[19] K.W. Shim, D.H. Kim, Cloning and expression of chondroitinase AC from *Bacteroides stercoris* HJ-15, Protein Expr. Purif. 58 (2008) 222–228.
[20] M.A. Price, L.E. Colvin Wanshura, J. Yang, J. Carlson, B. Xiang, G. Li, J.B. McCarthy, CSPG4 a potential therapeutic target, facilitates malignant progression of melanoma, Pigment Cell Melanoma Res. 24 (2011) 1148–1157.
[21] Y. Kim, H.G. Lee, N. Dmitrieva, J. Kim, B. Kaur, A. Friedman, Choindroitinase ABC I-mediated enhancement of oncolytic virus spread and anti tumor efficacy: a mathematical model, PLoS One (2014) e102499.
[22] E.J. Bradbury, L.D. Moon, R.J. Popat, V.R. King, G.S. Bennet, P.N. Patel, J.W. Fawcett, S.B. McMahon, Chondroitinase ABC promotes functional recovery after spinal cord injury, Nature 416 (2002) 636–640.
[23] A.W. Barritt, M. Davies, F. Marchand, R. Hartley, J. Grist, P. Yip, S.B. McMahon, E.J. Bradbury, Chondroitinase ABC promotes sprouting of intact and injured spinal systems after spinal cord injury, J. Neurosci. 26 (2006) 10856–10867.
[24] J.M. Massey, C.H. Hubscher, M.R. Wagoner, J.A. Decker, J. Amps, J. Silver, S.M. Onifer, Chondroitinase ABC digestion of the perineuronal net promotes functional collateral sprouting in the cuneate nucleus after cervical spinal cord injury, J. Neurosci. 26 (2006) 4406–44014.
[25] X.R. Chen, S.J. Liao, L.X. Ye, Q. Gong, Q. Ding, J.S. Zeng, J. Yu, Neuroprotective effect of chondroitinase ABC on primary and secondary brain injury after stroke in hypertensive rats, Brain Res. 1543 (2014) 324–333.
[26] A. Didangelos, M. Iberl, E. Vinsland, K. Bartus, E.J. Bradbury, Regulation of IL-10 by chondroitinase ABC promotes a distinct immune response following spinal cord injury, J. Neurosci. 34 (2014) 16424–16432.
[27] P.L. Steyn, P. Segers, M. Vancanneyt, P. Sandra, K. Kersters, J.J. Joubert, Classification of heparinolytic bacteria into a new genus, *Pedobacter*, comprising four species: *Pedobacter heparinus* comb. nov. *Pedobacter piscium* comb. nov., *Pedobacter africanus* sp. nov. and *Pedobacter saltans* sp. nov. Proposal of the family Sphingobacteriaceae fam. nov, Int. J. Syst. Bacteriol. 48 (1998) 165–177.
[28] K. Liolios, J. Sikorski, M. Lu, M. Nolan, A. Lapidus, S. Lucas, N.C. Kyrpides, Complete genome sequence of the gliding, heparinolytic *Pedobacter saltans* type strain (113T), Stand. Genomic. Sci. 5 (2011) 30–40.
[29] E. Lojkwoska, C. Masclaux, M. Boccara, J. Robert-Baudouy, N. Hugouvieux-Cotte-Pattat, Characterization of pelL gene encoding a novel pectate lyase of *Erwinia chrysanthemi* 3937, Mol. Microbiol. 16 (1995) 1183–1195.
[30] Z. Zhang, Z. Xiao, R.J. Linhardt, Thin layer chromatography for the separation and analysis of acidic carbohydrates, J. Liq. Chromatogr. Relat. Technol. 32 (2009) 1711–1732.
[31] N. Sugiura, Y. Setoyama, M. Chiba, K. Kimata, H. Watanabe, Baculovirus envelope protein ODV-E66 is a novel chondroitinase with distinct substrate specificity, J. Biol. Chem. 286 (2011) 29026–29034.
[32] T. Ke, L. Zhangfu, G. Qing, T. Yong, J. Hong, R. Hongyan, L. Shigui, Isolation of *Serratia marcescens* as a chondroitinase-producing bacterium and purification of a novel chondroitinase AC, Biotechnol. Lett. 27 (2005) 489–493.
[33] V. Kale, Ó. FriÐjónsson, J.Ó. Jónsson, H.G. Kristinsson, S. Ómarsdóttir, G.Ó. HreggviÐsson, Chondroitin lyase from a marine arthrobacter sp. MAT3885 for the production of chondroitin sulfate disaccharides, Mar. Biotechnol. 17 (2015) 479–492.
[34] W. Han, W. Wang, M. Zhao, K. Sugahara, F. Li, A novel eliminase from a marine bacterium that degrades hyaluronan and chondroitin sulfate, J. Biol. Chem. 289 (2014) 27886–27898.
[35] K. Hiyama, S. Okada, The mode of action of two chondroitinase-AC preparations of different origin, J. Biochem. 80 (1976) 1201–1207.
[36] R.J. Linhardt, Analysis of glycosaminoglycans with polysaccharide lyases, Curr. Protoc. Mol. Biol. 48 (2001), III:17.13B:17.13B. 1–17.13B.16.
[37] K.A. Jandik, K. Gu, R.J. Linhardt, Action pattern of polysaccharide lyases on glycosaminoglycans, Glycobiology 4 (1994) 289–296.
[38] J. Zaia, C.E. Costello, Compositional analysis of glycosaminoglycans by electrospray mass spectrometry, Anal. Chem. 73 (2001) 233–239.
[39] A. Zamfir, D.G. Seidler, H. Kresse, J. Peter-Katalinić, Structural investigation of chondroitin/dermatan sulfate oligosaccharides from human skin fibroblast decorin, Glycobiology 13 (2003) 733–742.
[40] H. Desaire, J.A. Leary, Detection and quantification of the sulfated disaccharides in chondroitin sulfate by electrospray tandem mass spectrometry, J. Am. Soc. Mass Spectrom. 11 (2000) 916–920.
[41] C. Flangea, A.F. Serb, C. Schiopu, S. Tudor, E. Sisu, D.G. Seidler, A.D. Zamfir, Discrimination of GalNAc (4S/6S) sulfation sites in chondroitin sulfate disaccharides by chip-based nanoelectrospray multistage mass spectrometry, Cent. Eur. J. Chem. 7 (2009) 752–759.
[42] S. Yamada, K. Yoshida, M. Sugiura, K. Sugahara, One-and two-dimensional 1H-NMR characterization of two series of sulfated disaccharides prepared from chondroitin sulfate and heparan sulfate/heparin by bacterial eliminase digestion, J. Biochem. 112 (1992) 440–447.
[43] T.N. Huckerby, R.M. Lauder, G.M. Brown, I.A. Nieduszynski, K. Anderson, J. Boocock, P.L. Sandall, S.D. Weeks, Characterization of oligosaccharides from the chondroitin sulfates, Eur. J. Biochem. 268 (2001) 1181–1189.
[44] R.M. Lauder, T.N. Huckerby, I.A. Nieduszynski, I.H. Sadler, Characterisation of oligosaccharides from the chondroitin/dermatan sulphates: 1 H and 13C NMR studies of oligosaccharides generated by nitrous acid depolymerisation, Carbohydr. Res. 346 (2011) 2222–2227.
[45] J. Egea, A.G. García, J. Verges, E. Montell, M.G. López, Antioxidant: anti-inflammatory and neuroprotective actions of chondroitin sulfate and proteoglycans, Osteoarthr. Cartilage 18 (2010) S24–S27.
[46] M. Jin, T. Iwamoto, K. Yamada, H. Satsu, M. Totsuka, M. Shimizu, Effects of chondroitin sulfate and its oligosaccharides on toll-like receptor-mediated IL-6 secretion by macrophage-like J774. 1 cells, Biosci. Biotechnol. Biochem. 75 (2011) 1283–1289.
[47] N. Igarashi, A. Takeguchi, S. Sakai, H. Akiyama, K. Higashi, T. Toida, Effect of molecular sizes of chondroitin sulfate on interaction with L-selectin, Int J. Carbohydr. Chem. (2013) 9, Article ID 856142.
[48] P. Du Souich, A.G. García, J. Vergés, E. Montell, Immuno-modulatory and anti-inflammatory effects of chondroitin sulphate, J. Cell Mol. Med. 13 (8a) (2009) 1451–1463.

Carbohydrate Polymers 159 (2017) 11–19

Contents lists available at ScienceDirect

Carbohydrate Polymers

journal homepage: www.elsevier.com/locate/carbpol

Research Paper

Physicochemical, antioxidant and biocompatible properties of chondroitin sulphate isolated from chicken keel bone for potential biomedical applications

Aruna Rani, Rwivoo Baruah, Arun Goyal*

Department of Biosciences and Bioengineering, Indian Institute of Technology Guwahati, Guwahati 781039, Assam, India

ARTICLE INFO

Article history:
Received 20 September 2016
Received in revised form
30 November 2016
Accepted 5 December 2016
Available online 6 December 2016

Keywords:
Chicken keel bone cartilage
Chondroitin sulphate
TGA
DSC
MTT assay
Antioxidant activity

ABSTRACT

Chicken keel bone cartilage was explored for cheaper and sustainable source for isolation of chondroitin sulphate (CS) for its future use in tissue engineering and pharmaceutical industry. HPSEC analysis displayed two peaks of 100 kDa for CS-keel polysaccharide and 1 kDa for protein. DLS analysis of CS-keel displayed polydispersity. CS-keel yield was 15% and 53 ± 5% uronic acid content. The quantified percentages of UA-GalNAc4S and UA-GalNAc6S disaccharide in CS-keel were 58% and 42%, respectively. FT-IR identified CS-keel to be chondroitin 4-sulphate. ^{1}H NMR of CS-keel confirmed the presence of N-acetylgalactosamine and Glucuronic acid. FESEM demonstrated layer structure and AFM displayed the size of CS-keel fibres. DSC, TGA and DTG studies of CS-keel showed T_d at 243 °C. *In vitro* cell proliferation assay and morphological analysis of mouse fibroblast L929 cell lines confirmed the biocompatibility of CS-keel. CS-keel (5 mg/ml) exhibited ~49% antioxidant activity against DPPH and 22% against superoxide radical protecting from oxidative damage. CS-keel demonstrated better (70.3%) emulsifying activity than commercial sodium alginate (60.2%).

1. Introduction

The waste by products from slaughter house and poultry industries can serve as the major sources of cartilage. Cartilage mainly constitutes glycosaminoglycans (GAGs) and collagens (Garnjanagoonchorn, Wongekalak, & Engkagul, 2007; Vázquez et al., 2013). GAGs are heteropolysacchrides made up of disaccharide repeats of D-galactosamine/D-glucosamine and D-glucuronic acid/L-Iduronic acid. GAGs are abundant in the cartilages (Iozzo, 1998). The cartilage matrix is composed of fine mesh of collagen embedded with hyaluronic acid (HA), chondroitin sulphate (CS), various glycoproteins and proteoglycans (PGs). CS is composed of N-acetyl galactosamine (GalNAc) and glucuronic acid (GlcA), linked by β-(1 → 3)-glycosidic bond, while the two disaccharides are linked by β-(1 → 4) linkage. CS has been classified as chondroitin 4-sulphate (CS-A), chondroitin 6-sulphate (CS-C) and dermatan sulphate (DS/CS-B) with sulfation at C4 and C6 positions of GalNAc residue, respectively and C4 of GalNAc/C2 of GlcA for DS (Schiller & Huster, 2012).

CS is a part of connective tissues and involved in major biological processes such as resiliency, structural integrity of cartilage and maintenance of synovial fluid in the bone joints owing to its polyanionic structure (Henrotin, Mathy, Sanchez, & Lambert, 2010; Luo, Fosmire, & Leach, 2002). Low molecular weight CS is used as oral nutraceutical supplement for joint disorder treatment (Raynauld, Pelletier, Abram, Delorme, & Martel-Pelletier, 2016). The beneficial effects of CS have been reported for joint pains, stiffness and swelling in osteoarthritis patents (Hochberg et al., 2015; Raynauld et al., 2016). CS alone or in combination with HA or chitosan were used to formulate scaffolds that mediate and accelerate the regeneration of damaged tissues, bone repair, cartilage and cutaneous wounds (Bianchera et al., 2014). CS-hydrogels are appealing materials for biomedical application as they enhance wound healing by reepithelialization and neovascularization (Bianchera et al., 2014). CS also acts as free radical scavenger and decreases DNA fragmentation, protein degradation and cell death rate (Campo, Avenoso, Campo, Ferlazzo, & Calatroni, 2006; Henrotin et al., 2010). The partially purified CS was also used as food preservative and emulsifying agent (Hamano et al., 1989; Vázquez et al., 2013).

Abbreviations: GAG, glycosaminoglycan; GalNAc, N-acetyl galactosamine; GlcA, D-glucuronic acid; CS, chondroitin sulphate; DS, dermatan sulphate; C4S, chondroitin 4-sulphate; C6S, chondroitin 6-sulphate; DPPH, 1-diphenyl-2-picrylhydrazyl; MTT, [3-(4,5-dimethylthiazol-2-yl)-2,5-diphenyltetrazolium bromide; NMR, nuclear magnetic resonance; DLS, dynamic light scattering; DSC, differential scanning calorimetery; TGA, thermogravimetric analysis.

* Corresponding author.
E-mail address: arungoyl@iitg.ernet.in (A. Goyal).

http://dx.doi.org/10.1016/j.carbpol.2016.12.015
0144-8617/

CS is commercially available from various sources such as, bovine cartilage, bovine trachea and shark fin. The increasing demand and the high cost of CS has led to the exploitation of shark and bovine which impart a strong impact on the ecological balance (Field, Meekan, Buckworth, & Bradshaw, 2009; Vázquez et al., 2013). CS has been isolated from other sources *viz.* ray fish and crocodile cartilages (Garnjanagoonchorn et al., 2007), broiler chicken carcasses (Nakano, Pietrasik, Ozimek, & Betti, 2012; Srichamroen, Nakano, Pietrasik, Ozimek, & Betti, 2013), duck trachea (Vittayanont & Jaroenviriyapap, 2013), chicken keel cartilage (Luo et al., 2002; Khan, Ashraf, Hashmi, Ahmad, & Anjum, 2013), Bony fishes (Maccari, Galeotti, & Volpi, 2015) and sea cucumber (Zou, Pan, Dong, He, & Wang, 2016). Production of bioengineered chondroitin using a non-pathogenic *E. coli* strain by metabolic engineering approach has been reported (He et al., 2015). However, the bioengineering approach has the disadvantages of relatively high cost and the lack of commercializable sulfation method for CS production. All these reasons make it essential for researchers to seek for more different animal sources of CS isolation. CS is also in high demand for its applications in tissue engineering, pharmaceutical, cosmetic and food industries. This makes it essential to rigorously characterize the physicochemical, biocompatible and antioxidant properties of CS. Most of the reports however, have focused on isolation and partial characterization of CS. This is the first study on the isolation, complete physicochemical and structural characterization of a CS from chicken keel bone cartilage that displayed biocompatible, antioxidant and emulsifying potentials. These preliminary results will facilitate further exploration of CS-keel for emulsifying and antioxidant activities under *in vivo* studies.

2. Materials and methods

Keel bone cartilage of chicken was collected from the waste of a local slaughter house, Guwahati, Assam, India. Papain from *Carica papaya* was purchased from Himedia Pvt. Ltd., India. Chondroitin 4-sulphate sodium salt (C4S) from bovine trachea, Chondroitin 6-sulphate sodium salt (C6S), D-Glucuronic acid (GlcA), Potassium bromide (KBr), 1-diphenyl-2-picrylhydrazyl (DPPH), MTT [3-(4,5-dimethylthiazol-2-yl)-2,5-diphenyltetrazolium bromide, Chondroitin 4-sulphate disaccharide (UA-GalNAc4S) and UA2S-GalNAc were purchased from Sigma-Aldrich, USA. Chondroitin 6-sulphate disaccharide (UA-GalNAc6S) was purchased from Dextra Laboratories Ltd., U.K.

2.1. Isolation of CS from the keel bone cartilage

CS was isolated from keel cartilage using the method of Lauder, Huckerby, & Nieduszynski (2000). One hundred gram of cartilage was diced and boiled for 15 min to remove the meat and connective tissues. The remaining cartilage was washed with Milli-Q water and wet weight was taken. This was digested with papain (1U/100 mg tissue) in 100 ml of 0.1 M sodium acetate buffer, pH 6.8 containing 2.4 mM EDTA and 10 mM cysteine HCl and incubated at 65 °C for 24 h. GAG containing CS was precipitated from soluble fraction by adding 4 vols of ethanol and the solution was cooled to 4 °C and allowed to stand overnight. It was centrifuged at 13,000 ***g*** and 4 °C for 30 min and the pellet was resuspended in minimum volume of 50 mM sodium acetate buffer (pH 6.8). The CS-keel was precipitated by dropwise addition of 2 vols of ethanol with constant stirring at 25 °C. The solution was cooled to 4 °C and allowed to stand overnight for recovery of CS-rich precipitate which was resuspended in 5 ml of 50 mM sodium acetate buffer (pH 6.8) and dialyzed overnight against distilled water. The dialysed CS was lyophilized. The residual amino acids were removed by treating 18 g of lyophilized CS-keel resuspended in 5 ml Milli-Q water with 0.05 M NaOH and 1 M sodium borohydride at 45 °C for 12 h. CS-keel was precipitated by neutralizing with 5 ml, 1 M sodium acetate. The CS-keel precipitate was resuspended and dialysed against Milli-Q water to remove the excess salts and finally lyophilized for further use.

2.2. Determination of molecular weight of CS-keel by HPSEC and particle size by DLS

The molecular mass of CS-keel (1 mg/ml) was determined using high performance size exclusion chromatography (HPSEC) system consisting of Phenomenex Polysep-GFC-P6000 column connected with a guard column Phenomenex Polysep-GFC-P and Prominence, UFLC (Shimadzu, Japan) equipped with RI detector. 10 μl samples each of CS-keel, standards and reference (1 mg/ml) were loaded and eluted using 0.1 M $NaNO_3$ with a flow rate of 0.5 ml/min. C4S and C6S (Sigma Aldrich, USA.) each at 1 mg/ml were used as reference. The standard dextran T20, T40, T70, T100, T200 and T500 (1 mg/ml) were used as standards to calculate the molecular weight of CS-keel. The particle size of CS-keel (1 mg/ml in 0.1 M $NaNO_3$) was determined by Dynamic Light Scattering (DLS) (Zetasizer nano, Malvern, UK).

2.3. Composition analysis of CS-keel

The CS-keel polysaccharide was purified by HPSEC. A stock solution (10 mg/ml) of isolated crude CS-keel was prepared. 50 μl of CS-keel solution was applied to Phenomenex Polysep-GFC-P6000 column connected with a guard column Phenomenex Polysep-GFC-P and Prominence, UFLC (Shimadzu, Japan) equipped with RI and UV detector. The UV detector was set at 280 nm to identify the peak specifically for the protein. The peak corresponding to CS-keel (100 kDa) was eluted and collected. This process was repeated 10 times for collection of enough CS keel for Carbazole assay. The eluted purified CS-keel fractions were mixed and lyophilised. The protein content of the purified and lyophilised CS-keel was estimated by method of Lowry, Rosebrough, Farr, & Randall (1951) using bovine serum albumin (BSA) as standard in the concentration range, 25–500 μg/ml. The carbazole assay is used for quantification of uronic acid present in GAG and is based on the quantitative concentration-dependent colour reaction between carbazole and the uronic acid. The uronic acid content of purified lyophilised CS-keel was estimated by carbazole method (Frazier, Roodhouse, Hourcade, & Zhang, 2008). C4S and GlcA were used as standards at a concentration range, 4 – 40 μg/ml

2.4. Quantification of CS disaccharides in CS-keel by enzymatic digestion

The enzymatic depolymerisation of CS-keel was achieved by using chondroitin AC lyase (*Ps*PL8A) from *Pedobacter saltans* (Rani and Goyal, 2016). The digestion of CS-keel with 5 μg/ml of *Ps*PL8A was carried out in a 1 ml reaction mixture containing, 5.0 mg/ml CS-keel in 50 mM Tris-HCl buffer, pH 7.2 and incubating the reaction at 39 °C for 24 h (Rani and Goyal, 2016). 1 ml reaction mixture was then treated with 1 ml absolute ethanol and centrifuged at 13000*g* at 25 °C for 10 min to precipitate the undigested CS-keel (Rani and Goyal 2016). The glucuronic acid content in the un-digested and the digested sample in the supernatant was quantified by carbazole assay (Frazier et al., 2008). The sample was analysed by Electron Spray Ionization (ESI) mass spectrometer (Waters, Q-TOF Premier) in both MS and tandem MS (MS/MS) mode. ESI–MS and tandem MS analyses were carried out in negative ion mode, where the parameters for ESI–MS analysis were; capillary voltage 3 eV, collision energy 5 eV, ionization energy 1 eV, desolvation temperature 250 °C and the source temperature of 80 °C. The tandem MS analysis was

carried out by nanospray ionization using the voltage 3 eV, collision energy 20 eV and collision-induced dissociation was performed on ion of interest using the argon gas. The detection and quantification of disaccharide composition was analysed by electronspray tandem mass spectrometery (Desaire & Leary, 2000a). The relative abundance of product ions for pure isomeric standards (UA-GalNAc4S and UA-GalNAc6S) were used in a binary system. The disaccharide composition of digested CS-keel was quantified based on the MS/MS spectra of all standards (Desaire & Leary, 2000a).

2.5. Fourier transform infrared (FT-IR) spectroscopic analysis of CS-keel

FT-IR spectroscopy was used for determining the functional groups present in CS-keel. CS-keel was pressed into KBr pellet (sample: KBr, 1:100) using 15 Ton Hydraulic Press. FTIR spectrophotometer (Perkin Elmer, Spectrum Two, USA) was used to obtain the spectrum in 4000–500 cm^{-1} region in the transmission mode with 32 scans per min. The spectral resolution was 4 cm^{-1}.

2.6. ^1H NMR spectroscopic analysis of CS-keel

CS-keel (5 mg/ml) was dissolved in D_2O (99.96%) (Merck, Germany) and ^1H NMR spectrum was acquired at 25 °C using 600 MHz NMR spectrometer (Bruker, Avance III-HD, USA) fitted with a 5-mm probe and equipped with topspin software (Bruker) for analysis.

2.7. Scanning electron microscopy (SEM) analysis of CS-keel bone

5 mg of CS-keel was fixed on the SEM stubs using double sided carbon tape, then coated with ~10 nm thick layer of gold. The samples were observed in a scanning electron microscope (Zeiss, Sigma, Germany) at an accelerating voltage of 2.5 kV at 500 x and 1000 x magnifications.

2.8. Atomic force microscopic (AFM) analysis of CS-keel

A stock solution of CS-keel (5 mg/ml) was prepared in Milli-Q water. The solution was diluted to make final concentrations of 0.01, 0.05 and 1.0 mg/ml. 10 μl of each diluted CS-keel solution was dropped on the surface of mica sample carrier and allowed to dry at 25 °C and analysed using semi-contact imaging mode. AFM analysis was performed using atomic force microscope (Agilent 5500, USA). The data obtained were processed using WSxM 5.0 Develop 7.0 software (Horcas et al., 2007).

2.9. Thermogravimetric Analysis (TGA) and Derivative Thermogravimetric Analysis (DTG) of CS-keel

The TGA and DTG of CS-keel was carried out using thermal analyser (Hitachi STA7200, Japan) operating at atmospheric pressure under nitrogen gas flow rate of 100 ml/min. The CS-keel (6.5 mg) was placed in a Al_2O_3 crucible and heated at a linear heating rate of 10 °C min^{-1} over a temperature range, 30 °C–600 °C and the corresponding weight loss was determined.

2.10. Differential scanning calorimeter (DSC) analysis of CS-keel

The DSC analysis of CS-keel was carried out using thermal analyser (STA 449-F3, Germany) operating at atmospheric pressure under argon gas at a flow rate of 100 ml/min. The CS-keel (3 mg) was placed in an Al_2O_3 crucible and heated at a linear heating rate of 10 °C min^{-1} over a temperature range, 25 °C–800 °C and enthalpy changes were determined.

2.11. In vitro cell proliferation assay of CS-keel

The mouse fibroblast cell line (L929) was procured from National Centre for Cell Science, Pune, India. The L929 cells were cultured in Dulbecco's Modified Eagle Medium (DMEM) low glucose medium supplemented with 10% (v/v) heat-inactivated fetal bovine serum (FBS) (Gibco), 50 μg/ml streptomycin and 50 IU/ml penicillin (Gibco) incubated at 37 °C under 5% CO_2. The effect of CS-keel on L929 cells viability was analysed by MTT [3-(4,5-dimethylthiazol-2-yl)-2,5-diphenyltetrazolium bromide] assay (Mosmann, 1983). The cells were seeded at a density of 2×10^4 cells/well in a 96 well plate and incubated at 37 °C in 5% CO_2 for 16 h for cell adherence. After incubation, the medium was completely removed and the cells were exposed to different concentrations (0.5 mg/ml to 5 mg/ml) of CS-keel dissolved in serum-free DMEM medium (incomplete). The incomplete DMEM medium without CS-keel was used as negative control. The plate was incubated at 37 °C in 5% CO_2 for 12 h and 24 h. MTT assay was done after 12 h and 24 h by removing the medium and washing the wells with 200 μl of 1 x phosphate buffer saline (PBS). 100 μl of MTT (0.5 mg/ml) was added to each well and plate was incubated at 37 °C in 5%CO_2 for 4 h. After the incubation, MTT was removed from the wells and the formazan formed was dissolved by adding 100 μl of dimethyl sulfoxide. The absorbance at 570 nm was monitored by a 96-well microplate reader (Tecan, Infinite 200 Pro, Switzerland). The cell viability (%) was calculated according to Van Meerloo, Kaspers, & Cloos (2011).

2.12. Microscopic analysis of CS-keel treated L929 cells

The surface morphology of L929 cells was observed after treating with CS-keel for 24 h. The L929 cells were maintained and seeded as described in the section 2.10. The cells were treated with 5 mg/ml of CS-keel dissolved in incomplete DMEM medium. The cells in only incomplete DMEM medium were used as control. After 24 h of treatment, the cells were observed under microscope (Nikon, TS100F, Japan) and photomicrographs were taken and processed using imaging software (Nikon NIS-Element).

2.13. DPPH radical scavenging activity of CS-keel

1-diphenyl-2-picrylhydrazyl (DPPH) scavenging activity was measured by the method of Lee et al., 2010. 100 μl of 0.5 mM DPPH in ethanol was mixed with 100 μl of different concentrations (0.25 mg/ml–5 mg/ml) of CS-keel dissolved in 50 mM Tris-HCl buffer (pH 7.2). The reaction mixture was incubated in dark at 37 °C for 30 min and 50 mM Tris-HCl was used as blank. The absorbance at 517 nm was measured using a microplate reader (Tecan, Infinite 200 Pro, Switzerland). The DPPH scavenging activity was calculated according to Lee et al., 2010.

2.14. Assay of inhibition of ascorbate autoxidation

The ascorbate inhibition assay was performed according to method of Lin and Yen (1999). 0.01 ml of varying concentrations (0.5 mg/ml–5 mg/ml) of CS-keel was added to 0.98 ml of 0.2 mM sodium phosphate buffer, pH 7.0 and 0.01 ml of 5 mM ascorbic acid solution (Sigma Aldrich, USA). A blank was set up in parallel to the reaction with distilled water in place of CS-keel. The 1 ml reaction mixture was transferred to the UV cuvette and incubated at 37 °C and the absorbance at 265 nm was observed as a function of time for 10 min on a UV–vis spectrophotometer (Varian, Cary 100). The percentage inhibition of ascorbate autoxidation was calculated as mentioned by Lin and Yen (1999).

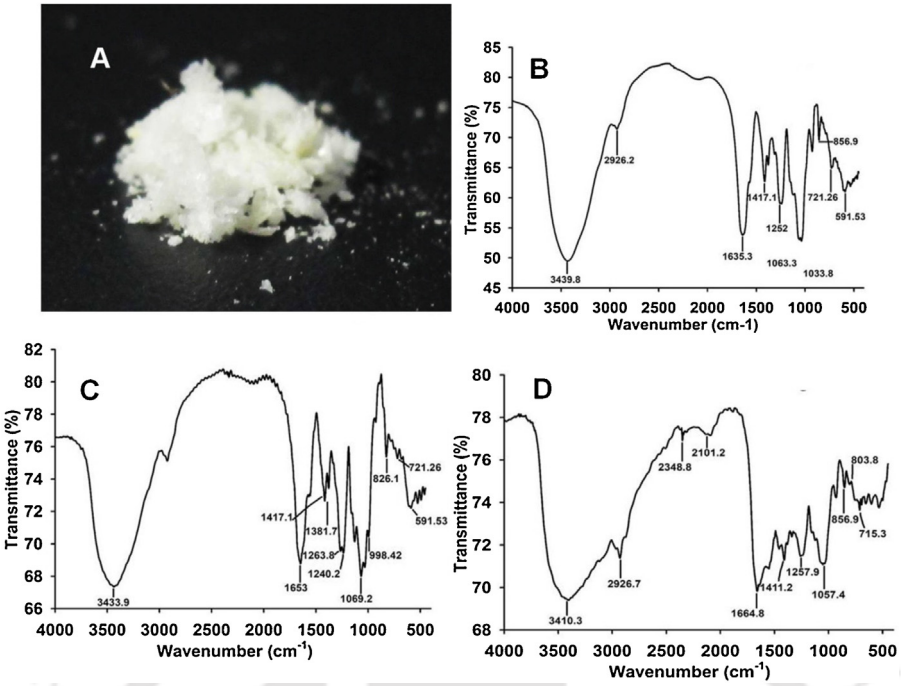

Fig. 1. (A) Digital image of isolated lyophillized CS-keel polysaccharide. FT-IR spectra of (B) standard chondroitin 4-suphate (C) standard chondroitin 6-sulphate (D) chondroitin sulphate isolated from chicken keel bone cartilage (CS-keel).

2.15. Emulsifying properties of CS-keel

The emulsifying property of CS-keel was analysed by method described by Bramhachari et al., 2007. 0.5 mg of CS-keel was dissolved in 0.5 ml of Milli-Q water by heating at 100 °C. The 1 x PBS, pH 7.4 was used to make up the reaction volume to 2 ml 0.5 ml of *n*-hexadecane was added to 2 ml reaction for emulsion formation and mixed by vigorous vortexing for 2 min. The absorbance at 0 min (A_0) was measured at 540 nm immediately after mixing the content. The reaction sample was incubated at 25 °C and decrease in absorbance (A_t) was recorded at 30 and 60 min. The negative control consisted of 2 ml of 1 x PBS and 0.5 ml *n*-hexadecane without CS keel, while the commercial guar gum was used as positive control. The emulsifying activity was calculated according to Bramhachari et al., 2007.

2.16. Statistical analysis

All experiments were performed in triplicates (n = 3). The results were presented as means of three determinations ± SD (standard deviation).

3. Results and discussion

3.1. Extraction and molecular weight determination of CS-keel

The chondroitin sulphate (CS) was isolated from the poultry waste of keel bone cartilage and 15% (g/g of cartilage) yield was achieved after lyophilisation (Fig. 1A). The molecular mass of references chondroitin 4-sulphate and chondroitin 6-sulphate were 70 kDa and 110 kDa, respectively as determined by HPSEC. The molecular weight of CS-keel was 100 kDa (Fig. S1). Another peak of 1 kDa appeared which might be due to the presence of small peptides or stretches of amino acids along with CS-keel. The protein contamination varies significantly depending on the source of cartilage. Two contaminating proteins, 77.8 kDa and 50.5 kDa were found in extracted GAG from chicken keel bone, which reduced the overall yield of CS content (Khan et al., 2013). The DLS analysis of CS-keel solution revealed polydispersity (Fig. S2). The CS-keel sample contained two peaks with hydrodynamic diameter of 255 nm and 44 nm which might be possibly corresponding to 100 kDa for CS-keel polysaccharide and 1 kDa for peptide peaks. The CS polysaccharide was reported to be polydispersed as well as large differences were also observed the average molecular weights of preparations from different sources (Hjertquist and Wasteson, 1972).

3.2. Compositional analysis of HPSEC purified CS-keel

The uronic acid content of HPSEC purified CS-keel as assayed by Carbazole method was 53 ± 5% (g/g of purified CS-keel). The protein content analysis of purified CS-keel showed that there was no trace of protein.

3.3. Quantification of CS disaccharides in CS-keel by enzymatic digestion

Mass spectrometry (MS) is being used as a powerful tool for structural analysis of isolated polysaccharides (Desaire & Leary,

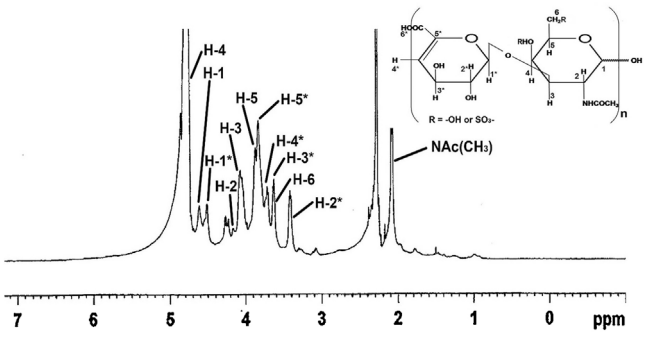

Fig. 2. ^{1}H NMR (600 MHz) of CS-keel polysaccharide.

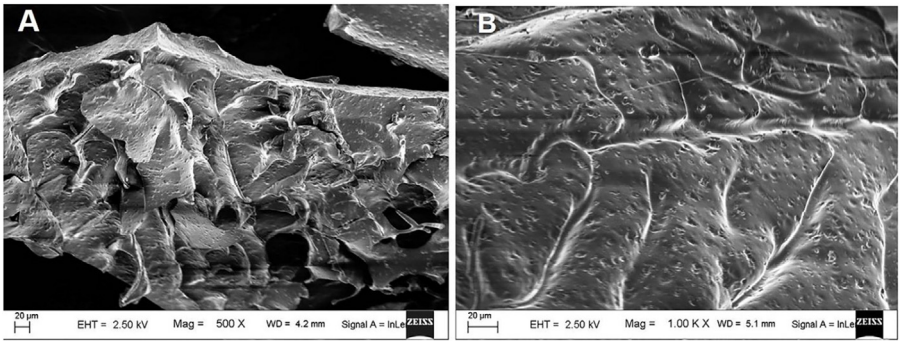

Fig. 3. FESEM images of CS-keel at magnifications (A) 500 x and (B) 1000x.

2000b). MS provides advantage in terms of accurate analysis and low sample consumption as compared to HPAEC and HPLC-UV detection (Desaire & Leary, 2000b). The CS-keel was treated with chondroitin AC lyase (*Ps*PL8A). After the enzyme reaction, the glucuronic acid contents of the digested and undigested CS-keel sample on quantification by carbazole method were 44 ± 4% and 10 ± 2%, respectively. The disaccharide composition of digested CS-keel was quantified by MS and MS/MS analysis. The MS analysis of three standard disaccharides UA-GalNAc4S (Fig. S3A), UA-GalNAc6S (Fig. S3C) and UA2S-GalNAc gave a major ion peak at *m*/*z* 458. The peak at *m*/*z* 458 was selected for MS/MS analysis for the three disaccharide standards. After MS/MS the UA-GalNAc4S (Fig. S3B), UA-GalNAc6S (Fig. S3D) and UA2S-GalNAc (data not shown) standards gave major peak at *m*/*z* 300, *m*/*z* 282 and *m*/*z* 237 respectively. The MS analysis of digested CS-keel sample gave major ion peak at *m*/*z* 458 (Fig. S3E). The MS/MS analysis of CE-Keel sample gave two peaks, one major peak at *m*/*z* 300 and other at *m*/*z* 282, which signifies the presence of UA-GalNAc4S, UA-GalNAc6S disaccharides in the sample (Fig. S3F). The absence of any peak at *m*/*z* 237 rules out the presence of UA2S-GalNAc in the CS-keel sample.

The quantification of disaccharides in CS-keel was done by using protocol described by Desaire and Leary, 2000a. The contribution of ions with *m*/*z* 282 and *m*/*z* 300 (as percentage of total ion current) were determined for the two standard disaccharide UA-GalNAc4S, UA-GalNAc6S from their MS/MS chromatograms. The binary equations were derived using these values

$$3.3XA + 55.5XB = C_{282} \quad (1)$$

$$73.5XA + 5.14XB = C_{300} \quad (2)$$

Where, A and B are the apparent percentages of UA-GalNAc4S, UA-GalNAc6S disaccharide in CS-keel sample, and C_{282} and C_{300} are the percentage contribution of two diagnostic ions in the sample. The value of A and B were calculated by inserting the values of C_{282} and C_{300} in the sample. A normalization factor was used as reported earlier (Desaire and Leary, 2000a) as many factors including the differences in the respective ionization efficiencies of the isomers might influence the peak intensities in the sample. The normalization factor for *m*/*z* 300 was 0.677, while for *m*/*z* 282 was 1.8 (Table S1). After normalizing, the observed values for A and B were then

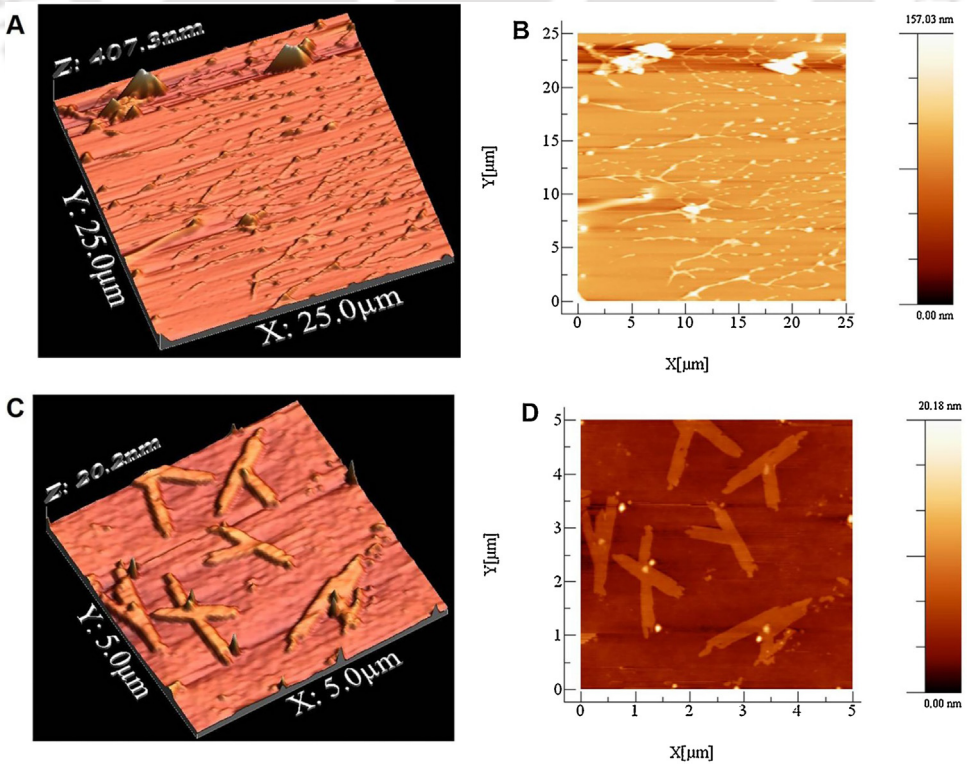

Fig. 4. AFM images of CS-keel (A) semi-contact mode 3D surface image at 25 × 25 µm, (B) 2D surface image at 25 × 25 µm, (C) Magnified 3D surface image at 5 × 5 µm, showing fibrous structure of CS-keel and (D) 2D representation of CS-keel at 5 × 5 µm.

Table 1
^{1}H NMR (600 MHz) chemical shift of CS isolated from keel bone cartilage.

Residue	Proton	^{1}H Chemical Shift (ppm)
GlcA	H-1*	4.51
	H-2*	3.41
	H-3*	3.63
	H-4*	3.71
	H-5*	3.84
	H-6*	–
GalNAc	H-1	4.61
	H-2	4.07
	H-3	4.03
	H-4	4.72
	H-5	3.87
	H-6	3.62
	NAc(CH_3)	2.08

* mark signifies the proton belonging to GlcA residue.

converted to the actual relative molar percentages of UA-GalNAc4S and UA-GalNAc6S disaccharide in CS-keel sample by dividing each normalized value by the sum of the two normalized values (Desaire and Leary, 2000a). The quantified percentages of UA-GalNAc4S and UA-GalNAc6S disaccharide in CS-keel sample were 58% and 42%, respectively (Table S1)".

3.4. Identification of type of chondroitin sulphate in CS-keel by FT-IR

The FT-IR spectrum of commercial C4S and C6S showed the corresponding peaks of sulphation at 856.9 cm^{-1} and 826.1 cm^{-1}, respectively (Fig. 1B & C). The isolated CS-keel spectrum displayed a distinct peak of sulphate group at 856.9 cm^{-1} indicating the polysaccharide being C4S (Fig. 1D). The peaks assigned for sulphation in present study corroborated with the previous findings by Garnjanagoonchorn et al., 2007 and Wang and Tang, 2009. The peaks for various other functional groups were analysed. The peak at 1411.2 cm^{-1} represented the coupling of C—O stretching vibration, OH variable angle vibration and existence of free COO^- groups. While the peaks at 1257.9 cm^{-1} and 1057.4 cm^{-1} signify S═O and –C—O-S stretching vibrations, respectively, as also reported earlier by Khan et al., 2013. The presence of the amide group in the CS-keel was depicted by the peak at 1664 cm^{-1} as shown earlier by Wang, Shen, & Lu (2003).

3.5. ^{1}H NMR analysis of CS-keel

The ^{1}H NMR spectrum of CS-keel was obtained at 600 MHz (Fig. 2). The characteristic signals of protons were assigned using previously reported chondroitin sulphate from porcine trachea, bovine trachea and shark cartilage (Mucci, Schenetti, & Volpi, 2000) and from *Scyliorhinus canicula* (Gargiulo, Lanzetta, Parrilli, & De Castro, 2009). The presence of broad range (3.4–4.6 ppm) of proton NMR spectrum confirms the polysaccharide nature of CS-keel (Table 1). CS-keel showed prominent signals of GlcA for H-1* and H-2* protons at 4.51 ppm and 3.41 ppm, respectively. The protons, H-3*, H-4* and H-5* of GlcA showed the resonances at 3.63 ppm, 3.71 ppm and 3.84 ppm, respectively. The protons of the GlcA ring resonate in the range, 3.4 –4.5 ppm, which is similar as previously reported (Mucci et al., 2000). Proton resonance at 2.08 ppm proves the existence of methyl group of N-acetylgalactosamine residue as also reported earlier by Gargiulo et al., 2009. The proton resonances of GalNAc residues, appeared in the regions, 3.6 –3.8 ppm and 4.0-4.7 ppm. H-5 and H-6 protons of GalNAc showed the signals at 3.62 ppm and 3.87 ppm, respectively and the rest of the protons in the 4.0-4.7 ppm region (Fig. 2). H-1, H-2, H-3 and H-4 protons of GalNAc gave resonances at 4.61 ppm, 4.07 ppm, 4.03 and 4.72 ppm as also reported earlier by Mucci et al., 2000.

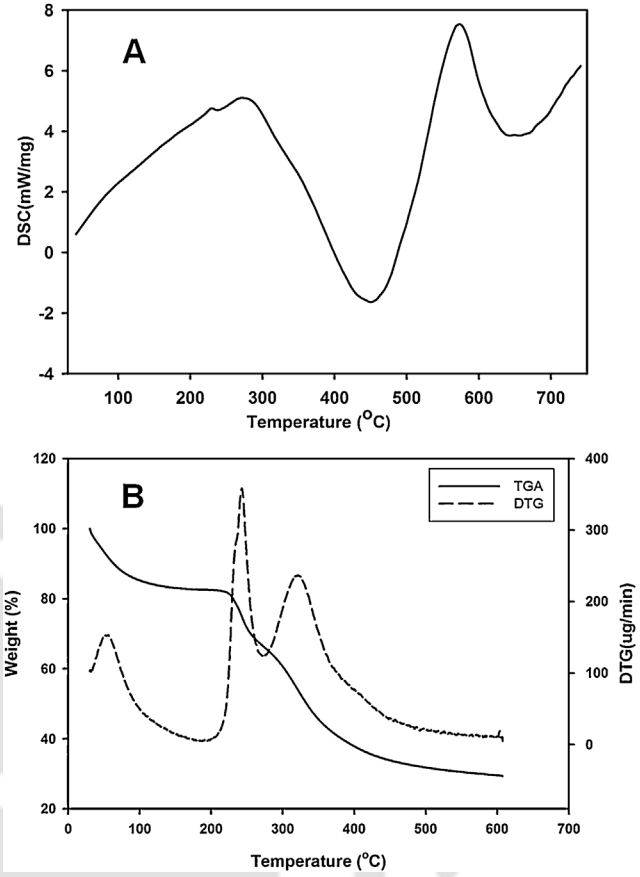

Fig. 5. Thermal property of CS-keel polysaccharide (A) Differential scanning calorimetery (DSC), (B) Thermogravimetric analysis (TGA) showing thermal stability up to 220 °C and Derivative Thermogravimetric Analysis (DTG) showing degradation temperature (T_d) of 243 °C.

3.6. Surface analysis of CS-keel by FESEM and AFM

Scanning electron microscopy was used for high resolution surface imaging of CS-keel. The surface morphology of CS-keel showed rough surface with several layers stacked upon each other (Fig. 3A). In the previous study of fucosylated chondroitin sulphate from sea cucumber *Acaudina molpadioidea* and *Holothuria nobilis* also showed the rough surface with several particles stacked together (Zou et al., 2016). The layer structure of CS-keel also showed the presence of depressions on the surface at regular intervals (Fig. 3B).

AFM is a powerful tool that enables the surface morphology of hydrated and soft samples (Jacoboni, Valdre, Mori, Quaglino, & Pasquali-Ronchetti, 1999). The AFM analysis of CS-keel bone revealed fibrous structures of irregular shapes arranged randomly throughout the surface (Fig. 4A & B). The fibrous structures were approximately, 20 nm in height and 300 nm in diameter with variable lengths (Fig. 4C & D). The distribution of fibrous structure present could be correlated with the concentration of CS-keel as with the increase in its concentration, the fibrous structure increased and was maximum at 1 mg/ml. Polysaccharides generally form chains of width 0.1 nm to 1 nm (Zou et al., 2016). The large variation in width of the structure could be attributed to the presence of associated core proteins, which form aggregates with CS-keel polysaccharide chain. The presence of associated proteins was also observed in the HPSEC analysis of CS-keel as mentioned earlier.

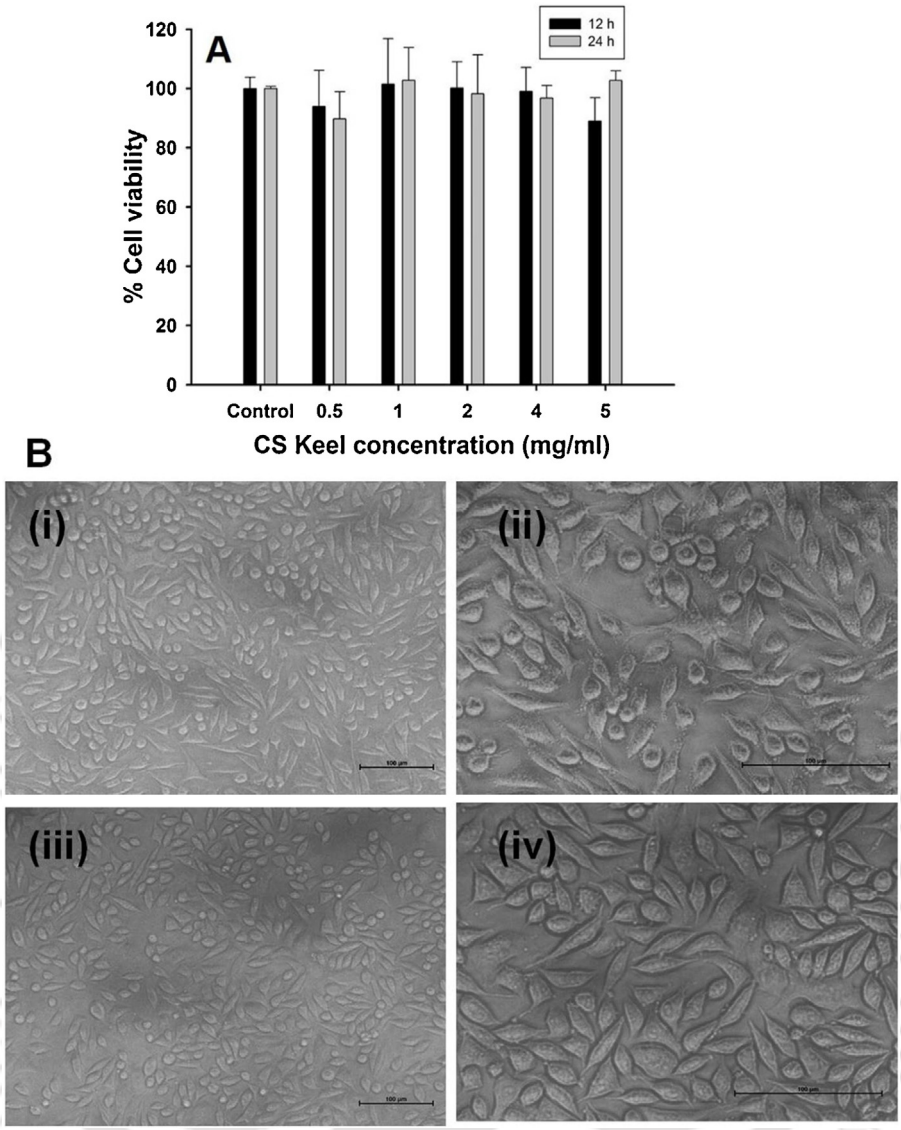

Fig. 6. Analysis of the **e**ffect of CS Keel polysaccharide on Mouse fibroblast L929 cells by (A) The *in vitro* cell proliferation assay (MTT) showing percent cell viability of L929 cells treated with varying concentration (0.5 mg/ml −5 mg/ml) of CS Keel, (B) Light microscopic images of, Untreated cells under (i) 20 x and (ii) 40 x magnification and CS-keel (5 mg/ml) treated cells for 24 h under (iii) 20 x and (iv) 40 x magnification.

3.7. *Thermal properties of CS-keel*

The thermal properties of CS-keel polysaccharide were studied by TGA, DTG and DSC. The DSC analysis showed, the thermal property of CS-keel resembles with the behaviour of polysaccharides. The thermal scan of CS-keel suggested the presence of an endothermic peak at 270.4 °C, which is due to bound water molecule in the CS-keel polymer chain (Fig. 5A). The exothermic peak at 451.5 °C is due to the irreversible process of polysaccharide degradation (Fig. 5A). These properties of CS-keel might be due to intermolecular or intramolecular hydrogen bonding and cross linking capacity (Moreno, Panero, Artico, & Filippini, 2008).

TGA of CS-keel depicted the weight loss of polysaccharide with increase in temperature. The weight loss of CS-keel was observed in three stages. Initial 15.0% weight loss of CS-keel occurred between 35 °C to 100 °C. The initial weight loss of polysaccharide CS-keel was associated with the loss of water and also suggested presence of high content of carboxyl groups which were bound to water molecules as also reported earlier (Wang, Zhao, Tian, Yang, & Yang, 2015). A sudden decrease of 43% weight of CS-keel was observed with in the temperature range, 220 °C–400 °C. The weight loss of CS-keel gradually decreased further and finally reached 28% at 600 °C (Fig. 5B). The Derivative thermogravimetric (DTG) curves showed two peaks, at 243 °C and 320 °C. Out of these two, the first sharp peak at 243 °C corresponded to the thermal degradation temperature (T_d) of CS-keel polysaccharide while the second peak at 320 °C might be due to the presence of protein (Fig. 5B). The thermal degradation of commercial chondroitin sulphate A isolated from bovine trachea occurred at T_d, 227 °C (Moreno et al., 2008). The relatively higher degradation temperature makes CS-keel a suitable material for tissue scaffolds and joint replacement therapies.

3.8. In vitro *cell proliferation assay of CS-keel polysaccharide*

The *in vitro* cell proliferation assay of CS-keel polysaccharide was determined using MTT. This is widely used method for estimation of cell viability, cytotoxicity and cell proliferation (Mosmann 1983). MTT is a yellow colour compound which on reduction by mitochondrial succinate dehydrogenase in the metabolically active cells yields a purple colour formazan (Van Meerloo et al., 2011).

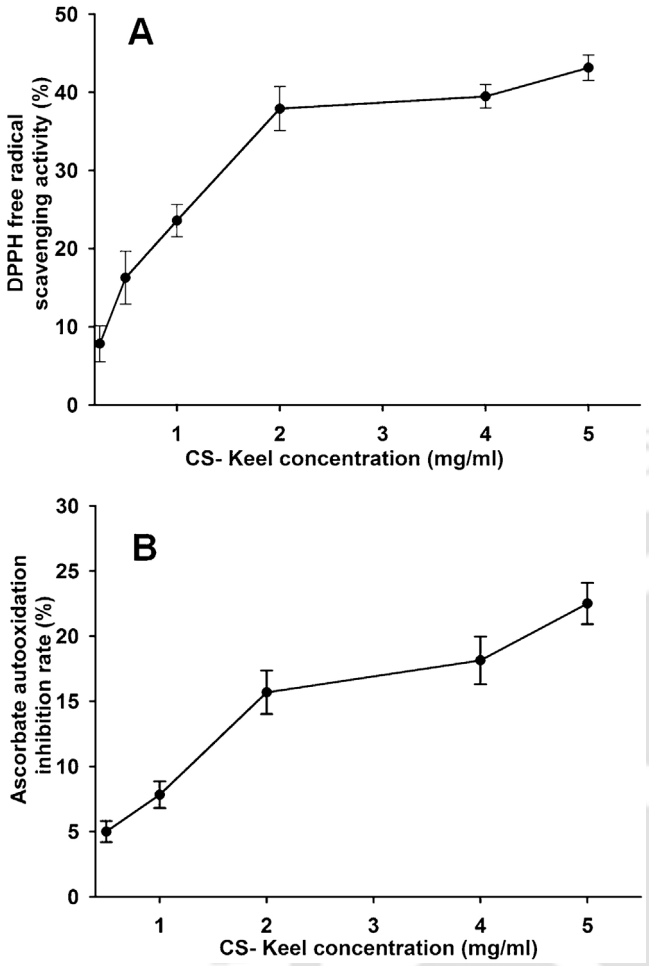

Fig. 7. *In vitro* antioxidant activity of CS-keel polysaccharide showing (A) DPPH radicals scavenging activity and (B) Inhibition of ascorbate autooxidation.

The mouse fibroblast L929 cells were treated with varying concentrations (0.5 mg/ml to 5 mg/ml) of CS-keel for 12 h and 24 h. The CS-keel was dissolved in serum free DMEM low glucose (incomplete) medium as the presence of serum in complete medium leads to the cell growth and interferes with the cell viability assessment (Barnes and Sato 1980; Van Meerloo et al., 2011). It was observed that CS-keel imparts no cytotoxicity on L929 cells with the time as well with increase of its concentration (Fig. 6A). The cell proliferation assay revealed that the viability of CS-keel treated L929 cells was 98% which was almost similar to the untreated cells at 5 mg/ml after 24 h. Hence the results concluded the biocompatible nature of CS-keel polysaccharide which makes it a prospective candidate for making tissue scaffolds in tissue engineering and as drug delivery agent for controlled release of drugs.

3.9. Microscopic observation of CS-keel treated L929 cells

The L929 cells under the normal condition exhibit spindle shape when adhered to the surface of culture plate (Theerakittayakorn and Bunprasert, 2011). The microscopic analysis of untreated and CS-keel treated L929 cells was carried out to study the morphological changes. The bright field microscopic analysis of L929 cells revealed that there was no detectable change in morphology of cells. Both, the untreated [Fig. 6B(i) & (ii)] and CS-keel treated cells [Fig. 6B(iii) & (iv)] exhibited the same spindle shape morphology. The surface morphology study analysis further supported the contention elucidated from the MTT assay that CS-keel polysaccharide is biocompatible.

3.10. Antioxidant properties of CS-keel

Antioxidant properties of CS-keel were assessed by DPPH and inhibition of ascorbate autooxidation method. The DPPH is a free-radical compound, which is widely used to assess the antioxidant nature of compounds. DPPH free radical scavenging activities of the antioxidant compounds is based on their hydrogen donating nature. It receives an electron or hydrogen radical (H•) from antioxidant and become stable in its reduced form. Therefore, the antioxidant activity of a compound can be expressed as its ability in scavenging the DPPH• free radical. The DPPH scavenging activity of CS-keel in the concentration range of 0.5 mg/ml to 5 mg/ml varied from 8% to 49% (Fig. 7A). In a previous study, the DPPH radical scavenging activity of antler CS, bovine cartilage CS and shark cartilage CS at a concentration of 5 mg/ml were measured as 51 ± 1%, 8 ± 0.1%, and 5 ± 0.1%, respectively (Kim, Gujral, Ganguly, Suh, & Sunwoo, 2014).

The inhibition of ascorbate autoxidation is the method to assess the superoxide radical suppression generated by oxidation of ascorbate. CS-keel showed inhibition of ascorbate autoxidation in the range, from 5.0 ± 0.8% to 22 ± 1.6% at concentrations from 0.5 mg/ml to 5 mg/ml (Fig. 7B). CS-keel can protect the oxidative damage caused by harmful superoxide radical. The results suggested that CS-keel possesses strong antioxidant activity preventing the oxidative damage caused by the reactive oxygen species and hence can be used as potential antioxidant agent in pharmaceuticals.

3.11. Emulsification capacity of CS-keel

The emulsifying property CS-keel was determined by its capability of stabilizing the emulsion of hydrocarbon in water. The emulsifying activity of CS-keel was measured at two different time intervals of 30 min and 60 min against *n*-hexadecane. CS-keel stabilized the emulsion of hydrocarbon and retained 72% and 70% of the emulsifying activity at 30 min and 60 min, respectively. The emulsifying activity of the two commercial emulsifiers, guar gum and sodium alginate were also calculated. Guar gum retained 81% and 74% of emulsifying activity after 30 and 60 min, respectively. While emulsifying activity of sodium alginate was 69% and 41% after 30 and 60 min, respectively. CS-keel exhibited comparable emulsifying activity than commercial emulsifier guar gum, while better than sodium alginate. Previously the emulsifying capability of commercial CS-A was studied as protein-polysaccharide complex involving lysozyme and CS-A (Kato, Sato, & Kobayashi, 1989). The overall finding of the present study suggested that CS-keel can serve as a potential emulsifier in the food industry.

4. Conclusion

CS polysaccharide was isolated from chicken keel bone cartilage. The composition, structure, surface and thermal analysis of CS-keel displayed that it can serve as a strong candidate in tissue scaffolds for biomedical engineering. *In vitro* cell proliferation assay showed the biocompatible nature of CS-keel. It possesses significant antioxidant activity against DPPH and superoxide radical and strong emulsifying property. Therefore, CS-keel can be used for functional food applications enriching the nutritional values. CS-keel also enables future prospects for analysis of its chondroprotective and anti-inflammatory properties for osteoarthritis treatment. Future challenges include its utilization in nanomedicine to develop an

efficient delivery vehicle for therapeutic agents, to further enhance its specificity and finally to have controlled drug release.

Conflict of interest

The authors declare no conflict of interest.

Acknowledgements

The research work and AR are being supported by Council of Scientific and Industrial Research (CSIR) Project No. 37(1672)/16/EMR-II to AG. The authors thank Central Instrumentation Facility for providing FESEM, NMR, AFM and DSC and Centre for Energy, of IIT Guwahati for providing TGA and DTG facility. The authors thank Prof. P. Goswami, Centre for Energy for providing DLS facility and Dr. N. Chaudhary, Department of Biosciences and Bioengineering, IIT Guwahati for helpful discussions in the MS data analysis.

Appendix A. Supplementary data

Supplementary data associated with this article can be found, in the online version, at http://dx.doi.org/10.1016/j.carbpol.2016.12.015.

References

Barnes, D., & Sato, G. (1980). Methods for growth of cultured cells in serum-free medium. *Analytical Biochemistry*, *102*(2), 255–270.
Bianchera, A., Salomi, E., Pezzanera, M., Ruwet, E., Bettini, R., & Elviri, L. (2014). Chitosan hydrogels for chondroitin sulphate controlled release: An analytical characterization. *Journal of Analytical Methods in Chemistry*, 2014.
Bramhachari, P. V., Kishor, P. K., Ramadevi, R., Kumar, R., Rao, B. R., & Dubey, S. K. (2007). Isolation and characterization of mucous exopolysaccharide (EPS) produced by *Vibrio furnissii* strain VB0S3. *Journal of Microbiology and Biotechnology*, *17*(1), 44.
Campo, G. M., Avenoso, A., Campo, S., Ferlazzo, A. M., & Calatroni, A. (2006). Chondroitin sulphate: Antioxidant properties and beneficial effects. *Mini Reviews in Medicinal Chemistry*, *6*(12), 1311–1320.
Desaire, H., & Leary, J. A. (2000a). Detection and quantification of the sulfated disaccharides in chondroitin sulfate by electrospray tandem mass spectrometry. *Journal of the American Society for Mass Spectrometry*, *11*(10), 916–920.
Desaire, H., & Leary, J. A. (2000b). Utilization of MS 3 spectra for the multicomponent quantification of diastereomeric N-acetylhexosamines. *Journal of the American Society for Mass Spectrometry*, *11*(12), 1086–1094.
Field, I. C., Meekan, M. G., Buckworth, R. C., & Bradshaw, C. J. (2009). Susceptibility of sharks: rays and chimaeras to global extinction. *Advances in Marine Biology*, *56*, 275–363.
Frazier, S. B., Roodhouse, K. A., Hourcade, D. E., & Zhang, L. (2008). The quantification of glycosaminoglycans: A comparison of HPLC, carbazole, and alcian blue methods. *Open Glycoscience*, *1*, 31–39.
Gargiulo, V., Lanzetta, R., Parrilli, M., & De Castro, C. (2009). Structural analysis of chondroitin sulfate from *Scyliorhinus canicula*: A useful source of this polysaccharide. *Glycobiology*, *19*(12), 1485–1491.
Garnjanagoonchorn, W., Wongekalak, L., & Engkagul, A. (2007). Determination of chondroitin sulfate from different sources of cartilage. *Chemical Engineering and Processing: Process Intensification*, *46*(5), 465–471.
Hamano, T., Mitsuhashi, Y., Acki, N., Yamamoto, S., Tsuji, S., Ito, Y., et al. (1989). High-performance liquid chromatographic assay of chondroitin sulphate in food products. *Analyst*, *114*(8), 891–893.
He, W., Fu, L., Li, G., Jones, J. A., Linhardt, R. J., & Koffas, M. (2015). Production of chondroitin in metabolically engineered *E. coli*. *Metabolic Engineering*, *27*, 92–100.
Henrotin, Y., Mathy, M., Sanchez, C., & Lambert, C. (2010). Chondroitin sulfate in the treatment of osteoarthritis: From in vitro studies to clinical recommendations. *Therapeutic Advances in Musculoskeletal Disease*, *2*(6), 335–348.
Hjertquist, D. S. O., & Wasteson. (1972). The molecular weight of chondroitin sulphate from human articular cartilage. *Calcified Tissue Research*, *10*(1), 31–37.
Hochberg, M. C., Martel-Pelletier, J., Monfort, J., Möller, I., Castillo, J. R., Arden, N., et al. (2015). Combined chondroitin sulfate and glucosamine for painful knee osteoarthritis: A multicentre, randomised, double-blind, non-inferiority trial versus celecoxib. *Annals of the Rheumatic Diseases*, annrheumdis-2014
Horcas, I., Fernández, R., Gomez-Rodriguez, J. M., Colchero, J., Gómez-Herrero, J. W. S. X. M., & Baro, A. M. (2007). WSXM: A software for scanning probe microscopy and a tool for nanotechnology. *Review of Scientific Instruments*, *78*(1), 013705.
Iozzo, R. V. (1998). Matrix proteoglycans: From molecular design to cellular function. *Annual Review of Biochemistry*, *67*(1), 609–652.
Jacoboni, I., Valdre, U., Mori, G., Quaglino, D., & Pasquali-Ronchetti, I. (1999). Hyaluronic acid by atomic force microscopy. *Journal of Structural Biology*, *126*(1), 52–58.
Kato, A., Sato, T., & Kobayashi, K. (1989). Emulsifying properties of protein-polysaccharide complexes and hybrids. *Agricultural and Biological Chemistry*, *53*(8), 2147–2152.
Khan, H. M., Ashraf, M., Hashmi, A. S., Ahmad, M. U. D., & Anjum, A. A. (2013). Extraction and biochemical characterization of sulphated glycosaminoglycans from chicken keel cartilage. *Pakistan Veterinary Journal*, *33*, 471–475.
Kim, C. T., Gujral, N., Ganguly, A., Suh, J. W., & Sunwoo, H. H. (2014). Chondroitin sulphate extracted from antler cartilage using high hydrostatic pressure and enzymatic hydrolysis. *Biotechnology Reports*, *4*, 14–20.
Lauder, R. M., Huckerby, T. N., & Nieduszynski, I. A. (2000). A fingerprinting method for chondroitin/dermatan sulfate and hyaluronan oligosaccharides. *Glycobiology*, *10*(4), 393–401.
Lee, B. J., Kim, J. S., Kang, Y. M., Lim, J. H., Kim, Y. M., Lee, M. S., et al. (2010). Antioxidant activity and γ-aminobutyric acid (GABA) content in sea tangle fermented by *Lactobacillus brevis* BJ20 isolated from traditional fermented foods. *Food Chemistry*, *122*(1), 271–276.
Lin, M. Y., & Yen, C. L. (1999). Antioxidative ability of lactic acid bacteria. *Journal of Agricultural and Food Chemistry*, *47*(4), 1460–1466.
Lowry, O. H., Rosebrough, N. J., Farr, A. L., & Randall, R. J. (1951). Protein measurement with the Folin phenol reagent. *The Journal of Biological Chemistry*, *193*(1), 265–275.
Luo, X. M., Fosmire, G. J., & Leach, R. M. (2002). Chicken keel cartilage as a source of chondroitin sulfate. *Poultry Science*, *81*(7), 1086–1089.
Maccari, F., Galeotti, F., & Volpi, N. (2015). Isolation and structural characterization of chondroitin sulfate from bony fishes. *Carbohydrate Polymers*, *129*, 143–147.
Moreno, J. S., Panero, S., Artico, M., & Filippini, P. (2008). Synthesis and characterization of new electroactive polypyrrole-chondroitin sulphate A substrate. *Bioelectrochemistry*, *72*(1), 3–9.
Mosmann, T. (1983). Rapid colorimetric assay for cellular growth and survival: Application to proliferation and cytotoxicity assays. *Journal of Immunological Methods*, *65*(1-2), 55–63.
Mucci, A., Schenetti, L., & Volpi, N. (2000). 1-H and 13-C nuclear magnetic resonance identification and characterization of components of chondroitin sulfates of various origin. *Carbohydrate Polymers*, *41*(1), 37–45.
Nakano, T., Pietrasik, Z., Ozimek, L., & Betti, M. (2012). Extraction, isolation and analysis of chondroitin sulfate from broiler chicken biomass. *Process Biochemistry*, *47*(12), 1909–1918.
Rani, A., & Goyal, A. (2016). A new member of family 8 polysaccharide lyase chondroitin AC lyase (PsPL8A) from *Pedobacter saltans* displays endo- and exo-lytic catalysis. *Journal of Molecular Catalysis B: Enzymatic*, http://dx.doi.org/10.1016/j.molcatb.2016.11.001
Raynauld, J. P., Pelletier, J. P., Abram, F., Delorme, P., & Martel-Pelletier, J. (2016). Long-term effects of glucosamine/chondroitin sulfate on the progression of structural changes in knee osteoarthritis: 6-year follow-up data from the osteoarthritis initiative. *Arthritis Care & Research*, http://dx.doi.org/10.1002/acr.22866
Schiller, J., & Huster, D. (2012). New methods to study the composition and structure of the extracellular matrix in natural and bioengineered tissues. *Biomatter*, *2*(3), 115–131.
Srichamroen, A., Nakano, T., Pietrasik, Z., Ozimek, L., & Betti, M. (2013). Chondroitin sulfate extraction from broiler chicken cartilage by tissue autolysis. *LWT-Food Science and Technology*, *50*(2), 607–612.
Theerakittayakorn, K., & Bunprasert, T. (2011). Differentiation capacity of mouse L929 fibroblastic cell line compared with human dermal fibroblast. *World Academy of Science, Engineering and Technology, International Journal of Medical, Health, Biomedical, Bioengineering and Pharmaceutical Engineering*, *5*(2), 51–54.
Vázquez, J. A., Rodríguez-Amado, I., Montemayor, M. I., Fraguas, J., González, M. D. P., & Murado, M. A. (2013). Chondroitin sulfate, hyaluronic acid and chitin/chitosan production using marine waste sources: Characteristics, applications and eco-friendly processes: A review. *Marine Drugs*, *11*(3), 747–774.
Van Meerloo, J., Kaspers, G. J., & Cloos, J. (2011). Cell sensitivity assays: The MTT assay. *Cancer Cell Culture: Methods and Protocols*, 237–245.
Vittayanont, M., & Jaroenviriyapap, T. (2013). Production of crude chondroitin sulfate from duck trachea. *International Food Research Journal*, *21*(2), 791–797.
Wang, P., & Tang, J. (2009). Solvent-free mechanochemical extraction of chondroitin sulfate from shark cartilage. *Chemical Engineering and Processing: Process Intensification*, *48*(6), 1187–1191.
Wang, L. F., Shen, S. S., & Lu, S. C. (2003). Synthesis and characterization of chondroitin sulfate-methacrylate hydrogels. *Carbohydrate Polymers*, *52*(4), 389–396.
Wang, J., Zhao, X., Tian, Z., Yang, Y., & Yang, Z. (2015). Characterization of an exopolysaccharide produced by Lactobacillus plantarum YW11 isolated from Tibet Kefir. *Carbohydrate Polymers*, *125*, 16–25.
Zou, S., Pan, R., Dong, X., He, M., & Wang, C. (2016). Physicochemical properties and antioxidant activities of two fucosylated chondroitin sulfate from sea cucumber *Acaudina molpadioidea* and *Holothuria nobilis*. *Process Biochemistry*, *51*(5), 650–658.

International Journal of Biological Macromolecules xxx (2017) xxx–xxx

Contents lists available at ScienceDirect

International Journal of Biological Macromolecules

journal homepage: www.elsevier.com/locate/ijbiomac

Insights into the structural characteristics and substrate binding analysis of chondroitin AC lyase (*Ps*PL8A) from *Pedobacter saltans*

Aruna Rani, Arun Dhillon, Kedar Sharma, Arun Goyal *

Department of Biosciences and Bioengineering, Indian Institute of Technology Guwahati, Guwahati 781039, Assam, India

ARTICLE INFO

Article history:
Received 26 June 2017
Received in revised form
12 November 2017
Accepted 13 November 2017
Available online xxx

Keywords:
Chondroitin AC lyase
Homology modelling
Saxs

ABSTRACT

The structure of chondroitin AC lyase (*Ps*PL8A) of family 8 polysaccharide lyase was characterized. Modeled *Ps*PL8A structure showed, it contains N-terminal $(\alpha/\alpha)_6$ incomplete toroidal fold and a layered β sandwich structure at C-terminal. Ramchandran plot displayed 98.5% residues in favoured and 1.2% in generously allowed region. Secondary structure of *Ps*PL8A by CD revealed 27.31% α helices 22.7% β sheets and 49.9% random coils. Protein melting study showed, *Ps*PL8A completely unfolds at 60 °C. SAXS analysis showed, *Ps*PL8A is fully folded in solution form. The *ab initio* derived dummy model of *Ps*PL8A superposed well with its modeled structure excluding some α-helices and loop region. Structural superposition and docking analysis showed, N153, W105, H203, Y208, Y212, R266 and E349 were involved in catalysis. Mutants N153A, H203A, Y212F, R266A and E349A created by SDM revealed no residual activity. Isothermal titration calorimetry analysis of Y212F and H203A with C4S polysaccharide, showed moderate binding by Y212F ($Ka = 9.56 \pm 3.81 \times 10^5$) and no binding with H203A, showing active contribution of Y212 in substrate binding. Residues Y212 and H203 or R266 might act as general base and general acid respectively. Residues N153 and E349 are likely contributing in charge neutralization and stabilizing enolate anion intermediate during β-elimination.

1. Introduction

Carbohydrates are dynamic molecules that are constantly synthesized and broken down in animal and plants. There are varieties of enzymes involved in the synthesis as well as breakdown of carbohydrates. The carbohydrate-active enzymes are grouped into different families based on amino acid sequence similarity and are listed in the continually updated carbohydrate-active enzyme (CAZy) database (www.cazy.org) [1]. The carbohydrate active enzymes belonging to the polysaccharide lyase (PL) class are relatively less explored enzymes. The PL family enzymes degrade the acidic polysaccharide such as pectin, glycosaminoglycans (GAG) and alginate. GAG are highly sulphated linear and anionic polysaccharide made up of repeating disaccharide units of hexosamine and uronic acid residues [2]. These GAG chains are linked through glycosidic linkage to serine residue of core protein and hence form proteoglycans (PG) [3]. GAG are classified into four major classes: Chondroitin Sulphate (CS)/Dermatan Sulphate (DS), Heparin/Heparan Sulphate, Hyaluronic acid (HA) and Keratan sulphate (KS). CS consisted of N-acetyl-galactosamine (sulphated at C4/C6) linked via β-(1 → 3) linkage to D-glucuronic acid and the two disaccharide are linked by β-(1 → 4) glycosidic bond [4,5]. CS lyase catalyze the cleavage of β-(1 → 4) glycosidic bond between hexosamine and uronic acid residue of CS by β-elimination and generate Δ4,5 unsaturated uronate oligosaccharides that exhibits absorbance maxima at 232 nm (A_{232}) [6,7]. The plausible mechanism proposed by Gacesa et al. in 1987 includes three steps: i) negative charge present on the carboxylate anion of glucuronic acid can be neutralized by positive charge amino acid/divalent metal ion, ii) Abstraction of C-5 proton by general base and iii) β- elimination of 4-O glycosidic bond.

The crystal structures of chondroitin AC lyase [3,8], Hyaluronate lyase [9], chondroitin ABC lyase [10] have been reported. The structural fold present in family 8 polysaccharide lyase is $(\alpha/\alpha)_{5,6}$ β toroid domain, that contains five α-helical hairpins and in some proteins a sixth hairpin is assembled from two additional antiparallel helices, one at the N-terminus and the other at the C-terminus of this domain. This domain is followed by a C-terminal antiparallel β-sandwich domain containing four β-sheets [3,11]. Chondroitin AC lyase from *Flavobacterium heparinum* consists of two domains, a N-terminal domain of around 300 amino acids arranged as α-helices and the C-terminal domain spanning 370 residues are configured as four antiparallel β-sheets. The N-terminal domain imparts the protein a double layered horseshoe structure $(\alpha/\alpha)_5$ toroidal

* Corresponding author.
E-mail address: arungoyl@iitg.ernet.in (A. Goyal).

https://doi.org/10.1016/j.ijbiomac.2017.11.087
0141-8130/

(doughnut-shaped) topology [3]. The putative catalytic residues His, Tyr, Arg, Glu and Cys have been previously proposed which act as general base by abstracting C-5 proton of uronic acid and the residues acting as general acid initially neutralizes the negative charge on the carboxylate ion [2]. The complete mechanism of the catalysis by chondroitin lyases is still not known. In the present study the 3-dimensional structure of *Ps*PL8A from *Pedobacter saltans* was developed by homology modeling. The structure of *Ps*PL8A in solution state was determined by SAXS. Secondary structure elements were evaluated by CD and Psipred analyses. The docking study of *Ps*PL8A with various CS ligands and site directed mutagenesis was performed to ascertain the catalytic centre and residues involved in *Ps*PL8A catalysis.

2. Material and methods

Chondroitin 4 sulphate, Trizma base, Sodium chloride, Calcium chloride, EDTA, phenyl methane sulfonyl fluoride (PMSF), Isopropyl-1-thio-β-D-galactopyranoside (IPTG), Kanamycin and Imidazole were procured from Sigma-Aldrich USA. Genomic DNA of *Pedobacter saltans* DSM12145 was purchased from Leibniz Institute DSMZ – German Collection of Microorganisms and Cell Cultures. *Escherichia coli* DH5α cells used for transformation of recombinant plasmid and *E. coli* BL-21 (DE3) cells for expression of recombinant proteins were purchased from Novagen (Germany).

2.1. Sequence retrieval and alignment of Ps*PL8A*

The protein sequence of *Ps*PL8A belonging to family 8 polysaccharide lyase (PL8) from *Pedobacter saltans* DSM 12145 was retrieved from the CAZy Database (http://www.cazy.org/PL8_bacteria.html). The sequence has a GenBank accession no. ADY54337.1. BLAST analysis of the query sequence was performed with known PDB structures from X-ray or NMR data [12]. The N-terminal signal peptide sequence was identified by using signalIP. *Ps*PL8A sequence was aligned with the previously reported sequence of chondroitin AC lyase sequences from *Pedobacter heparinus* (previously known as *Flavobacterium heparinum*) and *Arthrobacter aurescens*. Multiple Sequence alignment (MSA) was done by using Clustal omega (http://www.ebi.ac.uk/Tools/msa/clustalo/) available at EMBL-EBI page. The MSA sequence file was viewed under ESPript 3.0 to analyse the conserved and semi-conserved residues present in the sequence of *Ps*PL8A.

2.2. Homology modeling of Ps*PL8A*

The 3-Dimensional structure of *Ps*PL8A was modelled by using Modeller 9v12 (http://salilab.org/modeller/). MODELLER is used for homology or comparative modeling of protein three-dimensional structures [13]. The comparative protein structure modeling was done based on related known templates satisfying the spatial restraints [14]. The query sequence *Ps*PL8A was align with the best matched template of known protein sequence, PDB id: 1CB8_A from Pedobacter *heparinus*. After the optimization of molecular probability density by modeller, 15 independent models were generated. Further refining of structure was achieved by the loop optimization method in modeller. Discrete optimized protein score (DOPE) was generated for each model after loop refinement until a negative DOPE score was attained. The modelled structure with the least DOPE score was selected as best model for further studies.

2.3. Structure refinement and quality assessment of modelled Ps*PL8A*

The modelled structure with least DOPE value was refined and energy minimized by using 3Drefine: Protein structure refinement server (http://sysbio.rnet.missouri.edu/3Drefine/). The spatial structure of protein is critical for predicting the biological function on basis of its structure and docking studies [15,16]. The 3Drefine server utilizes iterative optimization of hydrogen bonding network along with atomic-level energy minimization on the optimized model for the refinement of modelled protein structure [16]. The structure generated after energy minimization was validated by using structure analysis and verification server (SAVES) at NIH–MBI laboratory page (http://nihserver.mbi.ucla.edu/SAVES/). The overall compatibility of 3D model generated with its own amino acid sequence was analysed by using Verify3D. ERRAT plot was generated which determines the overall quality of modelled structure. Ramachandran plot was generated using PROCHECK, where the possible and permitted torsional angles, backbone phi (ϕ) and psi (ψ) dihedral angles were defined. Protein Structure Analysis (ProSA) web Server (https://prosa.services.came.sbg.ac.at/prosa.php) was used to analyse steriochemical quality of modelled structure. Active site involves key amino acid residues which participate in the reaction mechanism. Generally, these residues are conserved within the family. Therefore, to identify the active site residues, we performed structure alignment of *Ps*PL8A with template protein (1CB8_A) of family PL8 using PyMOL (http://www.PyMOL.org). The topology diagram of modelled structure was generated by using PDBSum (http://www.ebi.ac.uk/thornton-srv/databases/pdbsum/Generate.html).

2.4. Secondary structure analysis of Ps*PL8A* by circular dichroism (CD)

*Ps*PL8A was cloned, expressed, purified and biochemically characterized in our earlier report [17]. The secondary structure of *Ps*PL8A was analysed using 0.332 μM of *Ps*PL8A in 50 mM Tris-HCl, pH 7.2. CD spectrum of *Ps*PL8A was recorded in the Far UV range (190–250 nm) on a spectropolarimeter (J-815, Jasco Corporation, Tokyo) at 25 °C using a sample cell with path length of 0.1 cm. The CD spectrum was collected at a scanning rate of 50 nm/min and 1 nm bandwidth with an average of six scans. The CD spectra was corrected for buffer contributions and the percentage of different secondary structures present in *Ps*PL8A were determined by using K2D3 server (http://k2d3.ogic.ca/). The molar residual ellipticity (mre) was calculated from the ellipticity (θ) values at each wavelength [18]. The mre values were analysed from 190 to 240 nm by K2D3 server.

2.5. Molecular docking studies of Ps*PL8A*

Molecular docking analysis of *Ps*PL8A was performed using Autodock Vina [19] (http://vina.scripps.edu/) along with the viewer MGLTools1.5.6 (http://mgltools.scripps.edu/). The ligands *viz.* chondroitin 4-sulphate disaccharide, chondroitin 4-sulphate tetrasaccharide and chondroitin 6-sulphate disaccharide were used for docking analysis. Ligand PDBs were obtained from pubchem (http://pubchem.ncbi.nlm.nih.gov) or ligands were drawn in chemsketch and converted to PDB files by OpenBabel 2.3.2a software. At first, the PDB files of protein and ligand were converted to PDBQT files by using AutoDock Tools. Thereafter, non-polar hydrogens were merged and their charges were assigned to carbon atoms. Grid box having dimension of 52, 92, 84 (*x*, *y*, *z* coordinates) with 0.375 Å grid point spacing and grid centre was designated at dimensions (x, y, and z): 23.05, 28.83, 44.96 was assigned around the active site. A scoring grid was calculated from the ligand structure

Please cite this article in press as: A. Rani, et al., Int. J. Biol. Macromol. (2017), https://doi.org/10.1016/j.ijbiomac.2017.11.087

to minimize the computation time. AutoDock/Vina was employed for docking using protein and ligand information along with grid box properties in the configuration file. All other parameters were set to default and the different conformations were generated. The best conformation was selected after evaluating the lowest binding energy of each conformation on the basis of scoring function used in Auto-Dock Vina. A more negative binding affinity indicates stronger binding. The docked conformation and interaction energies were saved and analyzed for protein-ligand complex with a lowest free energy of binding (ΔG). PyMOL (http://www.PyMOL.org) to find the hydrophobic interactions and polar contacts and Discovery studio visualizer-Accelrys was used to generate the 2D plots.

2.6. Protein melting studies of Ps*PL8A*

The protein melting curve of *Ps*PL8A was generated by subjecting the recombinant protein to varying temperatures and thereafter measuring the change in the absorbance at 280 nm (A_{280}) by a UV–vis spectrophotometer (Varian, Cary 100-Bio) following the method described previously [20]. A 30 μg of purified *Ps*PL8A in 1 ml 50 mM Tris-HCl, buffer, pH 7.2 was used. The absorbance at 280 nm (A_{280}) was measured by increasing the temperature at 5 °C per min from 25 °C to 100 °C using a peltier temperature controller. The protein solution was kept at a particular temperature for 3 min to attain the equilibrium and the melting curve of *Ps*PL8A was acquired. The melting curve of *Ps*PL8A was also studied in presence of 20 mM Ca^{2+} ion or 5 mM EDTA. A curve of absorbance at 280 nm versus temperature was plotted to generate the melting profile of *Ps*PL8A.

2.7. Structure analysis of Ps*PL8A in solution by small angle X-ray scattering (SAXS)*

2.7.1. SAXS data acquisition

The SAXS data for the *Ps*PL8A were collected using a one-dimensional CMOS Mythen detector (Dectris, Baden, Switzerland) on the SAXSpace instrument (Anton Paar GmbH, Graz, Austria). The radiation wavelength and the ratio of the sample to-detector distance were set to 1.5418 Å and 317 mm, respectively. For SAXS measurement, *Ps*PL8A (12 mg/ml) was used and passed through 0.22 μm filter (Millipore, USA). The sample was centrifuged at 24,000 ***g*** for 15 min at 4 °C prior to acquiring the scattering data. Two frames of 30 min at 10 °C were collected using 60 μl of *Ps*PL8A was used in a thermostated quartz capillary having 1 mm diameter. The images recorded on the CMOS Mythen detector were reduced in SAXStreat software to calibrate the position of the primary beam. SAXSquant software was used to subtract buffer contribution to obtain the scattering intensity I, as a function of momentum-transfer vector q ($q = 4\sin\theta/\lambda$ where λ and θ represent the wavelength of the X-rays and the scattering angle, respectively.

2.7.2. SAXS data processing

Initial data processing was done using PRIMUS software. The radius of gyration, Rg was computed from Guinier equation [21] and by indirect Fourier transform method using Gnom package [22]. The distance distribution function p(r) also was calculated using Gnom, and the maximum diameter, Dmax was obtained. The *ab initio* method was used to determine the low resolution shapes of the *Ps*PL8A from the scattering curve by Dammif [23]. The reconstructions of *Ps*PL8A were performed using 20 independent runs of Dammif. These solutions were subsequently checked by Damaver to create the final *ab initio* shape [24]. The modeled structures of the *Ps*PL8A were positioned in the envelopes using PyMOL.

2.8. Site-directed mutagenesis of Ps*PL8A by megaprimer PCR method*

2.8.1. Cloning of Ps*PL8A mutants*

Five mutants *viz.* N153A, H203A, Y212F, R266A and E349A were generated on the basis of the identified residues involved in active site of *Ps*PL8A. The site-directed mutagenesis was performed by megaprimer PCR approach [25]. Primers designed to introduce single amino acid mutation were prefabricated with *NheI* and *XhoI* restriction enzyme sites. The details of primers used for mutants are listed in Table S1. The PCR was carried out in two steps to introduce the single point mutations and 2037 bp amplicon was amplified for each mutant. The PCR amplification condition and reaction set up are given in Table S2 and Table S3, respectively. The PCR products and vector pET28a(+) were digested with *NheI* and *XhoI* enzymes and were ligated in 3:1 ratio of vector: insert. The ligation mix was incubated overnight at 16 °C. 5 μl of ligated product was transformed using 200 μl of *E. coli* DH5α competent cells prepared earlier. Cells were plated on LB agar plate containing kanamycin (50 μg/ml) and incubated at 37 °C overnight under static condition. The colonies were picked and grown on 5 ml LB broth containing Kanamycin at 37 °C 180 rpm for 12 h. The grown culture was centrifuged at 8000*g* at 4 °C for 10 min and the recombinant plasmid was isolated by Non-ionic detergent (NID) method [26]. The clone for the mutants *viz.* N153A, Y212F, H203A, R266A and E349A were screened by restriction digestion of respective plasmids.

2.8.2. Expression and purification of Ps*PL8A mutants*

E. coli BL21 (DE3) cells were used as host for expression of the mutants *viz.* N153A, Y212F, H203, E349A and R266A. The expression of R266A was not found in *E. coli* BL-21 cells, so its expression was further studied in *E.coli* BL-21 pLysS cells. The cells were grown in 100 ml LB medium supplemented with kanamycin (50 μg/ml) incubated at 37 °C with shaking at 180 rpm to mid exponential phase till the absorbance at 550 nm (A_{550}) reached 0.6. At this point isopropyl-1-thio-β-D-galactopyranoside (IPTG) was added to a final concentration of 1.0 mM and culture was incubated at 24 °C with shaking at 180 rpm. The cells were harvested by centrifugation at 8000 g and 4 °C for 10 min. The cell pellet was resuspended in 5 ml of 50 mM Tris-HCl buffer, pH 7.2 containing 1 mM phenyl methane sulfonyl fluoride (PMSF). The cells were sonicated (Sonics, vibra cells) by keeping on ice for 30 min with 10 s on and 15 s off pulse at 33% amplitude. The sonicated cells were centrifuged at 18,000 ***g*** and 4 °C for 45 min. The cell free supernatant was subjected to immobilized metal ion affinity chromatography (IMAC) for purification. The cell free extract was filtered through a 0.45 mm membrane and loaded on to a 1 ml HiTrap chelating column (GE Healthcare) equilibrated with 50 mM Tris-HCl buffer, pH 7.2 containing 300 mM NaCl and 60 mM imidazole. After extensively washing the column with 50 ml of same buffer the bound protein was eluted with 50 mM Tris-HCl buffer, pH 7.2 containing 300 mM NaCl and 350 mM Imidazole. SDS polyacrylamide gel electrophoresis (10.5% w/v) was used to assess the molecular weight and purity of recombinant *Ps*PL8A mutant proteins.

2.8.3. Activity assay of Ps*PL8A mutants with chondroitin 4-sulphate substrate*

The enzyme assay of wild type *Ps*PL8A and mutants were performed by incubating 0.15 μg of enzyme in 1 ml reaction mixture by containing 1 mg/ml of C4S substrate at optimum reaction conditions in 50 mM Tris-HCl buffer, pH 7.2 at 39 °C for 5 min. The unsaturated oligosaccharide product formation was monitored by an increase in the absorbance at 232 nm (A_{232}) as a function of time on a UV–vis spectrophotometer (Varian, Cary 100). The absorbance observed was converted to units using molar absorption coeffi-

Please cite this article in press as: A. Rani, et al., Int. J. Biol. Macromol. (2017), https://doi.org/10.1016/j.ijbiomac.2017.11.087

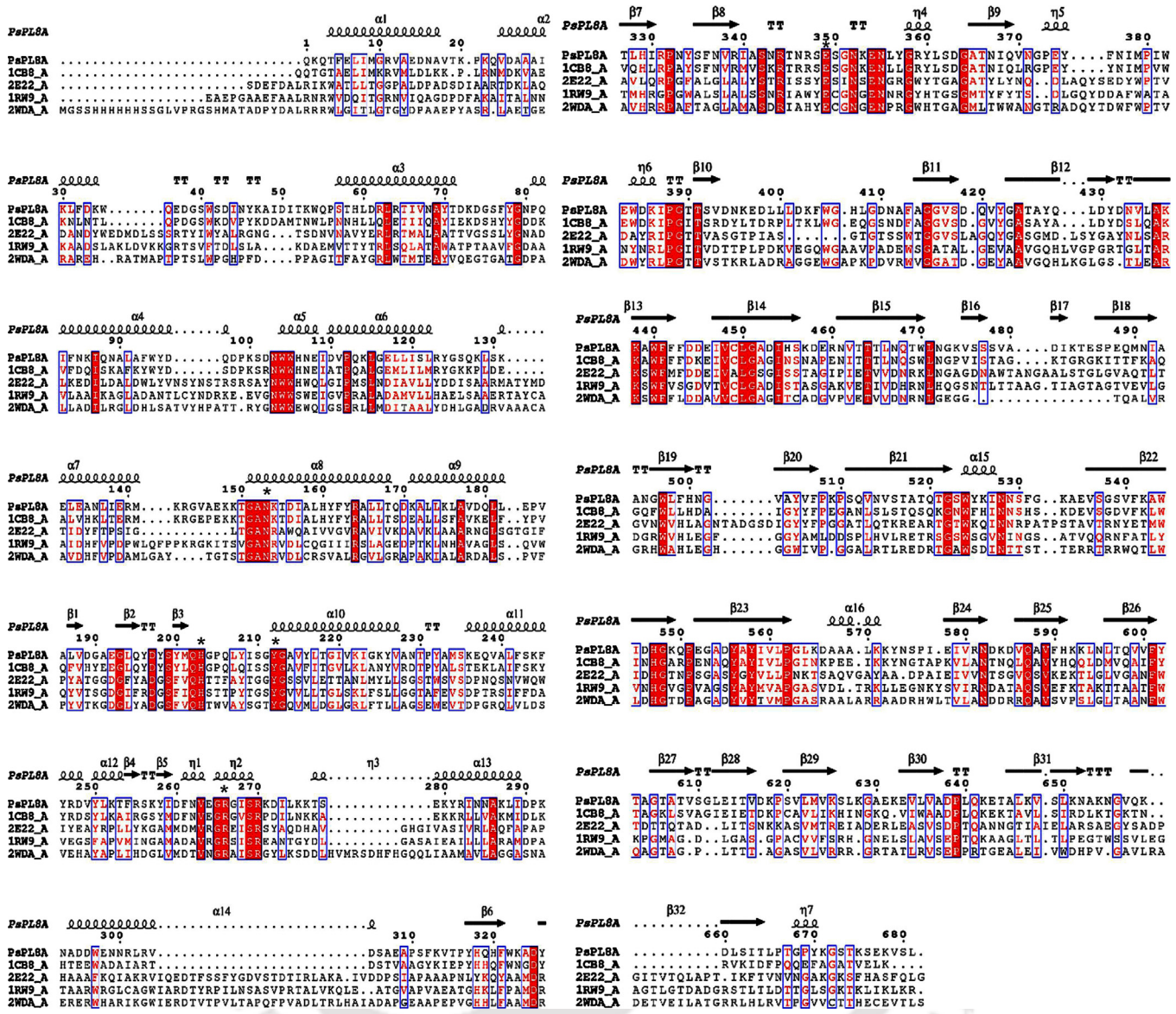

Fig. 1. Multiple sequence alignment of *Ps*PL8A from *Pedobacter saltans* with chondroitin AC lyases from *Flavobacterium heparinum* (1CB8_A), *Arthrobacter aurescens* (1RW9_A), *Streptomyces coelicolor* A3 (2WDA_A) and xanthan lyase from *Bacillus Sp* (2E22_A). The conserved residues are shown in red background and semi conserved residues are shown in box. Conserved catalytic residues are marked as asterisks. The figure was developed by EsPript3.0 (http://espript.ibcp.fr/). (For interpretation of the references to colour in this figure legend, the reader is referred to the web version of this article.)

cient (3800 M^{-1} cm^{-1}) for Δ4,5 unsaturated double bond formed in the reaction. One unit of enzyme activity was defined as amount of enzyme that liberates 1 μmol of unsaturated oligosaccharides product per min as calculated using a molar absorption coefficient (3800 M^{-1} cm^{-1}) [17,27].

2.8.4. Ligand binding studies of mutants by isothermal titration calorimetry (ITC)

The binding of *Ps*PL8A mutants, Y212F and H203A with C4S polysaccharide was quantified by ITC [28] (MICROCAL iTC 200, Malvern UK). Titration of mutant proteins and C4S polysaccharide was carried out using 50 mM Tris-HCl buffer, pH 7.2 at 25 °C. The reaction cell was filled by protein (Y212F or H203A) at a concentration of 80 μM, while the syringe was filled with 20 mg/ml (0.2%, w/v) of C4S polysaccharide.

Table 1
Secondary structure elements of *Ps*PL8A.

Secondary structure element	Percentage analysis by CD spectrum
α helix	27.31
β strand	22.70
random coils	49.99

3. Results and discussion

3.1. Sequence analysis of PsPL8A

The BLAST analysis of *Ps*PL8A sequence having GenBank accession no. ADY54337.1 from *Pedobacter saltans* displayed the sequence similarity with previously characterized chondroitin AC lyase. *Ps*PL8A showed 55% sequence identity and 95% query coverage with chondroitinase AC from *Flavobacterium heparinum* (1CB8_A). *Ps*PL8A further showed 26% and 25% sequence identity with chondroitin AC lyase belonging to *Streptomyces coelicolor* A3

Please cite this article in press as: A. Rani, et al., Int. J. Biol. Macromol. (2017), https://doi.org/10.1016/j.ijbiomac.2017.11.087

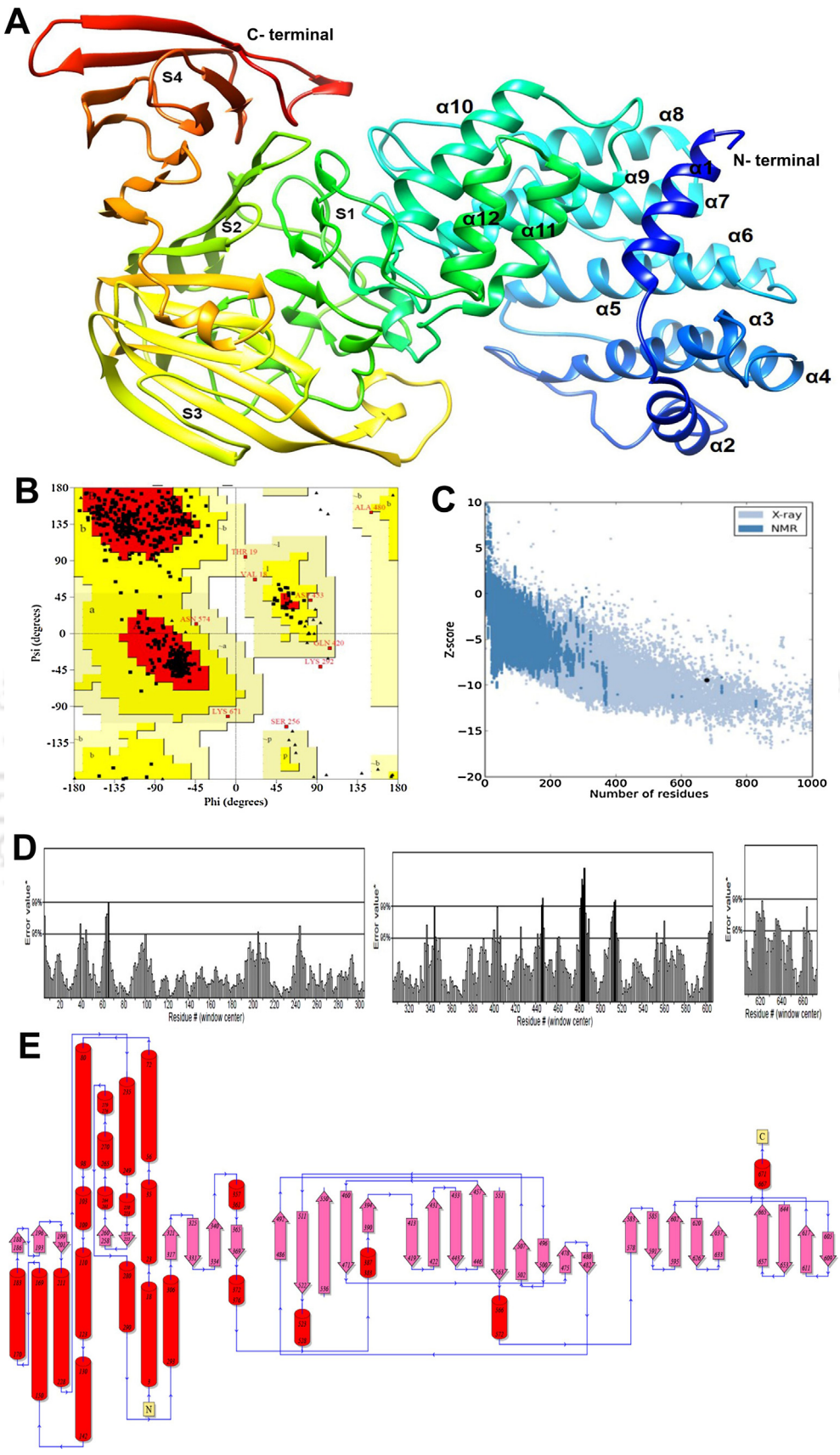

Fig. 2. Three dimensional predicted structure of *Ps*PL8A. (A) Modeled 3D structure. (B) Ramachandran plot. (C) ERRAT plot. (D) Z-score plot by ProSA-web server (E) Topology diagram of modeled *Ps*PL8A displaying the orientation of the secondary structures (thick arrows represent the β-strand and cylinders represent α-helix).

Please cite this article in press as: A. Rani, et al., Int. J. Biol. Macromol. (2017), https://doi.org/10.1016/j.ijbiomac.2017.11.087

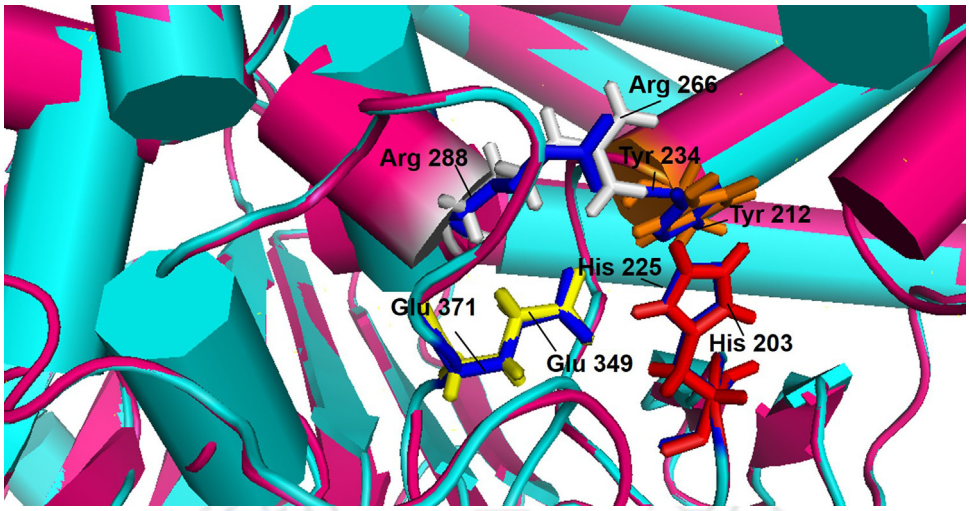

Fig. 3. Superposition of modeled structure of *Ps*PL8A (shown in magenta) with chondroitin AC lyase (1CB8_A) (shown in light-blue) from *Flavobacterium heparinum* showing the binding cleft. The residues from the binding cleft of *Ps*PL8A are marked as His203 (Red), Tyr212 (orange), Arg266 (Grey) and Glu349 (Yellow) and those from chondroitin AC lyase (1CB8_A) are marked in dark blue. The figure was generated using the PyMol program (http://www.pymol.org). (For interpretation of the references to colour in this figure legend, the reader is referred to the web version of this article.)

(2WDA_A) and *Arthrobacter aurescens* (1RW9_A), respectively. Multiple sequence alignment of *Ps*PL8A with the above mentioned chondroitin AC lyase sequences gave critical information about the conserved and semi conserved amino acid residue regions (Fig. 1). The SignalP 3.0 server deduced a N-terminal signal peptide sequence with a cleavage site between Ala22 and Gln23. The signal peptide consisted of 22 amino acids from N-terminal and consisted of a 679 amino acid *Ps*PL8A domain.

3.2. Homology modeling and structure validation of *Ps*PL8A

Modeled structure of *Ps*PL8A showed that it consists of two domains, a N-terminal domain having $(\alpha/\alpha)_6$ toroidal topology and C-terminal made up of antiparallel β-sheet folding structure (Fig. 2A). This $(\alpha/\alpha)_6$ toroidal fold and antiparallel β-sandwich structure are the conventional fold being assigned to the PL8 family [3,8,11]. The N-terminal of *Ps*PL8A is made up of nearly 330 amino acids forming a doubly layered horseshoe shaped or open toroid structure. The rest of 350 amino acids fold in a four layered β sandwich structure forming a C-terminal of *Ps*PL8A. The twelve alpha helices (α1-α12) in N-terminal are arranged in $(\alpha/\alpha)_6$ incomplete toroidal fold and these helices are linked with each other by the random coils. C-terminal is made up of β sheets with an exception of small α helix present between the β sheet S3 and S4. The chondroitin AC lyase from *Flavobacterium heparinum* also revealed the presence of small α helix in its C-terminal domain[3]. The N-terminal and C-terminal domain of *Ps*PL8A are linked by helix α12 and β sheet (S1) through the random coils. The quality of modeled structure after energy minimization was assessed on the tools available at SAVES server. Ramachandran plot developed by PROCHECK displayed that 98.5% residues were in the favoured region, 1.2% in the generously allowed region while only 0.5% of the residues were in the disallowed region (Fig. 2B). This implied that dihedral angles, phi (ϕ) and psi (ψ) of the modeled *Ps*PL8A structure have occupied favourable positions. The ERRAT plot also confirmed that modeled structure of *Ps*PL8A to be of satisfactory quality, with a quality factor of 90.89% (Fig. 2C). ProSA results indicate that the modelled protein is error free and reside in the X-ray zone with a score of −9.45 (Fig. 2D). The topology diagram of *Ps*PL8A is showed in Fig. 2E. The active site residues of *Ps*PL8A involved in catalysis were obtained by superposing the modeled *Ps*PL8A with the available structure of chondroitin AC lyase from *Flavobacterium heparinum* 1CB8_A. The superposition showed that the critical active site residues were conserved and aligned spatially. Asp153, His203, Tyr212, Arg266 and Glu349 were the active site residues of *Ps*PL8A (Fig. 3).

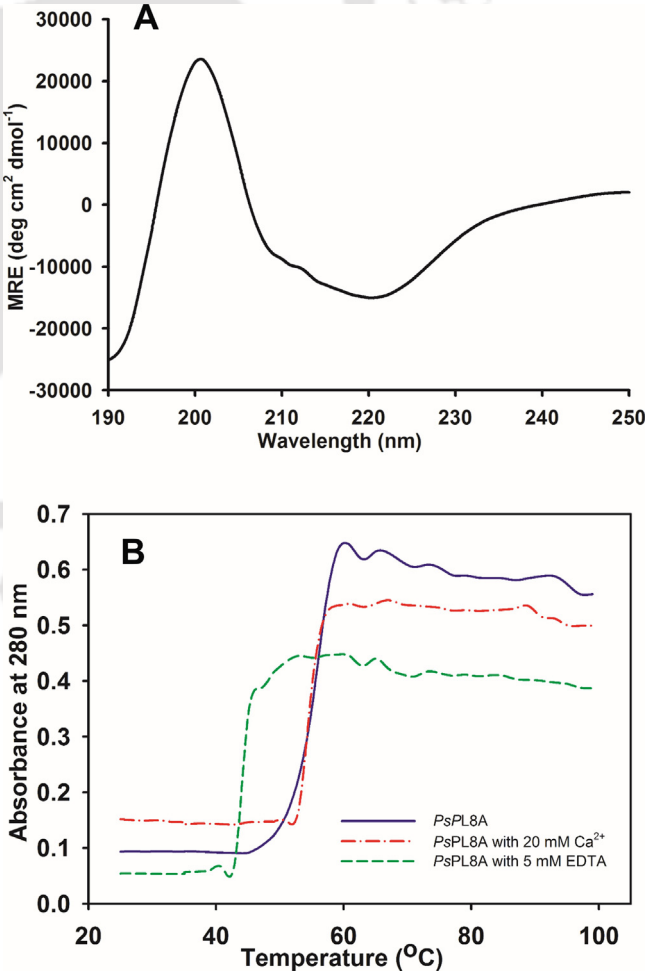

Fig. 4. (A) Far UV CD spectrum of *Ps*PL8A. (B) Protein-melting analysis displaying melting curve (—), in presence of 20 mM Ca^{2+} ions (-·-·-) and of 5 mM EDTA (—).

Please cite this article in press as: A. Rani, et al., Int. J. Biol. Macromol. (2017), https://doi.org/10.1016/j.ijbiomac.2017.11.087

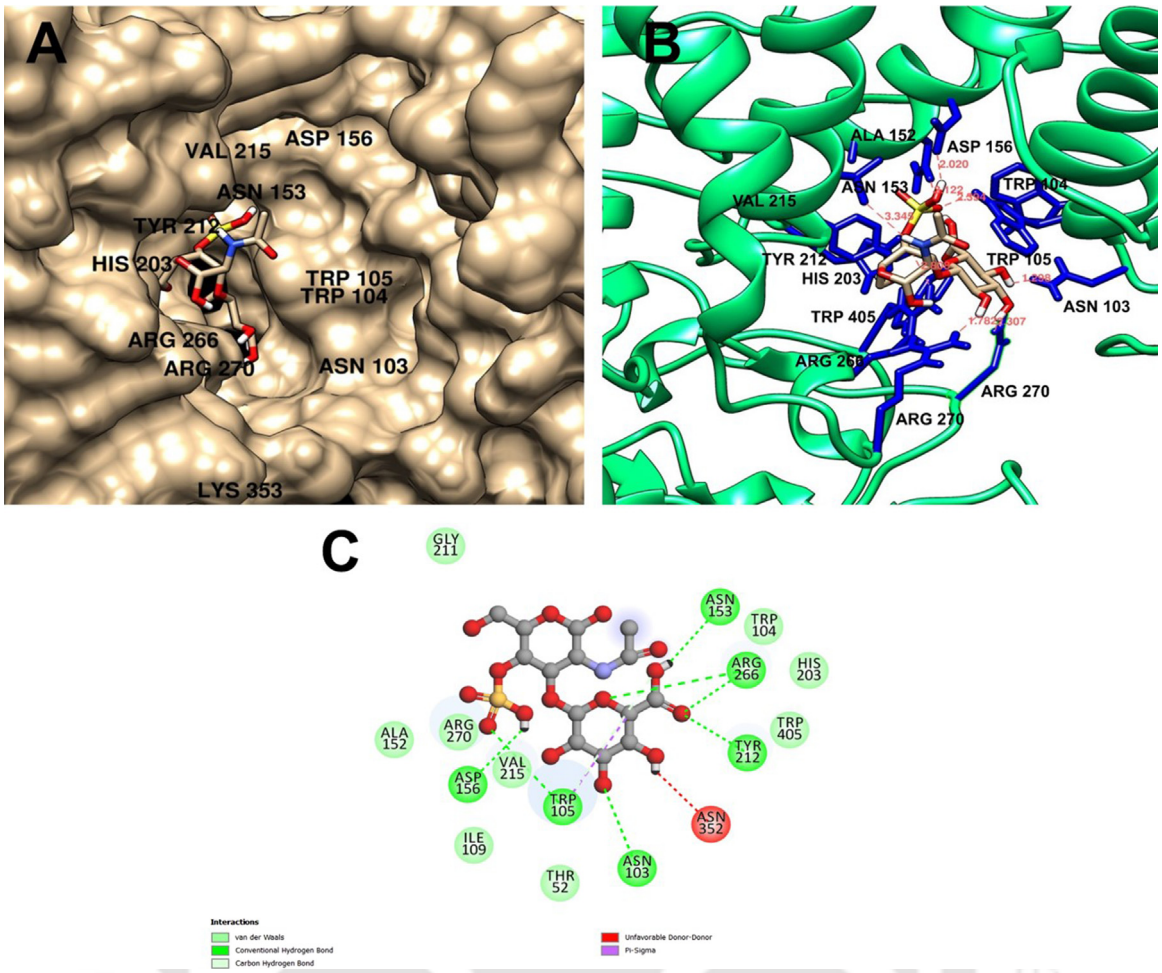

Fig. 5. (A) Surface view of the active site cleft of *Ps*PL8A showing the binding with ligand C4S disaccharide (B) C4S disaccharide interacting with the active site amino acid residues of *Ps*PL8A. (- - -) represents the hydrogen bond and the residues labelled are within 4 Å radius forming hydrophobic interaction with the ligand, (C) 2D Plot of C4S disaccharide interacting with the active side amino acid residues of *Ps*PL8A generated in Discovery studio visualizer-Accelrys.

3.3. Secondary structure analysis of PsPL8A by CD

Circular dichroism (CD) analysis was performed using K2D3 server and the CD spectrum of *Ps*PL8A was compared with the secondary structure of previously available proteins [29]. The CD spectrum of *Ps*PL8A revealed that it contains 27.31% α helices, 22.7% β sheets and rest 49.9% random coils (Fig. 4A) (Table 1). The results from the homology modeling of *Ps*PL8A also showed the presence of the α helices rich N-terminal domain and C-terminal consisting predominantly of β sheets. The overall structure of *Ps*PL8A matches well with previously solved crystal structure of chondroitin AC lyase form *Pedobacter heparinus* and *Arthrobacter aurescens* [3,8]. The result of CD analysis further consolidate the authenticity of modeled *Ps*PL8A structure.

3.4. Protein melting study of PsPL8A

The melting curve of *Ps*PL8A displayed a single peak at 60 °C. The protein starts unfolding at 45 °C and as the temperature increases it completely melts at 60 °C (Fig. 4B). In our previous biochemical characterization study of *Ps*PL8A [17], it was observed that the enzyme activity get enhanced by 2 fold in presence of 20 mM Ca^{2+} ions. Therefore, melting study of *Ps*PL8A was also studied in presence of 20 Mm Ca^{2+} ion, but there was no change in the melting temperature. This indicated that Ca^{2+} ion enhances only the enzyme activity of *Ps*PL8A but does not impart any structural stability to it. Melting study of *Ps*PL8A with 5 mM EDTA showed that it starts unfolding at 42 °C and gets completely melts at 52 °C. This 8 °C decrease in melting temperature of *Ps*PL8A in presence of EDTA might be due to chelation of the inherent divalent metal ion present in the protein structure.

Table 2
Amino acid residues of *Ps*PL8A showing polar interaction and residues within 4 Å of distance around the ligand at docking site.

Ligand	Binding Energy (kcal/mol)	Polar Interactions	Residues within 4Å
C6S disaccharide	−8.0	His 203, Gly211,Val 215, Arg266, Gly267, Arg270, Asn352, Trp 405	Asn 103, Trp105, Asn 153, Tyr 208, Tyr212, Gly265
C4S tetrasaccharide	−7.4	Asn103, Asn153, Tyr212, Arg266, Arg270, Asn 352,	Trp 105, Val215, Lys271, Ile 273, Trp 405, Phe531
C4S disaccharide	−7.2	Gly211, Ala214, Glu264, Gly267, Arg270, Lys275	Ile 51, Asn 103, Trp 105, His106, Tyr212, Val215, Arg266, Asn 352

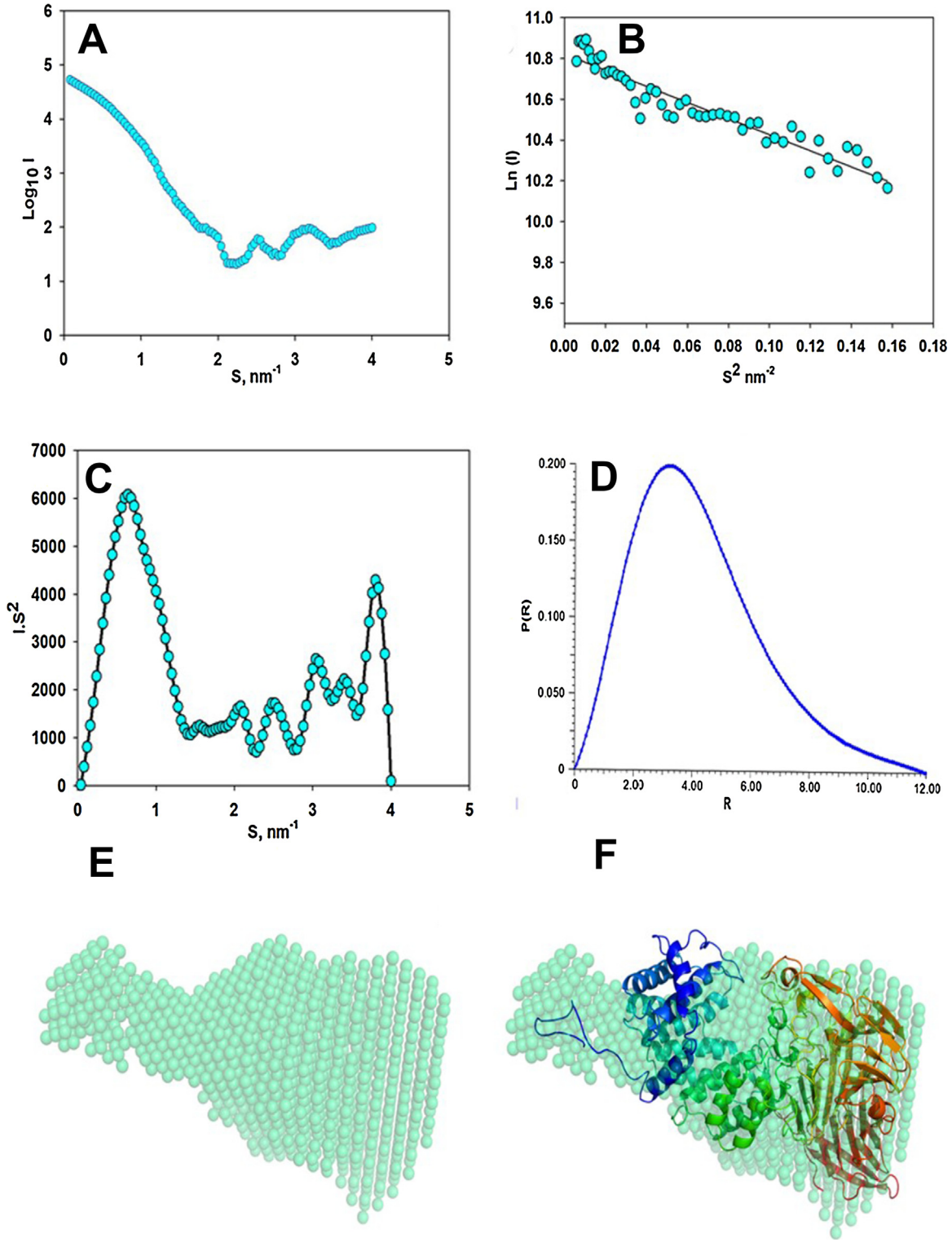

Fig. 6. Small Angle X-ray Scattering analysis of *Ps*PL8A (A) SAXS intensity profiles from samples of *Ps*PL8A, (B) Guinier plot of the SAXS intensities, *Ps*PL8A. The straight line was obtained by least-squares fitting in the region, (C) Kratky plots of the SAXS datasets confirmed the globular nature of the scattering *Ps*PL8A, (D) P(r) curves of the predominant scattering dataset of *Ps*PL8A plotted as a function of r, (E) *Ab initio* model of *Ps*PL8A generated by constructing independent dummy atom residue models using DAMMIF and averaging with DAMAVER. (F) Superposition of *ab initio* and modeled *Ps*PL8A. Images were generated using PyMol ver. 1.3 Schrödinger, LLC.

3.5. *Docking analysis and ligand binding interaction of* Ps*PL8A*

The previously reported cocrystal structure of chondroitin AC lyase from *Flavobacterium heparinum* with CS/DS oligosaccharide [8,33] and *Arthrobacter aurescens* [3] guided the location of catalytic core and conserved active site residues of *Ps*PL8A. The docking of *Ps*PL8A with C4S disaccharide (Fig. 5A), C6S disaccharide (Fig. S1A) and C4S tetrasaccharide (Fig. S2A) was performed to obtain best fit conformation of the ligands. The result of docking studies is summarized in Table 2. The docking analysis of *Ps*PL8A showed best binding affinity with C6S disaccharide with binding energy of −8.0 kcal/mol followed by C4S tetrasaccharide (−7.3 kcal/mol)

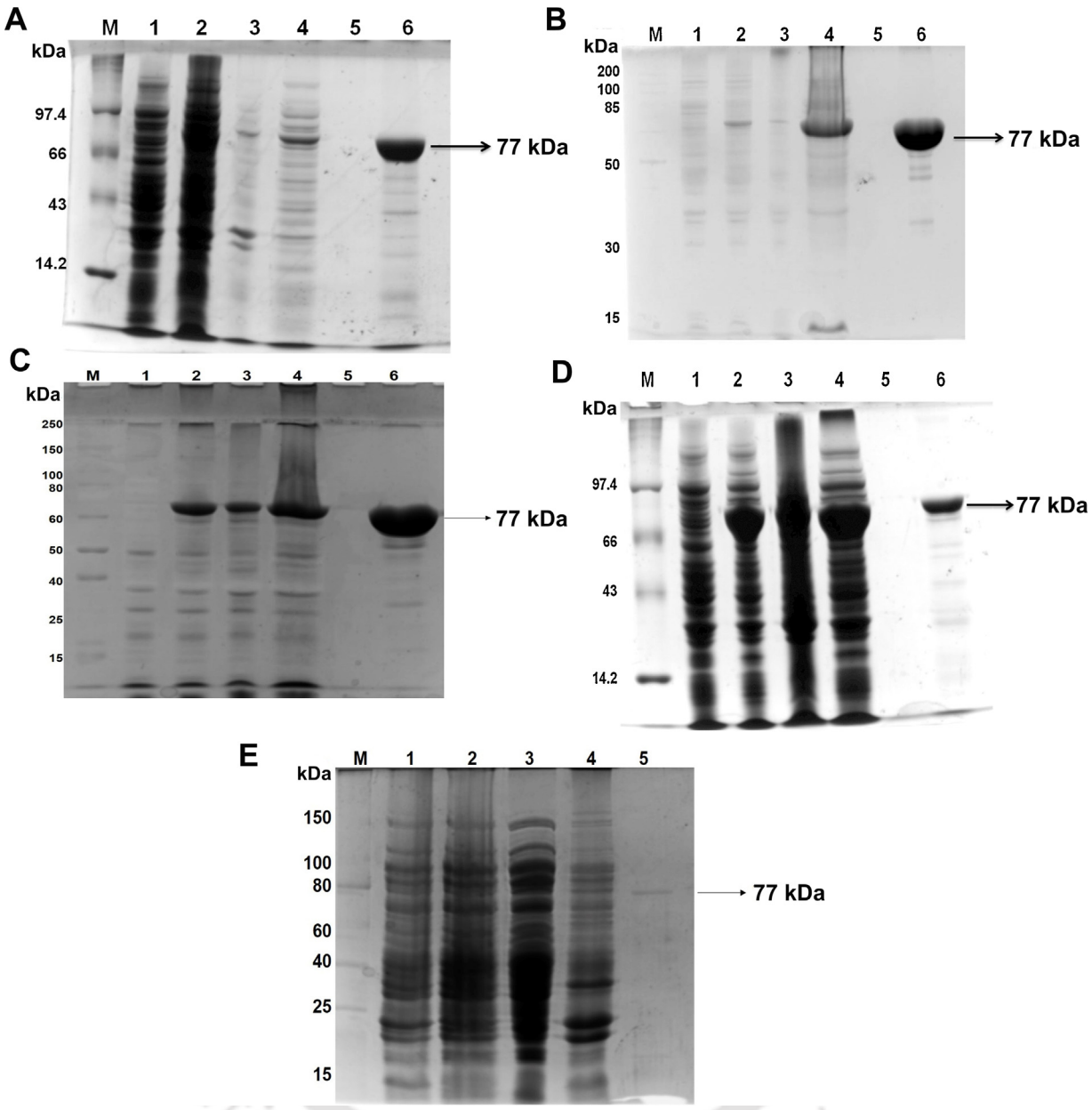

Fig. 7. SDS-PAGE (10.5%, w/v) gel showing over-expression and purification of *Ps*PL8A mutants using *E. coli* BL21 (DE3) cells; (A) N153A, (B) H203A, (C) Y212F, (D) E349A Lane 1: Uninduced BL21 (DE3) cells, Lane 2: Induced BL21 (DE3) cells, Lane 3: Cell pellet after sonication, Lane 4: Cell free extract, Lane 5: Last wash from the column and Lane 6: Purified recombinant *Ps*PL8A enzyme: Lane M: Protein marker, (E) Over-expression and purification of R266A in *E. coli* BL-21 pLysS cells.

and C4S disaccharide (−7.2 kcal/mol). The ligand binding study of *Ps*PL8A with C4S disaccharide revealed that substrate binding cavity is formed by α10, α11, α12 helices of N-terminal $(\alpha/\alpha)_6$ incomplete toroid domain and is enclosed by the loop region from the C-terminal (Fig. 5B&C). The catalytic core is majorly formed by the N-terminal α-helical domain and is broad enough to hold the CS polysaccharide chain. The presence of basic amino acids such as His203, Arg 266, Arg 270 and Lys 275 residues in the catalytic cavity might create the positive charge and hence contribute to the binding of acidic CS polysaccharide. The presence of basic residues (His225, Arg288, Arg292, Lys298 and Lys 299) was also observed in the catalytic core of chondroitin AC lyase from *Flavobacterium heparinum* [3]. His203 and R266 residues of *Ps*PL8A lies in the stretch of well conserved residues and corresponds to the His225 and R288 of chondroitin AC lyase from *Flavobacterium heparinum* [3]. The aromatic residues such as Trp105, Tyr208 and Tyr212 might help in the accommodation of the sugar ring of the CS substrate. The docking analysis of *Ps*PL8A was also studied with C6S disaccharide (Fig. S1B&C) and C4S tetrasaccharide (Fig. S2B&C). This docking study showed that polar interactions taking place between active site amino acid residues and the ligand molecule (Table 2). The docking result inferred that Asn153, His203, Tyr212, Arg266, Glu349 are the key catalytic residues of *Ps*PL8A. A similar catalytic tetrad including His225, Tyr234, Arg288 and Glu371 were reported in the chondroitin AC lyase from *Flavobacterium heparinum*. In addition to these critical active site residues, there are several other residues in *Ps*PL8A, such as Trp105, Tyr 208, Gly211, Val215 and Arg270 that are proximal to the CS substrate and hence could play a key role in positioning the substrate for enzyme action.

Table 3
Enzyme activity of *Ps*PL8A mutants.

Enzyme	Relative Activity (%)	
	Chondroitin4-Sulphate	Chondroitin 6-Sulphate
*Ps*PL8A (wild type)	100	100
N153A	0.66	ND
H203A	0.13	ND
Y212F	3.80	ND
R266A	0.38	ND
E349A	0.80	ND

ND: Not detected.

3.6. Structure analysis of Ps*PL8A* by small angle X-ray scattering (SAXS)

SAXS analysis of *Ps*PL8A was performed using scattering data collected at 12 mg/ml concentration (Fig. 6A). Guinier analysis for *Ps*PL8A indicate that the predominant shape by a radius of gyration (Rg) 3.19 ± 0.09 nm. Alternatively, Guinier approximation of a rod shape *Ps*PL8A implied an RC value of ~1.57 nm (Fig. 6B). The linearity of the Guinier plot in the low q-region shows that the scattered intensities follow the Guinier law and suggesting the length of *Ps*PL8A about 10 nm. The Kratky plot analysis of the *Ps*PL8A indicated that it is fully folded state in solution (Fig. 6C). The distribution profile of interatomic vectors [P(r)] evaluated by the indirect Fourier transform over a range of 0.01-0.3 concluded that the predominant solution shape of *Ps*PL8A are similar (modeled structure and ab initio generated model) and characterized by a D_{max} and Rg value of 12 nm and 3.3 nm, respectively (Fig. 6D). Experimentally obtained parameters matched with the modeled *Ps*PL8A structure parameters, which supported that the solution shape of *Ps*PL8A is in good correlation with modeled structure and its homologous crystal structures. Multiple independent cycles of *ab initio* modelling by DAMMIF were computed without symmetry restrictions and were averaged by DAMAVER to produce a low-resolution *ab initio* shape for *Ps*PL8A (Fig. 6E). The Dummy Atom Molecule of the *Ps*PL8A is elongated, and clearly reveals a single domain. The *ab initio* derived dummy atom model superpose well with the modeled *Ps*PL8A while, few α-helices and loop region protruding the dummy atom model of *Ps*PL8A derived from the SAXS Data. These regions outside the envelop may be due to the flexibility of the loops (Fig. 6F).

3.7. Construction of Ps*PL8A mutants by site-directed mutagenesis*

Based on the structural model of *Ps*PL8A and molecular docking studies with C4S disaccharide/tetrasaccharide, the putative catalytic residues N153, H203, Y212, R266 and E349 were selected for site-directed mutagenesis. The DNA sequence of 2037 base pairs encoding mutants N153A, H203A, Y212F, R266A and E349A was amplified by a two-step PCR megaprimer approach (Fig. S3). A single point mutation was introduced in each mutant. The *Ps*PL8A mutants were cloned in pET28a(+) expression vector and the positive clones were screened by restriction digestion (Fig. S3). The recombinant proteins were purified to apparent homogeneity level by immobilised metal ion chromatography (IMAC). The expression and purification of the five recombinant *Ps*PL8A mutants was analysed by SDS-PAGE (10.5%, w/v) gel and all showed a molecular size of approximately, 77 kDa (Fig. 7).

3.8. Binding and activity analysis of mutants and catalytic mechanism of Ps*PL8A*

The mutants N153A, H203A, Y212F, R266A and E349A were developed as mentioned in section 3.7, in order to probe the role of these residues in catalysis. The specific activity of all mutants was determined and compared with the wild-type *Ps*PL8A (Table 3). The

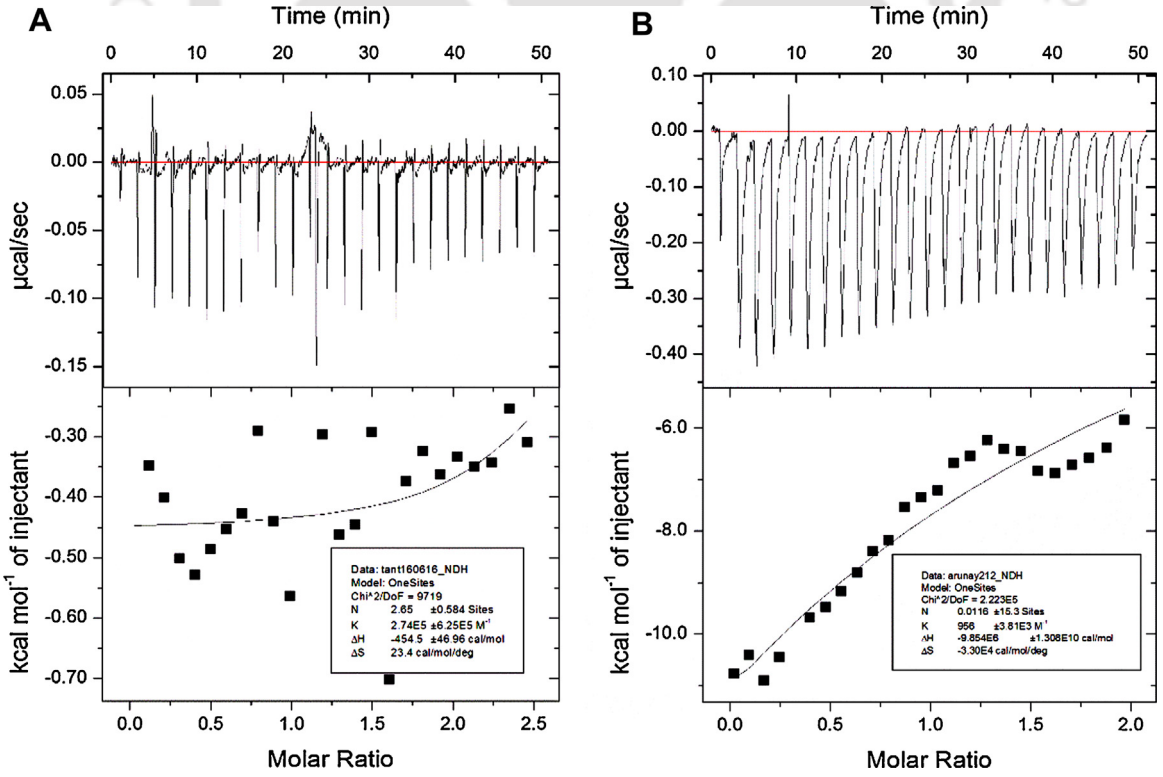

Fig. 8. Representative ITC data of *Ps*PL8A mutants with C4S polysaccharide (A) H203A (B) Y212F. The ligand C4S polysaccharide (20 mg/ml) in syringe was titrated with 80 μM of protein in the cell. The top half of each panel shows the raw ITC heat while the bottom half represents the integrated peak areas fitted to a single-site binding model with MicroCal Origin Ver. 8.0 ITC was carried out using 50 mM Tris-HCl buffer, pH 7.2.

results showed that the mutants N153A, H203A, Y212F, R266A and E349A gave 0.66%, 0.13%, 3.8%, 0.38% and 0.80% relative activity against C4S substrate taking the wild-type *Ps*PL8A activity as 100%. All the mutants showed no activity against C6S substrate when assayed under the same conditions. The complete loss in activity of the mutant proteins showed that these residues are critical and catalytic residues of *Ps*PL8A.

*Ps*PL8A showed an initial random endolytic mode generating higher C4S oligosaccharide up to dodeca-saccharide along with C4S disaccharide, while disaccharide was the major product observed after 1 h of catalysis as previously reported [17]. One of the plausible explanation for this mode of catalysis could be, since the catalytic cleft is formed by N-terminal and two-three loop region from C-terminal, the catalytic core of *Ps*PL8A is not rigid and the loops might be flexible enough for periodically opening and allowing the entry of CS chain inside to the catalytic groove. Such catalytic core was also reported for chondroitin AC lyase from *Flavobacterium heparinum* [30]. Initially as the substrate enters the catalytic core, *Ps*PL8A enzyme starts acting randomly and generates the higher oligosaccharide as well as the disaccharide, while with time it degrades all higher oligosaccharide to final disaccharide product, suggesting its more affinity towards disaccharide. The tunnel like catalytic core of cellobiohydrolase also showed the evidence of local conformational changes upon binding of the polysaccharide [31,32]. The crystal structure of endolytic chondroitin AC lyase from *Flavobacterium heparinum* showed the catalytic tunnel which is not rigid and having flexible loops [30] while, the catalytic core of exolytic *Arthrobacter aurescens* [8] was covered by the two loops, restricting the movement of only two to three sugar residues.

The binding of mutants Y212F and H203A with C4S polysaccharide by ITC analysis showed that H203A has no binding with C4S polysaccharide (Fig. 8A), implicating that mutation of His203 residue with alanine leads to the loss of activity as well as the ligand binding affinity. However, Y212F showed weak binding against C4S polysaccharide (Fig. 8B) as it also retained ~4% relative activity (Table 3). This revealed that Y212 residue is involved in the catalysis and substrate binding. Similarly, the crystal structure analysis of Y242F mutant of chondroitin AC lyase from *Flavobacterium heparinum* complex with CS-tetrasaccharide showed binding at the same position of catalytic site as that of the wild-type enzyme, suggesting the involvement of Tyr242 in catalysis and substrate binding [30]. In β-elimination a general base is required to abstract the proton from C-5 of the uronic acid, generating an enolate anion intermediate, followed by proton donation by a general acid or water molecule and concomitant release of the leaving group [6]. Three probable theories for catalytic mechanism of chondroitin AC lyase from *Flavobacterium heparinum* have been proposed [30] *viz.* i) His acting as general base while Tyr as general acid, ii) Tyr acting as both general acid and base iii) Tyr acting as general base and Arg as general acid. In other study it was suggested that Tyr242 acts as a general base in chondroitin AC lyase enzyme from *Flavobacterium heparinum* [7]. The structure comparison, mutagenesis and binding results of *Ps*PL8A indicated the roles of Y212 and H203 or R266 as probable general base and general acid, respectively. The residues N153 and E349 of *Ps*PL8A, are likely contributing to the charge neutralization and stabilization of the enolate anion intermediate during β-elimination.

4. Conclusions

The three dimensional structure of chondroitin AC lyase (*Ps*PL8A) of family 8 polysaccharide lyase from *Pedobacter saltans* was generated by homology modeling. The structure showed a N-terminal $(\alpha/\alpha)_6$ incomplete toroidal fold and a layered β sandwich structure at C-terminal. The secondary structure analyses of *Ps*PL8A displayed presence of more α-helices as compared to β sheets. SAXS analysis of *Ps*PL8A revealed a fully folded structure in solution form. The roles of key catalytic residues Y212 and H203 or Arg266 as probable general base and general acid, respectively were investigated by site-directed mutagenesis and binding studies by ITC. The structural characterization will enable to elucidate the complete mechanism underlying the mode catalysis of chondroitin AC lyase (*Ps*PL8A). However, the future challenge includes to determine the crystal structure of *Ps*PL8A by X-ray crystallography.

Conflict of interest

The authors declare no conflict of interest.

Acknowledgements

The research work and AR was supported by Council of Scientific and Industrial Research (CSIR) project no. 37(1672)/16/EMR-II to AG. The authors thank Prof. M.N Gupta and Ms. Joyeeta Mukherjee of Indian Institute of Technology Delhi for CD analysis. The authors also thank Dr. Ashish and Dr. Kunzes Dolma from Institute of Microbial Technology Chandigarh for SAXS analysis.

Appendix A. Supplementary data

Supplementary data associated with this article can be found, in the online version, at https://doi.org/10.1016/j.ijbiomac.2017.11.087.

References

[1] B.L. Cantarel, P.M. Coutinho, C. Rancurel, T. Bernard, V. Lombard, B. Henrissat, The Carbohydrate-Active EnZymes database (CAZy): an expert resource for glycogenomics, Nucleic Acids Res. 37 (Suppl. 1) (2009) D233–D238.
[2] C.S. Rye, S.G. Withers, Elucidation of the mechanism of polysaccharide cleavage by chondroitin AC Lyase from *Flavobacterium heparinum*, J. Am. Chem. Soc. 124 (33) (2002) 9756–9767.
[3] J. Féthière, B. Eggimann, M. Cygler, Crystal structure of chondroitin AC lyase, a representative of a family of glycosaminoglycan degrading enzymes, J. Mol. Biol. 288 (4) (1999) 635–647.
[4] V. Prabhakar, R. Raman, I. Capila, C.J. Bosques, K. Pojasek, R. Sasisekharan, Biochemical characterization of the chondroitinase ABC I active site, Biochem. J 390 (2) (2005) 395–405.
[5] A. Rani, S. Patel, A. Goyal, Chondroitin sulfate (CS) lyases: structure, function and application in therapeutics, Curr Protein Pept Sci 18 (2017), http://dx.doi.org/10.2174/1389203718666170102112805.
[6] P. Gacesa, Alginate-modifying enzymes: a proposed unified mechanism of action for the lyases and epimerases, FEBS Lett. 212 (2) (1987) 199–202.
[7] C.S. Rye, A. Matte, M. Cygler, S.G. Withers, An atypical approach identifies TYR234 as the key base catalyst in chondroitin AC lyase, Chembiochem 7 (4) (2006) 631–637.
[8] V.V. Lunin, Y. Li, R.J. Linhardt, H. Miyazono, M. Kyogashima, T. Kaneko, A.W. Bell, M. Cygler, High-resolution crystal structure of Arthrobacter aurescens chondroitin AC lyase: an enzyme–substrate complex defines the catalytic mechanism, J. Mol. Biol. 337 (2) (2004) 367–386.
[9] S. Li, S.J. Kelly, E. Lamani, M. Ferraroni, M.J. Jedrzejas, Structural basis of hyaluronan degradation by *Streptococcus pneumoniae* hyaluronate lyase, EMBO J. 19 (6) (2000) 1228–1240.
[10] W. Huang, V. Lunin, Y. Li, S. Suzuki, N. Sugiura, H. Miyazono, M. Cygler, Crystal structure of *Proteus vulgaris* chondroitin sulfate ABC lyase I at 1.9 Å resolution, J. Mol. Biol. 328 (3) (2003) 623–634.
[11] M.L. Garron, M. Cygler, Structural and mechanistic classification of uronic acid-containing polysaccharide lyases, Glycobiology 20 (12) (2010) 1547–1573.
[12] S.F. Altschul, W. Gish, W. Miller, E.W. Myers, D.J. Lipman, Basic local alignment search tool, J. Mol. Biol. 215 (3) (1990) 403–410.
[13] B. Webb, A. Sali, Protein structure modeling with MODELLER, Protein Struct. Prediction (2014) 1–15.
[14] A. Šali, T.L. Blundell, Comparative protein modelling by satisfaction of spatial restraints, J. Mol. Biol. 234 (3) (1993) 779–815.
[15] R. Méndez, R. Leplae, M.F. Lensink, S.J. Wodak, Assessment of CAPRI predictions in rounds 3–5 shows progress in docking procedures, Proteins: Struct. Funct. Bioinf. 60 (2) (2005) 150–169.
[16] D. Bhattacharya, J. Nowotny, R. Cao, J. Cheng, 3Drefine: an interactive web server for efficient protein structure refinement, Nucleic Acids Res. 44 (W1) (2016) W406–W409.

[17] A. Rani, A. Goyal, A new member of family 8 polysaccharide lyase chondroitin AC lyase (*Ps*PL8A) from *Pedobacter saltans* displays endo-and exo-lytic catalysis, J. Mol. Catal. B: Enzym. 134 (2016) 215–224.
[18] S.M. Kelly, T.J. Jess, N.C. Price, How to study proteins by circular dichroism? Biochimica et Biophysica Acta (BBA)-Proteins Proteomics 1751 (2) (2005) 119–139.
[19] O. Trott, A.J. Olson, AutoDock Vina: improving the speed and accuracy of docking with a new scoring function, efficient optimization and multithreading, J. Comput. Chem. 31 (2010).
[20] I.A. Dvortsov, N.A. Lunina, L.A. Chekanovskaya, W.H. Schwarz, V.V. Zverlov, G.A. Velikodvorskaya, Carbohydrate-binding properties of a separately folding protein module from β-1, 3-glucanase Lic16A of *Clostridium thermocellum*, Microbiology 155 (7) (2009) 2442–2449.
[21] A. Guiner, G. Fournet, C.B. Walker, Small Angle Scattering of X-rays, J. Wiley & Sons, New York, 1955.
[22] A.V. Semenyuk, D.I. Svergun, GNOM–a program package for small-angle scattering data processing, J. Appl. Crystallogr. 24 (5) (1991) 537–540.
[23] D. Franke, D.I. Svergun, DAMMIF, a program for rapid ab-initio shape determination in small-angle scattering, J. Appl. Crystallogr. 42 (2) (2009) 342–346.
[24] V.V. Volkov, D.I. Svergun, Uniqueness of *ab initio* shape determination in small-angle scattering, J. Appl. Crystallogr. 36 (3) (2003) 860–864.
[25] S.H. Ke, E.L. Madison, Rapid and efficient site-directed mutagenesis by single-tube 'megaprimer'PCR method, Nucleic Acids Res. 25 (16) (1997) 3371–3372.
[26] G. Lezin, Y. Kosaka, H.J. Yost, M.R. Kuehn, L. Brunelli, A one-step miniprep for the isolation of plasmid DNA and lambda phage particles, PLoS One 6 (8) (2011) e23457.
[27] K. Pojasek, Z. Shriver, P. Kiley, G. Venkataraman, R. Sasisekharan, Recombinant expression, purification, and kinetic characterization of chondroitinase AC and chondroitinase B from *Flavobacterium heparinum*, Biochem. Biophys. Res. Commun. 286 (2) (2001) 343–351.
[28] D.N. Bolam, H. Xie, G. Pell, D. Hogg, G. Galbraith, B. Henrissat, H.J. Gilbert, X4 modules represent a new family of carbohydrate-binding modules that display novel properties, J. Biol. Chem. 279 (22) (2004) 22953–22963.
[29] C. Louis-Jeune, M.A. Andrade-Navarro, C. Perez-Iratxeta, Prediction of protein secondary structure from circular dichroism using theoretically derived spectra, Proteins: Struct. Funct. Bioinf. 80 (2) (2012) 374–381.
[30] W. Huang, L. Boju, L. Tkalec, H. Su, H.O. Yang, N.S. Gunay, R.J. Linhardt, Y.S. Kim, A. Matte, M. Cygler, Active site of chondroitin ac lyase revealed by the structure of enzyme-oligosaccharide complexes and mutagenesis, Biochemistry 40 (8) (2001) 2359–2372.
[31] A. Varrot, M. Schülein, G.J. Davies, Structural changes of the active site tunnel of *Humicola insolens* cellobiohydrolase, Cel6A, upon oligosaccharide binding, Biochemistry 38 (28) (1999) 8884–8891.
[32] J.Y. Zou, G.J. Kleywegt, J. Ståhlberg, H. Driguez, W. Nerinckx, M. Claeyssens, A. Koivula, T.T. Teeri, T.A. Jones, Crystallographic evidence for substrate ring distortion and protein conformational changes during catalysis in cellobiohydrolase Ce16A from *Trichoderma reesei*, Structure 7 (9) (1999) 1035–1045.

Please cite this article in press as: A. Rani, et al., Int. J. Biol. Macromol. (2017), https://doi.org/10.1016/j.ijbiomac.2017.11.087